LASER LIGHT SCATTERING

AS

A PROBE OF BOVINE SPERM MOTILITY

A thesis

submitted to the Physics Department

of the

University of Waikato

in partial fulfilment of the requirements

for the Degree of

Doctor of Philosophy

MURRAY W. WOOLFORD

DECEMBER, 1980.

ABSTRACT

Laser light scattering measurements of sperm motility have traditionally assumed spermatozoa to behave as point scatterers at small forward scattering angles, and motile cells to exhibit an isotropic distribution of translation vectors. Such assumptions have lead to interpretations of fluctuations in the detected optical field as arising from Doppler-beats.

Experimental and theoretical results presented in this thesis show that for bull spermatozoa, the large dimensions ($>> \lambda$) and slab-like conformation of the rotating head result in large intensity fluctuations at the photodetector which call into question the role of coherence and render the Doppler-beat interpretation untenable.

A sharply peaked scattering lobe (width $\sim 20^{\circ}$) lying in the equatorial plane of the head is shown to give an intensity peak when the normal to the head plane becomes aligned with the scattering vector. Consequently only those motile cells swimming with appropriately aligned translation vectors contribute to the detected signal. Immotile cells, which are shown to exhibit geotaxis, become visible only to a detector aligned in the horizontal plane. A marked concentration dependence in the ratio of motile and immotile autocorrelation components is modelled on the basis of hydrodynamic interactions between motile and immotile fractions, which result in immotile cells being reoriented outside the range of visible alignments.

A complex opto-dynamic system is defined by a series of experiments which demonstrate that the traditional laser light scattering geometry gives only an empirical measure of the percent motile spermatozoa but may be used to obtain an absolute measurement of the head rotation rate.

Discussion is given to variations in the scattering geometry and sample chamber design which are more appropriate to the phenomenology within the system.

ACKNOWLEDGEMENTS

This research programme was carried out on study leave granted by the New Zealand Ministry of Agriculture and Fisheries. Equipment and resources made available by the Research Division of the Ministry were essential factors in the success of the project.

An extensive multi-disciplinary project such as this, inevitably depends on the direct and indirect contributions of many people. I hold in very high regard the patience, perseverance, understanding, co-operation and hard work of my colleagues and associates who have been associated with this research programme.

In particular, Messrs. P. Shannon and B. Curson of the New Zealand Dairy Board, Newstead Artificial Breeding Research Centre, have been key participants. They have provided vital technology in sperm physiology, diluents and technical procedures. Without their resources, their expertise, many hours of work, and enthusiastic participation, very little could have been achieved. I well recall the many long distance trips and quiet efficient preparation of samples which Brian Curson so willingly undertook.

The laser light scattering and computer facilities provided by Dr. J. D. Harvey at Auckland University for the earlier phases of the project, together with his contributions to the programme, particularly our co-operative studies in the later phases, have been of great significance. His participation and contributions have been highly valued.

Dr. R. A. Sherlock of the Physics Department, University of Waikato, has been most helpful in our frequent discussions and debates on the progress of the work. I am most grateful for his participation as project supervisor and his infinite patience in reading and commenting on successive stages of this thesis.

Professor D. F. Walls, also of the University of Waikato, has given enthusiastic support to the project from its earliest days and was originally responsible for generating local interest in laser light scattering methods.

At the Ruakura Agricultural Research Centre, Mr. D. S. M. Phillips, section leader of the Biophysics group, has been continually in touch with the project, incorporated it into the group's research programme, and accommodated the numerous problems which it has created in terms of research resources.

I would like also to acknowledge the contribution of Mr. J. K. Woolhouse of the Biophysics group who started the programme in the first instance with his M.Sc. thesis in 1976. This investigation has basically taken up where he left off. I thank him for his participation and contributions along the way, inclusive of the various vigorous discussions which occasionally arose. Very valuable contributions have also been made by my other colleagues. In particular, I appreciate the many hours of patience and fine work which Ken Buckle of our Biophysics group put into the fabrication of numerous sample cells and other pieces of equipment. Malcolm Stewart constructed the various items of electronic hardware and his input has been of valuable assistance.

In the last phase of the work, I very much enjoyed the collaboration with Dr. S. A. Hawley of the Eye Research Institute of the Retina Foundation, Boston, who joined our group as a research fellow.

To Peg and Bram Clark for their support and scrutiny of the manuscript, many thanks.

On a personal basis, a project such as this inevitably has a significant effect on one's own life. In many respects, it has been an enjoyable and fulfilling experience. In other ways, it has brought many strains and much pressure. I recognise the involvement of many people in this respect and therefore express my appreciation of the sacrifices they have made and the support they have given.

..... To all the animals

and

Rosaline.....

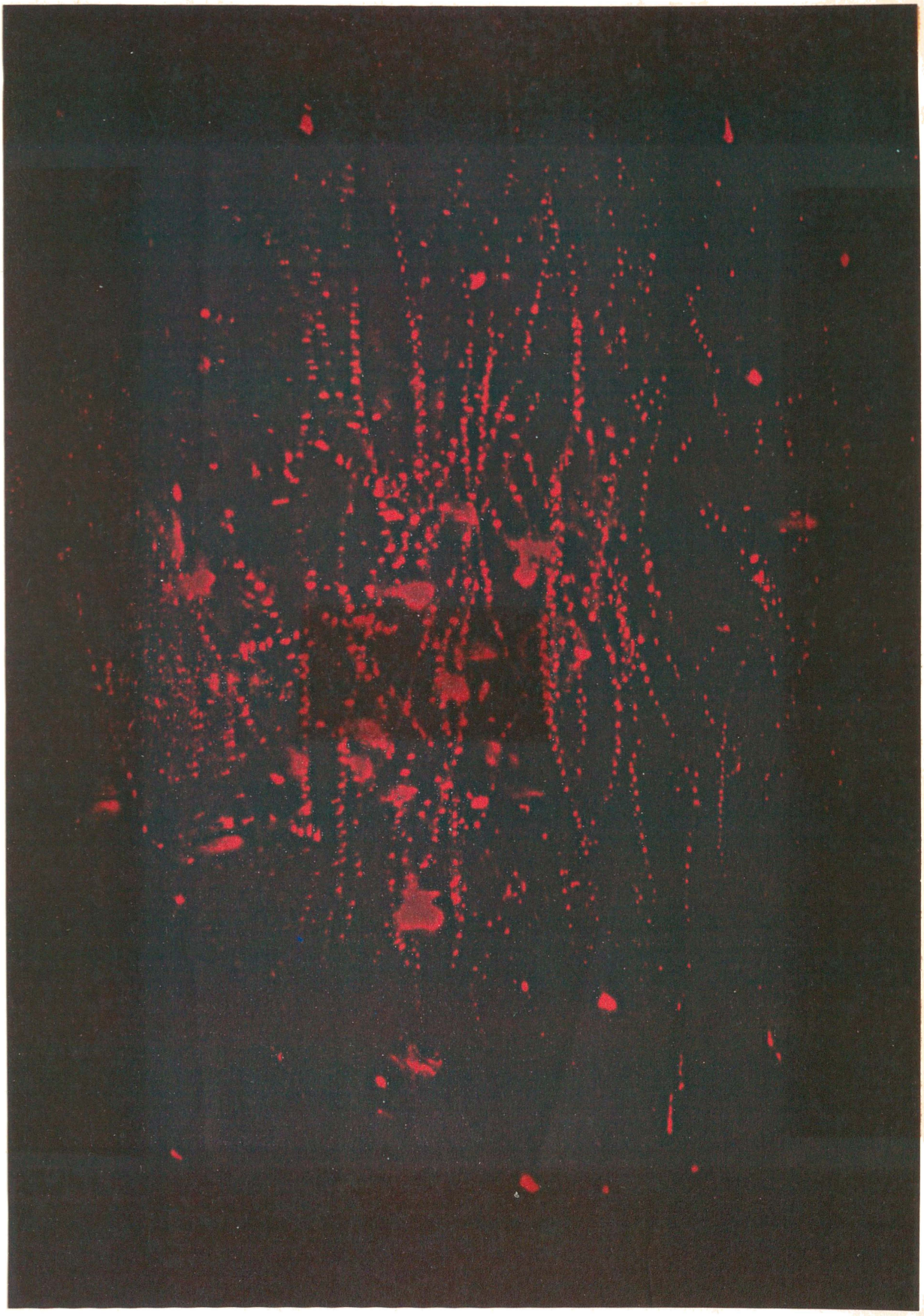

FRONT PLATE I

Swimming trajectories of motile bull spermatozoa and suspended immotile cells as viewed from their scattered light field.

TABLE OF CONTENTS

Page

Page

Page

Page

GLOSSARY OF ABBREVIATIONS

AAR	Autocorrelation Amplitude Ratio
ACA	Autocorrelation Function Amplitude
ACF	Autocorrelation Function
ADC	Analogue-to-Digital Converter
CEY	Cleared (Optically) Egg-Yolk Extender
DAC	Digital-to-Analogue Converter
DC	Mean Signal Amplitude
DLS	Differential Light Scattering
E. coli.	*Escherichia coli.*
EYC	Egg-Yolk-Citrate Based Extender
EYG	Egg-Yolk-Glycine Based Extender
FFT	Fast Fourier Transform
LBS	Light Beating Spectroscopy
NTR	Non-Translating
NZDB	New Zealand Dairy Board
TR	Translating
RLQF	Least Squares Functional Fitting Algorithm
TMV	Tobacco Mosaic Virus
UV	Ultra-Violet
VSP	Seminal Plasma from a Vasectomised Bull.

1.0 An introductory perspective

Reproduction is fundamental to the existence of all living species. Nature shows enormous diversity and imagination in the way that it is achieved and the study of the remarkable phenomena which are involved has long provided a research field of great scientific fascination.

Within the classification of living animals, which extends to over one million species (Rothschild, 1961), reproduction commences when a self-motile vehicle of genetic material, the spermatozoon, encounters the membrane of the female egg cell. In many species, enormous numbers of spermatozoa must be released by the male so as to achieve an acceptable probability that one normal sperm cell will encounter the female egg.

Manipulation and control of the various components of the reproductive process have become major scientific achievements with enormous implications for the social and economic structure of modern society. In animals, particularly sheep and cattle, widespread gains in the efficiency of agricultural production on a world scale have been achieved by controlling the selection of propagated characteristics, the timing of fertilisation and the source of genetic material. Methods of monitoring and quantifying the steps in these processes have in many areas reached a high level of technological development, while in other areas methods have remained as basic as the phenomena they observe.

Successful fertilisation demands that the male generates motile spermatozoa of sufficient numbers and sufficient motility to reach the site of the egg before environmental or energy factors result in their immobilisation. The *in vivo* motility of sperm cells is therefore a physical attribute of primary significance in the reproductive chain of events. Its significance relative to that of the biochemical environment however, is uncertain. Quantitative and objective measurements of 'sperm motility', both *in vivo* and *in vitro*, have proved to

be a challenging but largely unsuccessful scientific endeavour.

In general, subjective visual appraisals remain the most widely accepted method of characterising sperm motility.

Many different quantitative methods of varying levels of objectivity, have been devised and tested but in virtually all cases, have failed to find any general acceptance as routine assays of motility. Such methods have been found to be time consuming, useful only under specific conditions, or deficient in objectivity, repeatability or convenience. Discussion of these techniques, in terms of both their methodology and their applications, is given in Chapter 3.

The problem in objectively measuring sperm motility appears to lie in the diversity and complex behaviour which is a feature of many biological systems, together with the statistical problem of characterising a large microscopic population.

If translatory motion is the physical observable of primary interest, two general approaches are possible. We may either opt to measure the nett result of translation, the distance of migration over an extended period of time, or we may elect directly to characterise the kinetic parameters over a short timescale. Alternatively, indirect indicators of swimming 'vigour' may be used. The problem also arises as to the site of the measurement since spermatozoa were designed by nature to function in the egg's environment, which may or may not be a female body.

The migration distance method is the only technique which has been used in a mammalian *in vivo* situation where detailed observations of the population kinetics are not readily carried out. *In vivo* measurements would appear to be the most realistic measure of sperm motility in terms of fertilisation probability although we must accept the inevitability of environmental variations and the specificity they may impart to results. Further, such measurements clearly pose serious

impracticalities for use as routine assays and it is for these reasons, that much reasearch effort over the past thirty years has been directed towards the development of *in vitro* methods.

While *in vitro* techniques may lack the general attributes of the female environment, they do offer greater convenience and the opportunity of more closely controlling and standardising the measurement environment. The nature of this environment is very important and measurements made are specific to it, therefore raising the important question of the extent to which results may be extrapolated to the sperm behaviour within the female body.

Accepting these reservations in the fertilisation context, we must also consider the great value of *in vitro* measurements to laboratory studies of sperm preservation and storage, an area of central significance to artificial insemination.

However, it is remarkable that the progress of *in vitro* motility measurements beyond the level of traditional microscopic visual assessment, has been virtually non-existent in routine semen evaluations. There is no doubt that the eye is able to simultaneously take account of and assemble many factors and impressions and to semi-quantitatively express the result as a score. This is a time honoured method which, even if it is highly subjective, is reasonably rapid and convenient. In quantitative terms, however, there are definite limitations to the value of such a subjective method which gives poor resolution of motility changes and differences, and is subject very strongly to the visual acuity, skill and consistency of the observer.

While a variety of more objective *in vitro* approaches to the problem have been examined in the scientific literature (detailed in chapter 3) over a period of more than thirty years, none, other than variations in visual methods, have found significant application in artificial breeding laboratories. This tends to suggest that current techniques

have been found adequate and the need does not exist for higher resolution and objectivity. In view of major studies which have shown a poor correlation between fertility and sperm motility (e.g., Linford, Glover, Bishop and Stewart; 1976), this view is understandable. It is also true, however, that such experiments utilised existing motility assessment techniques most of which were variants of the traditional subjective methods.

From a physical viewpoint, what then are the requirements for a complete characterisation of motility in suspensions of spermatozoa? Although the experimental objectives may vary their relative importance, and swimming motions vary between species, we might consider:

(i) the fraction of sperm cells in the population which are motile (moving).

(ii) the ratio of normal or progressively motile cells to defective swimmers.

(iii) the frequency distribution of translational swimming speeds.

(iv) the distribution of uni-directional path-lengths.

(v) the frequency distribution of head-rotation rates or other characteristic internal motions.

In terms of fertility, any one of these dynamic characteristics may be of considerable importance.

Exactly which parameters are of significance in this respect is not known, since most are beyond experimental accessibility by visual methods. Measurements of these parameters would perhaps be of greatest relevance to fertility where carried out in a dilute environment where again visual assessments and most other methods have serious deficiencies.

This brings us then to the central theme of this thesis : the characterisation of the dynamics within a suspension of motile spermatozoa

by using laser light scattering. The concept in general is not new. The value of the laser beam as a probe of motion is well known since movement of an object which scatters the beam introduces a Doppler shift into the scattered light. This Doppler shift is proportional to the velocity component of the object in the direction of the scattering vector (fig. 1-5) and it enables one degree of freedom of the motion to be measured in absolute terms.

Applications of the system to macroscopic situations have become widespread since the pioneering experiments of Pecora (1964) and Cummins, Knable and Yeh (1964).

Measurement of the Doppler shift in the scattered light field (perhaps only 1 part in 10^{13} or 10^{14}) is the key to the technique and is carried out by light beating methods which are quite analogous to those commonly employed in the radio-frequency spectrum. Doppler shifted light in the scattered field is mixed with unshifted light (derived from the incident beam) in a non-linear photodetector to give a heterodyne beat frequency in the photocurrent equal to the Doppler shift. In addition, the light scattered from an assembly of moving scatterers generates a distribution of beat frequencies between the various Doppler shifted components so giving a measure of relative motion between the scatterers, the so-called homodyne or self-beat spectrum. All this was clearly possible, only through the extremely small line-width, the high degree of collimation and intrinsic brightness of the laser beam which therefore emerged as a powerful new remote sensing probe of motion.

Numerous applications suggested themselves, although the greatest potential appeared to lie in measurements of motion in microscopic systems where the high light intensity and the comparable dimensions of the scatterers and the wavelength allowed a significant scattered intensity to be obtained down to macromolecular particle sizes.

Applications to Brownian diffusion, electrophoresis, fluid dynamics, and other systems, were successfully implemented. Several useful reviews of such methods are available (e.g., Berne and Pecora, 1976; Cummins and Pike, 1976).

The application of the technique to the motility problem with spermatozoa and also bacteria followed logically since a spermatozoon swimming at a speed of 100μm/s along the scattering vector should give a Doppler shift of the order of 100 Hz. Such shifts are easily measured using light beating methods. The first report (Berge, Volochine, Billard and Hamelin; 1967) demonstrated substantial broadening of the Doppler beat spectrum by motile as opposed to immotile spermatozoa. In principle, it seemed there was the potential in the method to rapidly measure, in a quantitative and completely objective fashion, the kinetic parameters of the sample. A subsequent series of published light scattering experiments over the intervening thirteen years (reviewed in chapter 1) using largely bull, human and marine sperm, indicated that the Doppler beat spectrum gave a measure of the percent motile cells in the sperm suspension and a numerically plausible swimming speed distribution. A very significant advance appeared to have been made since these measurements were achieved over a remarkably short measurement timescale of a few minutes.

Although publication on the subject was not voluminous, several comprehensive studies have been reported (section 1.5). The closely related application to motile bacteria appeared to receive more attention and several excellent detailed analyses of the expected light beating spectrum for various swimming dynamics were published. In the case of motile bacteria the dynamics of the suspension were rather more complex and variable than for spermatozoa.

The basic problem in all of these experiments was the absence of any precise quantitative knowledge of what comprised the actual kinetic

parameters. The method could not be calibrated against or compared with other techniques since there were none which could make similar measurements over a similar timescale under the same environmental conditions.

The validity of the results, in the case of motile bacteria, rested with comparing the theoretically calculated behaviour of optical-dynamic models (i.e., through their predicted light scattering spectra), against the scattering data from real samples. Of particular interest, was the contribution of the internal motions of the bacterium to its Doppler beat spectrum. In the case of spermatozoa however, the simplest optical model was assumed, that of a point scatterer and on this basis the light scattering spectra yielded numerically plausible swimming speeds and levels of percent motile cells (ref. section 1.5). Spermatozoa were however, significantly larger than bacteria and the justification for the point scatterer optical model lay in the presumed invariance of the form-factor at small forward scattering angles.

The original light scattering studies which are described in this thesis, found their origin in the context of such contemporary thinking on the application of light scattering to spermatozoa.

The first experiments, (reported by Woolhouse, 1976), appeared to demonstrate that the percent motile cells in samples of bull spermatozoa, and the swimming speeds, could be measured by characterising the intensity autocorrelation function of the scattered light field.

Subsequent studies carried out by the author (M.W.W.) to quantitatively determine the relationship between the autocorrelation components and the percent motile cells, uncovered a remarkable dependence on sperm concentration and that result formed the starting point for the experimental sequence detailed in chapters 4 and 5 of this thesis.

The research to be described deals primarily with bull spermatozoa and was undertaken with the long term objective of assisting the

improvement of artificial breeding efficiency in New Zealand.

Artificial breeding of cattle, in dairy and beef breeds, has played an important role in improving animal production in New Zealand over the last twenty-five years. Currently in 1980, approximately 55% of the New Zealand national herd of 2.3 million dairy cows is artificially inseminated from a highly selected group of proven bulls. The system has many advantages for the farmer. Bulls need not be kept on the farm and the probability of improving the genetic merit of the herd is significantly improved.

The largest system is organised and serviced by the New Zealand Dairy Board (NZDB) which has developed a highly efficient bull selection system based on progeny testing. Production and ancestry records are used to locate the best cows in the country (in terms of milk production and other desirable characteristics) and these are mated to the top proven bulls in the NZDB team. The bull calf off-spring (about 150 per year) enter the NZDB sire proving system wherein they sire several hundred (perhaps >1000) daughters in special proving herds. The production and desirable traits in the daughters are evaluated over a four year period and compared with other cows in the herds.

From the initial 150 bulls about 5% are then selected each year to join the élite proven bull team and provide semen for widespread inseminations on a country-wide scale.

This small proven team of bulls (<30) are considered to represent the best overall compromise of all those traits which contribute to genetic merit in dairy cattle. Each year, over half of the cows in the New Zealand national herd (i.e., $\sim$ 1.2 million cows) are inseminated from these bulls within the ten week September - November mating period.

A unique aspect of the system through which this massive logistical feat is achieved, is the distribution of semen from a central collection and processing laboratory, in *liquid* form at ambient temperature.

Conventional practice in most other countries entails the use of deep frozen semen in 'straws'. Use of fresh semen distributed in liquid form is possible only because of specially developed sperm extenders and a highly organised country-wide distribution system over the short timespan of the mating season. The use of liquid semen is in fact essential to the system since the sperm losses associated with deep freezing of semen, require ten times more semen to be used than is possible with fresh (≤48 hrs) liquid semen to achieve the same conception rate. The NZDB have progressively developed liquid semen diluents which now allow average conception rates of ∿ 66% (at first service) to be obtained from insemination with 2 x 10^6 sperm in a 0.5ml dose.

Table I shows the improvements in artificial breeding efficiency achieved by the NZDB since the inception of the scheme in the early nineteen fifties.

	1953/57	1958/62	1963/67	1968/72	1973/78
Average conception rate (%)	58	63	66	65	66
Insemination dose (10^6 sperm)	>25	12.5-25 reducing to 6.25	6.25 reducing to 3.25	2.5	2.0
% inseminations to proven bulls	9	22	79	100	100

Table I. Conception rates (first insemination) and sperm dose levels in the NZDB artificial breeding scheme over the 27 year period from 1953, together with the percentage of inseminations to proven bulls.

In recent years since 1963, the conception rate has remained constant at ∿66% but has been achieved with substantially smaller sperm doses, therefore giving a substantial improvement in overall efficiency

of semen utilisation. The efficiency of the system is evident therefore, in considering that *one* average bull service of 5.05ml of semen at a concentration of 1.64×10^9 sperm/ml (refer table 2-3 later) is potentially capable of being used to inseminate 4000 cows.

Two aspects of this system are vitally important and were seen as potential areas of application for an objective high resolution motility assay which would operate at high sperm dilutions:-

(i) Quality assessment for individual ejaculates:

Prediction of conception performance is extremely important since a 5% decrease in conception rate for an individual ejaculate (the standard deviation is normally ∿3%) due to a poor service, could leave perhaps 100 cows not pregnant and a costly delay to the next insemination. Variations in motility associated with such conception rate changes are not resolvable by eye assessment methods and the potential value of a high resolution motility assay as a screening measure is therefore very great, particularly within the bull selection/proving programme.

(ii) Laboratory evaluation of sperm extenders:

The composition of the diluent is vitally important for sperm kept in dilute liquid suspension at ambient temperature for a period of 24-48 hours prior to insemination. Further improvements to diluents which allow greater storage times or higher sperm dilutions and the development of other storage methods, could be considerably expedited by the use of a high resolution assay method which allowed the effect of variations in the sperm storage environment to be rapidly and quantitatively measured.

Detailed reference to these ultimate applications is not made in the work described in this thesis, which had the primary objective of exploring the characteristics and specific problems associated with the

light scattering method. However, by way of completeness, brief details of a preliminary, but very extensive study, along the lines of application (i) above, are given in appendix V together with illustrative results.

The preceding pages have, therefore, set out the context and background of the experimental work to be described in later chapters. The work represents a project taking up a promising new probe of sperm motility, laser light scattering, against a background of potentially significant applications in New Zealand animal production.

The research is described (chapters 4, 5) as a series of self-contained experiments in an approximately historical sequence. The starting point in chapter 4 concerns the long held belief that at small scattering angles the sperm cells behave as point scatterers and that the percent motile cells is directly obtained, probably in an absolute sense, from the autocorrelation function of the scattered field. The swimming speeds and their associated autocorrelation component were not at that stage the primary issue.

Studies through chapter 4 generated results which could not be understood on the basis of the accepted optical-dynamic model and it became increasingly evident that a more detailed understanding of the behaviour of the sperm suspension was required.

With this in mind, a series of direct visual observations then form the basis in chapter 5 for a more realistic optical-dynamic model which enable a qualitative understanding of the previous results to be obtained.

A basic outline of light scattering, light-beating and previous applications to motile microorganisms, is given in chapter 1. Further groundwork is laid in chapter 2 with a discussion of those properties and behaviours of spermatozoa which may be considered as relevant to light scattering experiments.

An additional perspective is given in chapter 3 (part 1), with a description of the methodology of the various other techniques evaluated over the past thirty years for use as sperm motility assays.

Part 2 of chapter 3 then details the light scattering equipment and sample preparation methods used in the following experimental studies of chapters 4 and 5.

An interesting irony becomes apparent in the results of chapter 5, when it is realised that the historically accepted light beating interpretation of the detected field is untenable and in reality, that the method is closely similar to the photo-electric methods of twenty-five years before.

CHAPTER 1

AN INTRODUCTION TO LIGHT SCATTERING AND LIGHT BEATING SPECTROSCOPY WITH A REVIEW OF APPLICATIONS TO MEASUREMENT OF THE MOTILITY OF MICROORGANISMS.

"Life can only be understood backwards;

but it must be lived forwards."

..... Sören Kierkegaard,

1813 - 1855.

1.1 Static Light Scattering from Small Particles

A brief perspective of light scattering from micron and sub-micron sized particles and the way in which the scattering is related to particle size will provide an appropriate introduction to the discussions which are to follow.

Light scattering from particles was first suggested by Rayleigh (1871) as arising from oscillations of the electrons in the material induced by the incident electromagnetic field. The bound electrons in the particle act as dipoles which reradiate part of the incident energy in directions other than the direction of propagation. Usually, unless some absorption of energy takes place, the scattered wave is of the same wavelength as the incident wave.

Using the concept of an assembly of independent and very small dipole oscillators, Rayleigh (1881) extended the phenomenological model to a general theory of light scattering for particles of arbitrary shape and size but having a refractive index of close to unity. Later work (Rayleigh, 1910, 1914, 1918) derived specific solutions for spheres of arbitrary size.

Further work by Gans (1925) dealing with large particles having dimensions similar to or greater than the wavelength, lead to the Rayleigh-Gans theory of scattering.

Here we discuss briefly the phenomenological aspects of light scattering from particles in terms of the most important physical parameter, particle size relative to wavelength.

1.1.1 Small Isotropic Particles

Consider a particle with a characteristic dimension ℓ which is very small relative to the wavelength λ of an incident light beam.
(i.e., $\ell \lesssim 0.01\ \lambda$).

As proposed by Rayleigh, the particle acts as an oscillating electric

dipole and gives the distribution of reradiated intensity characteristic of a dipole, as is illustrated in fig. 1-1.

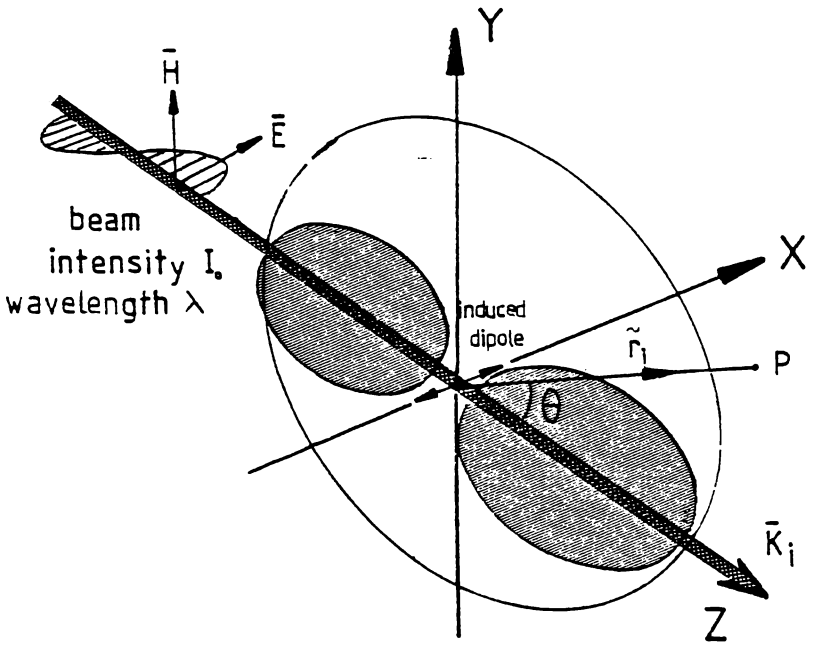

Fig. 1-1. The scattered intensity distribution for a very small particle ($\lesssim 0.01\lambda$) illuminated by an incident beam of intensity I_o and wavelength λ, having a defined electric field vector $\tilde{E}$.

Two significant features of the scattered intensity distribution are that no reradiation occurs in the direction of the dipole oscillations (X) and that the radiation is uniformly distributed in the plane (YZ) normal to the incident electric field vector.

Analytically the result is well known. The scattered intensity $i_{(r,\theta)}$ at any point P defined by position vector $\tilde{r}$ and angle θ (measured with respect to the on-going beam)

$$i_{(r,\theta)} = \{8\pi^2\alpha^2/\lambda^4 r^2\} \ (1 + \cos^2\theta) \ I_o \qquad (1.1)$$

where α is the polarisability of the particle (considered isotropic here) and I_o the intensity of the incident beam.

In the case of plane polarised light as illustrated in the figure where $\tilde{E}$ lies in the horizontal XZ plane, the intensity distribution is uniform with θ in the YZ plane, this corresponding to the first term in

equation 1.1 but has a $\cos^2\theta$ distribution in the horizontal XZ plane, this being the second term.

If the incident beam is unpolarised the entire radiation pattern is axially symmetric about the propagation vector $\tilde{K}_i$ following the orientation of the induced dipole moment and the dipole thus generates a radiation pattern with extended lobes in the forward and rear directions. However, as $\theta \rightarrow 90^\circ$ the scattered radiation becomes completely plane polarised in the vertical (YZ) plane, regardless of whether the incident beam is polarised or unpolarised. If the polarisability is anisotropic, then for a polarised incident beam, the scattered field will contain a depolarised component, (i.e., a component whose polarisation is perpendicular to that of the incident beam).

A scattering particle of extended dimensions was considered by Rayleigh to comprise an assembly of elementary dipole radiators. For a concentration ρ of such elements (per unit volume), Maxwell derived the dielectric constant ε for the mixture as

$$\frac{\varepsilon - \varepsilon_o}{\varepsilon_o} = \pi\rho\alpha \qquad (1.2)$$

and relation 1.1 may therefore be rewritten in terms of the optical constants of the system,

$$i_{(r,\theta)} = \frac{2\pi^2(n/n_o-1)^2}{\lambda'^4\ \rho\ r^2}\ (1 + \cos^2\theta) \qquad (1.3)$$

where N is the refractive index of the particle and n_o that of the medium λ' is the wavelength of the light incident on the particle.

We see here that the scattering depends strongly on the refractive increment $(n-n_o)$ between the region comprising the particle and the surrounding medium. The other significant effect is the very marked wavelength dependence of the scattering, an inverse fourth power relationship.

1.1.2 Particles $\gtrsim$ 0.1 λ

The preceding scattering model,that of an array of elemental dipoles, works well for particles of molecular dimensions, regardless of shape, but assumes the particle is optically isotropic.

However, as the linear dimensions of the scatterer increase above $\sim$ 0.1 λ (i.e., $\sim$ 50 nm), the distribution of scattered intensity departs from the $1 + \cos^2\theta$ description. This arises due to the significant phase differences which exist between the oscillating electrons in different regions of the particle.

The geometry of the particle then becomes important and it is necessary to add both the phases and the intensities of waves scattered from its various elements.

The problem falls into two general classifications:

(a) particles with refractive index n close to that of the medium n_o ($n \approx n_o$)

(b) particles of refractive index substantially different from that of the medium.

In case (a) where $n \approx n_o$, the problem merely involves summing the phase relationships from independent dipole oscillators over the particle volume, although the integration is complex for other than simple geometrical forms. Rayleigh (1910) solved the simplest case, that of spheres of arbitrary size.

However, in case (b) where n differs appreciably from n_o the particle must be considered as having higher order electric moments since the electric field amplitude is not uniform throughout the particle and internal phase changes may be large.

Mie (1908) produced an elegant solution for the case of spheres having radii $\gtrsim\lambda$ and of large refractive increment. Using spherical harmonics, the intensity was expressed as the sum of a series representing

the contributions from a complete set of induced electric multipoles and the refractive index and particle size appear in the coefficients of the series. The technique was to expand the incident plane wave, the scattered field and the field inside the sphere, in terms of electric and magnetic spherical waves. The boundary conditions at the surface of the sphere eliminate consideration of the coefficients of the internal field. The solution is exact and in the limiting case of very small spheres having $n \to n_o$, the Mie series reduces to the single dipole term of equation 1.1. An increased refractive index at large particle sizes implicates higher order multipoles and computations of the Mie series show that scattering increases significantly in the forward direction with increasing dimensions. This effect is evident in fig. 1-2 which shows the angular distribution of scattered intensity as calculated from the Mie series, for spheres dimensionally both much smaller than and comparable to the wavelength of the incident light.

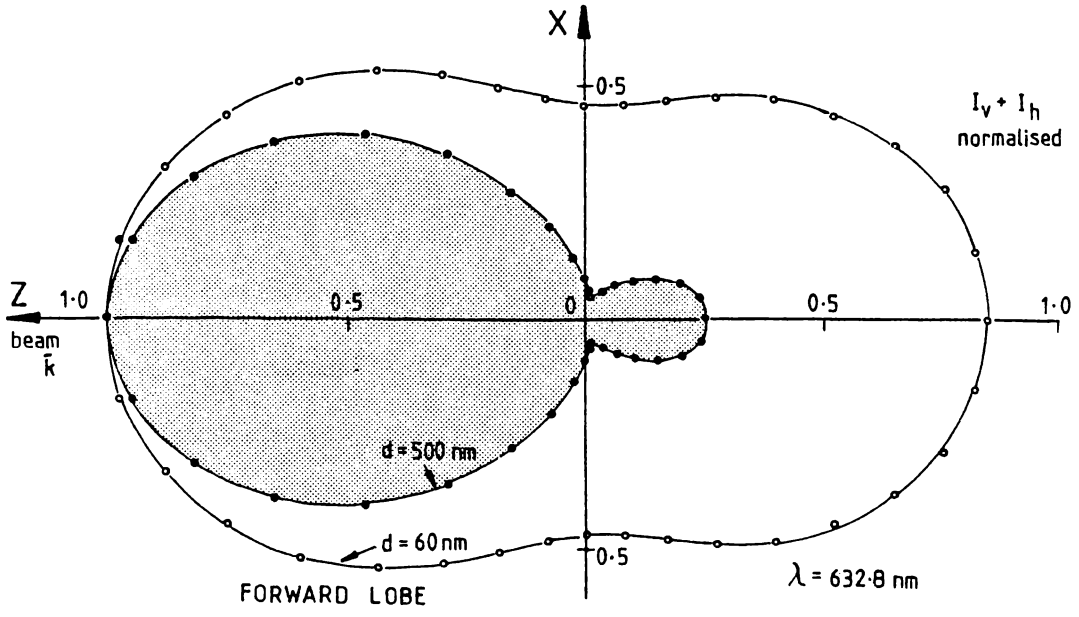

Fig. 1-2. Angular distributions of total scattered intensity for spheres of diameter 500nm and 60nm when illuminated by a beam of wavelength 632.8nm (calculated from the Mie series).

The substantial increase in forward scattering for larger spheres is clearly evident, the ratio of forward/backward intensities being 1.18 for spheres of 60μm diameter but 4.0 for spheres of 500nm diameter.

The solutions given by the Mie theory are exact and departure of experimental results from the theoretical predictions may be used as an indicator of sphericity for the scatterers or of their optical anisotropy. Blau, McCleese and Watson (1970) reported experimental measurements of the angular intensity distribution (at optical wavelengths) for spherical scatterers in the diameter range 7.5μm - 110μm and obtained excellent agreement with the Mie theory.

1.1.3 Polarisation

The small ($<<\lambda$) optically isotropic dipole element generates a scattered field which is completely plane polarised at a scattering angle of 90°, regardless of whether the incident beam is polarised or unpolarised. If however the polarisability of the element or particle is anisotropic, the scattered field at $\theta = 90°$ will not be completely polarised, and the degree of depolarisation gives a measure of the optical asymmetry. Large particles ($\approx\lambda$), even if optically isotropic, also give depolarisation at $\theta = 90°$ due to the increased significance of higher order multipoles which introduce localised non-linear polarisabilities.

1.1.4 Large Particles ($\ell>\lambda$)

When the scattering particle is significantly larger than the wavelength, a number of interacting effects may occur, in particular diffraction, refraction, reflection and interference. The scattered intensity distribution in this case, particularly where $\ell>>\lambda$, may be approximated by summing a set of rays passing through the particle (Van de Hulst, 1957). This approach requires that the refractive

increment be large and it can be shown that the Mie formulae asymptotically approach a localised ray model for $\ell >> \lambda$.

Summing the intensity at a point over a set of rays traversing the particle still requires, as in the Rayleigh approach, that the phases be added, although in many situations, even for very large particles, the phase effects may average out.

In addition, absorption of the incident and scattered fields may become important, particularly where the pathlengths are long. For scatterers in this multi-wavelength size domain, diffraction becomes important and in fact the large forward scattering lobe of fig. 1-2 (d = 500nm) essentially represents the diffraction pattern.

Van de Hulst points out that each Mie coefficient can be separated into two terms, one depending on the nature of the particle and the other independent of it. When the scatterer is large these two components may be usefully separated, one giving the Fraunhofer diffraction around the particle (and independent of its optical composition) and the other the scattering by reflection and refraction.

Diffraction in the forward direction peaks rapidly as the particle diameter moves into the multiple wavelength range. Fig. 1-3 for example, shows the angular width of the diffraction peak for particles of circular cross-section as a function of diameter and provides a perspective of the magnitude of the diffraction effect which will be useful in considering the light scattering from spermatozoa at a later stage.

The bull spermatozoon head, when oriented so as to give a maximum characteristic dimension of 8μm generates a diffraction peak half-width in the range 2° - 3°. When oriented edge-on to the incident beam the characteristic dimension shrinks to $\sim$ 1μm and the peak half-width broadens to $\gtrsim 20^\circ$.

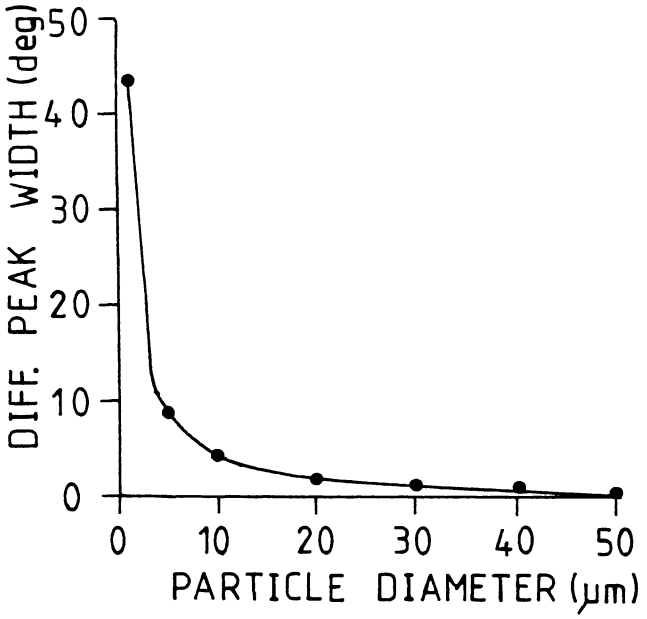

Fig. 1-3. Angular width of the principal diffraction lobe for a spherical particle as a function of diameter (λ = 632.8nm)

1.1.5 Rayleigh-Gans Scattering

A special case which is particularly appropriate for biological cells arises when

(a) the refractive increment for the particle is small

$$|n-n_o| << 1 \qquad (1.4)$$

and (b) the phase shift within the particle is small

$$\text{i.e., } (4\pi\ell/\lambda)|n-n_o| << 1 \qquad (1.5)$$

where ℓ is a characteristic linear dimension of the particle.

While (1.5) is a restriction on the particle size, the actual size range which meets these criteria depends on the refractive increment. That is,

$$\ell << \lambda/4\pi|n - n_o| \qquad (1.6)$$

Particles meeting these criteria can be considered weak scatterers

and the scattering may be modelled on the basis of a modification of the simple Rayleigh Theory discussed in section 1.1.1 being commonly referred to as Rayleigh-Gans scattering.

The intensity in this case is expressed as the Rayleigh limit for a small scatterer ($<<\lambda$) multiplied by a form factor which takes account of the distribution of phases throughout the volume V of the particle, i.e.,

$$i = I_o\{\frac{1 + \cos^2\theta}{2}\} \frac{K^4V^2}{r^2} \left(\frac{n-n_o}{2\pi}\right)^2 |P_{(\theta,\psi)}| \qquad (1.7)$$

$$\text{where} \quad P_{(\theta,\psi)} = \frac{1}{v}\int e^{i\delta}\, dV \qquad (1.8)$$

and $\delta = \underset{\sim}{k} \cdot \underset{\sim}{r}$ is the phase difference between waves scattered from two regions of the particle defined by the displacement vector $\underset{\sim}{r}$, and θ and ψ define the particle orientation.

I_o = intensity of the incident beam

and $K = 2\pi/\lambda$

The factor $P_{(\theta,\psi)}$ is a volume integral over the particle which for many regular geometries is readily evaluated.

An important result of significance in later discussions is that for $\theta \to 0, |P_{(\theta,\psi)}| \to 1$ and the simple Rayleigh scattering model of equation (1.3) applies.

1.1.6 Applications of Rayleigh-Gans Scattering

This particular scattering model has been extensively applied and has proved useful for biological cells such as bacteria. Bacteria are generally $\gtrsim\lambda$ in size and due to their 70-80% hydration have a refractive index comparable to that for water. Wyatt (1972a) refers to *Staph. aureus* as having a radius of 477 nm and a refractive index of $\sim$ 1.4.

On the basis of the Rayleigh-Gans criteria for such cells immersed in water;

$$n - n_o = 0.067 \text{ complying with relation} \quad (1.4)$$

$$\text{but } (4\pi\ell/\lambda)|n - n_o| = 1.3 \qquad (\lambda = 632.8\text{nm})$$

These values fail to satisfy the requirements of relation 1.5 and although the bacterial cells do not therefore comply with the Rayleigh-Gans criteria, the theory has still been found sufficient to give a reasonable description of the static scattering characteristics. The range of experimental parameters over which a scattering description is required (e.g., scattering angle), is an important consideration. An adequate scattering model may well be provided by the Rayleigh-Gans method over a limited range of parameters, even though the particle or cell does not comply fully with the approximation criteria.

The foregoing discussion of light scattering in terms of particle size is relevant to a wide range of applications ranging from molecular scattering through to colloidal particles and aerosols whose dimensions may range up to the sub-millimeter region.

The general objective of such applications is to characterise those physical features of the scatterers such as size, refractive index and conformation, in terms of the light scattering measurements. The angular distribution of scattered intensity for the two scattering planes, sometimes at different wavelengths, and the degree of depolarisation, enable these physical attributes of the scatterers to be characterised in a semi-quantitative fashion.

Such applications are generally known as *Differential Light Scattering* (DLS), an excellent review of which is given by Wyatt (1973). Applications of DLS to bacterial cells have been widely discussed by Wyatt and it appears that the Rayleigh-Gans scattering model provides

an adequate basis for understanding the angular distribution of light scattered from such cells.

As an example of such measurements on bacteria, and in view of forthcoming discussions of the dynamics of motile bacteria, fig. 1-4 shows typical DLS results for a sample of *Escherichia coli* suspended in water.

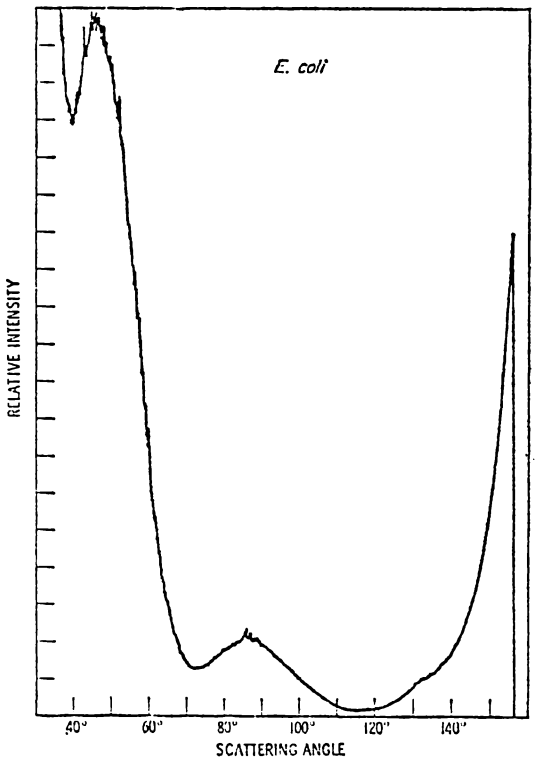

Fig. 1-4. DLS data showing the horizontal angular distribution of intensity for *E. coli* for a vertically polarised incident beam at λ = 632.8nm, (Wyatt, 1973).

Changes in cell conformation as produced by bacteriocidal agents, heat treatment or growth conditions, result in changes in the fine structure of these distributions; that is,changes in the secondary peak amplitudes and locations.

1.1.7 Conclusions

The preceding discussion has outlined the basic concept of static light scattering from particles when the average intensity and

polarisation of the scattered field is related to the particle size and geometry.

However in this thesis we are primarily concerned with the study of the motion of moving scatterers (self-motile micro-organisms) by measuring time dependent attributes of the scattered field - i.e., so called dynamic light scattering. Nevertheless, we do need to consider the implications for dynamic light scattering of the static scattering characteristics, and the following points arising out of the discussion in section 1.1 are noted for possible future reference:

(1) Time dependent changes in the scattered field intensity will occur for asymmetric scatterers when the scatterer reorients and the scattering cross-section changes.

(2) Such orientation effects will become more apparent with increasing particle size and similarly will vanish as the particle becomes very small relative to the wavelength.

(3) Optical anisotropy will generate orientational scattering effects regardless of particle size and will give depolarisation of the light scattered at 90°.

(4) Scattering from large particles ($\gtrsim\lambda$) (e.g., spermatozoa) is largely in the forward direction and may be considered as a combination of a diffraction field together with a field scattered from the structures of the cell. The diffraction lobe becomes of relatively small angular width ($<10^{\circ}$) for particles having diameters of more than a few wavelengths.

(5) In studying small angle (forward) scattering from large particles, polarisation of the incident beam will not be important since the forward scattered intensity is very similar for all planes of polarisation. Even at large scattering angles ($45 \rightarrow 90^{\circ}$) where plane polarisation of the

scattered light is most likely, depolarisation arising from optical anisotropy and particle size, is likely to occur. For a plane polarised incident beam, a depolarised scattered field may arise depending on the anisotropy of the polarisability tensor.

(6) Since a bull spermatozoon has a highly irregular geometrical form (section 2.4), the question arises as to the relative contributions to the scattered light arising from its two principal components, the head and the flagellum. In terms of the dimensional effects discussed in section 1.1 it seems likely that at small forward scattering angles, the scattered field will be generated largely by the head structure whereas with increasing scattering angle the field scattered by the long (50μm) thin (∿0.5μm) flagellum will contribute to a greater but indeterminate extent.

1.2 Kinetics of Scattering Systems by light beating spectroscopy

The studies of spermatozoa motility to be discussed in this thesis were based on a technique which only recently became experimentally feasible with the development of laser technology. The technique allows quantitative and absolute measurements of the motion of a microscopic particle by measuring the relatively small Doppler shift which the motion generates in the scattered light as seen by a stationary detector. Since for velocities of tens or hundreds of microns/sec. the Doppler shifts are very small, an extremely high spectroscopic resolution ($\sim 10^{13}$) is required. This has been achieved by light beating methods which, in principle, are exactly the same as those used in radio frequency technology for many years.

The high intrinsic brightness of the laser beam and its very small line width have made light beating methods experimentally simple and

have so provided a window into a region previously inaccessible to optical spectroscopy.

High performance scanning Fabry-Perot interferometers had realised a spectroscopic resolution limit of $\sim 10^8$ (Yeh and Keeler(1969) reported an instrumental resolution of 15 MHz) which fell short by orders of magnitude, of the performance required to study line shifts or widths in the region below 10^6Hz. Laser line widths of less than 1Hz have recently made this spectroscopic domain accessible with relatively simple equipment through the use of the light beating technique.

The general principle is that of combining light fields which differ in frequency due to Doppler shifts, in a non-linear photo-detector such that beats between the Doppler components appear as photocurrent fluctuations. In fact, for very small beat frequencies, the coherence and brightness of a laser source actually enables the beats to be observed visually in the scattered field.

Therefore, we have a light scattering technique which gives information not primarily on the size and structure of the scatterer as that discussed in section 1.1, but on the dynamics of the particle. The question, arises however, as to what extent the two types of light scattering technique overlap. Do the static scattering characteristics of a particle affect the dynamical information accessible by the Doppler beating technique?

Answering this question will prove to be the major concern in later chapters of this thesis.

1.2.1 Measuring the temporal features of the Scattered Field

Consider an assembly of particles illuminated by a coherent plane polarised monochromatic beam of constant intensity, having the electric vector in the vertical plane.

The total scattered field $E_{s(t)}$ at a detector located in the far field is

$$E_s(t) = \sum_i A_i(t)\, e^{ik_s.r_i(t)}\, e^{-iw_o.t} \qquad (1.9)$$

where $\tilde{k}_s$ defines the scattering geometry and is known as the scattering vector (see fig. 1-5).

$$\tilde{k}_s = \tilde{k}_i - \tilde{k}_f$$

$$\text{and} \quad |\tilde{k}_s| = \{4\pi n_o \sin(\theta/2)\}/\lambda_o \qquad (1.10)$$

$r_{i(t)}$ is the position vector of i_{th} scatterer w_o and λ_o are the frequency and wavelength respectively of the incident field and θ is the scattering angle as defined in fig. 1-5 and lies in the scattering plane defined by the incident beam and the scattered wave (XZ plane).

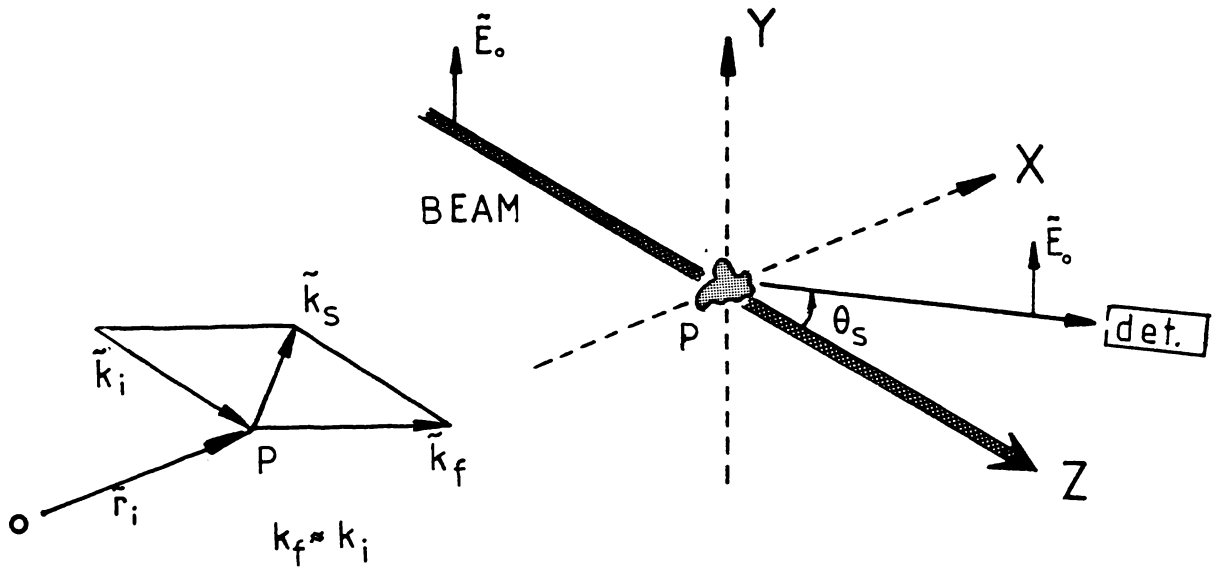

Fig. 1-5. Geometry of the light scattering system.
Generally $|\tilde{k}_f| \approx |\tilde{k}_i|$

Equation 1.9 relates to the vertically polarised scattered field which arises from the polarisation of the incident beam (in the ZY plane). An identical equation, however, may be written for any depolarised scattered field ($\tilde{E}$ lying in the ZX plane in the case of fig. 1-5) which

may be generated by optical anisotropy within the scatterer. In the case of spermatozoa the level of depolarisation is quite small and we shall not therefore consider this field component, although further reference will be made to it in the literature discussion of section 1.5.

The term $A_{i(t)}$ in relation 1.9 is the scattered field amplitude for the i_{th} scatterer and it is noted at this early stage, particularly in view of the previous discussion in section 1.1, that this may be time dependent for larger particles if the orientation changes.

The scattered field $E_{s(t)}$ is an observable and information regarding movements of the scatterer is contained in the time dependence of the phase relationships of the scattered field. This temporal information may be extracted by determining the time averaged autocorrelation function $G^{(1)}(\tau)$ for the optical field;

$$G^{(1)}(\tau) = \langle E_s^*(t) . E_s(t+\tau) \rangle \qquad (1.11)$$

For any assembly of point scatterers having known dynamics, $G^{(1)}(\tau)$ may be calculated directly from the time dependence of $\tilde{r}_{i(t)}$, (using equation 1.9). However, experimentally we can only measure the second order correlation, the intensity autocorrelation function, by analysing the photodetector output current I(t).

$$\text{i.e. } G^{(2)}(\tau) = \langle I(t) \; . \; I(t+\tau) \rangle \qquad (1.12)$$

$$= \langle E_s^*(t) \; . \; E_s(t) E_s^*(t+\tau) E_s(t+\theta) \rangle \qquad (1.13)$$

and $G^{(2)}(\tau)$ is related to $G^{(1)}(\tau)$ by a relation which depends on the mode of the light beating detection system.

An extremely important point to consider here, is that while the dynamics of the scatterers uniquely determine $G^{(1)}(\tau)$ and hence $G^{(2)}(\tau)$, the converse is not necessarily true. Measuring the temporal field autocorrelation at a single point in the scattered field; cannot give

a unique set of dynamical variables which characterise the motion of the scattering system. This highly significant point will be further considered in relation to the light scattering applications reviewed in sections 1.3 and 1.4 and the subsequent results of chapter 5.

However, if the scatterer motions conform to some defined dynamical model, then the temporal information contained in the autocorrelation function of the scattered field at a point enable some of the parameters of that model to be determined.

An example is Brownian motion of microscopic scatterers wherein the particles conform to a known and specifiable dynamical model and autocorrelation of the scattered field thus enables the diffusion constant to be determined. If the scattered field is a stationary Gaussian random process, $G^{(1)}$ and $G^{(2)}$ are related by the Siegert relation (Glauber, 1963).

$$g^{(2)}(\tau) = |g^{(1)}(\tau)|^2 + 1 \qquad (1.14)$$

where $g^{(1)}(\tau)$ and $g^{(2)}(\tau)$ are the normalised first and second order autocorrelation functions respectively.

This relationship requires that the field at the detector be the result of a large number of statistically independent contributions. By measuring $g^{(2)}(\tau)$ we can therefore obtain access to the kinetic information contained in the phase relationships between the components of the scattered field. In this case $I_{(t)}$ represents a summation over all the mutual beats between the individual Doppler components in the scattered field and the process is termed *homodyne* detection. In simpler terms $I_{(t)}$ (ignoring detector noise) results from the relative motions of the system of scatterers.

A further approach to examining the scattered field is to coherently combine it at the detector with a reference field, usually derived from

the same laser source.

The system is analogous to the radio-frequency mixing method where a selected local oscillator frequency is combined with the incoming signal.

In the light scattering case it may be shown (for example,Jakeman, 1974) that;

$$|g^{(2)}(\tau)| = |g^{(1)}(\tau)| \qquad (1.15)$$

and the first order correlation function of the scattered field may be measured directly.

This process is logically known as optical *heterodyne* detection and allows absolute translational speeds to be measured for the system of scatterers by way of their Doppler shifts.

Transformation from the time domain $g^{(1)}(\tau)$ to a frequency domain description of the scattered field, is via the Fourier transformation and the optical spectrum of the scattered field is thus given by;

$$I(w) = \frac{1}{2\pi}\int G^{(1)}(\tau)\, e^{iwt} d\tau \qquad (1.16)$$

where $I(w)$ is the scattered intensity at beat frequency w.

Experimentally therefore, determination of either the autocorrelation function or the power spectrum of the detected photocurrent, will give the distribution of Doppler shifts in the scattered field and hence allow information on the dynamics of the scattering system to be obtained.

As previously discussed, to acquire any physically meaningful information on the motion of the scatterers, a dynamical model is required. The detection system sees Doppler shifts Δw of magnitude $|\tilde{k}_s.\tilde{v}|$ (refer fig. 1-6).

That is, $\Delta w = \pm (4\pi n/\lambda_o)|\tilde{v}| \cos\psi \sin(\theta/2)$

Taking a typical velocity relevant to the motion of spermatozoa, say $|\tilde{v}| = 100\mu m/s$ with the velocity at an angle $\psi = 45^\circ$ to the scattering vector, then for a scattering angle $\theta = 10^\circ$, and $\lambda_o = 488nm$ the Doppler Shift is 34Hz, (n is the refractive index of the scattering medium).

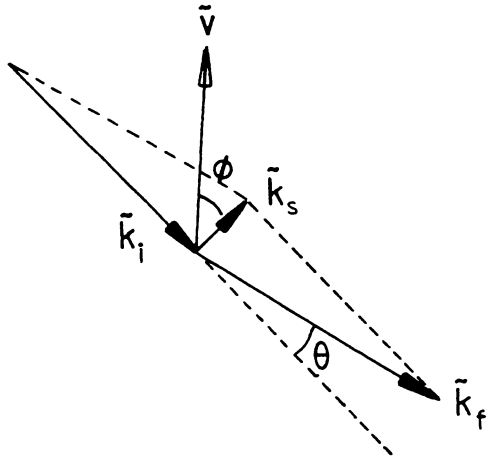

Fig. 1-6. Geometry for calculation of Doppler Shift in the scattered field $\tilde{k}_f$.

It is clear that there exists an infinite set of velocities all of which will give the same velocity component along $\tilde{k}_s$ and hence the same spectral information in the scattered field. Therefore, when observed at a single point, the scattered field gives information regarding only one degree of freedom of the scatterer's motion. If, however, the dynamical model is known, the phase information in the scattered optical field may be used to quantify, to some extent, its kinetic parameters.

In the case of Brownian diffusing particles, the model is a simple one, and light scattering has been highly successful in measuring the diffusion coefficient, the most important parameter associated with the motion (see, for example, Berne and Pecora, 1976). Similarly, electrophoretic or flow induced motion of scatterers along the same translational vector, is another dynamical model which has been conveniently studied by light beating methods, (e.g., Pike, 1970; Uzgiris, 1972; Harvey, Walls and Woolford, 1976).

The more complex case of an isotropic distribution of translational velocities may also be characterised in terms of the distribution of velocity components along the scattering vector (Nossal, 1971) although any departure from an isotropic distribution becomes exceedingly difficult.

The discussion to this point has concerned the phase content of the scattered field arising from motion of the scattering particle. There is also, however, the question of the static scattering parameters of individual particles, a background discussion on this question having been given in section 1.1. The particle size, wavelength, refractive increment and scattering angle all affect the amplitude of the scattered field at the detector. In terms of our primary interest in the temporal features of the scattered field for spermatozoa, these factors are unimportant unless one of them creates a time dependence in the amplitude. The factor of greatest concern in this respect is the particle geometry since the effective scattering cross-section may change if the particle undergoes a reorientation. In this situation, the field autocorrelation function may be expressed as the product of a phase component and an amplitude component. (Cummins, Carlson, Herbert and Woods, 1969).

For an assembly of N identical particles;

$$G^{(1)}(\tau) = N\langle A^{*}(t)\, A(t+\tau)\rangle \cdot \langle e^{-i\,\tilde{k}_s.\tilde{r}(t)} \cdot e^{i\,\tilde{k}_s.\tilde{r}(t+\tau)}\rangle \qquad (1.17)$$

The term $A^{*}(t)\, A(t+\tau)$ arises then from changes in the scattered amplitude resulting from reorientation while the phase component;

$\langle e^{-i\,\tilde{k}_s.\tilde{r}(t)} \cdot e^{i\,\tilde{k}_s.\tilde{r}(t+\tau)}\rangle$ is generated by changes in the particle position.

For point scatterers ($<<\lambda$) $A(t)$ = constant.

However, for particles in the region $\gtrsim\lambda$ the amplitude term will contribute to the autocorrelation function of the field if the conformation is anisotropic, and further confound the interpretation of the scattered field in terms of the dynamical parameters. It becomes necessary therefore to have two models, a dynamical model and a conformational scattering model.

Extensive theoretical consideration has been given to the effects of particle shape on the light beating spectrum, largely within the context of diffusion measurements on macromolecules and virus particles. Pecora (1968), Cummins *et al.*(1969) for example, considered the case of diffusing rigid rod-shaped scatterers, a conformation very relevant to macromolecules and biological cells. They computed the total spectrum for such scatterers undergoing simultaneous translational and rotational diffusion and showed that it comprised a series of Lorentzians.

The first term in the series corresponded to the spectrum expected for spheres and successive terms represented the contributions from higher order modes arising from the asymmetry of the particle. The important point was that at small scattering angles when using samples of Tobacco Mosaic Virus (TMV), which has an axial ratio of 17:1, the higher order terms vanished although the maximum linear dimension was only 0.3μm ($\sim$0.5λ). At larger scattering angles, samples of TMV gave light scattering spectra which were best fitted by two Lorentzians.

In general, the question of small asymmetric scatterers has been comprehensively treated and no further discussion is necessary at this stage. Berne and Pecora (1976) give an excellent and comprehensive summary of the problem as it applies to macromolecules. It is, however, appropriate to now become more specific and continue the discussion within the context of those types of scatterers with which we are primarily concerned, motile micro-organisms.

1.3 Applications of Light Beating Spectroscopy (LBS) to Motile Bacteria

A discussion of bacterial motility, as measured by laser light beating methods, is worthwhile and relevant since it gives a perspective of the particle size considerations and it is very close to the spermatozoa application with which we are concerned.

Use of the LBS method in quantifying the dynamics of motile microorganisms appears an effective answer to a long-standing biophysical problem. In principle, not only can the swimming speed distribution be measured, but it can be followed in close to real time, in marked contrast to other techniques which require hours of photographic analysis or data collection/analysis. A further advantage is that data may be collected from a large population of cells over a short timescale (minutes). That is, a speed distribution determined over a period of a few minutes may result from the motion of thousands of cells. Alternatively, by using appropriate dimensions and scattering geometry, dynamical information may also be obtained on the swimming motions of individual cells. The potential of the method therefore appears to be very great.

1.3.1 Conformation and Swimming Motions

The interpretation of light beating data requires both a realistic scattering model for the cell and a model of its swimming motions.

Bacteria are not always spherical in shape. This is certainly the case for many motile bacteria which tend to be rod-shaped or ellipsoidal, often having an axial ratio of 5 or more. The axial dimension ranges of *E. coli* for example, which is approximately rod-shaped, are length 1μm - 4μm and diameter 0.4μm - 0.7μm (Wyatt, 1968).

The most commonly observed axial dimensions of *E. coli* appear to be 3.0μm length and 0.54μm diameter, being of prolate spheroidal conformation. The refractive index has been measured as 1.4 in the cell wall

(thickness 0.01μm) and 1.35 in the cell interior. The flagella are generally short and of very small diameter (0.015μm) their contribution to the scattered light being justifiably neglected.

The dynamical model, however, is not generally characteristic or easily specified since the motion involves translation, internal motions during translation and frequent stops, 'twiddles' and reorientations which result in directional changes. Berg and Brown (1972) carried out a unique study of the motions of various strains of *E. coli*, using a tracking microscope (Berg, 1972) which followed the coordinates of individual cells in three dimensions. They analysed the motion of individual cells as being a random walk process, with a directional bias if the population as a whole was undergoing a displacement (as in chemotaxis). That is, individual cells move some randomly varying distance in a straight line, pause and reorient through a variable semi-random angle, then move off in a new direction, all at some characteristic speed which varies between cells. Keller and Segel (1971) discussed a one-dimensional step model of such bacterial motion. Other studies by Boon (1975) reviewed and evaluated the various dynamical models and their application to the chemotactic phenomena exhibited by bacteria. The point was made that the theoretical models while helpful, were simplistic in relation to the experimentally observed behaviour.

The three dimensional motion of a large number of random walk cells in the absence of chemotaxis is described by Roberts, (1974).

$$\frac{\partial n}{\partial t} = \mu \nabla^2 n \qquad (1.18)$$

where n is the concentration of cells and μ is a motility coefficient. The parameter μ (the motility coefficient) is analogous to the diffusion coefficient (Keller and Segel, 1971) and for motion in three dimensions

$$\mu = \lambda^2/6T = u^2T/6 \qquad (1.19)$$

where λ is the mean straight line path (i.e., we may refer to this as the distance over which the motion is correlated). Hence T is the

mean time between reorientations and u is the mean swimming speed.

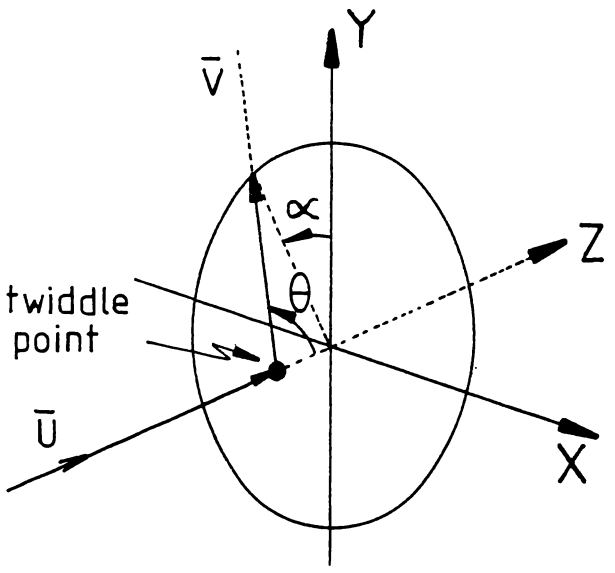

Fig. 1-7. Swimming model for motile bacteria. Initial and final velocity vectors are $\tilde{u}$ and $\tilde{v}$, respectively. (Roberts, 1974).

The change in motion at each reorientation involves six degrees of freedom and following Roberts (1974), it can be shown that if the cell delays for a time δt during orientation,

$$\mu = \frac{u^2(T-\delta t)^2(1+\cos\theta)}{6T(1-\cos\theta)} \qquad (1.19)$$

where θ is the mean angle of reorientation as defined in fig. 1-7.

The value of θ has been considered not to be a random variable, the random directional component arising largely from a random selection of azimuthal angle α (fig. 1-7).

Typical values for these various kinetic parameters, as ascertained from the experiments of Berg and Brown, are given in Table 1-1, for illustrative purposes and may later be compared with the information on spermatozoan dynamics given in chapter 5.

Bacterial Strain	AW405 (wild type)	Unc 602 (uncoordinated)	Che C497 (non-chemotactic)
Number bacteria tracked	35	10	14
Tracking time (min)	20	3.0	2.7
$\bar{u}$ (μm/s)	14 ± 3	14 ± 3	20 ± 5
θ (degrees)	68 ± 36	74 ± 33	33 ± 15
T (s)	1.0 ± 1.4	0.56 ± 0.51	6.4 ± 5.4
δt (s)	0.14 ± 0.19	0.14 ± 0.24	0.10 ± 0.13

Table 1-1. Kinetic parameters for various strains of *E. coli* (Berg and Brown, 1972).

The mobility coefficient μ was found to vary widely both between individual cells and between populations of cells such as to make the parameter quite meaningless. From a light scattering viewpoint, complications also arise from wobbling motions of cells during the 'straight-line' translation phase, and these were analysed by Boon, Nossal and Chen (1974). Of particular interest for light beating experiments is T, the time over which the motion remains correlated since this must must be greater than the characteristic decay time of the autocorrelation function if a measure of swimming speed is to be obtained.

1.3.2 Light Scattering Studies of Bacterial Dynamics

On the basis of the simple bacterial model discussed in section 1.3.1 it is apparent that extracting meaningful dynamical parameters from light beating measurements is not a trivial problem. It represents a different situation again from that of large asymmetric molecules undergoing a combination of translational and rotational diffusion. Nossal (1971) presented a theoretical investigation of the light scattering spectra to be expected from motile microorganisms having various swimming speed distributions. He pointed out that where the swimming motions are correlated over times which are long compared with the

autocorrelation decay time, (a reasonable assumption for motile bacteria) the light scattering spectrum gives the reduced distribution function P of directed velocities.

$$\text{that is} \quad S_{(\tilde{k},w)} = \frac{N|A|^2}{|\tilde{k}|} P\left(\left|\frac{w-w_o}{\tilde{k}}\right|\right) \tag{1.20}$$

where N is the number of contributing scatterers and A is a scattering amplitude factor.

Here, no time dependence in the amplitude A was considered and in fact Nossal, Chen and Lai (1971), and Nossal and Chen (1972b) when reporting the first experimental results for motile bacteria (*E. coli* K_{12}) based their interpretations on a point scatterer model.

For an isotropic velocity distribution among independently moving point scatterers, the swimming speed probability distribution $P_s(v)$ can be shown to be related to the normalised field autocorrelation function via the relationship (Nossal and Chen, 1972a).

$$\left|g^{(1)}(\tilde{k},t)\right| = \int_o^\infty \frac{\sin(kvt)}{(kvt)} P_s(v)\,dV \tag{1.21}$$

Taking the Fourier sine transform;

$$P_s(v) = \frac{2v}{\pi} \int_o^\infty \sin(kvt)\left[kt\left|g^{(1)}(\tilde{k},t)\right|\right] d(kt) \tag{1.22}$$

where k is the scattering vector and v the translational velocity.

In the experimental results, validation of the point scatterer and isotropic velocity *assumptions,* which are implicit in equation 1.21, rested with the observed kt scaling of the autocorrelation function with scattering angle over the range 20° - 70°. Here, relating back to the discussions of 1.1.2, we have an assumed dynamical model combined with the most elementary scattering model and the interpretation of the light scattering results can only be in terms of this model. The validity of these assumptions is therefore extremely important.

Fig. 1-8 gives the swimming speed distribution $P_s(v)$ obtained by Nossal and Chen (1972a) using equation 1.22, and shows a significant departure from a Maxwellian.

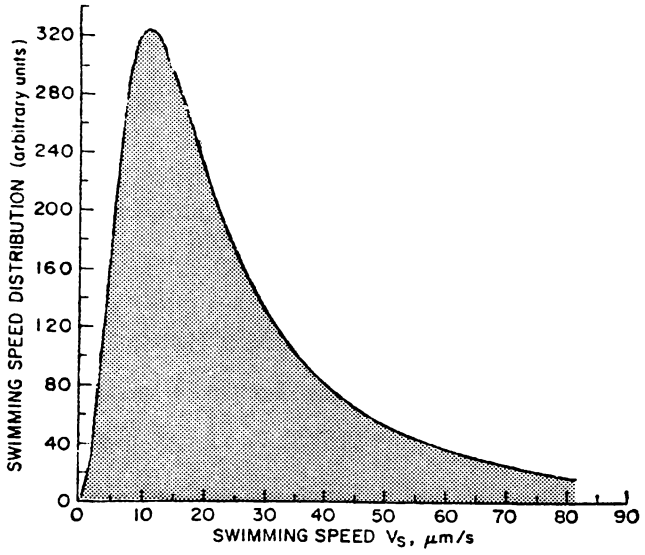

Fig. 1-8. Swimming speed distribution obtained by using equation 1.22 on light scattering data from motile *E. coli* (K_{12}) bacteria. (Nossal *et al.*, 1971).

A further assumption made in this experimental work was that the individual scatterers were independently motile and this was validated by the observation that no changes in the autocorrelation data occurred when the bacterial concentration was changed. Superimposed plots of the autocorrelation functions scaled as kt are shown in fig. 1-9 and clearly demonstrate that for these samples of bacteria, kt scaling was obtained.

Nossal and Chen (1972a) showed that *E. coli* cells, when rendered non-motile, behaved approximately as large Brownian scatterers. The autocorrelation functions departed slightly from the exponential form to be expected for point scatterers undergoing Brownian motion but the

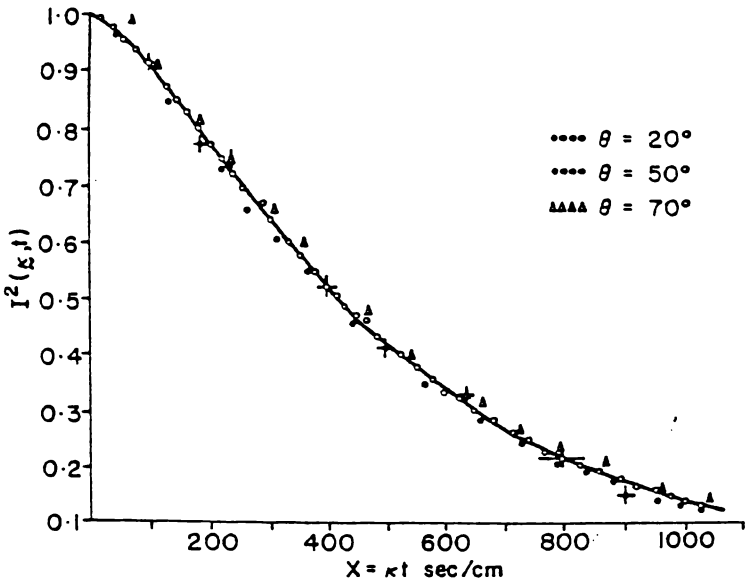

Fig. 1-9. Correlation functions for motile *E. coli* (k_{12}) bacteria plotted as a function of kt. (Nossal *et al.*, 1971).

difference was attributed to heterogeneous elements in the sample and possibly rotational effects. The diffusion coefficient was computed from these results to be 5 x 10^{-9} cm^2/s with the hydrodynamic radius of the equivalent sphere being 0.5μm.

Further, consideration was also given to mixed populations of motile and non-motile scatterers which were expected to give a spectrum of the form;

$$\left|g^{(1)}(\tilde{k},t)\right| = \alpha\left|g^{(1)}_{m}(\tilde{k},t)\right| + (1-\alpha)\, e^{-k^2Dt} \qquad (1.23)$$

where D is the diffusion coefficient, α is the fraction of the field autocorrelation amplitude arising from the motile cells, $g^{(1)}_{m}(\tilde{k},t)$ is the autocorrelation function of the motile fraction and the second term represents the Brownian-like contribution from the non-motile cells. Attention was also drawn to the need to fit and subtract the non-motile component so as to obtain the pure motile component. In addition it was suggested that the fraction motile cells (α) could be determined by subtracting autocorrelation functions taken at different scattering angles ($\theta_1 = 20°, \theta_2 = 40°$) (motile component vanishes due to kt scaling).

$$\text{i.e.,} \quad \Delta g^{(1)}(\tilde{k},t) = (1-\alpha)\left[e^{-k_1^2 Dt} - e^{-k_2^2 Dt}\right] \qquad (1.24)$$

and determining the peak value of ΔI max.

This allows α to be calculated from;

$$\Delta g^{(1)}_{max} = (1-\alpha)\left[K_r^{(k_1/\Delta k)} - k_r^{(k_2/\Delta k)}\right] \qquad (1.25)$$

where $k_r = k_2/k_1 \quad \Delta k = k_1 - k_2$

This technique is interesting to compare with methods to be described in chapter 4 for finding α in the case of spermatozoa where direct use is made of equation 1.23. The need to use this autocorrelation subtraction technique which is based on the different scaling properties for the motile and non-motile components, would appear to lie in the overlapping autocorrelation timescales for the two components. Any significant overlap would make it difficult to achieve an independent fit of one or other component.

Nossal and Chen in the same paper also gave autocorrelation functions generated by chemotactic behaviour. When a chemical gradient was established in the sample parallel to the scattering plane (XY plane in fig. 1-5), a periodic component appeared in the autocorrelation function. The periodic feature vanished when the gradient was perpendicular to the scattering plane, suggesting that the oscillation was generated by a general drift of cells along the gradient.

While these early experiments looked extremely promising, the assumption of a constant scattering amplitude seemed a little suspect, as Cummins (1973) pointed out, since the cells had dimensions of the order $\gtrsim\lambda$, were of asymmetric conformation and tended to wiggle while swimming. The relative importance of shape and wiggle during translation would probably vary significantly between strains as the data of table 1-1 indicate.

Boon, Nossal and Chen (1974) and, Berne and Nossal (1974), pursued this aspect of the problem at some length by calculating the expected light beating spectrum for motile rod-shaped scatterers of finite length but negligible width. Boon, *et al.*, (1974), drew attention to the possibility that the bacterial cell may be optically heterogeneous and due to scattering from internal structures may be optically much smaller than the physical dimensions suggest. This situation may have given the reasonable approximation to a point scatterer scaling behaviour which Nossal and Chen observed.

This possibility was consistent with internal structures evident in microscopic observations and Boon *et al.*, (1974) therefore in a detailed analysis, calculated the autocorrelation functions to be expected for a dumbbell-like model comprising two separated but relatively fixed point scatterers.

For a swimming speed distribution of Gaussian form the intensity autocorrelation function for dumbbell scatterers translating with their axes parallel to $\tilde{v}$, was derived to be;

$$I_{(\tilde{k},t)} = \left\langle J_o(Kvt) \right\rangle + \left[1 + J_o(kd)\right]^{-1} \sum_{n=1}^{\infty} (4n + 1) J_{2n}(Kd) \left\langle J_{2n}(Kvt) \right\rangle \quad (1.26)$$

where d = point scatterer spacing.

When planar wiggling motions were imposed simultaneous with the translation, the correlation function was expressed as;

$$I_{(\tilde{k},t)} \simeq \left\langle J_o(Kvt) \right\rangle \; f^{W}(K,t) \quad (1.27)$$

where $f^{W}(k,t) = \left[1 + 2J_o(Kd) + \left\langle J_o(K\beta d) \right\rangle\right] / \left[2 + 2J_o(Kd)\right]$ (1.28)

and $\beta = 2 \sin\left[\tfrac{1}{2}(\alpha(t) - \alpha(o))\right]$ expresses the nature of the wiggle, α being the instantaneous inclination of the dumbbell axis to the direction of translation.

Taking $\alpha_{(t)} = A \sin W_o t$

Boon *et al.*, derived the 'wiggle factor' as;

$$f^W(k,t) = \left[1 + 2J_o(Kd) + J_o(2Kd \sin [\tfrac{1}{2}A \sin W_o t])\right]/2[1 + J_o(Kd)] \qquad (1.29)$$

Intensity autocorrelation functions computed using equation 1.29 are shown for the same range of scattering angles for two sets of model parameters in fig. 1-10.

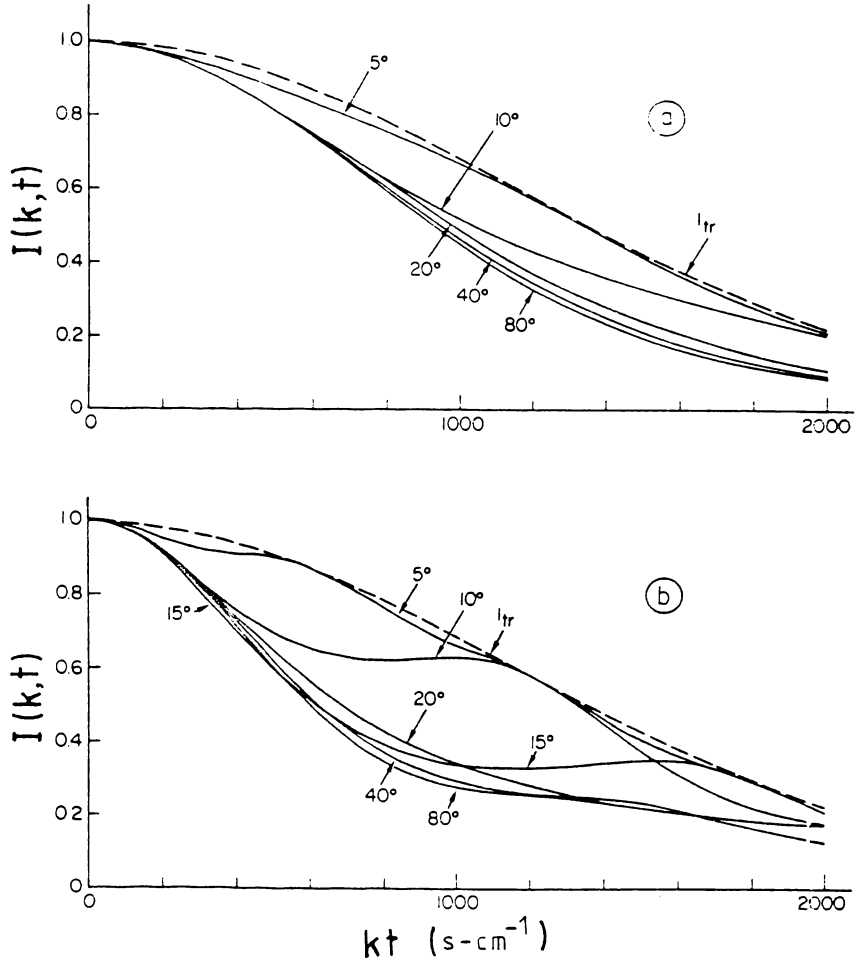

Fig. 1-10. Normalised intensity autocorrelation functions for motile 2-point dumbbell scatters at various scattering angles for a Gaussian speed distribution.

(a) $d = 1.5\mu m$ $\nu_{wiggle} = 5s^{-1}$, $v^{2\,\frac{1}{2}} = 15\mu m/s$, $\alpha_{max} = 30°$

(b) same parameters but $\nu_{wiggle} = 10s^{-1}$

(Boon *et al.*, 1974).

These curves may be compared with those obtained for real samples of *E. coli* K_{12} bacteria and shown in fig. 1-11.

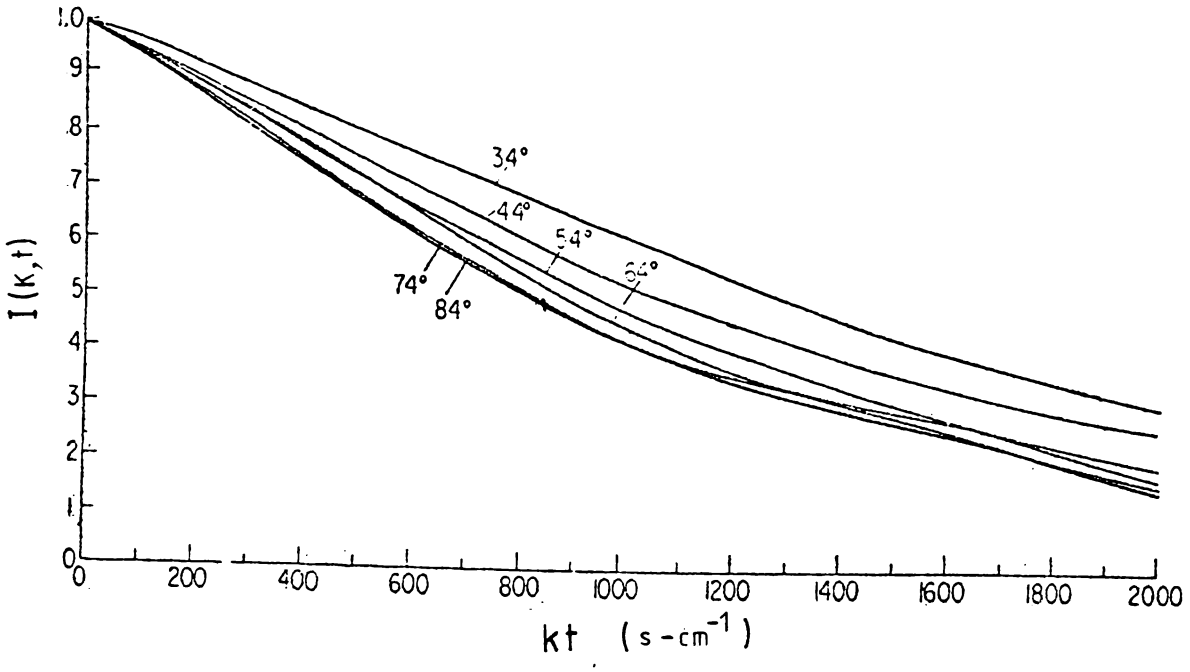

Fig. 1-11. Normalised intensity autocorrelation functions taken at various scattering angles (34° - 84°) for a sample of *E. coli* K_{12} in which wiggle motion had been enhanced by adding 7% Glycerol. Visual estimates suggested $\nu_{wiggle} \approx 2\text{-}3\ s^{-1}$ and $\alpha_{max} = 30°$. (Boon, *et al.*, 1974).

The general scattering angle dependence of these results is consistent with the calculated curves of fig. 1-10(a) and the following conclusions may be drawn from both the calculated and theoretical results;

(1) When $K \to o$ (i.e., experimentally when θ is small) the wobble factor $f^W \to 1$ and the correlation function arises from translation only.

(2) At large scattering angles the functions also scale as Kt although the decay time has been decreased by the presence of the wiggle factor.

(3) At intermediate scattering angles, substantial departure from Kt scaling occurs due to wiggle motion.

In looking back over these two early sets of experiments we find that the characteristic half-widths for Nossal's experimental data of fig. 1-9 are all of order $|\tilde{kt}| = 400$ s-cm^{-1} whereas those for the Boon, *et al.*, data (fig. 1-11) appear to range from $\sim$830 s-cm^{-1} up to an estimated 1300-1400 s-cm^{-1} over the same scattering angle range. If we assume that both experiments were carried out using the same wavelength, then since Kt scaling was observed in Nossal's data over the same angular range as that of fig. 1-11, it seems likely that the organisms used had a more vigorous mode of translation as opposed to wiggling or other internal motions.

The modelling component in the interpretation of light scattering data is therefore the key to physically useful applications of the method. Considerable exploration of the model parameters, as in the case of Boon, *et al.*, who essentially carried out a sensitivity analysis of a particular model (for scattering angle), is required to improve insight into the dynamical interpretation of the scattered light field.

Stock and Carlson (1974) refined the conformation model further by applying the Rayleigh-Gans approximation to rod and ellipsoidal shaped scatterers of bacterial dimensions.

$$\text{i.e.,}\quad A_{(t)} = A_o V \cdot {}^{1}/_{V} \int_{V} e^{i\tilde{k}.\tilde{r}_{(t)}}\, dV \qquad (1.30)$$

where $A_{(t)}$ is the time dependent form factor of a particle of volume V the motion of which is defined by the time dependence of $\tilde{r}_{(t)}$ for individual elements.

Their results are probably best discussed here in graphical form, the principal objective of the study being to examine the effect of a correlation between the cell orientation and its direction of translation.

The simple case of spheroids translating without wiggle having their major axis oriented along the translation vector is shown in fig. 1-12 as a function of scattering angle, for a mean swimming speed of $|\tilde{v}_s|$ = 20μm/s.

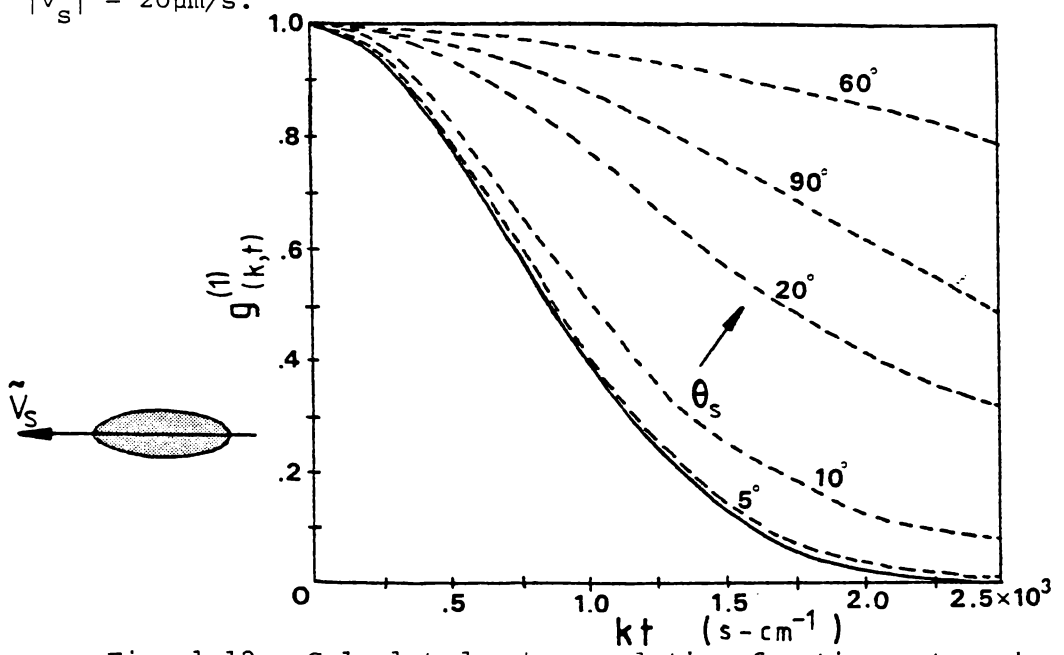

Fig. 1-12. Calculated autocorrelation functions at various scattering angles for spheroids of axes 1.5μm x 0.3μm translating without wiggle with their major axes aligned along the translation vector. (Stock and Carlson, 1974).

The departure from Kt scaling becomes very significant for scattering angles $\theta > 10°$ and it is also apparent that for $\theta \to 0°$ the autocorrelation function approaches that for a point scatterer (solid line in fig. 1-12) and the spectrum is determined solely by the translational motion.

A further extension of the model involved allowing the major axis of the spheroid to assume a Gaussian distribution of angles about the translation vector with $\sigma = \pm 20°$ and it is apparent that the departure from Kt scaling is substantially less than in the simple case of fig. 1-12.

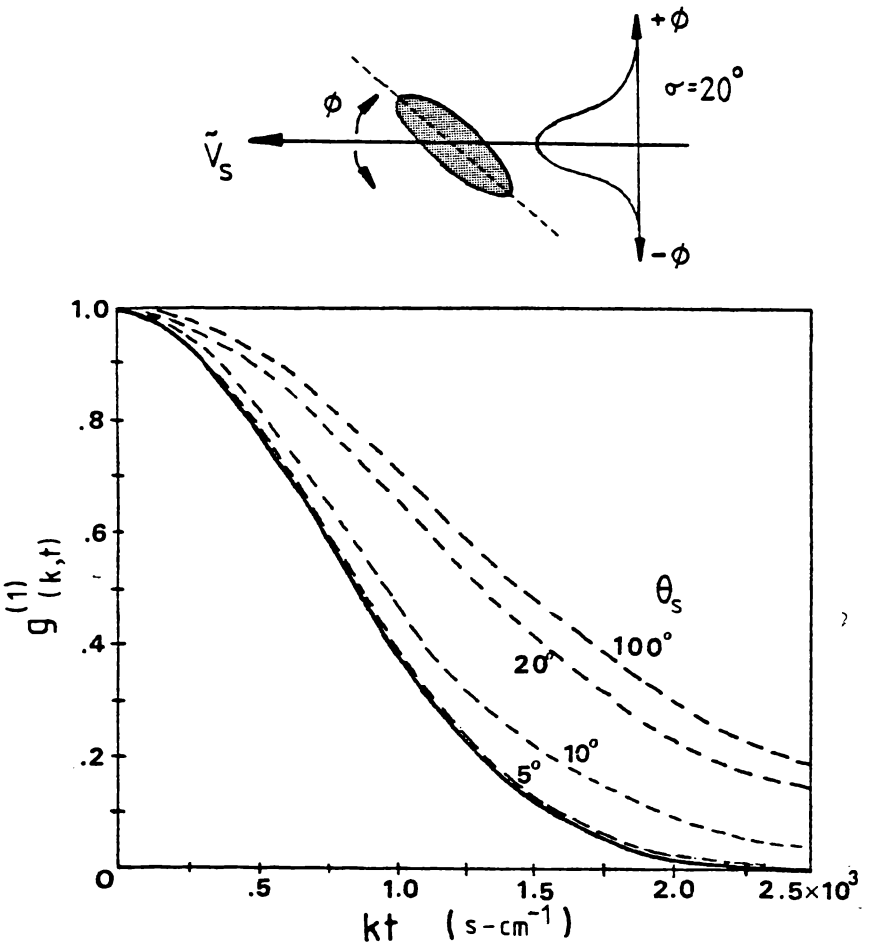

Fig. 1-13. Autocorrelation functions for the spheroids of fig. 1-12 but having a Gaussian distribution of major axis alignments peaked along the direction of translation. v_s = 20μm/s. (Stock and Carlson, 1974).

The effect of allowing the rod axes to be uncorrelated with the translation vector and to oscillate at a frequency of 10Hz and amplitude ϕ = 30° was also investigated. These data are given in fig. 1-14 but unfortunately the physical and dynamical parameters of the model differ from those of figs. 1-12 and 1-13 (in this case the model is that of rods of length 2.5μm with v_s = 10μm/s).

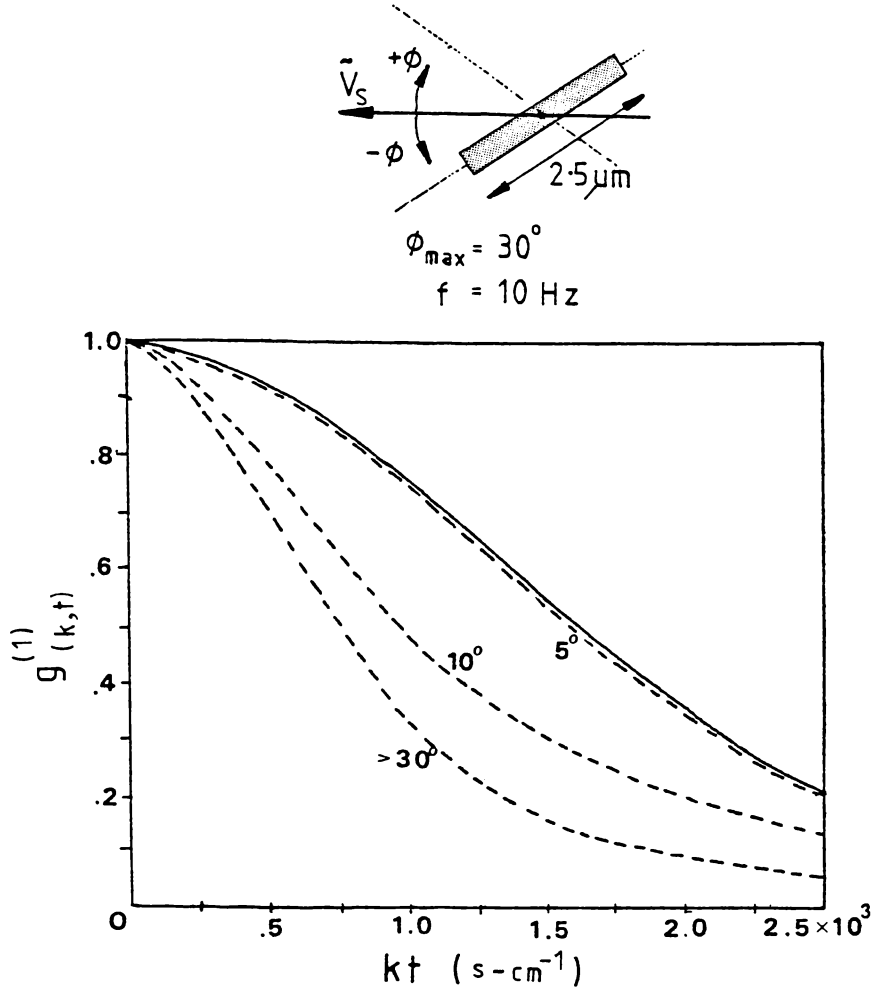

Fig. 1-14. Autocorrelation functions for rods with $\tilde{v}_s$ = 10μm/s ν_{rot} = 10Hz Amplitude = 30° (Stock and Carlson, 1974).

In this case the large angle decay time becomes shorter than for the spherical case although the absolute value of the mean swimming speed has been halved.

Finally, Stock and Carlson (1974) present experimental autocorrelation functions for *Salmonella typhimurium* at various scattering angles. This data (fig. 1-15) exhibits a similar angle dependence to that of fig. 1-14.

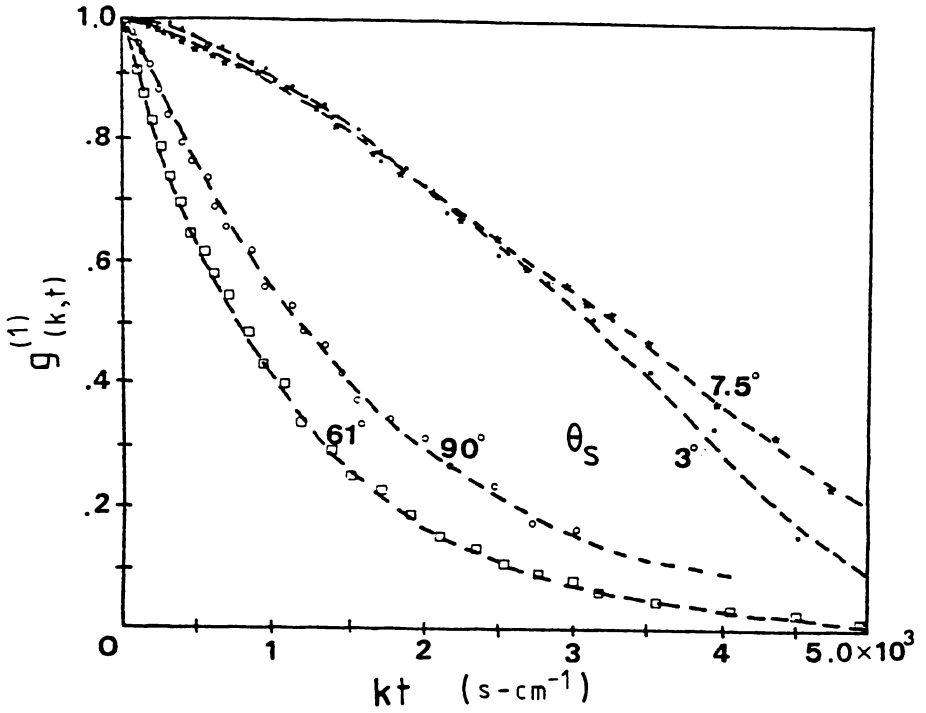

Fig. 1-15. Autocorrelation functions for *Salmonella typhimurium* for scattering angles 3° - 61° at 30°c.
(Stock and Carlson, 1974).

It was concluded that the magnitude of deviations from Kt scaling at higher angles may be used to indicate the extent of wobble or off-axial alignment of the translating bacteria. Comparing the functions of fig. 1-13 and 1-14 we might be able to define a parameter indicating the level of departure from Kt scaling; a shift towards increased decay constants on the basis of these models, would indicate axial wobble while deviations towards longer decay constants appear to be associated with an increased level of alignment along the translation vector. A combination of these two dynamical parameters would clearly be much more difficult to deconvolve and again the question of ambiguity arises in the interpretation of the autocorrelation data.

The experimental and computational data of Stock and Carlson appear to lie in a much lower translational velocity range than the early work

of Nossal *et al.*, since the characteristic half-width of the low angle functions in fig. 1-15 is $\sim$3000 s-cm^{-1}, large in comparison with the $\sim$400 s-cm^{-1}, evident in Nossal's data of fig. 1-9. The reason for the differences in Kt scaling characteristics between these reported experiments probably lies in the conclusion of Boon *et al.*, (1974), that for vigorous bacterial strains (as presumably Nossal and Chen used) having a strong and dominantly linear mode of movement, 'wiggles' and 'wobbles' superimposed on the translational motion will not result in significant irregularities in the correlation function or errors when light scattering is used for measuring the translational swimming speed. Substantial variation in the motile characteristics between cultures clearly exists and the level of response to chemotaxis is probably also closely related to the swimming properties.

If the low scattering angle data is to give translational information, it is a fundamental requirement of dynamic light scattering that the translation is correlated over a mean time which is substantially larger than the characteristic autocorrelation decay time (Berne and Pecora, 1976). Looking at table 1-1 (Berg and Brown, 1972) we see that the translational correlation time was in the range 0.56 - 6.45s showing an order of magnitude variation between bacterial strains.

Assuming λ = 632.8nm we can calculate the approximate decay times for the data of Stock and Carlson (1974) in fig. 1-15 and that of Nossal *et al.*, (1971) in fig. 1-9. For a scattering angle of 5° the values are given in table 1-2.

	Estimated K (cm^{-1})	Characteristic low angle Kt from data (s/cm)	Estimated τ^{-1}(s)
Nossal and Chen (1971)	1.15 x 10^4	0.8 x 10^3	0.070
Stock and Carlson (1974)	1.15 x 10^4	5 x 10^3	0.44

Table 1-2. Estimates of autocorrelation decay times for data of figs. 1-9 and 1-15.

On the basis of the data from Berg and Brown, (1972), T in table 1-1, the interpretation of the Stock and Carlson data at low scattering angles as being due to translation seems a little doubtful unless the sample was vigorously motile in a linear sense. The translational interpretation appears valid in the case of Nossal and Chen which may account for their Kt scaling result.

A completely different approach to light scattering studies of motility was reported by Schaefer and Berne (1972) and then Schaefer (1973), who looked at the time dependence of the scattering volume population by analysing the intensity fluctuations in the scattered light. If the region within the sample from which scattered light is collected by the detector, is small and contains fewer than ∿100 cells, a fluctuating amplitude term appears in the photocurrent spectrum.

These fluctuations, the mean value of which is represented by $\langle \delta N(o) \, . \, \delta N(t) \rangle$, occur on a timescale characterised by the time τ_n required for a particle to traverse the scattering volume. The intensity autocorrelation function then becomes,

$$G^{(2)}(\tau) = \langle N^2 \rangle A^4 \; g^{(2)}(\tau) + A^4 \langle \delta N(o) \, . \, \delta N(t) \rangle \qquad (1.31)$$

The second term has the effect, at least in the case of motile bacteria, of adding a 'long lived tail' onto the rapidly decaying phase component $g^{(2)}(\tau)$ (Cummins, 1973).

While we are not primarily concerned with this approach to motility measurement which uses number fluctuation spectroscopy, it has been cited here since the significance of the number fluctuation term is later considered in interpretations of results using spermatozoa in chapter 4 and is analogous to cinephotographic methods described in section 3.8.

1.3.3 Conclusions from Light Beating Spectroscopy studies using Motile Bacteria.

The published studies which have been discussed have all been based on the approach of defining dynamic light scattering models for motile bacteria, then comparing the scaling characteristics and functional form of computed autocorrelation functions with those obtained from real samples. Accepting that large variations in motility parameters occur between individual bacteria and strains of bacteria, the technique looks quite promising. However, the problem of validating the light scattering parameters as predictors of motion is clearly very difficult since independent measurements of the motion by other means are not readily carried out. The validation must therefore be indirect but it would certainly appear that the general features of the motion can be objectively characterised.

In terms of the measurable light scattering parameters the scattering behaviour studied in the literature suggests;

(1) Bacterial cells may be optically smaller than their physical dimensions suggest.

(2) At small scattering angles ($<5^{\circ}$) model calculations suggest that the autocorrelation function results from translation alone although there is little independent evidence that this is a safe assumption.

(3) Departures from Kt scaling at intermediate and large scattering angles are associated with axial wobble or reorientation.

(4) Shifts towards larger decay constants imply significant axial wobble while shifts to smaller decay constants imply an increasing degree of axial alignment.

(5) It appears difficult without ambiguity to individually characterise both axial alignment and wobble using the

autocorrelation data.

(6) The autocorrelation decay time must be considered relative to the time over which the swimming is correlated, which varies considerably from strain to strain.

Bull Spermatozoa, with which we shall be primarily concerned in chapters 4, 5, have a head which is an order of magnitude larger again than most motile bacteria, and is highly asymmetric. Consequently, while the swimming motions are substantially different, it seems likely that internal motions of the spermatozoon would potentially be of considerable significance.

1.4 Application of Light Beating Spectroscopy to Motile Algae

A recent light scattering study of considerable relevance is that of Ascoli, Barbi, Frediani and Murè (1978) who dealt with motile cells at the other dimensional extreme, those very large relative to the wavelength and in fact significantly larger than most spermatozoa.

Euglena gracilis is a flagellated alga of ellipsoidal shape which is self-motile with a complex roto-translatory motion. The axial dimensions of the cell are typically 60μm x 10μm x 10μm. Considered relative to the wavelength at 632.8nm, these dimensions are 95λ x 16λ x 16λ which certainly excludes it from consideration as a point-scatterer. Propulsion is provided by a single flagellum which beats around the body, the resultant motion being helical with a translational speed of ∿100μm/s, a rotational frequency of ∿2Hz and a translational velocity which is constant over distances of typically $\gtrsim$ 1 mm.

Ascoli, *et al.*, found that the intensity distribution of forward scattered laser light from a suspension of *Euglena* cells, when viewed directly on a screen, was remarkably non-uniform. Their photographs,

taken by placing a film about 20cm behind the sample in the forward scattering direction (film plane perpendicular to the incident laser beam), are reproduced in fig. 1-16.

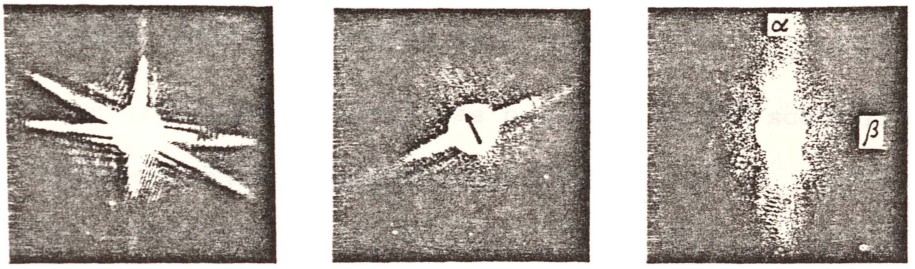

Fig. 1-16. Light scattering patterns from *Euglena*: (a) unoriented cells; (b) single cell; (c) oriented cells. The arrows indicate the direction of the orienting field. α is the position of the photodetector chosen to reveal the intensity modulations of the scattered light; β is the photodetector position chosen to reveal the Doppler shift of the scattered light. In all the pictures, the white spot masks the image of the direct laser beam (after Ascoli, *et al.*, 1978).

These photographs (exposure times were not given) show a sharply peaked scattered intensity distribution generated by the movement of individual cells, the intensity peak being in the plane perpendicular to the major axis of the cell. The intensity peak was observed to oscillate to some extent around the laser beam due to rotation of the major axis of the cell around its translation vector. The location of the photodetector, relative to the cell orientation, was therefore important and the field which it observed could be expected to be modulated by the internal motions of the cell if located near the peak.

The elegant technique employed to measure the dynamical parameters capitalised on the pronounced optical orientational effect through inducing parallel alignment of all translation vectors. This was

accomplished by means of a radio-frequency field (2MHz), the two detectors being located such that;

(i) the translation vector was perpendicular to the scattering plane (detector at α in fig. 1-16c).

(ii) the translation vector was parallel to the scattering plane (detector at β in fig. 1-16c).

In case (i) with the detector at α, the detected signal was demonstrated to arise largely from the periodically varying intensity generated by off-axial rotations of the cell and an associated sharp peak (at 1.8Hz) in the homodyne spectrum thus gave the cell rotation frequency. A further higher frequency peak (at $\sim$ 40Hz) was said to be associated with the flagellar beat frequency (possibly body wobble) and the location of both homodyne peaks was independent of scattering angle.

In case (ii) with the detector at β but using heterodyne detection, another prominent displaced spectral peak was obtained. This was identified as a Doppler peak and allowed the translational speed to be measured. With this configuration the detector did not see any significant intensity fluctuations from the internal motions although the scattered intensity was said to be very much lower.

With such a technique, the perturbation of the cell motion induced by the radio-frequency field used for alignment, may well be significant. Accordingly Ascoli, Barbi, Frediani and Petracchi (1978) showed that translation speed, rotation and flagellar beat frequency all increased with the radio-frequency field intensity and were closely associated with a temperature rise in the medium.

These results, particularly the asymmetry in the scattered field, are particularly relevant to the observations for bull spermatozoa later to be presented in chapter 5. It should also be pointed out, however, that the findings of Ascoli, *et al.*, (1978) and those presented

here in chapter 5, were quite independent. While different motile organisms are involved in the two studies, there are close similarities in the light scattering characteristics, which hold the key to interpreting measurements made on the scattered field.

As previously pointed out in the discussion of motile bacteria, the use of a single detector at a point in the scattered field has limitations in terms of the dynamical information which it can extract regarding the ensemble of scatterers. It may well be that bacterial motility, even without translation alignment, (as used by Ascoli, *et al.*, 1978), could be better characterised using two detectors. This essentially was what Nossal and Chen (1972b) demonstrated in their chemotactic studies and possibly their experiment, in particular the significance of their autocorrelation function corresponding to that from detector α in fig. 1-16c, could be further studied.

1.5 Applications of Light Beating Spectroscopy (LBS) to Spermatozoa

The first application of laser light beating spectroscopy to the motility of spermatozoa, was reported by Berge, Volochine, Billard and Hamelin (1967). These workers qualitatively demonstrated that spectral broadening of the scattered light was dependent on the motility of the sample, when using rabbit and fish sperm. Further experiments by the same group (Adam, Hamelin, Berge and Goffaux, 1969), showed similar light beating phenomena for bull spermatozoa.

Bull spermatozoa swim either with a predominantly linear trajectory or in circles of relatively large radii of curvature. The swimming motions are discussed in some detail in section 2.6, but in the present context the important point is that the translatory motion is generally correlated over long intervals, perhaps 10s or more, and the swimming speed is $\sim$ 100μm/s. The head dimensions of the spermatozoon and its conformation vary between species, and again further detail is given

in section 2.4. The cells are larger than motile bacteria and of oblate ellipsoidal conformation with axial dimensions of typically 8.6μm x 4.6μm x 1μm.

The optical model required for such an asymmetric scatterer (scattering from the flagellum has generally been ignored) and indeed also the dynamical model in terms of which the light scattering data is interpreted, have not until recently been rigorously studied. The general approach to the scattering model, has been to extrapolate the assumption from the bacterial studies that the cell approximates a point scatterer at small scattering angles.

A dynamical model of isotropically translating scatterers has been assumed without exception in the interpretation of small angle scattering data.

Again, as with motile bacteria, problems arise in validating the light scattering results since data from other methods is neither generally nor readily available. However, at least for bull spermatozoa, the range of the dynamical parameters is reasonably well known from other methods, and unlike bacteria, the variation between normal fresh samples under standard conditions, is not large. The motion would, therefore, appear to be much easier to characterise than the complex movements of bacteria.

A basic and highly significant publication for LBS spermatozoa studies, was that of Nossal (1971) who analysed the spectral broadening generated by motile micro-organisms (including spermatozoa) in some detail. The geometry and dimensions of the scatterers were ignored since the low angle point-scatterer model was assumed and particles were taken to be moving in total random directions. Using these assumptions, Nossal calculated the light beating spectra corresponding to various swimming speed distributions;

(i) a population of uniformly speedy cells.

(ii) a population of cells having speeds of equal probability up to a maximum V_s.

Each model also assumed 50% of the population were immotile and this was taken into account by expressing the autocorrelation function as a sum of two components;

$$G^{(1)}_{(\tau)} = N|A|^2\{\alpha\, G^{(1)}_{m(\tau)} + (1-\alpha)\, G^{(1)}_{i(\tau)}\} \qquad (1.32)$$

where $G^{(1)}_{m(\tau)}$ and $G^{(1)}_{i(\tau)}$ refer to the motile and immotile field autocorrelation components respectively and α the fraction of the population (N cells) which is motile. Under these conditions the translational models of (i) and (ii) generated the calculated scattering spectra shown in fig. 1-17.

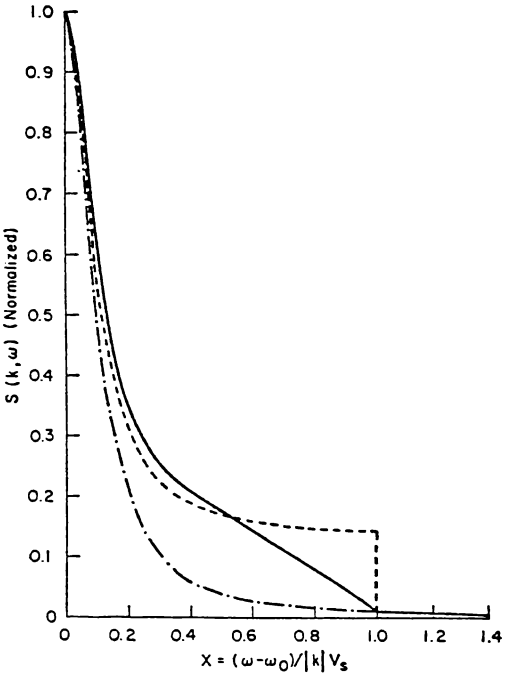

Fig. 1-17. Calculated spectra for;

(i)------ uniform swimming speeds.

(ii)——— swimming speed range having a uniform probability up to a maximum.

α as defined in equation 1.32 was given the value of 0.5.

(Nossal, 1971).

The modelling exercise was then extended by taking a swimming

speed distribution for bull spermatozoa which had been determined by other methods (photoelectric methods of van Herpen and Rikmenspoel, 1969);

$$P_{(\nu)} = B \exp\left[-\tfrac{1}{2}(\nu - \nu_s)^2/\sigma\right] \qquad (1.33)$$

(where ν_s = 102μm/s, σ = 35μm/s B a constant) and deriving from it the expected light beating spectrum on the basis of an isotropic distribution of translation vectors. These spectra are shown here in fig. 1-17 and the case utilising the experimental swimming speed distribution is shown in fig. 1-18. Nossal indicated that the parameters of P(ν) ($\bar{\nu}$ and σ) may be determined by varying the scattering angle. No experimental spectra were presented for comparison with that of fig. 1-18.

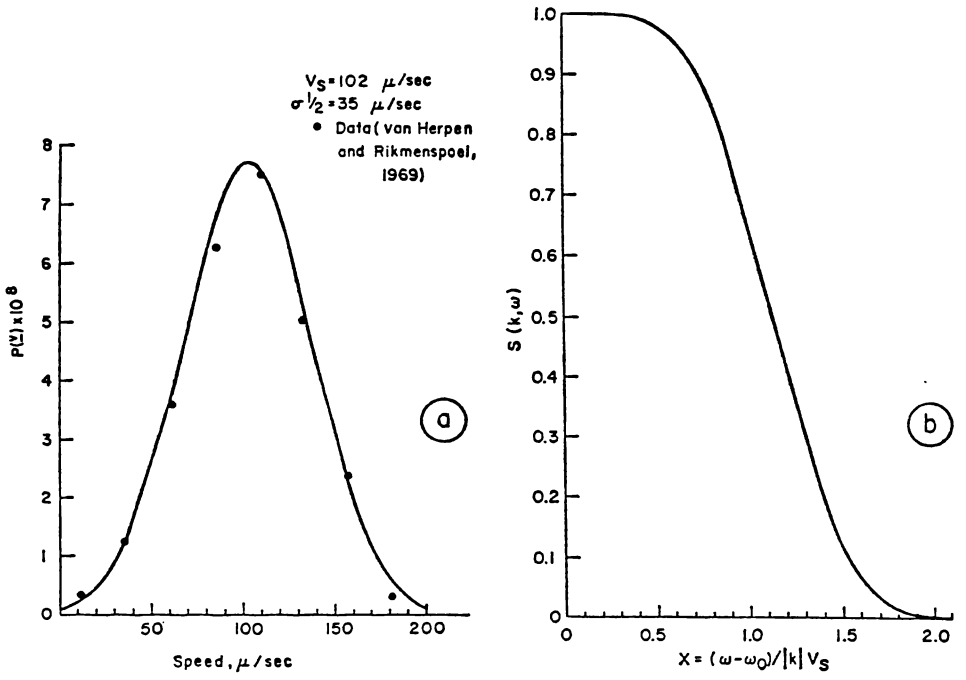

Fig. 1-18. Light scattering spectrum (b) calculated for the swimming speed distribution of (a), for bull spermatozoa. (Nossal, 1971).

A significant point is made by Nossal;

"..... *it seems that the general form of the distribution P(ν) needs to be known from other measurements in order to comprehend*

the light scattering data. However, once the general form of P(ν) is known, the laser scattering experiments can be employed to measure changes in characteristic parameters.".....

Nossal also constrained the applicability of his analysis to cases where $k\ell/4 \lesssim 1$ (ℓ being a characteristic linear dimension of the scatterer and k the amplitude of the scattering vector) since only under this condition (Pecora, 1968) is the point scatterer assumption a valid one. At higher scattering angles and dimensions where this criterion is not met, it was acknowledged that the scattering spectrum may contain additional components generated by the form factor of the particle.

Values of the factor $k\ell/4$, for particles having ℓ = 8.6μm (the maximum linear dimension of the bull spermatozoon head) are shown in fig. 1-19,

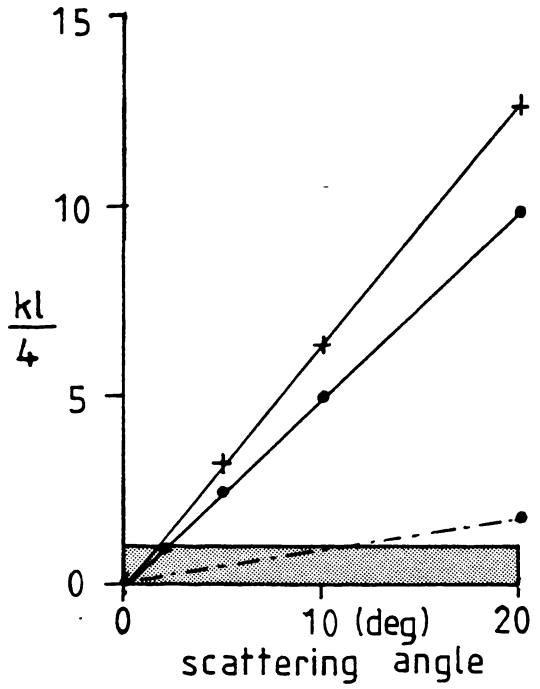

Fig. 1-19. Values of $k\ell/4$ as a function of scattering angle for an object of characteristic dimension 8.6μm, at two commonly used laser wavelengths.
+——+ 488 nm.
•——• 632.8 nm.
- • - • similarly for a 1.5μm particle at λ = 632.8 nm. The shaded region depicts $k\ell/4 < 1$.

and it is apparent that the criterion is only met at very small scattering angles ($\lesssim 2°$). For comparison, a plot is also given for a bacterial sized particle of dimension 1.5μm at λ = 632.8nm and in this case the criterion is met at angles $\lesssim 10°$ which is consistent with the scaling results previously shown in fig. 1-16 for *Salmonella typhimurium* (Stock and Carlson, 1974).

Unpublished studies by Woolhouse (1976) accepted the point scatterer approximation for bull spermatozoa and plausible RMS swimming speeds were plotted as a function of temperature. Further, kt, scaling of $g^{(2)}(k,t)$was obtained for 100% motile sperm over a wide range of scattering angles (11.3° - 51.8°) although the scaled autocorrelation functions appeared more exponential than Lorentzian in form.

A Fourier derived swimming speed distribution was obtained which peaked at a very low velocity ($\sim$ 15μm/s) and problems occurred with periodic artifacts arising from the transformation. While the magnitude of RMS velocities for the distribution appeared reasonable, the shape of the probability distribution was highly skewed and did not closely resemble that of van Herpen and Rikmenspoel (1969) in the higher range.

These studies, however, also explored the suitability of various diluent and sperm concentrations for light scattering studies and suggested on the basis of subjective but nevertheless very useful observations, that a concentration of 10^6sperm/ml in an optically cleared 0.25% Egg-Yolk extender was appropriate.

Possibly the most significant result from this work was the observation that a two-component autocorrelation function was obtained for a composite sample of live and dead spermatozoa. A rapidly decaying component arising from the motile fraction was observed to be superimposed on a relatively long timescale exponential-like feature apparently associated with the dead cells. The amplitude ratio (at τ = o) of the two autocorrelation components was suggested from qualitative observations,

as being a measure of the percent dead cells in the sample although no supporting data was presented. This proposal was consistent with the earlier predictions of Nossal (1971). A contemporary publication, at the time, by Cooke, Hallett and Barker (1976) also reported applications of photon correlation spectroscopy to motility evaluation using bull spermatozoa. Following Nossal's analysis, they analysed the field autocorrelation function as being a sum of two components.

$$g^{(1)}(\tau) = \alpha f_m(\tau) + (1 - \alpha) f_d(\tau) \qquad (1.34)$$

where f_m was the autocorrelation function for the motile cells and f_d that for the dead cells.

f_d was found to be of exponential form (see fig. 1-20(a)) but with slight departures from exponentiality said to arise from settling of the cells through the Gaussian intensity profile of the beam.

Fig. 1-20 shows autocorrelation functions for bull spermatozoa presented by Cooke, *et al.*, for (a) dead cells and (b) a mixed sample of dead and motile cells.

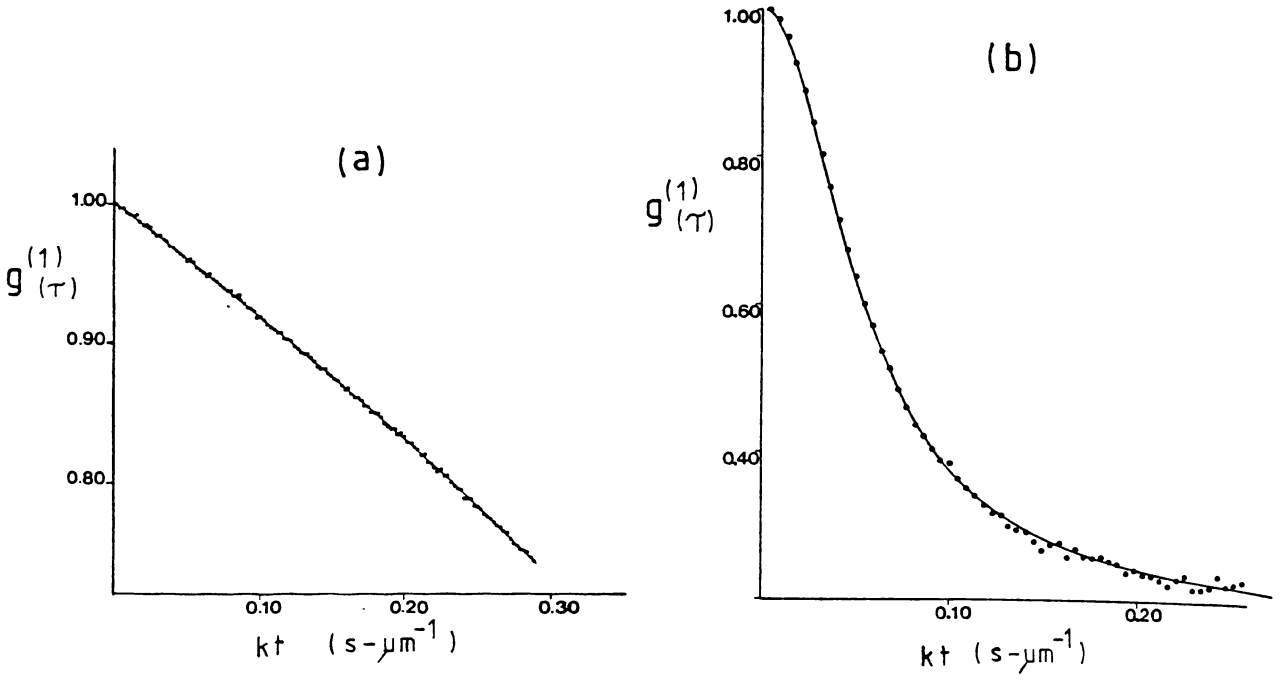

Fig. 1-20. $G^{(1)}(\tau)$ measured by Cooke, *et al.*, (1976) for (a) dead and (b) a mixture of dead and motile bull spermatozoa. Scattering angle was 10° in both cases and λ = 647nm.

For the experimental conditions given, it can be deduced that the characteristic half-width at half-height for the composite curve of (b) is $\sim$ 560 s-cm^{-1} in comparison with the equivalent value of $\sim$ 3500 s-cm^{-1} evident in fig. 1-16 for motile bacteria. In this case $k\ell/4 \sim 4.8$ and no details are given of the sperm concentrations employed nor is any corroborative data presented.

The functional forms in relation 1.34 and the data of fig. 1-20 were best fitted by a Lorentzian for the motile component (fig. 1-20b).

$$f_m(\tau) = \frac{\Gamma^2}{\Gamma^2 + (k\tau)^2} \qquad (1.35)$$

with $\Gamma = 12.05$

and an exponential for the dead component (fig. 1-20a).

$$f_d(\tau) = \exp(-\tau/\tau_d) \qquad (1.36)$$

where τ_d is the fitted characteristic decay time (no typical values were given).

The value of α in relation 1.34 was said to be sensitive to systematic errors in the background measurement and problems were encountered in defining the slow exponential form of f_d over short experimental times imposed by rapid settling of the cells. These problems are relevant to phenomena discussed in chapter 5 of this thesis. Further it is interesting to contrast the relatively high value of $\alpha = 0.811$ obtained by Cooke, *et al.*, (1976) for the data of fig. 1-20, with those α values given in the various results of chapter 4. Cooke, *et al.*, also derived a swimming speed distribution using the argument of Nossal and Chen (1972) that;

$$P_{(v)} \alpha V \int_0^\infty \text{Sin}(vKt)\,(Kt f_m)\,dt \qquad (1.37)$$

and extrapolating the function f_m so as to suppress oscillations in $P_{(v)}$ created by truncation effects in the sine transform Brigham (1974). This distribution is shown here in fig. 1-21 and clearly extends into

the high velocity region. The authors interpreted this distribution as representing not the speed of translation, which is generally

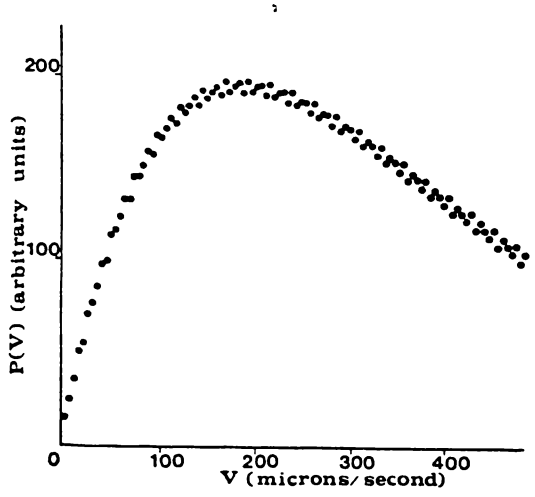

Fig. 1-21. Swimming speed distribution derived by Cooke, *et al.*, (1976), from the autocorrelation data as in fig. 1-20b.

accepted to have a mean value of $\sim$ 100$\mu m/_s$ (at 37°C), but as the instantaneous tangential velocity which was reasoned to be a factor of 2 greater. Transforming this data to give a distribution of translation speeds would then seem to give a reasonable mean velocity, although the high speed tail of the distribution differs somewhat from that determined by the photoelectric methods of van Herpen and Rikmenspoel and previously given in fig. 1-18. It is also similar in form to that obtained by Jonannet, Volochine, Deguent, Serres and David (1977), who, using the point-scatterer and isotropic velocity assumptions, derived a swimming speed distribution for human sperm which is illustrated here in fig. 1-22. In comprehensive studies this group also used light scattering to determine the absolute concentration and percentage of motile cells as well as total sperm concentration. Percent motile cells was determined by signal filtering techniques which compared the relative amplitudes of the low and high frequency domains which arise from immotile and motile cells respectively.

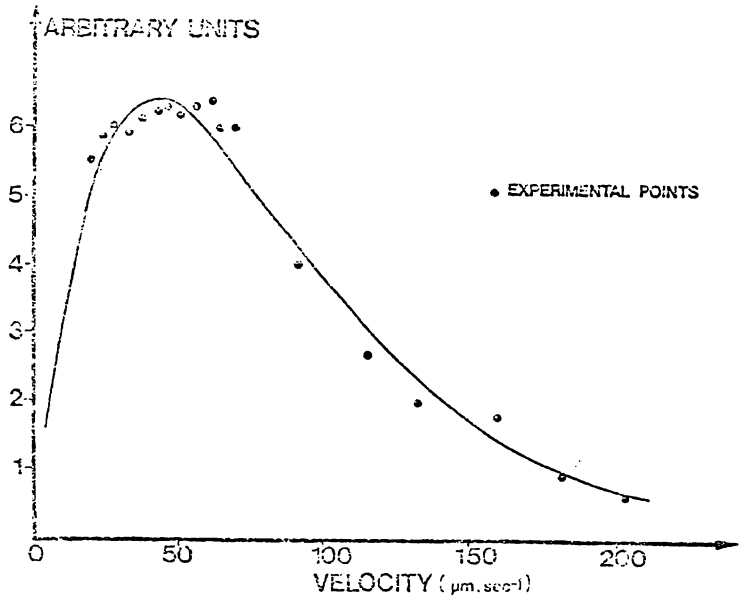

Fig. 1-22. Swimming speed distribution for human spermatozoa as determined from the point-to-point derivatives of the light beating spectrum.

. points determined from point to point derivatives of the photocurrent spectrum.

____ solid curve represents the best fit to the distribution of 1.40 with V_c = 44μm/s.

(Cummins, 1976).

The speed distribution of fig. 1-22 was derived from the heterodyne beat spectrum

$$I(w) = C \int_{w/k} \frac{P(v)}{kv} \, dv \qquad (1.38)$$

where C is a constant and $P(v)$ is the velocity distribution assuming an isotropic distribution of translation vectors. Differentiating (1.38) gives;

$$P(v) \alpha w \frac{d}{dw} \{I(w)\} \qquad (1.39)$$

Consequently by differentiating the heterodyne spectrum the points plotted in fig. 1-22 were determined. The best fit to the distribution

$$P(v) = \frac{1}{v_c^2} V \exp - (V/V_c) \qquad (1.40)$$

with V_c = 44μm/s, is also plotted.

This study produced a velocity distribution with a mean swimming speed which was in the accepted range for human spermatozoa. However, the extension of the distribution into the high speed range, as was also apparent in fig. 1-21 for bull sperm, is of dubious physical significance. Further, the tangential as opposed to translational velocity question was not discussed. Validation of the percent motile cells measurements involved comparisons with visual microscopic assessments. Of this and other experiments by the same workers, Cummins (1976) in a review of LBS applications to motile microorganisms commented;

> "..... *In the experiments of the Saclay group, there has been little attempt to analyse the complications of orientation dependence, wobbling motions, etc..... Nevertheless, they have made extensive comparisons of their results against measurements by other methods, and generally obtained good agreement.....*"

Cummins himself, in a later section of his review, briefly discusses orientational effects but only within the context of the motile bacterial results of Berne and Nossal (1974) and Stock and Carlson (1974).

Shimizu and Matsumoto (1977) appear to have selected sperm which were more appropriate to the constraints of Nossal's (1971) analysis. They studied abalone and pig spermatozoa, both of which have an approximately spherical head conformation, but make no reference to actual dimensions. The analysis followed the well established Fourier sine transform approach and swimming speed distributions were derived for both pig and abalone sperm. These gave 'most probable' and 'RMS' velocities of 135μm/s and 181μm/s respectively (for pig) and 41μm/s and 60μm/s for abalone. Concentrations employed were approximately 10^8 spermatozoa/ml. Using pig spermatozoa, kt scaling of the autocorrelation functions was obtained for scattering angles of 45° and 90°. Taking the characteristic

dimension of the head to be a conservative 2μm gives $k\ell/4 \approx 6.5$ at $\theta = 45°$.

A progressive increase in autocorrelation decay time was obtained when the sample temperature was incremented over the range 28.5°c - 56°c. The mean swimming speeds were plotted against temperature and showed a sharp peak at ∿ 39°c which was claimed to be physiologically reasonable. The average swimming speed of (181 ± 10) μm/s for pig sperm at 39°c was said to be in good agreement with that obtained by other methods and reported by Bishop (1962). However, Bishop (1962) gives no data for pig sperm and it seems that a general comparison with values across species was intended.

Using a rather different approach, Matsumoto, Shimizu, Shimada and Wada (1977), and then later work by Shimizu and Matsumoto (1980), looked at the homodyne autocorrelation function for the depolarised scattered field using very small scattering angles (< 2°). The depolarised scattered field intensity was found to be a factor of 30,lower than that for the polarised field, using samples of sea chestnut (*Anthocidaris crassipira*) sperm. For these cells the head was stated to approximate an ellipsoid of revolution with axial dimensions of 1μm x 0.5μm and this puts it back into the bacterial size domain previously discussed.

The depolarised autocorrelation function was considered to originate either from time dependent changes in the form factor of the head or from the flagellum. The measured 1.4mS autocorrelation decay time was not consistent with that expected for head motions (which showed a high degree of physical symmetry) and the conclusion was drawn that the depolarisation was generated by the flagellum. A distribution function was derived from the light scattering data and indicated a mean flagellar beat at 36Hz. The authors point out that other observations suggest frequencies of 30 - 40Hz.

The first large scale study of spermatozoa motility by LBS appears

to be that of Hallett, Craig and Marsh (1978) who analysed 88 samples of bovine semen from 39 bulls. In common with previous workers their analysis was based on the assumption of a point-scatterer model (at a scattering angle of 15°) and an isotropic velocity distribution. The experimental conditions indicate $k\ell/4 \approx 7.4$. However, the approach was more sophisticated in that the autocorrelation function was fitted as having three components arising separately from normal swimmers, defective or circular swimmers, and dead cells. Least squares methods were used to select the best functional fits to the individual components and to compare their relative amplitudes, as defined by the coefficients of 1.41;

$$g^{(1)}(\tau) = \alpha(f_\ell) + \beta(f_c) + (1 - \alpha - \beta)(f_d) \qquad (1.41)$$

where α = fraction of normal swimmers
β = fraction of circular swimmers
$(1- \alpha - \beta)$ = fraction of dead cells

The functions determined as best functional fits in 1.41 were;

Normal Swimmers f_ℓ

two possible functions were compared.

(i) $f_\ell = \exp(-K^2 + 2 \langle V_N^2/6 \rangle)$

a Gaussian

(ii) $f_\ell = 1/\{1 + [K \langle V_n \rangle \tau/2]2\}$

a Lorentzian

Circular Swimmers f_c

$$f_c = \{\frac{1}{K} \langle V_c \rangle \tau\} \operatorname{Cot}^{-1}\{\frac{1}{k\langle V_c \rangle \tau}\}$$

which gives a gamma distribution of speeds

$$P_{s(v)} = \frac{\langle Vc \rangle}{4\Pi} \exp\{- V/\langle V_c \rangle\}$$

f_d dead cells

$f_d = \exp(- \tau/\tau_c)$

an exponential

This was a very comprehensive and detailed study but one which appears to have been more preoccupied with the mathematical and analytical rigour of the fits than with the validity of the basic model and the phenomenology of light scattering and sperm dynamics. Typical data from the study is quoted here in table 1-3 taken over all 88 semen samples which were analysed.

Parameter	Average value	S.D.
α	0.29	0.17
β	0.24	0.16
$\alpha + \beta$	0.53	0.21
$\langle V_N \rangle$	384μm/s	110μm/s
$\langle V_C \rangle$	103μm/s	83μm/s

Table 1-3. Overall means and standard deviations (SD) for the 88 semen samples analysed by Hallett, *et al.*, (1978).

As in the earlier study of Cooke, *et al.*, (1976) the high speed values obtained from the normal swimming component, were interpreted as actually representing the tangential speed along a helical trajectory. This interpretation suggested an average translation speed of $\sim$ 180μm/s which, as they conceded, seemed to be slightly high. This is in fact a particularly high value when it is considered that the measurements were stated to be carried out at 30°c and that various measurements (see section 2.6) by other methods have given values in the range 94 - 123μm/s at 37°c.

The relatively large component (β) attributed to circular swimmers is interesting and may well have been due to sample temperature, handling, dilution methods (Shannon, 1980), or perhaps special swimming effects within the sample cell as later outlined in section 2.8.

No comment was made on the sperm sample concentrations used other

than that all raw samples were diluted by a factor of 2500. Considering the normal range of sperm concentrations found in ejaculates (section 2.3) this could mean any final concentration in the range (0.1 - 0.8) x 10^6 sperm/ml and this may later be compared to data in the results of chapter 4, section 4.3 in particular.

Attempts were made in this study (Hallett, *et al.*, 1978) to relate semen quality as assessed by the light scattering measurements to a visual scoring method used by trained technicians. Using the light scattering result $100*(\alpha+\beta)$ multiplied by the derived translation speed, a broad correlation was evident with scored visual assessments based on a motility factor (1 - 5) multiplied by the percent live cells.

Frost (1977) discussed the problems inherent in the Fourier sine transformation and suggested that the methods employed by Nossal and Chen (1971) were questionable. Using the method of Splines (Stock, 1976) Frost generated fits to various swimming speed distributions without performing a Fourier inversion. Further, methods were evolved for expressing the autocorrelation function in terms of the moments of different swimming speed distributions. Comparisons were then made of the efficiency of the two methods and the conclusion drawn that both techniques should be employed.

Swimming speed distributions for human spermatozoa were obtained experimentally (temperature 37.5°c and scattering angle 11.8°) on various timescales. Splines fits were made to the data and compared with those obtained by the method of Jouannet, *et al.*, (1977) who best fitted a function of the form;

$$P_{(v)} = \langle \frac{1}{V_c^2} \rangle \; V \exp\left(-V/\langle V_c \rangle\right) \qquad (1.42)$$

to their data for human spermatozoa $\langle V_c \rangle$ being a characteristic velocity.

Quite recent experiments reported by Finsy, Peetermans and Lekkerkerker (1979) on undiluted human sperm, were along the same lines

as previous work. The point-scatterer, isotropic velocity model was again assumed and the autocorrelation data was best fitted by

$$P_{s(v)} = (4v/\bar{v}^2) \exp(-2v/\bar{v}) \qquad (1.43)$$

A rather different experimental system was suggested by Dyott (1978) who proposed the use of a fibre-optic laser Doppler anemometer for studies of the motility of bull spermatozoa. This instrument, similar to that previously used by Tanaka and Benedek (1975) to measure blood flow, uses an optical fibre to deliver illumination to the measurement site and the *back-scattered* light is then collected and transmitted to the photodetector by the same optical fibre. The scattering volume within the sample from which significant scattered light could be collected, extended typically a distance of $\lesssim$ 1mm from the fibre end. The use of back-scattered light is interesting but the origin of light scattered from bull sperm at such angles is by no means clear. Results for spermatozoa did not appear as proposed in a subsequent publication (Ross, Dhadwal and Dyott, 1978).

It is not intended that the details of these various techniques be further investigated here. Various detailed descriptions are already available (e.g., Frost, 1977, Stock, 1976; and Cummins, 1976). The important point is that the methods of analysis which have been used (i.e., splines, moments or Fourier methods), operate on data derived as or from the intensity autocorrelation function of the scattered field. The swimming speed distribution for spermatozoa which these methods may produce must be interpreted as being a distribution of velocity components along the scattering vector. How this is related to the swimming velocity distribution of the ensemble of scatterers is dependent on the dynamical model assumed for the system. In this respect, all the literature discussed has assumed an isotropic velocity distribution for

the ensemble. The assumption has also been made, which is indeed a substantial simplifying assumption, that the autocorrelation function arises entirely from the phase relationships of the scattered field and contains no amplitude component (although studies on motile bacteria had examined the significance of amplitude effects). The particular geometrical form of the spermatozoa involved may well affect this amplitude factor although no attempt was made to examine the effect of sperm conformation as has been done in the case of motile bacteria.

The validity of these assumptions appeared to be implied by the fact that, *'the numbers came out right'*! Indeed, this fact has probably hindered the development of laser light scattering as a probe of sperm motility.

1.5.1 Conclusions from Light Beating Spectroscopy literature on Applications to Spermatozoan Motility.

The literature pertaining to spermatozoa motility measurements using laser light beating spectroscopy is not voluminous even though it extends over a ten year period. There are several possible reasons for this;

(i) that a seemingly simple application of LBS had apparently been established by several papers as a rapid and quantitative technique for motility measurement and research interest in the field had thereafter declined.

(ii) the multi-disciplinary effort required for such studies is not always readily arranged, coordinated or sustained. The highly variable level of artificial breeding or semen handling technology, particularly when dealing with other than bull semen, is likely to be a major factor and responsible for the lack of depth in experimental method seen in some papers.

(iii) that considerable experimental difficulty has been encountered and interpretation of LBS data has not been sufficiently well defined to allow confident publication.

A general categorised summary of the principal papers which describe applications of LBS to the study of spermatozoa motility, is given in table 1-4. The experimental details and parameters have been given where possible and the general similarity of approach is clearly evident.

Table 1-4. A summary of the principal features of light beating spectroscopy experiments seeking to measure the motility of spermatozoa.
* Craig, *et al.*, (1979) is discussed subsequently in section 1.5.2.

SUMMARY OF LITERATURE

Author(s)	Berge, *et al.*	Nossal	Jouannet, *et al.*	Woolhouse	Cook, *et al.*	Shimizu, *et al.*	Matsumoto, *et al.*	Hallett, *et al.*	Finsey, *et al.*	Craig,* *et al.*
Year	1967	1971	1976	1976	1976	1977	1977	1978	1979	1979
Journal	C.R. Acad. Sci.	Biophys. J.	Andrologia	M.Sc. Thesis	J. Mechanochem cell motility	I.EEE Trans on BME.	Opt. Comm.	Biophys. J.	Biophys. J.	Biophys. J.
Sperm Species used.	Rabbit Fish	Theoretical	Human	Bovine	Bovine	Abalone Pig	Sea Chestnut	Bovine	Human	Bovine
Diluent/Medium	-	-	Seminal plasma?	Cleared Egg Yolk.	(Hanks balanced salt solution)	Sea water Ringer-Lockes	Sea water	Hanks balanced salt solution.	Seminal plasma.	As for Hallett, *et al.*, (1978).
Scattering Model Assumed.	Reported exptl. observations.	Point scatterer	Point scatterer	Point scatterer	Point scatterer	Point scatterer	Optical asymmetries Flagellar origin.	Point scatterer.	Point scatterer.	An investigation of a Rayleigh-Gans model of the head. Acknowledge non-isotropic distribution of visible trajectories. Studied distribution of rotation rates
Dynamical Model Assumed.	Reported exptl. observations.	Isotropic	Isotropic	Isotropic	Isotropic	Isotropic		Isotropic.	Isotropic.	
Type of Swimming speed prob. distribution.	-	(i) all same speed (ii) const. probability up to v_{max}. (iii) distrib^{n} from photoelectric data.	$\frac{1}{v_c^2} v\exp(-\frac{v}{v_c})$	Fourier Sine Transform	Fourier Sine Transform.	Fourier Sine Transform.	Interval motions only.	(i) Gamma with 2 d.f. (ii) Normal. $\frac{4v}{\langle v\rangle^2}\exp(-\frac{2v}{\langle v\rangle}$	Gamma	$P(w) = \frac{4w}{\bar{w}^2} e^{-2w/w}$
Sperm concentration or dilution.	-	-	varied widely but >0.5 x 10^6/ml	Nominally 10^6/ml	1:29	$\sim 10^8$/ml	$\sim 10^7$/ml	1:2500	Undiluted	As for Hallet, *et al.*, *et al.*, (1978).
Absolute concentration controlled?	-	not an experimental study.	recognised effect of conc. on results.	Yes	No	Uncertain	Uncertain	No	No	No
Scattering Angle.	Small	-	8°	Up to 50°	10°	45° - 90°	< 2°	15°	10° - 20°	15°
$\lvert k\ell/4\rvert$ (estimated from available exptl. detail).	-	-	1.8	Variable	$\sim$ 4.8	-		$\sim$ 7.4		$\sim$ 7.4
Sample Cell Geometry.	Unspecified	-	Cylindrical 0.1 mm thick 17 mm^3 volume.	Rectangular path length 1 cm.	Air tight 1cm cuvette	Unspecified	Unspecified	Unspecified	Cylindrical $\sim$ 3 mm ID vol. 10 mm^3	Unspecified.
Wavelength	-	-	Unspecified.	450 - 514 nm	647.1 nm	632.8 nm	632.8 nm	632.8 nm	632.8 nm	632.8 nm
Parameters measured.	Spectral broadening observed.	Spectra computed for assumed $P_{(v)}$	Concentration $P_{(v)}$ $\langle v_c\rangle$ percent motile.	$P_{(v)}$ $\langle v\rangle$ and temperature depend nce.	$P_{(v)}$ time dependence of $\langle v\rangle$ end percent motile	$P_{(v)}$ $\langle v\rangle$ and temp. dependence	Periodicities from motion of optical anisotropies	$P_{(v)}$ various distributions percent normal swimmers, percent circular swimmers, mean speeds.	$P_{(v)}$ percent motile mean speed.	Derived autocorrelation functions for a Rayleigh-Gans model and a distribution of head rotation rates.

From the studies which have been reported, several prominent features merit serious consideration in view of data to be presented in chapters 5 and 6. These are:

(1) Without exception all workers (until the recent work discussed in 1.5.2) have assumed an isotropic velocity distribution within the sample. That is, all spermatozoa swimming through the scattering volume contribute equally to the detected signal, regardless of the orientation of the translation vector. This is a critical assumption in the deconvolution of the swimming speed distribution and unless it is valid all results presented in the literature for swimming speeds have no quantitative significance other than their apparent numerical plausibility. It seems a perfectly reasonable assumption that the velocity distribution should be isotropic and this has no doubt been reinforced by analogy with Brownian diffusion and motile bacteria. Much effort has therefore gone into the mathematics and computations of generating various reduced distribution functions for swimming speeds from the autocorrelation data and no consideration has been given to the possibility that the distribution of velocity components along the scattering vector could be generated by something other than a 3-dimensionally isotropic distribution.

(2) Another outstanding feature of the literature has been the assumption of a simple point scatterer model for sperm heads where most of the scattered light has been considered to originate. For spermatozoa of marine species (sea chestnut, abalone, fish and starfish) this may well be a reasonable assumption at small scattering angles since the dimensions are

comparable with motile bacteria which have been more extensively studied in this respect. For human, and in particular bull and ram sperm, the approximation hardly seems appropriate, particularly when the scattering angles employed have been in the range 8° - 20°. The significance of these large dimensions lies largely in the asymmetry of the head geometry which as previously discussed may introduce amplitude fluctuations into the scattered field when the cell changes its orientation. The human sperm head being smaller and more or less cylindrically symmetric, may not give such large fluctuations as might be expected for the large flat head of bull and ram sperm. However, it is still larger than, for example, *E. coli*, for which it has been demonstrated that the ellipsoidal shape modifies the light scattering spectrum even when no internal motions exist and generates departures from kt scaling at scattering angles $>5^{\circ}$. (Refer fig. 1-26). For bull spermatozoa one can only believe that the effects would be even greater due to the lack of axial symmetery and the larger dimensions.

(3) No significance has been attached to the absolute concentration of spermatozoa in the light scattering samples. This is surprising in view of the well known cooperative swimming effects which spermatozoa exhibit and which are later discussed in section 2.7. Interaction between swimmers could conceivably introduce additional components into the light scattering spectrum, perhaps by modifying the distribution of translation vectors.

(4) One very basic aspect of any measurement technique has received no mention, namely, does the method introduce any

perturbation of the observed system? In this case, does the light field influence the motion of the spermatozoa in view of the extremely high intensities which a focussed laser source is capable of generating? No mention of sample illumination levels is made in the literature although it is well known that spermatozoa have absorption bands in the visible region and show a sensitivity to light (see section 2.9). Most workers,however,appear to have made a concession to the possibility of photosensitivity by using the red 632.8nm He - Ne wavelength.

(5) Little attention has been given to interpreting and quantifying the characteristics of the slow autocorrelation component attributed to the dead cells. The assumption generally appears to have been made that dead cells behave simply as diffusing Brownian scatterers although one group have mentioned settling effects as generating distortions of the associated exponential (Cooke, *et al.*, 1976). Not even simple verifications of the Brownian particle model have been made such as by relating the equivalent *Stoke's radius* of the spermatozoon.

(6) The autocorrelation functions presented in the literature have all used extremely short timescales relative to that of the slow immotile component, (e.g., 7.9 mS for Hallett, *et al.*, 1978 with the largest being 133 mS for Cooke, *et al.*, 1976). This short timescale would appear to make the detailed form of the slow autocorrelation component more difficult to extract. The results of chapters 4 and 5 will demonstrate that useful information may be extracted from the amplitude and shape of this slow component which requires

measurements over a timescale of typically 0 - 1s to adequately define it at typical scattering angles ($\sim 10^{\circ}$).

In conclusion, while the literature dealing with light scattering measurements of spermatozoan motility has been found remarkably deficient and inexplicit in many respects, it has, however, convincingly demonstrated that motility can be rapidly and objectively characterised by light scattering methods. The development of the technique has clearly been impeded by a complete lack of alternative methods having a similar level of objectivity and rapidly of measurement, against which the light scattering measurements could be compared.

1.5.2 Contemporary studies using a more detailed scattering model for bull spermatozoa.

Craig, Hallett and Nickel (1979) in a recent comprehensive and detailed paper, closely examined the light scattering model for bull spermatozoa. From a computer modelling study in which the sperm head was considered as a Rayleigh-Gans ellipsoid, it was concluded that the electric field autocorrelation function for motile cells, was generated not by their translational motion but by axial rotation of the head. Their calculations were compared with experimental autocorrelation functions previously published by the same group (Hallett, *et al.*, 1978) which, at the time, had been otherwise interpreted, (table 1-4). Again, however, validation of the results from the Rayleigh-Gans model calculations rested largely with fits to the form of the experimentally obtained autocorrelation functions, no new independent experimental data being presented. This work pointed to the primary significance of the head rotation rate in generating the fast autocorrelation function and explained the absence of periodicities in the experimentally obtained functions by assuming a distribution $P_{(w)}$ of rotation frequencies in the population given by:

$$P_{(w)} = \frac{4w}{\bar{w}^2} \exp(-2w/\bar{w}) \qquad (1.44)$$

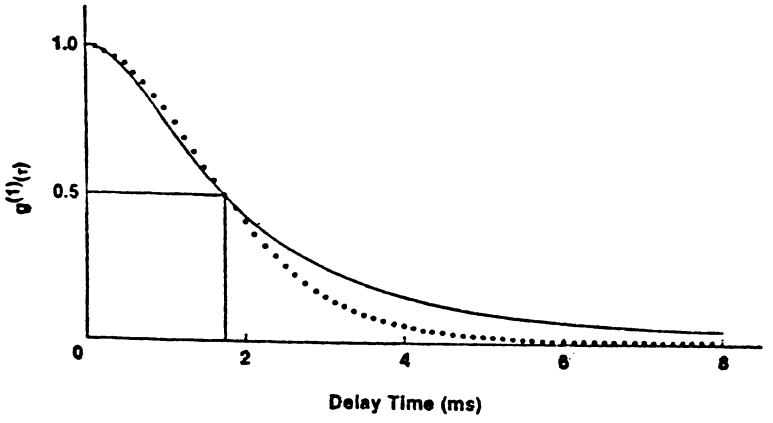

Fig. 1-23. A Lorentzian representing the experimentally obtained field autocorrelation function (solid line), together with a function computed on the basis of an ellipsoidal Rayleigh-Gans model (plotted points) using normal distributions for the swimming speeds and rotation frequencies (ellipsoidal semi-axes 0.5μm, 2.3μm, 8.3μm). The mean rotation frequency was 10Hz. (Craig, *et al.*, 1979).

Typical results from this work are shown in fig. 1-23 and the function was found to be unaffected by the mean swimming speed of the cells, a result which is clearly in conflict with the preceding literature.

This study has been separately considered in this literature review since it represents a significant contribution to the field of light scattering from spermatozoa and one which shows a radically different approach from previous work. The studies of Craig, *et al.*, (1979) independently arrived at one of the conclusions presented in both chapter 5 of this thesis and in an associated publication by Harvey and Woolford (1980). The two research programmes, however, arrived at their respective conclusions quite independently and in fact details of

the work by Craig, *et al.*, only became available following submission of the papers contained in Appendices II and III.

However, small differences in interpretation do exist between the work reported here and that of Craig, *et al.*, (1979) and these are further discussed in the conclusions of chapter 5.

CHAPTER 2

CHARACTERISTICS OF BULL SPERMATOZOA RELEVANT TO LIGHT SCATTERING.

"Wherever possible, logical constructions are to be substituted for inferred entities."

..... Bertrand Russell.

2.0 Introductory Remarks

Spermatozoa throughout the diverse range of animal and plant species vary enormously in shape, dimensions and functional characteristics. Rothschild (1962), whose early writings on the subject show a deep fascination with spermatozoan function, presented drawings of conformation for fifty-five species which illustrate this diversity. Some of these are reproduced here in fig. 2-1. The principal common feature is that they are all self-motile under the propulsive action of an active appendage termed the flagellum. The general application of laser light scattering to studying the dynamics of spermatozoa, is therefore a very broad one and techniques are highly likely to be species specific. Not only does the head shape vary in geometry and size but the structure, size and action of the flagellum varies widely. Flagellar lengths range from perhaps 4-5μm for small examples (e.g.,*Ciona intestinalis* and *Branchiostoma Ian ceolatum*) to several hundred microns for the larger specimens. In general, the length of the flagellum far excedes any linear dimension of the head but it is generally of very much smaller cross-section. The head, which is often elongated and not well defined, carries the genetic material and in many cases is known to generate the cell wall penetration necessary for fertilisation. Spermatozoa may be broadly categorised as being primitive or mammalian depending on whether fertilisation occurs, external or internal, to the female body. In general, mammalian spermatozoa have a larger head and an extended linear region posterior to it, referred to as the *mid-piece* and around which is located a mitochondrial sheath.

The question of geometry and dimensions of sperm cells assumes great importance in the context of the light scattering studies described in this thesis and in the generalisation of the techniques to other species. Previously reported light scattering studies of spermatozoa motility have frequently taken little account of even the general structure and

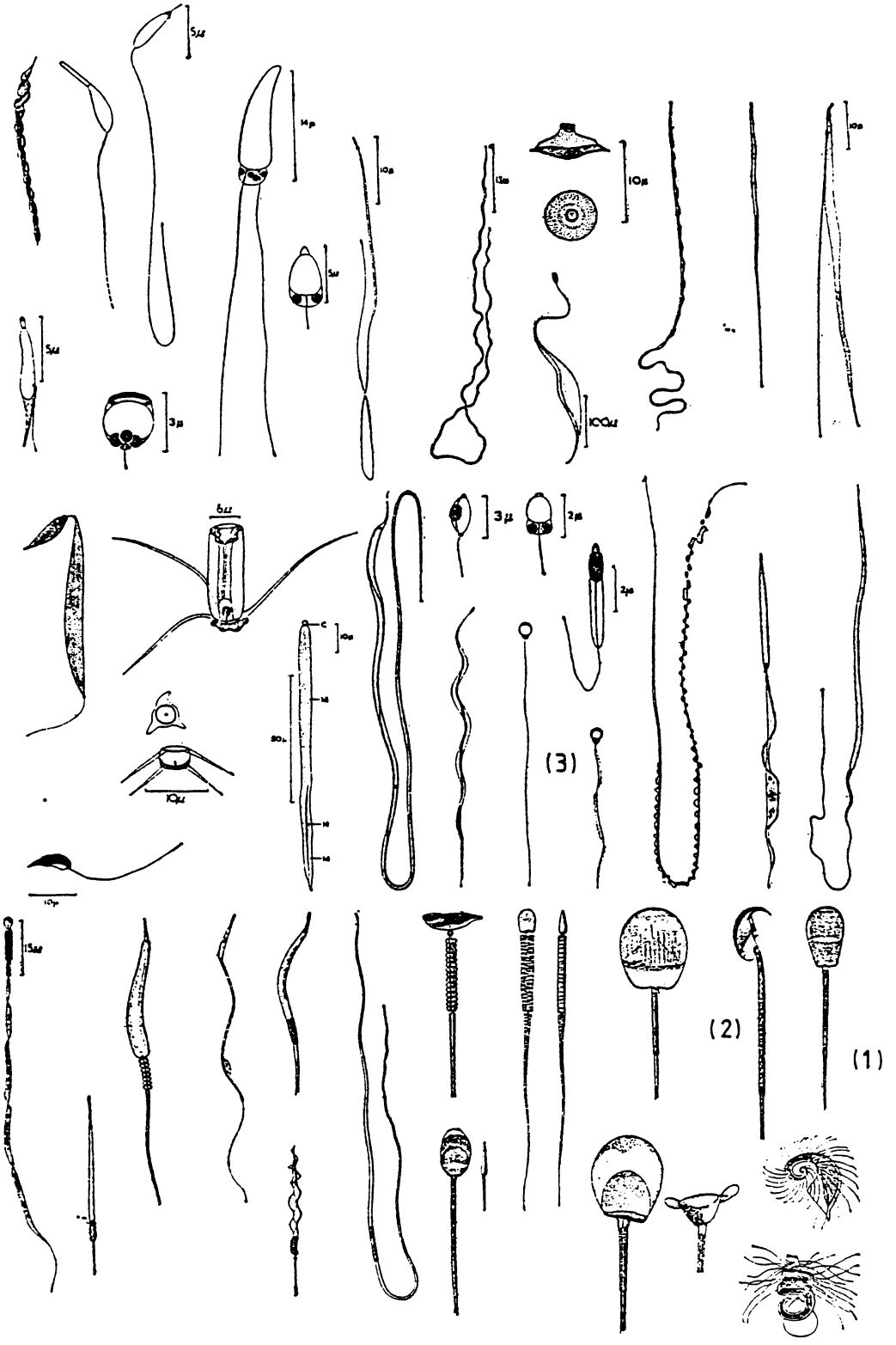

Fig. 2-1. Drawings of spermatozoa from a range of animal and plant species which illustrate the enormous variation in conformation and dimensions. The full extent of the flagellar length in some cases is not shown. Cells of relevance to these studies are:
1. bovine. 2. mouse. 3. fish.
(Rothschild, 1962).

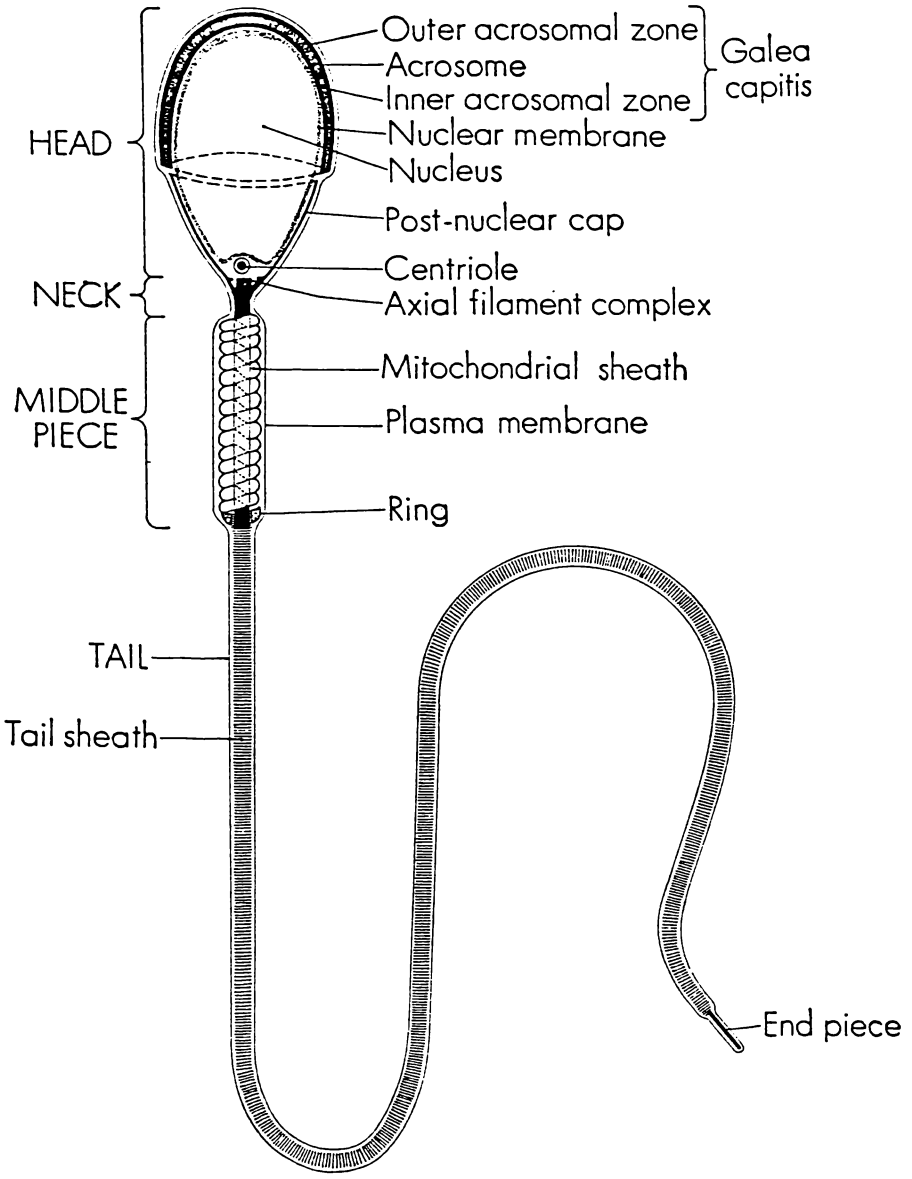

Fig. 2-2. The morphological components of the bovine spermatozoon. Note the extended nuclear mass and the thickened mid-piece region. Mann (1964).

dimensions of the cells. Recognising the significance of the geometric and structural detail for light scattering, this chapter will also be concerned with discussing other features of spermatozoa, swimming motions, morphology, photosensitivity and other characteristics which may also be relevant to such scattering. However, consideration will be restricted to those species of immediate practical interest, generally, bull, ram and human cells.

2.1 Morphology

The principal morphological features of the bull spermatozoa are illustrated in fig. 2-2 (Mann, 1964). The head, dimensions for which are discussed in section 2.4, contains a nucleus within a double layered membrane (Saacke and Almquist, 1964) which comprises closely packed chromatin (largely deoxyribonucleoprotein). In mature ejaculated cells the internal distribution of chromatin has been observed microscopically at high power to be highly homogenous (Szollosi and Ris, 1961; Hancock, 1966).

A cap-like structure known as the *Galea capitis* has been observed to cover the front half of the head, and containing the acrosome, it is sometimes referred to as the 'acrosomal cap'. The function and structure of this feature, other than its primary involvement in the egg penetration phenomenon, are not well understood.

Optical photomicrographs by Hancock (1952) are shown in figs. 2-3 and 2-4. The white light photographs of fig. 2-3 show that a marked delineation of the equatorial boundary of the acrosomal cap occurs in cells which were morphologically dead prior to staining. The posterior boundary of the cap is clearly evident in the photographs of fig. 2-3b, d and e. In the case of fig. 2-3e, complete detachment of the cap has occurred in the case of one head and there is evidence of partial detachment in other cases.

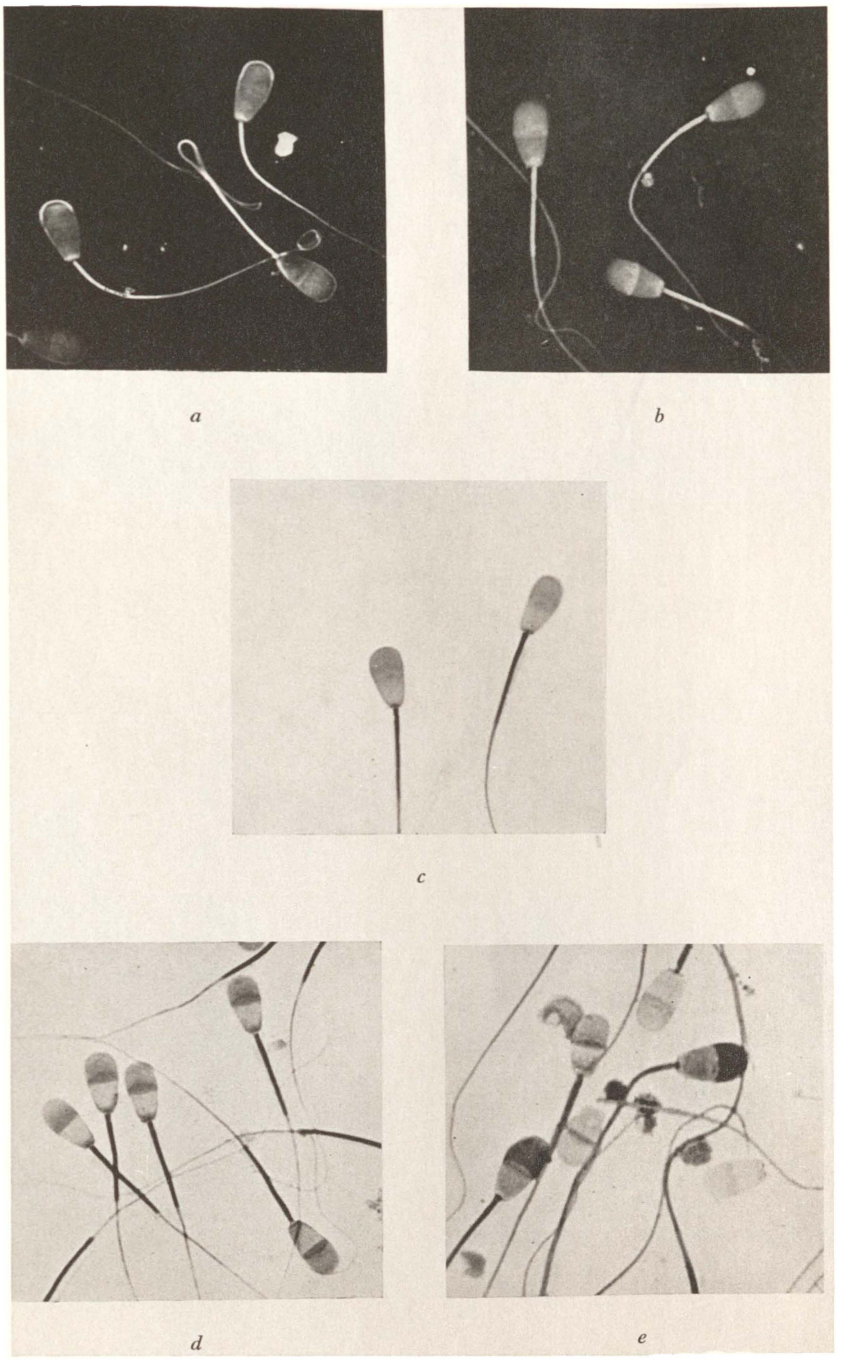

Fig. 2-3. Living and dead bull spermatozoa, after treatment with various stains. (Hancock, 1952).

(a) Live cells } Eosin - Nigrosin
(b) Dead cells } stain
(c) Live cells } Iron hemotoxylin
(d) Dead cells } stain
(e) Dead cells Giemsa stain: showing detachment of the acrosomal cap.

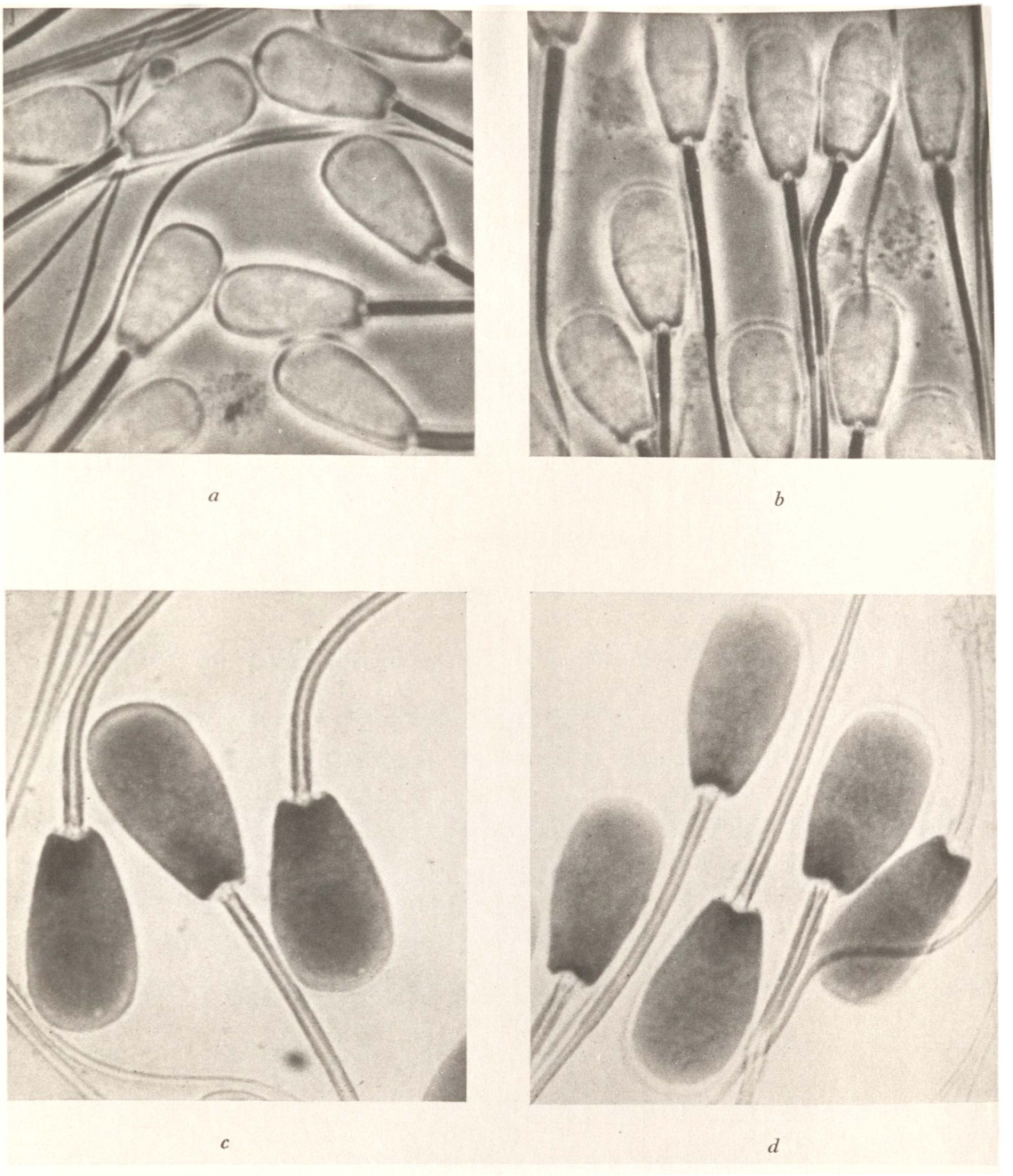

Fig. 2-4. Photomicrographs of bull spermatozoa illuminated from below with ultraviolet light, both with and without phase contrast optics. (Hancock, 1952).

(a) Living } cells Negative phase contrast λ = 275nm
(b) Dead magnification X 2350.

(c) Living } cells magnification X 3000, λ = 275nm.
(d) Dead

A shedded acrosomal shell is clearly evident. These photographs alone, suggest that the light scattering properties of the sperm head may differ between live and dead cells and that much of the scattering may occur, at least for dead cells, in the cell wall and cap.

Also of interest are observations of changes in the light reflection and/or refraction properties of the head surface when viewed with dark field illumination (Lindahl, *et al.*, 1952). These changes were thought to be associated with the degree of hydration of the lipid capsule surrounding the head and showed some correlation with sperm maturity. An increase in the relative density of the sperm with ripening was considered to indicate a loss of water and an associated increase in the relative hydration of the superficial layers. This is possibly evident in the photographs of Hancock, fig. 2-3a, which shows a bright halo around the acrosomal cap of live (prior to staining) cells, perhaps indicative of refractile characteristics of the hydrated layer. The effect is not apparent for dead cells.

Further photomicrographs, but taken with ultra-violet (λ = 275nm) illumination, are shown in fig. 2-4 for both direct and phase-contrast optics. The images suggest that significant scattering and/or absorption takes place in the bulk of the head at this wavelength.

Profound structural differences between live and dead cells are also apparent in the electron-micrographs (Hancock, 1952) of fig. 2-5. The head of the live cell shows a much more clearly delineated surface, while the surface of the dead cell appears irregular and diffuse.

Posterior to the head is a short thick segment, the middle-piece, and this encloses axial fibres which extend back through the flagellum. The mid-piece is characterised by the presence of a mitochondrial helix of two or three strands (Hodge, 1949 ; Wu and Newstead, 1963) and perhaps 100 turns, which surround the axial fibres. The mitochondria have been identified as the principal site of the cell's respiratory and oxidative

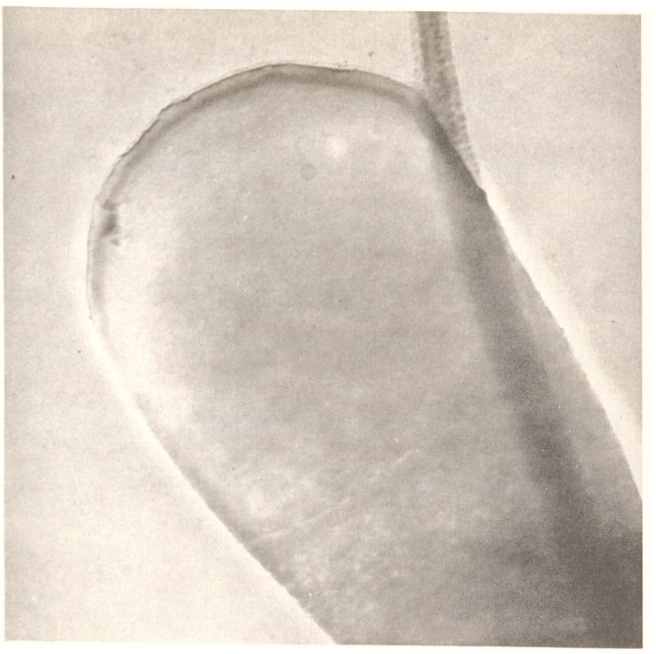

a

b

Fig. 2-5. Electron micrographs (magnification X 16000) (using gold-palladium) for bull spermatozoa, (a) live and (b) dead cells, showing the structural differences in the acrosomal cap which is much less prominent in dead cells.

(Hancock, 1952).

processes. Microscopically it is often difficult with bull spermatozoa to differentiate the mid-piece from the flagellum since it appears as a thickened proximal end to the flagellum, although significant and distinctive variations in the geometry of the mitochondrial sheath do occur between species.

The mid-piece, apart from its geometry and dimensions (which were taken into account in the scattering computations of Craig, *et al.*, 1979) is potentially relevant to light scattering not only from a dimensional viewpoint, but also because it appears to be the site of photochemical processes. Microspectrophotometry has been used to demonstrate the location of cytochromes or respiratory pigments in the sperm cell of the grasshopper *(nebenkern)*. Perry, Thorell, Akerman and Chance (1960) showed cytochromes to be concentrated in the cytoplasm of the mitochondrial region. Absorption bands corresponding to both oxidised and reduced cytochromes were detected and the total cytochrome concentration was determined to be about $\sim$ 50 x higher than in any other part of the cell. Absorption peaks were observed in the near ultraviolet ($\sim$ 330nm) and in the visible blue region (420 - 440nm) although the magnitude of the absorption was very small ($\sim 5 \times 10^{-3}$). No measurable absorption bands were observed in the cytoplasm or nucleus. Similar work for bull spermatozoa does not appear to have been reported. In this context, several studies have however shown that bull spermatozoa are sensitive to light and these are to be discussed in more detail in section 2.9. Such photosensitivity may be due to increased oxidative processes and the site of such reactions is likely to be located in the mitochondrial region.

The flagellum of all spermatozoa species has been the subject of considerable morphological interest for many years. This interest has centred around the tail structure, the internal structure of which is common not only across species but also between flagella and cilia. The biophysics whereby it generates bending and wave motions have been the

subject of an extensive literature, reviewed for example by Holwill (1966). The bending is accomplished by a particular type of filament structure known as the axoneme. The geometrical arrangement of the active elements within the axoneme referred to as microtubules, is unique across species. It comprises a symmetric geometrical array of 9 interconnected doublet microtubules surrounding and joined by cross-bridges to 2 centrally located microtubules. Detail of the structure and mechanisms involved has been the subject of an extensive literature which is outside the context of this discussion. Fig. 2-6 shows a cross-sectional view of the structures involved and considerable detail is given by Warner (1973).

In terms of their light scattering characteristics, flagella can probably be considered as long but extremely thin ($\lesssim$ 0.5μm) scatterers (Bishop, 1962).

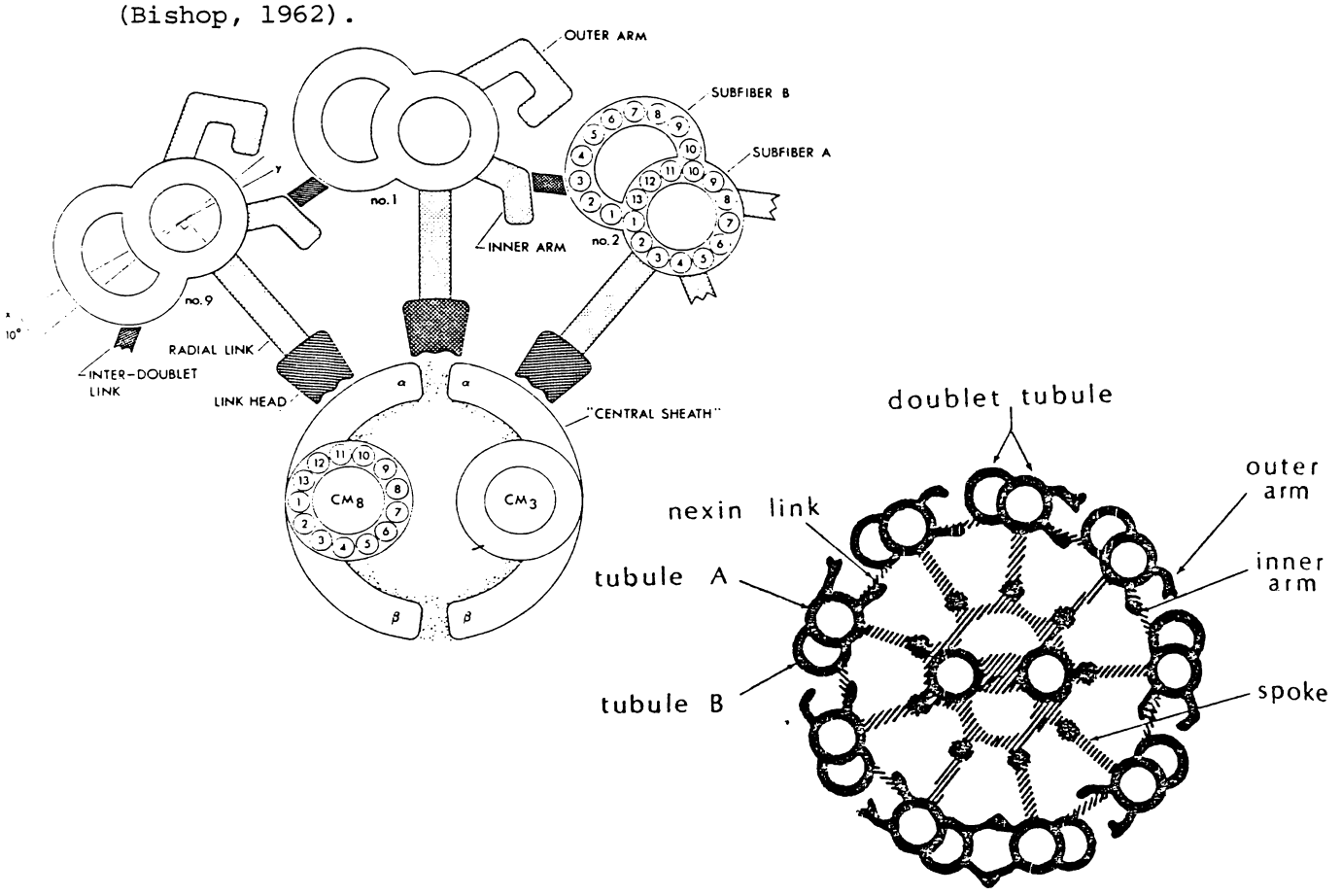

Fig. 2-6. A cross-sectional diagram showing the general structure of a so-called 9 + 2 axoneme (Warner, 1973); Brokaw, 1975)

2.2 Abnormal Conformations

Bull spermatozoa from the same ejaculate show a distribution of dimensions and shapes. In addition, pathological variations occur and a variable percentage of abnormal forms are observed. In some circumstances for bull spermatozoa, this percentage is sufficiently large to warrant rejection of the service for commercial artificial breeding purposes (Shannon, 1980).

Every conceivable deviation from the normal cell structure may be observed. Tapering cells, two-headed cells, multiple tails, giant cells, and multiple nucleii are perhaps the most commonly observed grossly pathological forms (Mann, 1964).

Campbell, Hancock and Shaw (1960) categorised bull spermatozoa into nine morphological classes and looked at the frequency of abnormal forms in 257 ejaculates from twelve Hereford and Friesian bulls. These classes defined by Campbell, *et al.*, are listed in table 2-1 with the corresponding frequencies of occurrence, and give a perspective of the incidence of abnormal cells.

Type of Abnormality	Percent Occurrence (%)	Correlation with % dead within bulls	Correlation of occurrence with conception rate
Malformed heads	1.4	N.S.	0.179^{*} (1)
Tailless heads	3.6	0.354^{***}	0.186^{*} (1)
Fractured necks	0.1	N.S.	N.S.
Malformed mid-pieces	1.2	N.S.	N.S.
Headless tails	2.4	0.314^{***}	N.S.
Bent tails	2.8	N.S.	N.S.
Coiled tails	0.5	0.166^{*}	N.S.
Neck beads	0.3	-0.209^{*}	-0.576^{*} (2)
Mid-piece beads	6.2	-0.227^{**}	N.S.
All abnormalities	18.5		

Table 2-1. Occurrence frequencies for various bull sperm abnormalities and correlations with percent dead cells and conception rates. (Campbell, *et al.*, 1960).
(1) - within bulls
(2) - between bulls (*, **, *** $P < 0.05, 0.01, 0.001$, respectively.)

In terms of light scattering experiments, the significance of these and other abnormal forms, lies in their frequency of occurrence and in the modifications of swimming motions or (in the case of dead cells) orientational dynamics which they may produce in the population. Often for example, morphological abnormalities may affect the symmetry of the flagellar beat and result in circular swimming motions. Headless tails and tailless heads, two of the most common pathological forms, are generally associated with dead cells.

Abnormal spermatozoa in ejaculates from high quality bulls are generally at an insignificant level (Shannon, 1980).

2.3 Ejaculate characteristics

At ejaculation, sperm in most species are mixed at very high concentration with a natural buffer - extender medium generated within the male, the seminal plasma. The volume and concentration of sperm within the ejaculate often vary widely.

Most reported LBS studies of motility have involved a dilution of the raw semen (refer table 1-4) and therefore data on the sperm concentration of the basic ejaculate are of considerable relevance.

Table 2-2 compares the observed ranges for ejaculate concentration and volume in three species of interest.

Species	Bull	Ram	Human
Volume (ml)	2 - 10	0.7 - 2	2 - 6
Concentration (10^9 sperm/ml)	0.3 - 2	2 - 5	0.05 - 0.15
Most frequent concentration (10^9 sperm/ml)	1.0	3.0	0.1

Table 2-2. Ejaculate volume and concentration for bull, ram and human semen. (Mann, 1964).

In practice, even among proven bulls of high fertility, semen can vary widely in both concentration and the content of dead cells. Table 2-3 shows more specifically typical ejaculate characteristics for proven bulls used in commercial artificial breeding service at the New Zealand Dairy Board's Newstead centre. These data were taken from records for the November 1979 period and are typical of the properties of the basic ejaculates used in preparation of samples for the LBS studies studies of chapters 4, 5.

	Mean Value	Standard Deviation	Overall Range	# of ejaculates
Concentration (10^9 sperm/ml)	1.64	0.43	0.66 - 2.82	80
Volume (ml)	5.05	1.74	1.25 - 9.25	78
Percent Live † (%)	84.0	6.9	70 - 97	38

Table 2-3. Ejaculate characteristics for highly selected bulls used for commercial artificial insemination service.
(by courtesy of New Zealand Dairy Board, Artificial Breeding Research Centre, Newstead).
† percentage of sperm eosinophobic immediately post-ejaculation (refer section 3.2).

The significant points regarding this data are:

(i) Samples of spermatozoa prepared by using a fixed dilution of the raw semen, will give a final sperm concentration which varies widely even for high performance bulls.

(ii) The normally high percentage of live cells which has implications for sample preparation where a known percentage of dead cells is required.

2.4 Dimensions

The geometry and dimensions of the bull spermatozoon will become

central to the theme of later discussions and some consideration of the available data on the topic is required.

Measurement of size for sperm cells is microscopically difficult since the dimensions are at the resolution limit of the optical microscope. Consideration must also be given to any fixing or preparation procedures since these may modify the dimensions *in vitro*.

Mukherjee and Dott (1960) using optical microscopy, measured the length and breadth of sperm heads (for five different bulls) both before and after preservation in two commonly used extenders egg-yolk-citrate (EYC), and egg-yolk-glycine (EYG). Over the five bulls, sperm head length was 9.27 $\pm$ 0.03 (SE)μm with a range of $\pm$ 0.31μm. Breadth of the head was 4.97 $\pm$ 0.02 (SE)μm with a range of $\pm$ 0.31μm. Significant variations occurred between bulls in terms of both head length and breadth. Further, variations in size occurred between different ejaculates from the same bull and a small decrease in dimensions ($\sim$ 1.1% in length and 3.9% in breadth) was observed after preservation for 72 hours in EYG but not after storage in EYC. Clearly the dimensional changes *in vitro* are small and probably of little importance in a light scattering context.

Veres (1964) reported electron-microscope measurements of sperm head dimensions and gave an electron densitogram of the sperm head. Dimensional characterisation of morphologically normal and abnormal sperm was discussed since abnormal forms were said to exhibit a marked axial asymmetry as illustrated in fig. 2-7. These data indicate a thickness at the midpoint of 1.1μm with a bi-convex cross-section.

The standard deviation of sperm head size for ejaculates from the same bull was $\pm$ 10% while between bulls it is given as $\pm$ 15%. The electron-density data, however, indicated a flat contour for the head surfaces. This was also supported by the observations of de la Torre and Salisbury (1964), also using electron microscopy, who concluded

that the nuclear mass (which substantially fills the entire head volume) was flat.

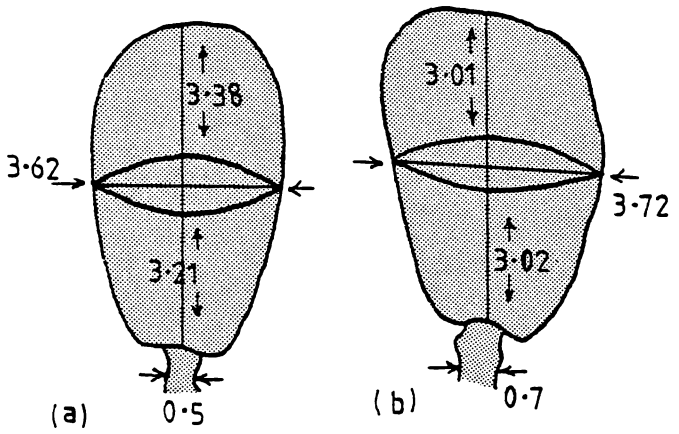

Fig. 2-7. Conformation of morphologically normal (a) and abnormal bull spermatozoa from electron microscopy. (Veres, 1964).

Nuclear size may well be the dimensional parameter of greatest significance to light scattering if scattering occurs principally from its closely packed mass of macromolecules of DNA size.

One of the techniques which has been used to measure nuclear size, is that of staining the DNA with Feulgen, the dimensions of the stained region being measured with an ocular micrometer or on a projected image. Baker and Salisbury (1963) used this method and determined the nuclear dimensions as 8.53 m $\pm$ 0.5µm in length, 3.98 $\pm$ 0.32µm in breadth, with increases of 4.7% and 5.3% respectively for dead (eosinophillic) cells. These dimensions indicate that the nuclear mass fills the majority of the head volume. The thickness of the nucleus over the head plane has also been studied using Feulgen - DNA staining with cytophotometric methods to map the optical transmission (Salisbury and van Dongen, 1965). However, as is pointed out by van Duijn and van Voorst (1971), Feulgen and other staining techniques change the dimensions and their ratios,

and planimetric methods are susceptible to optical errors.

Detailed quantitative electron microscopy was employed by Bahr and Zeitler (1964) to study dimensions, and their results are summarised in table 2-4.

Head	Length	8.83µm	± 0.25µm
	Area	31.3 µm	± 1.4 µm
Middle-piece	Length	11.0 µm	± 0.3 µm
	Width	0.63µm	± 0.02µm
Flagellum	Length	53.4 µm	± 1.2 µm

Table 2-4. Dimensional data from electron-microscopy. (Bahr and Zeitler, 1964).

Probably the most accurate and comprehensive dimensional data for bull spermatozoa are those of van Duijn and van Voorst (1971) who employed an optical image-splitting microscope having a resolution of ∿ 0.02µm. Mean values from their comprehensive measurements which gave useful dimensional distributions, are listed in table 2-5.

A transverse section given by van Duijn and van Voorst, based on their measurements, is shown in fig. 2-8 having sections of the head middle piece and tail superimposed for comparative purposes.

	Mean	S.D.(%)	Range between bulls (%)
Head length	9.09μm	4.21	3.91 - 4.45
Maximum breadth	4.66μm	6.09	5.17 - 6.79
Head thickness	1.03μm*	0.48%	-
Base width	2.10μm	12.93	9.41 - 14.30
Projected head area	34.2 μm^2	6.85	5.7 - 8.70
Head volume	32.7 μm^3	9.55	7.09 - 12.59

Table 2-5. Physical dimensions of sperm heads from image-splitting microscopy (van Duijn and van Voorst, 1971).

* by interference microscopy.

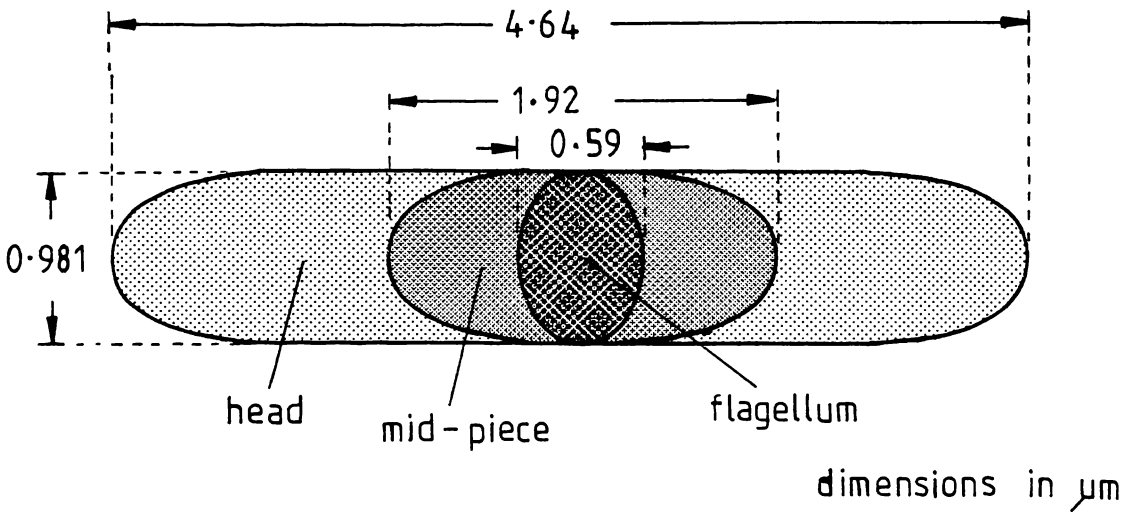

Fig. 2-8. Transverse sections of the principal components of a bull spermatozoon as determined by van Duijn and van Voorst (1971).

2.5 Physical and Optical Characteristics

Brief consideration is now given to various other properties of the spermatozoon which bear relevance to light scattering studies.

2.5.1 Refractive Index (n)

Van Duijn and van Voorst (1971) used an interference microscope to determine the refractive index of the sperm head. This instrument measured the change in phase-shift of light passing through the head, when immersed in two media of slightly differing refractive index.

At λ = 546nm the refractive index of the head was determined to be n = 1.42 $\pm$ 0.01 by interferometry and 1.416 $\pm$ 0.002 using immersion refractometry.

Wyatt (1968) however, had found that for bacteria the refractive index in the interior of the cell was $\sim$ 1.5 and increased to $\sim$ 1.7 at the cell wall. The optical characteristics for sperm heads are probably however, quite different, since the sperm head contains a homogeneous distribution of genetic material having high molecular weight.

The value of n for fixed and dried specimens of spermatozoa, increased to 1.548 $\pm$ 0.005 and was associated with a decrease in head thickness to 0.72 $\pm$ 0.01μm, suggested to be due to water loss. No change in refractive index occurred after 24 hours storage in an egg-yolk-citrate medium at 2°c.

This refractive index data is highly important to the validity of the Rayleigh-Gans approximation for sperm heads (see section 1.1.5) and will be further discussed in chapter 5. The Rayleigh-Gans criteria requires a refractive increment $|n - n_o| << 1$ and characteristic particle dimensions $\ell << \lambda/(4\pi[n - n_o])$. Using the data of van Duijn and van Voorst (1971) values of these criteria for sperm heads (n = 1.416) in a medium of refractive index 1.348 (citrate and egg-yolk based mediums) were determined as being $|n - n_o|$ = 0.068 and $\lambda/(4\pi[n - n_o])$ = 0.74μm (at λ = 632.8nm) respectively. The second criterion is not even approached

by either of the two major linear dimensions of the sperm head, although the Rayleigh-Gans approximation has been usefully employed to model scattering from bacteria (Wyatt, 1968).

2.5.2 Birefringence

Commoner (1949) discussed birefringence induced by cellular nucleic acids and van Duijn and van Voorst (1971) found sperm heads to be negatively birefringent to a small extent. Depolarisation has recently been reported in plane polarised laser light scattered from spermatozoa (Schimizu and Matsumoto, 1980) although at small scattering angles the depolarisation was only $\sim$ 3.3% and may well have resulted from the large cell dimensions (ref. sect. 1.1.4).

2.5.3 Light Reflection, Refraction and Absorption

Lindahl, Kihlström and Ström (1952) studied changes in what was termed light reflection from bull spermatozoa at varying stages of cell maturity. This amounted to measuring the light transmission through a suspension of cells as a function of concentration.

The reflected light intensity was measured using a 'modified' nephelometer (details not given) and was expressed relative to the concentration by measuring the extinction (at λ = 660nm) with a Klett electrocolorimeter. Experimental detail was sparse but it appeared that the reflected light intensity under standardised conditions showed a standard deviation of $\pm$ 10% between samples with extremes of $\pm$ 20%, the implication being that sperm samples vary significantly in their light reflecting characteristics.

Blokhuis (1961) reported that when the head plane of a spermatozoon swimming with a trajectory in the horizontal plane, is near parallel alignment with the vertical (and is viewed microscopically from above), the upper edge appears optically bright. He attributed this to light being conducted through the head via internal reflections. This

interpretation seems unlikely to be correct in view of the earlier observations of Gray (1958) which are subsequently discussed in section 2.6 and illustrated in fig. 2-11. The bright edge referred to by Blokhuis, which is clearly the same phenomenon as is shown in fig. 2-11, is much more likely to have resulted from specular reflection at the plane surfaces of the head, the angles of incidence and reflection (w.r.t. the normal) being close to 90° due to the small subtended angle of the microscopic illumination.

2.5.4 Specific gravity

The specific gravity of the spermatozoon is of relevance to sedimentation effects in light scattering experiments later to be discussed in chapter 5 and several workers have published measurements which are of interest. Van Duijn and van Voorst (1971) determined the solids content of the sperm head to be 47 - 55% depending on environmental conditions and this infers therefore, that the specific gravity probably depends strongly on the degree of hydration.

Lindahl and Kihlström (1952) measured the specific gravity distribution for spermatozoa from normally fertile bulls and related the measurements to the proportions of unripe, ripe and over-ripe cells present in the ejaculates. The technique involved centrifuging the cells in media of various specific gravities which were selected so as not to modify the volume of the cell, (e.g., umbradil-methylglucamine-salt solutions). Unripe cells had a significantly lower specific gravity than either ripe cells or over-ripe (normally non-motile) cells, and it appeared that the process of ripening was associated with a continuous rise in specific gravity. These were measurements on whole sperm cells and gave a distribution of specific gravities which peaked at 1.288 for a first ejaculate.

Later work by Lindahl and Thunqvist (1965) is of even greater

interest in that the specific gravities of the major components of the spermatozoon were measured. Bull spermatozoa were fragmented ultrasonically to yield isolated heads, mid-pieces (both with and without tails), and isolated tails. The specific gravities of these individual fractions were then determined using a 'Ficoll' density gradient and analysing the distribution of the various components along the gradient following centrifugation.

	Specific Gravity Range
Unfragmented	1.21 - 1.33
Mid-pieces with tails	1.04 - 1.07
Heads	1.25 - 1.35

Table 2-6. Specific gravity ranges for major physical components of bull spermatozoa (Lindahl and Thunqvist, 1965).

Data from Lindahl and Thunqvist (1965) are presented in table 2-6 and show the head as being of much higher specific gravity than either the mid-piece or the flagellum. The specific gravities for heads are relatively high and suggest that rapid sedimentation, probably with a head-down attitude, is likely to occur for dead cells, in media of lower specific gravity.

However, the results of Lindahl and Thunqvist (1965) are in disagreement with those of Lavon, Volcani, Amir and Danon (1966) who used two-phase centrifugation (Dannon and Marikovsky, 1964) and determined a density of 1.076 $\pm$ 0.003 for first ejaculate unfragmented bull spermatozoa.

These results will form a useful background to light scattering studies discussed in chapter 4 where it becomes apparent that sedimentation effects are involved.

2.5.5 Mass distribution

Bahr and Zeitler (1964) using electron microscopy, plotted the mass per unit length in a longitudinal scan over the length of a bull spermatozoon and the resultant mass distribution is shown in fig. 2-9 along with quantitative estimates of the mass distribution in table 2-5.

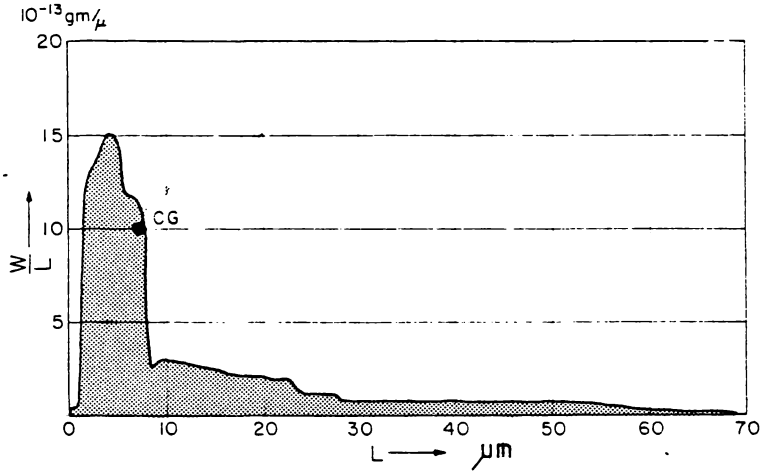

Fig. 2-9. Mass distribution along a longitudinal scan of a bull spermatozoon using electron microscopy. (Bahr and Zeitler, 1964).

The centre of mass appears to be located (CG) approximately 90% of the head length back along the major axis.

	Sperm	Head	Mid-piece	Flagellum
Percent of total mass	100	63.7	17.3	36.3

Table 2-5. Distribution of mass between the major components of the spermatozoon (Bahr and Zeitler, 1964).

2.6 Swimming Motions

The internal motion of the spermatozoon during swimming, and the trajectory that the cell follows, are of fundamental significance to light scattering experiments. A brief review of reported observations

and measurements of sperm motion, will therefore give a useful perspective of phenomena to be expected in such experiments.

The forward progression of a spermatozoon is generated by the propagation of waves or bending couples which originate at the mid-piece and progress distally along the flagellum (Bishop, 1962). Direct visual observations of the resultant head and flagellar motions is uninformative since the speeds and frequencies of the movements are too high. The tail wave frequency for example may be as high as 20 Hz.

The hydrodynamics of the swimming mechanics have been the subject of extensive theoretical analyses and modelling but it is beyond the scope of this section to discuss other than the phenomenology. Taylor (1951), Reynolds (1965) and Brokaw (1975) give detailed treatments of the mechanisms of movement while Nelson (1967) reviews the associated biochemistry and cytology.

Detailed micro-photography carried out by Gray (1958) provides some of the best direct observational evidence to date of the motions of bull spermatozoa. With continuous microscopic dark-field illumination, the swimming spermatozoon was found to appear as a triangular optical envelope which defined the displacement limits of the waving flagellum. Gray used multiple exposure micro-photography on stationary film with 1/80s between exposures, and syncronised flash illumination, to give a remarkable definition of the tail wave motion. These photographs are reproduced in fig. 2-10 for illustrative purposes and use dark-field microscopic optics.

The two spermatozoa in these exposures are not obviously rotating, the head appearing to remain in one plane. The tail wave is more or less sinusoidal with the amplitude increasing distally and the maximum lateral distance across the flagellar wave has been measured as 33μm in these photographs.

In the case of exposures 1-7, no lateral wobble of the head

Fig. 2-10. Multiple-exposure photomicrographs (on stationary film) with dark field flash illumination showing the flagellar and head motions for two bovine spermatozoa. The illuminating flashes are at intervals of 12.5mS, the sequence of exposures #1 → #7 referring to one spermatozoon, and #8 → #14 to the other. (Gray, 1958).

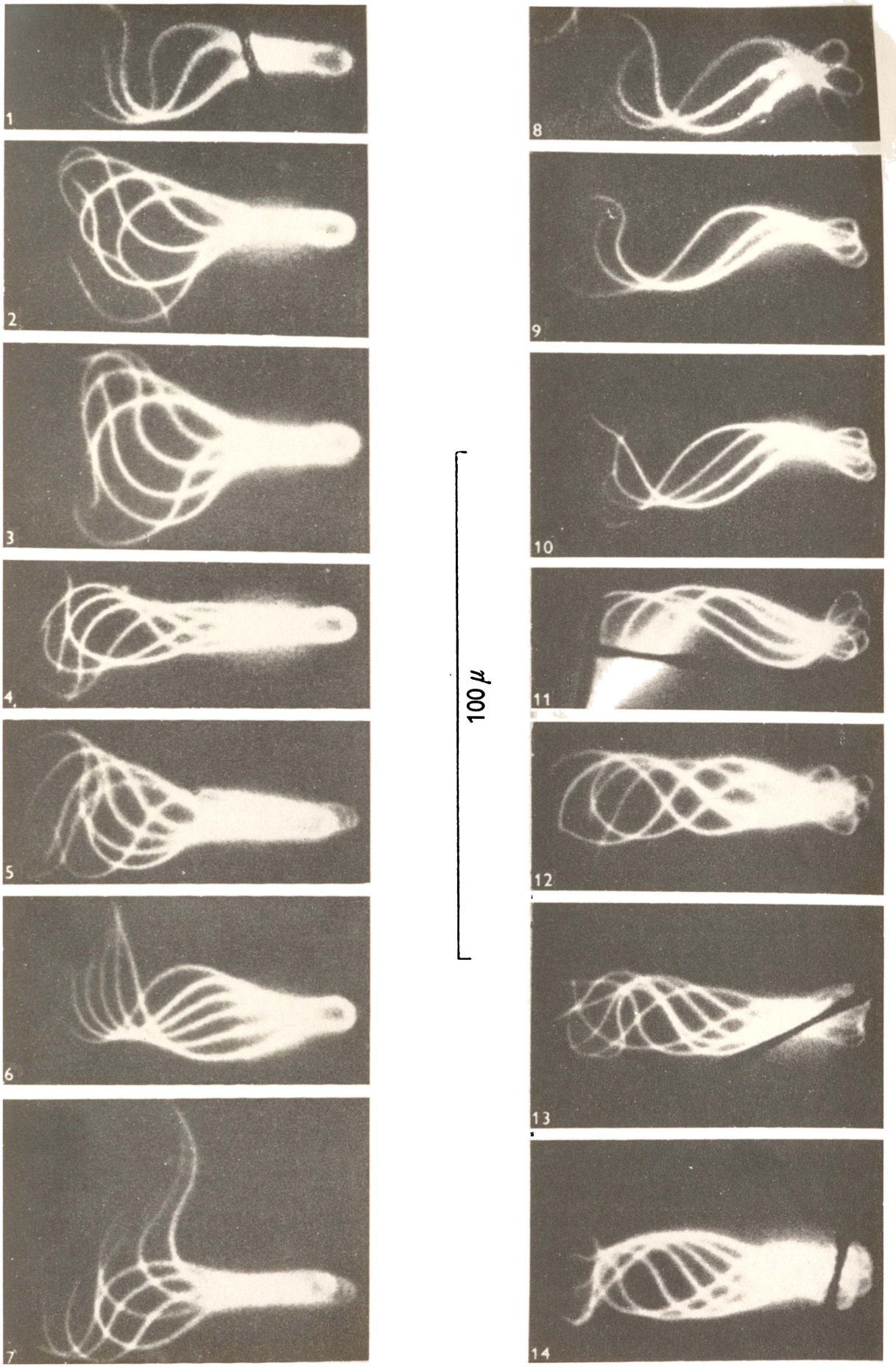

Fig. 2-10.

(transverse to the direction of progression) is apparent and it does not appear to be undergoing axial rotation (i.e., about the translation vector). However, for the cell observed in photographs 8-14, lateral wobble of the head in one plane does definitely take place but again, there is no clear indication of head rotation although each photograph covers a timespan of only $\sim$ 60mS (i.e., 5 exposures) in which time the head would have rotated $\sim$ 180° about its major axis.

According to Gray (1958), the elements of the flagellum execute their transverse movements in a plane which is parallel to the plane of the head and this certainly appears to be the case in fig. 2-10. It is possible that the plane of the flagellar wave in the exposures of fig. 2-10 is in fact rotating as is generally observed to be the case for normal motile cells. In the discussion reported in Rothschild (1953b), Walton commented on his visual observations of bull spermatozoa when their swimming motions had been slowed down in a viscous medium:

> *".....you find that the wave appears to be in two dimensions only. When you're looking at the sperm and you see the flat surface of the head, then you'll see the waves of movement in the tail; but if you're looking at the sperm with the head on edge then the tail will appear straight and motionless. You can see that these two appearances alternate as the head rotates. ....."*

Rothschild (1953b) also drew attention to an optical property of swimming spermatozoa which is of profound significance in the context of this thesis. He observed, as no doubt had others, that motile bull spermatozoa viewed microscopically with dark-field illumination exhibit a characteristic 'flashing' phenomenon. Mann (1964) presented a 1s time exposure photomicrograph from Rothschild's work, showing the trajectory of a single bull spermatozoon in the dark field. The track had a length of 103μm displaying ten bright linear flash segments distributed along

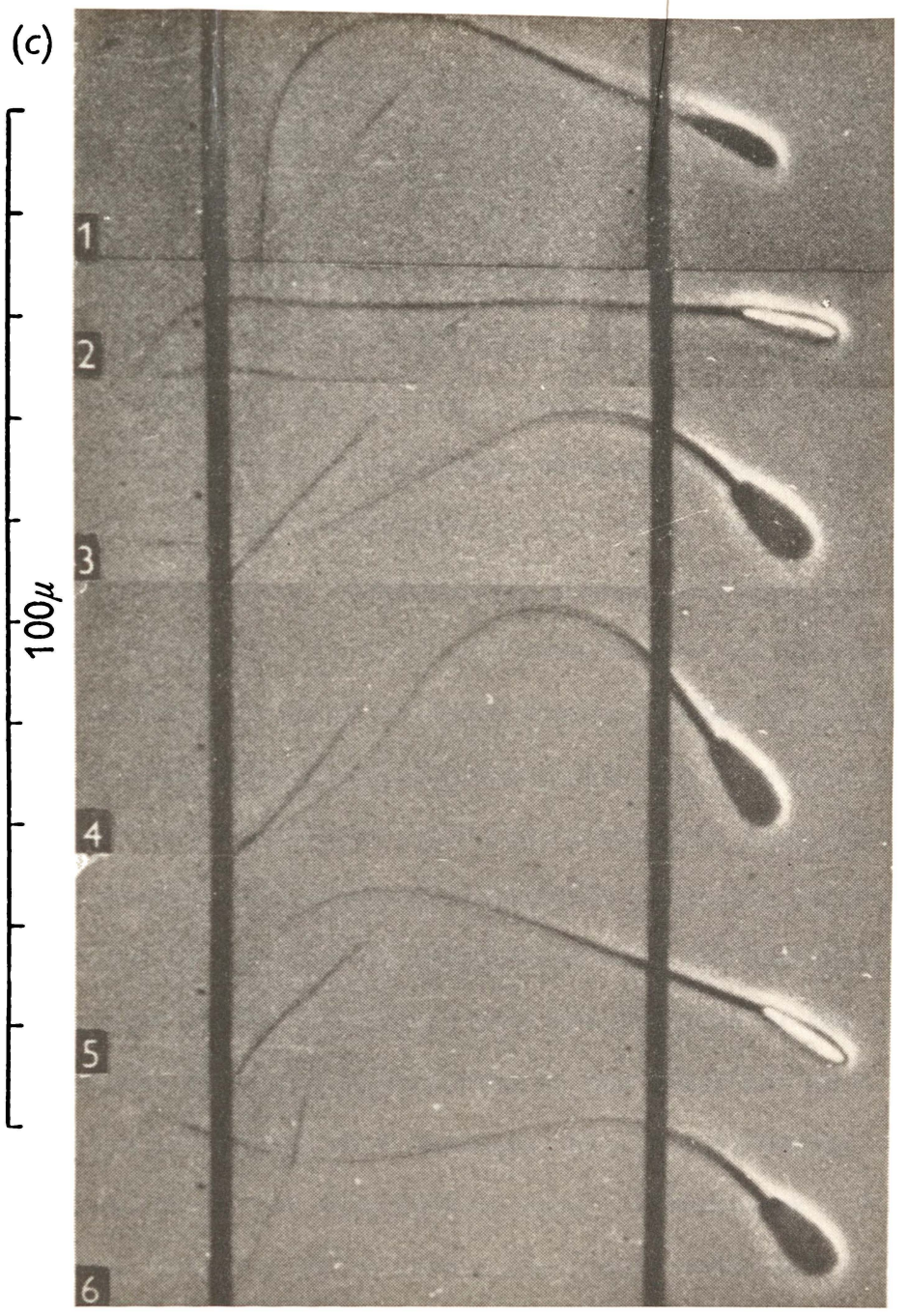

Fig. 2-11. Successive cine-photomicrographs (phase contrast with 3.5mS flash illumination and dark field optics) at 333mS intervals of a swimming bull spermatozoon. These show the characteristic bright flash which is seen when the head is approximately edge-on to the observer. Note also the tail wave amplitude is a maximum when the head appears flat.

(Gray, 1958).

its length. These flashes were attributed to light scattered from the relatively large and flat head when suitably oriented by the internal swimming motions. It was not clear whether the head motion involved a wobbling action or a complete rotation.

Gray (1958) also presented remarkable cinemicrographs (using with dark-field illumination) of a bull spermatozoon while apparently generating the time-exposure tracks observed by Rothschild. These photographic data are reproduced here in fig. 2-11. The two previously discussed phenomena, a predominantly planar tail-wave and the optical 'flashing' effect of the head, are both evident in these photographs. Gray concluded that cells swimming freely flashed at a frequency very similar to, and probably synchronous with, the flagellar waves. Further, Rikmenspoel and van Herpen (1957) had concluded, also from cinemicrographs, that the head, middle-piece and flagellar waves lie approximately in one plane, which is rotating in synchronism with the tail wave frequency. However, Gray (1958) considered that the rotation of the head was entirely a consequence of planar asymmetries in the flagellar wave and in fact presented a photograph of a headless cell, the flagellar wave of which was rolling about the longitudinal axis. Rikmenspoel (1962) subsequently agreed that rotating cells have a non-planar component in the tail wave which was thus supposed to generate the rotary motion. It was further observed that on time exposures the linear flash segment was sometimes aligned along the direction of translation, sometimes oblique to it and sometimes left a more complex herringbone-like pattern.

Movements with other than a closely axial wobble or rotation have not been commonly referred to for bull spermatozoa and there appears no detailed analysis of to what extent the head locus is helical. Certainly other species exhibit grossly off-axial rotations along their swimming trajectories. Phillips (1972) shows motions for various species with superimposed tracings from cinemicrographs for spermatozoa of the rat,

mouse, Chinese hamster, human, rabbit and opposum, all of which show distinctly off-axial movements. These tracings for two human spermatozoa are shown in fig. 2-12 and are interesting to consider in respect of the swimming speed distributions which might be obtained from LBS, (section 1.5.1).

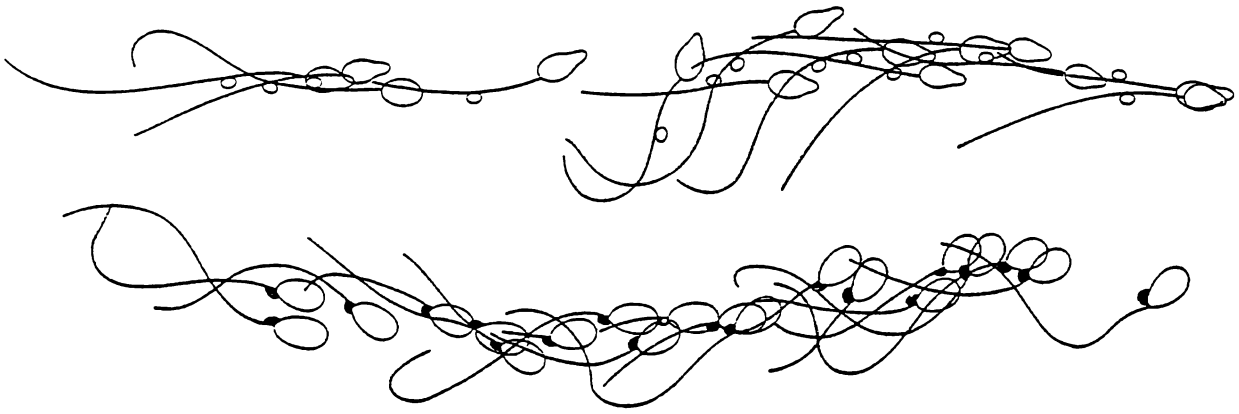

Fig. 2-12. Tracings of the movement of two human spermatozoa from cinemicrographs. Both cells have a protoplasmic droplet in one case on the neck, in the other case on the flagellum which provides a physical asymmetry and allows rotation to be identified (Phillips, 1972).

Note the wide variations in head orientation and alignment about the translation vector and its rotation all of which suggests a grossly helical trajectory.

However, in the case of bull spermatozoa, microscopic observation (by the author, M.W.W.) suggests that the rotation of the head is much more closely axial in fresh specimens which have not been excessively diluted. Irregular swimming motions with a marked helical trajectory can be observed in aged specimens and also at lower temperatures (i.e., $< 37^{\circ}c$). There are wide variations in swimming motions between cells and one can only consider the general characteristics displayed by a population.

Rikmenspoel (1965) arrived at typical values for the pitch and radius of the helical trajectory for bull spermatozoa as being 10μm

and 3μm respectively. With such a small radius, however, this amounts to little more than a rotation of the cell about a centre of pressure, possibly located somewhere near the centre of mass shown previously in fig. 2-9, with the major axis of the head inclined at a substantially constant angle but precessing around the direction of translation.

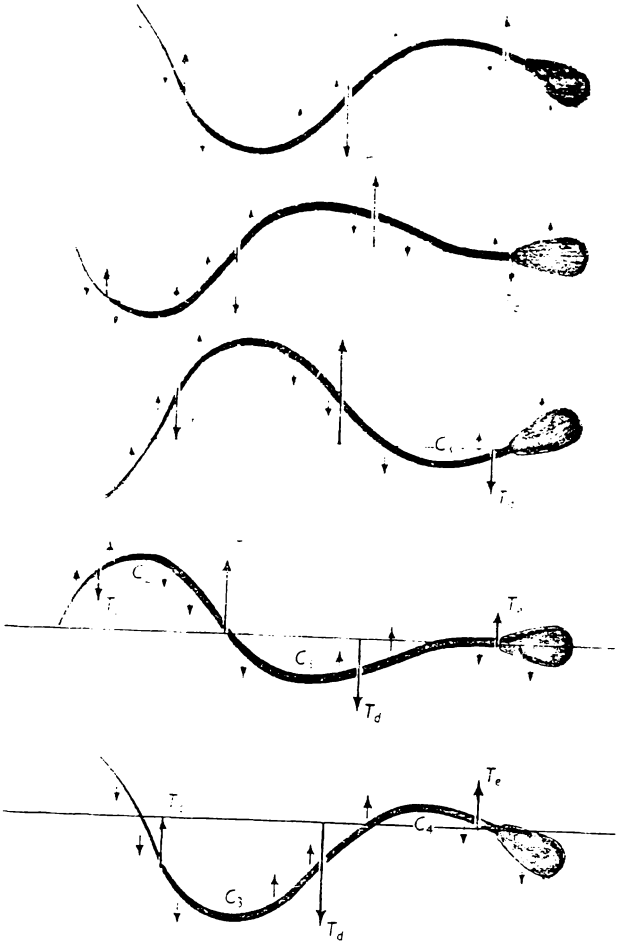

Fig. 2-13. Tracings from cinemicrographs of Gray (1958) showing lateral motions of the head and flagellum (refer back to fig. 2-10).

This motion can be easily visualised with the assistance of fig. 2-13 by imagining the head and tail-wave plane to be rotating about the translation vector which passes through a point, the centre of pressure, located just posterior to the head (refer back to fig. 2-9). Such a motion could readily account for the oblique flashes or herringbone track left on dark-field time exposures as the head passed through

appropriate planar alignments on opposite sides of its helical trajectory. The translational trajectories of bull spermatozoa were also closely studied in these early photographic experiments. Rikmenspoel and van Herpen (1957) tracked the movements of such cells and found that those of morphologically normal appearance could be roughly categorised into two classes (which thus provides an interesting contrast with the motile bacteria discussed in section 1.3.1 and the data of table 1-1. That is:

(i) Spermatozoa swimming in an orbit which is almost straight (having a radius of curvature $\gtrsim$ 1mm) and showing a periodic rotation about the direction of translation.

(ii) Spermatozoa swimming in almost closed circles and showing no axial-rotation (radius of trajectory in the range 25 - 25°μm) a lower swimming speed. Normally such cells comprise less than 10% of the population but according to Rikmenspoel the percentage of such cells is much higher in cold-shocked samples.

Observations of 150 cells showed the radius of curvature of the trajectory was distributed as:

Radius range	$r < 0.5$mm	0.5mm $< r <$ 1mm	$r >$ 1mm
percentage of cells	15%	24%	61%

Using high speed cinemicrophotography with pulsed dark field illumination, Rikmenspoel (1962) was able to quantify other dynamical parameters from frame-by-frame analyses. The swimming speed dependence of the tail-wave amplitude and rotation frequency are shown in fig. 2-14.

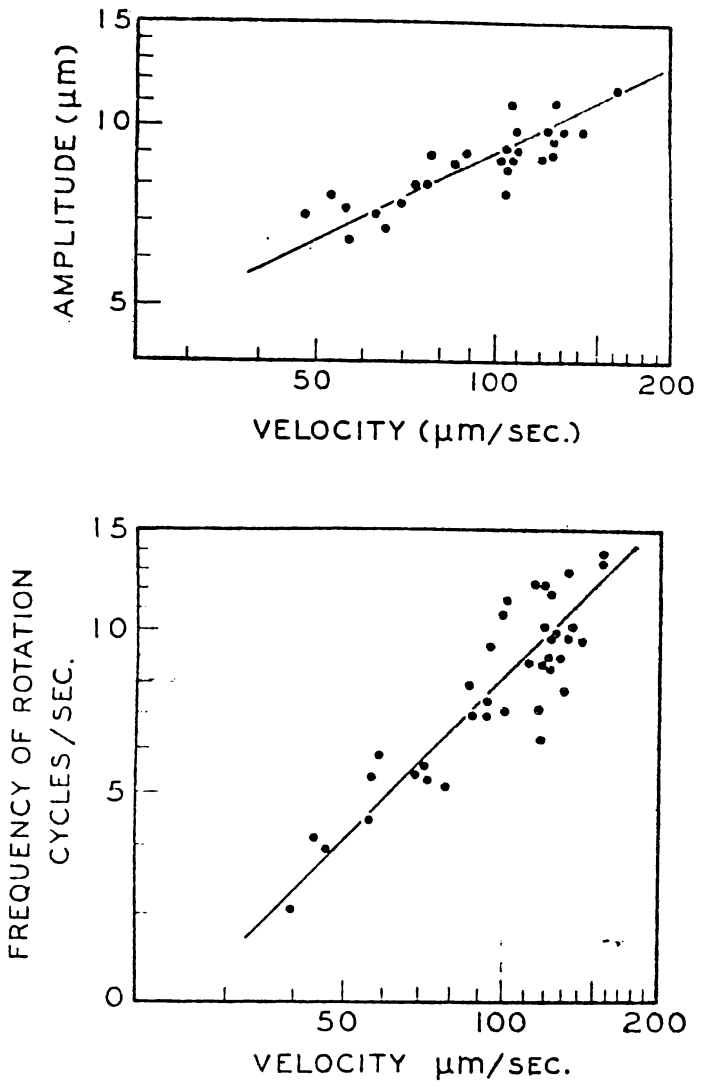

Fig. 2-14. Tail wave amplitude and cell rotation frequency for bull spermatozoa as a function of cell velocity. (Rikmenspoel, 1962).
Tail displacement is taken to be measured either side of the translation axis.

These data were fitted by the relationships;

$$V = pf_{rot} \qquad (2.1)$$

where V is the speed of translation, f_{rot} the frequency of cell rotation and p the pitch of the helical motion. From measurements on seven ejaculates (Rikmenspoel, 1962)

$$p = 11.9 \pm 0.7\mu m$$

The speed of the cell was found to be quadratically related to the mean amplitude of the tail wave

$$V = \varepsilon_{rot}\, b^2 \qquad (2.2)$$

where b is the mean tail wave amplitude (either side of the translation axis) and ε_{rot} was fitted as $1.2\mu m^{-1}s^{-1}$ which was interpreted as an efficiency factor for flagellar propulsion.

As categorised above, cells are often observed swimming in closely circular orbits and Rikmenspoel found that such cells, which often do not rotate, have a planar flagellar beat which has a lateral asymmetry of up to 30%. This asymmetry is closely related to the radius of the orbit as illustrated by the data of fig. 2-15.

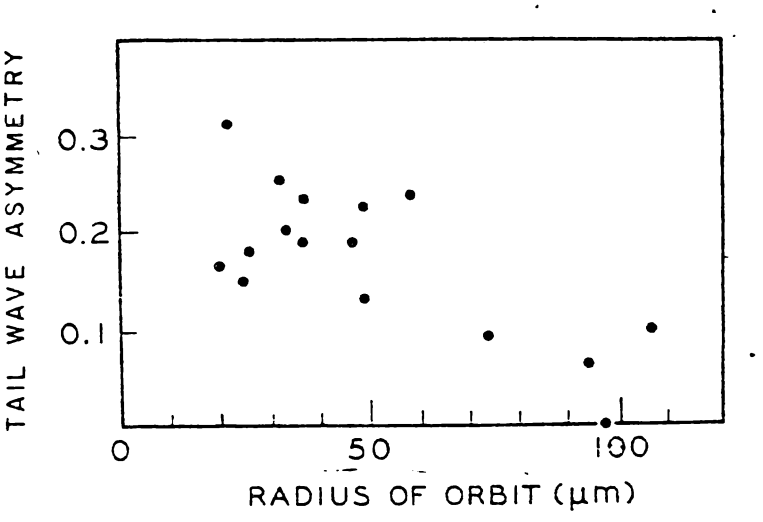

Fig. 2-15. Radius of swimming orbit as a function of tail wave amplitude asymmetry for bull spermatozoa. (Rikmenspoel, 1962).

Measurements of tail wave parameters have also been related to swimming speeds for ram spermatozoa. From measurements using high speed cinemicrophotography, Swan (1969) carried out a multiple regression analysis which showed swimming speed V was best predicted by the relationship;

$$V = \{f_t^{\,1.0 \pm 0.3}\, b_p^{\,1.7 \pm 0.4}\} \,/\, \{1.3 \pm 0.4\} b_d \quad \mu m/s \qquad (2.3)$$

where f_t is the tail wave frequency (Hz), b_p is the proximal wave amplitude 20μm behind the neck and b_d is the distal wave amplitude 40μm behind the neck.

This result is consistent with Rikmenspoel's observations for bull spermatozoa and in view of the conformational similarities of the two species of cell, may indicate rather similar swimming characteristics.

Taylor (1952) derived theoretical relationships between the various tail-wave parameters and concluded that a torque arising from the fluid motion created by the flagellum would tend to rotate the plane of the wave, the expression for the torque G per unit flagellar length being (for a tail of radius a);

$$G = 16\pi^3\eta a(f_t b^2/\lambda)\,[J_o(2\pi a/\lambda) - 0.5]/[J_o(2\pi a/\lambda) + 0.5] \qquad (2.4)$$

where η is the medium viscosity and λ is the wavelength on the tail.

The swimming speed distribution has clearly been an important factor in previous interpretations of light scattering autocorrelation functions (section 1.5). Therefore, to complete the general discussion of swimming motions for bull spermatozoa, a typical swimming speed distribution derived from traditional methods is given in fig. 2-16. This data is from Rothschild (1953) and was obtained by taking cinemicrographs at 25.8 frames/sec. and mapping the movements of 433 individual cells between frames. These swimming speeds were measured in an aqueous medium and are therefore higher than might be expected in the more viscous environment of cervical mucus (Tampion and Gibbons, 1962 measured a swimming speed of 55.6μm/s in bovine cervical mucus).

The mean and standard deviation of the swimming speeds for fig. 2-16, are 122.7μm/s and 38.6μm/s respectively and the distribution is seen to be slightly skewed in comparison with the normal distribution (solid line) having the same parameters.

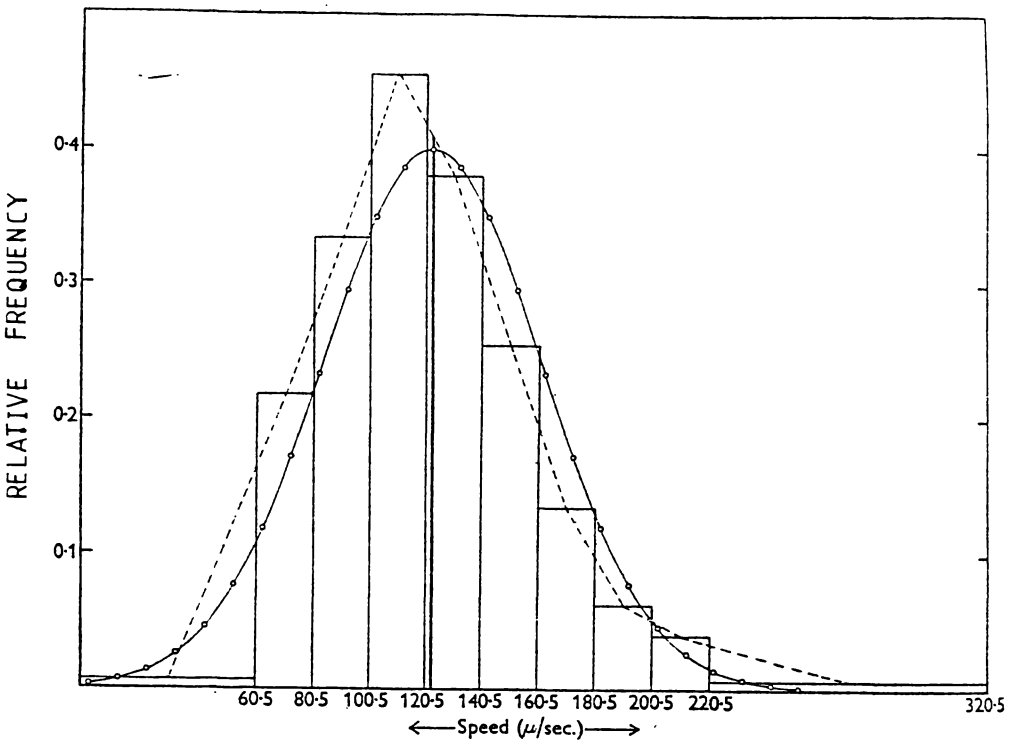

Fig. 2-16. Swimming speed distribution for bull spermatozoa with the solid line indicating the profile of a normal distribution with the same mean and standard deviation. (Rothschild, 1953).

It is however interesting to compare this distribution with that obtained by van Herpen and Rikmenspoel (1969) (previously presented in fig. 1-18) which it closely resembles in shape, but to contrast it with those derived by LBS methods, as fig. 1-21 for example. There is clearly a significant difference in the functional form of these swimming speed distributions.

2.7 Cooperative Swimming Behaviour

The preceding section discussed individual swimming motions of isolated spermatozoa. A logical sequel to this, is an outline of the collective behaviour of large numbers of swimming cells.

One of the most remarkable microscopic phenomena exhibited by spermatozoa, is that of 'wavemotion'. This is a pattern of flowing

waves evident in the semen at high concentration when viewed microscopically at low power. Waves of dark bands, obviously variations in optical transmission or scattering (depending on illumination), undulate through the semen and localized lineal variations in concentration or alignment of cells can be observed along those waves. The phenomenon is most marked at the high natural concentrations occurring in bull and ram semen, but is also observed in semen of other species when concentrated to similar levels (Walton, 1952).

The vigour of the wavemotion can vary significantly both within bulls and between bulls, and is commonly used as a measure of motility. Further, its frequency and strength are closely related to the vigour of the motile cells. Dead cells at the same concentration do not exhibit wavemotion effects.

No detailed analysis of the physical aspects of the effect appears to have been reported. However, when observed at high power it does appear to result from interactions between swimming cells, which generate a varying degree of order in cell orientations, and often sweep dead cells into the same alignments, generating localised regions of high concentration.

The effect is closely related to the concentration of the semen, becoming progressively weaker as the semen is diluted.

Wavemotion is illustrated in fig. 2-17 which shows photomicrographs of (a) strong and (b) weak wavemotion in undiluted bull semen together with dead sperm (c) at the same concentration. The phenomenon largely appears as a grossly heterogeneous and time dependent distribution of scattered light.

The existence of hydrodynamic interactions between swimming cells is highly likely in view of the small spacing of cells at ejaculated concentrations. For a random isotropic distribution of spermatozoa at a typical concentration of $\sim 10^9$ sperm/ml, the mean spacing is only

Fig. 2-17. Photomicrographs of (A) strong and (B) weak wavemotion in undiluted bovine semen, with the appearance of dead cells shown in (C).
(by courtesy of the New Zealand Dairy Board, Artificial Breeding Research Centre, Newstead).

(A)

(B)

(C)

Fig. 2-17.

10μm, about 20% of one spermatozoon length. This is well within the flagellar amplitude of neighbouring cells (fig. 2-14) and induced localised movements of the medium may result in alignment of swimming trajectories or otherwise generate localised correlations of motion.

Walton (1952) found that normal wavemotion could be completely disrupted by inducing a viscous shear or uniform flow within the sample. Under such hydrodynamic conditions, the cells become more or less uniformly oriented by *rheotaxis* (Bishop, 1960; Roberts, 1970) and the light scattering characteristics become more or less homogeneous. When the hydrodynamic shear ceases, cells revert to the characteristic wavemotion after a delay ($\sim$ seconds), which depends on the *motility*. Measurement of this relaxation time has in the past formed the basis of a motility instrument which is described in section 3.4.

Walton considered that the alignment of cells in the linear bands of this correlated motion was induced by hydrodynamic flows and there seems to be some support for this in the observation that dead cells are often seen to be swept into strands (Blom, 1946). However, a short range order, independent of flows, has been observed in dense suspensions of immotile sperm (Walton, 1952) and hydrodynamically coupled interactions (even without invoking flow induced alignment) undoubtedly exist at an even higher level between motile cells. Wavemotion is not generally observable at concentrations $\lesssim 10^8$ sperm/ml.

Light scattering motility experiments reported in the literature (table 1-4) have generally used diluted semen and the important question arises as to whether interactions occur between swimming spermatozoa at the sperm concentrations involved, and therefore whether the assumption of independently moving scatterers is really a valid one. If swimming cells are *not* independent, added complications may arise in interpreting the light scattering data. How low must the concentration be before cells can be considered as independently motile? No consideration of

this cooperative factor is evident in the literature on laser light scattering from spermatozoa, to date.

Observations carried out by the author (M.W.W.) in association with studies later detailed in chapter 5, showed correlations may exist between the motion of neighbouring cells at concentrations down to 10^7 sperm/ml.

The technique employed was to observe apparent impacts on the top surface of a 1mm deep sample cell placed on a heated microscope stage (relevant to the later studies of section 5.2). The microscope was used at 500 x magnification with a small depth of field and the focal plane set at the upper surface of the cell. This effectively removed from the field of view the population of cells normally swimming in close proximity to the surface (see later section 2.8). However, motile spermatozoa swimming out of the bulk of the medium and encountering the surface were readily distinguished as they briefly appeared in the focal plane at 'impact'.

Under these conditions there were definite correlations between the 'impacting' cells which appeared briefly in patches or clumps in the focal plane before reorienting and swimming just clear of the surface. Such effects were observed at a concentration of 10^7 cells/ml, although for the reasons detailed in section 2.8, the effective concentration of swimming cells in the bulk of the medium was probably less than this.

Reynolds and Rothschild (1963) observed that the effective diffusion coefficient of oxygen in a medium containing motile bull spermatozoa, was higher than normal (i.e., oxygen in a static medium) by an order of magnitude. This was attributed to mixing, resulting from large scale movements of the medium possibly generated by ordered sperm groups, even at dilutions of 1:20 ($\sim 5 \times 10^7$ sperm/ml). In this study, cinemicrographs were used to look for short range ordering of sperm locations and orientations by measuring the parameters shown in fig. 2-18.

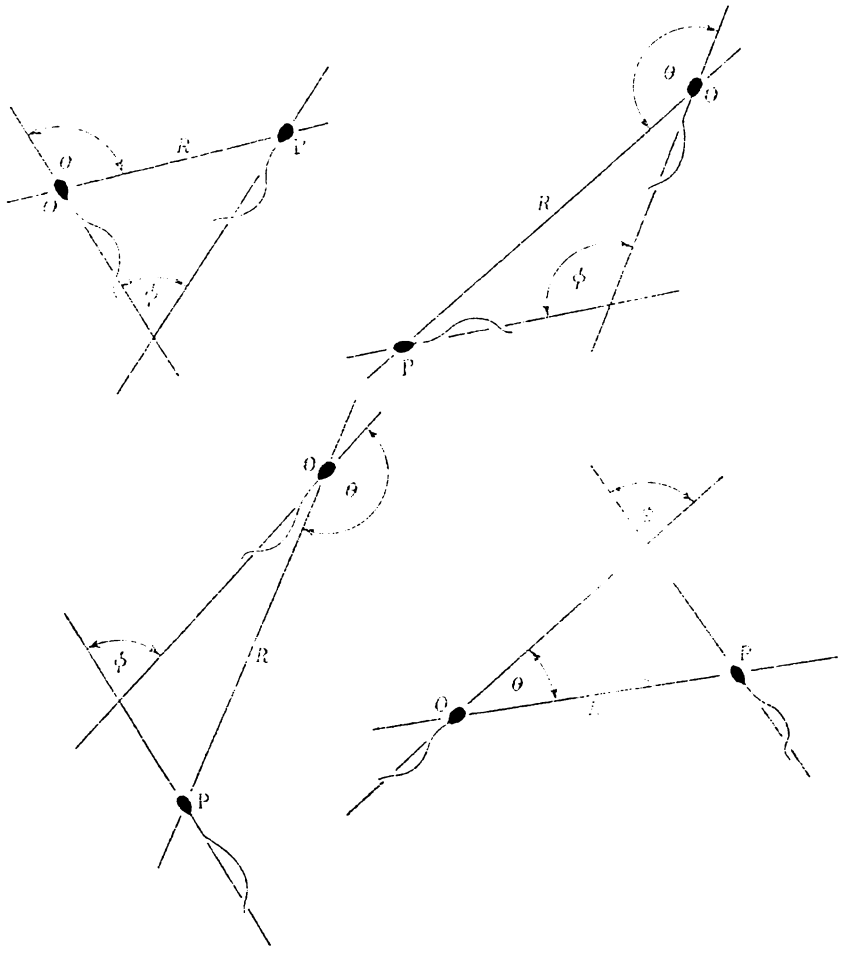

Fig. 2-18. Spacing and angular measurements made by Reynolds and Rothschild (1963) to identify correlated motions of spermatozoa.

The experimental distributions of the relative orientations ϕ and the pair separation R, differed significantly ($P < 0.05$) from the computed theoretical distributions for randomly distributed and isotropically oriented cells. Even at 4.2×10^7 cells/ml, $\langle\phi\rangle$ at 85.1° departed substantially ($P < 0.001$) from the expected value for random orientations of 90.0°. This parameter (ϕ) is an indicator of any tendency for neighbouring cells to swim parallel ($\phi < 90°$ parallel or $\phi > 90°$ anti-parallel). In addition, the distribution of pair separations was significantly skewed ($P < 0.001$) towards low values indicating that cells tend to swim in clumps. Observed frequencies of cells swimming with $\phi < 20°$ and R in the range 5 - 15μm were significantly higher than a random model would

predict.

The results of this study supported the concept of interactions and cooperative swimming between spermatozoa at relatively low concentrations, presumably through hydrodynamic coupling. (Weihs, 1975, considered the hydrodynamical aspects of fish schooling which may bear similarities).

A more recent experiment by van Duijn (1973) using photoelectric methods looked for clumping behaviour in the time distributions and velocities of cells generating signals when they passed the probe. For bull spermatozoa, the mean velocity of cells swimming in correlated groups was higher than that of isolated cells when diluted in the range 1:10 through 1:200 (concentrations of say $10^8 \rightarrow 5 \times 10^6$ cells/ml). The difference was only 3.7% in fresh samples but increased to 17% for aged specimens.

In the context of light scattering experiments it is not difficult to visualise the effect of such cooperative effects, particularly where high ($> 10^7$/ml) sperm concentrations are used. With a population of perhaps hundreds of cells contributing scattered light to a detector, short range ordering and localised fluctuations in concentration (perhaps plausibly on a timescale of order 1s) may introduce an additional amplitude term into the autocorrelation function, particularly if the scattering from individual cells is anisotropic.

2.8 Swimming Behaviour at Surfaces.

One of the most interesting characteristics of the swimming spermatozoon, and one which will be seen to be fundamental to understanding light scattering experiments, is its tendency to swim parallel to smooth plane surfaces.

Spermatozoa observed on a microscope slide under a coverslip often appear to be homogeneously distributed in the liquid medium. However,

when a short depth of focus, or a deep (> 200μm) sample cell is used, this is found not to be the case, particularly at higher dilutions ($< 10^7$ sperm/ml).

Observations and data later discussed in section 5.2 demonstrate that swimming spermatozoa rapidly become distributed within the sample cell in a grossly inhomogeneous fashion and exhibit a marked tendency to swim closely parallel with the internal surfaces.

The phenomenon is not frequently observed since motile samples of spermatozoa are generally examined at high concentration in a thin layer beneath a microscope coverslip, often with a relatively large microscope depth of focus.

Rothschild (1963) appears to have been the first to recognise, report and quantitatively analyse the effect. Using bull spermatozoa, he took cinemicrographs with a short depth of focus, at 20μm intervals through a haemocytometer chamber of depth 200μm. From analysis of the frames as a function of depth, the spatial distribution of spermatozoa between the two plane surfaces of the chamber was plotted and is shown here in fig. 2-19.

Rothschild's data indicates that a much higher localised concentration of motile spermatozoa was found in close proximity (< 40μm) to the internal surfaces of the chamber. The local sperm concentrations were higher at the floor and roof surfaces by factors of 6.75 and 5.0 respectively, relative to the concentration measured at the mid-point between them. The sperm concentrations employed were not specified.

The effect has also been observed in relation to the light scattering studies later discussed in chapter 5. The author (M.W.W.) first became aware of this phenomenon when microscopically observing spermatozoa in typical light scattering cells, and data illustrating these effects is later presented.

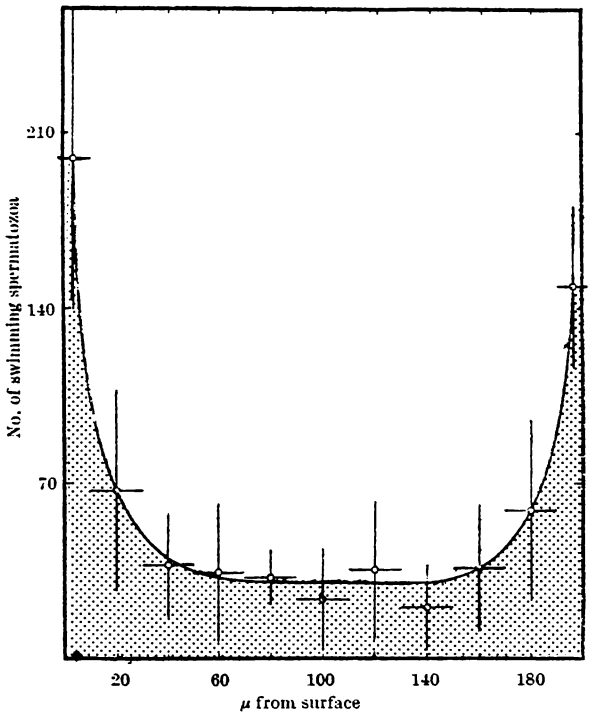

Fig. 2-19. Spatial distribution of motile bull spermatozoa within a haemocytometer cell. The bottom surface corresponds to the left of the distance axis and shows a higher surface concentration than the top surface located to the right.
(Rothschild, 1963).

However, it seems that prior to Rothschild's quantitative study, Gibbons (1962) had observed that when swimming spermatozoa contact with a surface they then tend to swim in circles (on the surface) having a characteristic radius and direction of rotation. The effect was said to be exhibited for sperm of quite varied conformation. In the case of sea urchin sperm, the head traced out a circle of diameter 50μm and orbited at $\sim$ 1 - 2 Hz with the plane of the tail wave remaining approximately parallel to the surface. Furthermore, the direction of rotation was the same for all cells, a quite remarkable phenomenon and later reference is made to this in section 5.8. Blokhuis (1972), found bull spermatozoa behaved in a similar fashion. Normal cells were found to swim in more

or less linear trajectories in the bulk of the medium but in slightly curved paths when on a surface.

Hancock and Paraschivescu (1965) found that the material of the microscope slide and coverslip surfaces affected the survival of sperm. Samples of boar semen which under glass lost all motility within a few minutes, survived for hours under a polyethylene coverslip of the same dimensions. The longer survival time was suggested to be associated with the surface permeability to carbon dioxide. However, it seems that motile spermatozoa also swim close to surfaces for hydrodynamic reasons.

Katz (1974) theoretically studied the influence of solid boundaries on the self-propulsion of microscopic organisms at very low Reynolds number ($<< 1$). The model considered was that of a thin wavy sheet swimming between two walls and was suggested as representing spermatozoa swimming cooperatively at high concentration. Complex biharmonic and lubrication theory analysis indicated that hydrodynamic forces result in the sheet swimming at a specific distance from and parallel to the wall. The analysis also suggested that the organisms may gain a propulsive advantage from its proximity to the surface such that the same swimming speed can be maintained with a lower energy input, the optimum distance from the wall being approximately twice the wave amplitude.

Subsequently, Katz and Blake (1974) pointed out that the wavy sheet model overestimates the wall effect since fluid disturbances are unrealistically constrained to decay in two dimensions only. The problem was then analysed by determining resistance coefficients (C_N and C_L) normal to and parallel to the tail, using hydrodynamic slender body theory but with the simplifying assumption that the flagellum was very thin and long (i.e., $r << \ell$). The conclusion was that the presence of a wall increases both C_N and C_L in the ratio $\gamma = C_N / C_L$ and that the effect of the wall becomes apparent at a spacing of about one bodylength, with same propulsive advantage being indicated.

It appears then, that there is some hydrodynamic basis for understanding why spermatozoa should swim on surfaces although clearly it is not understood in detail.

Rothschild (1963) considered that there was no evidence to suggest either adhesion or positive chemotaxis to glass and attributed the surface swimming behaviour to either hydrodynamic interactions with the surface or simply to inelastic collisions.

The important point regarding this surface swimming effect is that, particularly at high dilutions, it may generate an inhomogeneous distribution of motile spermatozoa in a sample chamber. In light scattering experiments therefore, the location of the observed scattering volume is important and if light is collected from cells swimming on surfaces additional complications will be involved in deriving the velocity distribution from the LBS data.

The wall swimming phenomenon could potentially therefore render the isotropic velocity assumption (table 1-4) invalid.

2.9 Effect of Light on Motility

If a light beam is to be used as a probe of motility, the light field in the observed region of the sample must not perturb the dynamics or survival of the spermatozoa over the timescale of the measurement. Even low power lasers of a few milliwatts generate high field intensities (a 2 mW beam with a diameter of 1 mm gives 250mW/cm^2) and in the LBS motility literature to date, no reference has been made to the biological effects of such light fields.

Three levels of perturbation would appear to be possible where only a small portion of a sample is illuminated by the beam, as in the later experiments of chapters 4, 5 and probably also those reported in the literature;

(i) Short term effects over a timescale of perhaps seconds

as the spermatozoon swims through the illuminated region.

(ii) Long term effects on the average motility parameters of the sample as progressively greater numbers of cells traverse the illuminated region and suffer potential motility change.

(iii) Photo-effects on the medium itself within the illuminated region, (i.e., chemical change or heating).

Since exposure to light is one significant environmental variable in artificial breeding technology, the literature contains a reasonable amount of data on photosensitivity, for bull sperm in particular.

Norman and Goldberg (1959), van Duijn (1961), Norman, Goldberg and Porterfield (1962), Wales and Choong (1963), Foote (1967) all reported experiments involving the effect of light on sperm survival or motility, *in vitro*.

The general conclusion which one may draw from these studies is that light has an adverse effect on both survival and motility, at least over a timescale of hours but depending on the light intensity and wavelength. Norman, *et al.*, (1962) concluded that the effect was due to a photosensitised oxidation and commented;

> "..... *Unlike most other cells and tissues which are inactivated and killed by exogenous photosensitive oxidations, bovine sperm did not require the presence of an exogenous photosensitive agent in the suspension medium at the time of illumination. Presumably, spermatozoa possess an intracellular photon-acceptor which can transfer its quantum to other energy absorbing cellular components* ....."

Mann (1964) considered the photosensitivity to result from the formation of an intermediary peroxide as a result of energy absorption via a cytochrome acceptor. Early experiments by Mann (1945) using thick washed suspensions of sperm together with microspectroscopy, had

demonstrated the presence of the absorption bands associated with cytochromes a, b, c, and later work by Perry, *et al.*, (1960) using grasshopper sperm located the main concentration of cytochrome as being in the mitochrondria.

Norman, *et al.*, (1962) quoted the absorption bands for bull spermatozoa as being in the wavelength ranges 540 - 560nm and 400 - 450nm (peaks are observed at 440, 480 and 550nm) and discussed the likely photo-reaction pathways and agents associated with the cytochrome system.

Foote (1967) showed that catalase added to sperm suspensions improved their survival when irradiated with visible wavelengths particularly at high dilutions. The suggested mechanism was that of reducing hydrogen peroxide levels.

A rationalisation of data from these survival studies with the photo-conditions pertaining to a typical LBS motility experiment, may give a useful insight into the likely significance of photosensitivity in light scattering experiments.

Norman, *et al.*, (1962) gave data on the *in vitro* survival of bovine sperm when illuminated by both fluorescent and incandescent water cooled light sources. Quoted light intensities were up to 10.8 lumens/cm^2 which corresponds to an energy flux of $\sim$ 17 mW/cm^2. This compares with approximately 140 mW/cm^2 for sunlight and a relatively high 1.27×10^3 mW/cm^2 for a low power 10 mW laser beam focussed to a beam diameter of 1 mm.

A typical laser source as used in LBS sperm motility experiments, therefore, gives a light field $\sim$ 70 times more intense than the upper limit of illumination used by Norman, *et al.*, a disturbing prospect at first sight. The dose-versus-percent motile sperm data obtained by Norman, *et al.*, (1962) is shown in fig. 2-20 along with data for non-irradiated controls. The post-radiation survival times for various irradiation intervals are shown in fig. 2-20. The composition of the diluent was found to have a substantial effect on survival, the presence of oxygen

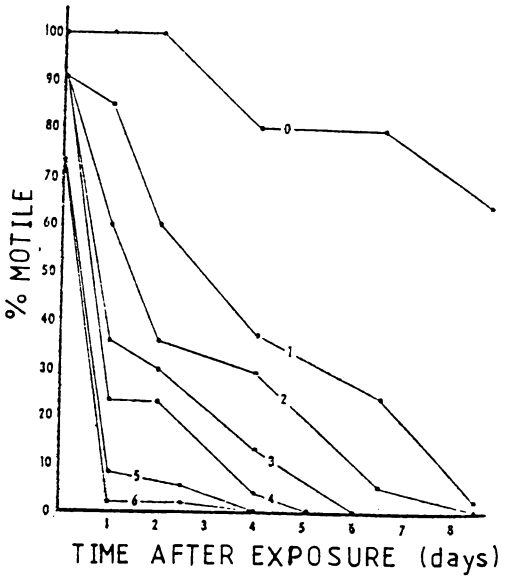

Fig. 2-20. Effect of varying periods (0 - 6hrs) of irradiation at (< 17 mW/cm^2) on the subsequent survival of bovine spermatozoa. (Norman, *et al.*, 1962).

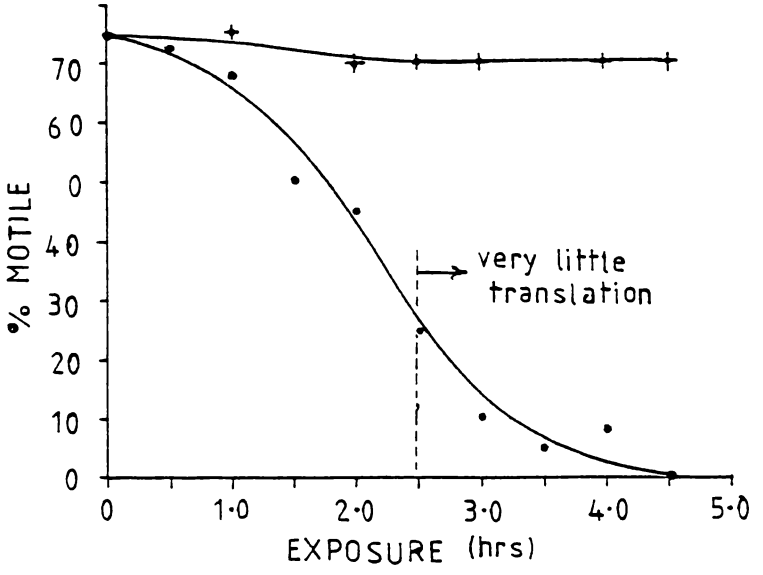

Fig. 2-21. Decline in percent motile sperm during exposure to light at 9.2 lumens/cm^2 (∿ 14.5 mW/cm^2) for unwashed sperm in a coconut milk extender at 24°c and an incandescent light source. (Norman, *et al.*, 1962).

hastening photoimmobilisation while the addition of catalase gave some protection.

In addition, by using a series of narrow band optical-filters, the action spectrum and an absorption spectrum were obtained for bovine spermatozoa, both of which are given in fig. 2-22.

(a)

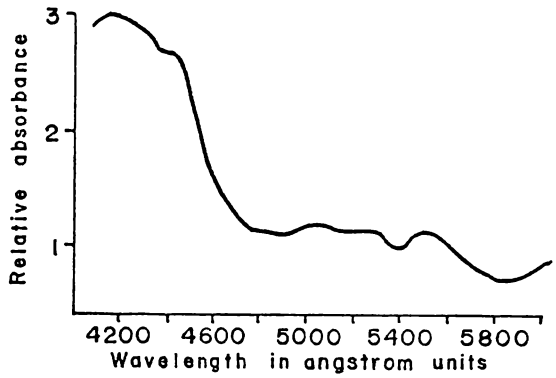

(b)

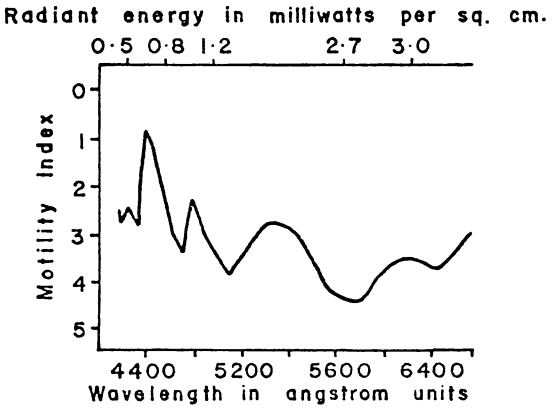

Fig. 2-22. (a) absorption spectrum for bovine spermatozoa.
(b) action spectrum for motility versus wavelength (motility scale 5 indicates maximal activity) (Norman, *et al.*, 1962).

A visible wavelength of ∿ 440nm generated the greatest degree of inactivation and it is clear that absorption is generally at a maximum in the blue region of the spectrum.

Shorter wavelengths, those in the ultraviolet, have also been shown to depress bovine sperm motility (Wales and Choong, 1963). The sperm were held in various milk based extenders and irradiated at wavelengths of 254nm and 366nm. The 366nm wavelength depressed motility more than that at 254nm and, in common with other workers, it was found that catalase gave some protection. Comparisons between experiments are difficult, however, since the actual light intensities at the location of the samples, have not been given.

What then do these results mean in terms of LBS motility experiments?

The detrimental effect of light on sperm motility when using very much lower intensities than in laser light scattering experiments, is indisputable. It would therefore appear that the blue-green region of the spectrum (where the argon-ion and He - Cd lasers operate) is the most damaging, and suggests that the use of He - Ne lasers (at 632.8nm) or Krypton lasers would be the most appropriate.

However, two mitigating factors may fortuitously reduce the problem within the geometry of the typical light scattering experiment, if due consideration is given;

(i) only a small volume of the sample is usually irradiated by the beam.

(ii) sperm absorb light only during transit through the illuminated volume.

Most radiation damage in biological cells can be considered in terms of the dose-time product. Let us, therefore, consider as a typical example, a light scattering sample cell of internal dimensions 35mm x 8mm x 1mm with a 1mm diameter laser beam aligned to give a path length of 1mm through it, (see, for example, type C vertical plane cell described in section 3.17.3). The illuminated volume is, therefore, cylindrical, of length 1mm, radius 0.5mm, the volume of which is $0.79mm^3$ or 0.3% of the total

sample volume.

Assuming further, that all spermatozoa swim with an isotropic distribution of planar velocities on the internal sample chamber surfaces (section 2.8), the average radiation dose per motile spermatozoon may be estimated.

Exposure time E = (# beam traversals) * (average beam transit time).

By transforming to a stationary spermatozoon and a moving circular spot of illumination,

$$E = \{T(A_i + Vd)/A_s\} * \{\pi d/4V\} \qquad (2.5)$$

where T is the total experimental time, A_i is the circular illuminated area of diameter d on the surface of area A_s, the mean speed of the spermatozoon being V.

For typical experimental parameters A_i = 0.79 mm^2, A_s = 280 mm^2, d = 1.0 mm, V = 0.1 mm/s and an experimental timescale of 600s, the average spermatozoon traverses the illuminated region 1.9 times and spends an average of 7.8s in the beam at each transit. For a worst-case situation of a 10mW beam the sperm cell receives a radiation dose of 1.9×10^4 mW-s/cm^2. In sample chambers of smaller volume the dose will clearly be higher, depending on the geometry and dimensions.

In the experiment of Norman, *et al.*, (1962) the total dose received over a 60 min. period was 5.3×10^4 mW - s/cm^2 and this resulted in a decrease of percent motile sperm from an initial 75% to 68%. This dose was higher by a factor of 2.8 than the dose of illumination received over the timescale of a typical light scattering experiment. In the example given the laser beam can be expected to affect the motility of the sample to a negligible extent.

While large approximations and numerous assumptions have been made in this argument, it does suggest that the laser light probe on an intensity-time basis, may not have the effect on sample survival which the large difference in intrinsic brightness might suggest.

Apart from the intensity level, the effect of the laser beam on sample motility is dependent largely on the ratio of illuminated sample volume to total volume and this is a matter of sample cell geometry. The issue has not received mention in the literature on LBS motility measurements for either bacteria or spermatozoa, although workers have, in general, used the apparently less damaging red wavelengths and appear to have assumed therefore, a minimal effect on motility. The incorporation of protective components in the extender medium, such as catalase and the exclusion of oxygen, may be useful in laser light scattering samples, but has received no mention.

2.10 Dilution Effects

In general, dilution of the sperm sample from the extremely high concentration of the initial ejaculate (see section 2.3) is necessary for most motility measurement techniques, with the exception of those that are based on wavemotion (section 3.1). Samples used in most reported LBS experiments have been diluted by a constant factor (in some cases unspecified) although this would inevitably result in variations between bulls or ejaculates, of the final concentration in the light scattering sample. Such variations in motile cell concentration, have serious physical implications for the measurement of percent motile cells, particularly in dilute samples, as is discussed in the results of chapter 5.

In addition, dilution of samples may well have biological effects as outlined in this section.

When a sperm sample is diluted, not only does the concentration of cells diminish, but so does the biochemical environment of the seminal plasma. Substantial dilutions are involved for light scattering studies. Hallett, *et al.*, (1978) diluted their samples by a factor of 2500 and the studies described in chapters 4 and 5 used dilution factors typically in the range 150 - 6000. Consequently the *biochemical shock* to the cells on dilution needs due consideration. It has been widely recognised for many years that sperm do not survive well at low concentrations, although the specific mechanisms involved have not been closely defined (Mann, 1964).

Blackshaw (1953) reported motility measurements at high dilutions for both ram and bull spermatozoa in various diluents. Rapid immobilisation over a timescale of several hours occurred at all dilutions (which gave final concentrations in the range (0.06 - 20) x 10^6 sperm/ml) but more particularly so at the low end of the concentration range. The medium or extender was found to play an important role, and maintaining a high level of seminal plasma at the lower concentrations was partially effective in preventing immobilisation. Other components added to the extender were also found to give partial protection against dilution: egg albumin, plasma albumin, plasma gamma-globulin, starch and glycogen, being examples.

The role of the seminal plasma in the dilution effect was also studied by Tampion and Gibbons (1963) who diluted bull spermatozoa to concentrations of 20 x 10^6 and 5 x 10^6 sperm/ml in both saline and seminal plasma. Dilution with seminal plasma (from the same ejaculate) gave a decrease in motility similar to that obtained with saline. However, there was no evidence of dilution effects for sperm swimming in bovine cervical mucus although the swimming speeds were

somewhat lower and the observations were not well controlled.

The decreased motility at high dilution *in vitro* may be due to either a sensitivity to decreased hydrodynamic interactions between sperm or (probably more likely) to changes in the biochemical environment brought about by the dilution process or the presence of other sperm cells. Clearly, if spermatozoa are to be diluted for light scattering experiments, dilution phenomena must be taken account of, particularly if the final concentration of the sample is not controlled (refer table 1-4 and section 2.3).

The dilution effect occurs across species and Rothschild (1948b) carried out extensive studies of dilution effects in sea-urchin spermatozoa (*Echinus esculentus*).

One of the most significant recent studies of the effect in bull spermatozoa is that of Shannon (1965), who measured the effect of added seminal plasma, added dead cells and gas-phase conditions on sperm survival at low and high storage concentrations (12.5 and 200 million sperm/ml respectively). Storage was at 5°c in egg-yolk based diluents and survival was determined at intervals by measuring the hours of incubation life for samples when raised to 37°c and defining over a 7 day period an index of survival, $\left(\frac{\text{Incubation life on Day 7}}{\text{Incubation life on Day 2}}\right)$. Typical results showed this index to be 0.81 for semen stored at 200 x 10^6 sperm/ml and 0.46 for semen stored at 12.5 x 10^6 sperm/ml. Adding 10% seminal plasma appeared to reduce livability and incubation life, an effect thought to be due to the involvement of a toxic, heat-labile protein.

The addition of dead sperm sought to test the possibility that dilution effects are created by the leakage of essential intracellular substances at high dilution. Adding dead cells to diluted samples had a marked detrimental effect on survival but did not increase the dilution effect.

Studies with both oxygenated and nitrogenated diluents, however, implicated the oxygen level as a major factor in both survival and dilution effects. The study indicated that the greater decline in incubation life for sperm stored at low concentrations could be due to the greater availability of oxygen and a resultant increase in H_2O_2 levels via oxidative metabolic pathways. Nitrogen saturation was particularly effective in prolonging the incubation life of sperm stored at low concentration and it was also demonstrated that periodically oxygenating sperm stored at high concentration (300 x 10^6/ml) gave survival times substantially lower than those obtained for diluted semen at 12.5 x 10^6/ml.

The key to the dilution effect, therefore, appeared to be oxygen availability in the diluent.

It is significant, however, that the dilution effects discussed here, and indeed those of general interest in artificial breeding, take place over a period of days, at low temperatures (from ambient down to 5°c). In the context of LBS motility studies however, we are primarily interested in temperatures of 30° - 37°c where cells are progressively motile, high dilutions (giving perhaps 10^6 sperm/ml or less), and time-scales of minutes. The conclusions which can be drawn from the data of Shannon (1965) about survival under these conditions, are very limited although no other more relevant data appears to have been published. Certainly a decline in motility due to oxidative mechanisms, over the timescale of a LBS experiment (minutes), seems unlikely, particularly if nitrogenated diluent and added catalase (Desjardins and Hafs, 1961; Vandemark, Salisbury and Bratton, 1949), are used for added protection. Sperm diluents for artificial breeding use have been developed through trials which, among other factors, select those ingredients which protect against dilution effects. The low sperm concentration, high temperature and high illumination level, may conceivably give dilution effects in LBS

experiments and the level of seminal plasma dilution and the composition of the extender medium may well be of considerable significance to such studies.

2.11 Toxic Effects of Dead Spermatozoa

Experimental procedures to be outlined in chapter 3 involve the addition of dead sperm to motile samples so as to vary the percent motile cells. The question arises, therefore, as to whether the addition of dead cells has a detrimental effect on the motile fraction.

Shannon and Curson (1972) looked at this question and concluded that dead cells did indeed have a toxic effect. Previously Shannon (1965) had shown that the addition of freshly killed dead sperm to diluted bull semen (at 12.5 x 10^6 sperm/ml) reduced sperm survival (section 2.10). Shannon and Curson, however, showed the toxic effect was due to the amino acid oxidase activity of dead spermatozoa. Acting on aromatic amino acids, the amino acid oxidase resulted in the formation of hydrogen peroxide which is highly toxic to sperm cells. The enzyme responsible was determined to be heat labile and to become degraded at pH < 3.0 or > 9.0. Semen treatments which destroyed or inhibited oxidase activity correspondingly eliminated or reduced the toxic effect of the dead cells. The effect, however, was enhanced at higher egg-yolk concentration (20% as *c.f.* 5%) in the diluent, possibly due to the increased substrate available for peroxide formation. Further, use of catalase in the extender at 4.5µg/ml dramatically reduced the peroxide induced toxicity, and nitrogen saturation of the extender could be expected to do likewise.

An important feature of the experiment, was that the toxic effects took place over a time span of tens of hours, even in the absence of oxidase inhibiting treatments (e.g., catalase). In an LBS experiment where the total timescale is perhaps ten minutes, a low concentration of egg-yolk is present (section 3.28) and catalase is used in the

diluent (in some cases nitrogenated), toxic effects caused by dead sperm are unlikely to be of any significance.

2.12 Diluents and Extenders

The question of media appropriate for dilution and preservation of spermatozoa is possibly still the central problem in artificial breeding across all species. This is certainly true for other than bull spermatozoa, for which sophisticated diluents have been developed. The nature of the diluent has received very little attention in the LBS motility experiments reviewed in section 1.5, most of which used only either seminal plasma or Hanks balanced salt solution.

To review the literature on sperm diluents is far beyond the objective of this section and a brief outline of the significant components of extenders used by the New Zealand Dairy Board in its artificial insemination services and which have also been used for the LBS studies described in chapters 4 and 5, is given in appendix I.

The value of egg-yolk-citrate (EYC) as a sperm extender has been well known for many years (Phillips, 1939; Salisbury, Zelaya and Vandemark, 1945). The addition of various other ingredients has resulted in the development of extenders which are even more effective in their long-term preservation of bull spermatozoa.

It is very common for bull sperm to be preserved at lowered temperatures ($\sim 5^{\circ}c$) and various substances in the egg-yolk (lecithin and lipoproteins) provide protection against the temperature decrease (Kampschmidt, Mayer and Herman, 1953) or cold shock (see section 2.13). Essential components also inhibit dehydrogenase reactions (Smith, Mayer and Merilan, 1956) and provide proteins, vitamins and enzymes. (Salisbury, 1957).

Bacterial growth in the diluent (Salisbury, Willett and Gunsalus; 1939) is highly undesirable and most diluents now include antibiotics.

EYC diluents developed by the New Zealand Dairy Board for use as *liquid extenders* at ambient temperature (i.e., rather than extenders for deep freezing of semen), include 2.5% n-Caproic acid and are known as 'Caprogen'. The formulation and preparation of Caprogen is specifically detailed in Appendix I.

Caprogen is widely used in the New Zealand Dairy Board artificial breeding system for the country-wide distribution of diluted (4×10^6 sperm/ml) bull sperm in liquid form, at ambient temperature over a time-scale of $\sim$ 48 hours.

2.13 Temperature Effects

Spermatozoa have clearly evolved to function with the best compromise between motility and survival, at the physiological temperatures within a cow's body (37 - 38°c).

As temperatures fall below this level, motility progressively decreases to zero, although it is found that sperm survive for longer periods at lowered temperatures, typically 5°c. Virtually indefinite survival is possible by deep freezing in liquid nitrogen, provided appropriate protective components are added to the diluents employed (e.g., Glycerol).

A rise of temperature to above 38°c, results in a short term increase in motility and, as might be expected, a premature ceasation of motility.

Of particular interest, however, is the irreversible damage which occurs when the temperature is *decreased* rapidly, so called cold-shock. In the absence of protective elements in the diluent (section 2.12), cells are particularly sensitive to rapid temperature decreases although rapid temperature rises have not been found to have the same adverse effects. Rapid heating of the sample (e.g., 20°c $\rightarrow$ 37°c in $\sim$ 2 min. period) in the light scattering chamber was not therefore considered to be of any real consequence.

2.14 Conclusions

The implications of the various properties and behaviours of spermatozoa, for LBS experiments, have been briefly indicated in each of the sections. However, a brief overall summary may be useful, considering the situation where samples of spermatozoa at high dilution are maintained at 37°c and illuminated by a laser beam for measurements of motility over a timescale of ∿ ten minutes or more. What are the significant effects which may influence the LBS results?

(1) Illumination of the sample by a low power laser beam (say, 10mW focussed to a diameter of 1mm) is unlikely to have any significant effect on the motility of the sample as a whole, provided the illuminated volume is small relative to the total sample volume (say < 1%). The use of catalase in the diluent gives additional protection against illumination effects.

(2) Wavelengths in the red region (say, 632.8nm or 647nm) appear to be the most appropriate, giving lower levels of absorption. Blue wavelengths may be acceptable due to a larger scattering amplitude.

(3) The sperm head, being large and flat, probably generates most of the scattered light, particularly at small scattering angles. The photographs of fig. 2-11 suggest a strong specular reflection from the head surface and, together with fig. 2-4, indicate that scattering and/or absorption occurs in the interior of the head. Amplitude fluctuations in the scattered field, as a consequence of head rotation, appear likely.

(4) The refractive index (and dimensions) of the head is such that the Rayleigh-Gans approximation is not really valid, although it may give approximate results.

(5) Dead cells may be expected to sediment rapidly, and the higher density of the head would indicate a head-down attitude in most media.

(6) Where samples are significantly diluted (say > 1000:1), the use of an extender medium giving protection against dilution effects is required.

(7) Correlations between the motions of swimming cells certainly occur at high concentrations and may be observed down to, or even below, 10^7 sperm/ml. The effect of correlated swimming on LBS autocorrelation functions is not clear.

(8) Motile spermatozoa tend to swim close to plane surfaces and the implications of this phenomenon for the spatial distribution of motile cells in the sample also needs clarification.

The literature relating to LBS measurements of spermatozoa motility has taken none of these factors into account and must therefore be considered an over-simplistic and superficial treatment of the problem. The studies using spermatozoa have not approached the more detailed analyses evident in reported applications to motile bacteria for which the scattering models and dynamics have been explored in some detail and related to the light scattering data.

In summary, we may conclude that there are clear indications (section 2.6) that the generally accepted model of a point-scatterer (at low scattering angles) with an isotropic velocity distribution, is inadequate for bull spermatozoa. Further, the swimming motions in the light scattering cell may not be either isotropic or independent.

CHAPTER 3

METHODOLOGY

..... *"The shortest answer - is doing."*

..... Lord Herbert,

1583 - 1648.

METHODOLOGY

PART 1

An outline and discussion of conventional methods of motility assessment for Spermatozoa.

3.0 Introductory Remarks

Thirty years ago Lord Rothschild succinctly summarised procedures which existed in the innumerable artificial breeding laboratories around the world:

> *....."At artificial insemination centres the 'goodness' or otherwise of a sample of bull semen is usually assessed by microscopical examination. So far as can be ascertained, the examiner allots a number of marks to a sample on the basis of its density, the number of active as opposed to inactive spermatozoa, the intensity of wave formation and the degree of activity of the active sperm present."*.....
>
> Rothschild (1950a)

Such methods still persist, probably because they are rapid and convenient and a trained and experienced eye appears to be better than the available alternatives. There is little evidence to suggest that more objective methods, having a higher resolution of motility differences, would be any advantage, but on the other hand it is also possible that such evidence does not exist because adequate methods of measurement have never been available.

Regardless of the biological significance of spermatozoa motility, the quantitative characterisation of the dynamics within a sample of spermatozoa is a challenging scientific problem. Completely to specify the sperm dynamics within a sample, many degrees of freedom are involved. As a reasonable compromise we might seek to measure:

(i) the percent motile cells.

(ii) the probability distribution of swimming speeds.

(iii) the translational trajectories.

(iv) the distribution of head rotation rates.

On the basis of the published literature to date (see chapter 1), it

would seem that LBS is at least potentially capable, of giving quantitative measurements of parameters (i) and (ii). However, a variety of other methods has been developed over the years, methods which measure directly or indirectly, one or more of these kinetic attributes of sperm suspensions. The simplest and most time-honoured of these techniques is the simple microscopic examination referred to by Rothschild. Using a microscope subjective scorings of bulk motility may be made or the motions of individual cells may be followed. In both cases, the work is tedious and highly subjective so that repeatability and resolution of differences are low, despite various innovative improvements to observational techniques. Measurements of swimming speeds, or vigour of motile cells, require tracking and timing of individuals or methods of quantifying the bulk motion of large numbers of cells. Head rotation rates are too fast to be followed by eye and have required more sophisticated techniques, generally either photographic or photoelectric.

In general, previously proposed laboratory methods of motility measurements on bovine semen all appear to have had serious limitations of extended measurement times, precision, repeatability or interpretation, and for these reasons have never found widespread acceptance.

This chapter, in part 1, gives more specific descriptions of these conventional methods (i.e., methods other than LBS) of measuring various features of sperm motility. The literature, however, is extensive and a detailed review is not possible; the basic principles of the methods are the prime objective.

Part 2 of the chapter then proceeds to detail the equipment and techniques employed in the laser light scattering studies with which this thesis is primarily concerned.

The principal reason for discussing conventional techniques, in addition to the LBS methodology, is to enable a comparative evaluation of the LBS technique to be made and indeed some discussion to this point

is given in the final summary and conclusions.

3.1 Wavemotion Scoring

Spermatozoa at ejaculate concentrations exhibit a remarkable flowing and swirling wave-like motion (Walton, 1952), which has for many years been used as a measure of motility. The phenomenon appears to result from cooperative swimming motions and has previously been discussed in section 2.7. Fig. 2-17 showed the visual appearance of ejaculates judged to have good, moderate and zero wavemotion.

The general procedure is for an experienced observer to view the wavemotion microscopically (at low power) in a small drop of undiluted semen, and to allocate a score, on typically a five-point scale, which characterises the vigour of the swirling and flowing motions. Clearly a subjective assessment is involved, the technical ability and experience of the observer being of great importance.

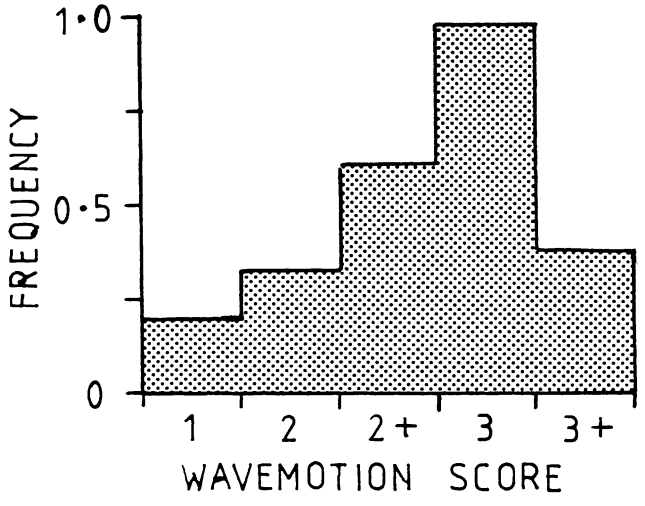

Fig. 3-1. Frequency distribution of wavemotion scores for 123 ejaculates from commercial A.I. bulls. (Data supplied by the New Zealand Dairy Board, Newstead research centre).

The procedure is commonly employed as a routine assessment of semen quality in commercial artificial insemination practice and, as

an example, scored wavemotion data from a mixture of proven and unproven bulls is given in fig. 3-1. Over the 123 ejaculates contributing to the distribution, the mean score was 2.7. Those scoring 1 and occasionally those scoring 2 were rejected for insemination purposes.

The technique is useful at ejaculate concentrations only and results are not readily interpreted in terms of sample behaviour after dilution.

3.2 Differential Staining

The percentage of morphologically dead spermatozoa may be determined by staining undiluted semen with *Eosin-Nigrosin* (Hancock, 1956). The staining procedure kills the sperm but the heads of those cells morphologically dead prior to staining, take up the pink coloured dye (i.e., *eosinophillic*) enabling a differential count of percent live cells, (which do not take up stain), to be carried out. As with wavemotion scoring, the method is widely used as a standard measurement on ejaculates used for insemination purposes and typical data have previously been given in table 2-3. This data showed that on the basis of *Eosin-Nigrosin* differential staining, fresh ejaculates have a percent live cells content with a mean and standard deviation of 84% and 6.9%, respectively.

Water soluble halogenated derivatives of *fluorescein, eosin B, eosin Y* and *erythrosin B,* will all stain dead spermatozoa (Mayer, Squires and Bogart, 1947). Hackett and Macpherson (1965) give a useful review of the preparation, methods and stains which may be used.

Much of the data later presented in chapters 4 and 5 of this thesis is based on estimates of the percent dead cells obtained by using *Eosin-Nigrosin* stain on the undiluted semen. One of the major problems with the technique is that in the presence of competition for binding sites on the cell membrane, the stain is not taken up effectively. This occurs in the presence of the protein component of the egg-yolk which has been

shown to bind to the plasma membrane (Watson, 1975) and so creates difficulties in measuring the percent live cells after dilution into egg-yolk based diluent.

The LBS method was therefore seen as a means of quantifying the percent motile cells in sperm samples after dilution in commercial egg-yolk based diluents.

3.3 Impedance Change Frequency (ICF)

One of the earliest attempts to objectively measure the motility of semen was described by Rothschild (1948a, 1949, 1950a). Samples of motile cells, at high concentration, were found to exhibit rapid fluctuations in the electrical impedance measured between two electrodes immersed in the sample. Both ram and bull semen showed the effect which was also found to be closely associated with wavemotion, samples showing no wavemotion giving no impedance fluctuations. The recording apparatus used platinised platinum electrodes and a 5KHz bridge circuit connected to an oscilloscope which displayed the rapid impedance fluctuations. Various schemes were then devised to quantify the signal. As Rothschild pointed out, the method was quite rapid ($\sim$ 5 min) and objective, and the electrode unit could be used as a probe which was immersed in the semen. The technique was not useful at high dilution (probably not $\lesssim 10^8$/ml) where no impedance fluctuations could be observed.

Rothschild (1950a) compared results using the electrical technique with those obtained by an expert technician from a scored visual assessment of motility. The two methods gave results which were highly correlated ($r = 0.899$, $P < 0.05$) and it was concluded that the electrical method could be substituted for visual assessments at artificial insemination centres, without adversely affecting conception rates. The technique was objective and therefore eliminated the variation in assessment skill between different technicians. Later work by Bishop, Campbell,

Hancock and Walton (1954) showed significant ($P < 0.05$) differences in ICF between bulls and breeds. Further, strong correlations ($P < 0.001$) were found between ICF, sperm concentration, and the percentage of live spermatozoa.

3.4 Optical - Rheological Methods

Wavemotion in undiluted semen also formed the basis of an objective method described by Glover (1968a; 1968b). A hydrodynamic shear (at rates up to 200 s^{-1}) was generated within the sample between two rotating glass plates and had the effect of completely disrupting the wavemotion, probably through forced rheological alignment of the cells. The variable of interest, was the time required for wavemotion to become re-established when the hydrodynamic shear was stopped. The re-establishment of wavemotion was detected optically by recording the light transmission through the sample as a function of time. Alignment of the cells by the shear would increase the optical transmission, which would then abruptly decline when wavemotion restarted. Highly motile samples showed re-establishment of wavemotion in $\sim$ 1s. As motility declined, the recovery time lengthened, becoming infinite for immotile semen.

Surprisingly enough, recovery times were found to be independent of the absolute sperm concentration within the range of 5:1 which normally occurs between ejaculates. Changes in light transmission were sufficient to allow the use of dilutions up to 1:20.

Good correlations were apparently obtained with expert visual assessments, but the comment was made that application of the technique in artificial insemination laboratories would require the development of an optically clear egg yolk extender. However, the method was apparently used as the basis for a 'Motility Meter' (Glover 1968a) which was subsequently tested by Linford, *et al.*, (1976) in a comparison of thirteen laboratory assays of motility, as predictors of semen fertility.

While being the only completely objective method in the study, results ranked it lower than several other tests.

3.5 Spectrophotometric Methods

The changes in light transmission with sperm alignment, have been used as the basis for a motility instrument with similar operating principles to the device described in section 3.4. Both dead sperm (Rothschild, 1962) and motile sperm (Bishop and Walton, 1960) will become aligned along the direction of a liquid flow, by any velocity gradient which is present.

This effect has formed the basis of an instrument which uses a conventional recording spectrophotometer or colorimeter, fitted with a specially designed cuvette (Timourian and Watchmaker, 1970). The semen was diluted and passed through a flow cell at a constant rate by an infusion pump. The general design of the system is illustrated in fig. 3-2.

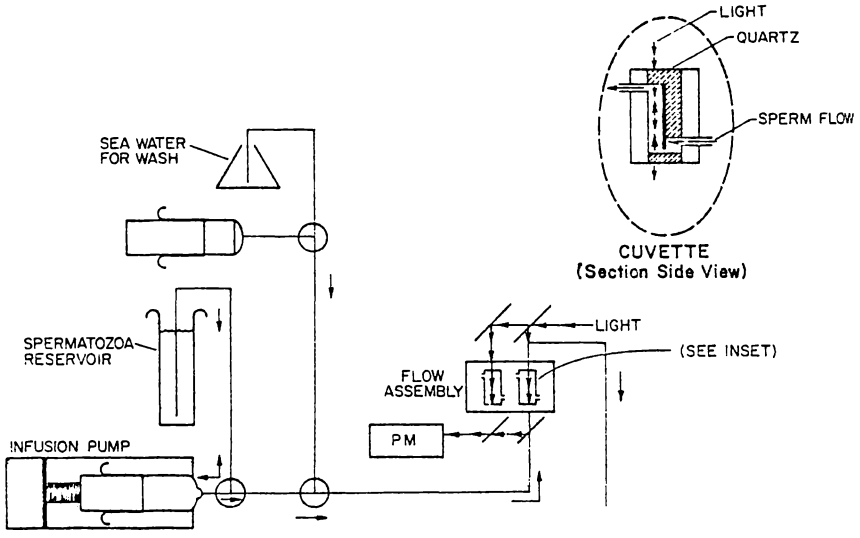

Fig. 3-2. Sample chamber, optical geometry and flow system employed by Timourian and Watchmaker (1970) for their spectrophotometric technique.

The light transmission in the direction of flow is recorded and this is a function of the degree of random alignment of the spermatozoa.

With the sample flow on,the cells become axially aligned and optical extinction is a minimum. When the flow is stopped abruptly, the cells reorient their translation vectors and relaxation back to random alignment occurs, with a resultant increase in extinction. The percentage change in optical transmission over the 30 s period (see fig. 3-3) following ceasation of the flow, is then taken as an index of motility.

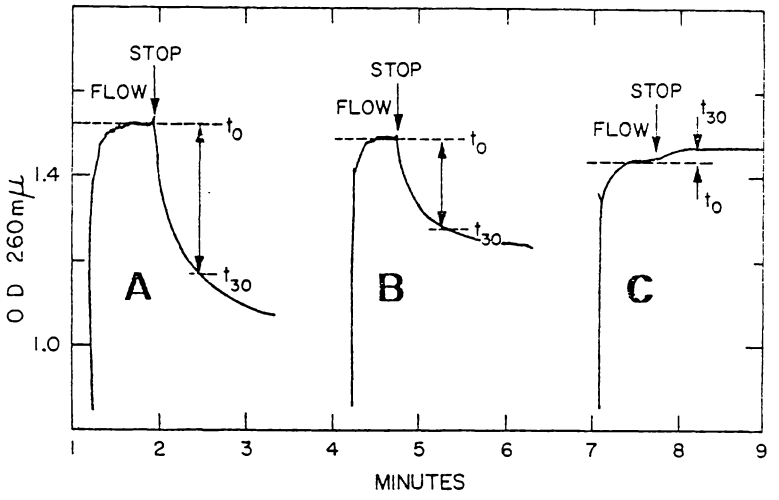

Fig. 3-3. Changes in optical transmission (OD) during flow alignment of spermatozoa and during the relaxation phase after the flow ceases. Recording A is for active spermatozoa, C for inactive spermatozoa and B for a mixture of A and C.
(Timourian and Watchmaker, 1970).

The dead cells apparently remain in their vertical orientation and so contribute very little to the increase in extinction when the flow ceases, although this vitally important aspect of the technique is not mentioned. The results of chapter 5 will indicate that, at least with bull spermatozoa, geotactic reorientation of dead cells would have occurred in Timourian and Watchmaker's apparatus when the flow stopped, had the sample flow direction been horizontally oriented. It is possible, however, that geotactic orientation is much slower with smaller sperm cells, such as from sea urchin, with which these studies were carried out.

The percent change in light transmission over a 30 s period was found to be directly related to the proportion of motile cells in the suspension. This was achieved by mixing inactive cells with an active sample in various proportions and is the same approach as is later described for the LBS studies of bull spermatozoa in chapter 4.

Subsequently Wall and Boone (1973) adapted the technique for use with a standard *Beckman Spectronic 20* Spectrophotometer operating at λ = 475nm and applied it to studies of rooster sperm. Atherton (1975) also successfully used the method, in a comparison of sperm motility between Angus and Hereford cattle and subsequently gave a detailed review of the technique (Atherton, 1979).

In comparison with the rotary shearing technique of Glover (1968a), the method represents a significant advance since it would appear useful down to much lower concentrations. While no discussion of actual concentrations used is given by Timourian and Watchmaker for sea urchin sperm, Wall and Boone (1973) state that their samples of rooster semen were diluted 1:1000, but that the actual dilution level was not critical. Atherton (1975) appeared to have used a similar dilution when studying bull spermatozoa.

3.6 Visual Timing Methods

Forward progressive movement has been generally considered as being the most important kinetic parameter characterising sperm motility. Consequently the measurement of translational speeds, by microscopic tracking and timing of individual cells was one of the earliest methods of motility assessment.

Moeller (1955), for example, reported measurements of swimming speeds *in vitro* for bull spermatozoa by clocking their travel over a measured distance in a microscope field. This was accomplished by selecting and timing individual spermatozoa which were swimming parallel to a

rotatable micrometer eyepiece, timing being typically over a distance of 700μm. Bias in the selection of cells to be timed, reaction times, scale alignment and deviation of the swimming track from the focal plane were all problems of some concern.

Harvey (1960) described a more sophisticated approach for use with human sperm, for which the swimming tracks are generally rather irregular. Individual cells were followed and timed across a number of squares of a grid system. A score was allocated to each square traversal along the trajectory depending on where the cell traversed the sides of the square and the total score over all squares traversed was closely related to the distance travelled along the curved trajectory.

While the technique was capable of giving useful results, in common with all other visual timing methods, it suffered the obvious disadvantage of being highly tedious and prone to bias.

Such methods have never been widely accepted as being appropriate routine measures of motility.

3.7 Migration Methods

A variation of the direct timing approach is to measure the migration of cells into a sperm-free region over a fixed period of time.

Early studies by Schwartz and Zinsser (1955) measured the maximum height to which sperm migrated vertically up a capillary tube. Along similar lines, Smith and Newmann (1961) inserted a 6cm length of polyethylene tubing (1.4mm diameter) filled with sperm-free buffer, upright into a sample of spermatozoa. After one hour, the tube was deep frozen, cut into 1cm segments and the sperm contained in each segment counted.

This general approach *in vitro* may well suffer from dilution effects as the more highly motile cells move into a progressively dilute environment and this is supported by the studies of Nevo and Mohan (1969), who observed dilution effects of this type.

Gassner, Goldzieher, Masken and Hopwood (1959) constructed a sandwiched sample cell having two chambers separated by a 10μm wire mesh between them. Bull spermatozoa diluted up to 1:100 were injected into one chamber and sperm-free seminal plasma into the neighbouring chamber. The system was then incubated at 37°c for periods of 15 - 60 min. and the concentration of sperm in the initially sperm-free chamber measured at intervals by withdrawing samples. The maximum transfer through the screen was typically only 1% over a 60 min. period, the transfer rate being taken as an index of motility. While the method was objective and had the advantage of looking at the motility of cells in bulk over a long period of time, the precision and convenience were limited by the technical manipulations required.

Migration methods have also been described by Lamar, Shettles and Delfs (1940), Rothschild (1949), Dott and Walton (1953) and Botella (1956).

In vivo adaptations of the migration principle have also been carried out by Phillips and Andrews (1937), Allison and Robinson (1972), and more recently, Tervitt (1980). Tervitt has carried out experiments in which ram spermatozoa were inseminated to the proximal cervix in oestrus ewes which were sacrificed after 60 min. The genital tract was removed and, after freezing, was sectioned to determine the distribution of spermatozoa along the tract. Allison and Robinson (1972) had previously used similar methods and demonstrated convincingly that the endocrine status of the inseminated animal had a marked effect on the survival of sperm in the reproductive tract.

Such methods, while having the very real advantage of being *in vivo* determinations, are impractical for other than special purpose studies and are subject to environmental factors which are difficult to control.

3.8 Photographic Methods

Photography has obvious appeal as a technique for analysing sperm motions and indeed some of the most significant results in this thesis were obtained using photographic methods. As a routine assay of motility photographic methods have never found acceptance, although, in special purpose studies, they have produced some of the most impressive results characterising sperm motions (section 2.7 on cooperative swimming, for example).

Rothschild and Swann (1949) and then, Rothschild (1951), took time-exposure photomicrographs of dilute sperm suspensions (using dark field illumination), on which the track lengths allowed the swimming speeds to be measured.

A more sophisticated variation of the same theme was tried by Troll and Goldzieher (1962), who superimposed photomicrographs taken at time Δt ($\sim$ 1 - 2 seconds) apart, one a positive and one a negative. This defined those cells which had changed position during the interval Δt, and by taking a whole series of consecutive exposures, the percent motile and the distribution of swimming speeds could be measured, albeit, with considerable work.

Difficulties in matching up the positive and negative images lead on to a further variation where multiple exposures were made on colour film through rapidly and cyclically changed filters. Moving cells thus appeared as multicoloured images or tracks while immotile cells appeared as a single colour. For example, using red and green filters in rapid succession gave a red-green track for moving cells and a yellow image for immotile cells. In terms of sample preparation, photographic procedures and image analysis, the technique was elegant but hardly a practical laboratory method.

Janick and MacLeod (1970) applied the time-exposure technique to human sperm since the short timescale of the measurement (1 sec exposures)

eliminated the problem of frequent directional changes which arises with human cells.

Various cinephotographic approaches have been attempted. The general philosophy has been that of plotting the changes in position of individual cells between frames. The technique as used by Rothschild (1950b) was said to be extremely time-consuming and requiring high film speeds to give continuous tracking. A simplified analysis technique which allowed sperm suspensions of any concentration to be analysed, was detailed by Rothschild (1953a). This involved determination of the fluctuations, between frames, of the number of cells in some defined region on the film. This was a stochastic approach, based on the *probability after effect* (Chandrasehkar, 1943), which relates the time dependence of the population in the defined region, to the mean swimming speed.

For a random spatial distribution of spermatozoa, the population of a small defined volume will have a Poisson probability distribution;

$$P_{(x)} = \frac{1}{x!} < n >^{x} \exp(-<n>) \qquad (3.1)$$

Where $P_{(x)}$ is the probability of finding x cells in the volume and $< n >$ is the average population.

If the number of spermatozoa, n, counted in a defined area of frame i is n_i at time t_i, then $\delta_i = |n_{i+1} - n_i|$ and $\tau = t_{i+1} - t_i$ and it was shown that

$$< \delta^2 > = 2< n >(1 - e^{-\lambda\tau}) \qquad (3.2)$$

where $< \delta^2 >$ and $< n >$ are the expected values of δ^2 and n respectively and the parameter λ which depends on the geometry, contains the mean speed of movement into and out of the volume.

For a circle of radius r and a mean swimming speed of $\bar{v}$,

$$\bar{v} = - \frac{\pi r}{2\tau} \ln \left(1 - \frac{\bar{\delta}^2}{2\bar{n}}\right) \qquad (3.3)$$

where $\bar{\delta}$ is the average change in population of the circular region between frames.

and $\bar{n}$ is the mean population of the region.

While highly ingenious and elegant, the technique still required considerable analysis per sample and has never found any general application. What is interesting about this method of Rothschild's, is that twenty years later Schaefer (1973) described exactly the same technique, but using the new technology of laser light scattering. Schaefer quantified the time dependence of the population in the defined volume, not by counting images on successive frames of a cinefilm, but by looking at the changes in the scattered light intensity using an autocorrelator. As the population varied so did the scattered light intensity at the detector, which through its collimation defined the geometry of the fixed volume. In the case of Schaefer's work the method was applied to dilute suspensions of motile bacteria (*E. coli*) and reasonable values for the mean speed were obtained (see section 1.3.2).

Extension of the light scattering version of the method (intensity fluctuation spectroscopy) to spermatozoa, (in particular ram and bull) for which the cinefilm method was intended, later proves to be confounded by a phenomenon which, ironically, was first observed by Rothschild. That is, the characteristic flashing effect generated by swimming bull spermatozoa in the microscopic dark-field. This could be expected to generate intensity fluctuations which may be significant relative to those generated by the population changes. Such a possibility will become apparent in later results, particularly sections 4.5 and the conclusions of chapter 5.

3.9 Image Analysing Methods

The use of *probability-after* statistics is particularly appropriate to computer-based image analysis. Katz and Dott (1975) used an image

analysing computer (*Quantimet* 720) to relieve the tedium of analysing the numerous cinefilm frames required in Rothschild's method. The imaging system scanned the microscopic field, using phase-contrast optics and counted the number of images in a specified rectangular area (typically 0.04mm^2), at typically 1.5 s intervals for a total period of 146 s.

Computations of the mean speed, using the method of equation 3.3, were then carried out on a small digital computer and compared with those from more conventional photographic track analysis. A standard error of 11% was quoted and the system was clearly expensive. Due to the level of automation, it held the promise of being a routine assay method, which was reasonably insensitive to sperm concentration.

3.10 Photoelectric Methods

These techniques are the most significant in this summary of conventional methods since they later prove to relate quite closely to the laser light scattering methods in which our primary interest lies.

Photoelectric methods have had considerable success in quantifying the dynamics of bull spermatozoa and have been particularly successful in research applications. The basic technique was first outlined by Bosselaar and Spronk (1952) whose apparatus is shown in fig. 3-4. A projection microscope with dark-field illumination formed a magnified (400 x) image on a screen (5) containing a small aperture (6).

A photomultiplier (9) placed behind the aperture received light from a defined region of the image, a region having dimensions similar to those of a sperm cell (inferred to relate to head dimensions). When the image of a sperm cell traversed the aperture, the detector generated a photocurrent fluctuation (fig. 3-4b) and such fluctuations were counted in a digital counter, after being digitised by a Schmitt trigger. Sperm concentration in the sample could also be measured by the simple expedient

(a)

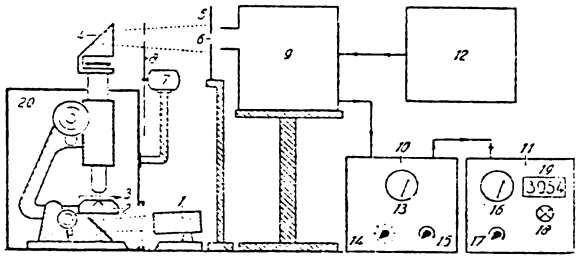

(b)

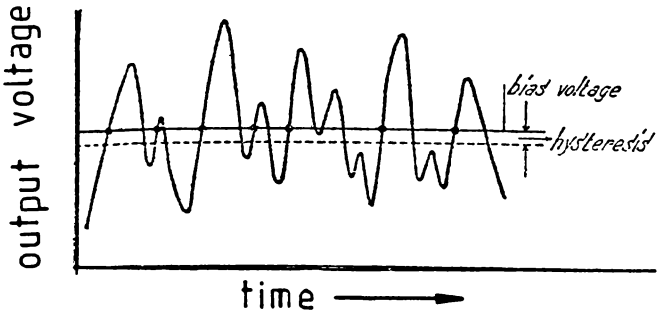

Fig. 3-4. Diagram of (a) the apparatus of Bosselaar and Spronk (1952) and (b) its output signal.

of using a lower power microscope objective lens and a large screen aperture, so collecting the light from a large number of cells; the mean photocurrent thus gave a measure of concentration.

In principle, this scheme is in fact very similar to the geometry of the laser light scattering systems discussed in the literature review of chapter 1, apart from the spread of effective scattering angles arising from the annular illumination cone, and the use of an incoherent light source. These two points will receive further consideration in the final conclusions of chapter 5.

Subsequently Rikmenspoel and van Herpen (1957) described a photoelectric technique which was really of the same geometry as that of Bosselaar and Spronk, and is shown here in fig. 3-5.

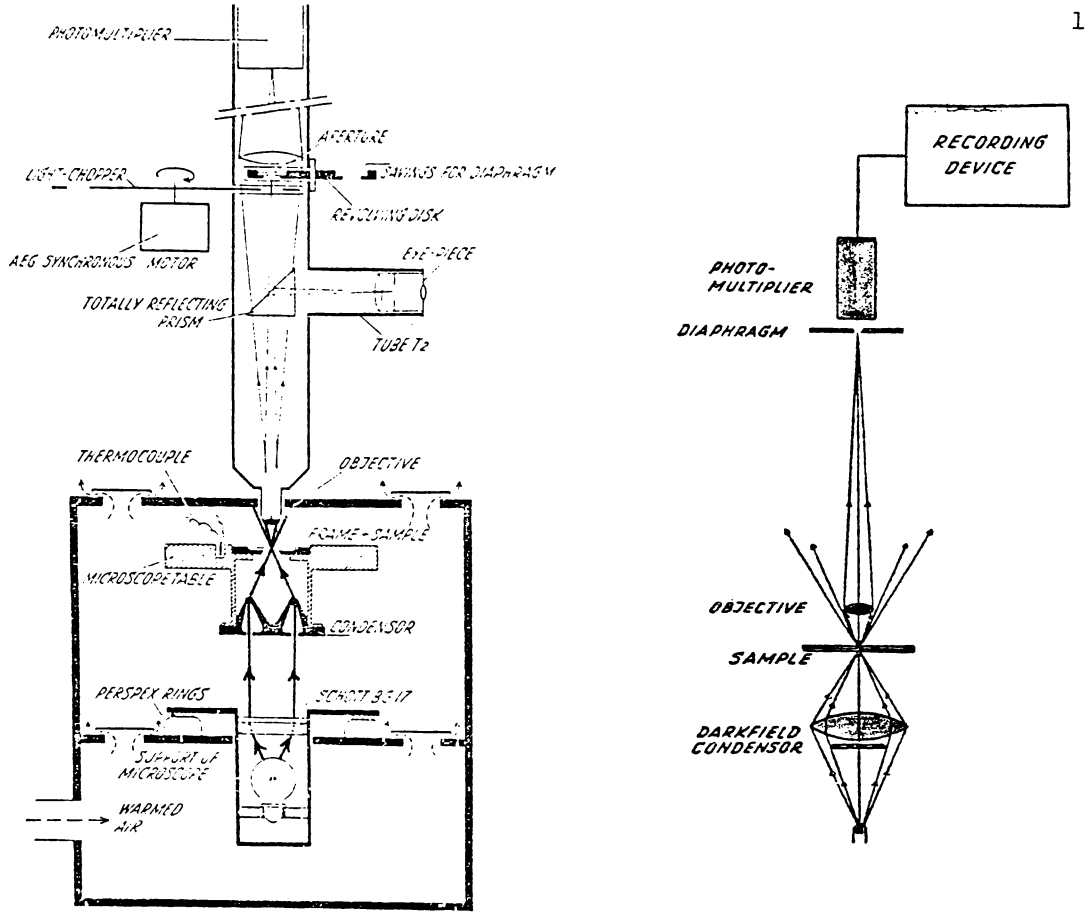

Fig. 3-5. Photoelectric apparatus employed by Rikmenspoel and van Herpen (1957). The layout is closely similar to that of Bosselaar and Spronk (1952).

Rikmenspoel and van Herpen attributed the large fluctuations in photocurrent which they recorded during a sperm transit, to the characteristic flashes seen in the dark field from the head of a bull spermatozoon as it rotates (Rothschild, 1953). Typical recordings of the detector output for the transit of rotating and non-rotating cells, are given in fig. 3-6.

The photocurrent recording for rotating cells (fig. 3-6a) could be divided into three sectors, a multiple-peak phase H generated by rotation of the head, a sector M said to be generated by the mid-piece and a low amplitude fluctuation T generated by the flagellum. Non-rotating cells generated lower amplitude photocurrent changes modulated at a high frequency (of $\sim$ 20Hz) over the M and T regions, probably representing twice the tail-wave frequency, and possibly generated by lateral displacements of the mid-piece. A phototube aperture diameter of 100μm was

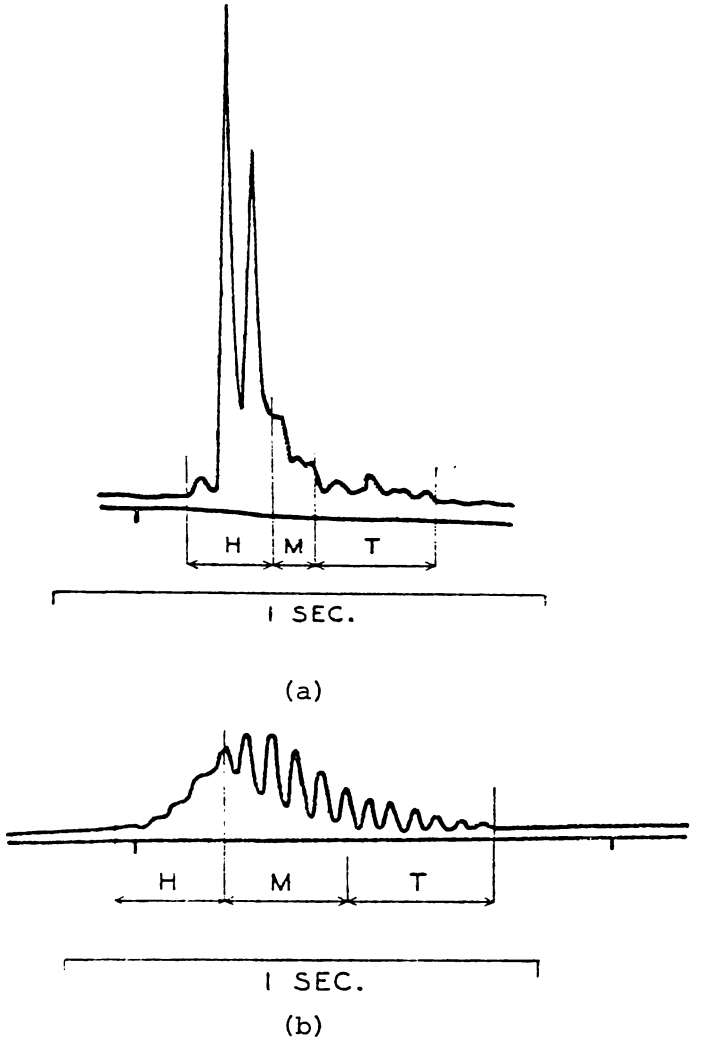

Fig. 3-6. Recordings of the detector output for the transit of the image from (a) a rotating spermatozoon (b) a non-rotating spermatozoon, across the detector aperture for the apparatus of fig. 3-5 (Rikmenspoel and van Herpen, 1957).

used and this again defines a scattering volume within the sample as is also the case in LBS studies, although of much smaller dimensions ($\gtrsim$ one head-length).

The swimming speed of an individual spermatozoon was determined from the aperture transit time and the rotation period of the head was derived from the interval between the peaks. The system was subject to the constraint that only one cell image traverses the aperture at any one time and this according to Rikmenspoel (1964) imposed an upper concentration

limit of 5 x 10^6 cells/ml.

Photoelectric measurements of swimming speeds were compared with those obtained by cinemicrophotography and the relationship is illustrated in fig. 3-7.

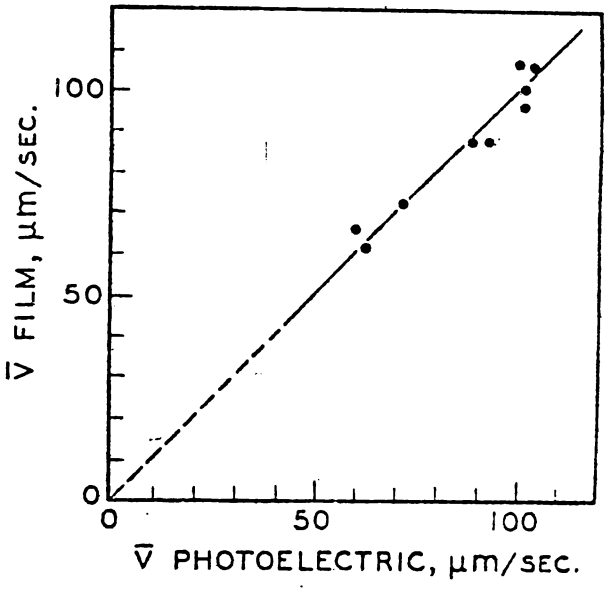

Fig. 3-7. Correlation between swimming speeds determined by cinemicrophotography and those determined by the photoelectric method for bull spermatozoa. Rikmenspoel and van Herpen (1957).

Here then, was an objective technique capable of measuring the distribution of both swimming speeds and head rotation rates as well as giving a measure of the concentration of motile cells. Further improvements took place when Rikmenspoel (1964) described an electronic analyser which determined the probability distribution of rotation rates and measured mean velocities provided they were > 50µm/s. This special purpose system was remarkably similar to a modern autocorrelator.

In general the photoelectric technique showed good correlations with data from photographic methods although in common with other instrumental developments it has found little general acceptance as an assay method in

artificial breeding laboratories.

3.12 Conclusions regarding Motility Measurement

A categorised summary of the various conventional approaches to motility assessment has been given in table 3-1. While the choice of an assay method clearly depends on the requirements constraints and objectives of the particular application, an interesting feature of the table is that none of the methods other than time-honoured wavemotion scoring, has found any significant routine application.

Probably the most extensive area of application of motility assays is in artificial breeding of cattle, which is now well established and highly organised, worldwide. Assessment of ram semen and possibly even human semen may also benefit from an appropriate instrumental technique. In this light, it is remarkable that although bull sperm concentrations are routinely measured in insemination laboratories using U.V. absorption spectrophotometers, no equivalent device has been available for measurement of motility.[1]

This may relate to the significance which is attached to motility. Obviously there is a real requirement to determine sperm concentrations in artificial breeding, since the sperm numbers in the doses or straws are important to both the conception rate and the number of inseminations per ejaculate.

The need for an accurate measure of motility is less obvious, other than in a general sense. Clearly semen of abnormally low motility will not achieve satisfactory conception rates, but whether accurate measurements of motility within the normal range are a meaningful indicator of conception performance is by no means clear. Visual assessments whether of wavemotion or activity in diluted samples have become the most widely accepted methods and in the circumstances this is hardly surprising.

[1] Very recent reports indicate a Doppler based instrument has become available.

MEASUREMENT TECHNIQUE	WAVEMOTION SCORING	IMPEDANCE CHANGE FREQUENCY	VISUAL TIMING	MIGRATION	RHEOLOGICAL	SPECTROPHOTOMETRIC
Semen Properties characterised.	Cooperative motion.	Electric resistivity.	Translation speed of selected cells.	Distance moved along tubes or # moved through screen in a fixed time.	Time to re-establish wavemotion after alignment constraint removed.	Change in optical transmission over fixed time after alignment constraint removed.
Level of Objectivity	Low	High	Low - medium	Moderate	Moderate	High
Concentration Range most appropriate.	Undiluted semen > 10^8/ml.	< 20 x diln. of semen.	Low, say 10^6/ml.	Undiluted down to 1:100 dilution.	Less than 1:20 dilution.	Less than 1:1000 dilution.
Concentration sensitivity of method.	Low with normal undiluted range.	Low over normal range of 1:5 in undil. semen.	Measured speeds lower at high dilution.	Low over range 7.5 - 800 x 10^6/ml.	Low over normal 1:5 range in undiluted semen.	Not highly critical.
Standard error or estimate thereof.	∿ 20%	< 5%	10 - 15%	$\pm$ 4%	7%	S.E. = $\pm$ 10%
Type of measurement.	Scored	Empirical	Absolute	Absolute	Empirical	Empirical
Volume undiluted semen required.	0.05ml	0.5ml but can use a probe in situ.	< 0.05ml	0.4ml	0.2ml	0.006ml
Estimated time required per sample for preparation and analysis.	2 min.	2-3 min.	20 tracks timed in 3 - 5 min.	15 - 60 min.	2 - 3 min.	4 min.
Appropriate applications of technique.	Routine assessment.	Routine assessment.	Very limited.	Very limited	Routine assessment	Research
Probable Extent of use in A.I. labs.	Widespread Routine use.	Very low.	Occasionally for human sperm.	Very low	Very low	Very low

Table 3-1. A general summary of the principal features of the various traditional techniques for measuring sperm motility.

MEASUREMENT TECHNIQUE	PHOTOGRAPHIC: TIME EXP.	PHOTOGRAPHIC: MULTIPLE EXP.	PHOTOGRAPHIC: CINE.	COMPUTERISED IMAGE ANALYSIS	PHOTOELECTRIC	*IN VIVO* METHODS
Semen Properties characterised	Length of image tracks (speeds and % motile)	Displacement between exposures (speeds and % motile)	Movement between frames (speeds and % motile)	Mean swimming speed and % motile	Distribution of swimming speeds and rotation rates, % motile cells.	Migration in the female reproductive tract.
Level of Objectivity	High	High	High	High	High	High
Concentration Range most appropriate	$\sim 5 \times 10^7$/ml	-	Bull sperm dil. 1:4 - 1:2	-	$< 5 \times 10^6$/ml but later mods permit up to 3×10^7/ml.	$\leq$ ejaculate or insemination concentrations
Concentration sensitivity of method	Determined by the distinguishability of tracks or images.			Affects statistics		High concentration required.
Standard error or estimate thereof	5 - 10%	-	Dept. on conc. $\sim$ 5%	$\pm$ 11%	Concentration $\pm$ 15% speed $\pm$ 7%.	Large
Type of measurement	Absolute	Absolute	Absolute	Absolute	Absolute	Absolute measure of distribution achieved in tract.
Volume undiluted semen required	$\leq$ 0.005ml	$\leq$ 0.005ml	$\leq$ 0.005ml	0.005ml	60µl	Large $\sim$ ejaculate volume.
Estimated time required for sample for preparation and analysis	> 10 min.	Hours	2¼ hrs.	2.5 min. computer sampling	Depends on concentration. At max. concentration $\geq$ 100s for data from 100 cells.	Hours
Appropriate applications of technique	- Appropriate only for research purposes -			Possibly routine assessment	Routine assessment and research.	Special studies highly dependent on endodrine status of female tract.
Probable extent of use in A.I. labs.	- Very low -			Virtually nil.	Several applied studies reported.	Nil.

Table 3-1. (Continued)

Considering movement and morphology, a trained eye is capable of taking into account many factors, which although subjectively appraised, collectively may give an appraisal of more value than any provided by a single instrument.

Similarly, differential *Eosin-Nigrosin* staining, because it is rapid and quantitative, and the consequences of a high proportion of dead cells seem obvious, has found widespread acceptance as a routine method.

The routine motility assessments used by the largest and most sophisticated artificial breeding systems still comprise wavemotion scoring on undiluted semen, differential staining to determine percent live cells, an appraisal of morphological form, and sometimes a visual estimate of motility in diluted semen.

The case for more accurate and objective routine measures of motility has not been proven, although clearly such methods may be seen as desirable for research purposes. However, it can also be argued that the relationship between motility and conception performance of semen has not been established, due to the lack of reliable and objective motility assays. Certainly those objective motility measures used in the field conception studies of Bishop, *et al.*, (1954) and Linford, *et al.*, (1976) did not represent the best of such technology.

The various techniques which have been developed are generally relevant to or look at different aspects of motility: high concentrations, or low concentrations, swimming speed distributions or mean speeds, rotation rates, percent motile cells. Of the methods discussed, probably the photoelectric technique is the most objective and gives the most information, although on the basis of the published literature laser light scattering also appeared capable of providing rapid and absolute measurements of the kinetic parameters.

METHODOLOGY

PART 2

Laser light beating spectroscopy:

Equipment and methods.

This section details first the equipment and then the procedures which have been used in obtaining results presented in Chapters 4 and 5.

3.13 Light Scattering Geometry

The optical geometry whereby a sample of spermatozoa is illuminated by a laser beam and the scattered light is collected at a known scattering angle is simple and well reported in the literature. A plan of the layout of the various components of the system is given in fig. 3-8.

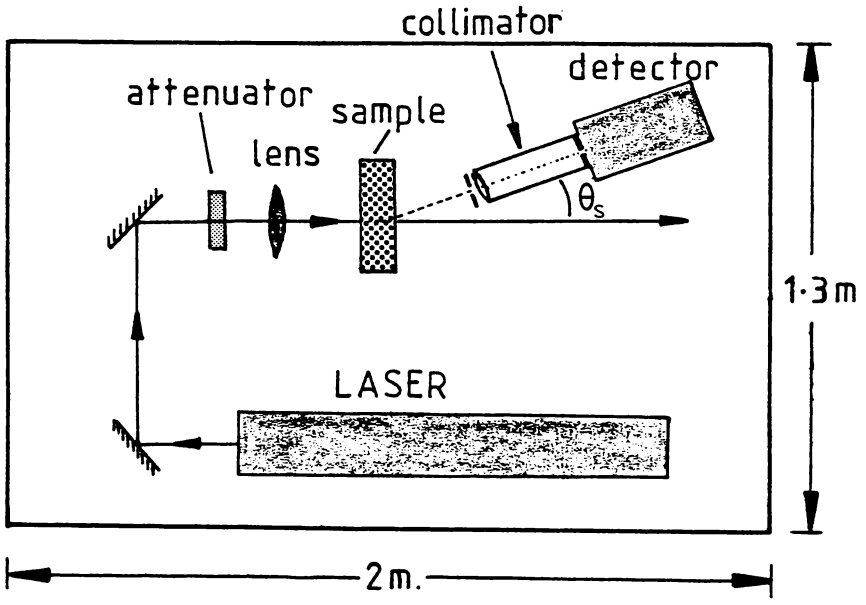

Fig. 3-8. Typical layout of the optical components of the system, as located on an anti-vibration table.

Since fluctuations in the scattered light intensity, which fall in the low frequency range up to 10Hz, are involved in these experiments, it was necessary to isolate the optical components from ground or building vibrations which often fall in this frequency range. The important requirement was to minimise relative movement of the components and this was achieved by locating the entire optical system on an anti-vibration table. This comprised a massive surface ground granite table of mass

$\sim$ 600kg supported on a high compliance suspension system comprising partially inflated pneumatic tubes. The resonant frequency of the table in the horizontal mode was $\sim$ 1Hz and in the vertical mode $\sim$ 2Hz. Spectral components arising from building vibrations was not found to be a problem under these conditions.

The spatial constraints imposed by the table made it necessary to redirect the beam as illustrated in fig. 3-8. Surface coated mirrors were used for this purpose and provided the reflecting surface was kept clean, no problems were encountered. Contaminated mirrors can create spatial intensity variations across the beam.

Beam intensity within the sample was varied either by adjusting the laser output power, or using a variable attenuator in the incident beam.

The beam diameter in the sample was set to required levels by appropriately locating the lens in front of the cell. The lens was normally of 10cm focal length.

The photo-detector was generally aligned at a small angle θ_s relative to the ongoing beam, in the horizontal plane. (typically $\theta_s < 20^\circ$). In some studies discussed in chapter 5, θ_s was arranged for special purposes to be in the vertical plane.

3.14 Lasers

A variety of lasers was used for the studies reported in this thesis; the particular instrument used often being dictated by availability or maintenance considerations. The wavelength employed was found to have no detectable effect on the data obtained, although noise modulation (either 50 or 100Hz, or high frequency) did occasionally cause problems, particularly with the He - Cd and He - Ne units.

Generally, blue or green laser lines were employed, although the 632.8nm He - Ne line was found best suited for photographic work. While fig. 2-22 in section 2.9 showed a substantial increase in absorption for

bull spermatozoa in the blue region of the spectrum, this is generally compensated for by being able to use lower beam powers through the $1/\lambda^4$ dependence of the scattered intensity (refer section 1.1.1) and the higher photo-detector sensitivity to blue wavelengths. Consequently, a lower beam intensity can be used for blue as opposed to red lines, for the same detected signal level. In fact, the inverse fourth power relation suggests a scattered intensity 2.8 times greater for the Argon-ion 488nm blue line in comparison with the He - Ne 632.8nm red line.

The lasers used at various stages of the study were:

(i) *Spectraphysics Model* 164 4 watt Argon-ion, generally operated at 488nm but occasionally at 514nm.

(ii) *Liconix Model* 403 Helium-Cadmium 14mW, operating at 441nm.

(iii) *Liconix Model* 405 Helium-Cadmium 50mW, operating at 441nm.

(iv) *Coherent Radiation CR*-4 4 watt Argon-ion, operating at 448nm or 514nm.

(v) *Coherent Radiation Model CR80*-2H, 5mW Helium-Neon, operating at 632.8nm.

Noise-free operation and a stable beam intensity were best achieved by using the Argon-ion lasers, operated in light-control mode wherein the output is stabilised by a photo-electric beam sensor and temperature regulated feedback electronics. All lasers operated in the TEM_{oo} mode.

In the case of the Helium-Neon and Helium-Cadmium lasers, beam intensity could only be controlled by using a variable neutral density attenuator plate. The attenuator plate was also necessary for the Argon-ion lasers since the best noise-free operation and stability were achieved with the plasma current set at relatively high levels, which generated much higher light intensities than were needed or desirable.

External attenuation, sometimes via two plates, was, therefore, necessary.

Light levels at the sample were generally no greater than 5mW, depending on other experimental parameters such as wavelength, scattering angle, detector apertures, sperm concentration, photomultiplier voltage. The Argon - ion lasers (the most commonly used) gave a plane polarised beam with the electric vector in the vertical plane and an amplitude ratio of $\sim$ 100:1.

3.15 Photodetector Systems

The photodetector system requires collimation so as to collect light at a specific scattering angle from a small defined volume within the sample. Early experiments were carried out using a double pinhole collimator. This comprised two pinholes of typically 0.2mm diameter spaced 1m apart, and this type of system has been widely used in reported experiments. It suffers the disadvantage that alignment of the detector on the sample, and hence the location of the scattering volume, must be inferred from signal changes as the collimator is tracked horizontally and vertically across the illuminated region of the sample. Alignment of the photodetector is therefore subject to an uncertainty in scattering volume location.

For this reason, the majority of experiments reported here, used an optical imaging collimator (Chu, 1974; Collins, 1976) in front of the phototube, the principal features of which are shown in fig. 3-9.

A large diameter lens ($\sim$ 5cm) of focal length 20cm was used to form a real inverted image of the illuminated region within the sample, on a screen. The object region and the image screen were both located at a distance of twice the focal length from the lens, so giving an unmagnified image. The image formed on the screen was the real size projection of the illuminated region within the sample at that particular scattering angle θ_s, and could be observed on the screen through a low power microscopic eye-piece.

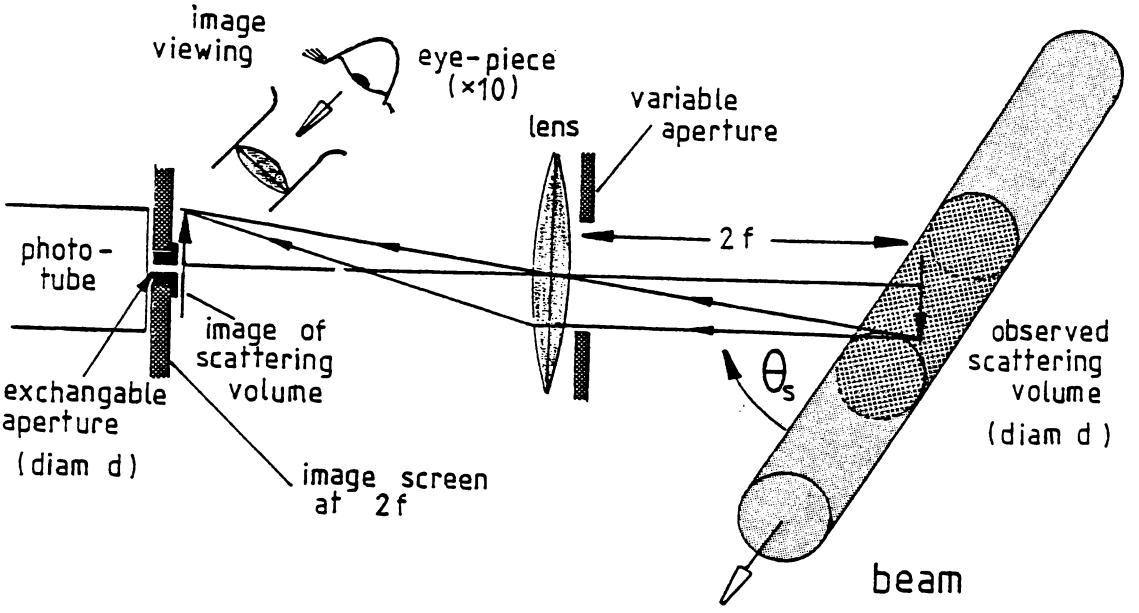

Fig. 3-9. Optics and geometry of the photodetector system.

This system was found to have enormous practical advantages over the conventional double pinhole system, in that it could be rapidly and accurately aligned. Having set the detector at the desired scattering angle θ_s relative to the beam (usually measured by simple triangulation), the detector was then moved towards or away from the sample so as to bring the projected image of scatterers within the illuminated region of the sample into sharp focus on the viewing screen. An Iris - diaphragm over the front of the lens allowed the aperture, and hence the depth of focus, to be varied. At minimum aperture ($\sim$ 1mm diameter) the depth of focus was several millimeters while at full aperture ($\sim$ 45mm) it was significantly less than the image depth, probably < 100μm.

Alignment and focussing were best carried out at full aperture, where the image was at maximum brightness and the depth of focus a minimum. Scattered light could then be collected from any desired location in the illuminated region by appropriately locating the phototube aperture on

the image. In addition, the volume of the region from which scattered light was collected, could be readily varied by changing the phototube aperture diameter (range employed was 50μm - 800μm).

The lens aperture had three major effects. It determined:

(i) the image brightness.

(ii) the depth of focus and hence and depth within the scattering volume from which light was collected.

(iii) the coherence over the dimensions of the image (see Chu, 1974).

Of these three effects, the first two are convenient experimental attributes of the system. However, the question of the coherence of the image, or at least the coherence of the light on the image reaching the phototube, has fundamental implications for light beating experiments. At large apertures coherence will be reduced and the signal/noise ratio of the beat signal degraded. It was, therefore, standard practice to set-up the detector alignment and focus at full-aperture and then stop-down the lens to minimum aperture when light scattering measurements were to be made, where depth of field was greatest and the coherence area was a maximum. The coherence region on the photocathode at minimum aperture (1mm) was of $\sim$ 230μm diameter. Wang and Snyder (1974), Cohen (1975), Chan and Ballik (1975) give detailed analyses of coherence in photodetection systems of various geometries.

The photodetector employed in all experiments was a Phillips 56AVP photomultiplier. This is not a refrigerated tube and provided more than adequate sensitivity and signal/noise. (Spectral response peak at 420nm, current gain 10^8 at 2.2kV and having a luminous sensitivity of 65μA/ℓm). The tube was normally operated with an anode voltage in the range 1100 - 1800v, depending on experimental conditions such as phototube aperture size, scattering angle, beam power and sperm concentration. The photo-multiplier was supplied with high-voltage from a regulated supply

(*Hewlett-Packard* Model 6516A; 0 - 3000 v at 0 - 6mA).

A polarisation analyser was not used in the detector optics.

3.16 Scattering Volume Geometries

The conformation and dimensions of the scattering volume defined by the detector were important.

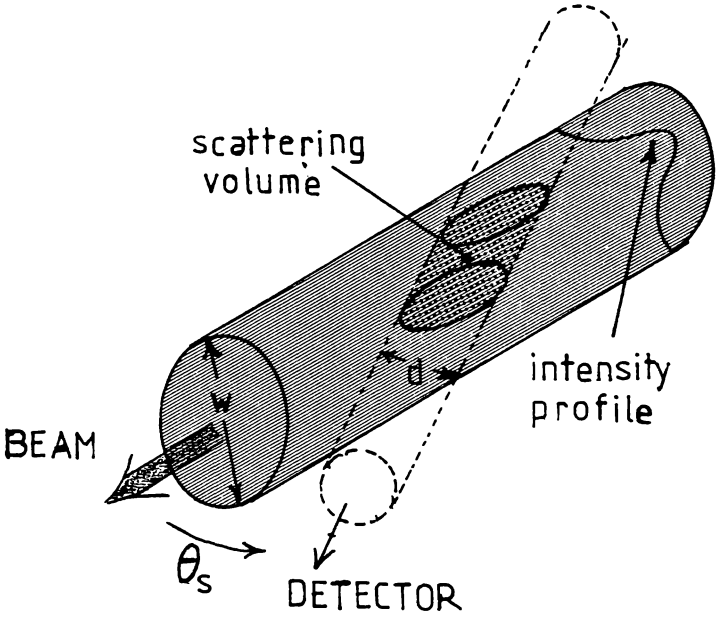

Fig. 3-10. Intersection geometry for the Laser beam and the solid angle effectively subtended by the photo-detection system.

The geometry of the illuminated region is illustrated in fig. 3-10 and for the case where beam diameter W > d, at small scattering angles θ_s, the scattering volume is substantially cylindrical, the diameter being that of the phototube aperture which is located on the image (refer fig. 3-9). Simple trigonometrical analysis shows the volume of intersection is given approximately by

$$S.\ Vol = \pi d^2 W / 4 \sin\theta_s \qquad (3.4)$$

for d << W

For a beam diameter of 1mm, a phototube aperture diameter of 200μm and a scattering angle of $\theta_s = 8°$, the scattering volume is then $0.23mm^3$. At a typical sample concentration of 10^6 sperm/ml the population of the observed scattering volume would then be 230 cells. However, the effective scattering volume (in terms of scattered intensity) may be less than this due to the Gaussian intensity profile across the beam and the particular depth of focus within the region.

A further important parameter, one which is imposed by the scattering cell design is the path length of the beam through the sample. In some sample cell designs (see section 3.17.1 and 3.17.2) this was selected to be 10mm and at small scattering angles ($\lesssim 5°$) the defined scattering volume would extend the entire length of the illuminated path through the sample.

Later cell designs (see section 3.17.3) used a short pathlength ($\sim$ 1mm) with the phototube aperture (0.8 - 1mm) being $\gtrsim$ beam diameter. This system, at low scattering angles ($\lesssim 20°$) allowed scattered light to be collected from the entire illuminated region within the sample although the implications for the coherence and signal/noise ratio of the detection system require an understanding of the intensity fluctuation nature of the signal, later discussed in section 5.6.

3.17 Sample Cell Design

During the course of these experiments, the design of the sample cell underwent several significant changes of geometry as the understanding of phenomena existing within the sample improved. The three basic sample cell designs are described here while the detailed philosophy behind them, particularly the later (type C) design, will become more evident in chapter 5. All sample cells were temperature controlled by immersion in a thermostatically controlled water bath,details of which appear in sections 3.18 / 3.19. In general, the basic cell structure was that of a standard

spectrophotometer cell, since these are commercially constructed to be of optical quality.

It is interesting to note that little significance has been attached to scattering cell geometry in the LBS literature reviewed in section 1.5.

3.17.1 Simple Open Cell (Type A Cell).

Early work was carried out using a rectangular spectrophotometer cell constructed of optical glass, open at the top and having internal dimensions of either 10mm x 10mm x 40mm or 10mm x 2mm x 20mm. In both cases, the beam path through the sample was oriented along the 10mm dimension as shown in fig. 3-11. The cell had the beam entry and exit windows polished and the detector was aligned to view the sample through the beam exit window.

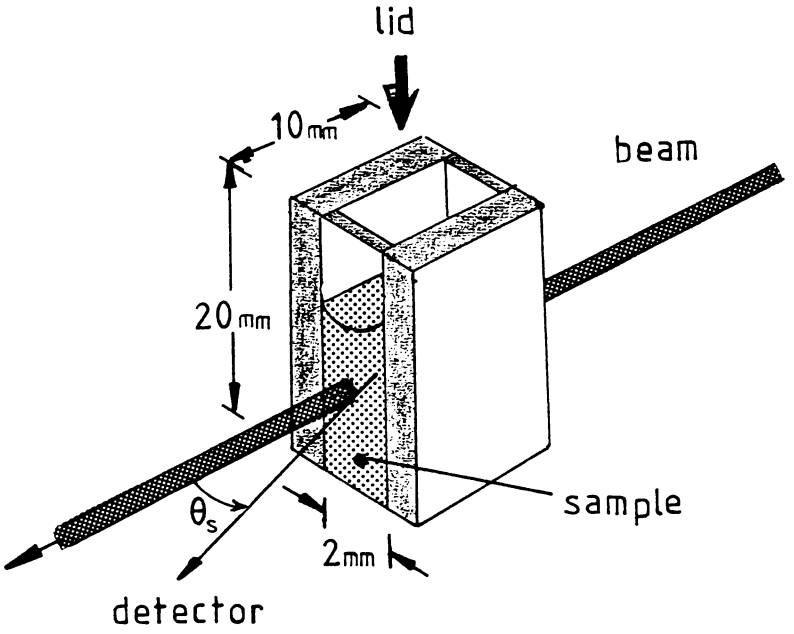

Fig. 3-11. Type A sample cell comprising an open topped spectrophotometer cell partially immersed in a water bath.

The cell was partially immersed (typically to depth 15mm) in a water bath, being located on a slotted pedestal so as to allow removal for

sample changing while retaining its previous physical alignment on replacement. The water bath was temperature controlled by recirculation from a remote reservoir (similar system to that of fig. 3-17 but unpressurised).

The sample cell was only partially filled with sample leaving an airspace of several millimeters beneath the loosely fitting lid. The sample surface was level to or slightly below that of the surrounding waterbath, and the laser beam was located centrally at half-depth within the sample.

This system, while used for preliminary studies, was found to have several disadvantages.

(i) The small airspace above the sample potentially allowed absorption of water vapour from the humid atmosphere existing within the enclosed waterbath with detrimental effects on sperm survival.

(ii) The sample would readily lose nitrogen and absorb oxygen with consequent detrimental effects on sperm survival.

(iii) The existence of a pronounced meniscus at the sample surface, which appeared to produce hydrodynamic disturbances within the sample due to surface tension fluctuations. (Such disturbances were very small but significant).

(iv) The problem of mechanical rigidity in the water bath and the need to remove and replace the cell when changing samples.

3.17.2 Horizontal Plane Immersed Cells (Type B)

In view of the problems encountered with type A sample cells, a totally immersed flow-through cell system was developed, the prototype of which is shown diagramatically in figs. 3-12 and 3-13. The photograph of fig. 3-14(d) shows the cell unit fixed to the lid of the water-jacket, the assembly being removable for cleaning purposes.

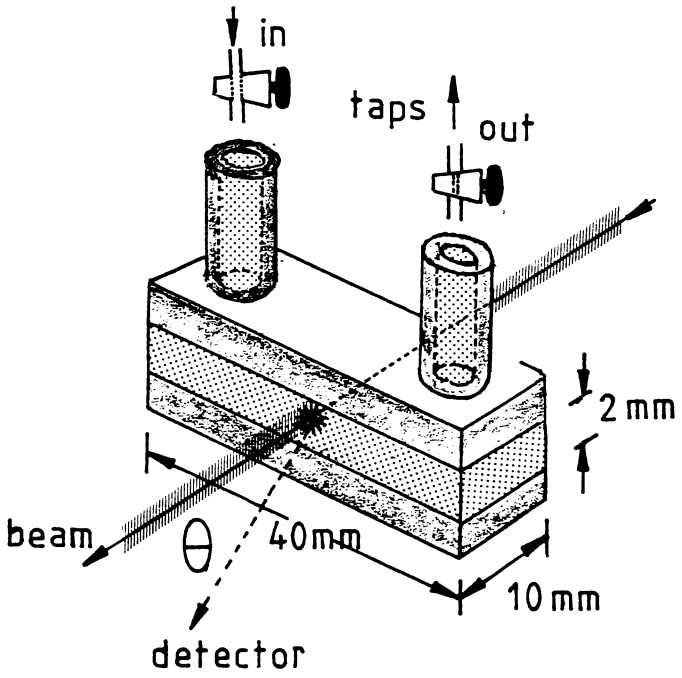

Fig. 3-12. Horizontal plane flow-through sample cell (Type B-1).

The actual sample cell comprised a standard glass spectrophotometer cell of internal dimensions 40mm x 10mm x 2mm. Holes of 3mm diameter were drilled at either end in the top surface of the cell and tubular pedestals cemented over them with an epoxy cement, to form the unit shown in fig. 3-12. These pedestals were then cemented to the glass lid coaxial with PVC sockets which carried small plastic *Lauer* tap fittings.

Unlike the Type A cell the Type B design was enclosed in a pressurised cylindrical water-jacket of internal diameter 90mm and volume 382ml (fig. 3-13) constructed from thick walled glass tubing of good optical quality. The water-jacket was pressure fed with water from a remote reservoir, a system which is further discussed in section 3.19.

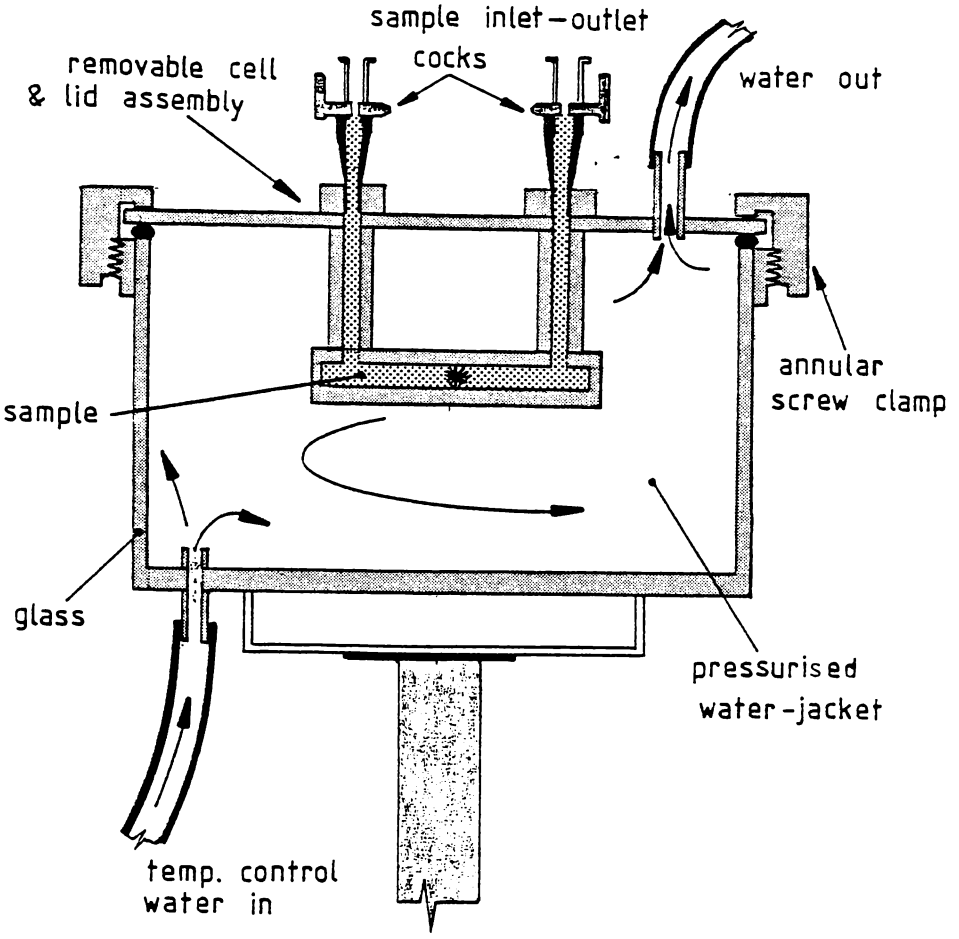

Fig. 3-13. Cross-sectional diagram of the type B-1 system showing the pressurised water-jacket with the flow-through sample cell fixed to the removable lid. Construction was entirely in glass but used a threaded annular lid clamp of PVC.

The sample was injected into the cell from a syringe connected to one of the *Lauer-lock* tap fittings then isolated by closing both taps. There was, therefore, no air/sample interface, and the sample was not subject to disturbances created by free surface effects or external pressures. Further, care was taken to exclude air-bubbles which were readily flushed through and out of the cell by the sample flow.

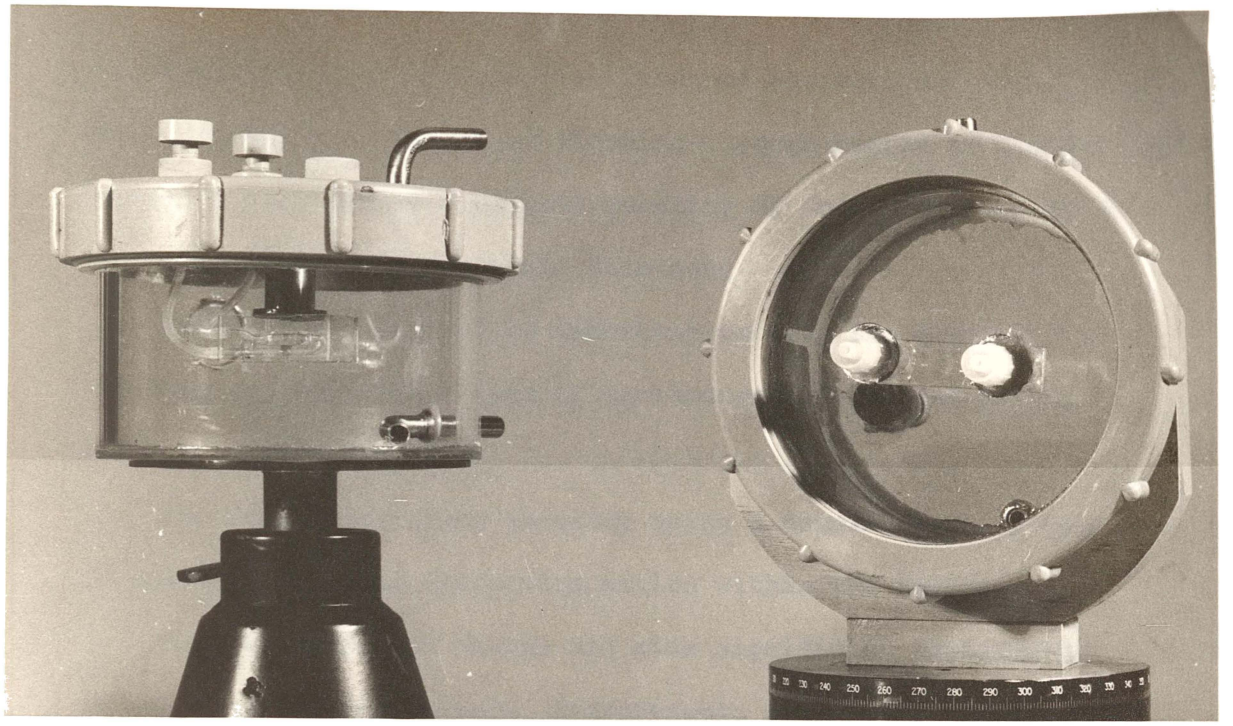

(a) (b)

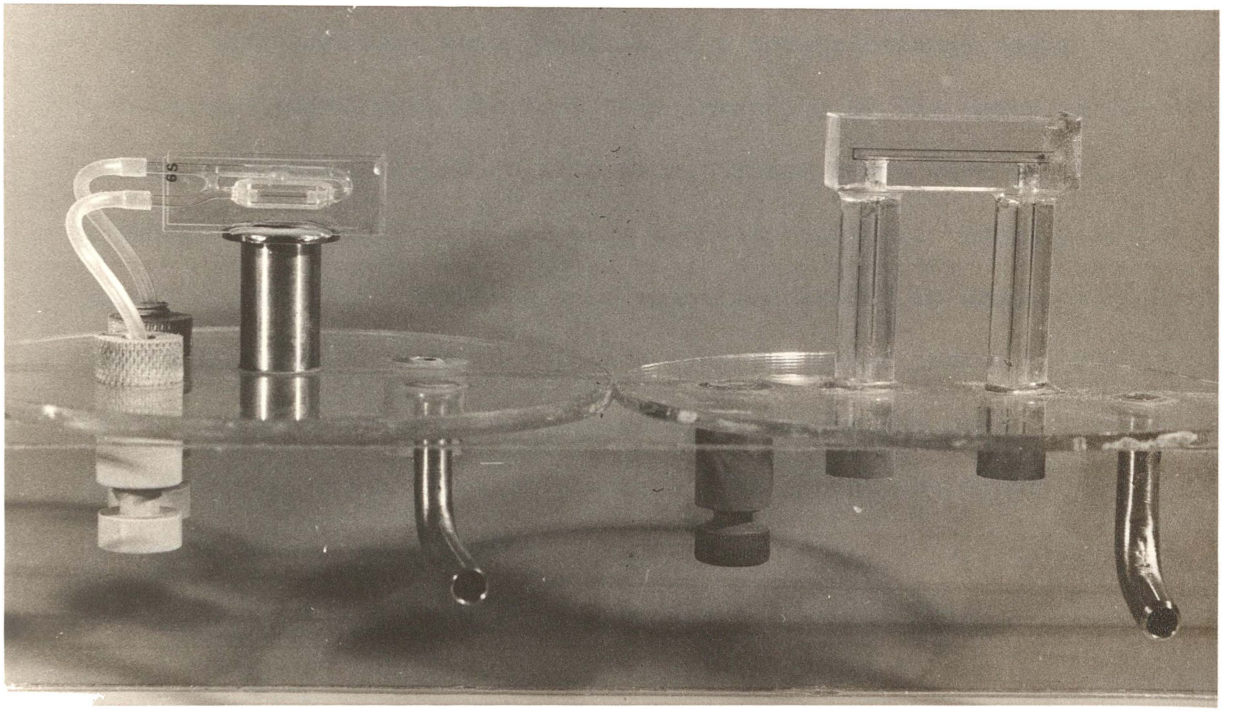

(c) (d)

Fig. 3-14. (a) Assembled sample cell and water-jacket for a horizontal plane type B-2 cell. Not the substantial pedestal and the cylindrical jacket geometry.

(b) Assembled sample cell and water-jacket for a vertical plane type C cell (3.17.3 and fig. 3-16). Note the plane water-jacket windows essential for later photographic studies.

(c) A type B-2 sample cell fixed to the removable water-jacket lid.

(d) The prototype B-1 sample cell fabricated with glass and epoxy cements.

Cleaning of the internal surfaces of the cell was important and was routinely carried out by flushing through buffer or a glass cleaning detergent followed by a liberal quantity of sodium citrate based buffer (Appendix I) as used in sample dilutions.

It was also found to be important to keep the external cell surfaces (windows in particular) free of contaminants deposited by the circulated water.

The horizontal plane geometry using a sample depth of only 2mm was intended to minimise convective motion within the sample.

The type B-2 cell design did give significant improvements in terms of experimental convenience, hydrodynamic stability, sample longevity and data quality.

It did, however, pose problems of a constructional nature which were largely concerned with the long term integrity of the epoxy joints used in the cell-pedestal-lid construction. These bonds were continuously immersed in the waterbath and were prone to failure. Irregularities in autocorrelation functions were sometimes traced to unsuspected microscopic pathways through these bonds from the water jacket to the sample, which generated hydrodynamic disturbances within the cell. Further, use of strong cleaning materials tended to hasten the deterioration of the epoxy bonds (fig. 3-14d).

A type of construction was therefore devised, which eliminated wetted epoxy joints yet retained the same general geometric design. This system utilised a standard flow-through spectrophotometer cell (*Beckman* type 41) which was fixed to a pedestal bonded to the water-jacket lid. (The same water-jacket system was used). Internal dimensions of the sample cavity gave a 10mm path length x 2mm deep and 20mm wide.

The sample was ducted via small bore thick walled nylon tubing from the *Lauer* tap fittings to the inlet and outlet tubes of the cell. Photographs of both this cell (referred to as the B-2 design) and the

previously described B-1 design, as mounted on the water-jacket lid, are shown in fig. 3-14. The assembled water-jacket cell (type B) system is also shown in fig. 3-14(a).

A further advantage of the B-2 cell construction was the thinner cell walls and smaller sample volume which allowed more rapid thermal equilibration and better temperature regulation of the medium and this was subsequently reflected in the improved stability in long time-scale autocorrelation functions.

3.17.3 Vertical Plane Short Pathlength Cell (Type C)

An improved understanding of sperm behaviour (as discussed in section 5.3), within sample cells, led to the conclusion that certain features of this behaviour could be capitalised upon by reducing the light pathlength and reorienting the major plane surfaces of the type B cell into the vertical plane. A simple variation in layout was therefore used wherein a *Beckman* Type 48 spectrophotometer cell, having its two principal plane surfaces polished, was mounted such that these surfaces were normal to the beam, as illustrated in fig. 3-15 and the photograph of fig. 3-14b.

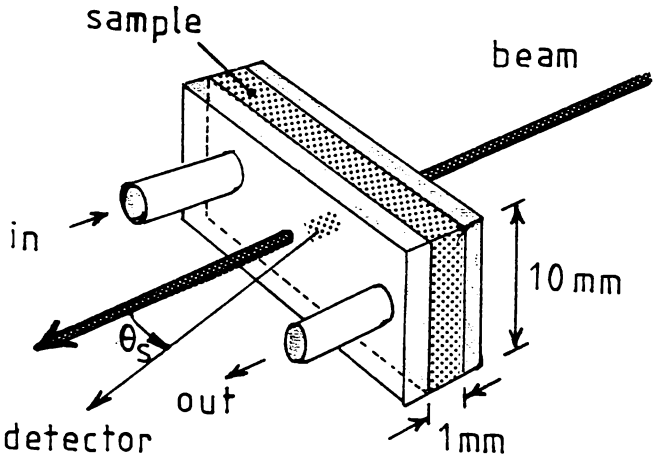

Fig. 3-15. Vertical plane short pathlength sample cell (Type C) finally determined to be the most appropriate cell geometry.

Pathlength in this cell was only 1mm and the design philosophy was that the photodetection system at small scattering angles (< 20°) collected light from the entire illuminated pathlength within the sample. Of particular importance was light scattered from motile spermatozoa in the two regions at the entry and exit windows of the cell.

The cell was used (section 5.13) with a phototube aperture d ≳ the beam diameter W. Although the vertical dimension was 10mm, the hydrodynamic stability of the medium appeared extremely good, possibly due to

the close spacing of the two vertical surfaces and their small thickness which gave a highly uniform temperature distribution throughout the medium.

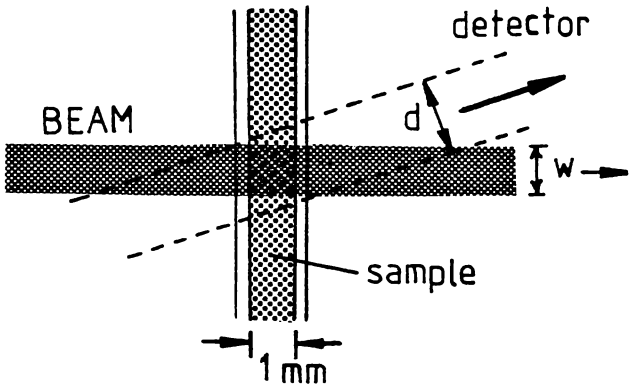

Fig. 3-16. Scattering geometry of the short pathlength vertical plane cell, a horizontal section. Note the illuminated region is entirely encompassed within the field of view of the detector.

It is perhaps of interest to point out at this stage, that the requirement for extremely high temperature stability, primarily concerns not the motile fraction of the sample, but the very slowly diffusing immotile cells.

While these various discussions of cell geometry, orientation and dimensions may seem unimportant, this is far from the case. Phenomena related to the dynamics of spermatozoa suspensions, which became apparent in chapter 5, will in retrospect make the significance of the cell geometry abundantly clear. It is also interesting that none of the reported literature on LBS studies of spermatozoa motility has made specific mention of cell design features.

3.18 Temperature Control System

Since these light scattering measurements were in many cases

concerned with the apparent Brownian motion of dead cells, even extremely slow convective disturbances in the medium would grossly distort their autocorrelation function. For example, in a typical experiment a horizontal convective drift component of even 1μm/s would be sufficient to significantly decrease the autocorrelation decay time for dead cells, and so distort the shape of the function. A highly uniform temperature distribution throughout the sample was therefore found to be essential.

Temperature control was achieved by recirculating filtered and heated water between a water-jacket surrounding the cell and a remote thermostatically controlled reservoir. With type B and C sample cells, the cell was completely immersed in the water-jacket and thus uniformly heated by the large thermal mass of water which was well mixed by the flow. The water-jacket was pressurised to approximately 35kPa which gave a recirculation flow rate of $\sim$ 1ℓ/min and this was found to give adequate thermal stability within the sample.

Water movement within the water-jacket was a potential source of mechanical disturbance for the cell assembly as a whole and for this reason the sample cell unit and ducting (fig. 3-14) were mounted with extremely high rigidity. Even so, mechanical movements of the cell could be induced if the water flow rate was increased to above normal levels.

An essential requirement of the water recirculation system, was found to be the exclusion of contaminant particles down to sub-micron sizes. Such contaminants could introduce intensity fluctuation components into the detected signal, these being on the same timescale as the signals of interest, presumably arising from fluctuations in the optical transmission through the water. Effective filtration was found difficult to achieve and maintain and considerable development went into devising an adequate system. A schematic diagram of the final recirculation and filtration system is shown in fig. 3-17.

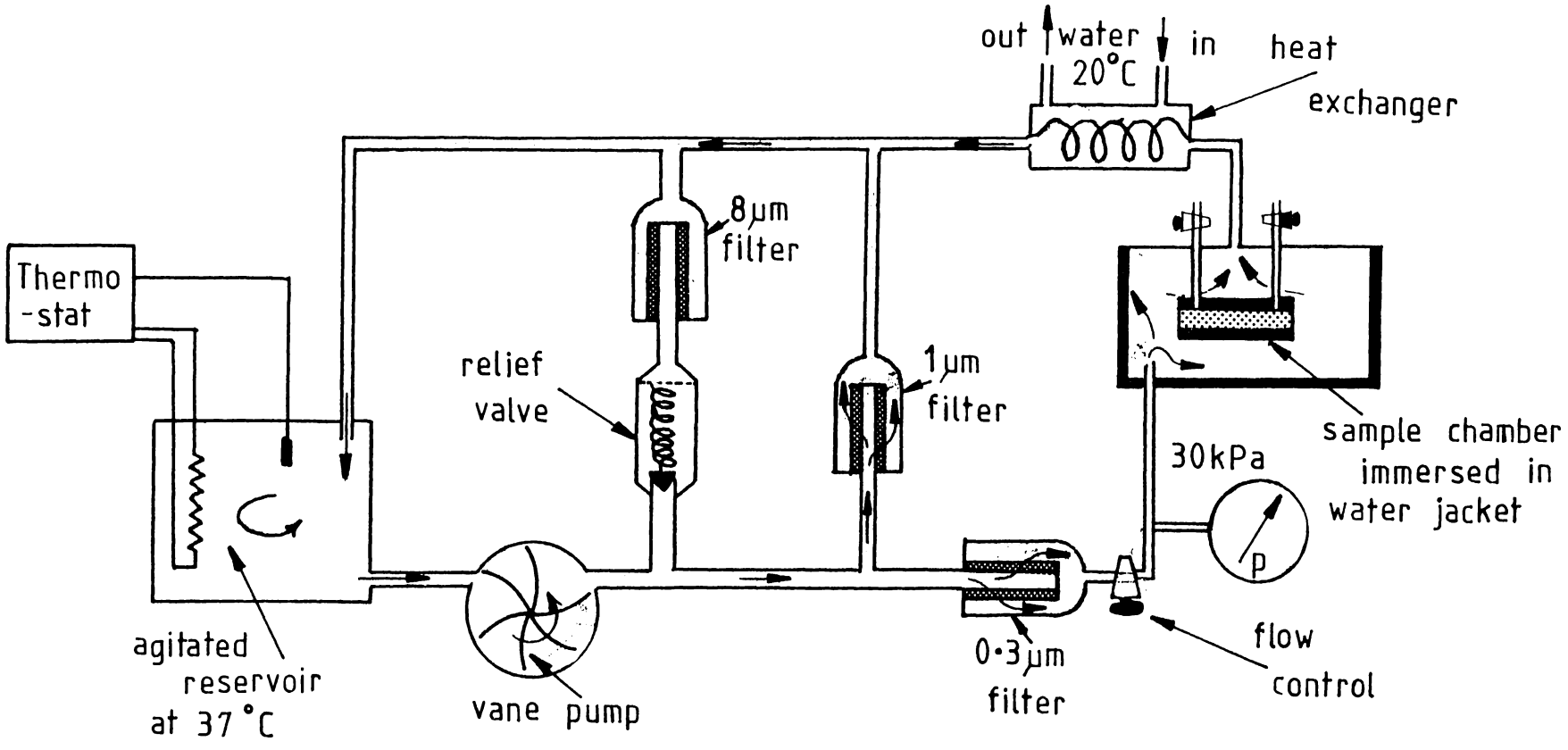

Fig. 3-17. A schematic diagram of the temperature control and filtration system. Water from the thermostatically controlled reservoir is continuously recirculated at a high flow rate through the 1μm filter in the bypass leg and a smaller flow is taken off through a 0.3μm filter to supply the water jacket.

The temperature control of the reservoir was achieved using a *Haake* Model FJ or a *TECAM* Control Unit Controller which both gave long term temperature control of approximately $\pm$ 0.1°c. Water was drawn from the reservoir by a rotary vane-pump (driven by a 350 w electric motor) and continuously recirculated via a *Whatmann's Gamma-12* filter cartridge containing a 1μm element. A lower flow was also taken from the delivery side of the pump via a 0.3μm filter and plastic tubing to the water-jacket. The return water was passed through a small heat exchanger wherein a counter-flow of tap-water at $\sim$ 17°c removed heat from the system to offset the heat input arising from viscous effects in the vane-pump.

The level of contaminants in the water jacket was readily observed in the laser beam and was checked prior to and during experiments. Temperature in the water-jacket was continuously monitored during experiments, using a Digitec Model 5810 digital thermometer having a resolution of $\pm$ 0.01°c. Temperature stability over the $\sim$ 10 min. timescale of a light scattering measurement was typically $\pm$ 0.02°c.

Bacterial growth in the water system was a long term problem, the plastic tubing apparently providing a substrate. This made it difficult to achieve adequate filtration unless a bacteriocidal substance was added to the water and the system was frequently cleaned out. In addition, problems were encountered with the adherence of contaminants to the external cell surfaces which required frequent cleaning. Such external cell contamination increased the background scattering at the windows and was particularly troublesome during the photographic studies of chapter 5.

3.19 Water-jacket Geometry

The glass water-jacket surrounding the sample cell was of cylindrical geometry (diameter 90mm) the sample cell being located approximately

at the centre. This allowed a wide range of scattering angles to be employed. A photograph of this type of water-jacket with a Type B-2 sample cell in place, is shown in fig. 3-14a. However, refraction of the scattered light passing through the curved walls resulted in some distortion of the image formed at the photo-detector screen. This was not normally a problem since the principal features of the image were still readily distinguished, particularly at small lens apertures. Photographic studies, as discussed in chapter 5 could not, however, be carried out with such image distortion. For the initial photographic studies plane circular windows were inserted into drillings in the wall of the water-jacket, and later a redesigned water-jacket, having large plane entry and exit windows, was used. This later design of water-jacket with a type C sample cell is shown in the photograph of fig. 3-14b.

3.20 Thermal Equilibration

With all three sample cell designs, thermal equilibration of the sample was necessary before data collection. Observations of the time dependent changes in the autocorrelation function (viewed in real time) following injection of a sample of non-motile scatterers (i.e., polystyrene latex spheres) was used as an indicator of medium stability. In addition, observation of the speckle pattern created by the forward scattered light on a screen was useful in directly monitoring the stability of the medium. Movement of the medium was clearly evident as directed anisotropic disturbances in the speckle pattern. Using these methods, convective heating disturbances were found to persist for periods of $\gtrsim$ 5 min in type A sample cells, but for $\lesssim$ 2 min in the type B and C designs where the sample was in better thermal contact with the water-jacket.

In the case of the fully immersed type B and C designs, thermal equilibration not only occurred over a much shorter timescale but

occurred with an abrupt cessation of motion as observed in the speckle pattern. The effect appeared consistent with some form of hydrodynamic phase transition.

Using the technique for observing motion of the medium by visually studying the speckle pattern, it was found possible to observe the effects of localised heating of the sperm extender medium through absorption, at higher beam powers.

3.21 Signal Amplification

With the optical geometry employed and the large scattered intensity from sperm cells at small forward scattering angles, the phototube output was not in the photon-event mode but was a fluctuating analogue voltage with a high signal-to-noise ratio. In this respect, the signal differed from most other experiments, as reviewed in chapter 1, which used a digital approach to signal analysis. Consequently, the detector output was amplified by a variable gain voltage amplifier (gain 1x - 100x) with a frequency response 0 - 30kHz, (initially a *Tecktronix Model 7A22*, later a specially designed amplifier based on a *Datel AM201 series* instrument amplifier).

The principal requirement of the signal amplifier was that the D.C. off-set level remain stable over the timescale of a light scattering measurement. A frequency response extending down to 0Hz was necessary since the signal arising from immotile cells was in the very low frequency domain, typically 0 - 2Hz. However, the upper frequency cut-off was not critical since signal frequency components did not extend beyond 1KHz.

3.22 Time-domain signal analysis

The amplified signal was analysed in the time-domain by an analogue autocorrelator. This instrument was a *Hewlett-Packard Model 3721A* correlator operated in the autocorrelation summation mode or occasionally in quasi-real-time using exponential time averaging. This

instrument is particularly suitable for the analysis of analogue signals. It gives 100 point autocorrelation functions with the delay time between channels (dwell time) being selectable over the range 1s - 1μs. For analysis of the detected signal from sperm samples, dwell times of 10 ms/ch or 33.3 ms/ch were used, where either the slow component generated by immotile cells, or the composite two-component (motile and immotile components) function, was to be analysed. Where the short-timescale component arising from the motile fraction was to be studied dwell times of either 1 ms/ch or 0.333 ms/ch were usually most appropriate.

The autocorrelator could be set to analyse for a specific period by pre-setting the total number of signed samples required. For example, the most commonly used settings involved 32768 samples at 10 ms intervals giving a total data collection time of 328 seconds.

As previously mentioned in section 3.21, D.C. stability of the signal amplifier over periods of this order was necessary to minimise baseline drift in the autocorrelation function since the correlator input was D.C. coupled to preserve the low frequency signal components. With good amplifier stability and correct amplifier off-set adjustment for the particular signal level, baseline displacement of the autocorrelation function over a 328s sampling period was typically + 5% of the full scale range. Such baseline displacements were removed by software routines during subsequent analysis of the autocorrelation function. Changes in mean signal level over the timescale of the signal sampling interval resulted in a non-zero D.C. signal level with an associated baseline displacement. Following the completion of signal sampling, the 100 data values specifying the autocorrelation function could be input to a digital computer (see 3.24) which was interfaced directly with the experimental system. The correlator data and commands, were routed through a multiplexed 16 - bit general purpose interface (Harvey, 1976).

In some experiments data sampling by the correlator and processing of the previous autocorrelation function by the computer system proceeded simultaneously.

3.23 Frequency Domain Signal Analysis

The majority of experimental work utilised autocorrelation analysis of the detected signal partly because it was more appropriate to the very low-frequency components generated by immotile cells and partly due to an initial lack of frequency domain instrumentation and software. However, at a later stage of the study, Fast-Fourier-Transform (FFT) software (Lobb, 1976) and analogue signal sampling facilities were implemented on the computer system to give a spectral analysis facility.

Signal sampling was carried out by a 10 bit analogue-to-digital (ADC) converter (*Datel EH10B*) fitted with a sample-and-hold (*National LH0053*). The ADC was interfaced to the computer via the same multiplexed interface that controlled and handled data from the correlator. ADC sampling was initiated by the computer and ran continuously at maximum conversion speed ($\gtrsim$ 10KHz). The sampling rate was then effectively varied by having the computer sample, the ADC output at selected intervals, timed by a real-time clock in the computer.

The software design (Harvey, 1976) was such that batches of 1024 signal samples were collected. These were transferred to the computer memory and the interface immediately set back into the sampling mode while FFT analysis of the signal samples was carried out. Using typically a 1KHz signal sampling rate and batches of 1024 samples, quasi-real-time spectral analysis was possible with the 1.3s transform time for the FFT algorithm. A time averaged spectrum (over, say, 3-5 min) was usually required for an adequate signal/noise ratio.

In comparison with the autocorrelation technique this FFT system had the disadvantage that signal frequencies below 1Hz (the maximum

sampling time was 1.024s at 1kHz), those from the dead cells, contributed little to the spectrum. Lower sampling frequencies did not solve the problem unless a low pass filter was used, since the high frequencies (arising from the motile fraction) were then likely to generate aliasing effects.

However, frequency domain analysis was useful for various studies, some discussion of which arises in the latter part of chapter 5.

3.24 Computer system and data handling

The series of experiments described in chapters 4 and 5 required a computerised data analysis, storage and retrieval system. Each experiment generated a series of 100 - point autocorrelation functions along with numerous experimental parameters and alphanumeric identification characters.

This data was handled by a 16-bit mini-computer (*Computer Automation LSI - 2; 2/20G*) having 32K words of memory and peripherals comprising a dual floppy disk drive, a visual display unit for system control and a general purpose 16-bit multiplexed interface which allowed selection of data input/output channels and data control. Data input could be commanded from the autocorrelator channels or from the ADC. Data output via digital-to-analogue (DAC) converters was used to operate a high resolution *Hewlett-Packard Model 1335A* storage display. This storage display facility allowed autocorrelation functions and frequency spectra to be displayed.

Autocorrelation functions read from the correlator and FFT spectra, together with alphanumeric comments and experimental parameters could be stored on floppy-disk and retrieved for later inspection and analysis. All autocorrelation functions presented in this thesis were directly plotted by the computer system from the disk file onto an X - Y plotter, after appropriate scaling of axes.

It is interesting to record that the experimental programme

associated with this thesis generated a floppy disk data library totalling approximately 10 megabytes.

3.25 Analysis of Autocorrelation Functions

The principal data analysis requirement was the fitting of a base-line displaced exponential to the slowly decaying component of the autocorrelation function. This was carried out by an iterative linear-ising least squares functional fitting algorithm, henceforth referred to as RLQF (Tindel, 1977; listing appendix VI).

The efficiency of this algorithm is illustrated in the results of table 3-2 which show the fit parameters determined by RLQF for various levels of random noise and baseline displacement imposed on a 100pt exponential function generated by the functional form $y = \exp(-2.0t)$ over the range $0 < t < 1.0$, (i.e.,similar to the numerical range of a typical autocorrelation exponential).

That is, the algorithm has been used to fit the synthesised noisy data generated by;

$$y = \{A*\exp(-\alpha*t) \pm E\} + B \qquad (3\text{-}4)$$

with A = 1.0, α = 2.0 and B = -0.10, 0.00, +0.05, +0.10 and +0.20 where E is a random number from a Gaussian distribution having zero mean and standard deviations (σ) of 0, 0.01, 0.025 and 0.05. These numerical ranges were selected as covering the range of variation observed in experimental autocorrelation functions. The fits were carried out using a weighting factor $W_{(t)}$ for the data values

$$W_{(t)} = \exp(-\alpha t)$$

the value of α being determined from a first approximation fit to the data.

The results given in table 3-2 represent the means of fits to four independent noisy functions so as to reveal any bias introduced by the algorithm.

Noise σ	Parameter fitted	Max. RMS fit error	True Baseline Location				
			-0.100	0.000	+0.050	+0.100	+0.200
0.00	B	$< 10^{-6}$	-0.111	0.000	0.048	0.091	0.167
	α	$< 10^{-6}$	2.000	2.000	2.000	2.000	2.000
	A	$< 10^{-6}$	1.000	1.000	1.000	1.000	1.000
± 0.01	B	± 0.012	-0.114	-0.002	0.046	0.089	0.165
	α	± 0.041	1.984	1.987	1.988	1.988	1.989
	A	± 0.015	0.995	0.995	0.995	0.995	0.995
± 0.025	B	± 0.026	-0.119	-0.002	0.043	0.086	0.162
	α	± 0.10	1.958	1.968	1.970	1.971	0.973
	A	± 0.033	0.989	0.990	0.990	0.990	0.990
± 0.05	B	± 0.044	-0.127	-0.013	0.037	0.081	0.157
	α	± 0.194	1.924	1.945	1.942	1.944	1.947
	A	± 0.053	0.980	0.978	0.981	0.981	0.981

Table 3-2. Values of B, α and A for the function 3-4 as determined by RLQF for various levels of Gaussian noise and baseline displacement. The shaded region of the table denotes determinations relevant to the range of variation observed in experimental data.

These data show that for the range of experimental functions (shaded area, $\alpha = 2.0$, $\sigma < \pm 2.5\%$, $0 < B < 0.1$) the maximum error in baseline determination is < 14% and in the decay constant determination < 2%, both parameters being underestimated.

Noise in the experimental autocorrelation functions depended on the total signal sampling time in relation to the sampling rate. Typically, for a 10mS sampling interval, total sampling times of 2.75 - 5.5 min. gave low noise functions with a baseline displacement of < 5%.

3.26 Logistics of Experimentation

The light scattering experiments detailed in this experimental programme were initially carried out using the light scattering and computer facilities made available by Dr. J. D. Harvey of the Physics Department, University of Auckland. However, the samples of spermatozoa were collected and processed at the Newstead Artificial Breeding Research Laboratory of the New Zealand Dairy Board, approximately 140km distant from the light scattering facility.

After preliminary processing (section 3.27), the sperm samples were transported in bulk at high concentration in a high strength extender medium (5% egg-yolk) to the laboratory facility in Auckland. For a typical experiment, the semen would be collected in the early morning (0400 - 0600 hrs), processing completed by 0900 hrs and transported to Auckland, arriving possibly at 1100 - 1200 hrs. On arrival the semen would be 4 - 6 hrs old and the possibility clearly existed that a decline in motility would have occurred prior to the commencement of experimentation. Further, many of these studies depended upon differential staining estimates of the percent dead cells which were carried out on the fresh semen at the Newstead laboratory immediately following collection and prior to dilution into the extender. It had to be assumed that changes in the percent live cells had not occurred during transport. In some cases microscopic monitoring of samples on arrival and during experimentation revealed noticeable deterioration in motility although generally sample deterioration appeared negligible over experimental periods.

However, the logistics of this programme did impose definite limitations on the scope of experimental work. In the later phases of the study, establishment of the necessary laser and computer facilities at the Ruakura Agricultural Research Centre (neighbouring the Newstead laboratory), expedited the progress of the programme by allowing more frequent and extensive experiments with freshly collected and processed semen.

3.27 Semen Collection and Processing

Semen used in these studies was from performance proven Jersey and Friesian bulls. These were the product of selection within the NZDB sire proving programme on the basis of numerous factors, including fertility.

Semen collection was carried out by trained technicians using a heated artificial vagina and conforming to standard commercial practice. After collection and examination by experienced technicians, for acceptable morphology and wavemotion, a differential eosin-nigrosin stain and microscopic count was carried out on the semen to determine the percentage of morphologically live cells. The ejaculate was then diluted with optically cleared and nitrogenated Caprogen extender containing 5% egg yolk (Appendix 1), to a specific holding concentration, normally in the range 20 - 100 million sperm/ml, then sealed under nitrogen for interim storage and transport (see also table 4-1).

Typical ejaculate concentrations, as measured using a *Spectronic 20* U.V. absorption spectrophotometer, for services from these bulls were previously given in table 2-3. Unlike other experiments reported in the literature (which generally used a fixed dilution factor), the experiments reported in chapters 4 and 5 all relate to a specific absolute sperm concentration, and this was based on the initial concentration determination carried out on the undiluted semen. Staining counts of the percent morphologically live cells were generally in the range 80 - 90% and statistical data were previously given in table 2-3. Experiments reported by Hallett, *et al.*, (1978) were carried out with samples having an average of 65% motile on the basis of a visual assessment.

3.28 Sperm extenders

All experiments were carried out using a further dilution from the

holding concentration to give a final sample with a specific sperm concentration (and percent live cells) in an extender of specific egg-yolk content.

The extender medium used for holding and transport was invariably NZDB Caprogen which had been optically cleared and contained egg-yolk at the 5% level. The formulation of Caprogen (Shannon, 1973; Macmillan and Watson, 1975) is given in Appendix I. It is an extender which is particularly suited to maintaining sperm in liquid suspension as required by the NZDB distribution system in the mating season (previously outlined in the Introductory Perspective of page 1). For light scattering studies it was prepared as per standard practice, but filtered to 0.22μm to remove large contaminants and protein aggregates which may otherwise contribute to the scattered field (section 4.4). All primary sperm dilutions utilised Caprogen prepared in this fashion, using freshly prepared and filtered cleared egg-yolk (CEY).

Further dilution to the experimental concentrations was carried out with 5% CEY and citrate buffer (appendix I). For example, to give an experimental sperm concentration of 2×10^6/ml in 0.25% CEY from a holding concentration of 10^8/ml in 5% CEY, a primary dilution of 1:1.5 with 5% CEY would be followed by a secondary dilution of 1:19 with citrate buffer (see also the dilution scheme of table 4-1).

All 5% CEY diluent and sodium citrate buffer was filtered through 0.22μm membrane filters either during or immediately prior to use in dilutions.

Final sperm concentrations in light scattering samples varied depending on the objectives of any particular experiment, but were generally less than 10^7 sperm/ml. Similarly the final CEY concentration depended on the study but was usually < 1%, most commonly 0.25%. With short path-length light scattering cells, CEY concentrations of up to 5% were used;

while in other studies, including the photographic experiments, minimal CEY levels were used (< 0.05%) through high dilutions with sodium citrate buffer.

Contaminants, in particular protein aggregates in the egg-yolk were a potential source of background scattering and the relative level of this background signal was checked frequently. After 0.22μm filtering remaining or newly formed protein aggregates were effectively solubilised by the final sodium citrate dilution.

Seminal plasma as a diluent for bull spermatozoa was considered unsatisfactory. It was not readily available in large quantities, was found to require extensive filtration and gave inferior sperm survival under light scattering conditions.

3.29 Mixtures of live and dead Spermatozoa

For many of the experiments detailed in chapter 4 it was necessary to prepare samples of spermatozoa having a known total concentration and containing a known percentage of dead (*eosinophilic*) cells. This was achieved by mixing an appropriate proportion of dead cells at high concentration with a highly motile sample.

Dead cells were obtained by repeatedly and rapidly cooling samples of motile cells to $\sim 0^{\circ}c$. Cold shock of this type is well known as a means of inducing rapid cell immobilisation and was observed not to grossly affect the cell conformation. The procedure was carried out at high concentrations ($\sim 10^8$/ml) so that only small volumetric additions of dead cells were required to substantially alter the proportion of dead cells in the final sample.

Fresh semen typically contained 15% ($\pm$ S.D. = 6.9%) dead cells (table 2-3) on the basis of an *eosin-nigrosin* differential stain and this count, carried out prior to the initial dilution, was used as a basis for computing the required addition of dead cells. The extent to which this

count changed on dilution to the experimental concentration was not known and could not be measured (*eosin-nigrosin*) staining was not satisfactory in the presence of egg-yolk) although microscopic examination of specimens was routinely carried out to detect any gross changes. Consequently, the calculation of the percent dead cells in mixed samples was subject to any error in the determination of percent dead cells in the basic ejaculate, together with an uncertainty arising from immobilisation of cells on dilution to the final concentration. Such errors, although considered to be relatively small, remained an unknown factor in many experiments since microscopic checks on samples could only reveal large changes. Such an error would not have altered the general features of the results.

Section 2.11 discussed toxic effects of dead cells arising from amino acid oxidase activity which resulted in hydrogen peroxide formation. With fresh dead cells maintained under nitrogen, the short timescale of the experiments was unlikely to have resulted in the accumulation of significant levels of H_2O_2. Dead cells (and their diluent) when mixed with the motile fraction, became highly diluted, as would also be any H_2O_2 components which had accumulated in the suspension.

3.30 Sample cell flushing

Great care was taken to ensure that residues were not left in the sample cell which would influence the survival of subsequent samples. The protein components of the CEY extender were found to adhere strongly to the internal window surfaces. Other contaminants, including dead sperm cells, also gave problems and required strong cleaning materials to remove them from the internal surfaces of type B and type C sample cells.

General procedure was to flush the cell through with $\gtrsim$ 10ml of sodium citrate buffer between samples, the buffer being 0.22μm filtered at the point of injection. Prior to experimental sessions the cell would

be cleaned with chromic acid which effectively removed all internal contaminants and then flushed with several hundred ml of filtered water, followed by 10 - 20ml of buffer.

It was found that great care had to be taken to exclude traces of residual cleaning materials and other contaminants from the sample cell.

CHAPTER 4

RESULTS AND DISCUSSION : Part 1

..... "The universe is full of magical things,

patiently waiting for our wits to grow sharper".....

Eden Phillpotts

4.0 Introductory Remarks

Initial studies, largely those described in this chapter, were primarily concerned with interpreting the features of the autocorrelation function in terms of the percent immotile cells, an extremely important motility parameter and one not readily measured by traditional techniques, particularly at high dilutions. As previously discussed in 3.2, staining techniques for measuring the percent live cells are not effective after dilution of samples into egg-yolk based extenders. This, together with the uncertainty introduced by immobilisation of cells on dilution points to the value of a method which can rapidly measure the percent motile spermatozoa in dilute samples.

Nossal (1971), as discussed in section 1.5, had proposed that the autocorrelation function from a mixture of motile and non-motile scatterers would be of a two-component form (equation 1.32) and this was subsequently observed by Woolhouse (1976). Cooke, Hallett and Barker (1976) commented on the LBS studies of motile bacteria by Nossal and Chen (1972):

> ....."*We have adapted this procedure to the study of spermatozoan motility. The technique allows the determination of the fraction of swimming cells in a given sample as well as their swimming speed distribution. The former quantity is especially important in deciding upon an optimum dilution of spermatozoa for artificial insemination. The technique has been developed to the point where this information can be readily extracted with good reliability.*".....

Consequently, it appeared that the percent immotile cells should be directly obtainable from the amplitude ratio of the autocorrelation components. In fact, Hallett, *et al.*, (1978) had fitted their autocorrelation data with three components said to arise from normal motile swimmers, circular swimmers and immotile cells, the percentage of each type being given by the respective amplitude ratios (equation 1.41).

However, such measurements are difficult to verify due to a lack of alternative measurement techniques and in general it had to be inferred from microscopic observations that results were 'plausible'.

Consequently, rather than attempt to relate light scattering results to other assay techniques (no appropriate methods being available) the approach taken in this work was to prepare samples containing a calculated proportion of live cells by adding appropriate numbers of dead cells to a highly motile (> 80% live) suspension. In this way both the absolute concentration and the percentage of motile spermatozoa could be varied independently. This general technique then forms the basis of the studies described in this chapter, and had not previously been used in other reported LBS measurements on spermatozoa, although Woolhouse (1976) had qualitatively described a close relationship between the percent dead cells in samples prepared in this way and the apparent autocorrelation amplitude ratio.

The initial approach of the experimental work therefore differed from that of most other workers who had been primarily concerned with fitting the motile autocorrelation component so as to extract information on swimming speeds. The view was taken that it was important to be sure that the relative proportions of motile and immotile cells could be characterised before studying the motile fraction, the analysis of which was beginning to appear a well established technique.

4.1 Autocorrelation Functions: General Features

One of the features of autocorrelation functions discussed in following sections, is the relatively long timescale involved. Sampling intervals were typically 10mS or occasionally 33.3mS giving a 100 point function with a total timescale of 1s or 3.33s, respectively. The longest timescale function given in the LBS sperm motility literature is that of Cooke, *et al.*, (1976) reproduced in fig. 1-20(a) which, from the given

experimental parameters, can be calculated to have a timescale of $\sim$ 130mS. Other data such as that of Hallett, *et al.*, (1978) appears to have used even shorter timescales, less than 20mS. It may well be that such workers have in fact collected data on a longer timescale in order to get a satisfactory exponential fit to the dead component, although if this is the case details have not been given. This is surprising since it will become apparent that the timescale of the correlation function is extremely important in characterising the long timescale component associated with the immotile cells and recognising the presence of hydrodynamic instabilities in the sample medium.

As a general introduction, and to give a perspective of the form of the correlation functions which are the primary concern of this chapter, fig. 4-1 shows two normalised and baseline corrected autocorrelation functions on a timescale of 10mS/ch for samples of bull spermatozoa. The upper exponential-like function was generated by an aged sample (apparently 100% dead or immotile cells) while the two-component function was that for a fresh sample containing a mixture of motile and immotile cells.

The most significant feature is the two-component nature of the function for the composite motile/immotile sample, showing a prominent and rapidly decaying peak associated with the presence of motile spermatozoa. The slowly decaying exponential feature was observed to progressively increase in amplitude as the spermatozoa aged, until the 'motile peak' vanished completely. These particular autocorrelation functions (ACF's) were formed over a 328s signal sampling period with the experimental scattering parameter $k = 2.27\mu m^{-1}$ (note the functions of Cooke, *et al.*, in fig. 1-20 appear to relate to $k \approx 2.26\mu m^{-1}$ and covered only a small fraction of the total timescale shown in fig. 4-1).

The motile peak on this timescale is defined by only a few channels and gives no information other than its amplitude. When examined on a

shorter timescale the motile peak is of the familiar form shown in fig. 4-2, similar to functions published by other workers. The function

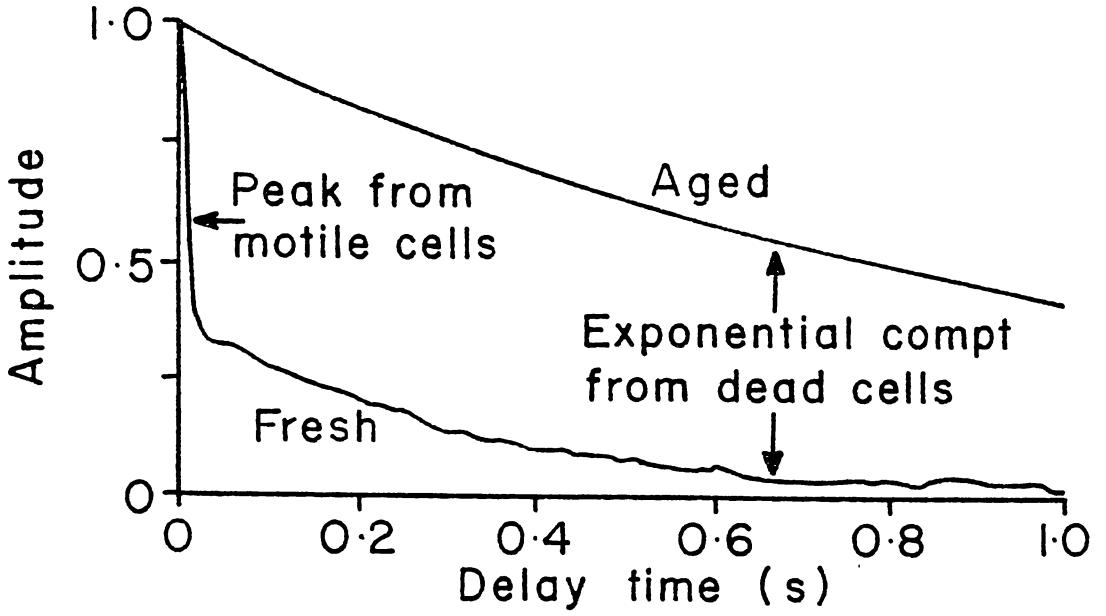

Fig. 4-1. Autocorrelation functions for fresh (2 hrs post collection) and aged (incubated 72 hrs at 37°c) bull spermatozoa. $K = 2.27\mu m^{-1}$, $\lambda = 514.6nm$ (from Woolford, *et al.*, 1980).

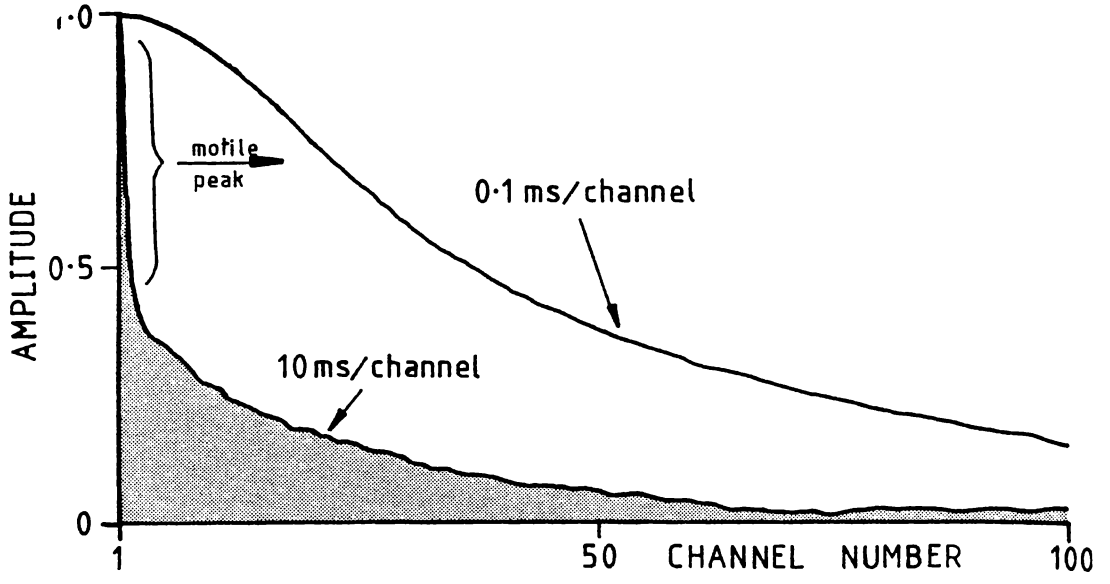

Fig. 4-2. Autocorrelation functions over both long ($0<\Delta t<$ 1.0s) and short ($0<\Delta t<$ 10ms) time scales for the same sample of spermatozoa. The short timescale function defines the functional form of the sharp motile peak evident at 10ms/ch. ($K \sim 2.3\mu m^{-1}$).

is apparently of Lorentzian form having a characteristic half-width at half-amplitude of ∿ 4mS. On this timescale the exponential generated by the immotile cells appears virtually as a baseline displacement of the peak. We will not, for the moment, be concerned with the functional form of this motile component, other than its amplitude and the delay range over which it significantly overlaps the slow exponential.

The significant parameters which characterise the composite ACF taken over a long timescale, such as that of fig. 4-1, are:

(i) the characteristic decay time of the exponential tail.

and (ii) the amplitude ratio of the two components, relative to their respective baselines, amplitudes being determined at $\Delta t = 0$.

as illustrated in fig. 4-3.

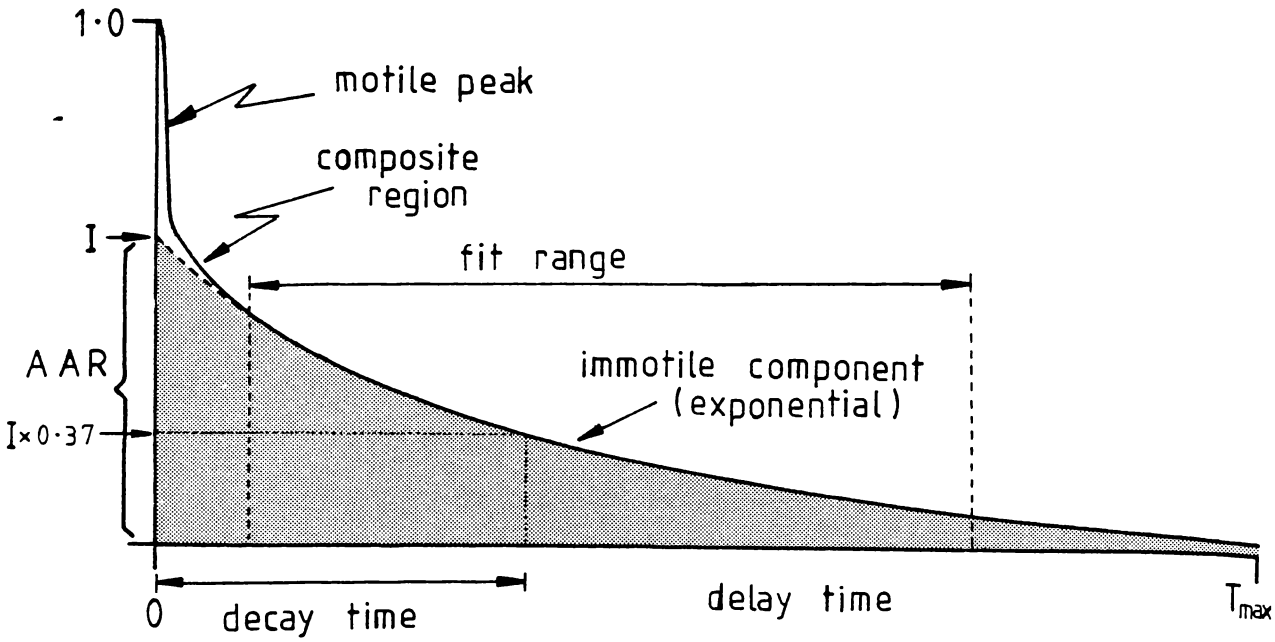

Fig. 4-3. Diagrammatic definition of the significant features of the two-component ACF, defining the autocorrelation amplitude ratio (AAR) and the fit range.

The composite region shown in fig. 4-3 represents the timescale over which the motile component contributes significantly (say > 1%) to the amplitude of the function.

This timescale was found to be 50 - 100ms but depended on the age of the sample. Aged specimens, presumably containing a higher proportion of irregular or circular swimmers (discussed by Hallet, *et al.*, 1978), were found to generate an ACF with an extended overlap region (extending to t = 100ms) and one such example is shown in fig. 4-4. The function in this case was fitted over the range 0.1s < t < 0.8s using RLQF (refer section 3.25), the characteristic decay time and amplitude of the exponential fit being 328ms and 0.65, respectively and the exponential fit is shown superimposed on the function. The third component is clearly evident over the range up to t = 100ms.

The time development of a third component is illustrated in the superimposed correlation functions of fig. 4-5. In this case, all autocorrelation functions are on the same timescale as that of fig. 4-4, but the fitted slow exponential has been subtracted and the residual function plotted. For this sample, which had poor longevity, the progressive development of a motile-associated third component extending over the delay range 0 - 200ms, is clearly evident. Similar functions in fig. 4-6 for a highly motile sample of good longevity, show no evidence of the development of a third component over the 50 min timespan of the functions.

The third component, which was found to be insignificant for fresh samples, was deduced from parallel microscopic observations to result from a fraction of defective swimmers.

Hallett, *et al.*, (1978) appeared to have characterised the same component in their studies, but at a much higher level since their results suggested 24% of cells to be defective swimmers, averaged over all samples. The study described here in section 5.1 used deactivated spermatozoa which is also relevant to the question of this intermediate

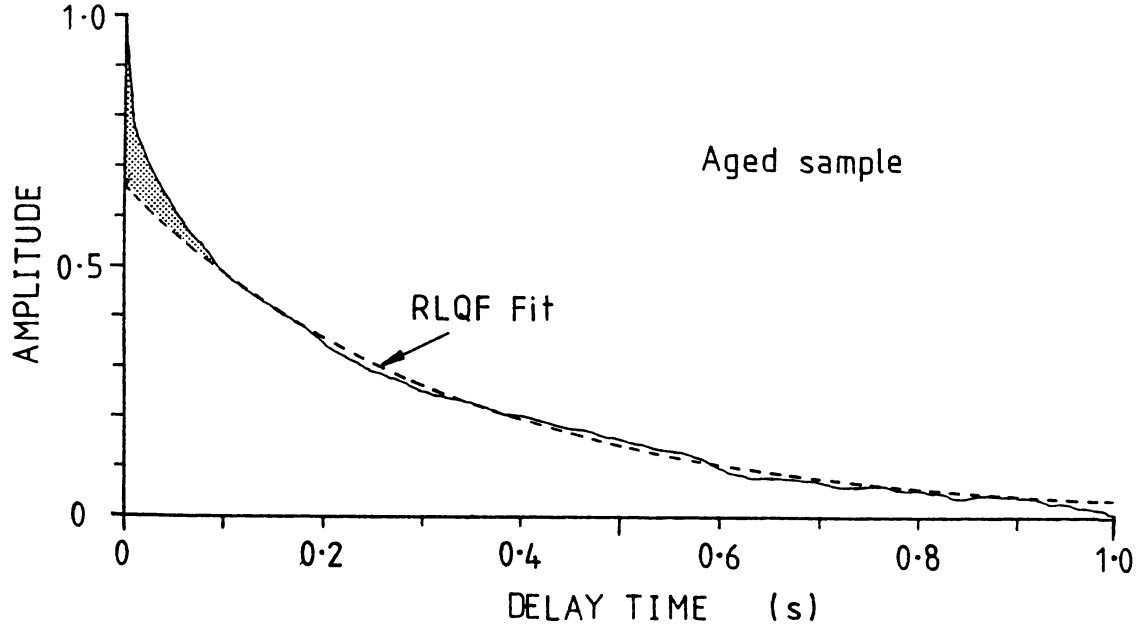

Fig. 4-4. An example of an RLQF exponential fit (dotted line) to the tail of the ACF (solid line), which illustrates the departure from exponentiality in the overlap region t < 100mS. This ACF was from an aged sample of spermatozoa and the overlap region was more extensive than is normally the case for highly motile samples.

timescale component.

So as to avoid errors introduced by this intermediate timescale region, fitting to the exponential tail of the autocorrelation function was generally over the range 0.1s < t < 1s and used a weighting factor W in the RLQF algorithm; W α exp (- At) where A was the approximate decay constant of the tail estimated from a first fit.

Returning then to the parameters which were extracted from the autocorrelation functions, the parameter of principal interest was the amplitude ratio of the autocorrelation components, henceforth referred to as the autocorrelation amplitude ratio (AAR) (illustrated in fig. 4-3). Accepting that defective swimmers, if any, are part of the motile

component, the AAR is simply defined as the amplitude ratio of the immotile component to the total amplitude, at $\Delta t = 0$.

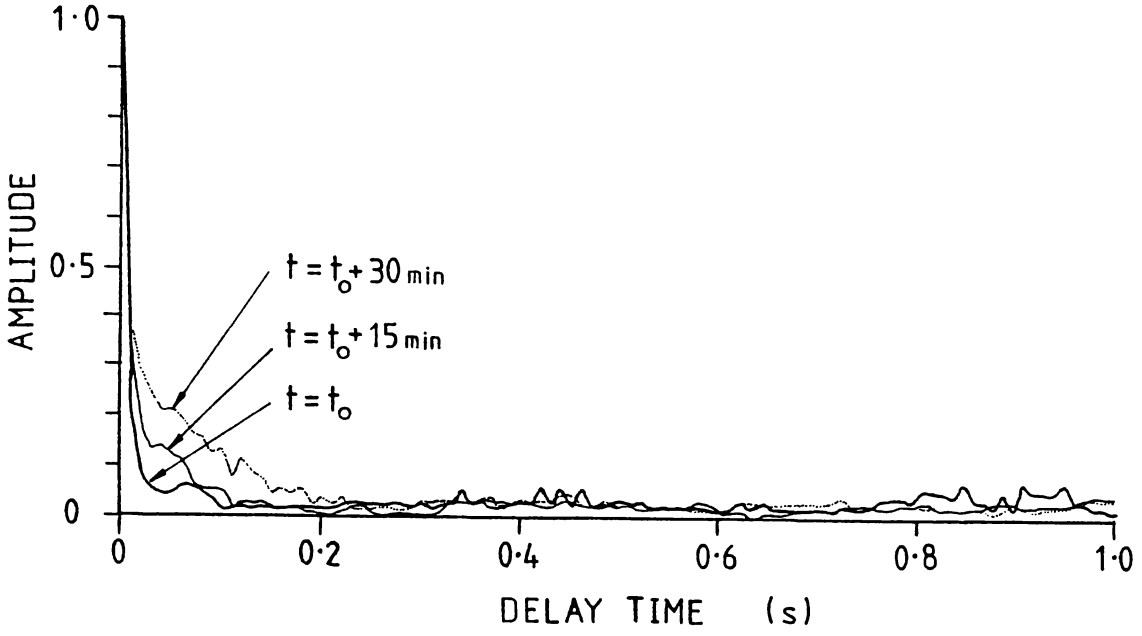

Fig. 4-5. Autocorrelation functions with the RLQF fitted exponential component subtracted. These functions are approximately 15 min apart and relate to the same spermatozoa sample. The growth of a third intermediate timescale component as the sample ages, is clearly evident and was characteristic of samples showing poor longevity. Sample concentration was 2 x 10^6 sperm/ml in 0.01% CEY.

As illustrated in fig. 4-3, this is the amplitude I of the slow exponential component for a normalised ACF when the baseline has been removed. Thus by determining the AAR we do not seek to distinguish between different types of motion, but to characterise the percentage of immotile or dead cells. For this reason in what follows, the term most commonly used is percent dead or percent immotile as opposed to percent live which may incorporate widely differing levels of motility, and the relevant LBS experimental measurement of percent immotile is the AAR.

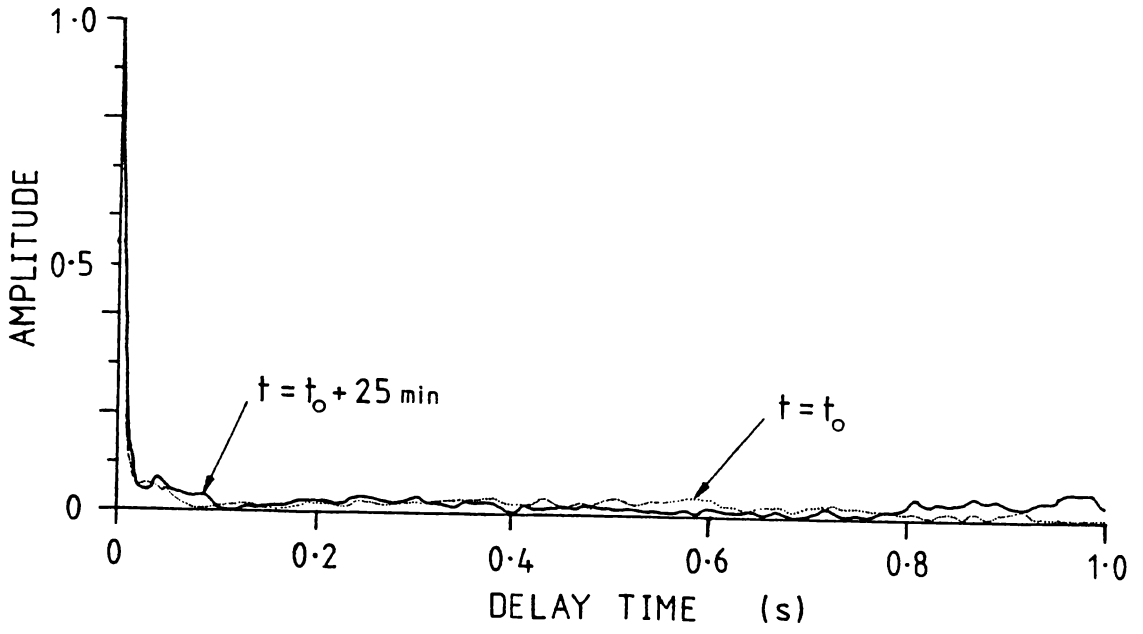

Fig. 4-6. Two sequential autocorrelation functions taken under similar conditions to those of fig. 4-5, but using a sample showing good longevity. There is no detectable change in the region of the intermediate timescale (0 - 200mS) over the 25 minute timescale of the experiment. (Sample concentration was 2 x 10^6 sperm/ml in 0.01% CEY).

Accurate determination of the AAR depended on the accurate location of the baseline by the fitting algorithm. Consequently slow signal fluctuations, arising from contaminants, motions of the medium or electronic problems, could distort the slow component and introduce baseline errors which would, in turn, give an erroneous AAR.

A further type of fitting error (although not common) sometimes arose from apparent truncation of the exponential. Where total signal sampling times were short, or interaction effects occurred, the ACF occasionally had the appearance as illustrated in fig. 4-7, and in such cases when heavy weighting of the data was not realistic, the fit range

was restricted.

An extreme example is later discussed in section 5.10 and illustrated in fig. 5-35.

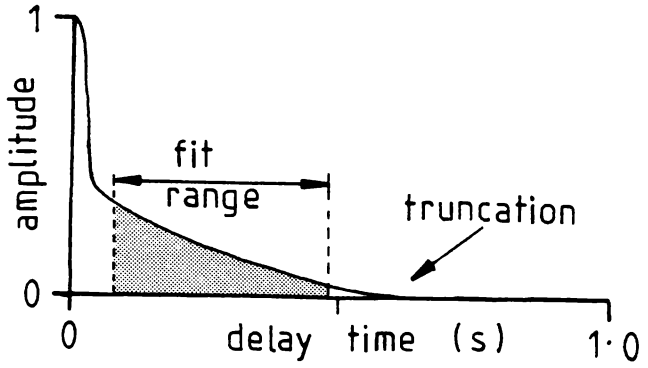

Fig. 4-7. Showing a restricted fit range which was used where data in high channels was excessively noisy or for physical reasons the exponential became truncated. (See also fig. 5-35).

4.2 AAR - Percent Dead Relationship: Preliminary Studies

The argument advanced by Nossal (1971) then subsequently implemented experimentally by Cooke, *et al.*, (1976) and Hallett, *et al.*, (1978) for bull spermatozoa suggested the AAR to be directly related through either a linear or a square law (see later discussion of section 4.8.1) relationship to the percent immotile cells, depending on whether the detection mode was *heterodyne* or *homodyne*, respectively. On this basis, preliminary studies were carried out where the AAR was measured at various levels of percent dead cells obtained by mixing appropriate numbers of live and dead spermatozoa (section 3.29). Such experiments (several were carried out), used a standard total (live + dead) concentration of 10^6 cells/ml in 0.25% CEY and a type A sample cell system (section 3.17.1). The AAR was determined by fitting methods as discussed in section 3.25.

The results were variable. Two experiments showed a one-to-one correspondence between the AAR and the percent dead cells (as might have

been expected for heterodyne detection) while others showed varying degrees of curvilinearity in the relationship. The results of two typical experiments are shown in fig. 4-8 for introductory purposes only. The reasons for the variability in the relationship were not clear, although various factors such as sample degradation (due to storage and transport logistics) and the detection mode were thought to be involved.

Little mention has been made to this point of the origin of the two autocorrelation components. Rather, at that stage it had been assumed that the fast decaying component arose from the isotropic motility of the live cells and the slow exponential component arose from the Brownian diffusion of immotile cells, the view also adopted in the literature.

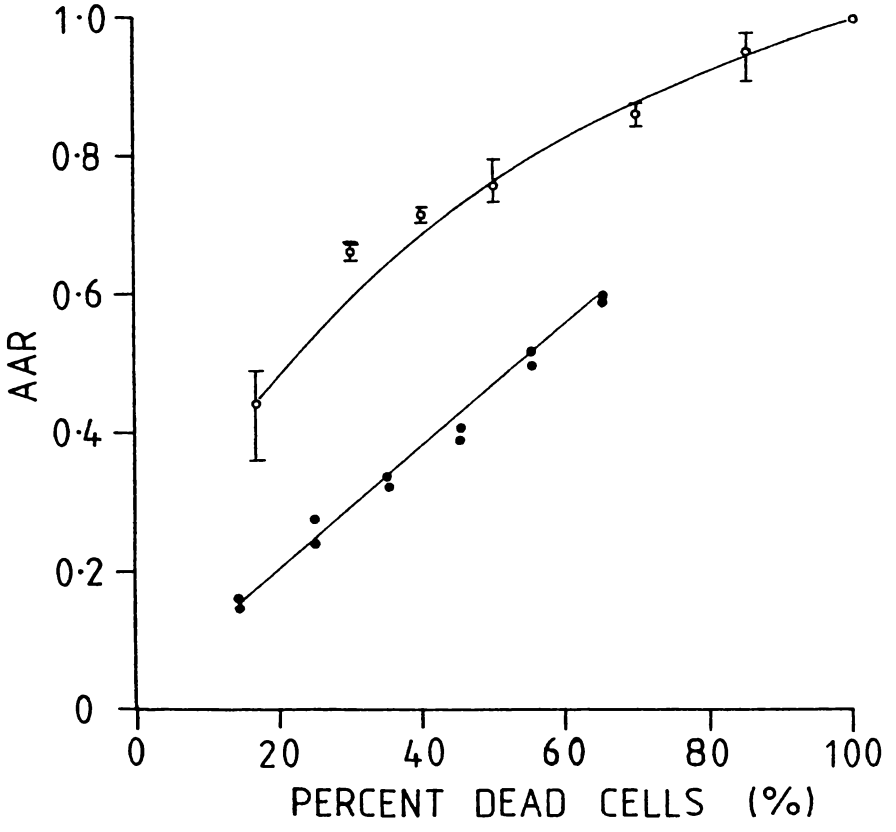

Fig. 4-8. A plot showing the relationship obtained between the AAR and percent dead cells (by mixing) in two early experiments. In both cases the total sperm concentration was 10^6/ml for all points ($K \sim 2.99 \times 10^4$ cm^{-1}). (The mean value and the range are plotted).

The exponential form of the slow component appeared consistent with a diffusion related origin and the calculated diffusion coefficient for a decay constant of 2 s^{-1} (typical in the data) was 1.1 x 10^{-9} cm^2/s. This was assuming a homodyne detection mode which was the most likely, considering the relative scattered intensities from the spermatozoa and from potential sources of local oscillator signal. The diffusion constant was clearly difficult to verify since the sperm head being of asymmetric geometry could not easily be related to the equivalent hydrodynamic radius of 2.97μm computed from the above diffusion coefficient, assuming a viscosity for the medium equal to that of water at 37°c. This hydrodynamic radius gave an equivalent volume of 110μm^3 as against the known volume of the sperm head of ∿ 32μm^3. The larger than expected hydrodynamic radius was plausibly attributable to the effect of the flagellum, a further indeterminate variable of the system.

With this preliminary experimental background and the objective of elucidating the variability in the AAR - Percent dead relationship, a significant experiment was carried out (as described in the next section) and the unexpected result from this experiment really forms the starting point for the arguments presented in this thesis.

4.3 Concentration Dependence of the AAR - Percent Dead Cells Relationship

4.3.1 Background

The preliminary results of section 4.2 along with studies which later came to notice from other groups, indicated that a well defined relationship should be expected between the AAR and the percent immotile cells. However, in the published work there had been no systematic definition of the relationship between the AAR and the percent immotile spermatozoa as given in fig. 4-8. These early studies (e.g., fig. 4-8) had been carried out at a standard sample concentration of 10^6 sperm/ml.

The experiment described in this section had the objective of further defining this relationship and any concentration dependence which it may show.

4.3.2 Methods

The AAR was measured for levels of 15, 45, 85% dead cells at each of five total (live + dead) concentrations over the range (0.25 - 5) x 10^6 sperm/ml.

A type A sample cell (fig. 3-11) was used, the temperature was controlled at 37°c, the scattering angle was 8° and the scattering vector amplitude 2.4μm^{-1}. The 448nm line of an Argon - ion laser was used with the beam waist focussed to approximately 0.75 - 1mm diameter and a phototube aperture of 200μm diameter.

Since the primary objective was to define any AAR/concentration dependence and in view of the extended timescale of the experiment, samples were processed by incrementing the concentration while holding the percent dead cells constant. Checks were also made at intervals for any decline in the motility of the basic bulk sample over the 12 hour timescale.

Samples for light scattering measurements were prepared immediately prior to use by diluting both the fresh sample and the 100% dead sample (both held at high concentration in 5% CEY) with freshly filtered 5% CEY to 20 x the desired final concentration. Appropriate proportions of the two were then mixed to give the desired percentage of dead cells (in 5% CEY), and the mixture was then diluted 1:19 to the desired final sperm concentration in 0.25% CEY. This dilution procedure is shown schematically in table 4-1 and was generally followed in most of the subsequent experiments of a similar nature.

4.3.3 Data Collection and Analysis

During the thermal equilibration phase immediately following sample

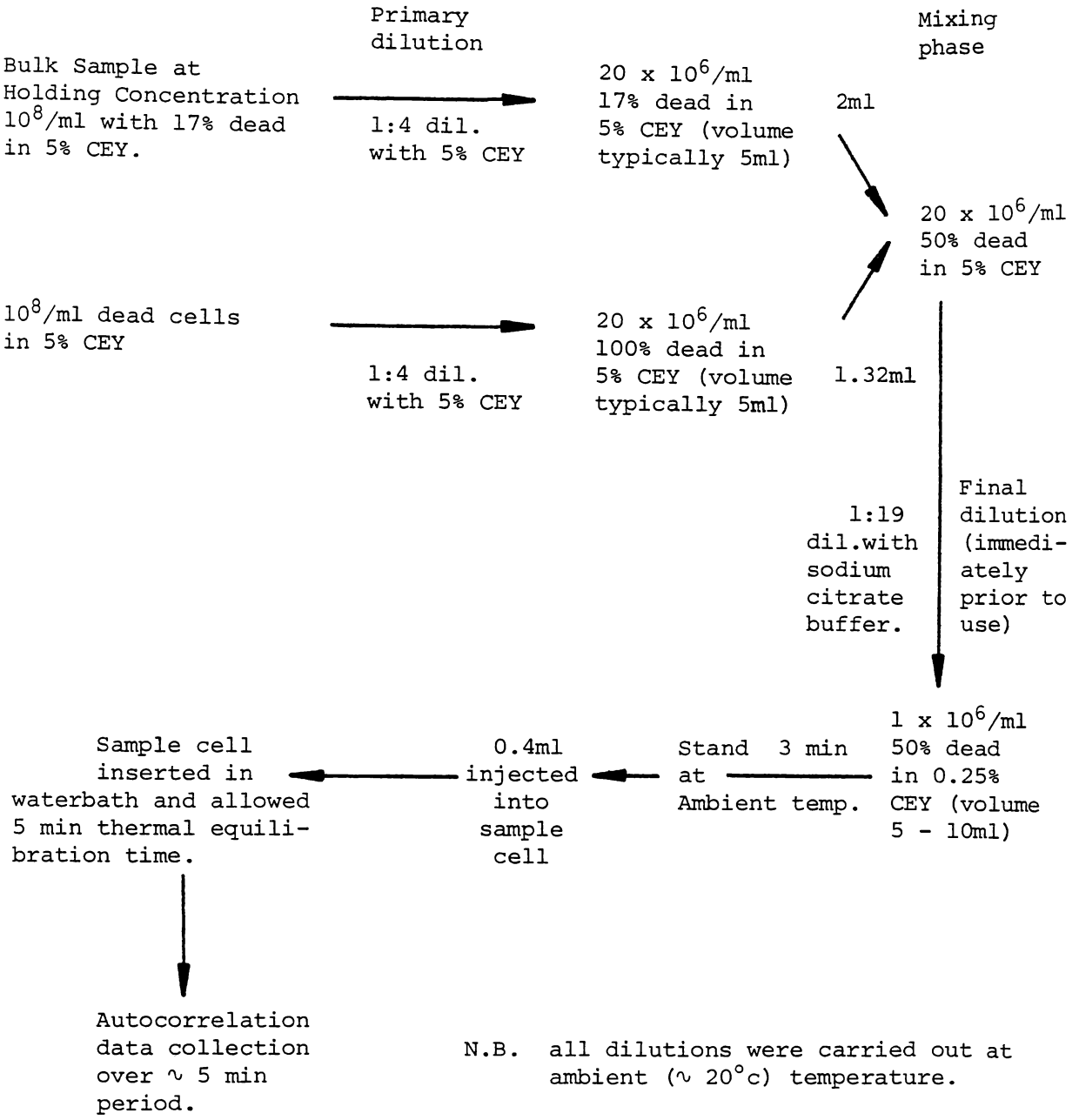

Table 4-1. A summary of the dilution scheme and mixing procedure used in most experiments. Actual concentration levels depended on the particular study. The time required for sample preparation and signal analysis allowed only ∿ 5 samples to be processed per hour.

injection, the signal level at the correlator input was adjusted to the correct amplitude range and to give an approximately zero D.C. level

using the amplifier offset. Close monitoring of the D.C. level was necessary due to the very low frequency signal components which made the true zero of the signal difficult to estimate. Following thermal equilibration autocorrelation analysis was carried out over a 328s period using a 10mS sampling interval. Three sample replicates and hence three autocorrelation functions were taken at each set of sample parameters (i.e., total concentration, percent dead) and were stored on floppy disk (section 3.24).

Analysis of the autocorrelation functions was by the RLQF least squares algorithm as described in sections 3.25 and 4.1.

4.3.4 Results

The AAR was found to depend strongly on sperm concentration as shown in fig. 4-10, this same data giving the set of curves in fig. 4-9 which plot the AAR as a function of the percent dead cells. For lower (< 50%) levels of percent dead cells, it is clear that the AAR shows a very marked curvilinear decline with increasing sperm concentration. Concentration dependent changes in two sets of autocorrelation functions which contributed to these curves are shown in figs. 4-11 and 4-12.

The standard deviation from the AAR mean, taken over all data points was $\pm$ 0.043 and the high level of repeatability of the technique is further illustrated by the range bars shown in the data of fig. 4-10. The data was also suggestive of an increase in the decay constant of the slow exponential component, with increasing sperm concentration, although the variability in the decay constants at higher concentrations precluded any definite conclusions.

This experiment in the same general format was subsequently repeated several times with scattering cells of type A and B design. On each occasion the results were substantially the same as the set presented here

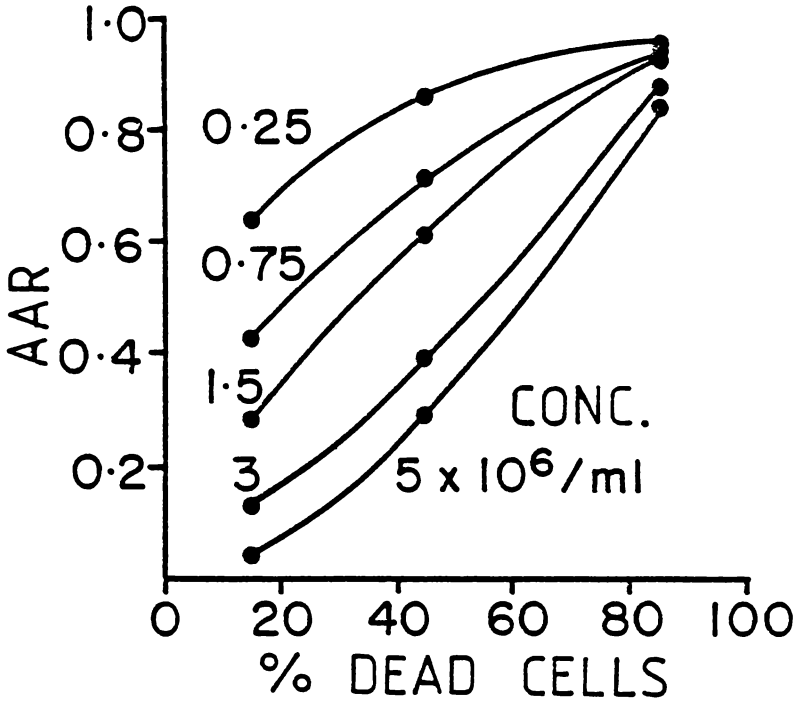

Fig. 4-9. AAR as a function of percent dead spermatozoa over the concentration range 0.25 - 5 x 10^6 sperm/ml.

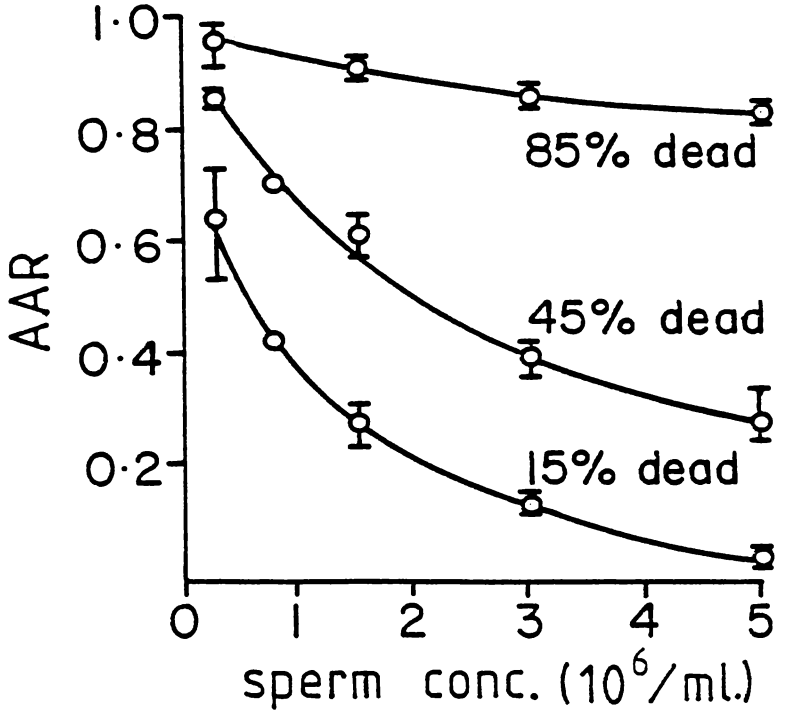

Fig. 4-10. AAR as a function of total sperm concentration, at three levels of percent dead cells. (This is the same data as that of fig. 4-9). Points show the mean and range of three replicates.

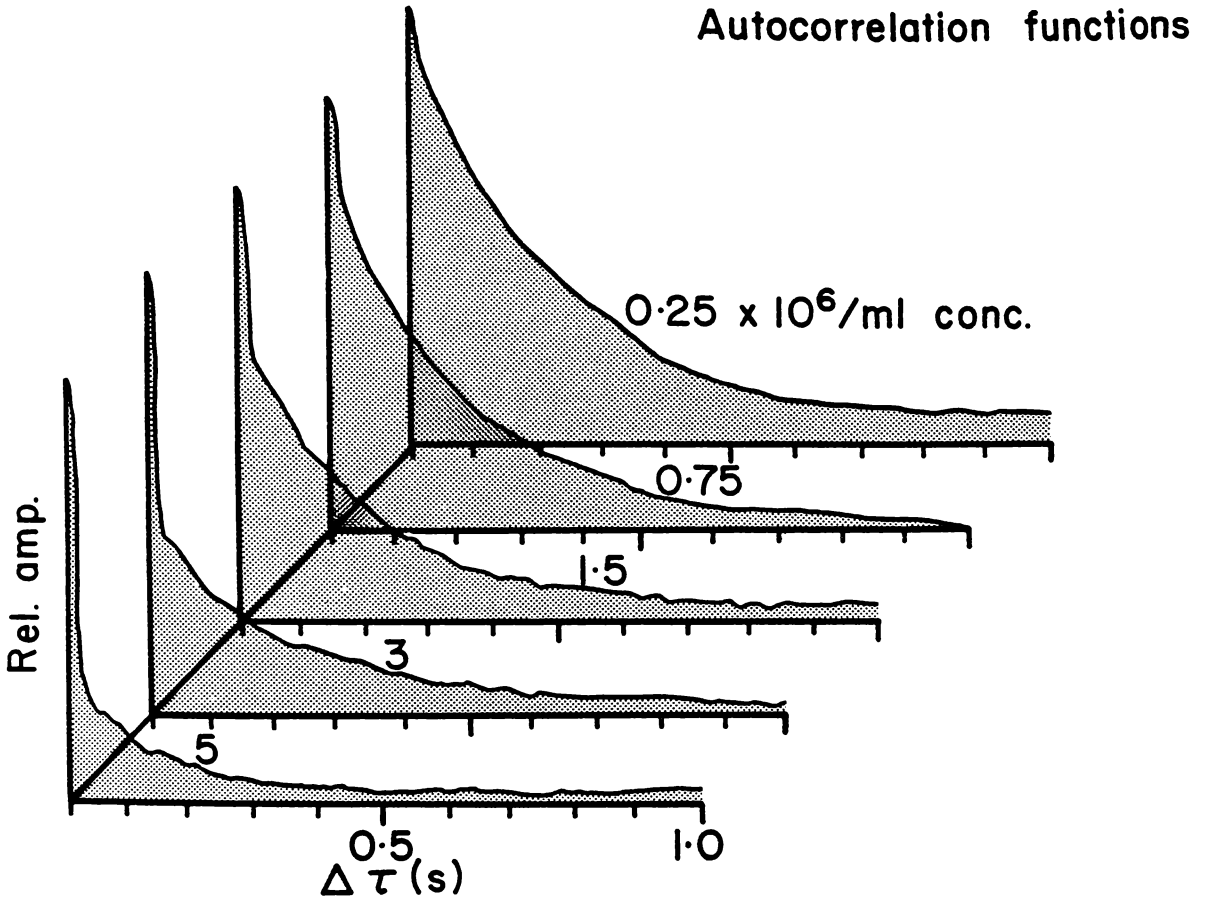

Fig. 4-11. Changes in the autocorrelation functions with total sperm concentration for a fixed level of 45% dead cells.

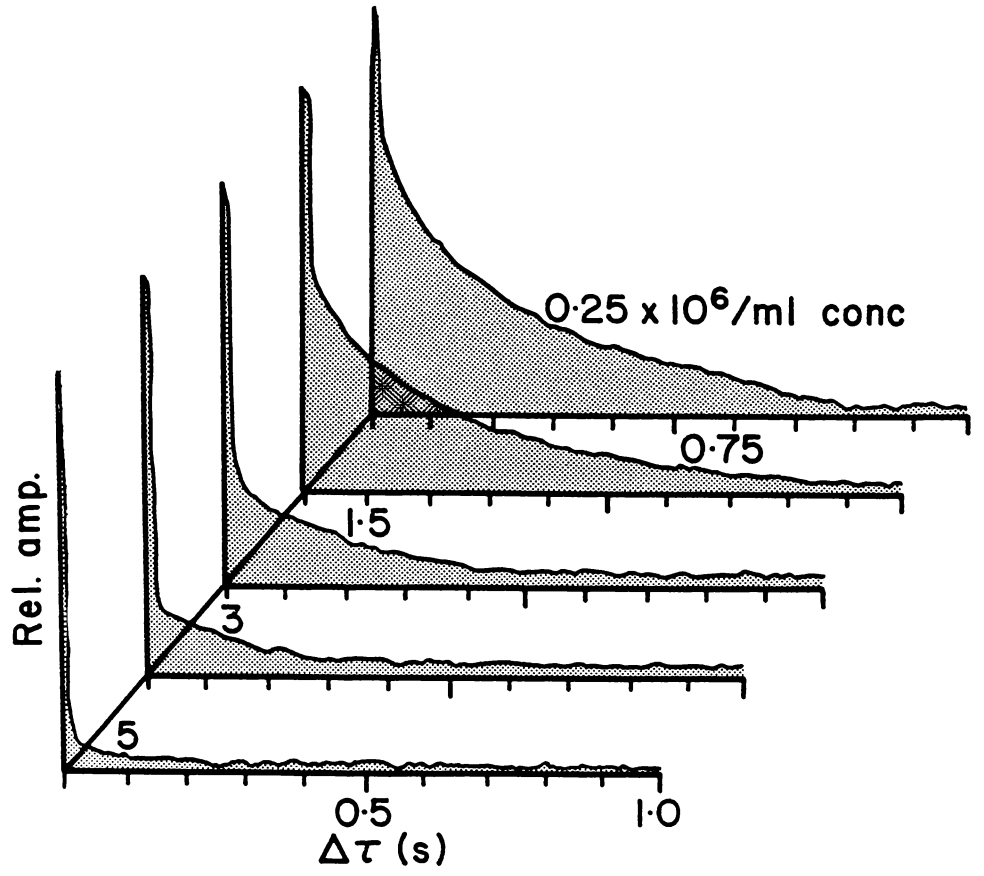

Fig. 4-12. As for fig. 4-11 but at a higher level of motility, all samples containing only a nominal 15% dead cells.

4.3.5 Discussion

The results of this experiment were disturbing to say the least, since published work had *appeared* to generally assume that the AAR gave an absolute measure of the percent dead cells in the sample, by extrapolating the argument of Nossal (1971) to spermatozoa. With the exception of Jouannet, *et al.*, (1977) little attention has been given to sperm concentrations employed in light scattering samples although in several cases the dilution factor (but not the final absolute concentration) was quoted.

It was not clear from the results of section 4.3.4 whether the amplitude changes were occurring in the motile associated ACF component, the immotile associated ACF component, or both.

Several hypotheses were considered to explain the substantial change in the AAR, and hence the apparent percentage of immotile cells, with total concentration:

(i) that the increase in AAR with decreasing total sperm concentration, represented a real increase in the percent immotile cells in the sample, a manifestation of the classical dilution effect. Possibly dilution effects which were normally observed over a timescale of hours (section 2.10), could be enhanced by the environmental conditions in the light scattering cell.

(ii) that background scattering from large contaminant particles in the medium (e.g., protein aggregates in the egg-yolk) became increasingly prominent with decreasing sperm concentration and effectively contributed to the apparent amplitude of the slow ACF component.

(iii) that the detected signal arose, not from homodyne or heterodyne detection of phase components in the scattered field, but from intensity fluctuations generated by variations in the scattering volume population (e.g., after Schaefer, 1974).

(iv) that an increasing collision frequency between motile and immotile cells with increasing total concentration, resulted in a proportion of the immotile population being physically displaced and appearing to the detection system as motile cells.

While a combination of such effects was also quite possible, subsequent experimentation set out to examine these possibilities individually.

The general conclusion from the experiment of section 4.3 was that, while the AAR gave a measure of the percent immotile cells, the relationship was not a simple one and depended on additional parameters which had apparently not been considered in other experiments.

4.4 Scattering from the Extender Medium

4.4.1 Background

Hypothesis (ii) in section 4.3.5 potentially implicated the 0.25% CEY sperm extender medium in the concentration dependence of the AAR through low frequency contributions from contaminants or protein aggregates. The presence of contaminants seemed unlikely since care was taken to filter the extender to 0.22μm prior to use. While the possibility of rapid reaggregation of proteins existed, such aggregates would need to have been up to 6μm in diameter to contribute a diffusion signal on the timescale of the slow ACF component.

However, it was found that the curves of fig. 4-10 could be reasonably well fitted by a function of the form

$$AAR = (D_{(\rho)} + B) / (L_{(\rho)} + D_{(\rho)} + B) \qquad (4.1)$$

where $D_{(\rho)}$ = the autocorrelation amplitude generated by dead or immotile cells (and $\alpha\ \rho$)

$L_{(\rho)}$ = the contribution of the motile component.

and B = a constant background component on the same timescale as $D_{(\rho)}$

Quantitative studies of the ACF contribution arising from typical levels of CEY were therefore carried out.

4.4.2 Methods

The sample cell design and general experimental procedures were as previously discussed in section 4.3.3. The experimental method was that of comparing absolute amplitudes of autocorrelation functions generated by various light scattering samples. All autocorrelation functions comprised the same number of signal samples and were hence collected over the same sampling time. The beam intensity, photo-detector sensitivity and system gain were maintained constant across all samples so allowing ACF amplitudes to be compared. The beam intensity was monitored by a small photodetector throughout each run. Samples comprised:

(i) 100% immotile sperm at concentrations of 0.15, 0.45 and 1.0×10^6/ml in 0.22μm filtered 2% sodium citrate buffer.

(ii) 0.25% CEY filtered to 0.22μm and containing no sperm. Freshly prepared, < 24 hrs old.

(iii) 81% motile sperm at concentrations of 2×10^6/ml and 0.5×10^6/ml in 0.22μm filtered, 0.25% CEY.

4.4.3 Results

The autocorrelation amplitudes are given in table 4-2 expressed relative to that for 100% immotile sperm at 10^6/ml in buffer.

Sample	0.25% CEY (fresh)	100% immotile sperm			81% motile	
Sperm Concentration (10^6/ml)	-	0.15	0.45	1.0	0.5	2.0
Medium	0.25% CEY	buffer	buffer	buffer	0.25% CEY	0.25% CEY
Autocorrelation Amplitude (1)	0.008	0.122	0.456	1.00	0.245	0.285

Table 4-2. Relative autocorrelation amplitudes for the principal components of light scattering samples of spermatozoa.

(1) Mean of three independent measurements.

The data shows the relative signal level from the 0.25% CEY medium to be virtually negligible showing a potential 6.6% contribution to the slow ACF component for a typical case of 15% immotile cells and a total concentration of 10^6/ml. A background signal of this magnitude (B in equation 4-1) could not have generated the concentration effects evident in fig. 4-10. However, associated trials using aged (> 24 hrs. old) CEY at 0.25% and unfiltered fresh material gave an autocorrelation component of significant amplitude (depending on age) and a typical example is shown in fig. 4-13 which compares the amplitudes for filtered and unfiltered material.

In this case, filtering achieved a 4.7 x reduction in the autocorrelation amplitude. It is interesting to note that the autocorrelation component generated by CEY, particularly when aged and unfiltered, is a two component function on a similar timescale to that generated by samples of spermatozoa (fig. 4-12). This suggests the presence of particles with

dimensions in the micron size range although in fresh material the scattering arises largely from very small scatterers which autocorrelation decay constants indicated to have a hydrodynamic radius of ∿ 30μm. The relative contribution at small forward scattering angles and CEY levels of 0.25 - 1.0% was found to be negligible for fresh material.

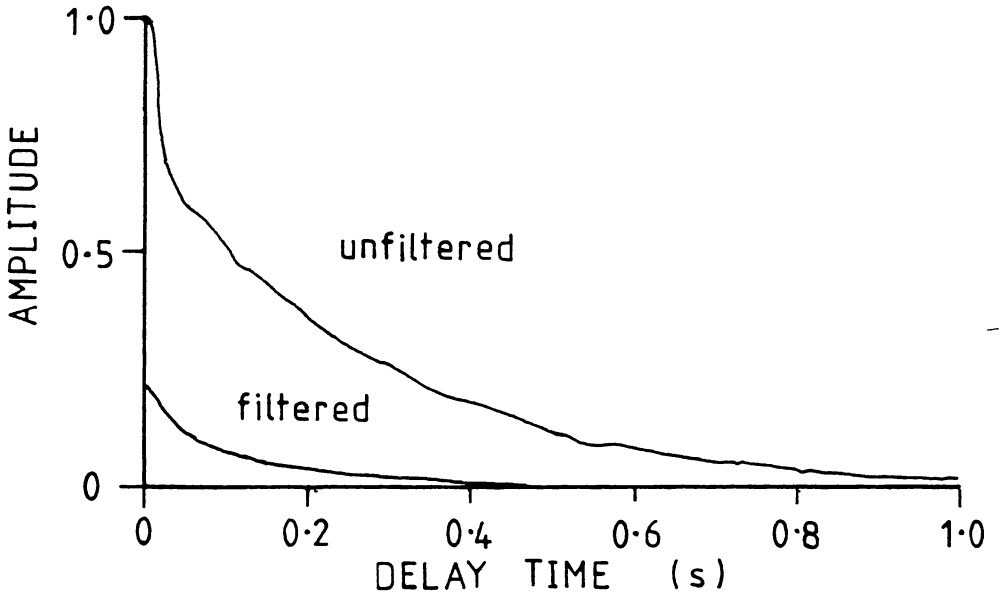

Fig. 4-13. Autocorrelation functions for aged (∿ 48 hrs. old) and unfiltered 0.25% CEY and the same material after filtering to 0.22μm.

Referring back to table 4-2 it is apparent that while 100% immotile samples gave autocorrelation amplitudes which were approximately proportional to the concentration of immotile cells, such was not the case with the 81% motile samples which might have been expected to show a greater difference in amplitude between the 0.5 x 10^6 and the 2 x 10^6/ml concentrations. Further, the relative ACF amplitude of 0.285 for the 2 x 10^6/ml concentration (which contained a nominal 0.38 x 10^6/ml *eosinophillic* cells) was substantially lower than that obtained (0.456) for a suspension of 0.45 x 10^6/ml dead sperm in buffer.

4.4.4 Conclusions

Freshly prepared 0.22μm filtered CEY extender at the 0.25% CEY level gave a negligible scattered intensity in comparison with that from sperm suspensions at typical forward scattering angles in the sperm concentration range of interest. The concentration effects evident in the data of figs. 4-9 through 4-12 could not therefore be understood on the basis of a constant background scattered intensity giving a diffusion signal on the same timescale.

Aged and unfiltered CEY generates both fast and slow autocorrelation components having a similar timescale to that obtained from motile spermatozoa. Attention to filtering of the extender and the use of freshly prepared material is therefore essential in preparing sperm samples for light scattering experiments.

There is evidence in the data of table 4-2 that motile samples give lower amplitude autocorrelation functions than do samples of dead cells, and this suggested that when motile, spermatozoa generate a lower amplitude signal. This particular point is highly significant in relation to results which follow in chapter 5 and it will be interesting to further consider this result in the context of the discussion in section 5.12.

4.5 Fluctuations in Scattering Volume population

4.5.1 Background

As proposed in the discussion of section 4.3.5, it appeared possible that the AAR concentration effect of fig. 4-10 was attributable to an increasing intensity fluctuation component, on the same timescale as the slow ACF component, arising from fluctuations in the scattering volume population. Schaefer (1974) had proposed this intensity fluctuation spectrum as a means of measuring the mean swimming speed of motile microorganisms (section 1.3.2) and published an ACF for swimming bacteria having a timescale similar to that for functions generated by spermatozoa

in these studies. With a decreasing motile sperm concentration, population fluctuations in the scattering volume (and hence fluctuations in scattered intensity) could be expected to increase and provided they were on the appropriate timescale, would enhance the slow ACF component thus giving an increase in AAR. The effect may be expected to substantially increase at low concentrations and could possibly generate relationships such as fig. 4-10. However, as previously discussed in section 3.16, at a total concentration of 10^6/ml and using a detector aperture of 200μm, the estimated scattering volume population was 230 spermatozoa. While it seemed unlikely with populations of this order that substantial fluctuations would occur, particularly sufficient to generate a marked intensity fluctuation component in the spectrum, the possibility was put to the test.

4.5.2 Methods

The procedure adopted was to vary the scattering volume population by changing the observed volume while holding the sperm concentration constant. This was achieved by varying the diameter of the phototube aperture the beam being of larger diameter than the maximum aperture diameter (refer fig. 3-10). The scattering volume therefore, was a long cylinder with a variable diameter.

In this experiment the scattering angle was 12.4°, the wavelength 488nm and the scattering vector amplitude 3.71×10^4 cm^{-1}. A type B-1 scattering cell was used (fig. 3-12),(note this had the same pathlength as the type A cell used to collect the data of fig. 4-10), with the detector system shown schematically in fig. 3-9.

The detector was used at minimum lens aperture with phototube apertures having diameters over the range 50μm - 600μm.

Sperm samples (a fresh sample was used for each aperture change) were at a standard concentration of 10^6 sperm/ml in 0.25% CEY and prepared

as outlined in table 4-1. Correlation functions were all taken using a sampling interval of 10mS, five functions being taken at each aperture diameter.

The diameter of the beam in the cell was approximately 2mm as measured by injecting a sample of small (0.091μm diameter) polystyrene latex spheres to outline the illuminated volume.

4.5.3 Results

Estimated scattering volume populations over the range of aperture sizes utilised are given in table 4-3. The corresponding mean AAR values (with range bars) are plotted in fig. 4-14 as a function of aperture diameter.

	Aperture Diameter (μm)				
	50	150	200	400	600
Scattering Volume† (mm^3)	0.016	0.141	0.251	1.0	2.3
Population of motile sperm	14	120	213	850	1955

† Assuming a scattering volume length of 8mm.

Table 4-3. Estimated scattering volume and motile cell population.

While a small linear change in AAR occurred over the range of selected aperture diameters, the variation was found to be in the opposite direction to that which would have been expected had number (and hence intensity) fluctuation effects become significant in the low population range.

4.5.4 Conclusions

Varying the mean population of motile cells observed by the photo-detector over a range from 14 to 1955 spermatozoa, had no significant

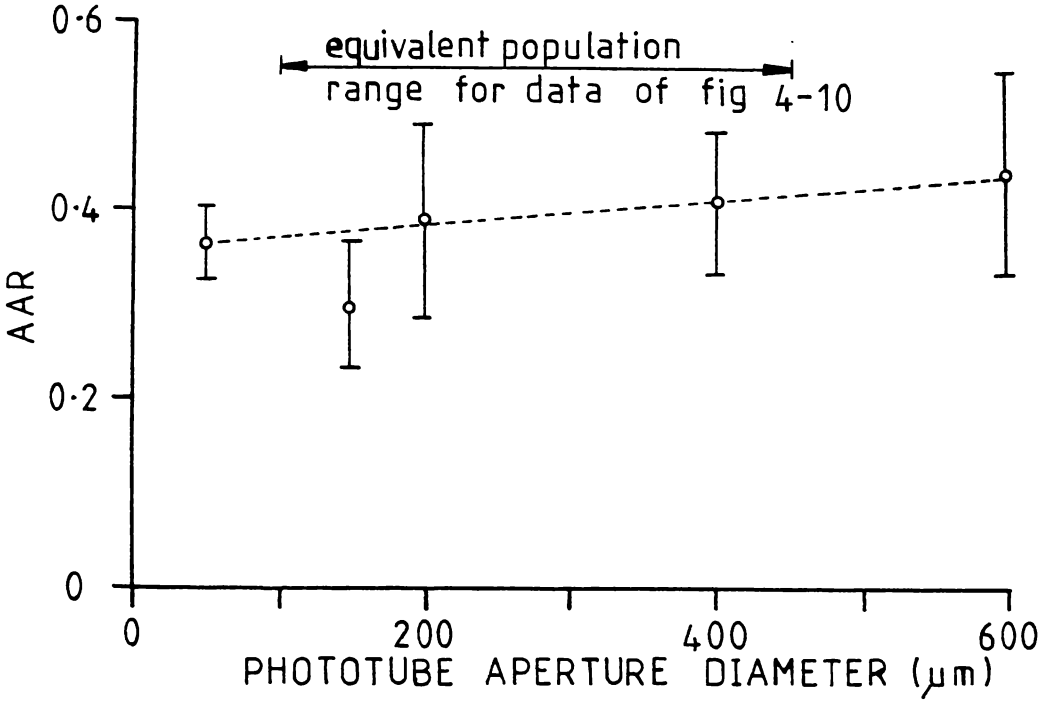

Fig. 4-14. Mean (bars denote range of six replicates) AAR values for a sample of 10^6 sperm/ml (nominal 85% motile) using a range of phototube aperture diameters.

effect on the AAR other than an ∿ 18% linear change which could not possibly account for the gross variations in AAR with concentration which were evident in fig. 4-10.

4.6 Effect of Sample Temperature on AAR

4.6.1 Background

The principal objective of the research programme of this stage was still centred on understanding the concentration dependence of the AAR which the experiments associated with section 4.3 had revealed. If, as was proposed by hypothesis (iv) in the discussion of 4.3.5, collisional phenomena between motile and immotile cells were involved, it might reasonably be expected that the concentration effect would be less marked at a

lower temperature where microscopic observation showed that motile cells moved less vigorously and the percentage of motile cells was lower.

Measurements of the AAR concentration dependence were therefore carried out and compared at *low* and *high* temperatures, specifically at 37°c and at the midpoint between ambient (∿ 20°c) and 37°c, namely 28.4°c.

4.6.2 Methods

The same basic experimental system was used as in previous studies. The sample cell was of the B-1 design, and the photodetector aperture 400μm. The scattering angle was 13.5°, wavelength 488nm (Argon - ion laser) giving a scattering amplitude of 4.04×10^4 cm^{-1}.

The autocorrelation functions comprised 32 * 1024 signal samples at 10mS intervals giving a 328s signal analysis time per sperm sample. A standard 5 min thermal equilibration time was allowed prior to signal analysis. Sperm samples, following standard practice, comprised dilutions from a basic high concentration bulk sample of 10^8 sperm/ml in 5% CEY, with 18% dead (*eosinophillic*) cells on the basis of a differential stain immediately following collection.

Dilutions (mixed immediately prior to use) followed the general scheme of table 4-1 to give total sperm concentrations (live + dead) over the range 0.25×10^6/ml through to 5.0×10^6/ml, in a medium containing 0.25% CEY. The sequence of sample concentrations was analysed first at a temperature of 28.4°c and then at 37.0°c.

In view of the dramatic result obtained in the first attempt at the experiment, the study was repeated and both sets of results are presented here.

4.6.3 Results and Discussion

Two data-sets are presented. Firstly (fig. 4-15a), that from the primary experiment and secondly (fig. 4-15b) that from a replicate of

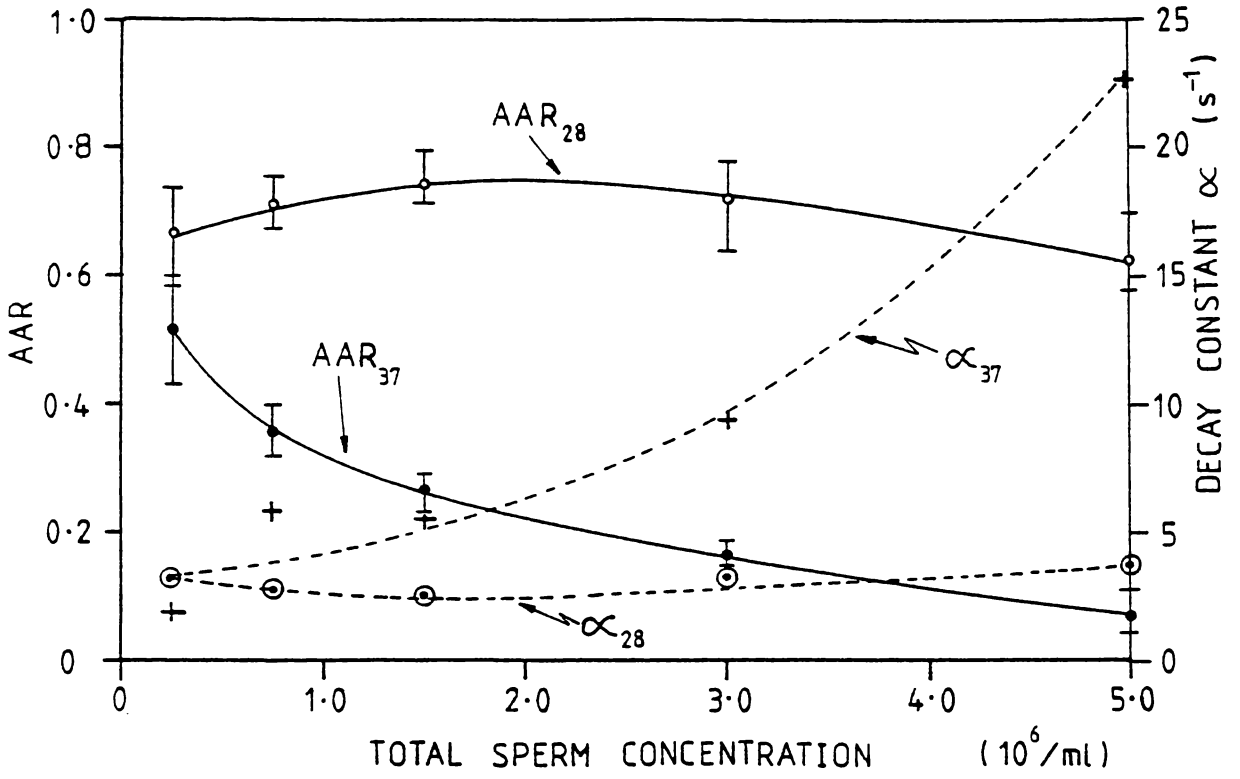

Fig. 4-15(a). Concentration dependence of the AAR and autocorrelation decay constant at 28.4°c and at 37°c for a suspension of 82% live cells.

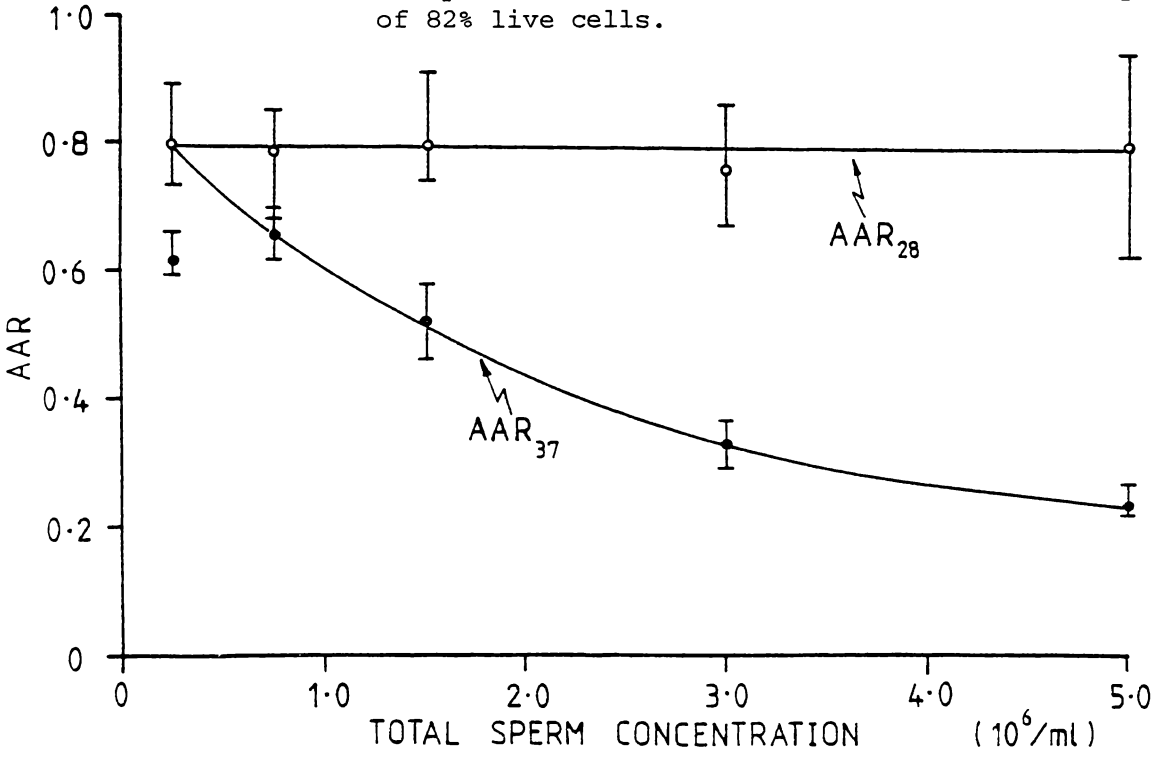

Fig. 4-15(b). A repeat experiment showing AAR trends only. Data points show mean value and range.

the experiment which sought to confirm the initial result.

In both studies, AAR values at 37°c showed the now familiar curvilinear decline with increasing total sperm concentration. It is interesting also to note, that although a type B-1 sample cell was used for these studies, the AAR - concentration curve is closely similar to the 15% dead curve in fig. 4-10 which was obtained using the earlier type A sample cell system.(i.e., the data at 37°c).

The prominent feature of these data is the absence of any significant AAR - concentration interaction at a sample temperature of 28.4°c. At this lower temperature, the AAR remained substantially constant at 0.7 - 0.8 over the entire concentration range. Furthermore, due to the improved hydrodynamic stability in the sample which was achieved with the type B-1 immersed cell design, it was possible to extract with a lower variability, decay constants for the slow ACF component as a function of both concentration and temperature. While in the first experiment of section 4.3 an apparent increase in decay constant was mentioned, in the current experiment a substantial rise in decay constant occurred with increasing concentration (fig. 4-15a) at a sample temperature of 37°c. The decay constant increased by a factor of $\sim$ 10 x over the concentration range 0.25 - 5.0 x 10^6 sperm/ml. It was also highly significant that at a sample temperature of 28.4°c, where no concentration dependence of the AAR was observed, the decay constant of the slow ACF component remained at a constant low value which was comparable to that obtained at the lowest concentration in the 37°c measurements. The viscosity ratio for water between these two temperatures is $\eta_{28.4}/\eta_{37}$ = 1.19 and could therefore be expected to contribute very little to these decay constant changes through its effect on the diffusion coefficient of the immotile cells (assuming the viscosity changes of the extender medium over the temperature range are similar to those of water).

The variability of the AAR data (as indicated by the range bars) was

generally greater at the lower temperature, probably as a result of impaired autocorrelation statistics for the more slowly decaying exponential (autocorrelation in lower frequency ranges requires extended sampling times to obtain the same variance).

The data from these experiments appeared to be consistent with two hypotheses;

(i) that the concentration dependence of the AAR at 37°c was a real effect due to an increasing proportion of cells which were rapidly (within minutes) rendered immotile with progressively higher sperm dilutions. Those spermatozoa sensitive to dilution were immotile at the lower temperature of 28.4°c and therefore no concentration - AAR interaction was obtained at this temperature.

(ii) that with increasing concentration, collisional interactions between motile and immotile cells became progressively more frequent. This may have resulted in immotile spermatozoa being sufficiently perturbed, by either direct encounters or by longer range hydrodynamic coupling, to cause at least a proportion of them to appear momentarily to the photo-detection system as motile cells, and a further proportion to appear as if undergoing enhanced Brownian motion.

Interaction effects should have been characterised by;

(a) a reduced AAR - concentration interaction at lower temperatures where swimming speeds are lower and the proportion of swimmers significantly less.

(b) an increased decay constant for the slow ACF exponential with an increasing population of motile cells and hence an increased level of hydrodynamic perturbations, possibly throughout the medium.

The data of figs. 4-15(a) and (b) is certainly consistent with hypothesis (ii), particularly on the basis of the decay constant results, but

the data may be understood by a combination of both hypothesised mechanisms. It appeared unlikely that the result could be explained by hypothesis (i) alone, since this could not readily account for the changes in ACF decay time.

4.7 Further sample temperature effects

4.7.1 Background

As a follow-up to the temperature/concentration studies of the preceding section, it was decided to:

(i) define the relationship between the AAR and sample temperature at a fixed total concentration of spermatozoa.

(ii) determine the form of the AAR/percent immotile relationship at a temperature of 28.4°c.

4.7.2 Methods

The same equipment and experimental conditions as previously described in section 4.6.2 were used with the exception that the scattering angle was reduced to 10° (this was not expected to have any significant effect) and hence the scattering vector amplitude $k \sim 3\mu m^{-1}$. In the case of phase (i) a fixed sample concentration (total) of 10^6 sperm/ml in 0.25% CEY was prepared and the sample temperature incremented in steps ∿ 4°c. A freshly diluted sample was injected on attaining each temperature level and a period of 11 min. was allowed for thermal equilibration before autocorrelation data was collected. The extended equilibration time (previously at 37°c 5.5 min was used) was found necessary at the lower temperatures where convective motions appeared to take longer to heat the sample, presumably due to the higher viscosity.

In the case of part (ii), the AAR - percent immotile study, the standard procedure for this type of experiment as first detailed in section 4.3.2 was followed, but with the modification that it was carried out at

sample temperatures of both 37°c and 28.4°c. This sector of the extended study therefore examined the AAR - percent immotile relationship in the 1 x 10^6/ml region of figs. 4-15(a) and (b) where samples of ∿ 82% live cells had been employed.

4.7.3 Results and discussion

By way of illustration, fig. 4-16 shows the changes which occur in the autocorrelation function from immediately following sample injection to the establishment of thermal equilibrium. This particular set of functions corresponds to a final sample temperature of 24.7°c and each function represents the cumulative result of a 5.5 min. signal sampling period. At lower temperatures such as this, the establishment of thermal equilibrium in the sample was observed to take a longer period of time and the oscillatory features evident in functions #1 and #2 are characteristic of convective disturbances in the medium. All functions are relative to the true zero baseline.

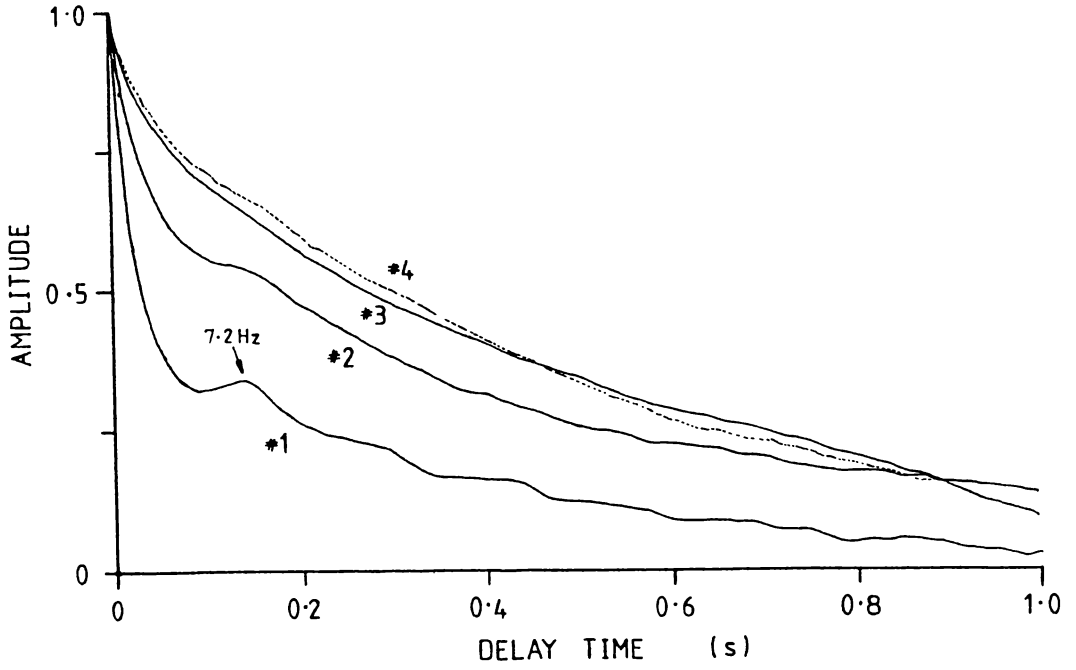

Fig. 4-16. Consecutive autocorrelation functions each of 32 * 1024 samples (i.e., duration 5.5 min.) immediately following sample injection. Final sample temperature was 24.7°c.

The progressive approach to a steady-state autocorrelation function is clearly evident, requiring a timescale of $\gtrsim$ 11 min. at this temperature.

Results corresponding to part (i) of the study are given in fig. 4-17 and showed a curvilinear decrease in the AAR as the sample temperature was increased over the range 24.7°c - 41°c. This was consistent with parallel microscopic observations which (qualitatively) also showed substantial changes in the level of motile cells over the same temperature range.

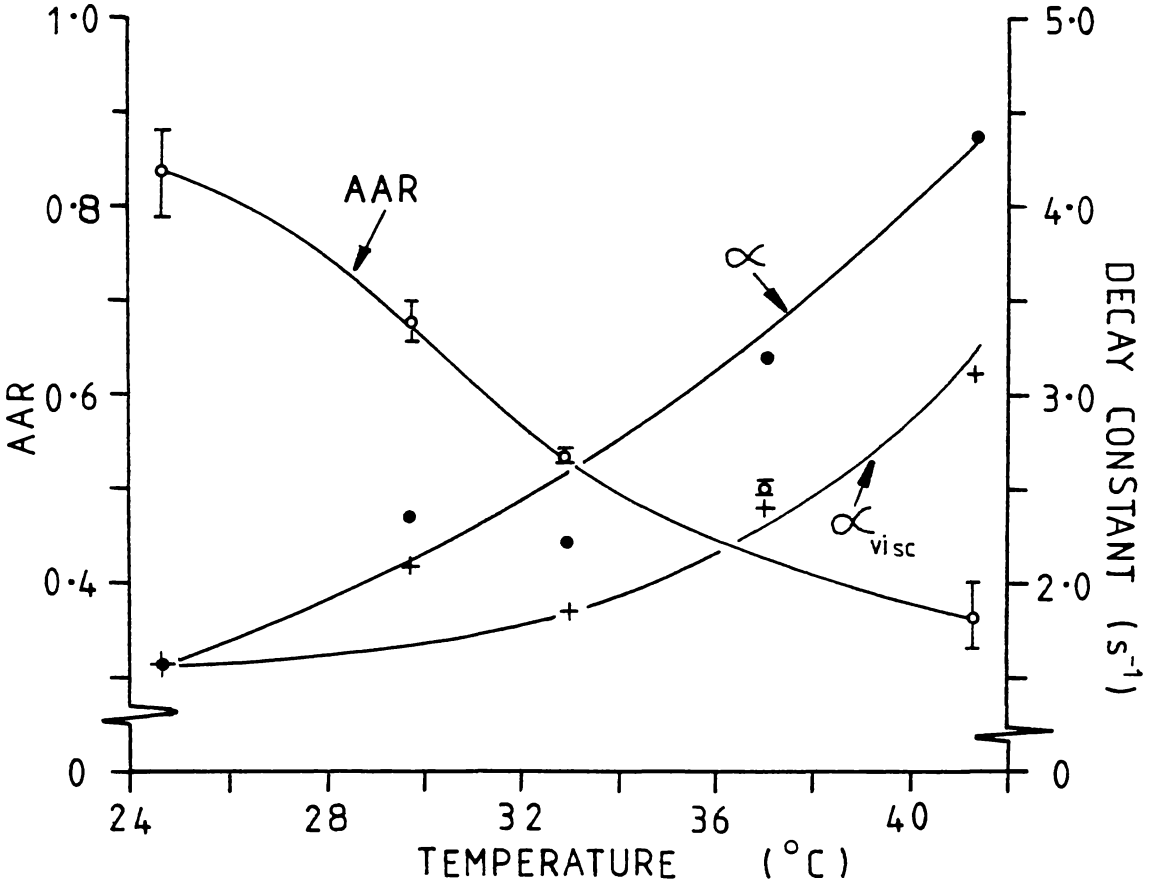

Fig. 4-17. Temperature dependence of the AAR at a fixed sample concentration of 10^6 sperm/ml in 0.25% CEY. Changes in the ACF decay constant are shown both with (α_{visc}) and without correction for medium viscosity.

While the duplicates in AAR determinations were in close agreement, large variations occurred between duplicate decay constant values. However, the trend apparent in the means was strongly suggestive of an increase in

decay constant over the temperature range, even after correction for viscosity changes. In referring back to the previous results of fig. 4-15(a) it is apparent there that the change in decay constant between 28.4°c and 37°c at a concentration of 10^6/ml was relatively small and of the same order as that apparent in fig. 4-17.

Results from part (ii) of the experiment are shown in fig. 4-18.

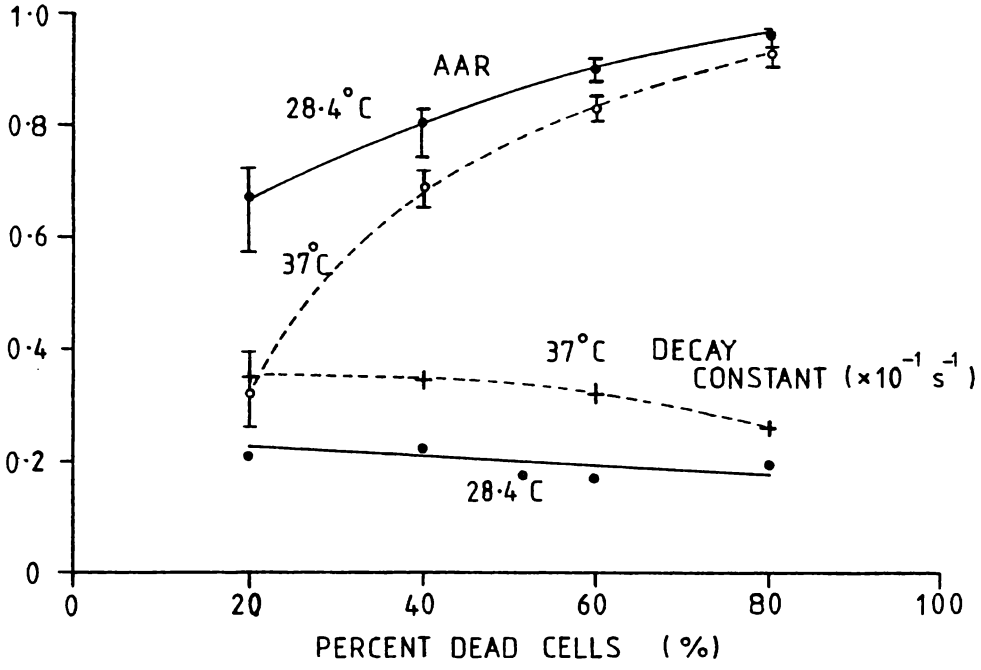

Fig. 4-18. Results from part (ii) of the experiment showing the AAR - percent immotile relationship at both 37°c and 28.4°c. The decay constants were substantially constant over the range at both temperatures.

The percent immotile scale as drawn is not true in an absolute sense at 28.4°c and the form of the relationship is what might be expected if at the lower temperature an increased percentage of spermatozoa were immotile. The results were consistent with the data of fig. 4-17. The decay constants for the slow ACF component were consistently lower at

28.4°c and those at 37°c showed a small decline as the relative level of motile cells declined. A decrease in sample temperature generated a rise in the AAR as did also a decrease in concentration in the data of fig. 4-10. In general these results were consistent with interaction effects between motile and immotile spermatozoa.

These experiments quantitatively demonstrated that the light scattering AAR changed substantially with sample temperature. It is therefore interesting to reflect on the experiments of Hallett, *et al.*, (1978) who used a sample chamber thermally regulated at 30 $\pm$ 0.5°c and over all 88 semen samples which they studied, obtained on average, 53.5% motile cells as derived from their AAR measurements. The data of fig. 4-17 suggest an equivalent value of $\sim$ 35% motile at 30°c on the basis of the relative amplitude of the motile ACF component but is specific to the sample used.

4.8 AAR - Concentration interaction at higher concentration

4.8.1 Background

Previous data (figs. 4-10, 4-15) had revealed a remarkable concentration dependence of the AAR in the concentration range 0.25 - 5.0 million sperm/ml. Of the possible explanations for the effect, the two most likely appeared to be;

(i) a real dilution effect wherein a proportion of cells became rapidly immobilised on dilution to the light scattering concentration.

(ii) interaction effects, wherein swimming cells perturb immotile cells such that they either appear to the photo-detector as being motile, or undergo an enhanced Brownian motion, or both.

In the circumstances, it seemed that a further experiment aimed at exploring the phenomenon in the higher concentration region, would be informative. If, in fact a real dilution phenomenon had been involved

in fig. 4-9, then it might be expected that at higher concentration levels (say > 5 x 10^6/ml), the AAR - concentration interaction would be markedly diminished and tend towards the predicted relationship between the AAR and the percent dead cells. The objective of exploring the high concentration behaviour of the slow ACF component was also of interest since as is apparent in fig. 4-12, the exponential feature of the ACF became much less well defined at a concentration of 5 x 10^6 sperm/ml (15% immotile).

The traditional model, (first suggested in a general sense by Nossal (1971), for a mixture of motile and immotile scatterers, and subsequently used experimentally by Cooke, *et al.*, (1976); Hallett, *et al.*, (1978)) predicted a two component autocorrelation function (ignoring interactions)

$$G^{(1)}_{(\tau)} = (1-\alpha)\, G^{(1)}_{\ell(\tau)} + \alpha\, G^{(1)}_{d(\tau)} \qquad (4\text{-}1)$$

where $G^{(1)}_{(\tau)}$ is the normalised autocorrelation function of the optical field, $G^{(1)}_{\ell}$ and $G^{(1)}_{d}$ are the motile and immotile components respectively, and α is the fraction of immotile cells. G_{ℓ} may be further divided into two components to account for normal and abnormal swimming fractions as was done by Hallett, *et al.*, (1978).

However, the actual determination of α is through the measurement of the second order autocorrelation function $G^{(2)}_{(\tau)}$ which is what the auto-correlator computes from the photocurrent. Measurements of α therefore depend on the relationship between $G^{(1)}_{(\tau)}$ and $G^{(2)}_{(\tau)}$ which as outlined in section 1.2.1, depends on the mode of photo-detection. For a homodyne experiment (and most of these studies were in a homodyne mode due to the absence of a local oscillator source)

$$|g^{(2)}_{(\tau)}| = 1 + |g^{(1)}_{(\tau)}|^2$$

and to determine $\alpha = G^{(1)}_{\ell(o)} / G^{(1)}_{(o)}$

square roots of the second order autocorrelation data points must be taken

before the AAR is determined. That is;

$$\alpha \approx [G^{(2)}_{d(o)} / G^{(2)}_{(o)}]^{\frac{1}{2}} \qquad (4.1)$$

and hence $\alpha \approx (AAR)^{\frac{1}{2}}$ (4.2)

(although to be strictly rigorous, the square roots of data points must be taken before fitting to determine the AAR).

It should be noted at this stage, that the AAR as defined in section 4.1 and discussed in section 4.2, is strictly the ratio $G^{(2)}_{d(o)} / G^{(2)}_{(o)}$ and has not been interpreted as being the actual percent dead cells. The important point, is that the previous data of fig. 4-9 shows the closest approach to the expected homodyne AAR - percent immotile relationship at the highest concentration of 5×10^6 sperm/ml. This then was a point strongly in favour of the real dilution effect hypothesis (case (i) in the discussion of 4.3.5) and the current experiment was intended to explore this possibility further, looking for a possible asymtotic approach to the square law relationship predicted for a homodyne experiment.

4.8.2 Methods

Experimental methods were very similar to those previously described in section 4.3.2 with the exceptions that a type B-1 sample cell was employed, the scattering angle was 8° and the scattering vector amplitude 2.39×10^4 cm^{-1}. The detector aperture was of 400μm diameter and a standard 5.5 min. thermal equilibration period was allowed prior to data collection.

Samples were prepared at total (live + dead) concentrations of 1, 5, 10, 15 x 10^6 sperm/ml (and higher) in 0.25% CEY with levels of percent dead cells over the range 20% - 100%. All autocorrelation functions comprised 32 * 1024 signal samples at 10mS intervals.

4.8.3 Results and Discussion

The relationships between the AAR and the percent dead cells at total concentrations of 10^6 sperm/ml and 5 x 10^6 sperm/ml were very similar to those previously obtained (fig. 4-9), the data being presented here in fig. 4-19.

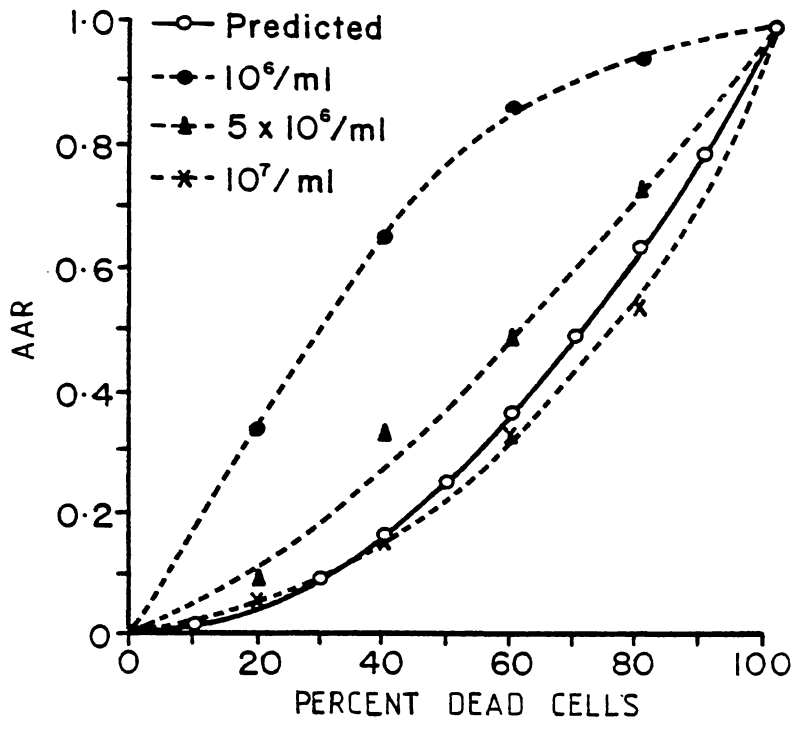

Fig. 4-19. AAR - percent dead cells relationship at three concentration levels (dotted lines) together with the curve predicted by the relationship of equation 4.2 (solid line).

At 10^6 sperm/ml the apparent relative contribution from the dead cells was substantially greater than at 5 x 10^6 sperm/ml, and at 10^7 sperm/ml the relationship closely approached that theoretically predicted for a homodyne detection mode. There was no question that the detection mode was homodyne rather than heterodyne for these measurements.

The autocorrelation functions, with increasing sperm concentration

showed a decreasing prominence of the slow exponential component to such an extent, that at a level of 1.5×10^7 sperm/ml, the slow component was undetectable for levels of less than 80% dead cells, even when using shorter autocorrelation timescales. Consequently only one data point (i.e., at 80% dead) was obtained at a sample concentration of 1.5×10^7 sperm/ml and it would therefore appear that 10^7 sperm/ml represents the upper concentration limit for the technique.

Of further interest is the concentration dependence of the slow ACF decay constant. Fig. 4-20 shows the decay constant plotted as a function of the concentration of motile spermatozoa in the sample, a reasonably linear relationship. The duplicate points at both 2 and 4×10^6 motile sperm/ml arise from combinations of concentrations and percent dead cells which result in the same absolute concentration of motile cells. For example, 20% dead at 5×10^6 total sperm/ml gave 4×10^6/ml motile spermatozoa as did also 60% dead at 10^7 cells/ml. This agreement in the corresponding decay constants tends to support the validity of the live-dead sample mixing technique and to some extent militates against the existence of a real dilution effect, at least between concentrations of 5 and 10 million sperm/ml. The data of fig. 4-20 show a clear cut relationship between the concentration of motile spermatozoa and the decay constant of the ACF exponential and this supports the concept of enhanced Brownian motion of the dead cells through medium disturbances created by the swimming fraction. Taking the decay constant of 1.59 s^{-1} obtained with the lowest concentration of motile spermatozoa, the diffusion coefficient was computed to be 1.39×10^{-9} cm^2/s, giving an equivalent hydrodynamic radius of 2.35μm. However, as will be discussed further in section 5.10.4 careful measurements on 100% immotile cells in a highly stable medium gave a decay constant of 0.963 s^{-1} at $|k| = 1.98 \times 10^4$ cm^{-1} indicating a diffusion coefficient of 1.23×10^{-9} cm^2/s and a hydrodynamic radius of 2.66μm.

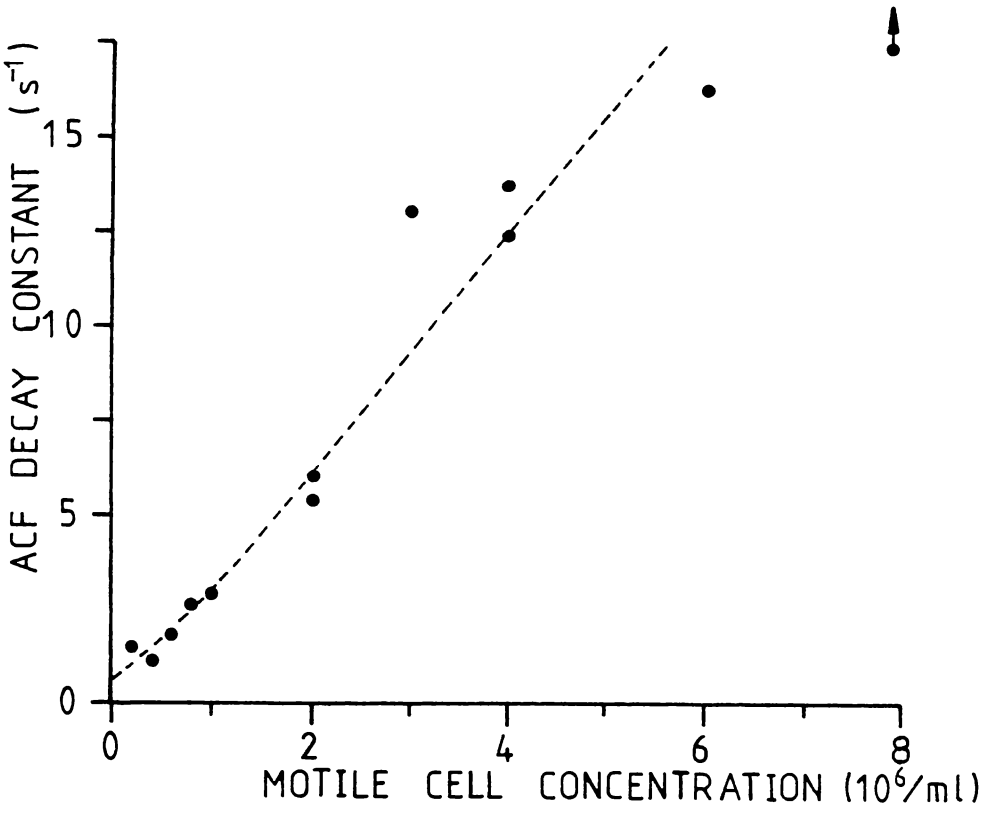

Fig. 4-20. The relationship between the slow ACF decay constant and the estimated concentration of motile spermatozoa.

These data suggest that even in the lower concentration ranges of motile cells used in this experiment (< 10^6/ml), dead cells were experiencing a detectable level of *enhanced* Brownian motion. The increase in AAR with decreasing total concentration (at a fixed level of percent motile cells) could have been partially attributable to translational displacements of immotile spermatozoa occurring in direct collisions with passing motile cells. At any given instant a specific proportion of immotile cells would be undergoing such perturbations and that proportion would clearly depend directly on the absolute concentration of motile spermatozoa.

However, if this were the case, the 10^7 sperm/ml curve of fig. 4-19 would then represent the relationship between the AAR and the *apparent* percentage of immotile cells not the true percentage of immotile cells

on which the theoretically expected curve (solid line) was based. If the observed approach of the relationship at 10^7 sperm/ml to the expected theoretical form is to be accorded any significance, then direct collisional interactions cannot be invoked as an explanation of the decrease in AAR at higher concentrations. Certainly it appeared likely that an enhancement of Brownian effects (presumably at long range) was responsible for the increase in decay constant as the level of motile cells rose, but on the results of this experiment, direct collision induced displacements of immotile cells seemed an unlikely explanation of the concentration effect. A dilemma arises however, when one considers that at 1.5×10^7 sperm/ml the slow ACF component had vanished completely other than at a level of 80% dead cells, an observation consistent with an extremely high level of perturbations and probably a high frequency of direct collisions. This presented something of a paradox since although interactions were likely to exist between the motile and non-motile fractions (there was definite evidence at a concentration of 15×10^6 sperm/ml) the AAR - percent dead relationship agreed with that derived on the basis of a no - interaction model, departures at low concentrations being real dilution effects.

Two conclusions were drawn from these results:

(i) that the AAR - concentration effect may indeed be a real one, there being no significant evidence to the contrary.

(ii) that the two autocorrelation components may not arise from the assumed mechanisms of cell translation and diffusion and that the basic model of the system may therefore be inappropriate.

Hypothesis (i) was supported by the results of the temperature dependence studies in section 4.6. In the case of hypothesis (ii) the evidence at this point indicated that the slow exponential component could very plausibly arise from diffusion of dead cells since the diffusion coefficient and hydrodynamic radius appeared to be reasonably consistent

with the known dimensions of the sperm head, where 100% dead cells were used or where levels of motile cells were low.

However, the nature of the fast autocorrelation component had little supporting evidence for its origin other than the numerical plausibility of the simple *low-angle point-scatterer isotropic velocity* model which had been proposed in the literature. The data of table 4-2 had indicated that motile cells apparently generated a substantially lower autocorrelation amplitude (in an absolute sense) than did dead cells at the same concentration level and this possibly pointed to an inadequate scattering model for the motile spermatozoon.

4.9 Attempts to reveal a Real Dilution Effect

4.9.1 Background

As discussed in section 2.10, spermatozoa are widely known to be sensitive to dilution and to not survive readily over a timescale of hours or tens of hours at low concentrations. The effect arises it seems from an accumulation of toxic substances in the medium due to the action of oxidative metabolic pathways and the effects can be substantially reduced by saturating the medium with nitrogen and/or adding catalase (ref section 2.10).

In the experiments described up to this point the 0.25% CEY medium had been nitrogenated and did contain catalase and on the basis of what was known about dilution effects, immobilisation of large numbers of spermatozoa over the 11 minute timescale of a light scattering experiment seemed most unlikely. In view of the AAR data obtained (section 4.8.3), some further study of the possibility of a real dilution effect was indicated, although it was not readily apparent as to how any such effect could be demonstrated independently of any confounding instrumental or optical effects. No adequate parallel measurements by other techniques were possible, other than microscopic examination of the diluted samples

for gross changes.

One possibility involved the level of seminal plasma which in a typical light scattering sample at a concentration of 10^6 sperm/ml, has been diluted by a factor in the range 1000 - 2000 from the level in the ejaculate. While the CEY medium used in these studies serves to replace the seminal plasma and has a similar activating effect on the cells (Shannon, pers. comm.), it seemed possible (Rozin, 1960) that the high dilution of the seminal plasma component which occurred in preparing a sperm sample, was generating a rapid immobilisation of a proportion of the population. Consequently a series of AAR - concentration dependence studies, very similar to those of sections 4.3 and 4.8, was carried out using samples both with and without additional seminal plasma in the light scattering diluent.

4.9.2 Methods

Experimental procedures and parameters were as previously described for section 4.3.

A large programme of experiments was carried out with the objective of investigating not only the effect of diluent composition but also identifying any differences between bulls in the AAR - dilution effect. Some of these experiments were carried out using the type C sample cell design, the philosophy behind which is enunciated in section 5.13.1 and due to the shorter path-length this design allowed the use of higher CEY concentrations in the diluent (up to 5%).

A comprehensive specification of these experiments is not intended for reasons of space and of relevance to the general theme of this chapter. The two basic comparisons in the study involved determining the AAR - concentration relation for;

(i) extender media both with and without a constant added level of seminal plasma[1] (VSP).

(1) Seminal plasma from a vasectomised bull.

(ii) different bulls.

4.9.3 Results and discussion

Fig. 4-21(a) → (c) show the AAR - concentration curves for spermatozoa in various types of media, both with and without a constant added level of VSP. In the case of fig. 4-21(a) the two media extremes, in terms of their potential activating effect (Shannon, pers. comm.) are shown. The minimal CEY medium, diluted from the 5% level at the sperm bulk concentration of 200 x 10^6/ml, varied from 0.025% - 0.25% over the sperm concentration range while the other experimental medium comprised 5% CEY with 10% VSP. The displacement of the two curves in this case suggests that a certain level of media - related inactivation of the live fraction did in fact occur but the general nature of the AAR - concentration remained the same.

Fig. 4-21(b) shows the result for samples in a 2% sodium citrate buffer, both with and without 10% VSP. The minimal difference suggests a sperm sample with a relative insensitivity to seminal plasma dilution. In the case of fig. 4-21(c), it appeared that even with use of 5% CEY as the diluent, some immobilisation, or other changes, had occurred due to seminal plasma dilution.

In all three sets of data, even with added seminal plasma, a marked AAR - concentration interaction was obtained and this was suggestive of the presence of other concentration dependent phenomena in the light scattering samples of spermatozoa. A variability between bulls in the magnitude of both the AAR and the AAR - concentration effect was also observed. Typical data showing this variability is given in table 4-4 for semen from six different bulls.

It is apparent from the data of this table that the ratio of the AAR measurements at the two concentrations ranks approximately as the percentage *eosinophilic* cells and the greatest percentage increase in AAR

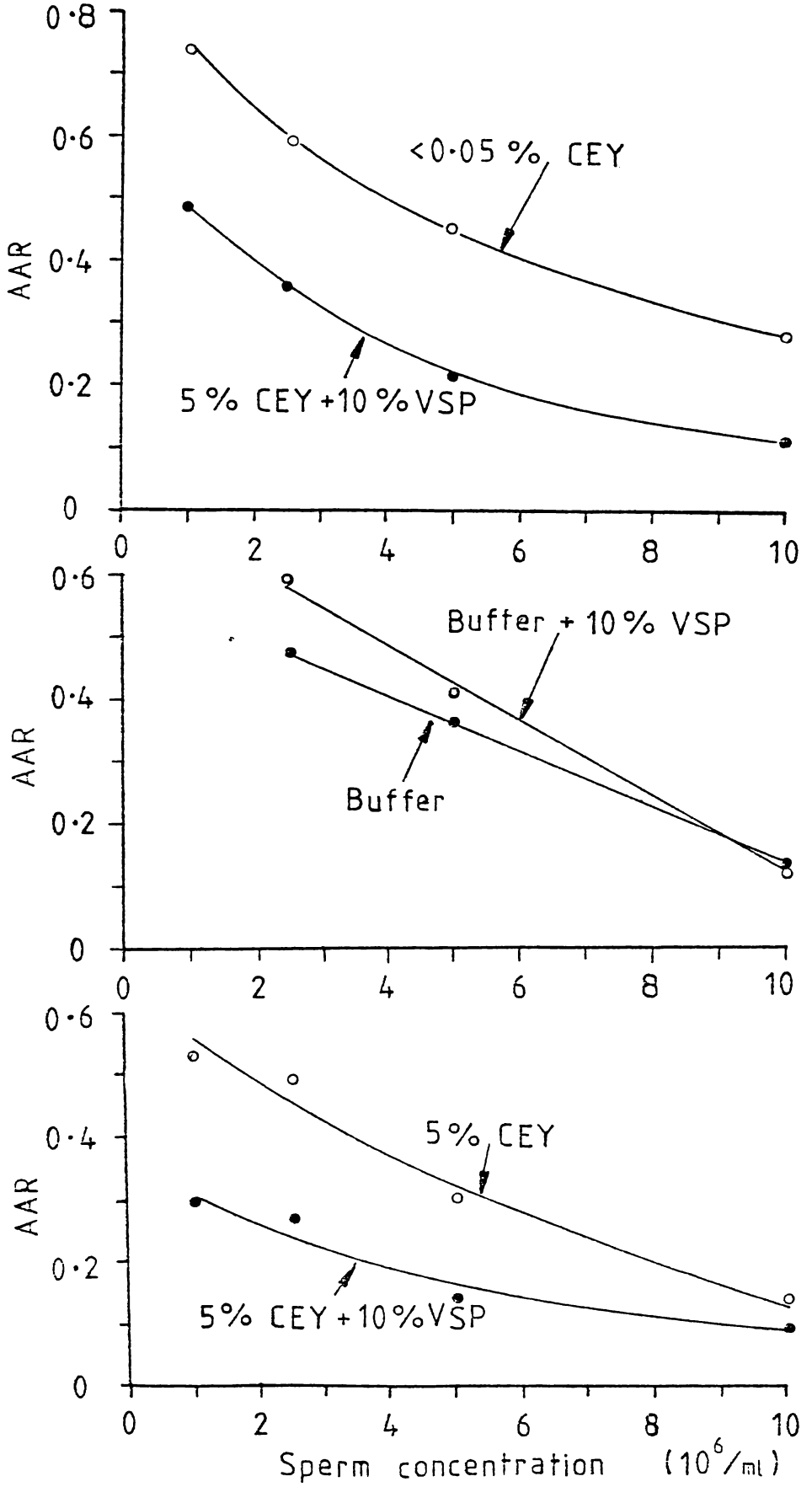

Fig. 4-21. The AAR - concentration relationship in various media. A between bull effect is superimposed on these illustrative data.

Bull #	% dead on *Eosin* Stain Count	AAR 0.5×10^6/ml	AAR 2.0×10^6/ml	(AAR)0.5 / (AAR)2.0
73464	12	0.414	0.245	1.69
74252	12	0.279	0.157	1.78
73444	15	0.414	0.233	1.78
74281	16	0.497	0.359	1.38
74213	25	0.437	0.463	0.944
71421	33	0.804	0.636	1.26

Table 4-4. AAR determinations at total sperm concentrations of 0.5×10^6 and 2.0×10^6 sperm/ml in 0.25% CEY for semen from six different bulls. The *eosin-nigrosin* stain counts of percent dead cells on the undiluted semen, are also given.

on dilution occurs for the most motile samples. Further, the AAR at 2×10^6 sperm/ml ranks reasonably well with the percent dead cells.

The general conclusions drawn from these results were;

(i) on dilution to the sperm concentration range used for light scattering measurements, a proportion of motile spermatozoa became immobilised due to environmental changes such as seminal plasma dilution. Such cells could be activated by adding VSP.

(ii) the general form of the AAR - concentration relationship is probably not generated primarily by such immobilisation effects, but by other as yet unidentified phenomena within the sample.

(iii) the fractional change in the AAR on dilution varies between bulls being greatest for samples of high apparent motility.

(iv) the AAR as measured at a sperm concentration of 2×10^6/ml ranks closely as the percent *eosinophilic* cells in the original ejaculate.

4.10 Changes in the short timescale ACF component with sample dilution

4.10.1 Background

Previous experiments, particularly that of section 4.8 and the data of table 4-2, had thrown increasing doubt on the accepted interpretation of the two autocorrelation components. Since it appeared that the AAR - concentration effect may partially be due to a rapid immobilisation of a proportion of the motile cells when diluted, it also appeared possible that some effect on the fast autocorrelation component may be evident. That is, if complete immobilisation of some spermatozoa occurs on dilution, others may well show a decline in swimming speeds.

4.10.2 Methods

The short timescale ACF component (collected at a signal sampling interval of 100μs) was compared at two dilution levels, after fitting and removal of the slow exponential component over the corresponding timescale (i.e., 0 - 10mS). The semen sample used, was one which showed a substantial difference in the AAR between the two sperm concentrations employed (1×10^6 and 4×10^6 total sperm/ml) which was indicative of the existence of an AAR - concentration effect for that particular sample.

The nature of the high frequency motile generated signal was also examined in the frequency domain using FFT spectral analysis (section 3.23). Spectra were taken at widely differing concentration levels ($0.2, 1.0, 10.0 \times 10^6$ total sperm/ml) for a sample having 15% *eosinophillic* cells.

The ADC sampling rate was 1KHz signal samples being transformed in sequential 1024 point batches to give an averaged spectrum in the frequency range 0.5 - 512Hz. Generally 110K signal samples were taken corresponding to a total signal sampling time of $\sim$ 1.9 min. for each spectrum.

Spectra were taken over the above sperm concentration range both with and without 10% VSP added to the 0.25% CEY diluent.

A type B-2 sample cell was used with a scattering angle of 8°.

4.10.3 Results and discussion

Standard long timescale autocorrelation measurements (10mS/ch) made on the sample are given in table 4-5 and the residual short timescale components after subtraction of the slow exponential components are shown in fig. 4-22. These autocorrelation functions were interpreted as being generated by the motile population within the sample.

	Concentration (10^6 sperm/ml)	
	1.0	4.0
AAR	0.556	0.252
Decay Constant (s^{-1})	5.26	7.81

Table 4-5. AAR and decay constants for the slow ACF component associated with the motile related functions of interest in this experiment.

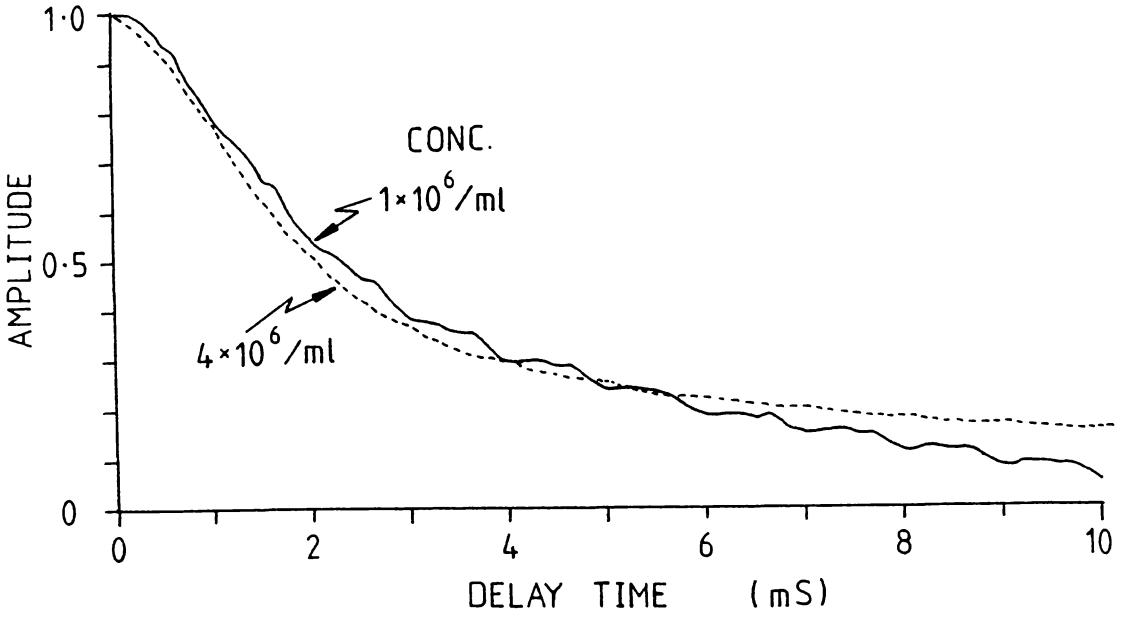

Fig. 4-22. Superimposed and normalised plots of the ACF component generated by the motile fraction after subtraction of the fitted slow exponential component, over the corresponding timescale, for concentration levels of 1 x 10^6 and 4 x 10^6 sperm/ml.

Comparison of characteristic widths for the two autocorrelation functions in fig. 4-22 leads to the conclusion that there was no substantial difference between the functions at these concentration levels and that the increased dilution of the sample had little effect on the swimming speed distribution or the dynamical variable responsible for the form of the fast autocorrelation component. The timescale of these autocorrelation functions is appropriate to the frequency range of the spectra given in fig. 4-23 which allowed the effect of dilution on the motile component to be examined from another perspective.

In the absence of 10% VSP in the diluent the frequency spectrum showed a decreasing prominence of the high frequency region both in its relative power level and its high frequency limit, with decreasing sperm concentration (fig. 4-23B). The upper frequency limit decreased from $\sim$ 350Hz at 10 x 10^6 sperm/ml to $\sim$ 200Hz at 0.2 x 10^6 sperm/ml. However, frequencies < 2Hz were attenuated due to the batch sampling mode of the FFT spectral analysis system and changes in the amplitude of the low-frequency peak with decreasing concentration do not correctly reflect changes typically observed in autocorrelation functions (e.g., figs. 4-11, 4-12).

However, the changes evident in the spectra of fig. 4-23B would appear to reflect real changes in the motility of the sample since the spectra of fig. 4-23A with 10% VSP added to the diluent (at the same sperm concentrations), show a less obvious decline in the high frequency domain with sperm dilution.

On this basis, the concentration dependence observed in the previous plots of fig. 4-21 both with and without VSP in the diluent, can only be accounted for by changes in the amplitude of the low frequency ($\lesssim$ 2Hz) domain to which the autocorrelation function is sensitive but which is effectively filtered out of the spectra of fig. 4-23.

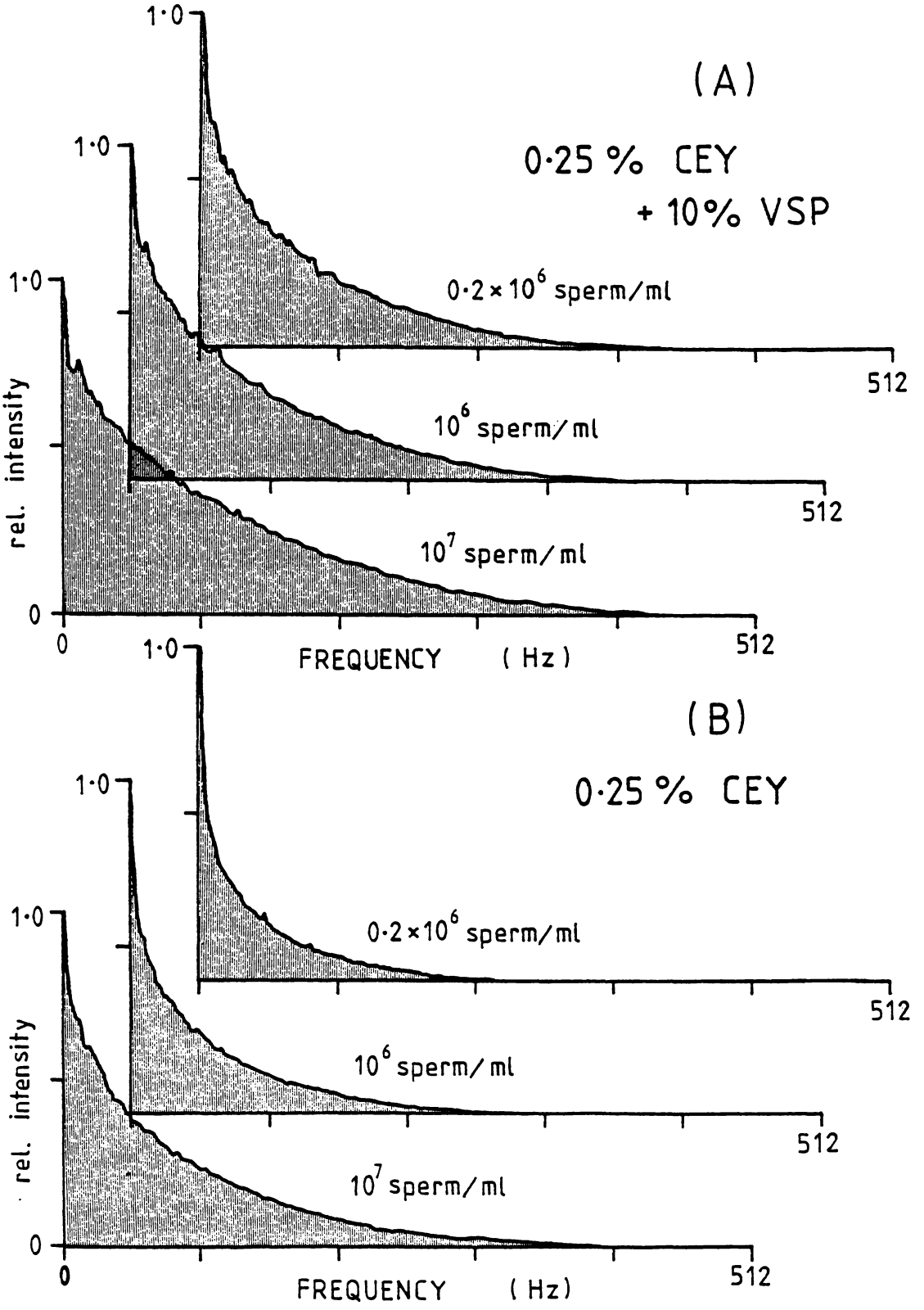

Fig. 4-23. Frequency spectra over the concentration range 0.2×10^6 - 10×10^6 sperm/ml both with (A) and without (B), 10% VSP in the 0.25% CEY diluent. The spectra have been normalised to the low frequency peak in each case.

These results also militated against the possibility that a fraction of the dead cells were appearing as motile cells due to interaction effects, since in these circumstances, significant changes in the shape of the fast component could reasonably be expected with interactions generating a wide distribution of immotile cell perturbations.

4.11 The effect of scattering angle

4.11.1 Background

Studies described to this point had utilised a scattering angle in the range 8° - 13.5°. In view of increasing doubts over the origin of the autocorrelation components, an exploratory series of experiments was carried out to define the effect of scattering angle on the magnitude of the AAR and the decay constant of the exponential ACF component.

Had the AAR been giving a true measure of the percent immotile cells there should have been no scattering angle dependence, provided that there was no background scattering from small particles which might become increasingly prominent at large scattering angles. Consequently experiments were carried out wherein, using a fixed concentration of spermatozoa, the scattering angle was varied over wide limits and the characteristic changes in the slow ACF measured. Some of the key results only are presented here.

4.11.2 Methods

(i) Scattering angle - AAR

Using samples of standard concentration, 10^6 sperm/ml in 0.25% CEY, autocorrelation functions were collected at scattering angles in the range 9.7° - 62.5° (measured to $\pm$ 0.5°). The scattering angle was varied by selecting the appropriate incident beam orientation via a system of prealigned mirrors and lenses, the location and orientation of the beam within the sample having been pre-adjusted in each case. Autocorrelation

functions were collected at sampling rates which allowed the slow ACF exponential to be defined, the AAR being determined by the standard RLQF fitting procedures.

(ii) Angle dependence of the decay constant for the slow ACF component

Scaling of the slow ACF component with scattering angle was found to be subject to considerable variations in the presence of motile spermatozoa. Consequently the scaling of the decay constant was examined using samples of 100% immotile sperm. Samples comprised 10^6 sperm/ml (100% immotile) suspended in 0.25% CEY and the exponential decay constant as determined by RLQF fits was measured over angles in the range 4.6° - 71.3°. In addition, the autocorrelation amplitude relative to that for 0.22μm filtered 0.25% CEY (sperm free) was determined so as to define the relative significance of the background scattering level.

Further, studies were carried out using suspensions of 5.17μm diameter polystyrene latex spheres diluted to a concentration (in 0.22μm filtered water) comparable microscopically with that of dead sperm at 10^6 sperm/ml. Autocorrelation functions were collected so as to calculate the diffusion coefficient and hydrodynamic radius.

In both sections of the study a B-1 sample cell was employed, with a photodetector aperture of 400μm.

4.11.3 Results and discussion

Results of the AAR - scattering angle studies are shown in fig. 4-24 and 4-25. A substantial decline in the AAR occurred with increasing scattering angle over the range 9° - 62° although the magnitude of the variation over the range of scattering angles usually employed in experiments, say 8° - 15°, was only $\sim$ 10%. The reason for the AAR angle

dependence was not immediately clear, other than the possibility of a background signal from small particles (protein aggregates) in the medium which may have imparted an increasing contribution to the fast ACF component as the angle was increased. Referring to section 3.16 it will be seen that the scattering volume in such an experiment would vary with angle as $\propto /\mathrm{Sin}\theta_s$, as would also its population of spermatozoa. With the type B-1 sample cell and a beam diameter of 1mm, the population at 10^6 sperm/ml can be estimated to vary from $\sim$ 1260 cells at $\theta_s = 5^\circ$ down to $\sim$ 145 cells at $\theta_s = 60^\circ$. However, the study of section 4.5 showed only a relatively small variation in AAR for a variation in scattering volume population over a similar range and therefore it seemed most unlikely that the results of fig. 4-24 could be accounted for by changes in the scattering volume population with scattering angle.

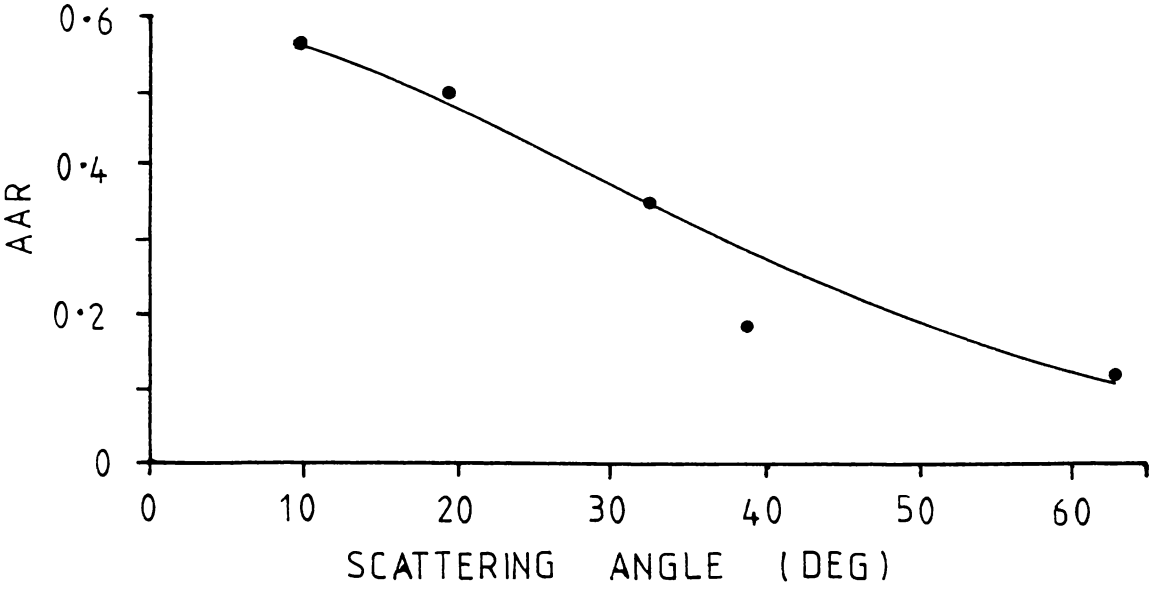

Fig. 4-24. Scattering angle dependence of the AAR. Sample 10^6 sperm/ml in 0.25% CEY.

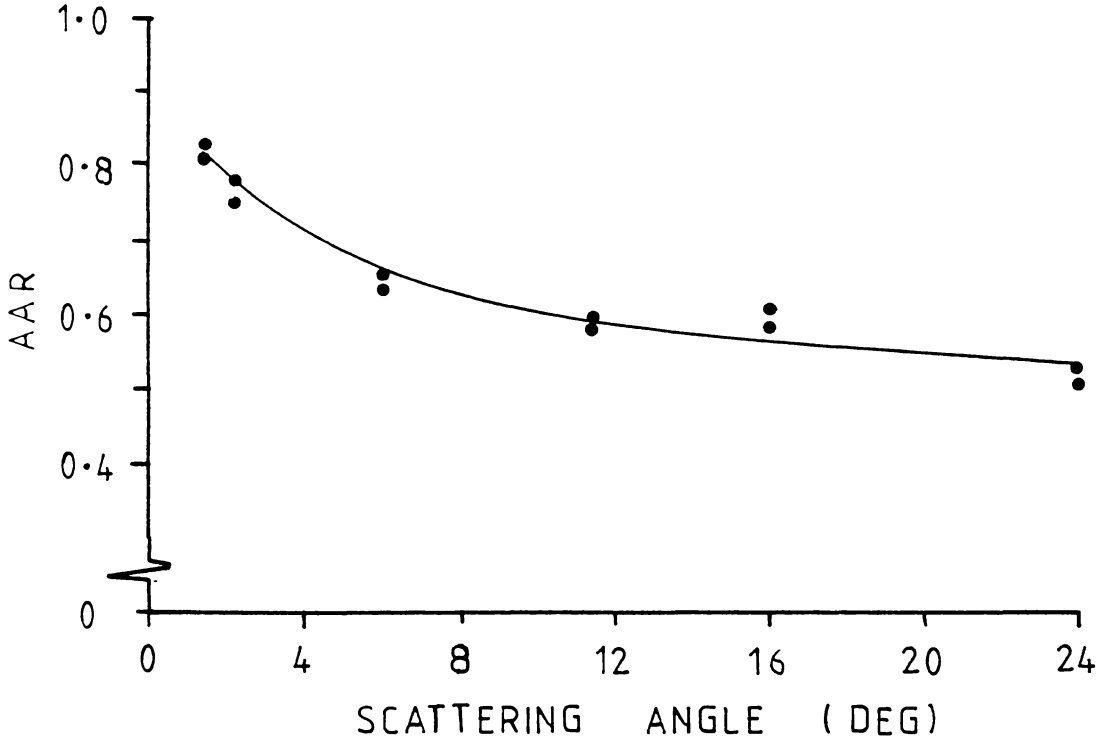

Fig. 4-25. Scattering angle dependence of the AAR over a smaller range of angles covering those commonly used in previous experiments. In this case the sample concentration was 2 x 10^6 sperm/ml in 0.25% CEY. Measurements were duplicated at each angle (on separate samples) and both data values are plotted.

Further results using samples of 100% immotile spermatozoa in buffer are given in table 4-5 and fig. 4-26. For these data the autocorrelation functions (ACF) at all scattering angles were well fitted by exponentials, the decay constants of which showed k^2 (i.e., with $\sin^2(\theta/2)$) scaling with scattering angle, as is generally obtained for Brownian diffusing scatterers (Berne and Pecora, 1976).

From the data of fig. 4-26, the diffusion coefficients for the 5.17μm (diameter) polystyrene latex spheres and for the immotile spermatozoa were calculated to be 1.305 x 10^{-9} cm^2/s and 0.690 x 10^{-9} cm^2/s, respectively. The equivalent hydrodynamic radii are respectively 2.50 ± 0.20μm and 4.74 ± 0.44μm. Clearly the computed hydrodynamic radius for the polystyrene

latex spheres was in excellent agreement with the manufacturers' specification of a 2.585μm (± 2%) radius. However, the calculated effective hydrodynamic radius of 4.74μm for spermatozoa seemed unexpectedly large and that calculated from the data of fig. 4-27 (another experiment using 100% immotile sperm) gave a higher value again, 5.76μm.

The data of table 4-5 shows the presence of a substantial background signal (observed to be in the high frequency range) which became significant at scattering angles in the range 22.6° - 71.3°.

Scattering Angle	Mean Decay Constant (s^{-1})	AAR	Background Noise - signal ratio[1]
4.6°	1.78	1.021	0
12.2°	2.17	1.008	∿ 0.002
22.6°	5.62	0.983	0
49.0°	24.7	0.949	0.17
71.3°	50.2	0.914	0.96

Table 4-5. Angle dependence of the autocorrelation decay constant, the AAR and the background contribution from the 0.25% CEY medium for a suspension of 100% immotile spermatozoa.

(1) *Background noise* to *signal* ratio defined as:

$$\frac{\text{ACF Ampl. for 0.25\% CEY}}{\text{ACF Ampl. for } 10^6\text{/ml sperm in buffer}}$$

At high scattering angles, this background signal, generated by scattering in the 0.25% CEY medium, appeared on the autocorrelation functions as a small high frequency 'pip' similar to that generated by motile cells, but of much shorter decay time. This signal rose to ∿ 17% of the autocorrelation amplitude for 10^6/ml sperm at a scattering angle of 49° and to 96% at a scattering angle of 71.3°.

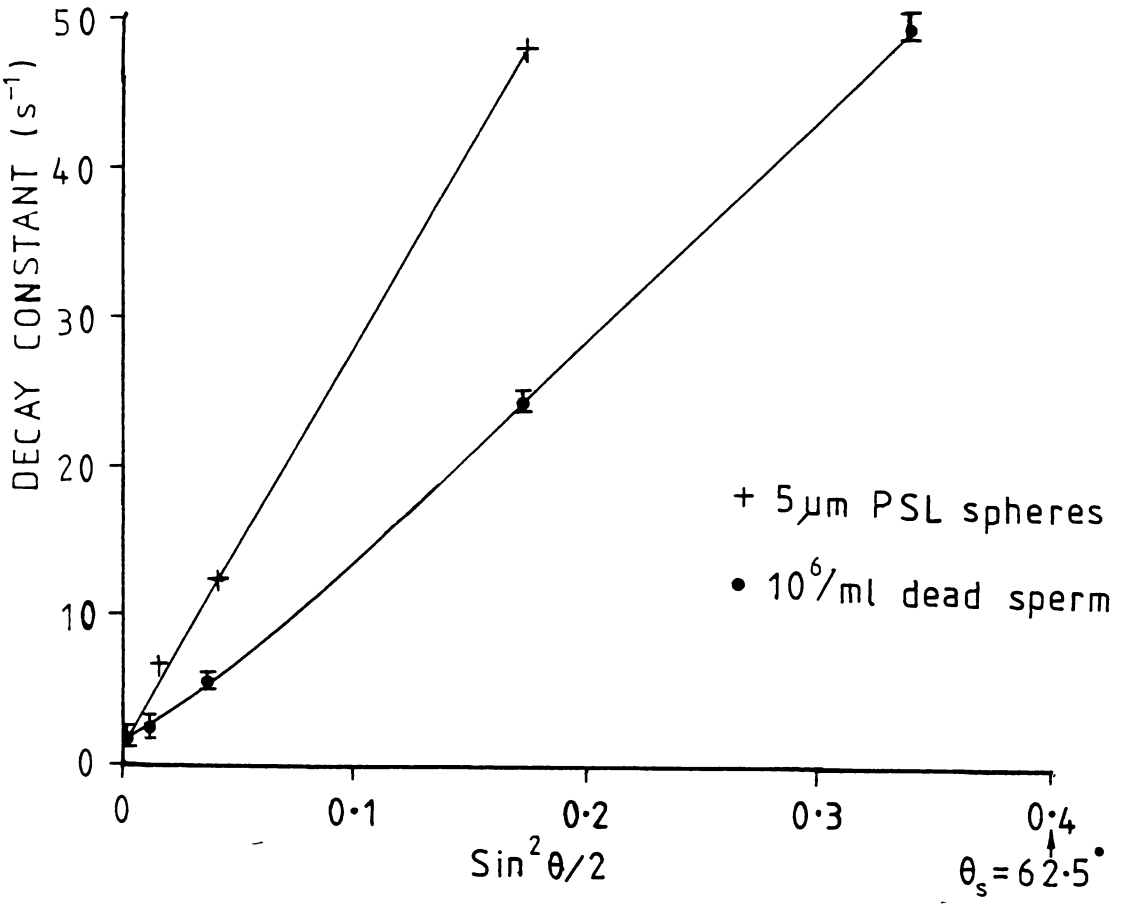

Fig. 4-26. The ACF exponential decay constant for 100% immotile sperm (suspended at 10^6/ml in 0.22μm filtered 2% sodium citrate buffer) and for a suspension of 5.17μm diameter polystyrene latex spheres (λ = 488nm).

The percent standard deviation of the data for the 5.17μm PSL spheres was $\sim \pm$ 8.2% taken over all data points (6 replicates at each value of θs). For the spermatozoa data in fig. 4-26 the mean and range are shown.

The conclusions drawn from the experiment were:

(i) a decrease in AAR occurs with increasing scattering angle although the reasons for it were not clear.

(ii) the AAR varies by only $\sim$ 10% over the most commonly used range of scattering angles 8° - 15°.

(iii) at higher scattering angles ($\gtrsim$ 25°) a high frequency scattering signal from the 0.25% CEY medium becomes significant.

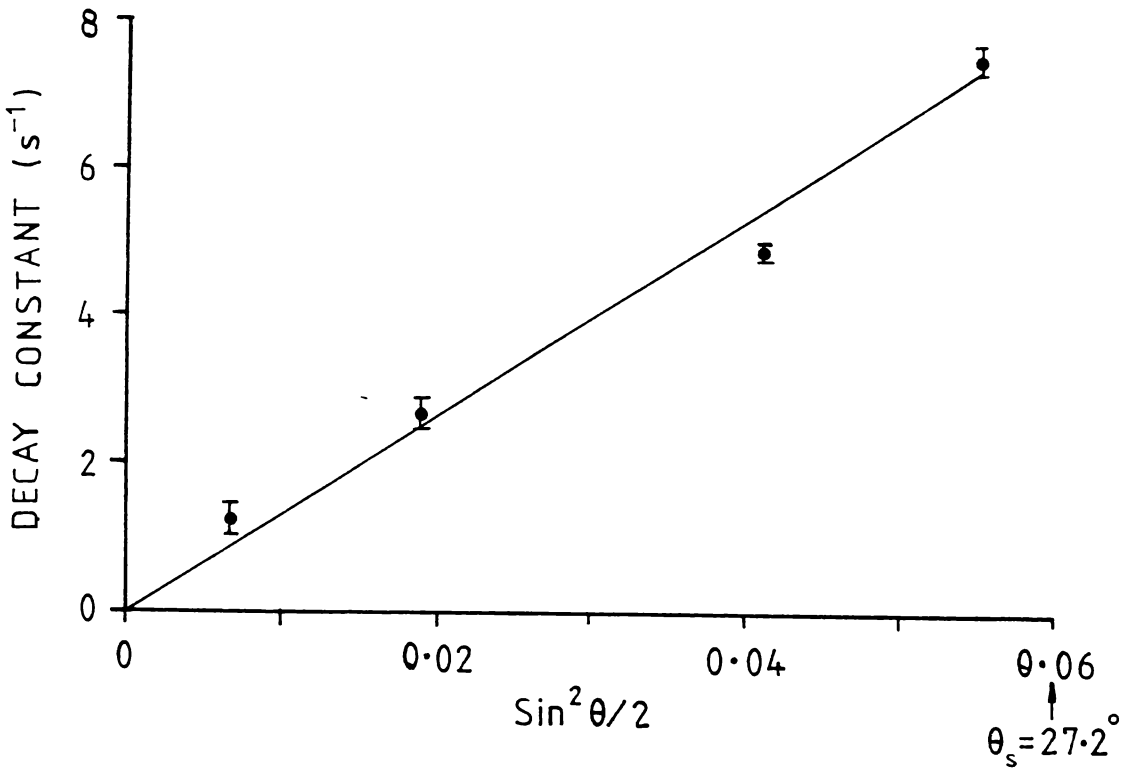

Fig. 4-27. ACF decay constant for 100% immotile sperm over a smaller scattering angle range (9.5° - 27.2°) than that of fig. 4-26. This data is from a different experiment to that of fig. 4-26 but the hydrodynamic radius computed from it is similar (mean and range of replicated measurements is plotted).

(iv) Autocorrelation functions for 5.17μm diameter polystyrene latex spheres gave an equivalent hydrodynamic radius of 2.5μm for a homodyne detection mode, confirming that this is the detection mode which the light scattering operates in when collecting light from spermatozoa at concentrations of the order of 10^6/ml.

(v) The diffusion coefficient of dead spermatozoa is substantially less than that of 5μm spheres and the equivalent hydrodynamic radius is larger than might be expected on the basis of head dimensions, although the flagellum may have a bearing on the hydrodynamic behaviour.

(vi) The autocorrelation function generated by dead spermatozoa is closely exponential and its characteristic decay constant scales with scattering angle as $Sin^2(\theta/2)$ in the absence of motile cells.

Such scaling appears to be consistent with the slow ACF arising from homodyne detection of the scattered field for scatterers undergoing Brownian motion.

4.12 Time dependance effects

4.12.1 Background

During the course of the preceding studies, it was known that the autocorrelation function exhibited time dependent changes. Both short timescale (0 - 10 min) and long timescale (0 - 60 min) changes were observed. For example, the set of autocorrelation functions shown previously in fig. 4-16 typifies changes (albeit at a lower temperature) immediately after sample injection, presumably arising from convective heating and stabilisation of the sample. In general, immediately following sample injection, the slow ACF component was observed to exhibit a higher than normal decay rate, sometimes a minor periodic feature, and always a lower AAR value. In many cases, the AAR would then show a progressive increase with time, possibly over a timescale of 15 - 30 min or more, which suggested immobilisation of a proportion of the spermatozoa, or other phenomena, were developing in the sample. In fact Cooke, *et al.*, (1976) had reported a logarithmic decline in the percent motile spermatozoa (as inferred from AAR changes) over a timescale of 200 min after allowing for settling effects. They found that the sample had to be agitated in the light scattering cell prior to taking a measurement.

In the experiments discussed to this point, a decrease in the detected signal level with time was often noted, particularly where spermatozoa were suspended in buffer. A detailed study of the time dependence of both the AAR and the total signal level was therefore carried out in various

media and at a later stage (section 5.13.1) in a light scattering cell of different geometry.

4.12.2 Methods

The general technique employed, was to inject a sample of spermatozoa (initially at ambient temperature) into the light scattering cell (maintained at 37°c) and immediately commence collection of closely consecutive autocorrelation functions, each formed by a fixed number of signal samples. In the data presented in the following figures each autocorrelation function comprised 16 * 1024 signal samples at 10mS intervals, corresponding to a total signal sampling time for each function of 164 s. When sampling for each function was complete the computer read the autocorrelator bins and the autocorrelator was immediately reset and restarted, after which the previous dataset was stored and/or analysed. The sperm sample was not agitated between successive functions.

The factors of principal interest were the AAR, sometimes the slow ACF exponential decay, and the absolute total amplitude of the autocorrelation function. This latter factor was a measure of the total signal power (since $\alpha\ E^2_{sig}$). By maintaining both the incident beam power and the photo-detector/amplifier system gain constant, the time dependence of the signal level could therefore be followed by comparing absolute amplitudes of autocorrelation functions. (Note that in chapter 5, section 5.5, another system of achieving this was to be employed which was more appropriate over shorter timescales). So as to detect any variation in incident beam intensity over the experimental timescale, the laser output was continuously monitored using a simple photodiode and a digital read-out. Laser beam stability was generally better than $\pm$ 1% over a 60 min experimental run. The amplitudes of consecutive autocorrelation functions could then be directly compared after removal of any baseline displacement revealed by the least squares exponential fit.

During the course of the study various sperm dilution media were examined for their effects on the time dependence of measurements. These experiments used a sample cell of the type B-2 design, having a depth of 2mm (fig. 3-12). Further studies of the same type, but using a sample cell of revised design, are later to be discussed in section 5.13.

Studies of sperm distribution within the sample cell over the time-scale of the parallel light scattering experiments were also carried out. These studies involved direct microscopic observation within a heated sample cell of similar geometry to that used in the light scattering studies (see later 5.2.2).

4.12.3 Results and discussion

(i) Trends in Autocorrelation Parameters

Typical time changes in three autocorrelation parameters of interest, amplitude, AAR and decay constant are shown in fig. 4-28 for a motile sample of spermatozoa at a total concentration of 2 x 10^6/ml in 2% sodium citrate buffer. A curvilinear increase in the AAR from an initial value of $\sim$ 0.4 to a plateau level of $\sim$ 0.75 took place over a timescale of 10 - 12 min. Autocorrelation functions formed over 164 s intervals commencing at elapsed times of t = 0, 5.5, 11, 19 min are shown in a superimposed plot in fig. 4-29. Over the $\sim$ 40 min period of the data, an almost linear decline in the autocorrelation amplitude (ACA) was observed, amplitude levels being expressed relative to that of function # 1. A period of $\sim$ 8 min with a reasonably constant ACA was followed by a substantially linear decline to zero amplitude at $\sim$ 38 min. The auto-correlation decay constant also declined from an initial value of 2.8 s^{-1} to a stable value of $\sim$ 1.3 s^{-1} but showed fluctuations beyond an elapsed time of 25 min.

Initially it was considered that the changes in the AAR and the decay

constant were symptomatic of a real decline in the percent motile cells. (the interaction between the two variables was previously discussed in section 4.8.3 and refer also later to fig. 5-33) which could very plausibly arise from rapid sample heating and thermal shock on injection, illumination and various other potentially detrimental factors. The dramatic decline in signal level as evidenced by the downward trend of the ACA, was strongly suggestive of a sedimentation effect and it was found that agitating the sample gave a temporary restoration of signal level.

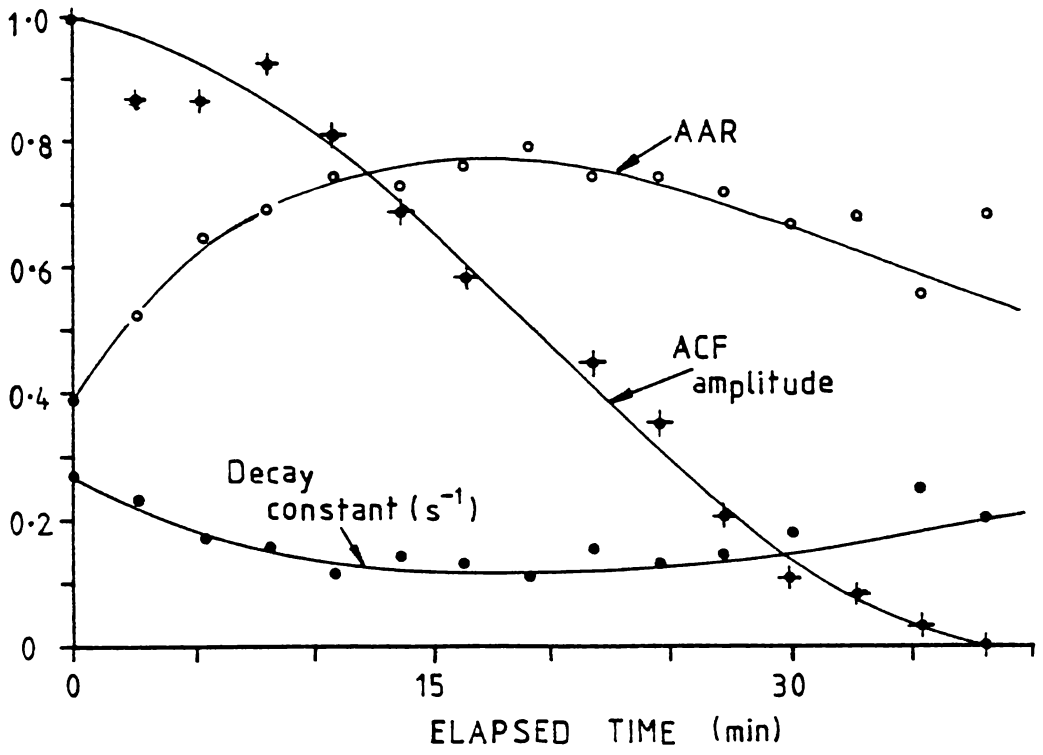

Fig. 4-28. Time dependence of autocorrelation parameters for spermatozoa at a total concentration of 2 x 10^6 sperm/ml suspended in buffer. AAR and relative ACF amplitude read directly on the vertical scale, the decay constant values x 10 give units of s^{-1} (scattering angle = 5.4°, λ = 441nm and K = 1.79 x 10^4 cm^{-1}).

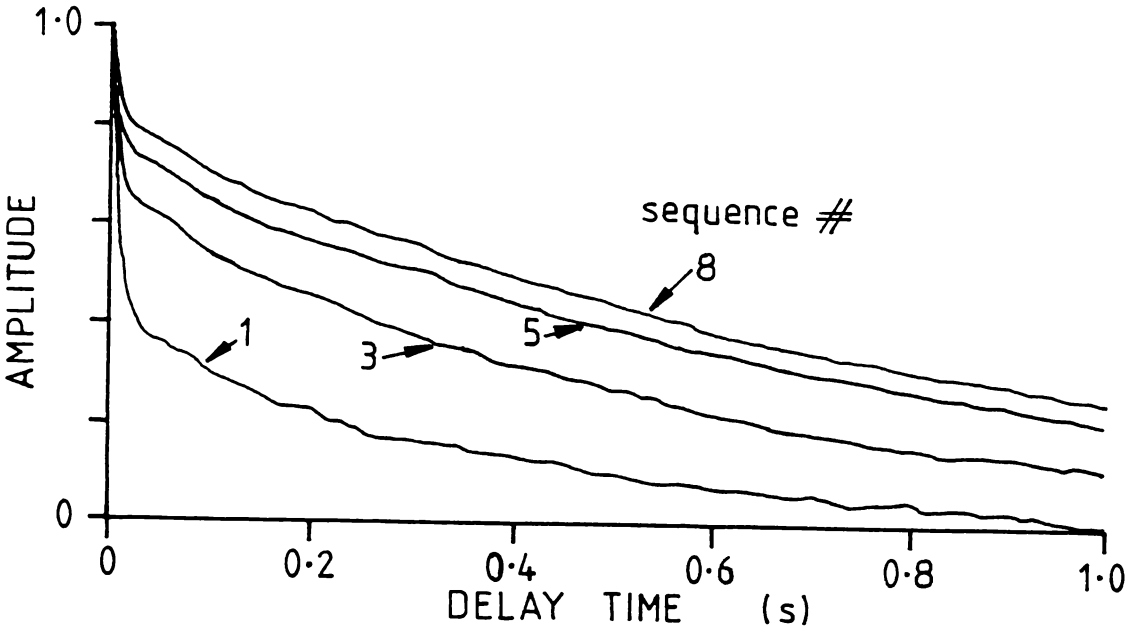

Fig. 4-29. Autocorrelation functions corresponding to data points # 1, # 3, # 5, and # 8 in fig. 4-28. The functions are normalised and plotted relative to zero baseline.

The optical alignment was such that the beam of diameter ∿ 1mm was located centrally in the cell (type B design, depth 2mm) and the photo-tube aperture (diameter 0.4mm) was centralised on the image (see fig. 4-30).

In fig. 4-28, the downward trend in the ACA appeared to commence at ∿ t = 600s at which point the upper level of dead cells in the sample (initially at the cell roof) would have sedimented into the upper region of the scattering volume. If the subsequent decline corresponds to the sedimentation of dead cells through the 400μm depth of the scattering volume, this suggests a sedimentation rate of ∿ 0.3μm/s which is in order

of magnitude agreement with that measured by Roberts (1972) of 0.42μm/s (after correction to 37°c).

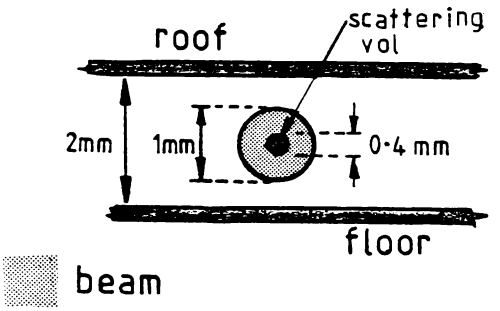

Cross-section of sample cell showing the approximate dimensions relevant to sedimentation effects.

However, a curious feature of this proposed phenomenon was that the apparent and progressive sedimentation of dead cells through and out of the scattering volume, was not accompanied by any substantial decrease in AAR (a minor downward trend only, was evident) as the relative levels of motile and immotile cells in the scattering volume, presumably changed. In fact, the AAR remained substantially constant over most of the ACA decline. The obvious explanation appeared to be that the decline in the population of motile cells occurred at the same rate as the sedimentation of dead cells, due to a slight downward swimming bias. In fact Roberts (1972) studied the tendency of human sperm to swim downwards suggesting that from an initially uniform distribution a stable vertical sperm concentration gradient would become established. The actual random walk downward swimming bias for human sperm was given as $\sim$ 5μm/s. The auto-correlation decay constant, which had previously been closely associated with the presence of motile spermatozoa (fig. 4-20) had declined to its minimum level over the same interval that the AAR rose, suggesting that either immobilisation of motile cells was occurring, or that the scattering volume was being depleted of motile cells.

Events within the sample clearly required closer examination.

(ii) Microscopic Observations

Direct visual observations were carried out to assess the magnitude of sedimentation effects for dead spermatozoa. A flat specimen cell of depth 1mm (type B geometry) was placed on a heated microscope stage, temperature controlled at 37°c. A suspension of 100% dead spermatozoa at 10^7/ml in 2% sodium citrate buffer, was injected into the cell and the vertical distribution of cell numbers qualitatively observed at ∿ 5 min intervals.

The spermatozoa were observed to progressively accumulate on the floor of the cell and after a period of 30 min, virtually no cells could be found in suspension. This demonstrated relatively rapid sedimentation at a speed of ∿ 0.5 - 0.6μm/s.

(iii) Effect of specific gravity of the medium

Attempts were made to reduce the effect of sedimentation which indirectly the results of (i) and more directly the conclusions from (ii) had demonstrated to be present within the sample. This involved the use of suspending media of higher specific gravity for time dependence experiments of the same design as that corresponding to fig. 4-28. The same techniques and experimental conditions as previously outlined in 4.12.2 were employed, with the exception that the media used for sperm dilution were;

(a) 2% sodium citrate buffer (Appendix I), 0.22μm filtered and containing 7% FICOLL and having a specific gravity of ∿ 1.04.

(b) 2% sodium citrate buffer (also 0.22μm filtered) but prepared by using D_2O in place of H_2O and having a relative density of ∿ 1.11 (use of D_2O in the buffer, in preliminary experimental runs and microscopic studies appeared not to have any toxic effect on the sperm sample).

These suspending media, together with the results of fig. 4-28,

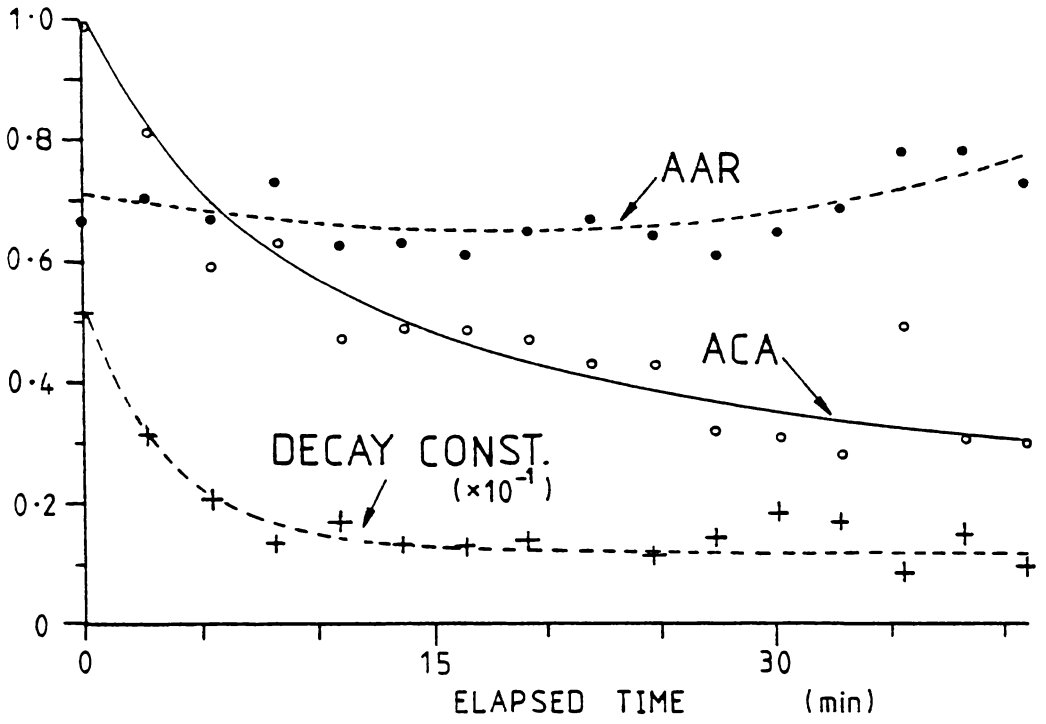

Fig. 4-30. Time dependence of autocorrelation parameters for sperm at 2 x 10^6/ml in 2% sodium citrate buffer containing 7% Ficoll.

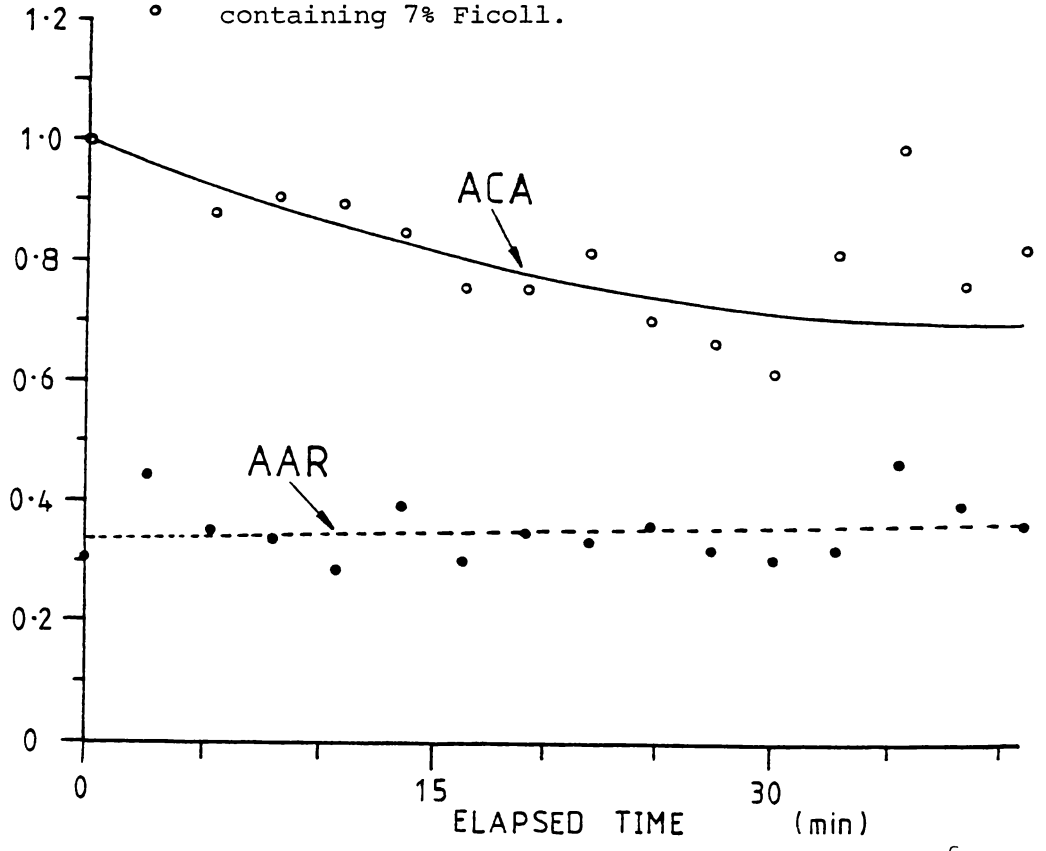

Fig. 4-31. A dilution of the same sample also at 2 x 10^6/ml but in 2% sodium citrate buffer prepared with D_2O and having a specific gravity of ∿ 1.11.

need to be considered relative to the unusually high specific gravity of the bull spermatozoa discussed in section 2.5.4.

The resultant data is shown in figs. 4-30 and 4-31 and relates to exactly the same experimental techniques, parameters and sperm samples as does that of fig. 4-28. In both media of high specific gravity the AAR remained substantially constant over the 35 min. experimental run although at significantly differing levels.

The fall-off in the ACA was substantially less in the D_2O medium than in the lower density Ficoll which, while it showed a rapid initial drop, did not approach the virtual zero signal level which had been obtained with citrate buffer in fig. 4-28.

No initial rise in the AAR occurred in either of the high specific gravity media. In addition, a very interesting feature was the large differences in AAR values between the two media, the D_2O medium giving values in the range $\sim$ 0.3 - 0.4 while those in the Ficoll medium were $\sim$ 0.6 - 0.7. There appeared to be a medium relative density interaction with the AAR and the nature of this was not immediately clear. Again, a large drop in ACA (in these cases to 50% of its initial value) was not accompanied by any change in AAR.

4.13 Interim Summary and Conclusions

LBS measurements (the AAR and associated decay constant) of the percent immotile cells in samples of spermatozoa have been described in some detail in chapter 4. These LBS parameters have not been those most widely discussed in the related light scattering literature. Rather, the interpretation of the fast autocorrelation component associated with the motile fraction has been the topic of central interest (section 1.5). Those few measurements of the percent immotile spermatozoa which had been reported using LBS, appeared to have assumed that the AAR gave an absolute measure of the percent motile cells. In these cases the technique was

largely based on an extrapolation of the Nossal (1971) discussion, and extended the two-component autocorrelation to be expected from a mixture of motile and immotile point scatterers, to the case of spermatozoa suspensions.

Initially, the studies reported here also proceeded on that basis. However, the results which have been presented in this chapter (sections 4.3 and 4.8) found that the AAR was highly concentration dependent, a most unexpected result at the time! Such an effect had not been reported in the literature and consequently the published studies appeared to have attributed no particular significance to sample concentration (see table 1-4).

The early data of fig. 4-10 clearly demonstrated that, particularly in high motility samples (those with a high percentage of motile cells), the AAR was very sensitive to the total concentration of the sample in the lower range (i.e., $< 10^6$ sperm/ml). The effect was closely related it seemed, to the absolute concentration of motile spermatozoa since the data of fig. 4-20 appeared to suggest that perturbations of the immotile cells (resulting, it seemed, in enhanced Brownian motion), possibly at long range, induced by either the individual or the collective motions of the motile fraction.

Obviously the question of the spacing between adjacent spermatozoa was of interest although the *low Reynolds number* regime ($\lesssim 10^{-3}$) in which the cells swim, made the understanding of spacings in terms of hydrodynamic interactions not at all obvious. Fig. 4-32 shows the variation in mean spacing between adjacent cells over the concentration range which was of interest in fig. 4-10. The linear spacing increases rapidly at the lower concentrations and possibly this could account for the substantial rise which occurred in AAR at concentrations $< 10^6$/ml in fig. 4-9 and below 5×10^6/ml in fig. 4-19.

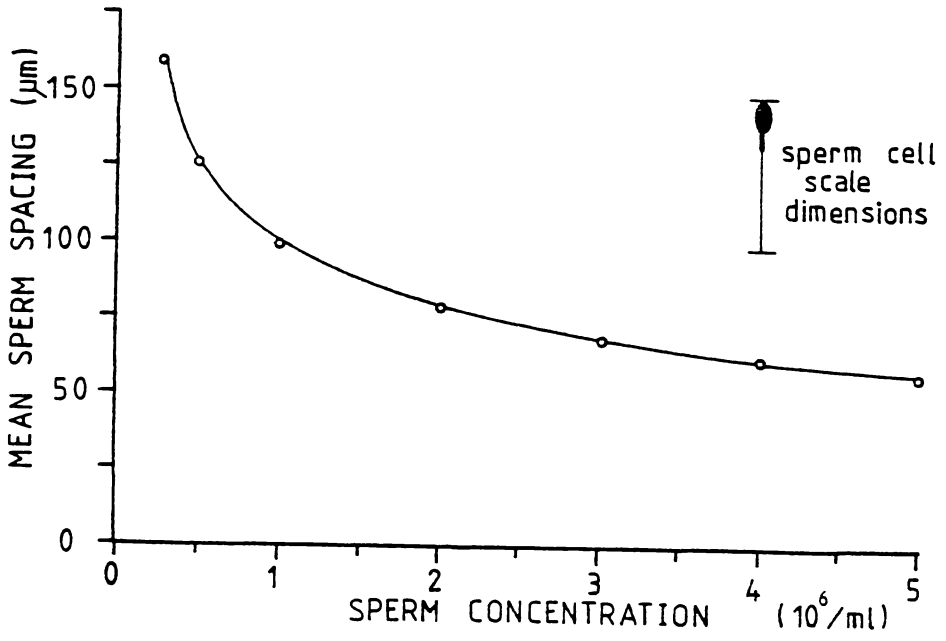

Fig. 4-32. A plot of the mean spacing between adjacent spermatozoa over the concentration range of interest, with the scale dimensions of a bull spermatozoon superimposed for comparison.

It was also possible, however, that the concentration - AAR interaction resulted at least partially from a real dilution effect, with a proportion of motile cells becoming rapidly immobilised on dilution to the light scattering concentration. This aspect was examined in section 4.9 and indeed it was shown that the AAR decreased and activity, as seen in the frequency spectrum, increased (i.e., implying an increase in percent motile cells) if 5 - 10% seminal plasma was added to the diluent. This appeared to be a result of some significance, since traditionally dilution effects (as discussed in section 2.10) had only been observed with conventional motility observation techniques and over timescales of hours, not minutes as was the case in the context of these light scattering experiments. There was also the possibility that the addition of seminal plasma had not only increased the percentage of motile spermatozoa,

but had also increased the vigour (swimming speeds) of the motile fraction. The motile fraction through these effects could be expected to increase its interactions with the immotile fraction. Whether this was the case was uncertain, but it did seem that even with added seminal plasma the general trend of the AAR with concentration was the same.

The complete absence of alternative quantitative techniques made the clarification of the situation difficult and it was for this reason that the approach of separately exploring the effect of the individual experimental parameters, was adopted. Table 4-6 gives a brief tabulation of the principal effects uncovered in the resulting programme of experiments in chapter 4. Many of these results could not be understood on the basis of the simple point-scatterer absolute correlation amplitude interpretation and it became increasingly obvious that the sperm sample model needed revision in terms of both its physical, biological and, probably, optical components.

Those results from chapter 4 which were not readily understood in terms of the accepted model, are tabulated in table 4-7 and form an appropriate point at which to terminate this chapter.

The general conclusions which were drawn from this phase of the experimental programme were:

(i) little significance could be attributed to the AAR as a quantitative and absolute measure of the percent immotile cells in suspensions of bull spermatozoa.

(ii) undefined phenomena existed within the light scattering sample which induced a pronounced concentration dependence of the AAR. Probably such factors were of optical or physical origin and had the effect of varying the relative scattered intensity levels from motile and immotile cells.

(iii) the slow ACF component was probably generated by Brownian motion of immotile cells and in the absence of motile cells, its amplitude was proportional to the immotile cell concentration.

Experimental Variable	Brief summary of association with light scattering measurements
Percent Dead cells.	AAR increases when proportion of dead cells in sample increases. Shape of curve dependent on sperm concentration.
Total (live + dead) sperm concentration.	Increasing concentration over range 0.25×10^6 - 10^7/ml gives $\sim$ exponential decrease in AAR.
Temperature.	AAR rises as temperature decreases and no interaction with concentration observed at 28.4°c but is observed at 37°c.
Semen from different bulls.	Showed variability in AAR between bulls, particularly at 2×10^6/ml and variable sensitivity to dilution.
Scattering Angle.	AAR decreased with increasing scattering angle.
Scattering Volume dimensions.	No significant change in AAR over a large range in estimated scattering volume population.
Diluent.	Scattering from CEY diluents did not contribute to the ACF at scattering angles < 25° if filtered to 0.22µm.
Time in sample cell.	Changes in both ACA and AAR due to sedimentation and other undefined effects. Use of higher specific gravity extender stabilised the AAR.
Decay Constant of slow ACF component.	Decreased AAR usually associated with an increased decay constant implying enhanced Brownian motion of dead cells.
Slow ACF component Angle Scaling.	Decay constant of slow exponential component scaled as $\mathrm{Sin}^2\theta/2$ supporting the Brownian diffusion model.

Table 4-6. A general summary of the major effects indicated by the data of chapter 4.

	Observed Effect	Ref.
1.	A hydrodynamic radius for dead cells, large relative to the linear dimensions of the sperm head (i.e., $\sim$ 4.7μm).	section 4.11.3
2.	A substantially higher scattered intensity from dead cells than from the same concentration of motile cells.	table 4-2
3.	A sharp rise in AAR at low (< 10^6/ml) concentrations where interaction effects decline, this being supported by the approach of the slow ACF decay constant towards that of dead cells.	fig. 4-10 fig. 4-19 fig. 4-20
4.	Approach of the AAR - percent dead relationship towards the ideal Nossal model for homodyne detection at 10^7 sperm/ml concentrations but disappearance of the slow ACF component at > 1.5 x 10^7 sperm/ml.	fig. 4-19
5.	No apparent change in the timescale of the motile - related ACF component on dilution from 4 x 10^6 - 1 x 10^6 sperm/ml.	fig. 4-22
6.	AAR - concentration interaction vanished at a temperature of 28.4°c.	fig. 4-15
7.	Large changes in the ACA without any substantial effect on the AAR.	fig. 4-28
8.	AAR appeared to depend on the relative density of the suspending medium.	fig. 4-30 fig. 4-31
9.	A progressive decrease in AAR with increasing scattering angle, not attributable to increased background scattering from diluent.	fig. 4-24 fig. 4-25

Table 4-7. A summary of those observations in the data of chapter 4, which could not be understood on the basis of the simple point scatterer - absolute correlation amplitude ratio model outlined by Nossal (1971) when extrapolated to bull spermatozoa.

(iv) the origin and behaviour of the fast component of the ACF was uncertain although there was little reason to believe that it was of other than *Doppler* origin.

(v) the existence of interactions between motile and immotile cells in the sperm sample was possibly involved in concentration effects. The presence of interactions was implied by changes in ACF decay constants which suggested enhanced Brownian diffusion.

(vi) a real immobilisation of a proportion of the spermatozoa appeared to occur on dilution. Variations in the biochemical environment appeared to be involved.

CHAPTER 5

RESULTS AND DISCUSSION : Part 2

..... *"The great tragedy of science -*

the slaying of a beautiful theory by an

ugly fact" .....

T. H. Huxley, 1825 - 1895.

5.0 Introductory Remarks

The results of chapter 4 presented something of a dilemma since, in common with the published work on the technique, attempts were being made to reconcile the experimental light scattering data with a conceptual model of the system which was clearly not providing a good basis for understanding. On this model the spermatozoa were considered to act as point scatterers at the small scattering angles employed and to move with an isotropic velocity distribution. There are often definite limits to the macroscopic understanding that one can derive about a biological system without some insight into its detailed behaviour on a microscopic scale, and this often proves to be exceedingly complex. In this context, the major difficulty in the studies of chapter 4, was not knowing what was really taking place within the sample. Further, as was emphasised at an early stage in this thesis (section 1.2.1), the intensity and phase information as analysed at a single point in the scattered light field, can only be interpreted in terms of the kinetics of the scattering ensemble of particles on the basis of a dynamical model. The analysis of changes in the detector photocurrent cannot uniquely characterise either the dynamics or the scattering properties of the particles.

The key result of chapter 4 was the unexpected AAR - concentration interaction which inspired a series of experiments in an attempt to understand it. However, these studies made it increasingly clear that a better understanding was required of how spermatozoa behaved both physiologically and physically in the environment of the light scattering cell. No attention had been given to this in the literature, other than in relation to sedimentation effects (Cooke, *et al.*, 1976). It appeared that the slow ACF component was a linear function of the concentration of dead cells (table 4-2) when motile cells were not present. This observation together with the calculated equivalent hydrodynamic radius, albeit rather large, tended to support the *Brownian diffusion of dead cells*

models as the origin of the slow component.

However, the source of the fast ACF component was less certain, particularly since there was the disturbing indication that the intensity contribution from motile spermatozoa (table 4-2) was significantly less than that from the same concentration of dead cells. The question arose as to whether the motile-generated ACF component was in fact generated by the translation of the cells. To some extent, up until now, this had not been treated as an important issue since it was the ratio of intensities from the motile and immotile fractions which was the measurement of interest and unless there was some substantial difference in the way in which motile and immotile cells scattered light, the exact origin of the scattering should not have been involved.

Compelling evidence of interactions between motile and immotile cells appeared in the LBS results and while it is well known that spermatozoa exhibit cooperative effects at high concentrations (section 2.7) such effects were not expected at concentrations $<< 10^7$/ml and had certainly not been referred to in the literature on applications of LBS to spermatozoa.

A new approach to the problem was required, an approach which examined more directly the fundamental aspects of spermatozoa behaviour in the light scattering environment and closely considered the previously accepted model of the system. This chapter is concerned with a series of experiments which adopted this philosophy and the revised model of the system which they ultimately generated.

5.1 Light scattering from vigorously translating and weakly translating spermatozoa

5.1.1 Background

Previous published LBS studies on various species of spermatozoa had derived swimming speed distributions or mean speeds from the LBS spectra or autocorrelation functions (section 1.5).

It is difficult to validate such measurements since no convenient and quantitative techniques are available which can be used in parallel with the LBS experiments. Photographic or photoelectric techniques (ref. section 3.8 and 3.10) could possibly have been used but great care would need to be taken to ensure that the sample cell and other factors were exactly the same for both techniques. The relative timescales involved in such methods would largely render the comparison impractical. Some light scattering experimentalists compared their derived numerical values for speeds with those generally accepted for spermatozoa while others looked, for example, for changes in derived swimming speeds as a function of sample temperature. Neither approach could completely verify that the LBS technique was in fact measuring the translational speed distribution.

What did seem possible, however, was to check that samples having *widely differing translational characteristics* gave an appropriate difference in the LBS autocorrelation function or frequency spectra. That is, in the limit, a comparison of the autocorrelation functions from vigorously translating spermatozoa with those from wiggling or otherwise active but non-translating cells. The difference in autocorrelation characteristics between motile cells and dead cells was well known, and is implicit in all the results of chapter 4. However, the effect of varying levels of translation was a new question and one through which this experiment sought to substantiate the origin of the fast autocorrelation component.

The results obtained in the first phase of this study suggested that further information might be obtained by varying the scattering geometry. It was for this reason that results are also presented in this section for alignment of the detector at scattering angles in, not only the horizontal plane (as was usual) but also in the vertical plane.

5.1.2 Methods

This experiment was made possible by the development of techniques for washing and removing a very high percentage of the seminal plasma and protein from samples of bull spermatozoa, which were then suspended in 2% sodium citrate buffer. (Shannon and Curson, pers. comm.) This washing procedure involved repeated differential centrifugation in a Ficoll density gradient, the specific preparative procedure being unimportant in the context of this LBS experiment other than that it resulted in sperm suspensions which showed a complete absence of progressive translation at 37°c.

Viewed microscopically at 37°c in sodium citrate buffer, a high percentage of spermatozoa were still obviously active, but exhibited internal motions only, wiggling, rotating or vibrating. However, by adding even minute quantities of seminal plasma (< 1%) or egg-yolk diluent to the buffer, the cells became reactivated and exhibited normal translation (Shannon and Curson, pers. comm.)

Samples of washed and deactivated spermatozoa were prepared in this way at the Newstead Artificial Breeding Research laboratory of the N.Z. Dairy Board, from a semen service containing 15% dead (*eosinophillic*) cells. For LBS measurements the sample was diluted to 10^6 sperm/ml in 2% sodium citrate buffer, (0.22μm filtered). A type B-2 light scattering sample cell was used, temperature controlled at 37.0°c and the standard 5.5 min thermal equilibration period allowed. The laser wavelength used was the 441nm He - Cd line, the scattering angle being 8° with a scattering vector amplitude of $k = 2.65 \times 10^4$ cm^{-1}.

Autocorrelation functions were collected for both non-translatory samples and for reactivated dilutions of the same sample. Microscopical examination of sub-samples from the light scattering dilutions, were carried out (at the experimental concentration) to verify the status of translatory activity. Care was taken to completely flush the LBS sample

sample cell between samples since small residual traces of protein or seminal plasma could have re-mobilised the non-translatory samples of washed cells.

Autocorrelation functions were collected at both high and low signal sampling rates (sampling intervals of 0.333mS and 10mS, respectively). The long timescale functions (32 * 1024 samples at intervals of 10mS) allowed the results to be related back to those obtained in the experiments of chapter 4 while the short timescale functions (128 * 1024 samples at 0.333mS sampling intervals, giving a total signal sampling time of only 43.65s) spanning the delay range 0 - 33.3mS were necessary to define the shape of the fast ACF component.

An additional experimental variable was incorporated after some preliminary experimentation. The experiment was carried out with the photodetector aligned at a scattering angle of 8° in both the horizontal (as normal) and the vertical scattering planes (scattering plane being that defined by the beam and the detector).

5.1.3 Results

In contrast to a dramatic difference in microscopic appearance between the translating and non-translating samples, a disproportionately small difference was observed in the AAR values, and in the general appearance of the long timescale (0 - 1s) autocorrelation functions, (shown here in fig. 5-1) when using horizontal detector alignment. From microscopic examination (under a coverslip on a microscope slide at 37°c) there was no question that in the deactivated samples virtually no motile cells were translating but a high proportion were executing wiggling, vibrating or circulatory movements. On the other hand, the reactivated samples all showed vigorous translation among a high percentage of the population, yet the AAR values were 0.679 (± 1%) and 0.420 (± 1.1%) for the non-translatory and translatory samples, respectively. The decay constant of

Fig. 5-1. Long timescale autocorrelation functions for translating and non-translating spermatozoa, with the photodetector aligned in the horizontal plane and in the vertical plane at a scattering angle of 8° in both cases.

Fig. 5-2. Autocorrelation functions taken under the same conditions as those of fig. 5-1 but at a higher signal sampling frequency so as to define the short timescale peaks seen in fig. 5-1 and generated by the motile spermatozoa.

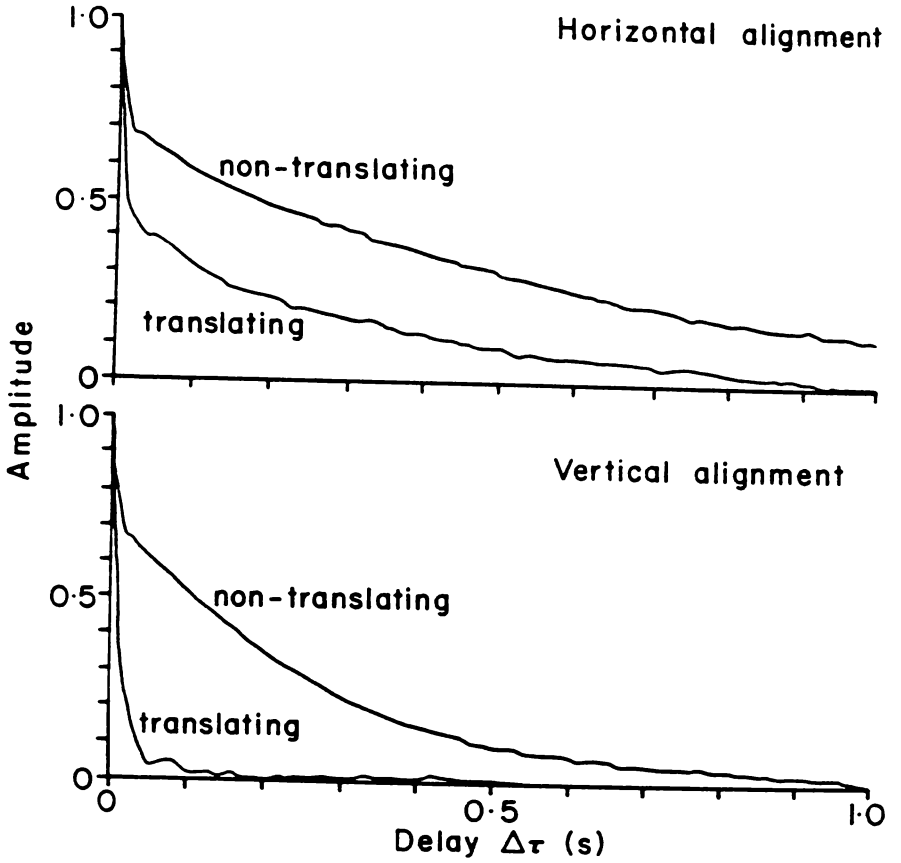
Horizontal alignment
non-translating
translating
Amplitude
1·0
0·5
0
Vertical alignment
non-translating
translating
0
0·5
1·0
Delay Δτ (s)

Fig. 5-1.

Fig. 5-2.

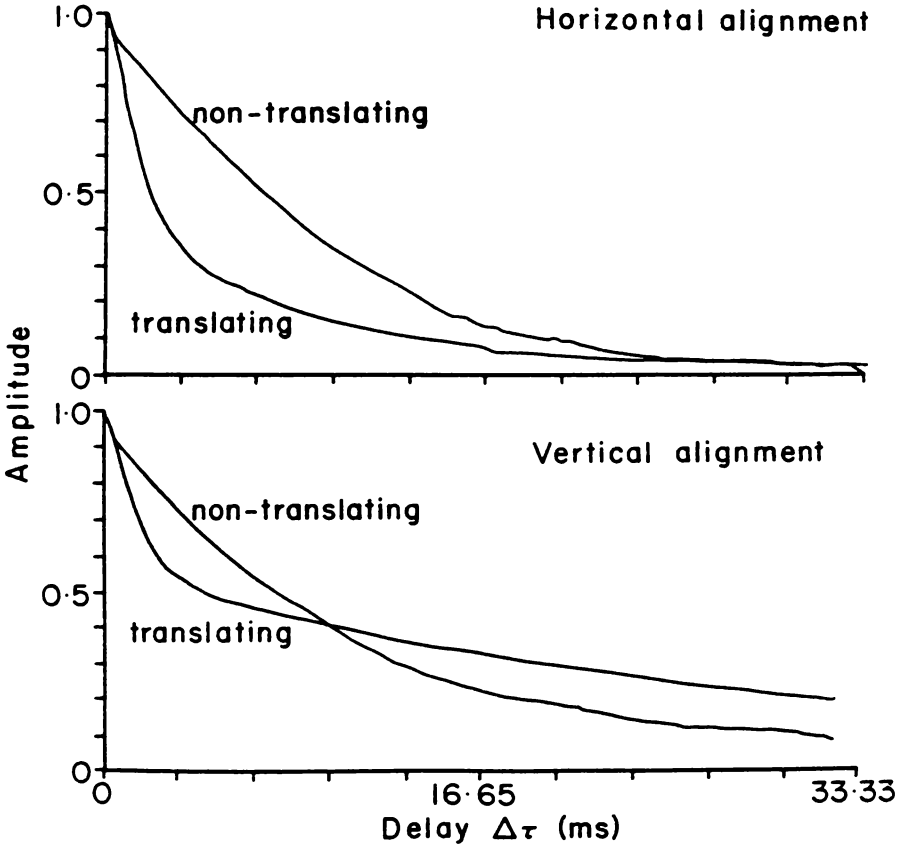
Horizontal alignment
non-translating
translating
Amplitude
1·0
0·5
0
Vertical alignment
non-translating
translating
0
16·65
33·33
Delay Δτ (ms)

the slow ACF exponential showed the differences previously noted to be associated with the presence of motile spermatozoa, being 1.66 $\pm$ 0.03 s^{-1} and 2.96 $\pm$ 0.08 s^{-1} for the non-translatory (NTR) and translatory (TR) respectively.

It had been expected on the basis of the differences in translation that a greater difference in AAR would be obtained and that the motile component for the NTR sample would generate a defective swimmer component such as was apparent, it seemed, in the correlation functions presented earlier in fig. 4-5. The relatively small shift in AAR was so unexpected that the possibility was examined that the active but non-translating cells in the scattering volume may have been photo-stimulated back into translational motion by the laser irradiation. However, observations of autocorrelation functions at very high and at very low levels of light intensity, failed to show any significant changes for NTR samples.

The short timescale autocorrelation functions (fig. 5-2) for horizontal detector alignment did show a significant difference in functional form for NTR and TR samples. For the TR samples the function was characteristic of the motile related component obtained in previous LBS experiments and shown for an even shorter timescale (0 - 10mS) in fig. 4-22. The functions of fig. 4-22 showed a characteristic width at half-amplitude of $\sim$ 2.1mS and that of the TR sample in fig. 5-2 (horizontal) a width of $\sim$ 1.9mS. However, the function for the NTR sample showed a significantly increased half-width at $\sim$ 7mS.

A quick check of the swimming speeds associated with these widths on the basis of an isotropic velocity point scatterer model (after Frost, 1977) gives r.m.s. velocities of 344µm/s and 49µm/s for the TR and NTR samples, respectively. The TR value is of the same order as that published by Hallet, *et al.*, (1978), for bull spermatozoa, which was said to arise from motion along a helical path, the actual translational velocity being much lower (the above 344µm/s would on their argument, give a true

translational RMS velocity of 162μm/s).

Certainly in fig. 5-2, the NTR sample showed a significant broadening of the autocorrelation function (giving a much reduced rms true translational speed of ∿ 23μm/s it seemed) although the residual width (7mS) was still not appropriate to the zero translation status observed microscopically in the samples and further, the function was of exponential form. A further significant result was obtained, however, when the same experiment was carried out with the photodetector aligned in the vertical plane at the same scattering angle (8°), the correlation functions for this case also being given in figs. 5-1 and 5-2.

On the long autocorrelation timescale (0 - 1.0s), much the same result was obtained for the NTR spermatozoa samples as had been obtained with horizontal alignment. That is, an AAR of ∿ 0.8 and the usual two component structure of the ACF. However, in the case of the TR, samples the familiar slow exponential component had vanished completely, having shrunk to or been replaced by a rapidly decaying feature with indications of a periodic component (fig. 5-1). For the short timescale data (fig. 5-2), the function for the NTR cells looked virtually identical to that obtained with horizontal alignment, both being of exponential form and having characteristic decay constants of 83.3 s^{-1} and 94.2 s^{-1}, for the horizontal and vertical cases, respectively.

The fast function (0 - 33.3mS) for the TR samples, however, had a rapidly decaying component with a similar decay rate to that observed on the same timescale for TR cells and horizontal alignment. This rapidly decaying component was clearly superimposed on the secondary damped cosine feature which was apparent in fig. 5-1 at Δt < 0.2s. The two component form, is also apparent in the family of correlation functions given in fig. 5-3 which shows a progression over intermediate timescales between the functions of figs. 5-1 and 5-2 (for TR spermatozoa with vertical alignment).

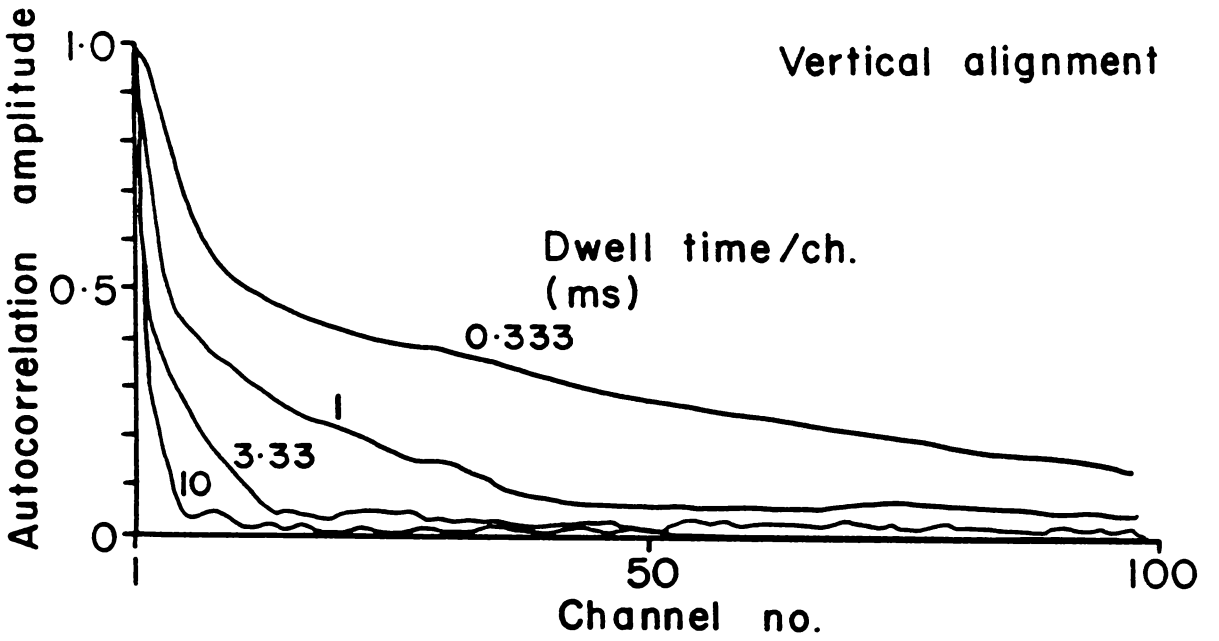

Fig. 5-3. Autocorrelation functions on various timescales showing the two component nature for motile spermatozoa and vertical alignment. Compare these functions with those corresponding in figs. 5-1 and 5-2 (all functions are normalised).

Fig. 5-4. Autocorrelation functions for a sample of vigorously motile bull spermatozoa using both horizontal and vertical alignment of the photodetector at a scattering angle of 8°. Note the disappearance of the exponential feature with vertical alignment and the appearance of a rapidly decaying cosine feature.

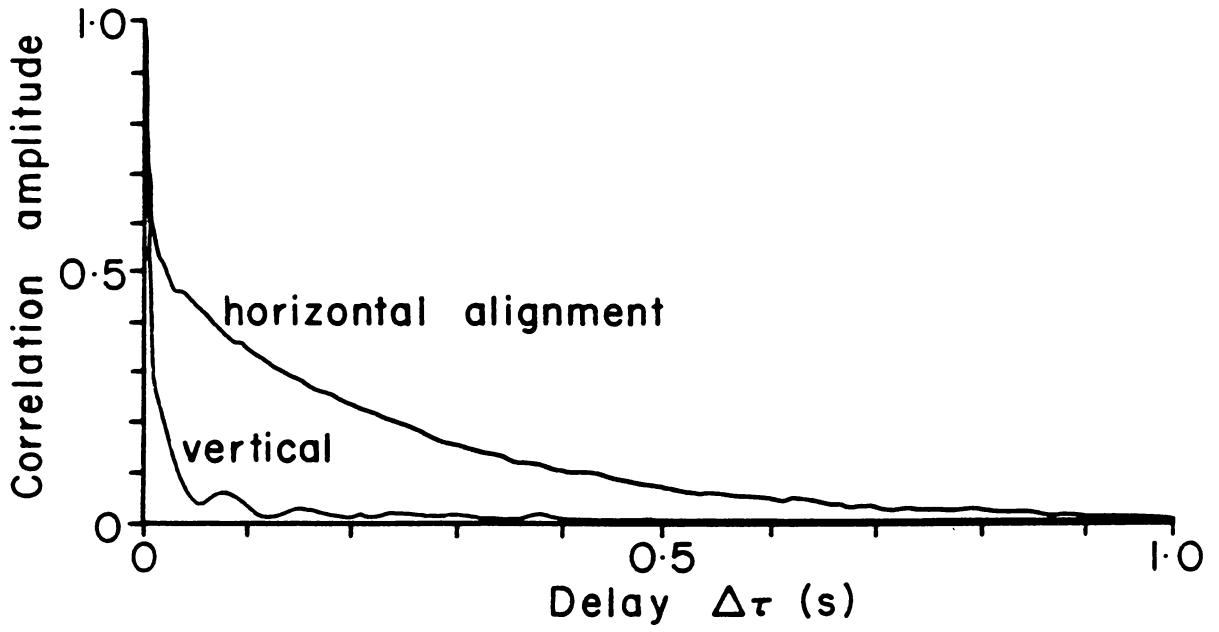

By collecting autocorrelation functions over a longer signal sampling time (∿ 11 min) as a followup, better definition of the form of the vertical alignment function with TR cells was obtained (fig. 5-4). This function clearly showed no trace of a slow exponential component with vertical alignment. Rather, it appeared to have either shrunk to, or been replaced by, a rapidly decaying cosine feature on a timescale of < 200mS, as had previously been suspected. The period of this oscillatory feature was determined to be 77mS and there appeared, therefore, the possibility that the cosine feature was associated with the sperm head rotation, the period being approximately half that observed by Rikmenspoel (1962) for bull spermatozoa swimming at 100μm/s (relates also ultimately to section 5.6.2).

5.1.4 Discussion and Conclusions

These were dramatic and unexpected results, the significant features being summarised as:

(i) non-translating spermatozoa (i.e., wigglers and circular swimmers) generate a rapidly decaying autocorrelation component, which is however broadened in comparison with that from translating cells, but is of approximately exponential form and not apparently consistent with a translational origin.

(ii) with vertical alignment of the detector, the ACF component normally associated with the immotile spermatozoa in the conventional horizontal scattering alignment, vanishes completely, being replaced by a highly damped cosine feature on a timescale 0 - 200mS.

(iii) AAR values for vigorously translating and for non-translating spermatozoa do not show differences consistent with the observed differences in translation.

Nowhere in the literature (sections 1.3 - 1.5) had any mention been made of the significance which might be attached to the plane of detector

alignment (in regard to spermatozoa studies), other than the studies of Nossal and Chen (1972). In their work with motile bacteria, periodic autocorrelation functions were obtained from the biased random-walk dynamics associated with chemotaxis and this suggested that the periodic feature of fig. 5-4 could possibly originate from geotaxis (Roberts, 1972). However, this explanation seemed unlikely since the experiments with spermatozoa were carried out in a homodyne mode which can detect only relative motion of scatterers, and even if the detection mode had been heterodyne, a vertical bias in the motile sperm velocities of 31μm/s would have been required to generate the observed periodicity (sedimentation velocity had previously been found to be < 0.6μm/s).

How then were these results to be interpreted? The most reasonable conclusions appeared to be:

(i) if, in fact, the slow exponential component of the long timescale autocorrelation functions did actually arise from the dead cells (previous studies had suggested that it did, i.e., chapter 4), then the inevitable conclusion was that a very marked orientational asymmetry existed in the light scattered by dead cells. It appeared on this basis that with vertical alignment, the dead cells did not scatter light to the detector.

(ii) wiggling and irregularly moving cells, the NTR fraction, gave similar results with both planes of detector alignment suggesting that the *supposed* rotational optical anisotropy of dead cells was destroyed by the irregular motions.

(iii) the motile fraction appeared to generate the same very short timescale component with both planes of alignment, possibly supporting to some extent, the point-scatterer Doppler model.

(iv) the decay times for the rapidly decaying autocorrelation component, while similar in both planes, gave RMS swimming speeds which even after correction for possible helical trajectories, were too high in comparison with known values from other methods, (fig. 1-18, for example) and militated

against the point scatterer - Doppler model. This, together with a suspected gross optical anisotropy on the basis of (i) above, and the disturbing new cosine component apparent in the vertical alignment case of fig. 5-4 which was possibly associated with the motile fraction, strongly suggested that the motile fraction was subject to the same optical anisotropy as was the immotile fraction.

(v) in view of (iv) it seemed that the fast ACF component may not arise, at least in part, from a Doppler beat effect but may result from intensity changes in the scattered field.

Further studies were therefore indicated to clarify the origin of both autocorrelation components.

5.2 Spatial distribution of spermatozoa in light scattering sample cells

5.2.1 Introduction

Previous experiments had created serious doubts regarding the behaviour of spermatozoa in the light scattering cell and the manner in which the cells scattered light. During these experiments, samples had frequently been viewed microscopically but always in a very thin suspension ($\sim$ 100μm) on a microscope slide (at 37°c) under a coverslip with bright-field illumination from below. Under these conditions, no unusual behaviour or phenomenon was readily apparent, the motile cells appearing to conform to an isotropically oriented distribution of translation vectors, both speed and direction being substantially constant over a timescale of several seconds.

With increasing suspicions, however, that *things were not what they seemed,* a programme of microscopic observations was undertaken under physical conditions which more closely approximated the scattering environment. One such aspect of this study was to confirm that the distribution

of translation vectors remained isotropic in a suspension of extended linear dimensions as in a typical light scattering cell.

5.2.2 Methods

These microscopic studies involved the swimming behaviour of bull spermatozoa in a sample cell of the type B-1 design (fig. 3-12) when located on a thermostatic microscopic stage, controlled at 37°c. The microscope stage was of extremely large thermal mass relative to the light scattering cell (being a copper block of dimensions 12cm x 7cm x 6mm) and heated the cell placed on it, through the bottom surface. The cell, while of the B-1 type conformation, was of only 1mm depth (but very deep relative to the depth of a suspension under a microscope coverslip) and had thinner glass windows than previous designs to allow improved thermal contact with the heat source. In fact, the cell was of the same geometry later used to construct the type C sample cell of fig. 3-15.

So as to prevent convection in the medium arising from heat losses at the upper surface, the cell was generally covered by an enveloping lid of expanded polystyrene, to give a more uniform temperature distribution, the sample being viewed microscopically from above through a small hole in the cover.

Microscopy was carried out using an *Olympus Model BH* microscope with both bright and dark - field illumination. For the results reported here, a 10 x objective lens was used, this having a working distance of 5.4mm and giving a depth of focus of $\sim$ 120μm when used with 10 x eyepieces the overall magnification being 100 x.

The key observations were recorded photographically through the appropriate microscope attachment and used time exposure methods. The camera, a 35mm single lens reflex (*Pentax SP1000*) was located on the camera tube of the microscope using a special purpose *Pentax* fitting screwed into the camera body in place of the normal lens. The objective

lens of the microscope directly formed a real image at the film plane via the interposed prismatic system which allowed simultaneous viewing.

While sperm swimming motions could be readily observed visually, it was found in initial studies using bright-field illumination from below, that good photographic contrast was not easy to achieve. Photography later carried out using dark-field illumination gave improved results.

The objective of using time exposure photomicrographs was that of defining motile sperm numbers and translational orientations via their swimming tracks at various focal planes down through the sample.

Film speed and exposure times varied, depending on the particular conditions of the experiment. Colour slide film of 64 ASA was frequently used, this appearing to allow the greatest latitude in exposure levels. It was found necessary to use faster film (125 ASA) when using dark field illumination.

Two sets of photographic results are presented in this section and they both seek to demonstrate the vertical distribution of spermatozoa over the 1mm depth of the sample cell and the planar swimming behaviour. The exposures (1s in both cases) were taken as part of a sequential series at $\sim$ 100μm intervals down through the sample.

The procedure was to inject a sample into the cell at a concentration of 10^7/ml in 0.22μm filtered sodium citrate based buffer and close off the inlet/outlet tubes. A period of 5 min. was allowed for thermal equilibrium to become established and after this was confirmed microscopically, the photographic exposures were taken using the calibrated fine-focus control on the microscope to increment the focal plane in steps from the top surface down to the bottom surface of the cell.

5.2.3 Results and Discussion

The set of prints shown in fig. 5-5 shows time exposure photomicrographs (1s exposures) of spermatozoa motions with the focal field aligned

ROOF

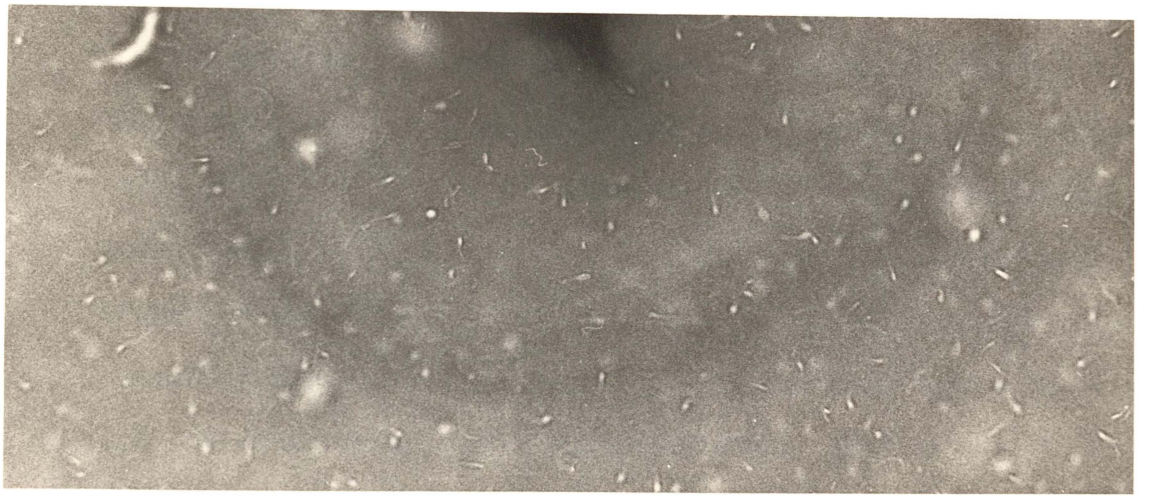

MID-
POINT

FLOOR

Fig. 5-5. Time exposure (1s) photomicrographs with bright-field illumination at the roof, mid-point and floor of the sample cell. Note the predominantly curved swimming tracks. Dead spermatozoa appear as sharply defined white dots.

Overall magnification of these prints ∿ 72 x, that is a 6mm track corresponds to a translational velocity of ∿ 83μm/s.

close to the roof, midpoint and floor of the sample cell, with bright-field illumination. In this case the exposure was on 64 ASA colour slide film and the prints were made directly from the slides on high contrast black and white paper.

The trajectories of motile spermatozoa are seen as curved white tracks and dead cells appear as white dots. In this case the tracks are curved due to the characteristic tendency to circular swimming associated with an aged sample.

The most obvious feature of these exposures is that all the swimming tracks appear in the exposures taken at the surfaces. No discernible tracks occur in the mid-cell exposure. However, if spermatozoa swimming in the centre of the cell had a more isotropic distribution of translation vectors, a large percentage would swim rapidly through the focal field at a range of angles and hence not leave tracks characteristic of those observed as swimming in the surface planes. Some of the blurred images in the mid-cell exposure may indeed be such spermatozoa swimming rapidly through the focal field. However, concurrent visual observations at these three locations in the cell demonstrated clearly that few motile spermatozoa were to be found in the bulk of the medium, virtually all swimming cells being found close to the top and bottom surfaces of the sample cells, as is demonstrated in the photographic exposures. The swimming cells showed a marked tendency to remain swimming in the plane of the surface rather than colliding elastically with it. An extremely marked spatial stratification of motile spermatozoa was thus observed, with a large percentage of the cells swimming in close proximity to the cell surfaces. Furthermore the spatial stratification of motile sperm was found to occur over a timescale of minutes, the time taken for thermal equilibration and for the spermatozoa to swim into contact with a surface.

This observation was found to be supported by the little known studies of Rothschild (1963b) which were subsequently discovered in the literature.

As previously described in section 2.8, Rothschild carried out cine-microphotography and found a grossly non-uniform distribution of motile sperm numbers between two plane surfaces spaced 200μm apart.

Dead cells are imaged in fig. 5-5 as quite sharply defined white dots. It is apparent on this basis, that a substantial number of dead cells were present on the floor and also in the mid region of the sample cell. Very few such images are seen in the exposure taken at the cell roof and this was consistent with sedimentation of dead cells which were observed to progressively accumulate on the bottom surface.

It is also interesting to note that the density of swimming tracks is rather similar at the top and bottom surfaces, although it was observed that as the sample aged the motile population at the top surface progressively diminished.

A further point of some significance, was the observation that spermatozoa swimming on the surfaces, were in fact swimming just clear of the surface, perhaps by 10 - 20μm. This could be ascertained for example, by focussing collectively onto the dead spermatozoa which were lying on the floor of the cell. In this condition the motile spermatozoa swimming on the bottom were seen to be slightly out of focus and the focal field had to be shifted up by 10 - 20μm to bring them into sharp focus.

Further prints taken under similar experimental conditions, but using dark-field microscopic illumination and a fresh highly motile sample of spermatozoa, are shown in fig. 5-6.

The same general features are apparent in these photographs as were in fig. 5-5. In this case however, the swimming tracks are much more linear and there appear to be fewer immotile spermatozoa. Here there is some slight evidence in the exposure taken at half depth, as by the blurred undefined images, that some spermatozoa were swimming through the focal field. Visually, a much smaller proportion of motile spermatozoa were present in this region than at the surfaces. Further, and of great

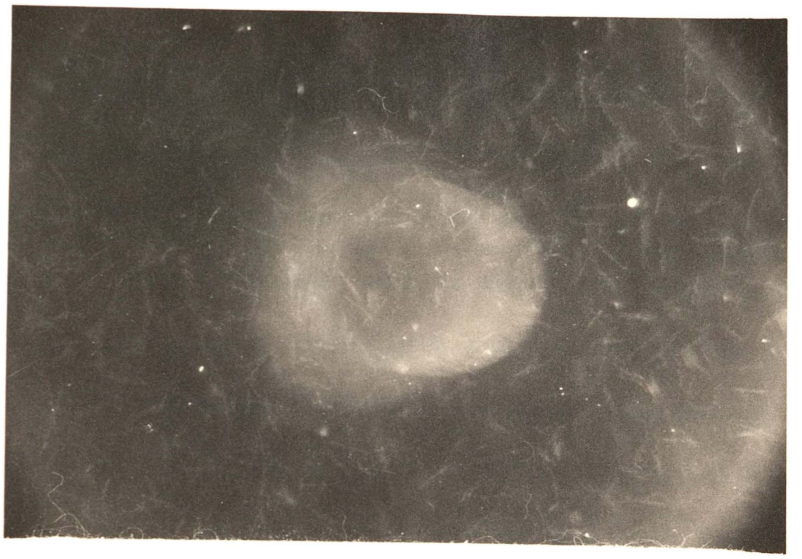

ROOF

HALF DEPTH

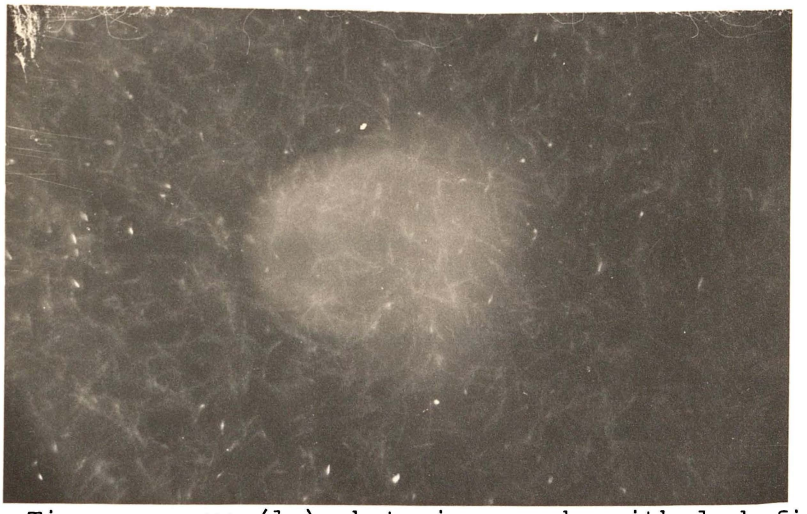

FLOOR

Fig. 5-6. Time exposure (1s) photomicrographs with dark-field illumination showing the high concentration of swimming spermatozoa at the surfaces of the cell. Note the intensity modulations along the tracks. Overall magnification of these prints is ∿ 72 x.

importance, an intensity modulation is evident along the tracks. Although the photographic resolution is not high, the tracks appear to comprise a structured linear set of dots or 'duck-footed' images. This is a consequence of the flashing effect which spermatozoa exhibit when swimming in the microscopic dark-field and the phenomenon was clearly observed visually. Rothschild (1953) discussed the effect and Grey (1958) later captured the phenomenon on film (section 2.6 and fig. 2-11). This phenomenon was studied more closely in the work described in the following section.

5.2.4 Conclusions

These simple visual and photographic observations had very considerable implications for the interpretation of, not only the LBS results of chapter 4, but for the interpretations previously proposed in the literature (section 1.5) for studies with spermatozoa.

The main features were:

(i) an extremely marked spatial stratification of the motile fraction, with spermatozoa apparently migrating rapidly to, and staying in close contact with, the internal surfaces of the sample cell.

(ii) motile cells with dark-field illumination presented a flashing appearance with a large apparent intensity ratio.

(iii) dead cells sedimented out of suspension, progressively accumulating on the floor of the cell.

from which was reasonably concluded:

(1) the grossly inhomogeneous distribution of motile cells and the highly anisotropic orientation of translation vectors (due to planar swimming motions) immediately refuted the validity of any assumption of an isotropic distribution of velocities as had been an essential feature of various published analyses. This might reasonably be expected to

also apply to species other than bull spermatozoa.

(2) the actual distribution of translation vector orientations contributing to light scattering data, would depend on the region within the sample cell where the observed scattering volume was located.

(3) short timescale scattering intensity and AAR changes can be expected from any region within the cell while the stratification of motile spermatozoa occurs.

(4) the final equilibrium value of the AAR would depend on the location of the observed scattering region within the sample. Higher AAR values could be expected in the mid-region of the sample than at the cell roof for example.

(5) the flashing effect when spermatozoa were observed with dark field illumination could well have considerable significance for the interpretation of the fast motile related ACF component which may consequently show a significant intensity fluctuation component.

Such conclusions immediately threw new light on previous results and added another small piece of understanding.

5.2.5 Further microscopic observations of motile spermatozoa swimming on surfaces

(i) *Smooth surfaces oriented in the vertical plane.*

The possibility existed, although considered unlikely at the time, that the marked surface swimming behaviour could have been induced by convective motions of the medium in a cell which was heated through the floor. In such circumstances, the surface swimming effect may have been maintained by way of spermatozoa being swept onto the surfaces by vertical convective flows of the medium. In the sample cell used, this was unlikely to have been the case since such effects would have been evident in the motion of the dead cells. Convective motions could be observed in sample cells of greater depth, one reason why a minimal depth of 1mm was employed. So as to further resolve the convection

possibility the swimming behaviour at vertical surfaces was examined. Using a similar flat shallow sample cell, a small piece of glass was seated within the cell, this piece of glass having a smooth vertical surface which became immersed in the sample. Spermatozoa were observed (microscopically) approaching and encountering the surface.

Exactly the same type of behaviour was observed as had been on horizontal smooth surfaces (section 5.2.3). A spermatozoon swimming out of the bulk of the medium would effectively become captured by the surface and remain swimming parallel to, but just clear of it. These collisions with the surface appeared completely inelastic and the previous observations on such collisions given in 2.7 were made at this time.

Several unsuccessful attempts were made to photograph swimming on vertical surfaces. Using bright-field illumination in the microscope, insufficient contrast was obtained and the use of dark-field illumination was even less appropriate with this geometry due to the extremely high level of scattering from the surface itself, with the large angles of incidence.

(ii) *Curved Surfaces.*

So as to acquire further insight into the nature of the wall swimming effect, swimming behaviour at edges and at regions of surface curvature was observed. In general, spermatozoa tended not to follow a surface the contours of which, fell away from its track. Other than for curves of very large radius of curvature the cells tended to swim away tangentially back into the bulk of the medium. This suggested that the effect was of hydrodynamic origin as originally concluded by Rothschild (1963b) and Maude (1963), and not a charge or chemotactic phenomenon. It seems likely that when in close proximity to a surface, the flagellar wave becomes modified such as to preclude the cell from acquiring a force component normal to the surface. The effect has

previously been discussed in section 2.8.

(iii) *Rough Surfaces.*

Movement of spermatozoa in the vicinity of microscopically rough surfaces was also observed. Surfaces having irregularities with characteristic dimensions of perhaps 50 - 200μm were used, and it was found that the same uniform wall swimming effect did not occur. While spermatozoa frequently became trapped in the valleys of the surface, it appeared much easier for them to acquire a velocity component away from the surface and to swim back into the bulk of the medium.

(iv) *Motile - motile interactions.*

Collisional interactions between motile spermatozoa swimming on a smooth vertical surface often appeared to induce a change in trajectory and deflect one or both cells back into the bulk of the medium. The phenomenon was difficult to observe due to the vertical distribution of cells on the surface. It is,however,relevant to the subsequent model discussed in section 5.12.

5.2.6 General discussion: wall swimming effects

Visual and photographic observations reported in this section (5.2) established that:

(i) a large percentage of motile spermatozoa became constrained to swim close to the smooth internal surfaces of the sample cell after colliding inelastically with a surface. The effect occurs at sperm concentrations typical of light scattering experiments.

(ii) surface swimming cells do not follow the contour of an undulating surface which falls away from the trajectory and will swim off tangentially back into the medium.

(iii) the wall swimming effect is likely to be somewhat diminished at rough surfaces (depending on the scale of the surface irregularities) although spermatozoa do become trapped in

valleys.

(iv) on smooth surfaces the cells appear to swim close to, but not in contact with, the surface and $\sim$ 10 - 20μm distant from it. This may be due to hydrodynamic interactions between the flagellar beat and the bounding surface.

(v) interactions between surface swimming cells may redirect a spermatozoon back into the bulk of the medium. The effect may therefore be diminished at high concentrations, and more apparent at low concentrations.

No published work on sperm motility studies by LBS had taken account of, or made mention of, such wall swimming effects (refer sample cell geometry in table 1-4). It is also noted with interest that the photo-electric technique of Rikmenspoel and van Herpen (1957) had constrained the spermatozoa to swim in a thin film of medium (presumably to restrict velocities so as to be co-planar with the detector aperture) where such wall swimming effects would not have lead to problems of distribution within the sample.

Analysis of the spatial distribution given by Rothschild (1963b), previously given in fig. 2.19, indicated that 68% of the motile spermatozoa in the 200μm deep chamber, were to be found within 20μm of the surface and 35% more swimming cells were observed on the bottom surface than on the top surface.

Looking at the variation in concentration at the three key locations within the cell, and expressing the localised concentration relative to the average concentration $\bar{\rho}$ over the whole volume we find:

Average concentration over whole sample volume	1.00 $\bar{\rho}$
Concentration at mid-depth in cell	0.43 $\bar{\rho}$
Concentration at top surface of cell	2.14 $\bar{\rho}$
Concentration at bottom surface of cell	2.87 $\bar{\rho}$

Table 5-1. Localised concentrations of bull spermatozoa at the top surface, mid-point and bottom surface of a 200μm deep chamber, expressed relative to the average concentration $\bar{\rho}$. (From Rothschild's distribution of fig. 2.19).

Rothschild did not specify the absolute concentration of spermatozoa used in his experiments, but did state that a dilution of 1:30 was used which suggests an absolute concentration in the range 30 - 60 million sperm/ml. (The results of figs. 5-5, 5-6 were at 10 million/ml).

If the ratio of wall swimmers to medium swimmers is strongly dependent on motile-motile interactions, the internal surface area of the cell, relative to both the sample volume and the motile concentration, would become important.

Commenting on Rothschild's observations, Maude (1963), pointed out that the low Reynolds number for a swimming spermatozoon ($\sim 10^{-3}$) indicates a form of creeping flow between the sperm and the surface. Resistance to motion of the spermatozoon, both towards and away from the surface, then arises due to the required displacement of the medium into or out of the boundary layer. Subsequently Katz and Blake (1974) and Katz (1974) also acknowledged the tendency of spermatozoa to swim in close proximity to solid boundaries such as microscope slides and coverslips. They considered the presence of the wall to introduce an anisotropy into the decay of fluid disturbances created by the flagellum, thus modifying the resistance coefficients normal to and tangential to the wall.

It is perhaps interesting that the wall swimming phenomenon is not more widely known and the probable reason is that suspensions of sperm are most often viewed at high concentration in a thin liquid suspension under a coverslip. Although the effect can be observed under these conditions if an observer is looking for it, it generally either misses the eye, or the depth of focus in the microscope field is too great to reveal it.

The phenomenon was clearly important in relation to the kinetic model of spermatozoa suspensions in light scattering cells.

5.3 Sperm behaviour within the typical laser light scattering geometry

5.3.1 Introduction

The observations of section 5.2 revealed *in vitro* swimming behaviour and optical properties of bull spermatozoa (fig. 5-6) which were obviously highly relevant to light scattering experiments. These studies however, were still not directly within the environmental conditions and geometry of such experiments. With dark-field microscopic illumination, which was the closest approach to the optical geometry of laser light scattering, the image was actually formed by collecting scattered or reflected light from a convergent annular sheet of illumination. Unlike the light scattering detector which collects light at a single point in the field scattered from a linear beam, the microscope objective lens collects all light from within a conical solid angle, (hence a range of scattering angles) and from a converged annular source. Such a system displays axial symmetry in terms of the contribution of the scattered field to the image.

In view of the results from sections 5.1 and 5.2 and their indication that the optical and dynamic behaviours of spermatozoa were inadequately understood, it was considered inappropriate to directly extrapolate the microscopic optical geometry (and hence the associated effects which have been described) directly to the laser light scattering system. Therefore, further microscopic and photographic experiments were carried out with the objective of defining exactly what the photodetector observed within the familiar geometry of LBS experiments. Direct observation is a most powerful experimental tool.

5.3.2 Methods

The approach taken was to simply replace the photodetector system with a low-power microscope aligned at a typical forward-scattering angle and to directly view the scattered light from samples of spermatozoa.

There were several experimental difficulties in doing this. Generally a short path length vertical plane cell of type C (fig. 3-15) was employed. (This design is further discussed in section 5.13.1) although initial studies had used type B cells. So as to minimise refractive distortions of the image, it was necessary to orient the plane surfaces of the water-jacket and cell to be normal to the axis of the microscope. A new water-jacket geometry, having large plane glass windows, was constructed for this purpose and is shown diagrammatically in fig. 5-7 and photographically in fig. 3-14b.

The viewing microscope was of low power and had a long working distance since the sample had to be viewed through approximately 3cm of water-jacket.

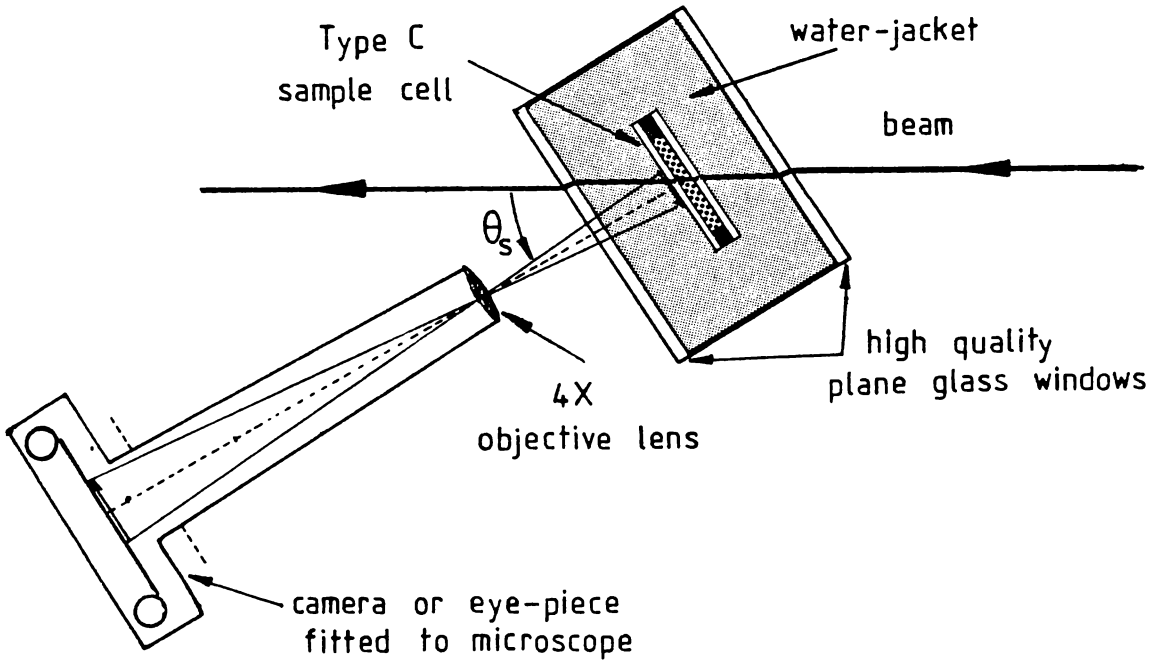

Fig. 5-7. Alignment of the sample cell, water-jacket, beam and camera/microscope for photographic/visual studies of spermatozoa within the light scattering system.

An objective of 4 x and a focal length of 5cm was generally employed in combination with an eyepiece in the range 6x - 10x. For purposes of

taking photomicrographs, the eyepiece was removed and the camera (*Pentax SP1000*) mounted directly onto the eyepiece-tube of the microscope, using the appropriate *Pentax* fitting. As with the studies of section 5.2 this allowed the objective to form an image directly on the film plane and the magnification was adjusted by using a variable length extension tube on the camera. This technique was necessary since although a higher power objective would have given sufficient magnification without the need for extension tubes, the smaller working distance of the lens would not allow the sample to be viewed through the water-jacket. A low-power objective with a long working distance was therefore the most appropriate, with the required magnification being achieved by increasing the distance to the film plane.

The image formed by this technique was, with careful alignment, of useful quality in terms of resolution and contrast. The depth of sharp focus was estimated to be 200μm. It was found that, at least for photographic purposes, the use of an egg-yolk diluent, even at low concentration, gave background scattering which significantly degraded the contrast on time exposures. For photographic purposes, therefore, samples were diluted with filtered sodium citrate buffer. It was also necessary to use appropriate dilutions (usually high) of the spermatozoa so as to give well defined individual swimming tracks over the exposure interval. Dilutions to 0.1×10^6 sperm/ml appeared the most appropriate for this purpose for exposures in the range 5s - 120s. Achieving the optimal combination of beam power, sperm concentration, film speed and exposure time required considerable experimentation.

The best photographic contrast was achieved using the red light from the 632.8nm He - Ne line. Contaminant particles within the water-jacket were a major problem since these adhered to the external sample cell surfaces. In the external beam entry and exit regions of the cell window, such contamination would scatter sufficient light to significantly degrade

photographic images of the region. Photographic observations at scattering angles > 20° were not generally successful due to contrast degradation by background scattering.

5.3.3 Results

The data in this section comprise the set of time exposure photomicrographs presented in figs. 5-8 through 5-12

These photographs represent directly, as closely as it was possible to achieve, scattered field intensity information received by a LBS photodetector, over the exposure period.

The diameter of the illuminated region was typically 500 - 700μm in these exposures, although it is difficult to precisely define the extent of this region, due to the Gaussian intensity profile across the beam. The Gaussian intensity profile is obvious in fig. 5-8 in particular, where there was some degree of over-exposure in the central region.

These time exposure photomicrographs are one of the most significant individual pieces of data in this thesis. They exhibit phenomena in the scattered light field from bull spermatozoa, which have very important implications for the measurement of motility by light beating spectroscopy. To some extent the situation is well described by the old saying.....

..... *one picture is worth a thousand words* .....

The general features in these and other time exposure photographs, supported by visual microscopic observation are:

(i) motile spermatozoa leave swimming tracks defined by a sequence of sharply defined dots or intensity peaks generated as the head rotates.

(ii) at typical LBS scattering angles the scattered light originates largely from the head region although an interference structured image of the flagellum, possibly the mid-piece, is evident for immotile cells. At larger angles ($\gtrsim 30°$) scattering from the flagellum becomes apparent.

Fig. 5-8. A time exposure of 20s at a scattering angle of 18° for 10^5 sperm/ml of sodium citrate buffer. The illuminated region is ∿ 700μm in diameter. Note that many of the dead cell images are out of focus. (page 312a).

Fig. 5-9. A 15s time exposure taken at a scattering angle of 18°. Sperm concentration is 10^5/ml and the illuminated region is ∿ 500μm in diameter. (page 312b).

Fig. 5-10. Long term time exposure photomicrographs (a = 120s, b = 180s) at a very low light level and a sperm concentration of 10^5/ml. Scattering angle is 17° to illustrate the very slow sedimentation and drift of dead cells. Note evidence of intensity fluctuations from the immotile cells and the background forest of intensity fluctuation from the wall swimming motile fraction. (page 312c).

Fig. 5-11. A short time exposure (1s) photomicrograph for spermatozoa at 10^5/ml in sodium citrate buffer. Scattering angle is 25°. Note the out-of-focus tracks arising from spermatozoa swimming on the rear window of the cell. (page 312d).

Fig. 5-12. An enlarged time exposure photomicrograph taken at a scattering angle of 18.8° and a concentration of 10^5 sperm/ml. (time exposure 20s).
The discrete nature of the images and the high intensity ratio is clearly apparent. (page 312e).

All original exposures *64 ASA Kodachrome*

Fig. 5-8

Fig. 5-9

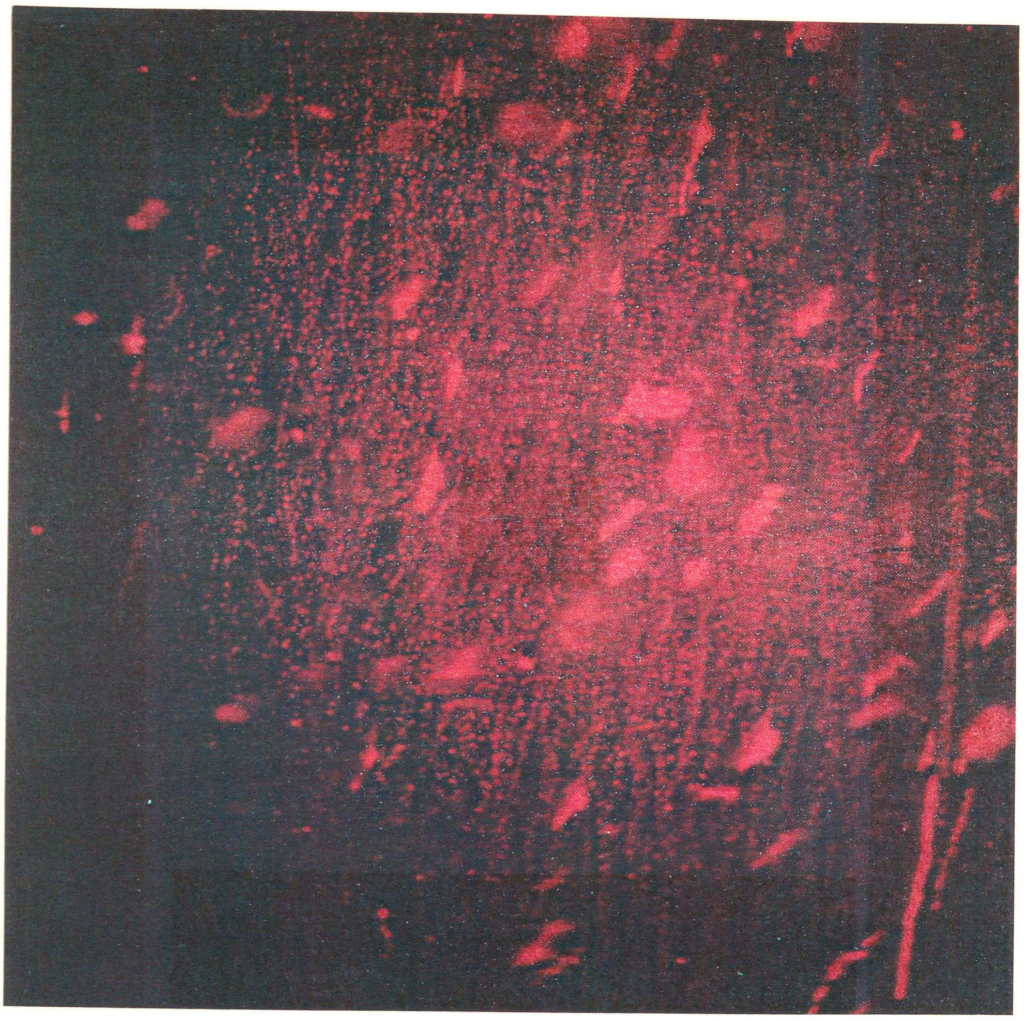

(a)

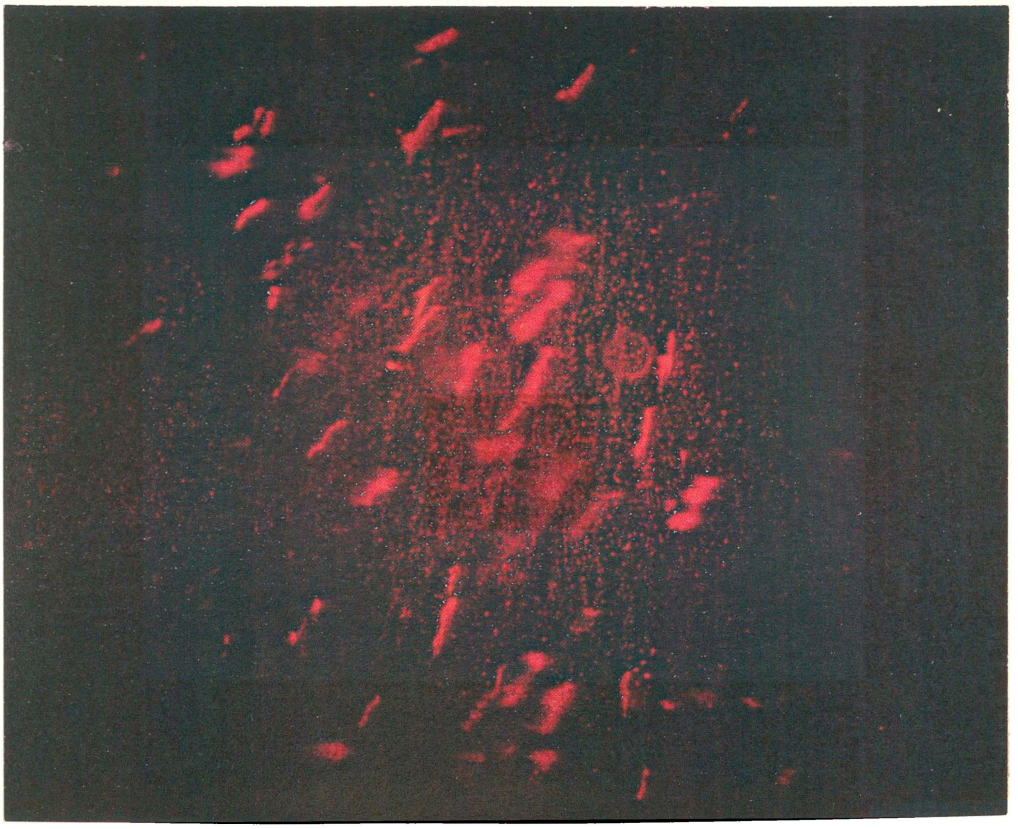

(b)

Fig. 5-10

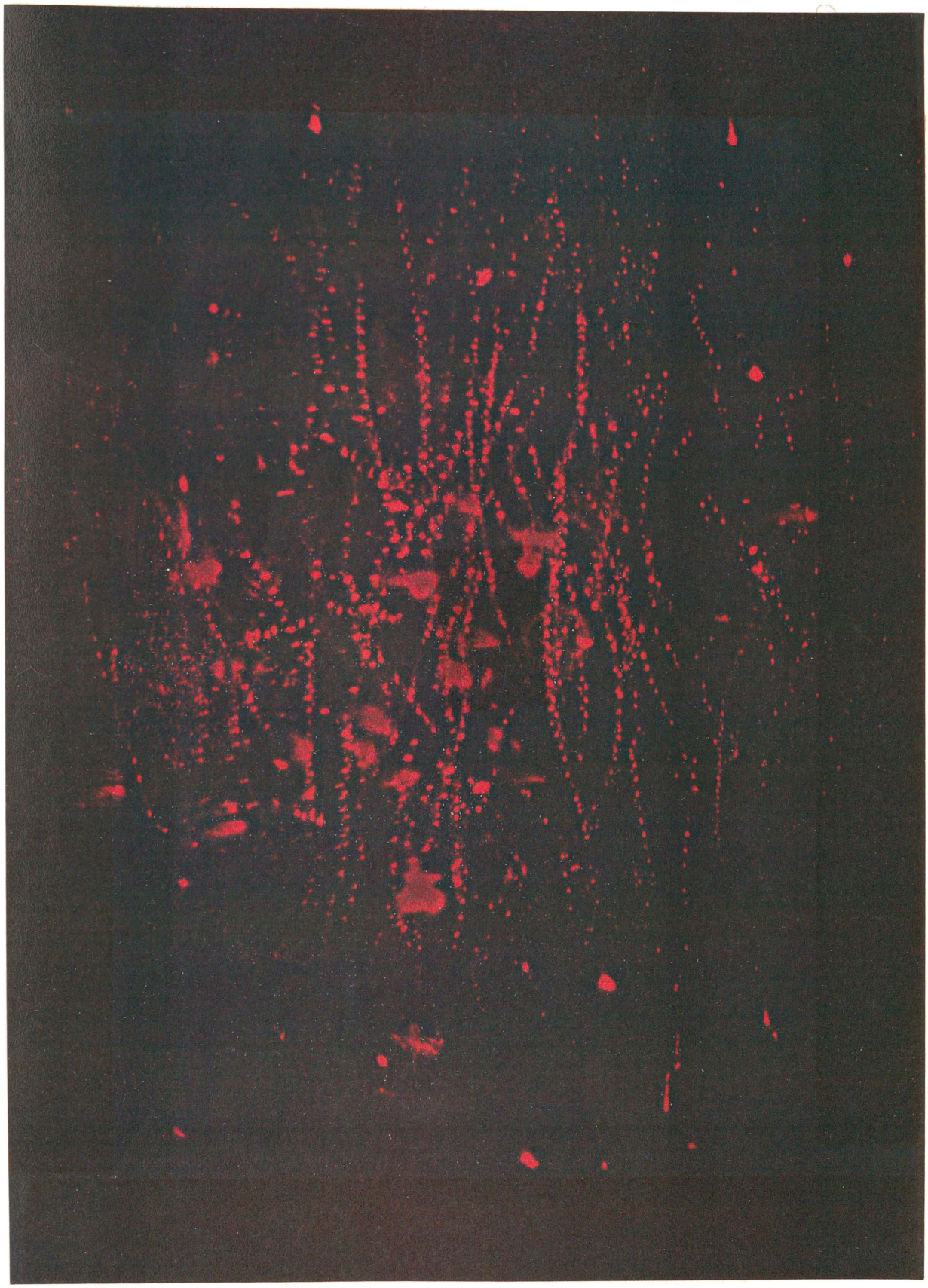

Fig. 5-11

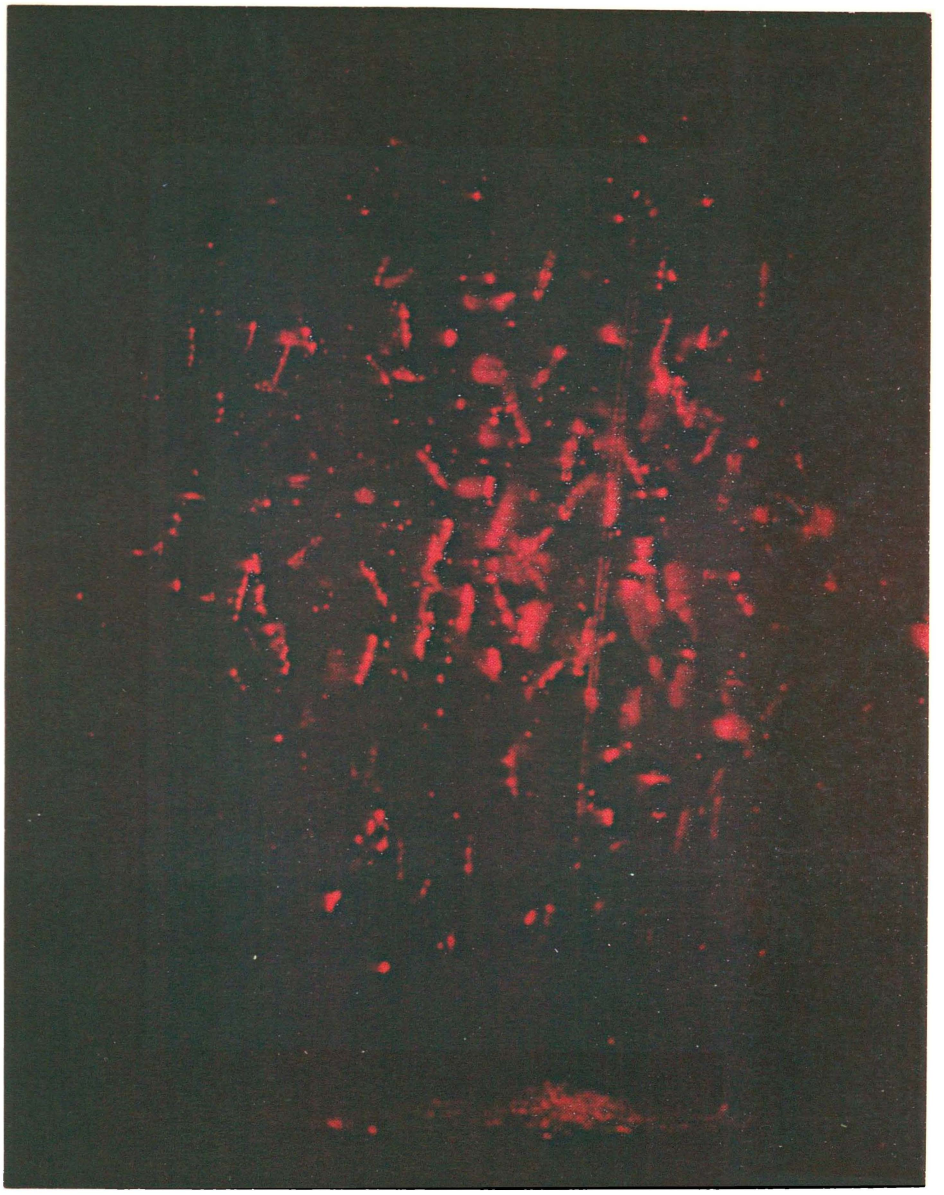

Fig. 5-12

(iii) the swimming tracks exhibit a high degree of alignment in a vertical direction (the scattering plane for these photographs was horizontal) and are far from being isotropically distributed.

(iv) swimming tracks are reasonably linear but small changes in direction do occur.

(v) dead cells are seen as bright diffuse flares, being generally out of focus and over-exposed.

(vi) the swimming tracks of motile spermatozoa appear to remain in the same focal field (that of the cell window) along their entire length while the images of most dead cells appear out of focus.

(vii) visual observations at blue wavelengths (441nm), where photography was not satisfactory due to significant background scattering at the high sperm dilutions, verified that the same phenomena occurred.

Further studies of the apparent vertical orientation of the swimming tracks were carried out, since although optical anisotropy was suspected, geotaxis of motile cells was also a likely explanation of the effect (Roberts, 1972). The photomicrographs of figs. 5-8 through 5-12 were taken with the microscope and camera aligned at the selected scattering angle in the horizontal plane and the photographs are oriented so that the vertical direction is up and down the page. This alignment geometry is illustrated in fig. 5-13(a). To resolve the geotaxis question observations were also carried out with the microscopic viewing angle aligned in the vertical plane as in fig. 5-13(b). Using similar scattering angles in the two scattering planes, the results were:

(1) for horizontal (X Z) alignment results were as previously detailed in (i) - (vii) above and as seen in fig. 5-8 through 5-12.

(2) with vertical alignment, the swimming tracks appeared exactly as in figs. 5-8 through 5-12 when rotated through 90°.

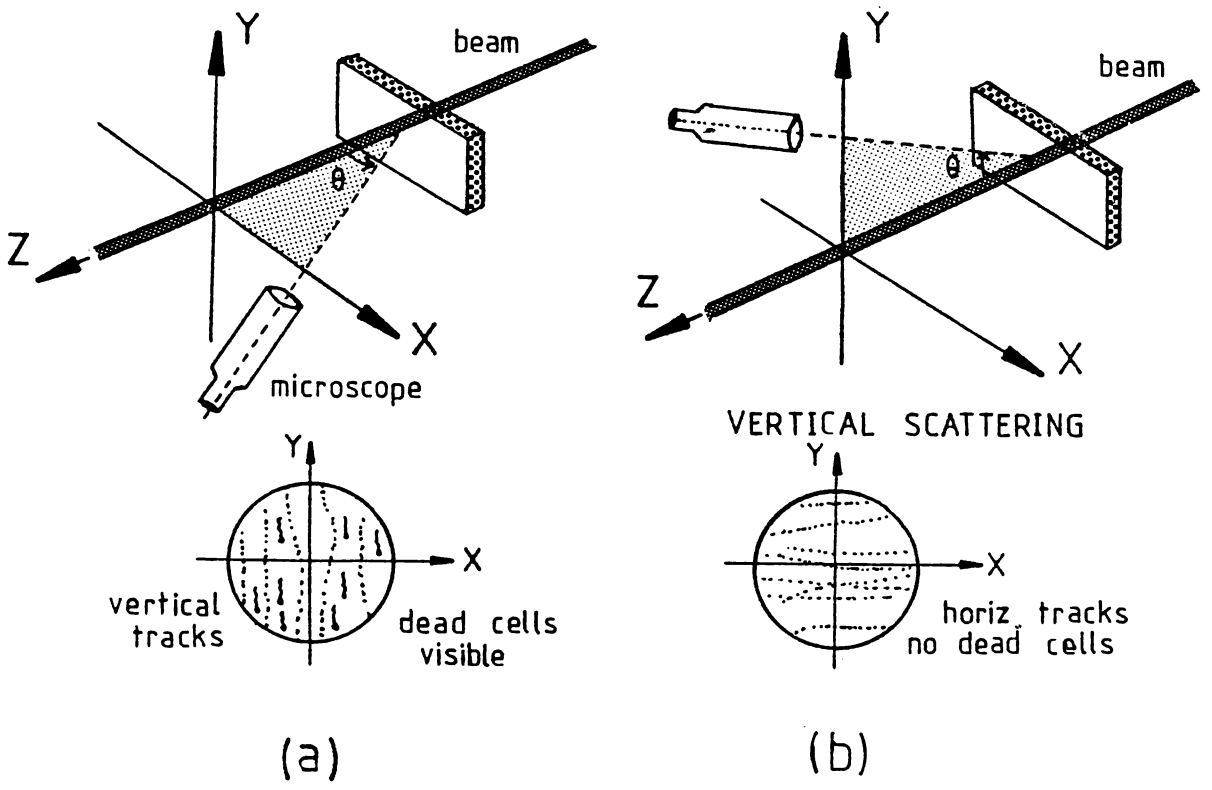

Fig. 5-13. Diagrammatic illustration of the effect of the scattering plane (XZ or YZ) on the orientation of swimming tracks in the viewing microscope field. (θs was typically 20°).

That is, to a vertically aligned viewing microscope, the swimming trajectories appeared to be within approximately ± 20° of the horizontal.

(3) No dead cells could be observed with vertical alignment of the microscope whereas with horizontal alignment of the microscope dead cells were clearly apparent but were always seen to be vertically oriented, head down.

When it therefore became apparent that a very considerable optical anisotropy was involved, further direct visual attempts to explore the effect with dead cells were made. Occasionally a dead spermatozoon could be found with the head or tail adhering at a point to the glass window of the sample cell. It was found that by simply displacing the suspending

medium in the cell (by the simple expedient of pinching the inlet and outlet tubing), the spermatozoon could be rotated by $\sim \pm 90^{\circ}$ about the point of attachment as shown in fig. 5-14.

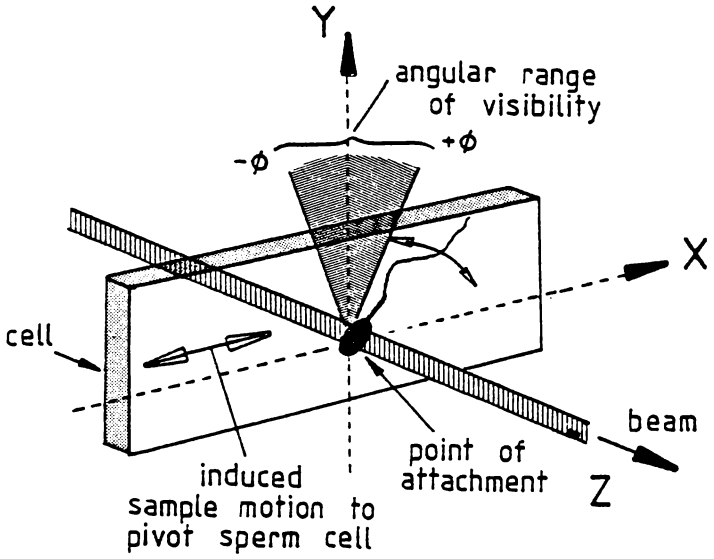

Fig. 5-14. Rotation of a spermatozoon about a point of attachment by displacement of the medium to demonstrate the optical anisotropy.

By manipulating the orientation of a single spermatozoon in this way, it was found that at a horizontal scattering angle of $\sim 17^{\circ}$, scattered light was only visible when the major axis of the spermatozoon was aligned within approximately 25° - 30° of the vertical. When the spermatozoon was oriented outside this angular range, total extinction of the scattered light appeared to occur.

Further evidence of this dramatic optical anisotropy came from observing the occasional motile spermatozoon which was swimming in a circular trajectory. These were rotating cells swimming in a circular trajectory of large radius of curvature. As is illustrated diagramatically in fig. 5-15 for a horizontally aligned microscope, the scattered light showed complete extinction over sectors of the swimming track where the spermatozoon was oriented at angles $\alpha \gtrsim 25^{\circ}$ - 30° from the vertical. The effect was particularly dramatic with the cell completely vanishing

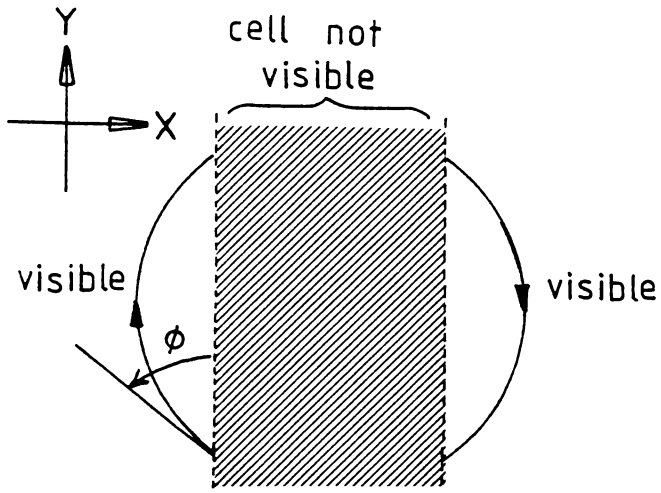

Fig. 5-15. A diagramatic representation of the segments of their trajectory over which circular swimming cells are visible in a horizontally aligned microscope. (ϕ is the maximum visible tilt-angle.)

from view and then subsequently reappearing in another region of the field on the same circular trajectory.

5.3.4 Discussion and Conclusions

The microscopic observations and the photomicrographs presented in this section, together with the previous wall-swimming observations of section 5.2, appeared to provide a new basis for interpreting laser light scattering experiments using bull spermatozoa. The observations demonstrated that the original *point-scatterer isotropic velocity* model was completely unrealistic. A new model based on a set of remarkable phenomena was required to represent a very complex opto-dynamical system. At least some of the earlier LBS results could be understood on the basis of these phenomena, while at the same time new questions were presented. To summarise and draw conclusions from this new information:

(1) motile spermatozoa exhibit a spectacular flashing effect as they swim, this clearly being of the same origin as the

flashing seen when they are observed in the microscopic dark-field. Within the optical geometry of the laser light scattering system the flashes are much more discrete, appearing as sharply defined point images on photographic time exposures, the image diameter being of the order of 30% of the spacing between them.

Flash images generated by bull spermatozoa with conventional dark-field microscopic illumination are generally elongated images, giving what has been referred to as a *duck-footed* track (Rothschild, 1953b). It is interesting to re-examine fig. 5-6. in this respect and also Mann (1964) presents a good dark-field time-exposure photomicrograph (taken from Rothschild's work) showing the dark-field track of a bull spermatozoon at high magnification. In comparison the laser light scattering geometry generates flashes which are not only more discrete, but show a much larger intensity ratio and are more closely colinear with the trajectory. In fig. 5-6, the dark-field tracks appeared in many cases as a zig-zag shape with an intensity modulation along the image. This probably resulted from a helical head motion and represented the variation in scattered intensity along the length of its trajectory. Whether the locus of the rotating head follows a true helical path and exhibits a precessional effect or whether it rotates about the centre of mass which follows a linear path, is not clear. It appeared that within the geometry of the laser light scattering system, the scattering peak or flash occurs at a particular point on the head rotation cycle, possibly that orientation shown in the remarkable photomicrographs of Gray (1958) and previously reproduced in fig. 2.11. Such flashes in the laser system give the closely colinear

sequence of dots evident in the time exposures and are possibly a consequence of the very small divergence of the illuminating laser beam as opposed to the convergent annular ray system of the microscopic dark-field optics.

What then are the implications of the large scattered intensity fluctuations, as seen by the photodetector to arise from individual spermatozoons, for the interpretation of the fast ACF component? Does this autocorrelation component really arise from the phase correlations in the scattered field, or, as seems more likely, does it arise from the large rapid intensity fluctuations created by individual rotating motile spermatozoa?

(2) A marked orientational effect arises as a consequence of a gross optical anisotropy in the scattered field from the spermatozoon. An observer or a photodetector looking into the sample at a small forward scattering angle, sees predominantly those spermatozoa which are swimming at angles closely distributed about the normal to the plane defined by the beam and the observer (but for additional qualification see (3) following). A photodetector therefore, will not collect light from all motile cells.

If, as seems unlikely, the fast autocorrelation component does arise from Doppler induced phase relationships in the scattered field, then the range of velocity components along the scattering vector would be substantially less than for an isotropic dynamical model. In fact, those spermatozoa which appear to contribute the greatest intensity to the detected signal (those swimming normal to the scattering plane) would give no Doppler shift. Clearly, apart from the significance

of the intensity fluctuations, this orientational phenomenon also calls into question the interpretation of the fast ACF component as being of Doppler origin due to the restricted range of velocities contributing to the light beating spectrum.

(3) The focal detail of the swimming tracks in figs. 5-8 through 5-12, together with the previous results of figs. 5-5 and 5-6, strongly suggest that the visible motile spermatozoa swim on the window surfaces of the sample cell. Microscopically this was observed to be the case and it was possible to focus onto two distinct groups of cells, those swimming on the front window and those swimming on the rear window (within the type C cell geometry).

This imposes a further constraint on the dynamical model; that depending on the scattering volume location, the detector may collect scattered light largely from those spermatozoa swimming in a plane normal to the incident beam, which are also following trajectories falling close to the normal to the scattering plane. The velocity distribution for a centrally located scattering volume may be quite different.

(4) Dead cells appeared to become oriented vertically during sedimentation. The rate of sedimentation was not apparent to the eye in the microscopic field since they could be expected to move only one head length ($\sim$ 10μm) in 10 - 20s. Examination of figs. 5-9 and 5-10 in particular, shows some of the bright, and slightly out-of-focus dead cell images to be elongated in the vertical direction to an extent which is consistent with sedimentation over this timescale. Also of interest, is evidence in some cases of intensity variations along the image. This could be expected to occur, in view of point (1) above, if the head of the spermatozoon were to rotate or wobble as

it sedimented, possibly induced by motile cell perturbations.

(5) The gross optical anistropy has the effect that dead spermatozoa, when they do become vertically oriented are not visible to an observer or photodetector aligned in the vertical scattering plane (ZY plane in fig. 5-13). This then would appear to be why in fig. 5-4, the slow ACF component vanished completely with vertical alignment of the photodetector. The immotile cells through orientation to vertical alignment, head-down, had become invisible to the photodetector. Further, the magnitude of the effect suggested both time dependent and concentration dependent interactions with the AAR and a possible explanation for many of the results obtained in chapter 4. This will be further taken up in more quantitative terms in section 5.12.

(6) Whereas the motile fraction were observed to be swimming on the internal window surfaces of the sample cell, the immotile spermatozoa were generally distributed throughout the medium. Many of the dead cell images in the photomicrographs are seen not to be in the focal field of the surface swimming motile cells.

These observations and conclusions form the basis of a new opto-dynamical model for laser light scattering from bull spermatozoa.

5.4 Measurements from time-exposure photomicrographs

5.4.1 Introduction and Methods

The previous section presented a qualitative description of phenomena observed in light scattering samples of bull spermatozoa, the observations of fundamental significance being the flashing of the sperm head and the orientation of swimming tracks.

So as to quantify the orientation effect as far as possible for real samples of normally motile spermatozoa, a series of time-exposure photomicrographs (including front plate I) was taken and the distribution of swimming track orientations measured. This was achieved by approximate fits of linear trajectories to all distinct and definable tracks, the inclination of the track then being measured with respect to a defined cartesian axis. All defined tracks were observed to lie within the same focal plane and were consistent with spermatozoa which were swimming in close contact with the windows of the sample cell.

The microscope and camera were aligned at a scattering angle of 18.8° in the horizontal plane, and the photographic techniques were as described in section 5.3.2. Time exposures were in the range 20 - 30s and the sample was illuminated by a 632.8nm He - Ne laser. The correct combination of beam intensity, exposure time, film speed and sperm concentration was essential to give photographs with well defined and distinct tracks of sufficient length for definition of the translation vector.

5.4.2 Results

The angular inclination of the swimming track with respect to the normal to the scattering plane is referred to henceforth as the *tilt-angle* and is defined diagramatically in fig. 5-16.

The frequency distribution of tilt angles determined from 171 swimming tracks is shown in fig. 5-17. Analysis showed that 78% of the spermatozoa which left defined tracks on the film were swimming at tilt angles $< 20°$,

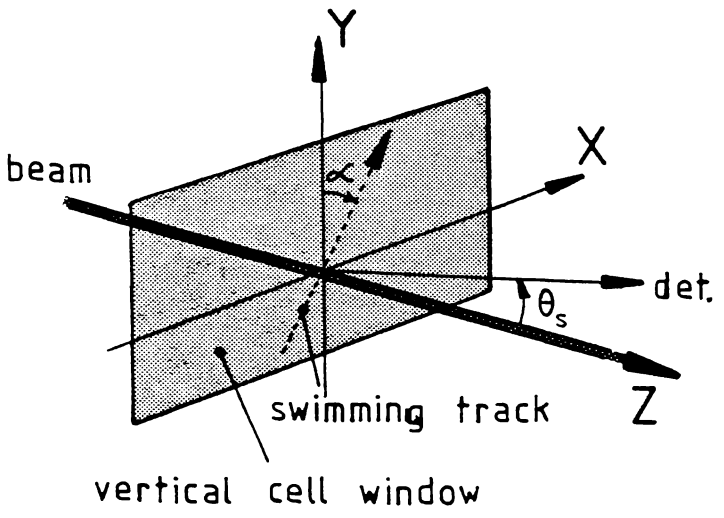

Fig. 5-16. Definition of the tilt-angle α. The Y-axis is normal to the scattering plane (XZ) in which the scattering angle θ_s is measured. Spermatozoa appeared to swim predominantly in the XY plane, that of the cell windows.

while 88% were at angles < 30°. No tracks could be found at tilt-angles > 55°. The standard deviation of observed tilt-angles was 17.4°.

Whether the high shoulder on the distribution represented a real broadening of the central peak was uncertain although some secondary structure in the distribution may well exist. The high shoulder and the minor peak at tilt angles 30° - 40° may represent such structure and there is some theoretical support for this in the following calculations of section 5.7, and evident in the tilt-angle plots of fig. 5-24.

5.4.3 Discussion

Assuming that the existence of a definable swimming track on the film emulsion represents a scattered intensity above some minimum detectable level, and assuming in addition, that the real distribution of actual velocities lying in the XY swimming plane is isotropic (refer observations of fig. 5-13), the data of fig. 5-17 suggests that the photodetector (in this case it was the film) only receives significant scattered light from

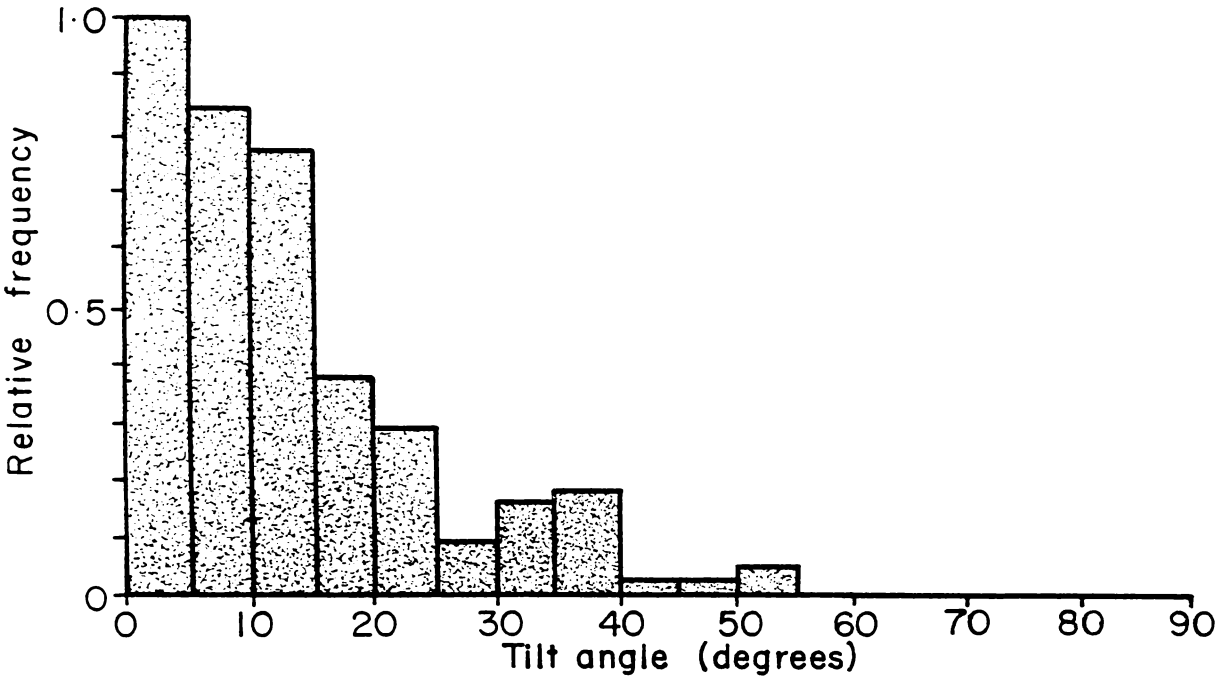

Fig. 5-17. Distribution of tilt-angles as determined from 171 tracks on six time-exposure photomicrographs. The scattering angle at which the observations were made was 18.8°. The standard deviation of observed tilt angles was 17.4°. (Harvey and Woolford, 1980).

about 20% of the motile spermatozoa. This obviously had an extremely important bearing on the interpretation of the AAR in LBS measurements which, in the presence of such large orientational effects, could not possibly give an absolute measure of the percent motile spermatozoa.

It might also be noted that in fig. 5-6, with microscopic dark-field illumination, the distribution of swimming track orientations is completely random and this is readily attributed to the axial symmetry of the optical geometry.

5.5 Orientational effects with dead cells

5.5.1 Background

Previous results had demonstrated that a vertically aligned photodetector did not apparently *see* dead cells since no slow exponential ACF component was obtained (fig. 5-1). On the other hand, a horizontally aligned detector did (see fig. 5-4) generate a slow exponential component, the amplitude of which had earlier been shown to be approximately linearly related to the concentration of immotile cells (table 4-2). This was also consistent with microscopic observations in both the horizontal and the vertical scattering planes (i.e., fig. 5-13) which, in a subjective sense, showed dead cells to be observable only when the microscope was aligned in the horizontal scattering plane. A common feature to both the autocorrelation studies of section 5.1 and the visual studies of section 5.3 was the time delay between sample injection and measurement or observation. Since the head is much more dense than the flagellum and contains most of the mass, (fig. 2.9) the spermatozoon will tend to sink head first, a well known effect (Roberts, 1970). Consequently the thermal equilibration period in these experiments allowed time for the dead or immotile cells to orient from what was initially a random distribution of orientations immediately following injection, to a uniform vertical alignment wherein they became invisible to the vertically aligned detector or observer.

An experiment was therefore devised to examine the time dependence of this effect by following of the signal amplitude generated by dead cells, from the instant of sample injection. The objective was to measure the supposed relaxation time from initially random orientations to uniform vertical alignment under the action of the gravitational torque acting on the cells. This was to be achieved by looking at the signal amplitude as a function of time for photodetectors aligned in both the horizontal and

and the vertical planes.

5.5.2 Methods

A suspension of 100% dead (cold shocked) spermatozoa in 2% sodium citrate based buffer (0.22μm filtered) was diluted to a concentration of 10^6/ml.

The sample, initially at ∿ 20°c was injected into a type C light scattering cell (fig. 3-15) temperature controlled at 37°c and the mean signal amplitude at the photodetector output immediately monitored over total timescales of 15 min. in one experimental run and 30 min. in another. The time trend in signal amplitudes was determined for both horizontal and vertical alignment of the photodetector at a scattering angle of 8° using separate experimental runs. Phototube aperture diameter was 800μm, and geometry as later detailed in section 5.13. Signal amplitude was measured by directly sampling the amplified photodetector output voltage at 1mS intervals, using an analogue-digital converter interfaced to the computer system (sections 3.23, 3.24). The computer collected consecutive batches of 10 * 1024 signal samples (at 1mS intervals) and with concurrent processing, computed the mean value over each 10.24s sampling interval. Arithmetic processing was concurrent with sample collection only after each batch of samples had been transferred to a processing array, and this ensured the best possible continuity of signal sampling the data transfer gaps being only ∿ 10mS. The laser beam intensity was monitored over the experimental period so as to detect any drift in laser output power.

5.5.3 Results and Discussion

Figs. 5-18 and 5-19 show plots of the mean signal amplitude over successive 30s sampling intervals following sample injection, plotted over a period of 15 min in one experiment, and 30 min in another experiment. For vertical alignment of the detector, the amplitude showed an immediate

exponential-like decline following sample injection, falling to a stable level of approximately 8% of its initial value over a timescale of 4 - 5 min. Conversely, with horizontal alignment of the photodetector, an exponential-like increase in amplitude occurred, but over a longer timescale (∿ 8 - 9 min). The final signal amplitude in this case was approximately 6.4 times the initial value at sample injection.

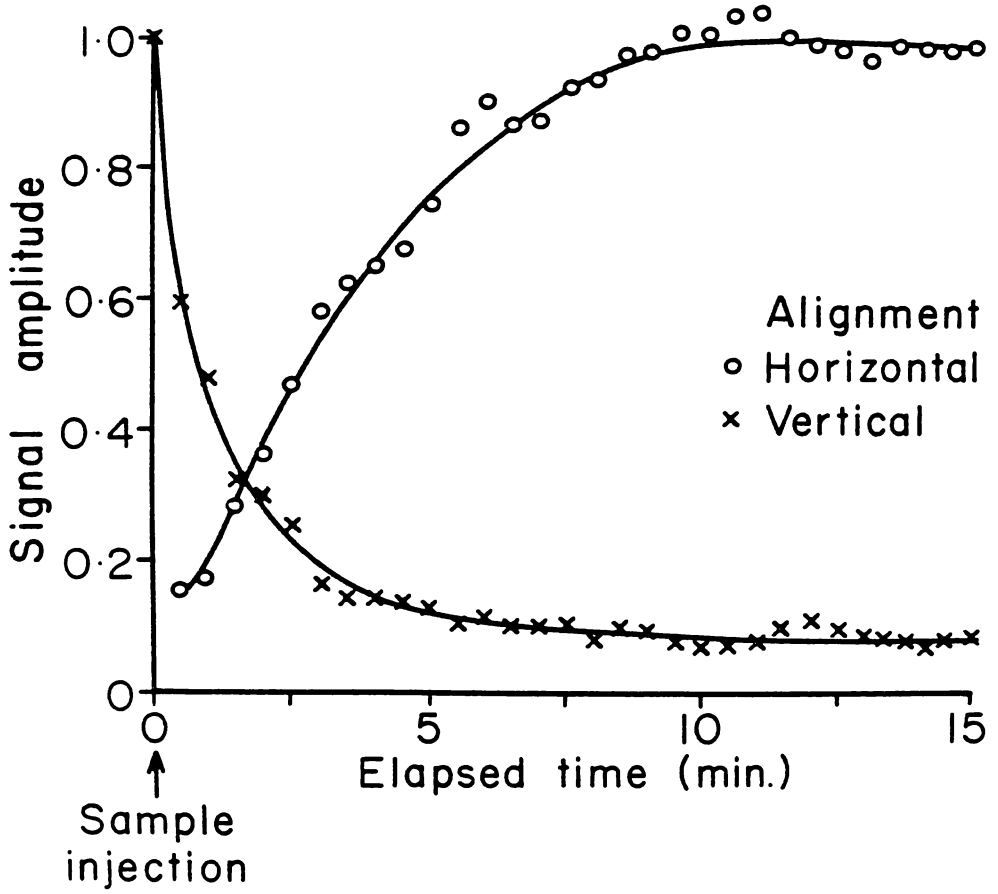

Fig. 5-18. Time dependence of the signal amplitude for both horizontal and vertical alignment of the detector at a scattering angle of 8°. (Harvey and Woolford, 1980).

Assuming that the sample initially had completely random alignments of spermatozoa (reasonable in view of the preparation and mixing procedure), the data indicates that in the final condition, where presumably the dead cells were uniformly aligned in the vertical direction, the

intensity ratio for the two detector alignments was ∿ 79.4.

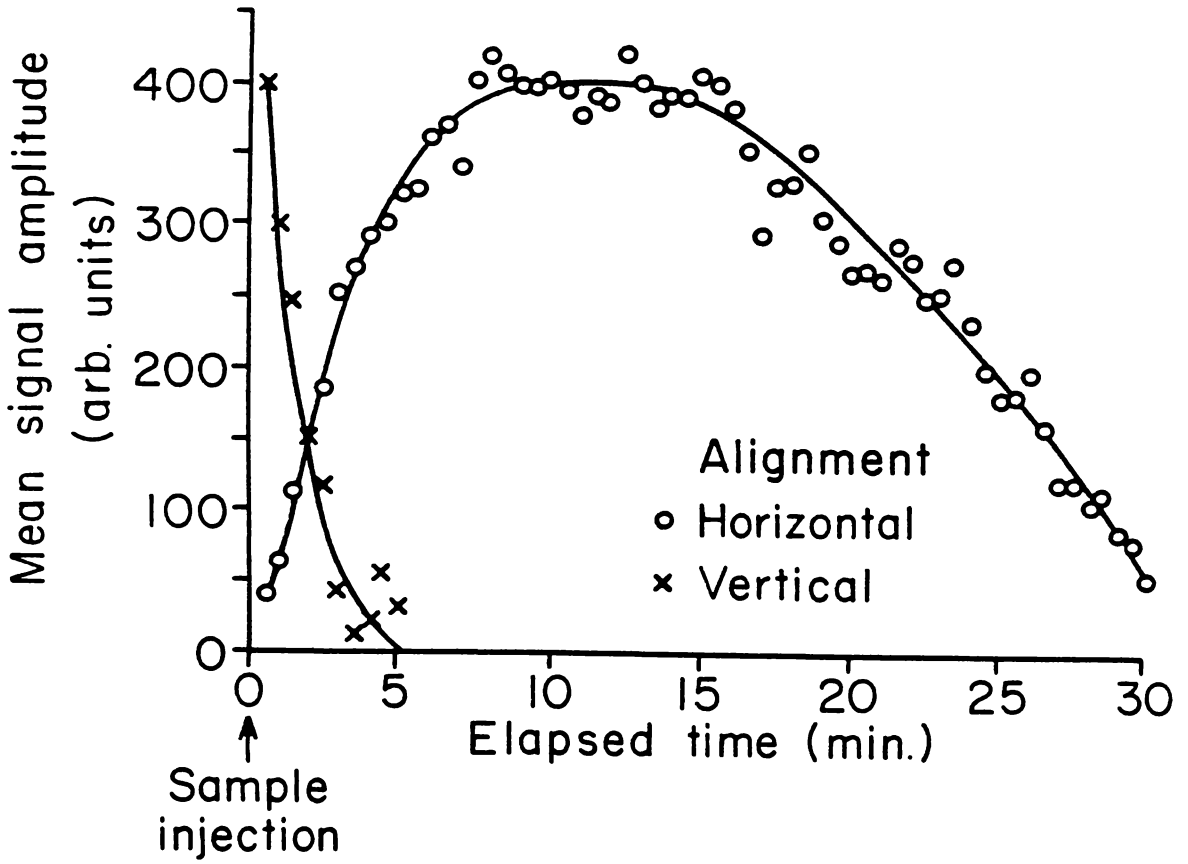

Fig. 5-19. Results from another experimental run showing the time dependence of the mean signal amplitude over a longer timescale. Note that over a 15 min. period the time dependence is very similar to that of fig. 5-18.

It is interesting to relate this result to the observations of Ascoli, *et al.*, (1978), regarding the gross spatial asymmetry in the scattered field from *Euglena gracilis*, which were discussed in section 1.4.

The data of fig. 5-19 refers to an experimental run of exactly the same design as that for fig. 5-18, but, in this instance, the scattering volume had been located close to the roof of the type C sample cell.

The decline in amplitude after a period of ∿ 15 min. (for horizontal detector alignment) appeared to result from sedimentation of the upper levels of the spermatozoa through and out of the scattering volume. Relating the estimated 32 min. decline to zero over this phase to the time required for the cells to sediment, the diameter of the observed scattering volume (800μm), gives a sedimentation rate of 0.42μm/s (refer also section 4.12.3).

Interpretation of these results of fig. 5-18 in terms of sperm orientational motions is not straightforward. The $(1 - e^{-x})$ rise in amplitude for horizontal alignment is readily understood, together with results of microscopic observations, as resulting from a progressive accumulation of spermatozoa within the visible range of tilt-angles after rotation to a *head-down* attitude. The rapid decline in amplitude with vertical detector alignment is not so readily interpreted as this might be expected to remain substantially constant for a period while cells with an initial *head-up* attitude reorient through the range of visible tilt-angles. It is possible that the sharp decline can be understood by considering the intensity change should the head (which is flat) rotate towards an edge-on attitude while sedimenting. Results of section 5.7 will later show that the light scattered from the sperm head peaks in intensity in two narrow lobes located in the equatorial plane of the head.

For orienting spermatozoa with the plane of the head distributed approximately around the vertical plane, these scattering lobes would not be visible to the detector. Consequently the rapid exponential decay evident in figs. 5-18 and 5-19 for vertical photodetector alignment, would result from rotation of the head plane about its major axis, towards the vertical plane, during the orientation of the cell towards vertical alignment.

Roberts (1972) stated that a bull spermatozoon geotactically oriented

at a rate given by

$$(d\theta/dt) = - 0.015 \sin\theta$$

at 24°c, where θ is the angle between the long axis of the head and the vertical. This gives a peak orientation rate of 0.015 rad/s which could be expected to be somewhat higher at 37°c, the viscosity ratio being 0.76 for water. The rise in amplitude in fig. 5-18 suggests an average orientation rate over π radians in $\sim$ 7 min, or 0.0075 rad/s which is plausible when compared with the data of Roberts (1972).

5.5.4 Conclusion

Orientation of immotile cells towards a uniform vertical alignment will introduce a time dependence into the amplitude of the low-frequency component of the detected signal having a relaxation time of 7 - 8 min. for a horizontally aligned detector and 3 - 4 min. for a vertically aligned detector. The increase in signal amplitude in the horizontal case arises from the cumulative arrival of all immotile cells in the visible range of tilt angles. This phenomenon would introduce a time dependence into the AAR over these timescales which would depend on the relative density and viscosity of the suspending medium. Referring back to fig. 4-28 we see that a substantial rise in AAR occurred after sample injection, the timescale being comparable with that obtained in fig. 5-18, the same suspending medium having been used in both cases. The data of fig. 4-31, where a high relative density medium was used (D_2O) could be understood on the basis of a very much slower orientation rate, and this is consistent with the lower AAR values obtained.

The light scattering AAR can therefore be expected to depend strongly on the degree of vertical alignment among the immotile spermatozoa. With horizontal alignment of the photodetector, all immotile cells potentially contribute light to the detector after orientation into the visible

range of tilt angles. However, the extent to which this alignment occurs could reasonably be expected to depend on the frequency of any direct interactions between motile and immotile fractions which result in reorientations of the immotile cells. We have therefore, a phenomenological basis for understanding the concentration dependence of the AAR studied at some length in chapter 4.

A further important optical effect which is superimposed on these geotactic phenomena, is discussed in the next section.

5.6 The origin of the autocorrelation components

5.6.1 Background

In view of the phenomena uncovered by the preceding experiments, close examination of the source of both the motile and immotile autocorrelation components was called for. A pure Doppler origin for the motile component in particular seemed most unlikely in view of the gross asymmetry (although as yet undefined) of the scattered field which should clearly superimpose an amplitude component on the Doppler beat spectrum. Such amplitude effects were clearly evident in photographic studies. Intensity fluctuations could similarly be expected for dead cells if, during sedimentation, they underwent axial rotation or perturbations.

Examination of the time-exposures in figs. 5-8 through 5-12, showed that the flashes originating from individual cells were highly periodic and evidence of this periodicity should have been found in the fast ACF, even if a distribution of rotation rates was involved. In general, however, such autocorrelation periodicities were not observed, although at various times very weak periodicities on an appropriate timescale had appeared to be present. In the case of the autocorrelation function of fig. 5-4 taken with vertical detector alignment, a damped cosine feature was clearly evident and the period of this $\sim$ 75mS was consistent with the estimated flash rate in the time-exposures of figs. 5-8 to 5-12 and with the

expected rotation period for swimming cells. The nature of the fast autocorrelation component required therefore to be examined more closely.

5.6.2 Photodetector signal generated by single motile cells

So as to further examine the nature of the fast ACF, the scattering geometry and concentration were adjusted so as to give, on average, only one motile cell in the scattering volume at any given time. This was achieved by reducing the waist size of the beam to typically 100μm and using a phototube aperture of the same diameter (a vertical plane type C scattering cell was used). The photodetector was aligned at the normal scattering angle (8°) in the vertical plane so as to exclude any interference from immotile cells (most of which were vertically aligned and hence invisible to the detector system). At a sperm concentration of $< 10^5$ sperm/ml the photodetector output comprised discrete events as individual motile cells traversed the scattering volume. These events, when observed on a monitoring oscilloscope were found to comprise a train of sharply defined pulses, examples of which are illustrated in fig. 5-20(a) - (c). The individual pulses are seen to be extremely sharp and appeared to be generated twice per rotation of the spermatozoon on the basis of reported rotation rates (Rikmenspoel, (1962) who reported rotation rates of 7 - 9Hz for bull spermatozoa swimming at 100μm/s). The general envelope of the pulses appeared to represent the Gaussian intensity profile of the beam. A tendency towards alternating relative amplitudes of adjacent pulses could plausibly be attributed to a slight rotational asymmetry arising from off - axial rotation of the head and was taken as being further evidence for two intensity peaks per rotation. The pulse width was difficult to estimate on the timescale shown in figs. 5-20. Other measurements collaboratively carried out and outlined in appendix IV, used computer averaging to determine a mean intensity profile and showed a mean peak width at half-height of 7.1mS.

The intensity peaks evident on the time-exposure photomicrographs of figs. 5-8 through 5-12 can obviously be reconciled with the recordings of fig. 5-20.

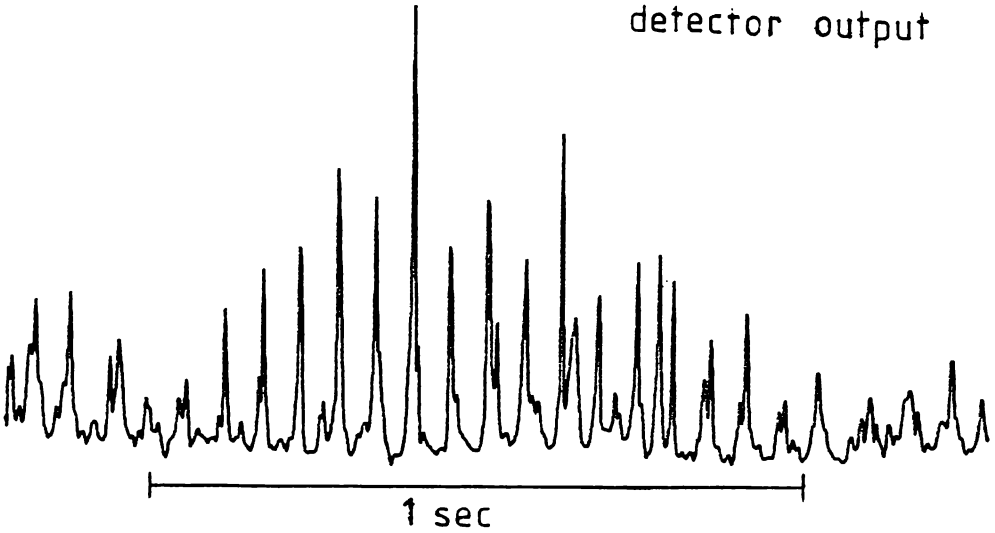

Fig. 5-20(a). Interval between peaks 58mS, probably half the head rotation period. Note the alternation in the relative peak amplitudes, possibly symptomatic of slight off-axial head rotation.

The photodetector output at normal scattering volume populations can therefore be considered to comprise the summation of possibly hundreds of pulse trains such as figs. 5-20, all in random phases, and exhibiting a distribution of flash periods. This was strikingly evident in fig. 5-8 for example, and it can be intuitively seen that the characteristic time component of such a signal, as would be extracted from the autocorrelation function, is the time dependence of flash intensity profile. The average characteristic decay time for an individual intensity peak (taken from Appendix IV) is of the order of 2.15mS, which is consistent with the timescale of the fast ACF components previously shown in figs. 4-22 and 5-2.

It is interesting at this point to compare the recordings of fig. 5-20 with those obtained by Rikmenspoel and van Herpen (1957) and previously shown in fig. 3-6, although more attention is given to this in the final conclusions. The peaks from the laser light scattering

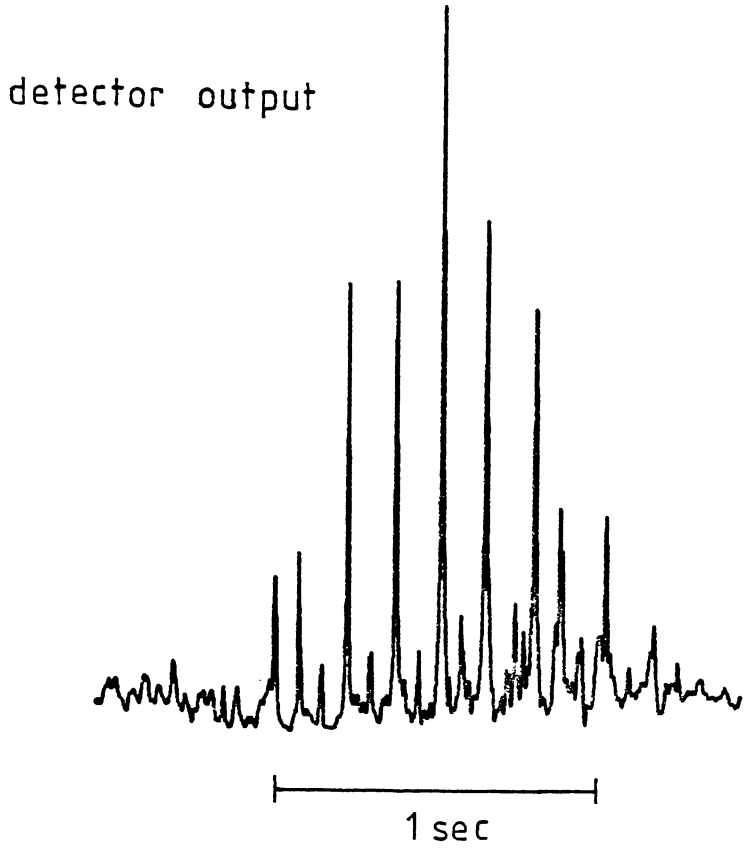

Fig. 5-20(b). Interval between major peaks 147mS. But note here the small amplitude peaks equidistant between the large peaks, suggestive of a head with a grossly off-axial rotation or helical motion. Taking account of the small peaks suggests a head rotation period of 147mS which is consistent with the flash periods of figs. 5-20(a) and 5-20(c).

geometry are much more sharply peaked, probably due to the higher degree of linear collimation of the light source and hence the smaller uncertainty in scattering angle for light contributing to the image.

In view of the recordings of fig. 5-20 and the associated evidence, the significance of coherence in this supposed application of laser light *beating* spectroscopy, is open to serious question, and this is further emphasised in the following sections 5.6.3 and 5.7.

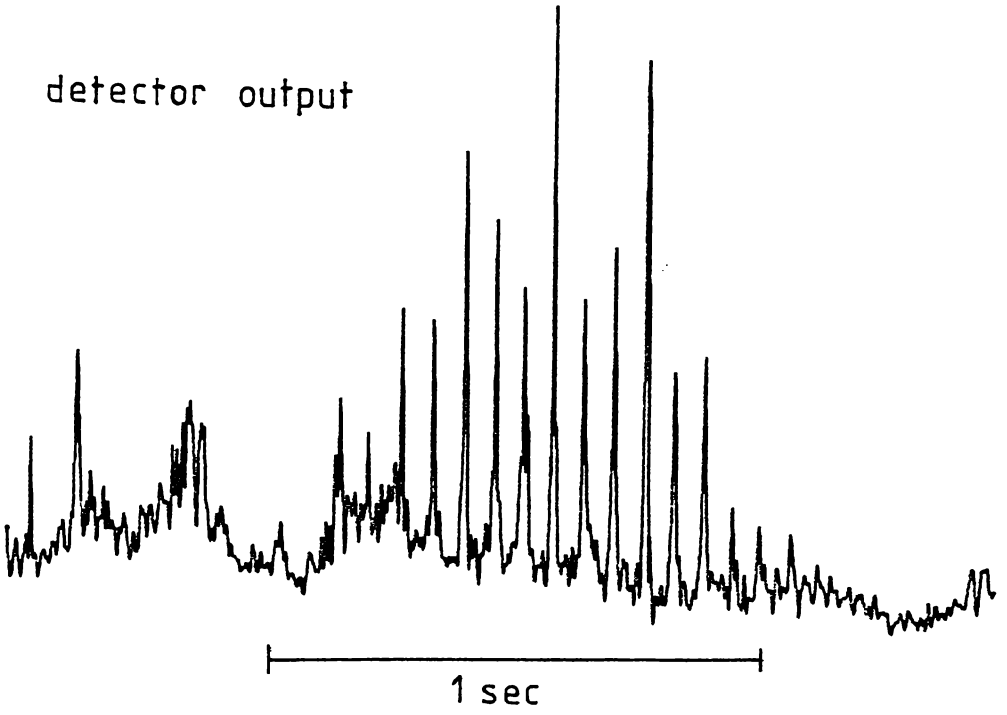

Fig. 5-20(c). Interval between peaks is 62mS. Here the baseline is somewhat more variable probably due to contaminants in the sample. Note again the tendency for peaks to alternate in relative amplitude as in recording (a).

Footnote: The scattering volume diameter used in these recordings was 100μm and the sample cell geometry was type C (fig. 3-15), with vertical alignment of the photodetector. The scattering volume transit time is seen to correspond to translational velocities of ∿ 100μm/s in all cases although it is difficult to estimate accurately due to the Gaussian beam intensity profile.

5.6.3 The origin of the slow ACF component

The data of section (4.11.3) showed that the slow ACF component scaled with $\sin^2(\theta_s/2)$ as is the case for light beating correlation functions from diffusing scatterers. The equivalent hydrodynamic radius for the head of a bull spermatozoon computed from these data was somewhat larger than might be expected at typically 4.7 - 5.7μm. Results were consistent with an enhanced Brownian diffusion where motile cells were present, through the increased autocorrelation decay constant.

One check that the slow ACF component did arise at least partially from *Brownian-induced* phase information in the scattered field, was to attempt a light scattering experiment of the usual geometry, but using an incoherent thermal light source. In such an experimental situation, the intensity attributes of laser light sources rapidly become apparent. With some considerable experimental difficulty, such an experiment was carried out. The biggest problem was obviously that of achieving an incident beam of sufficient intensity with good collimation to give an acceptable signal/noise ratio. A 75 watt quartz-halogen bulb energised by a 12v D.C. power supply was used as the source. Using a pinhole and lens collimation, a beam having a reasonably small divergence ($\lesssim 10^\circ$) was focussed into a sample of spermatozoa in a type C sample cell. The photodetector was aligned at the typical scattering angle of 8° and contained an 800μm diameter phototube aperture. With a high detector and system gain it was possible to obtain an output signal which appeared similar to that when using a laser source, but had a low level of shot noise superimposed.

Fig. 5-21 shows an autocorrelation function obtained from a suspension of 100% dead spermatozoa at a concentration of 5×10^6/ml in sodium citrate buffer. The fast decaying peak is due to shot-noise. This ACF displays the same slow exponential decay, so familiar from previous experiments which used a coherent laser light source. This particular

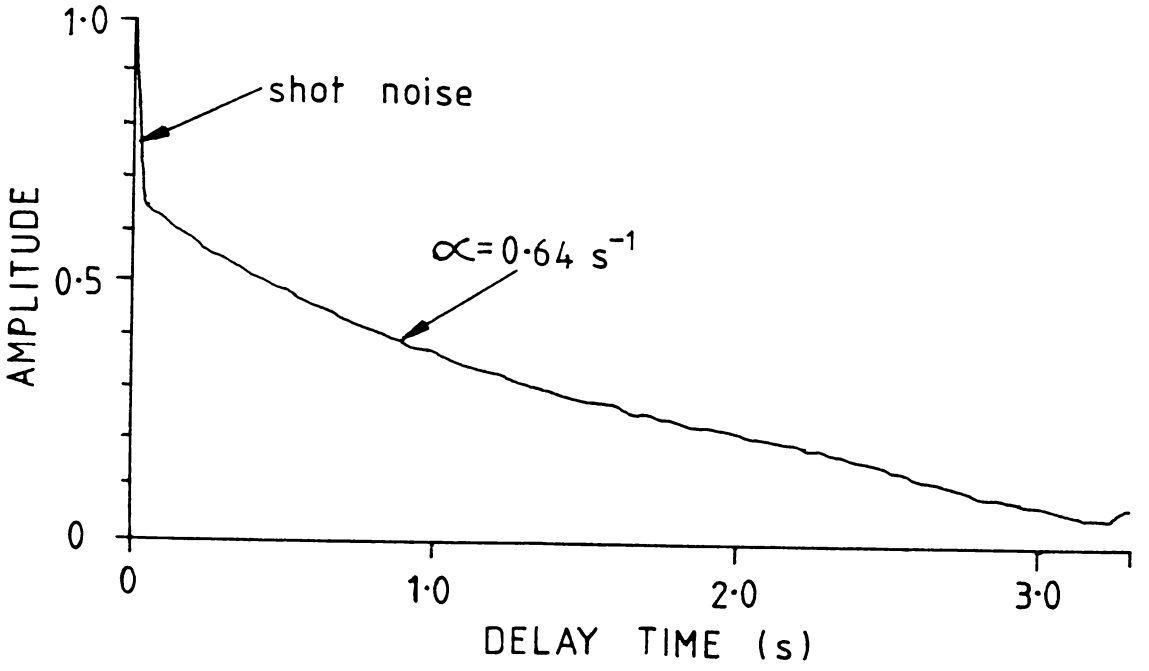

Fig. 5-21. An autocorrelation function obtained using an incoherent light source to illuminate a suspension of 100% dead cells.

The peak close to t = o arises from shot noise.

function was formed over an 18.2 min. period at a correlator sampling interval of 33.3mS. The decay constant of 0.64 s^{-1} is of the same order as that obtained for 100% dead sperm with laser sources (e.g., 0.963 s^{-1} to follow in section 5.10.4).

Fig. 5-22 shows a further autocorrelation function using incoherent light, in this case for a mixed sample of motile and immotile cells. The function was taken at 10mS/ch and required a signal sampling time of 11 min. A small rapidly decaying oscillation of period $\sim$ 60mS, and bearing a close similarity to that observed in the coherent light example of

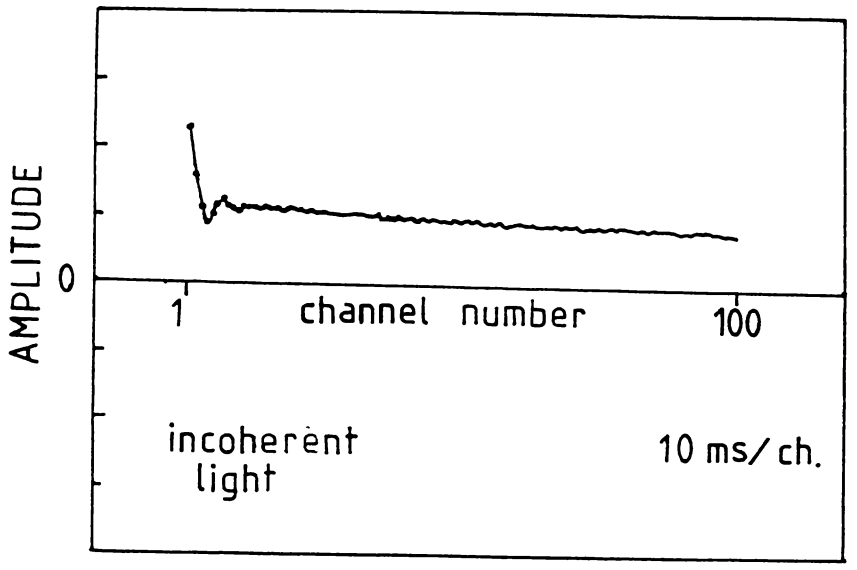

Fig. 5-22. An autocorrelation function obtained for a mixed sample of motile and immotile spermatozoa on a timescale of 10mS/ch and showing the familiar two-component nature, but with a significant periodicity. (Photographed directly from autocorrelator display).

fig. 5-4, was obtained. This period is closely related to the 'flash' period of single cells in figs. 5-20. This then appeared to be the equivalent of the microscopic dark-field illumination case but within the geometry of the laser light scattering experiment wherein light is collected at a single point in the scattered field, and not throughout an axially centred conical solid angle as in the case of an objective microscope lens (see also fig. 3-5).

The inevitable conclusion from this experiment, together with the recordings of fig. 5-20 was that both fast and slow autocorrelation components probably arise largely from intensity fluctuations as the heads of bull spermatozoa rotate or otherwise orient about the major axis of the head. In the case of motile cells, such intensity fluctuations have been amply demonstrated in fig. 5-20 and the photographic results of fig. 5-8. Dead cells however, now also seem likely candidates for

intensity fluctuations which would seem to be on a longer timescale, probably several seconds. It has been well demonstrated that dead cells sediment head down and are thus visible to a horizontally aligned photodetector. If any conformational asymmetry exists on the flagellum, it is very likely that such sedimentary cells will rotate as they sink and so generate long timescale intensity changes which may be partially or even entirely responsible for the slow ACF component. Alternatively, interactions with motile cells may result in small axial rotations of the head, sufficient to generate a substantial intensity change at the detector. Further reference to this is made in the conclusions of 5.7.4.

5.7 Sperm head scattering calculations

The methods and results which follow have been previously outlined by Harvey and Woolford (1980) as given here in Appendix II.

5.7.1 Background

Evidence presented in preceding sections pointed to the gross inadequacy of the *point-scatterer* model for bull spermatozoa when illuminated by a well collimated laser light source, and observed at a small forward scattering angle of 8°.

Attempts were therefore made to define a more realistic scattering model which accounted for the observed rotational and orientational effects.

The question of the scattering model for bacterial cells had received considerable attention by Wyatt (1972) in the development of techniques to characterise conformational changes. The parameter of interest in these studies had been the scattered intensity as a function of scattering angle and some discussion was given in section 1.1.6 on the techniques involved.

Wyatt had employed the Rayleigh - Gans approximation (section 1.1.5) for bacterial cells which are somewhat smaller than the bull spermatozoon

and have a refractive index reasonably close to that of water. On this model the scattering angle dependence of the scattered intensity was reasonably well fitted, at least at smaller angles, say $\lesssim 90°$. In these studies it was the precise functional form of the scattered intensity versus scattering angle relationship which was important over a relatively large range of angles.

Computations discussed in this section, applied the same Rayleigh - Gans approach to bull spermatozoa although in this case, due to the much larger linear dimensions involved, the validity of the approximation is more questionable as formerly discussed in section 1.5 and illustrated in the plotted criteria of fig. 1-19. At $\lambda = 632.8$nm the scattering angle would need to be $\lesssim 2°$ to meet the criterion.

However, such calculations were seen as being likely to give an order of magnitude result which would possibly facilitate an understanding of the previously described phenomenology. In addition, a second model was examined using a ray-tracing approach which is more relevant to such large scatterers and the results were compared. The objective was to calculate the scattered intensity at typical forward scattering angles for a model bull spermatozoon head as a function of axial rotation (i.e., around the translation vector) and tilt-angle.

5.7.2 Computational Methods

In this scattering regime, the absolute dimensions of the particle and its shape became important and this has been strongly suggested by the previous evidence. For this reason, the dimensions of the bull spermatozoon and its shape were discussed in some detail in section 2.4. So as to arrive at a practical computational method, two simplified geometrical models of the sperm head were employed (scattering from the flagellum was neglected):

(i) a flattened ellipsoidal conformation having axes of both 8.0μm x 4.5μm x 1.0μm and 8.0μm x 4.5μm x 2.0μm.

(ii) a flat elliptical multi-element slab of the same elliptic axes but of constant thickness, 1μm.

Scattering from the mid-piece and the flagellum was ignored on the basis of photographic and observational evidence.

Two computational strategies were employed and these have also been described by Harvey and Woolford (1980):

(i) the Rayleigh - Gans approach which was of an analytical nature (using the flattened ellipsoid model).

(ii) a ray tracing technique as outlined by Van de Hulst (1962).

These are now described in further detail.

(1) *Rayleigh - Gans*

The scattered far-field amplitude A for a scatter of large dimensions can be written;

$$A_{(\underset{\sim}{k})} = A^{\circ} \, P_{(\underset{\sim}{k})} \tag{5-1}$$

where A° is the Rayleigh limit for small angle scattering (section 1.1.5) and $P_{(\underset{\sim}{k})}$ is a form factor given in the Rayleigh - Gans approximation as;

$$P_{(\underset{\sim}{k})} = \frac{1}{V} \int_{V} e^{i \, \underset{\sim}{k} \cdot \underset{\sim}{r}} \, dV \tag{5-2}$$

where $\underset{\sim}{r}$ is the position vector of an element dv of the particle volume V and $\underset{\sim}{k}$ is the scattering vector. This form factor expresses the phase summation for the scattered field over the volume of the particle and for an asymmetric scatterer depends on its orientation.

Van de Hulst (1962) gives an analytic expression for $P_{(\underset{\sim}{k})}$ in the case of an ellipsoidal particle;

$$P_{(\underset{\sim}{k})} = \frac{1}{V} \int_{-d}^{d} e^{ikp} \, A_{(p)} \, dp \tag{5-3}$$

where d, referring to fig. 5-23, is the perpendicular distance from

the centre of the ellipsoid to a tangent plane normal to the scattering vector $\underset{\sim}{k}_s$ and p is the perpendicular distance to an arbitrary plane normal to $\underset{\sim}{k}$ which intersects the ellipsoid over an area $A_{(p)}$.

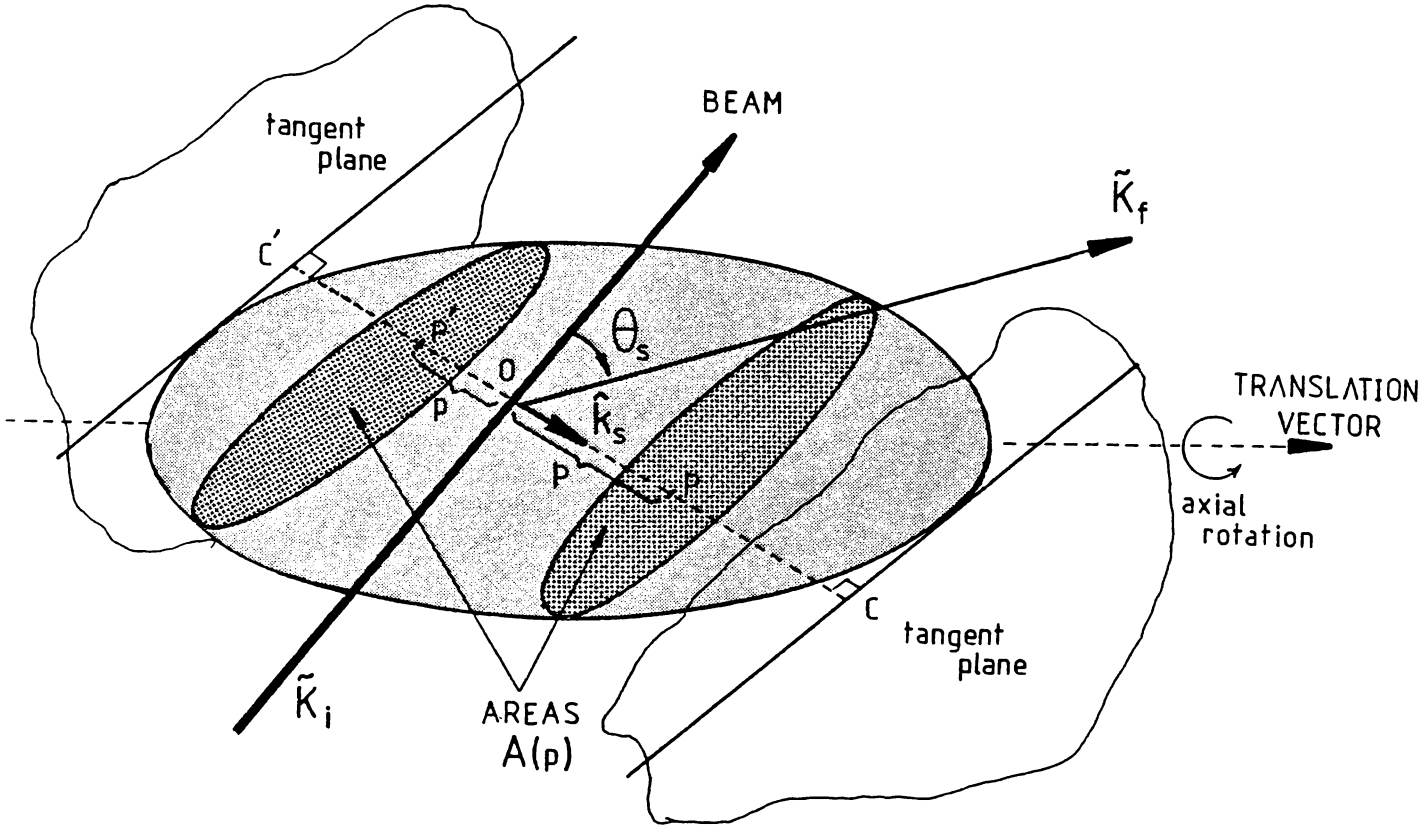

Fig. 5-23. Geometry associated with Van de Hulst's technique for evaluating the scattered amplitude in the far-field for an ellipsoid, using the Rayleigh - Gans approximation.

where θ_s is the scattering angle

$$OC' = OC = d$$

$$OP' = OP = p$$

$\hat{\underset{\sim}{K}}_s$ is the unit scattering vector

and OC' and OC are normal to the tangent planes.

The integration (5.1) is therefore over the elliptic areas of intersection for p from -d to +d.

If the ellipsoid has semi-axes, a, b, c and is thus defined in cartesian co-ordinates by;

$$\frac{x^2}{a^2} + \frac{x^2}{b^2} + \frac{Z^2}{c^2} = 1$$

then the equation of the plane $A_{(p)}$ is $\ell x + my + nZ = p$

(where ℓ, m, n are direction cosines of the normal to the plane of intersection) and the area of intersection is given by;

$$A_{(p)} = \pi abc(d^2 - p^2)/ r^3 \qquad (5\text{-}4)$$

where $d^2 = a^2 \ell^2 + b^2 m^2 + c^2 n^2$

Using this result in the integral (5-3) yields;

$$P_{(\underset{\sim}{k})} = (9\pi/2\ [kd]^3)^{\frac{1}{2}} J_{3/2}(kd) \qquad (5\text{-}5)$$

a result first derived for ellipsoids of revolution by Guinier (1939). Note that d is time dependent as the particle rotates about its axis.

It is interesting to note that for any given orientation of the ellipsoid, this is the same result, (Van de Hulst, 1962), as for a sphere of radius d (fig. 5-23). Consequently, an ellipsoid of axes 8.0μm x 4.5μm x 1.0μm, rotating about its major axis, when is aligned normal to the scattering plane, will appear to a photodetector in the far field as a sphere whose radius in varying between 4.0μm and 0.5μm.

Computation of the relative scattered intensity was then carried out by evaluating integral (5-3) over the limits of $\pm$ p for each orientation of the head model, over:

(i) an axial rotation of the head through an angle π about its major axis.

for each of

(ii) a range of tilt angles (fig. 5-16) for 0° to 90°.

For all calculations the major axis of the head model was considered to lie in the plane normal to the laser beam, thus taking account of the wall swimming phenomena, although a simple transformation would cover any arbitrary orientation of the translation vector.

The average intensity at each tilt-angle was determined after summing the calculated field amplitudes over stepped axial rotations of the head through π radians, commencing with the plane of the head parallel to the incident beam and rotating the normal to the head towards the scattering vector.

For the calculations as a function of tilt-angle the mean intensity so calculated bears little relation to the scattered field seen by the detector which contains the prominent intensity peaks. The maximum amplitude of the intensity peak could have been used as the characterising parameter, although the average intensity over the π axial rotation gives an equally valid indicator of the effect of tilt-angle. The variation of intensity over the head rotation is given separately in the results.

(2) *Ray tracing elliptical slab model*

Scattering from objects which have characteristic dimensions very large compared with the wavelength can be described by considering the incident wave to comprise a parallel set of rays (Van de Hulst, 1962). The resultant scattering pattern is then calculated by tracing and summing the amplitudes and phases of rays passing through and reflected from the particle structure together with the diffracted amplitude.

This strategy was carried out for a parallel sided elliptical slab model with varying degrees of attenuation for rays refracted through the head.

An array of 38 x 38 rays was considered incident on a square area containing the specified head shape. This conformational array was then rotated about its major axis at each selected tilt-angle and a numerical

summation of the individual ray amplitudes A_i and phases ϕ_i carried out.

hence $$A \alpha \sum_i A_i e^{i\phi_i} \quad (5\text{-}6)$$

where A_i in the case of a transparent slab may depend on the attenuation along the path through the slab.

Results from these numerical evaluations are presented here for the cases of both a transparent elliptical slab (i.e., zero attenuation) and an opaque elliptical slab.

The contribution of diffraction to the scattered field at typical scattering angles will depend on the scattering angle and the projected dimensions of the head, which vary with axial rotation. Reference to fig. 1-3 shows that the forward diffraction lobe is relatively narrow and will contribute significantly to the scattered field at a typical $\theta_s = 8°$ only when virtually edge on to the incident beam.

A wavelength of 632.8nm was assumed in all calculations.

5.7.3 Results and Discussion

(i) *Effect of tilt-angle on scattered intensity.*

The calculated relative scattered intensities (over a π axial rotation of the head for the ellipsoidal models) at typical forward scattering angles (5° - 20°) are shown in fig. 5-24 as a function of tilt-angle (fig. 5-16) over the range 0° - 90°. The data relate to the geometric models and two computational methods discussed in 5.7.2. The prominent peak in the intensity at zero tilt-angle arises from a strong equatorial peak in the curve of intensity versus head rotation angle (about its major axis) generated by specular reflection (fig. 5-25). This reflective peak becomes very strong at zero tilt-angle and occurs when the normal to the head plane lies along the scattering vector.

The average scattered intensity at all typical forward scattering angles is found to be dominated by this reflective peak and for this reason the results of all three opto-geometric models are very similar.

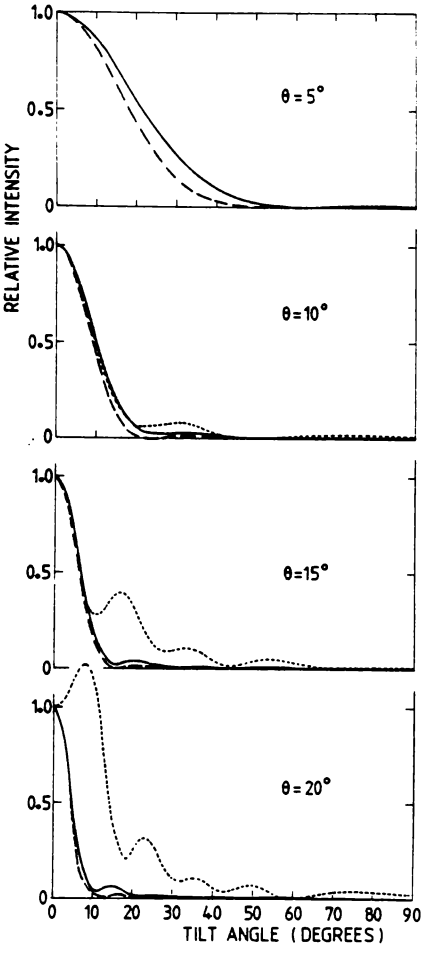

Fig. 5-24. Average scattered intensity at various scattering angles (θ) as a function of tilt-angle (α in fig. 5-16) for three opto-geometric models of the sperm head. The intensity is the average over a π rotation of the head about its major axis for the transparent ellipsoid models.

———— ellipsoid of semi-axes 4.0μm,2.25μm,0.5μm

---------- ellipsoid of semi-axes 4.0μm,2.25μm,1.0μm

- - - - - - opaque elliptical slab of semi-axes 4.0μm and 2.25μm, with a thickness of 1μm.

(Harvey and Woolford, 1980)

It is apparent in the results of fig. 5-24, that the intensity versus tilt-angle relationship becomes more sharply peaked at larger scattering angles, the width at half-intensity decreasing from $\alpha = 21.5^\circ$ for a scattering angle of 5° to $\alpha = 4.4^\circ$ at a scattering angle of 20°. Where the thickness of the head is such that phase differences in light scattered from the two opposite sides of the head are insignificant, both the Rayleigh - Gans model, the transparent and opaque elliptical slab models, all give virtually the same result, the reflective peak dominating the average intensity in all cases. However, in the case of the *Rayleigh - Gans thick-ellipsoid* model (i.e., thickness 2μm) where internal phase differences did become significant, secondary structuring and broadening

of the intensity versus tilt-angle relationship occurred as is apparent at scattering angles of 15° and 20° in fig. 5-24. While this *thick* model may appear unrealistic on a geometric basis, (section 2.4 suggested the head thickness was ∿ 1μm) it could be a more reasonable approximation if the refractive index was significantly higher than the value of 1.42 discussed in section 2.5, since this would increase phase-shifts of rays passing through the head.

The general form of the computational results in fig. 5-24 is seen to be in agreement with the experimental data presented previously in fig. 5-17.

However, the width of the experimental intensity versus tilt-angle distribution in fig. 5-17 is seen to be somewhat greater (∿ 15° at half-intensity) than that for the 1μm thick Rayleigh-Gans ellipsoidal model and also that for the opaque ray-tracing slab model (both ∿ 4.4°). This disagreement could result from the very marginal compliance of the opto-geometric model with the Rayleigh-Gans criteria and the results for the 2μm thick ellipsoid could be seen as supporting this possibility. However, in view of the ray-tracing fit it is also possible that the experimental distribution is broadened by slight helical motions of the sperm head as it rotates. Small off-axial rotations with the major axis inclined at perhaps 10° - 15° to the direction of translation would possibly impart significant broadening to the distribution of visible tilt-angles in this way. It is also a matter of observation that generally the head rotation is slightly off-axial, possibly rotating about the centre of mass located at the rear of the head (fig. 2-9).

(ii) *Intensity variation with head rotation.*

Fig. 5-25 shows the intensity distribution at a scattering angle of 20° for a 180° rotation of *transparent* elliptical slab head of various dimensions. The dimensions most relevant to bull spermatozoa are those of elliptical semi-axes 4.0μm and 2.3μm with a slab thickness of

1μm and the intensity profile is shown as the shaded region. The peak is seen to occur at a head rotation of $\theta_s/2$, that is with the normal to the head plane lying along the scattering vector.

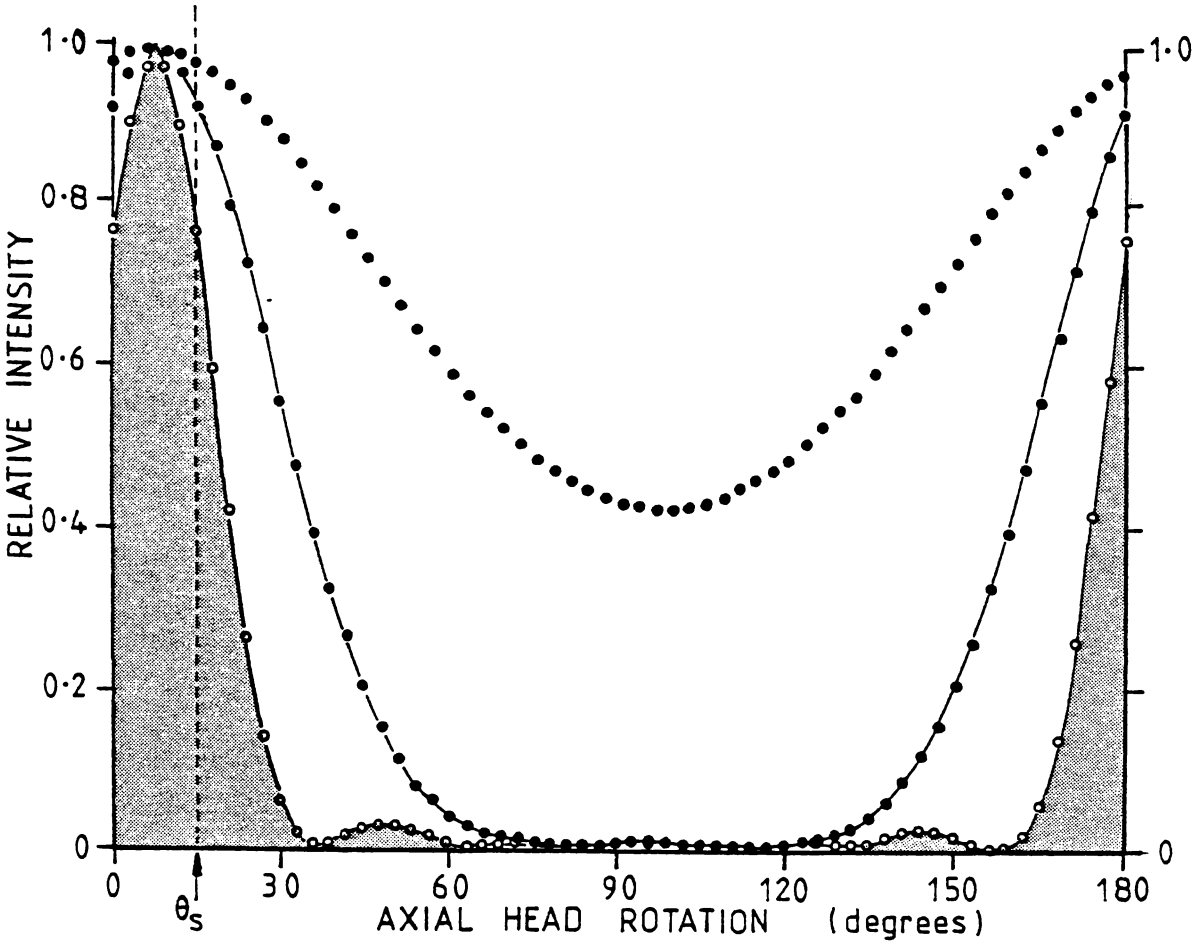

Fig. 5-25. The calculated far-field intensity distribution over a π radian axial rotation of a model sperm head of various dimensions. The optical model in all cases is that of a transparent elliptical slab. The dimensions of the slab are;

● ● ● ● ●	1.0μm x 0.57μm	semi-axes	0.25μm thickness
●—●—●—●	2.0μm x 1.15μm		0.5 μm
o—o—o—o	4.0μm x 2.3 μm		1.0 μm

The dotted line represents the scattering angle of 15° (for all cases) and the intensity profile appropriate to the linear dimensions of the bull spermatozoon is shown shaded.

As the linear dimensions of the head diminish the peak broadens, although a significant change in intensity is still evident at one quarter

of the normal head dimensions. The intensity peak profile for the opaque slab model is not shown since due to the small range of visibility over the head rotation ($0 \rightarrow \theta_s$) the trends are less illustrative and close agreement occurred with the transparent case over this range.

It is interesting to compare these intensity profiles with the photographic evidence of figs. 5-8 through 5-12 and the early work of fig. 2-11.

For a head model of spermatozoa dimensions the intensity peak shows a characteristic angular width of 19.3° at the half-intensity level. These calculated peaks can be compared with the experimentally derived peaks of fig. 5-20 and also the computer averaged flash intensity profile of Appendix IV. The peaks of fig. 5-25 at a flash period of $\sim$ 60mS (as derived from peaks in fig. 5-20) would have a width at half-intensity of 6.4mS which compares very favourably with the width at half-intensity of the experimental flash profile in Appendix IV of 7mS.

The extension of these calculations to derive the intensity autocorrelation function is clearly possible. For a single motile spermatozoon, from the calculations of fig. 5-25 and the experimental recordings of fig. 5-20 a strongly periodic autocorrelation function could be expected and indeed an example averaged over individual cell transits of the scattering volume is given in Appendix IV from collaborative studies.

Such is not found to be the case for large scattering volume populations where the simultaneous superposition of multiple pulse-trains such as fig. 5-20 leads to strong damping of the periodicity. To calculate the autocorrelation function in this case needs further definition of the dynamics of the scattering volume population the scattering volume geometry, the beam intensity profile and the number of pulses in each flash sequence. For these reasons the autocorrelation function has not been calculated, efforts having been directed towards exploring the basic characteristic of the system, the intensity fluctuation with head rotation.

It is also clear that dead cells will generate similar intensity changes on rotation. If a dead cell is sedimenting head down, then it will become visible to the photodetector only over a small range of head orientations about its major axis. For intensities at the detector of > 10% of the peak, the calculations of fig. 5-25 suggest that the cell will be visible over only 41.5° of each 180° axial rotation. At any given instant the detector would therefore collect light from only 23% of the vertically aligned dead cells. Furthermore, the sharp intensity profile will render the scattered field very sensitive to minor disturbances of the cell as by sedimentary rotation and/or Brownian forces.

5.7.4 Conclusions

Both the distribution of scattered intensity over a sperm head rotation, and the associated intensity versus tilt-angle relationship, are reasonably well modelled by applying either Rayleigh-Gans or ray tracing methods to geometrical models of ellipsoids and flat elliptical slabs respectively.

In general the head of the spermatozoon acts as a rotating mirror with a sharply peaked scattering lobe, the transverse angular dimensions of which are defined by the tilt-angle versus intensity relationship of fig. 5-24 and the peak widths of fig. 5-25. While the analysis has assumed spermatozoa to be swimming in a plane normal to the incident beam, it is clear that cells swimming in the bulk of the medium will generate an intensity peak at the detector if at some stage of the rotation, the normal to the head plane becomes closely aligned with the scattering vector. This can occur for cells swimming in any plane normal ($\sim$ within the tilt-angle limits) to the scattering vector as illustrated in fig. 5-26. In this case the two shaded planes represent the tilt-angle limits for the observable swimming plane in the bulk of the sample.

Fig. 5-27 shows the more general case for cells swimming in any direction within the sample although the fraction of motile cells not

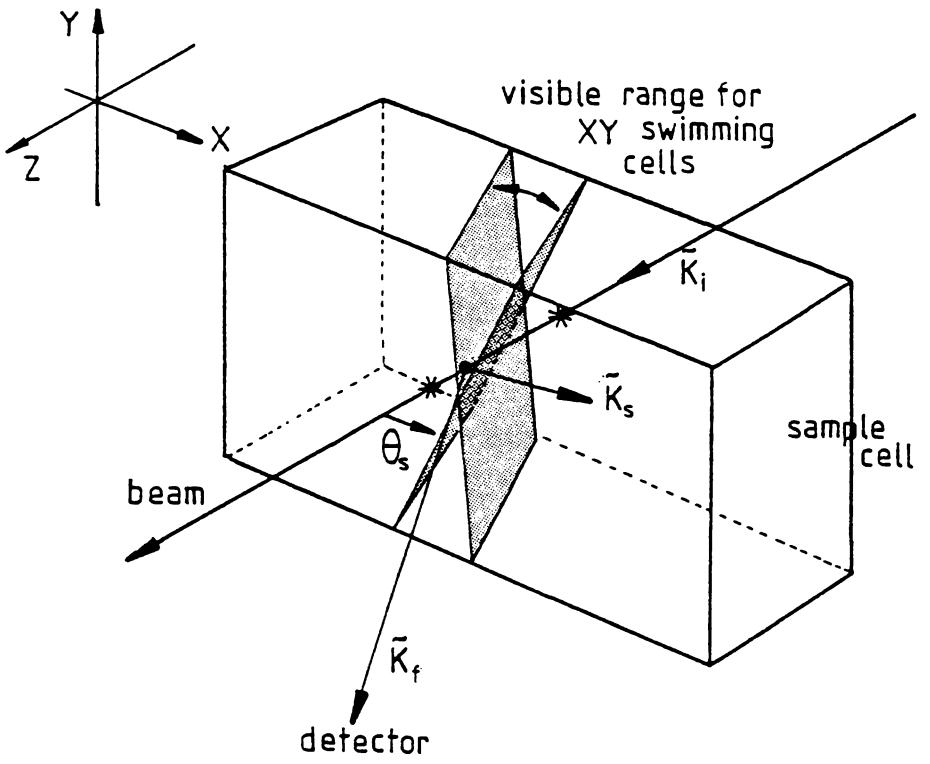

Fig. 5-26. A diagramatic illustration of the range of axial alignments or swimming planes visible to the detector. Cells whose trajectories do not intersect the shaded planes become visible to the detector at some point of their axial rotation.

Fig. 5-27. A three-dimensional illustration of the range of swimming trajectories visible to the detector, those velocity vectors $\tilde{v}$ falling within an angle $\alpha < \alpha_{max}$ to the plane normal to the scattering vector $\tilde{\kappa}$.

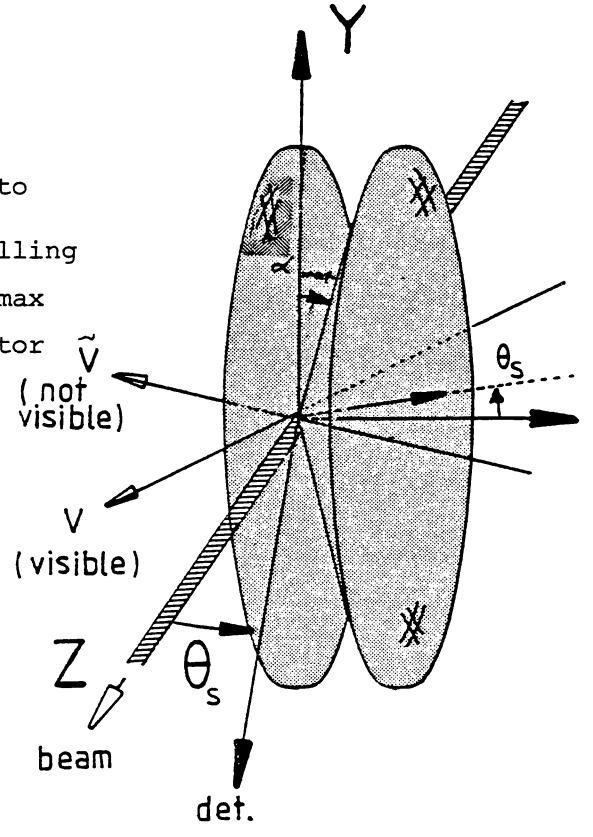

swimming on the cell surfaces is uncertain (see section 5.2.6). The actual peak amplitude of the intensity lobe, as $\tilde{v}$ (in fig. 5-27) is rotated about $\tilde{K}_s$, will be dependent on the orientation of the major axes of the head, relative to the detector. An oblate spheroidal head, for example, would give an axially symmetric intensity lobe as $\tilde{v}$ rotated about $\tilde{K}_s$.

Referring back to figs. 5-8 through 5-12, it is not clear whether some images represent spermatozoa swimming out of the window plane, through the bulk of the medium. The apparently constant focal position of the images, together with visual observation suggests that the images are largely of cells swimming on the cell walls.

The results of the calculations have shown very clearly that a sharply defined intensity peak occurs as the head rotates. The angular width of the intensity lobe is comparable with the value of 18° obtained experimentally (figs. 5-20). The characteristic width of the fast autocorrelation component (figs. 4-22 and 5-2 for example) is in the range 2-4mS at half-amplitude and this is consistent with the intensity profile of the scattering lobe (Appendix IV) as seen by the detector, which typically has a half-width of ∿ 3.5mS. Similarly dead cells, sedimenting head down, will only contribute light to the detector when axial rotation brings the normal to the head plane within ∿ 20° of the scattering vector. However, the slow autocorrelation component is of exponential form and may not be generated by a progressive rotation of the scattering lobe across the detector. If complete rotations were involved, the timescale of the slow autocorrelation component (decay time ∿ 1s for 100% dead suspensions) would suggest a rotation period of ∿ 40s in which time the cell would have sedimented ∿ 12μm or 1.5 head lengths. While such rotation is certainly a possible explanation for some of the dead cell images left on time exposure photographs. Many photographic images appear as diffuse flares and are more consistent with Brownian or other disturbances

which generate intensity fluctuations through very small movements of the head and so move the profile of the scattering lobe across the detector in a more or less random fashion, generating an exponential correlation function. The decrease in decay time of this function in the presence of motile spermatozoa is then easily understood as an enhancement of the basic Brownian induced random motions of the head, as a consequence of long range hydrodynamic coupling. The angular rotations involved need only be very small (a few degrees) to generate significant intensity changes.

This model of the slow ACF component does not however, appear to be consistent with the k^2t scaling previously evident for suspensions of dead cells in fig. 4-25, unless a fortuitous scaling of the scattering lobe width also occurs with scattering angle.

5.8 Studies with starfish spermatozoa

5.8.1 Background

Ample evidence has been presented that the large dimensions of the head of the bull spermatozoon and its flattened elliptical conformation, result in a gross asymmetry of the scattered light field. An important consequence is a flashing effect as the head rotates. It was, therefore, of interest in a comparative sense, to briefly study the scattering from smaller more symmetric spermatozoa using the same autocorrelation and photographic techniques. The published literature (table 1-4) on LBS studies of sperm motility, had in some cases used smaller species of more symmetric conformation. Consequently autocorrelation and photographic observations were carried out within the same light scattering geometry, using *cushion starfish (Patiriella regularis)* spermatozoa which have a spherical head of diameter in the range 1 - 2μm and a very thin flagellum of thickness $\lesssim$ 0.3μm.

5.8.2 Methods

Sperm samples were prepared by removing the gonads from live starfish,[1] flushing residual tissue away with saline and placing them in a 10ml tube of freshly filtered (0.22μm) seawater. Generally some degree of ejaculation took place spontaneously and the water thereby became cloudy with sperm at extremely high concentration.

The sample was then allowed to stand for a few minutes, passed through a 10μm millipore membrane filter to remove residual cellular debris, and diluted with 0.22μm filtered seawater to an appropriate concentration. A type C light scattering cell was employed, temperature controlled at 20°c ($\pm$ 0.1°) and aligned with its windows normal to the beam for data collection but normal to the microscope for photographic studies.

The level of dilution employed was adjusted to give cell concentrations having the microscopic appearance of being comparable with those employed for bull spermatozoa, probably in the range 1 - 5 x 10^6/ml for autocorrelation studies and somewhat less than this for photographic work.

It was noted that many samples prepared in this fashion had a very high percentage of immotile cells.

Time-exposure photomicrographs and autocorrelation functions were taken using the same techniques as previously defined.

5.8.3 Results

Results comprise the time exposure photomicrographs of figs. 5-28 and 5-29 together with the power spectrum and autocorrelation function of fig. 5-30.

Microscopically, starfish spermatozoa were found to exhibit the same marked surface swimming behaviour as bull sperm (section 5.2) in the low concentration range employed. However, the starfish spermatozoa in these samples were found to swim on the surfaces in circular trajectories having

[1] Kindly supplied by the Dept. Biochemistry, University of Otago.

a small radius of curvature, possibly 30 - 40μm, and at a frequency of ∿ 1 - 2 revolutions/sec.

The important point about these visual observations was that the head of the spermatozoon appeared as a bright luminescent point source showing no discernible scattered intensity fluctuations as it followed its circular trajectory. There was therefore, no orientational effect in the previous sense (section 5.7) since of a scattering angle of ∿ 20°, the head appeared to be of the same intensity along the entire length of its circular path.

These effects are readily apparent in the time-exposure photomicrographs of figs. 5-28 and 5-29. Complete circular trajectories are evident in fig. 5-29 and the short exposure tracks of fig. 5-28 are seen to be circular segments showing a uniform intensity along their length.

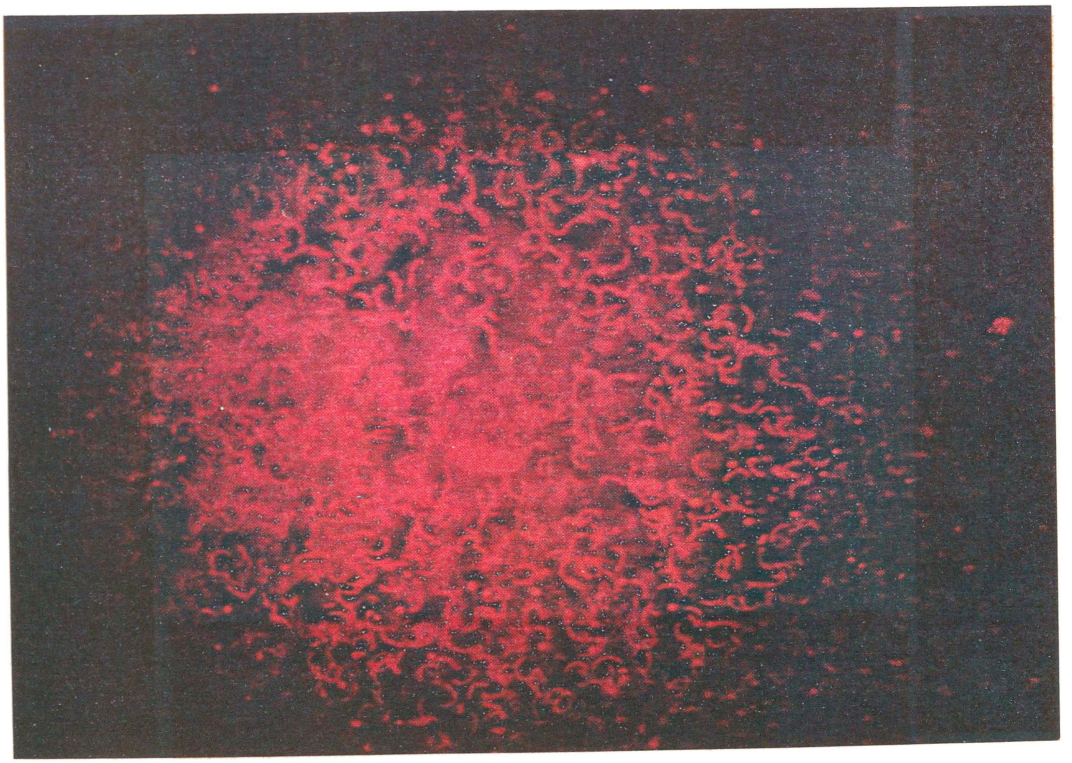

Fig. 5-28. A 0.25s time exposure photomicrograph of a dilute sample of starfish spermatozoa taken at a scattering angle of ∿ 20° (= 632.8nm) (64 ASA Kodachrome)

Fig. 5-29. Similar to fig. 5-28 but an exposure of 1s showing complete circular swimming trajectories. In both photographs the bright dots are immotile cells and the illuminated region is approximately of diameter 600 - 700μm. (64 ASA Kodachrome).

The autocorrelation function in fig. 5-30 is seen to be of the familiar two component form previously described for bull spermatozoa. The slow exponential feature, arising from the dead fraction, has a decay constant of 2.8 s^{-1} and is on a similar timescale to that previously obtained for dead bull spermatozoa ($\sim$ 1.0 s^{-1} for 100% immotile cells).

This decay constant at the scattering angle of 8° indicates a diffusion coefficient of 3.9 x 10^{-9} cm^2/s (assuming homodyne detection) which corresponds to an equivalent hydrodynamic radius of 0.55μm (temp. = 20°c), which is in good agreement with the known geometrical dimensions. Further, the fast signal component arising from the motile cells is characterised in fig. 5-30 by the power spectrum. This was obtained by direct signal sampling with FFT spectral analysis by the computer system (section 3.23).

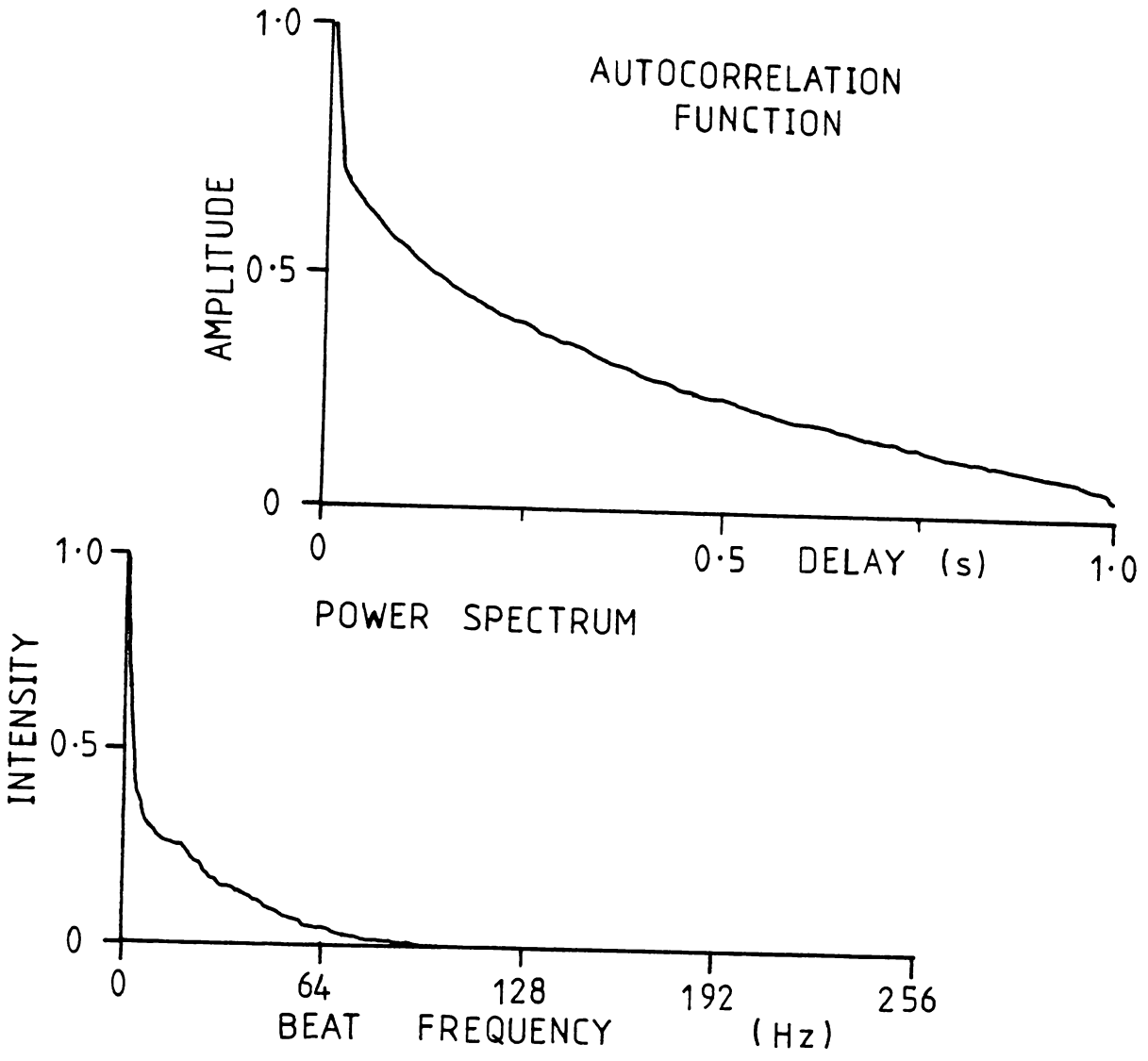

Fig. 5-30. An autocorrelation function on the same timescale as those collected for bull spermatozoa and a power spectrum formed by direct signal sampling and FFT methods. ($K \sim 1.9 \times 10^4$ cm^{-1}) scattering angle 8°.

The mean frequency of the spectrum is 43.2Hz and the peak beat-frequency is seen to be ∿ 80Hz. The large low frequency peak ($f \lesssim 6$Hz) is associated with the dead fraction which is further characterised by the autocorrelation function.

The highest frequency component in the spectrum, with homodyne detection and the swimming geometry apparent in fig. 5-28 and 5-29 should

correspond to the Doppler beat component for pairs of spermatozoa generated when moving along the horizontal segment of their circular trajectory, hence giving the maximum velocity components along the scattering vector.

The peak spectral frequency of 80Hz, under these conditions was calculated to be generated by pairs of spermatozoa, individually having tangential swimming speeds of 133μm/s. The circular rotation rate in the photographic data appeared to be ∿ 2Hz and on the basis of the computed tangential swimming speed, this would mean a radius of curvature of approximately 10μm. Qualitative agreement, therefore, was obtained between the observed swimming dynamics and the peak swimming speed calculated from the light beating result.

5.8.4 Conclusions

Starfish spermatozoa, being of substantially smaller dimensions than bull spermatozoa, and having a high degree of spherical symmetry, appear to behave at typical forward scattering angles as point scatterers, and the light scattering spectra can be validly interpreted as arising from Doppler shifted components in the scattered field.

However, within the sample cell system employed, the swimming dynamics were found to be far from those of an isotropic velocity distribution model. The cells swim predominantly in circular trajectories lying in the planes of the internal surface of the sample cell. Whether this observation has any implications for the results of other workers who have utilised similar spermatozoa in LBS experiments and interpreted their results on the basis of an isotropic velocity model, is not clear.

It is also interesting to consider that human spermatozoa, on which several LBS studies have been carried out (table 1-4), are intermediate in dimensions and conformal symmetry between the two species of sperm considered in these results and might be expected to show some of the same

phenomena.

Zorgniotti, Hotchkiss and Wall (1958) published high speed cine-photomicrographs (568 frames/sec) of swimming human spermatozoa. Their frames, using phase-contrast optics, showed the extent of the dense nuclear material where the refractive index was significantly higher than the surrounding medium, and presumably significant scattering would take place. Some variation is apparent in the size of this region (through the associated brightness when viewed in phase contrast) although the implications for the scattered intensity such as we have been concerned with, are not immediately clear.

5.9 Photographic studies of interactions between motile and immotile spermatozoa.

5.9.1 Background

Indirect evidence during the earlier studies of chapter 4, suggested strongly that dead or immotile cells were perturbed or even bodily displaced, by the relatively vigorous motions of the motile fraction. In the data of fig. 4-20 for example, the decay constant of the slow ACF component increased linearly with the concentration of motile cells, consistent with an enhanced Brownian diffusion of the immotile fraction induced by hydrodynamic coupling from swimming cells.

Two forms of interaction appeared possible at that stage:

(i) direct, or close encounters, between motile and immotile spermatozoa which induce rapid large amplitude displacements of the immotile cell. Such interactions were seen potentially as contributing to the AAR - concentration effects of sections 4.3 and 4.8. Since the displaced cell would momentarily appear as if motile.

(ii) a stirring or large scale disturbance of the suspending medium generated by the collective hydrodynamic disturbances generated by the motile fraction. Such disturbances could potentially enhance Brownian motions.

In view of the orientational phenomena discussed in this chapter, a further interaction mechanism becomes possible and we therefore also have:

(iii) Direct encounters or 'near-misses' between a motile spermatozoon and an immotile spermatozoon which result in a *reorientation* of the immotile cell to an attitude outside of the visible range of tilt-angles (fig. 5-16), hence modifying the number of visible immotile cells and so the light scattering AAR value.

The effective range for this latter type of interaction was likely to be very much larger since a torque applied via the flagellum from movements of the medium would be just as effective as direct interactions with the head. The presence of the flagellum would effectively increase the interaction cross-section.

The level of all three processes (i - iii) could be expected to be closely related to the concentration of motile cells. However, spermatozoa swim in a fluid environment at an extremely low Reynolds number ($\sim 10^{-3}$) where viscous effects dominate fluid motion and localised fluid disturbances might be expected to have a short range effect only. The collective effect of localised disturbances, created by a large number of motile cells in a fluid environment of restricted dimensions, or the collective effect of 'creeping flow' fluid displacements, was quite uncertain. With this in mind, a study was undertaken to determine whether, under typical sperm concentration and sample dimension conditions, interactions between motile and immotile cells can be directly observed, and whether their involvement in the ACF features could be more directly verified.

5.9.2 Methods

The general principle of the method was that of defining movements of the suspending medium by using small polystyrene latex (PSL) spheres[1] embedded in the medium (i.e., $\sim$ 1μm in diameter) as markers, and examining

(1) *DOW Chemical*.

the sample with time-exposure photomicrographs (Holwill, 1966).

Studies were carried out using a haemocytometer cell of depth 100μm, seated on a heated microscope stage and temperature controlled at 37°c. The haemocytometer chamber was filled with suspensions of either:

(i) 1μm diameter PSL spheres at an empirically adjusted low concentration.

or (ii) 1μm diameter PSL spheres at the same concentration with motile bull spermatozoa present in the suspension at a concentration of 10^7 sperm/ml.

both suspensions being in a 2% sodium citrate based buffer (0.22μm filtered).

The spermatozoa were from a highly motile (motile cells appearing normally vigorous) sample containing 15% *eosinophillic* cells in the raw ejaculate.

The PSL sphere concentration was adjusted so as to give a satisfactory density in the microscope field for imaging purposes, the same concentration then being used for photographic exposures both with, and without, spermatozoa in the suspension.

The 1μm diameter PSL spheres were effectively embedded in the medium This allowed any induced disturbances to be defined on time exposure photomicrographs, by either linear or incremental displacements of the sphere images or, alternatively, blurring of the image which could be taken to indicate enhanced Brownian motion.

The photographic and microscopic equipment and techniques were as previously outlined in section 5.2.2 for dark-field illumination of the sample. The 1μm diameter spheres were sufficiently large to be clearly visible with dark-field illumination but were not so large as to show significant sedimentation over the experimental timescale. Time exposures on 64 ASA Kodachrome slide film were taken to define the motion of the spheres and hence that of the medium, both with and without motile spermatozoa present in the suspension.

As previously discussed (section 5.2), a substantial percentage of motile cells swim on the internal plane surfaces of the sample cell. So as to exclude the spermatozoa swimming tracks (i.e., as in fig. 5-6) from the image, and to look solely at the motions of the medium (i.e., the PSL spheres) remote from the swimming cells, the focal field was adjusted to be at mid-depth in the 100μm deep cell. An indeterminate number of motile cells would have swum through the focal field during the exposures but, visually, most motile cells were somewhat remote from this region, being close to the upper and lower surfaces of the chamber and outside the focal field (refer fig. 5-5). Time-exposure photomicrographs were taken over a wide range of timescales so as to further verify the existence of interaction effects by looking for changes in sphere image definition with exposure time.

5.9.3 Results

The data comprise representative pairs of time-exposure photomicrographs presented in figs. 5-31 through 5-33 for exposures of 2, 5, 10s, respectively. At each exposure time, the density, location and definition of sphere images, may be compared in the presence (exposure b) and absence (exposure a) of spermatozoa.

Fig. 5-31 (exposure time 2s) in the absence of spermatozoa (exposure a) shows PSL spheres to be sharp, well defined point-images, randomly distributed and reasonably monodisperse. There is no evidence of bulk motion or localised motion of the medium, over the timescale of the exposure.

In the presence of 10^7/ml motile spermatozoa (exposure b), the number of sharp non-displaced sphere images is markedly less and close examination shows the presence of many diffuse images. This was taken to indicate a high level of sphere perturbation over the exposure interval.

Fig. 5-32(b) at a longer 5s exposure time reveals more detail of the

perturbation events. The sphere concentration is seen to be the same at all three exposure levels, by comparing all (a) photographs after allowing for the exposure time, which affects the general brightness of both the field and the images.

At the 5s exposure level, the sharpness of the spheres-only images in exposure (a), is still very similar to that at a 2s exposure (fig. 5-31(a). In the presence of spermatozoa, however, (fig. 5-32b), the number of sharply defined point images of spheres is markedly less than in (a), diffuse images arising from sphere motions are much more numerous and the increased incidence of multiple images (apparently of the same sphere) are all suggestive of significant effects over the 5s timescale. In many cases closely spaced or grouped images appear to indicate repeated small discrete displacements of the same sphere due to closely consecutive perturbation events and this in fact becomes even more evident in the 10s exposure of fig. 5-32(b). Again the 10s exposure for spheres-only in 5-33(a) shows excellent stability of the medium over the timescale of the exposure (10s) and no significant evidence of Brownian effects. The presence of spermatozoa clearly had a very significant effect on the hydrodynamic stability of the medium although in the case of this experiment, it was at a relatively short range (50μm) from spermatozoa swimming at the surfaces.

The presence of point images of spheres, even at an exposure level of 10s, suggests that major perturbations arise from localised interactions rather than from a long range general stirring of the medium.

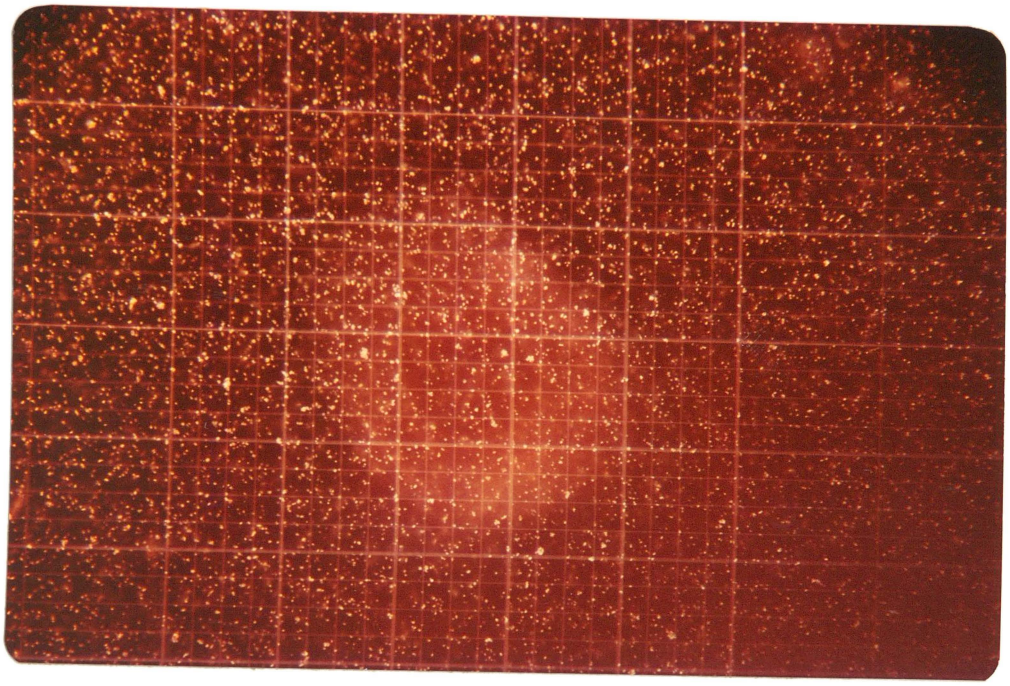

Fig. 5-31 (a). 1μm PSL spheres only in a sperm-free medium; exposure 2s.

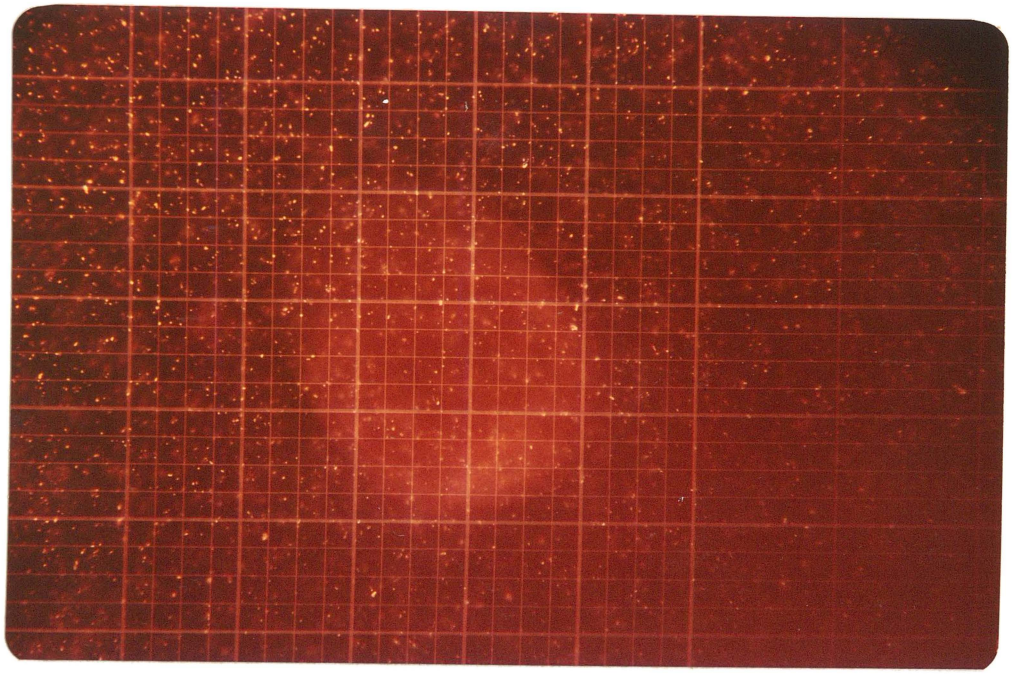

Fig. 5-32 (b). 1μm PSL spheres at the same concentration as in (a) but with 10^7/ml motile spermatozoa present in the suspension; exposure 2s.
The heavy rulings represent 100μm squares, the fine rulings 25μm squares.

64 ASA Kodachrome.

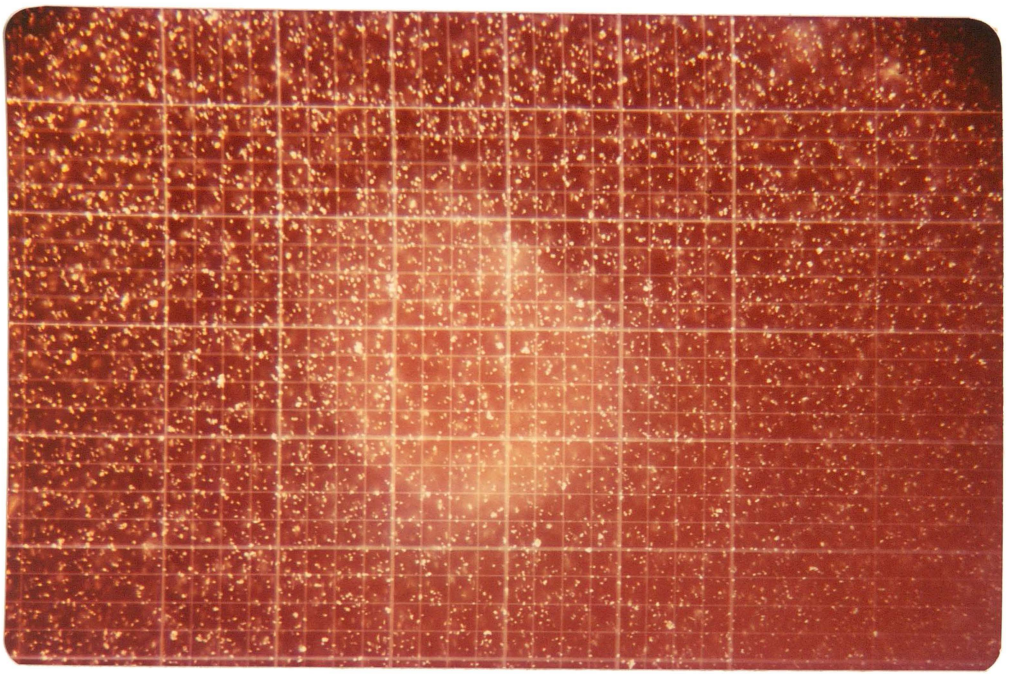

Fig. 5-32(a). 1μm PSL spheres only in a sperm-free medium; exposure 5s.

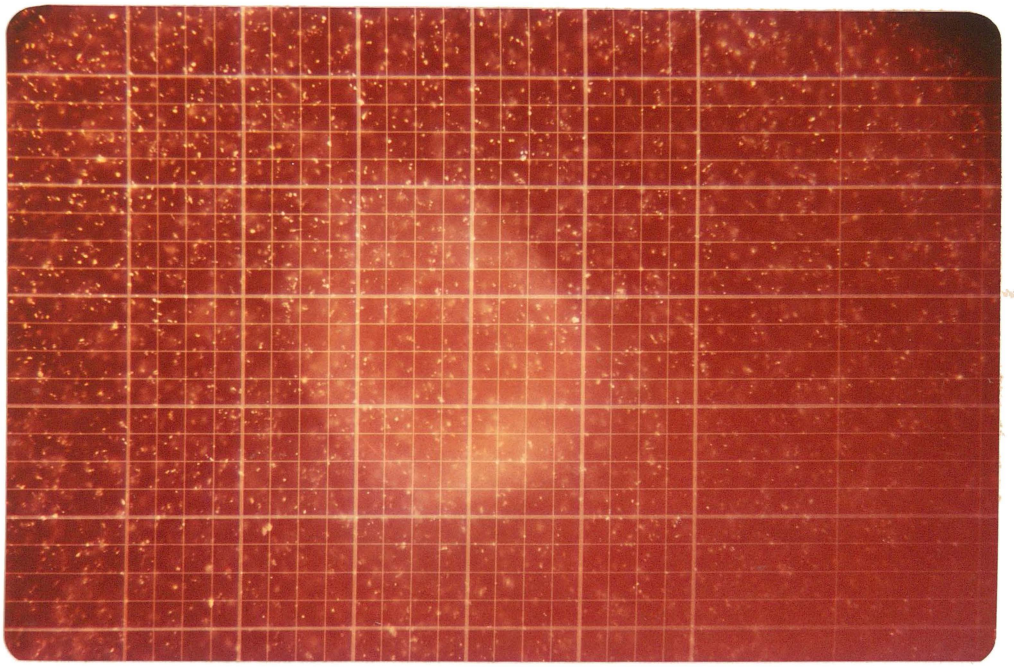

Fig. 5-32(b). 1μm PSL spheres at the same concentration as in (a) but with 10^7/ml motile spermatozoa present in the suspension; exposure 5s.

64 ASA Kodachrome.

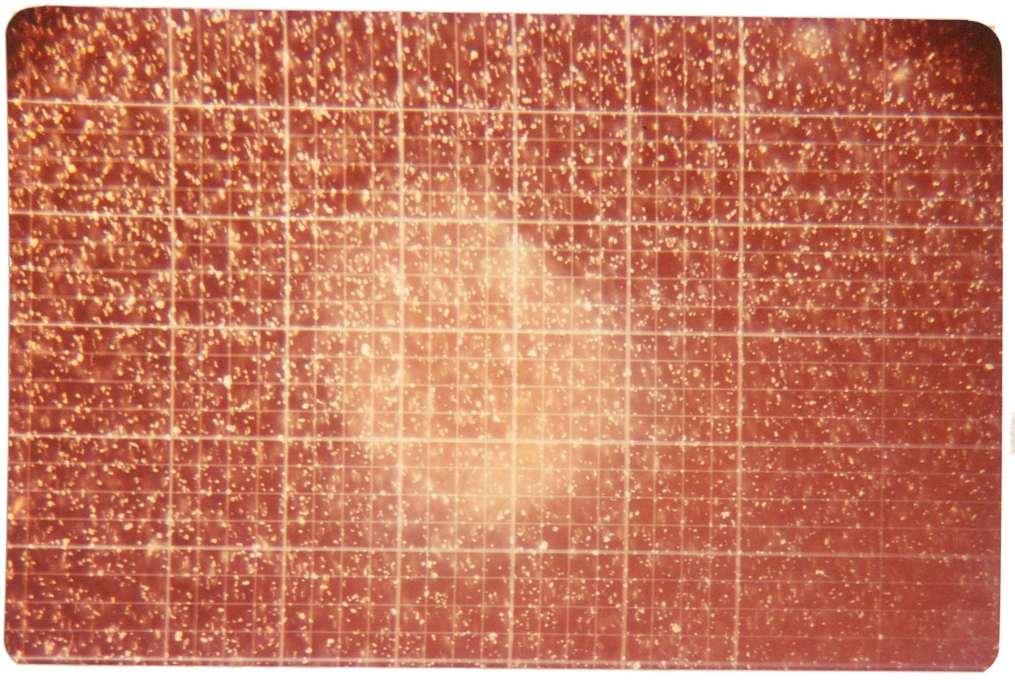

Fig. 5-33 (a). 1μm PSL spheres only in a sperm-free medium; exposure 10s.

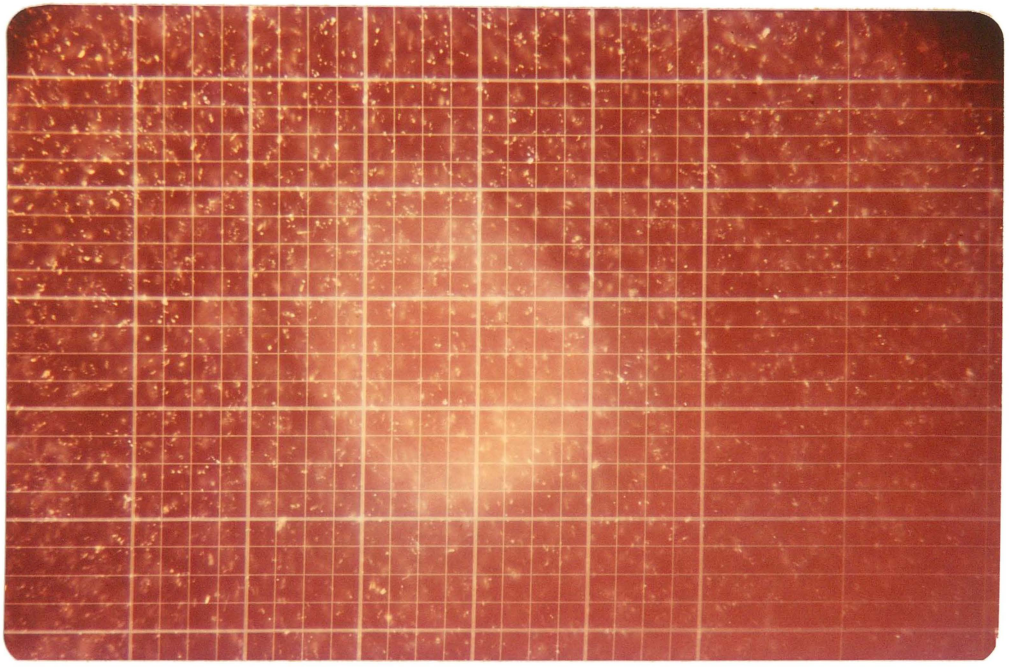

Fig. 5-33 (b). 1μm PSL spheres at the same concentration as in (a) but with 10^7/ml motile spermatozoa present in the suspension; exposure 10s.

64 ASA Kodachrome.

perturbations arise from localised interactions rather than from a long range general stirring of the medium.

5.9.4 Conclusions

In a sample cell of thickness 100μm, with an indeterminate percentage of spermatozoa swimming within a distance of 20μm from the surfaces (Rothschild, 1963), localised disturbances of the medium occurred throughout the mid-region of the sample due to interactions with passing spermatozoa. While the depth of the suspension in terms of surface swimming effects was relatively small, the observed perturbations occurred over a very short timescale (2 - 10s) and this might be considered in the light of following data in fig. 5-39. In light scattering sample cells, (e.g., type B-1, B-2, C) the spacing of the surface swimming motile fraction from the central regions of the medium is much greater, perhaps 10x - 20x. However, the percentage of motile cells traversing the bulk of the medium can be expected to be rather similar and the timescale over which the sample is observed in LBS experiments, is much longer (typically 300s in comparison with the 10s of fig. 5-33). The probability of a hydrodynamic disturbance, induced by the nearby passage of a motile spermatozoon, at any given point in the centre of the sample is, therefore, probably quite high.

5.10 Light scattering studies of interaction effects

5.10.1 Background

Direct evidence has been presented (section 5.9) showing the existence of medium perturbations at a range of 50μm from wall-swimming spermatozoa, although it appeared likely that the major disturbances were localised and possibly created by spermatozoa swimming in the bulk of the medium. While indirect evidence of such perturbations had been seen in

earlier light scattering studies, (fig. 4-20 for example), direct experimental confirmation of the existence of the phenomenon was not available.

While hydrodynamic interactions between motile and immotile spermatozoa indisputably occur at very high sperm concentrations (section 2.7), the important question was whether or not such interactions were contributing to light scattering measurements which were carried out at lower concentrations, bearing in mind the concentration - AAR effects evident in figs. 4-10 and 4-19.

Previous experiments, such as those of sections 4.2 and 4.8, had varied the ratio of motile to immotile spermatozoa while retaining fixed total concentrations. Interpretations of changes in the ACF decay constant as being due to interactions were thus confounded by changes in the absolute concentrations of both motile and immotile fractions.

An experiment was therefore indicated, wherein a variable population of motile spermatozoa was introduced to swim among a fixed population of immotile cells. By varying the motile population (but accepting that they would not be uniformly distributed) the effect on the dynamics of the supposed random three-dimensional distribution of dead cells could, therefore, be more convincingly studied.

5.10.2 An interaction model

Consider a homogeneous localised distribution of motile and immotile spermatozoa (say in the mid-region of the suspension) having concentrations of $(\alpha\ \rho_\ell)$ and ρ_d respectively, where ρ_ℓ and ρ_d are the average concentrations taken over the whole sample volume and α is a factor which takes account of the depletion of motile cells in the bulk of the medium due to surface swimming effects. Consider also that away from internal surfaces, the distribution of translation vectors is isotropic and that the mean swimming speed is $\bar{v}$.

The motile spermatozoa are then taken to have a characteristic circular

interaction cross-section of area σ, normal to the translation vector, over which the rotating flagellar wave imparts sufficient motion to the medium to perturb the orientation of any dead cells present. This interaction radius may extend very little beyond the amplitude of the flagellar wave ($\sim$ 9 - 10μm from fig. 2.14) due to the extremely small Reynolds number regime of the environment ($R_e \lesssim 10^{-3}$) and in this approximate treatment is considered to effectively include any extended region around the immotile cell, within which the transit of a motile cell will result in a perturbation.

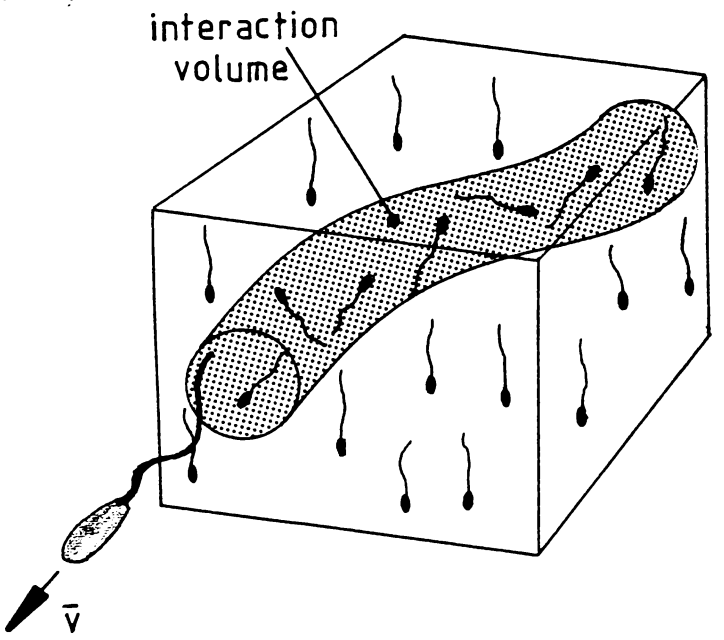

Fig. 5-34. The interaction volume per second of a motile spermatozoon. The tubular volume is of radius r_i and length $\bar{v}$.

The total interaction volume V_i traced out collectively by the swimming cells in a unit volume, per second, is given by;

$$V_i = \alpha \rho_\ell \bar{v} \sigma \qquad (5\text{-}5)$$

where $\sigma = \pi r_i^2$

Therefore the number N_i of immotile cells experiencing interactions per unit volume per second is;

$$N_i = V_i \rho_d = \alpha \rho_\ell \rho_d \bar{v} \sigma$$

and the fraction Δn_i of immotile cells experiencing interactions per unit volume per second is therefore;

$$\Delta n_i = \alpha \rho_\ell \bar{v} \sigma \qquad (5\text{-}6)$$

which is independent of the concentration of dead cells. This is an important characteristic of this interaction model which will be examined further in section 5.11.

If we consider the frequency of perturbations in the sample as a whole to have the effect of enhancing the Brownian induced motion of immotile cells, then we can use the slow ACF decay constant as an indicator of interaction rate. Whether an interaction results in a small amplitude disturbance of the cell or a complete reorientation, will depend upon the range at which the encounter takes place and hence different levels of perturbations will have associated cross-section levels.

For any given level of perturbation in the observed scattering volume we can expect that the frequency will be linearly related to the concentration of motile spermatozoa, the mean swimming speed and the interaction cross-section.

5.10.3 Methods

The general method in this light scattering study of interactions was that of varying the absolute concentration of an introduced population of motile spermatozoa swimming through a fixed concentration of immotile cells, the decay of the slow ACF component being the experimental observable of interest.

The same general sample collection, processing and dilution techniques were used as previously described in section 4.3.2. In this case, however, the final *immotile cell concentration* was adjusted to be 2×10^6 sperm/ml and the *motile cell concentration* was varied over the range $0 - 1.74 \times 10^6$ sperm/ml (i.e., 53 - 100% immotile cells). The high concentration of immotile cells enabled good autocorrelation statistics to be obtained in

the presence of a high level of perturbations, due to an enhanced scattering volume population of dead cells. Previously in highly motile samples the immotile population had been low and the level of interaction presumably high giving poor slow ACF component statistics (e.g., see definition of slow exponential component in fig. 4-12).

A type C sample cell was employed and a scattering angle of 8° giving $k = 2.39 \times 10^4$ cm^{-1}. Correlation functions were taken using a signal sampling interval of 33.3mS, functions comprising 16 * 1024 samples and so giving a total data - collection time of 546s. The standard 5.5 min. thermal equilibration period was allowed prior to data collection.

It should be emphasised that data collection over these time intervals for autocorrelation functions on this lengthy timescale required extremely high hydrodynamic stability of the medium.

5.10.4 Results and Discussion

Typical autocorrelation functions obtained over the concentration range 0 - 1.74×10^6 motile sperm/ml are shown in fig. 5-34, and the progressive departure from the zero motile cells case is clearly apparent. Two principal effects on the immotile component are evident;

(i) an increase in the decay constant as the motile cell concentration was increased.

(ii) an apparent truncation of the slow exponential feature after a reasonably well defined delay time, the cut-off point being better defined at the higher motile cell concentrations.

The AAR values showed a decrease with increasing motile cell concentration, although the determination of the absolute AAR values depended on the baseline definition, either that shown as being common for all functions in fig. 5-35, or that shown as fitted to the truncated exponential feature in fig. 5-36.

The slow ACF decay constants, relating to the truncated exponential

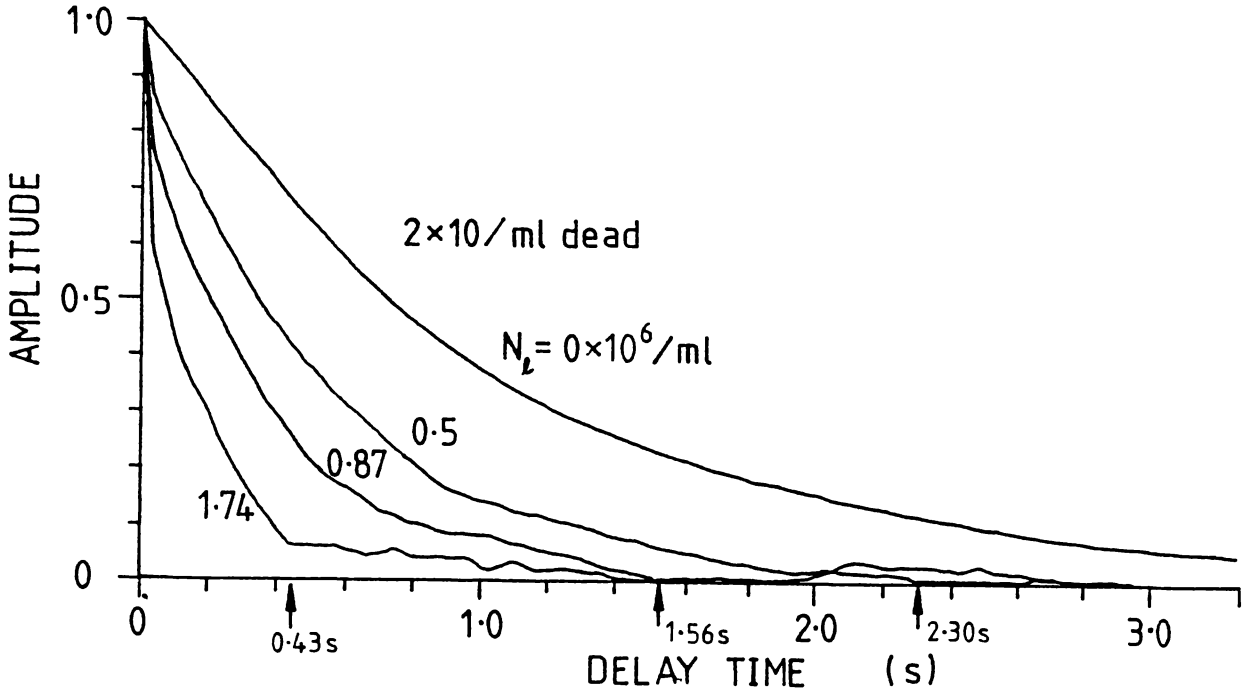

Fig. 5-35. Superimposed autocorrelation functions, all on the same timescale, for various concentrations of motile spermatozoa swimming among a fixed population (2 x 10^6/ml) of immotile spermatozoa (K = 2.39 x 10^4 cm^{-1}).

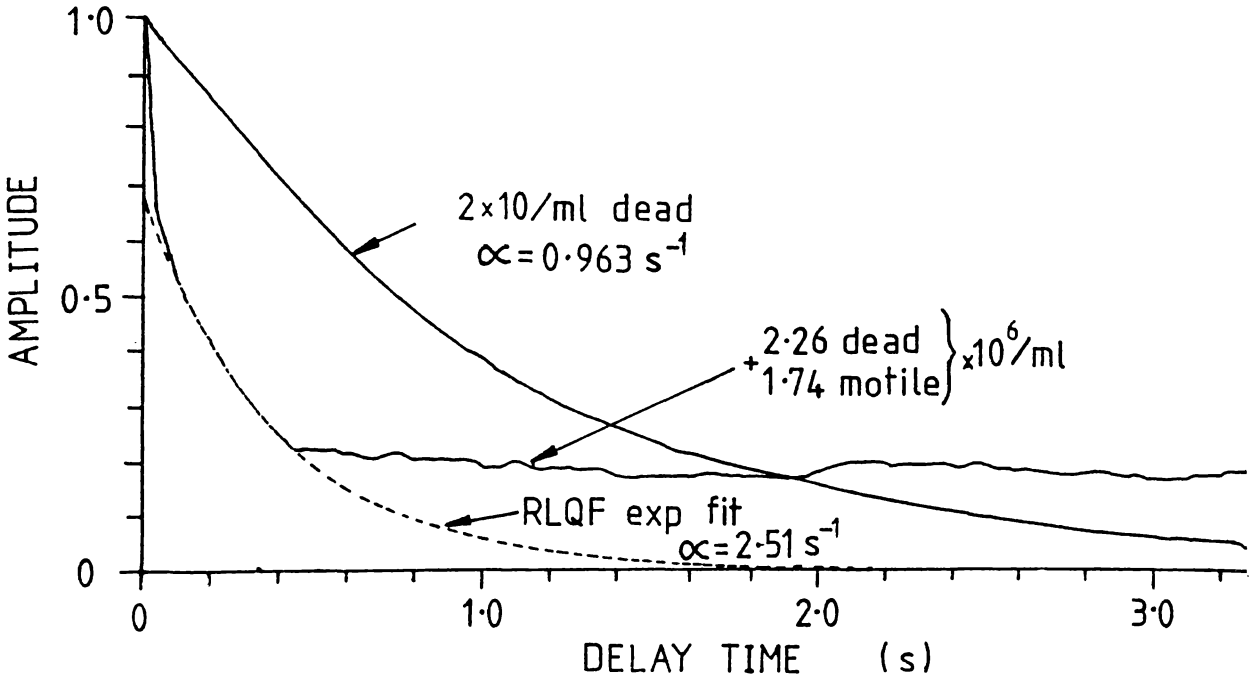

Fig. 5-36. The autocorrelation function for 1.74 x 10^6 motile sperm/ml shown relative to the true baseline of the exponential feature. For comparative purposes the function for a 100% immotile sample is superimposed.

segments, are shown plotted in fig. 5-37 as a function of the inverse cube of the mean motile sperm spacing (assuming a random distribution), that is, the mean volume per motile cell. This factor is an inverse function of the motile cell concentration just as the decay constant is the inverse of the decay time. This, therefore, is consistent with equation (5-6) which shows the interaction rate as being proportional to the motile cell concentration.

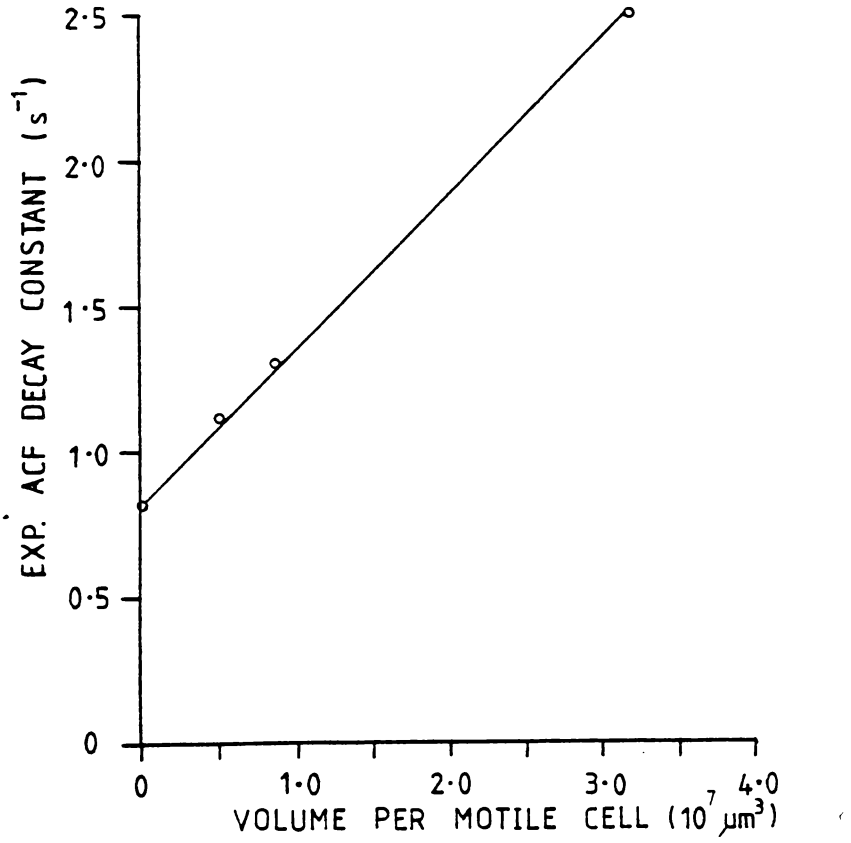

Fig. 5-37. The slow ACF decay constant for the exponential segments of the functions in fig. 5-35 plotted as a function of the mean volume per motile spermatozoa.

The truncation of the slow ACF exponential components in fig. 5-35 appeared to occur at reasonably well defined delay times which are seen in fig.5-38 to vary with motile cell concentration in a slightly curvilinear fashion. It would seem possible that the correlation time

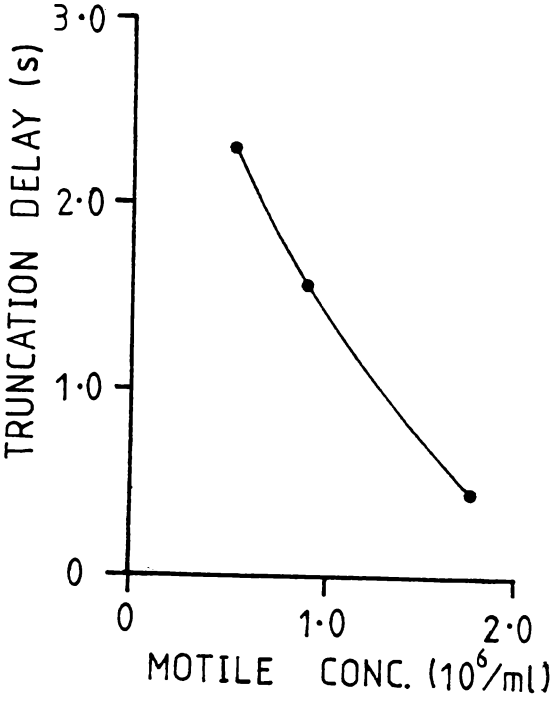

Fig. 5-38. The estimated truncation delay time (s) for the three 'motile' functions of fig. 5-34, plotted as a function of motile cell concentration.

corresponding to these truncation points represents a characteristic interval determined by the frequency of interactions experienced by an immotile spermatozoon. The exponential segments can then be interpreted as having a characteristic decay time determined by long range interactions which enhance random, small amplitude, motions of the cell, but being truncated at a delay corresponding to the mean collision interval, per cell.

5.11 Concentration dependence of the AAR as an interaction effect.

5.11.1 Background

As previously discussed (5.10.1), early experiments which demonstrated an AAR - concentration interaction, varied the ratio of motile to immotile cells at a fixed total concentration. Section 5.10 has shown evidence of interaction effects in a fixed immotile concentration of immotile cells, closely associated with the absolute concentration of motile cells. If the AAR - concentration effect does arise from motile-immotile interactions which reorient the immotile cells, then relation (5-6) indicates that the level of interaction should be independent of the concentration of dead

cells. Consequently, if the concentration of motile cells is held constant, the interaction factor will remain constant if immotile cells are added to the suspension. In this situation, the AAR should show a linear relationship to the percent immotile cells provided the absolute concentration of motile cells is maintained constant, and the slope of the line will be determined by the frequency of interactions. However, the absolute value of the AAR can be expected to depend upon other factors. Some of these are probably independent of the absolute concentration of immotile cells, the percentage of motile cells which are visible to the detector, for example, while others such as the wall swimming effects and other points which have previously been discussed, may be additional sources of concentration effects.

An experiment was thus carried out wherein the AAR was measured for various levels of percent immotile cells which were obtained in this instance by adding appropriate numbers of immotile spermatozoa to a fixed concentration of motile cells.

5.11.2 Methods

Sample preparation, mixing and dilution followed the general procedures previously discussed (e.g., table 4-1). Immotile cells, freshly killed by cold-shock, were added at high concentration (2×10^8/ml) to a fixed concentration of motile spermatozoa in appropriate numbers to give the desired percent motile cells in the sample. The total sample concentration varied depending on the number of cells added. Experimental runs were thus carried out using two levels of motile cell concentration, 1×10^6/ml and 4×10^6/ml. The basic motile sample was determined to be 83% live (*eosinophobic*) immediately following collection and immotile cell additions were calculated taking account of the nominal 17% dead cells in the motile sample.

The percent dead cells was thus varied over the range 17 - 50% at

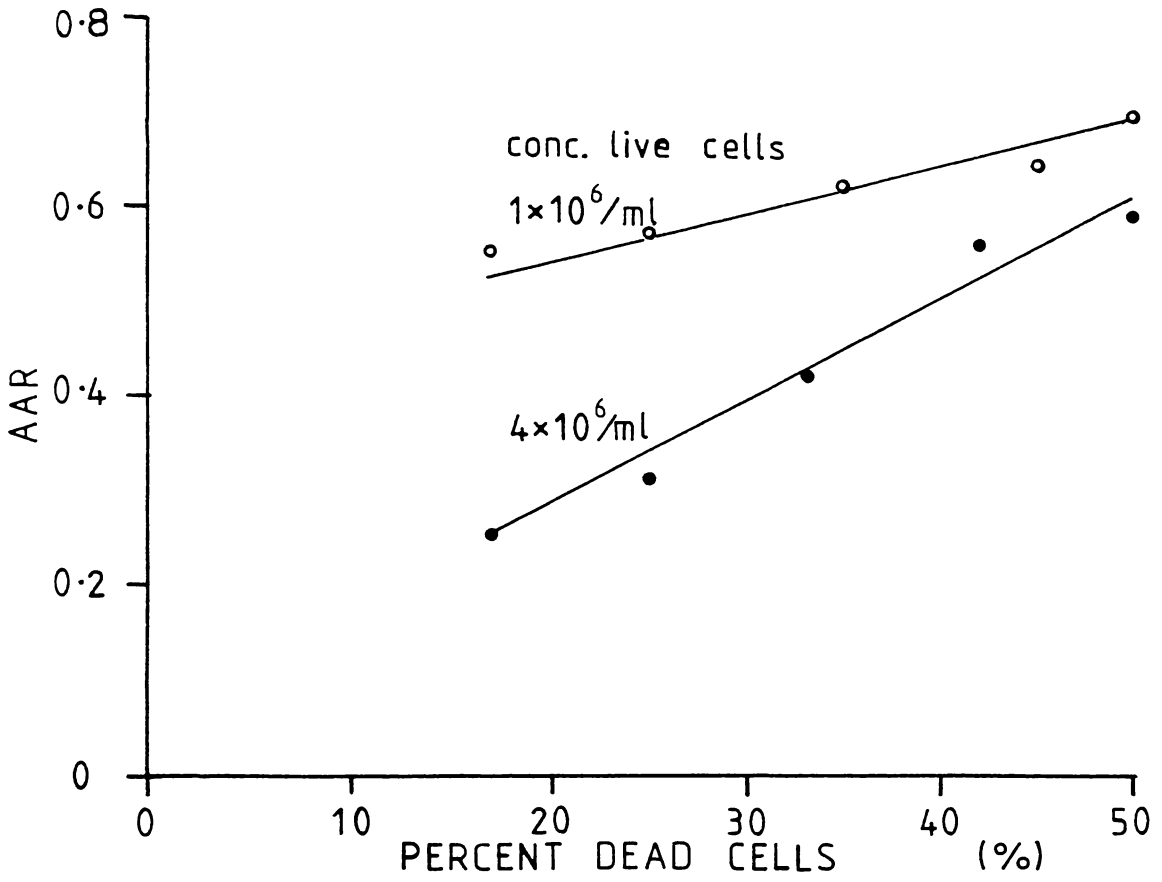

Fig. 5-39. The AAR as a function of percent dead cells at each of two fixed motile cell concentrations.

	Decay Constants (s^{-1})	
Concentration motile	1 x 10^6/ml	4 x 10^6/ml
Percent motile		
83%	5.26	7.81
75%	3.15	8.88
65%	2.98	8.34
50%	3.64	7.92

Table 5-2. Decay constants for the slow ACF exponential components over the range of percent motile cells employed at each of the two motile cell concentrations.

fixed motile cell concentrations of both 1 x 10^6/ml and 4 x 10^6/ml.

Autocorrelation functions were collected using a signal sampling interval of 10mS for a total of 32 * 1024 samples (328s sampling time) and analysis followed general procedures previously discussed.

5.11.3 Results and Discussion

As is evident in fig. 5-39 a substantially linear relationship, was obtained between the light scattering AAR values and the percent dead cells at both motile cell concentrations. The associated slow ACF exponential decay constants (table 5-2) appeared to depend, not on the percent dead cells, but on the level of motile cells.

The decay constant values at ρ_ℓ = 4 x 10^6/ml fall closely about a mean value of 8.24 s^{-1} and those at < 83% motile with ρ_ℓ = 10^6/ml show a mean value of 3.26 s^{-1}. The higher value at 83% motile was of doubtful significance but may have resulted from a higher level of interaction.

The data of fig. 5-39 can be usefully compared with the previous relationships of figs. 4-9 and 4-19, bearing in mind that the total concentration (live + dead) in the samples used in this experiment ranged from 1.2 x 10^6 - 2 x 10^6/ml for ρ_ℓ = 1 x 10^6/ml and 4.82 x 10^6 - 8 x 10^6/ml for ρ_ℓ = 4 x 10^6/ml.

These results are clearly consistent with a fixed frequency of interactions on a per cell basis for each motile cell concentration and provide convincing evidence that the AAR - concentration interaction arises from such interactions.

5.12 A system model incorporating orientational optical and spatial phenomena

Using the previously described phenomena associated with light scattering by suspensions of spermatozoa, it is possible to summarise the behaviour of the system in a simple optical and dynamical model which

predicts the form of the AAR - concentration interactions of figs. 4-9, 4.19 and 5.39.

The principal effects on which the model is based are:

(i) *The conformation of the sperm head is such that both motile and immotile cells are only visible to the detector within a certain range of head orientations relative to the scattering vector.*

(ii) *Hydrodynamic interactions at sufficiently short range between motile and immotile spermatozoa, may result in a reorientation of the immotile cell either into or out of the range of visibility to the photodetector.*

(iii) *In the absence of interactions, immotile cells orient towards a vertically aligned head-down attitude, at a specific average rate.*

(iv) *The scattering volume if located in the bulk of the sample, becomes depleted of motile cells which accumulate on the internal surfaces of the cell, an equilibrium situation becoming established wherein the flux of cells swimming onto the surfaces equals the flux of cells leaving the surfaces due to motile-motile interactions (etc.)*

Considering each of these effects in turn, parameters, functional relationships and probable values may be established which in sub-section (v) will be used in numerical calculations of the model behaviour.

(i) *Range of visible orientations.*

This is simply characterised by the maximum visible tilt-angle α_m. At tilt-angles $\alpha < \alpha_m$ the intensity peak and hence the relative contribution to the detected signal has been shown to vary widely (fig. 5-24). However, a simplifying assumption will be made that the contribution to the detected signal is uniform for all visible cells, that is those with $\alpha < \alpha_m$. Typically $\alpha_m \sim 20^\circ$ experimentally (fig. 5-17) but calculations show that it can also be expected to depend on scattering

angle (fig. 5-24). Considering the geometry of fig. 5-40, for a suspension of randomly oriented spermatozoa, the fraction visible to the detector is in the ratio of the bounded surface areas delimited by α_m and this proportion is defined by;

$$\rho_v/\rho = \text{Sin } \alpha_m \qquad (5\text{-}7)$$

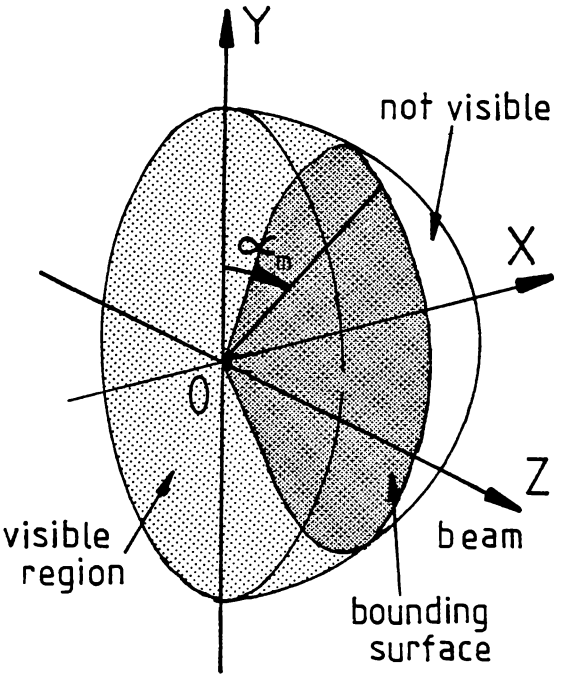

Fig. 5-40. Geometry of visible tilt-angle range.

where ρ_v is the concentration of visible cells and ρ is the overall concentration.

At $\alpha_m = 20°$ this gives $\rho_v/\rho = 0.34$. Using the experimental result at $\theta_s \approx 20°$ gave $\rho_v/\rho \approx 0.2$. In addition, at any given instant only $\sim$ 10% of cells within the visible range of tilt-angles are visible due to the relative orientation of the scattering lobe about the major axis of the head. The angular width of the scattering lobe is only $\sim 18°$ thus allowing the head to scatter light to the detector over only $\pi/10$ of each π axial rotation. If, however, it is assumed that immotile cells sedimenting head down within the visible range of tilt-angles rotate (albeit slowly) as do visible motile cells, then over an extended observation period the mean scattered intensity at the detector will be the same for either a motile or an immotile cell.

It also seems probable that the range of visible tilt-angles for motile cells (that determined experimentally in fig. 5-17) will be greater than that for immotile cells, due to off-axial head rotation during swimming. The theoretical calculations of fig. 5-24 suggested maximum visible tilt-angles of $\sim 10^{\circ}$ - 15° at typical experimental scattering angles.

(ii) *Interactions*.

Section 5.10.2 showed that the probability P_i of an immotile cell experiencing an interaction in a 1s interval is given by;

$$P_i = \rho_\ell \bar{v} \sigma_i \qquad (5\text{-}8)$$

where ρ_ℓ is the localised concentration of motile cells, $\bar{v}$ the mean swimming speed and σ_i the cross-sectional area of the interaction region.

The experimental evidence, as from the effect of motile cell concentration on the slow ACF decay constant (e.g., fig. 5-37 and table 5-2), suggests that the characteristic correlation time for the motion of immotile cells is indeed determined by ρ_ℓ. However, the interaction cross-section for a reorientational perturbation of the dead cell which may orient it to an attitude outside of the visible range of tilt-angles is not known, although the time exposures of fig. 5-31 through 5-33 indicate that major medium disturbances on a wide scale do occur in the bulk of the medium.

Such interactions have two characteristic variables of interest, the frequency of occurrence and the amplitude of the resultant reorientation.

The frequency of occurrence as defined by the probability that an immotile cell will experience an orientational interaction in a 1s period (equation 5-7), is plotted in fig. 5-41 over a range of typical motile cell concentrations, and likely radii of the interaction cross-section. For example at a motile cell concentration of 10^6 sperm/ml, for an interaction radius of 20μm, an immotile cell would experience an interaction

every ∿ 10s. In general, at experimental concentrations, there is little evidence of autocorrelation truncation (resulting from major interactions) over the usual autocorrelation timescale of 0 - 1s. The autocorrelation functions of fig. 4-12 may possibly show evidence of truncation due to interaction effects and there was evidence of such effects in the functions of fig. 5-37.

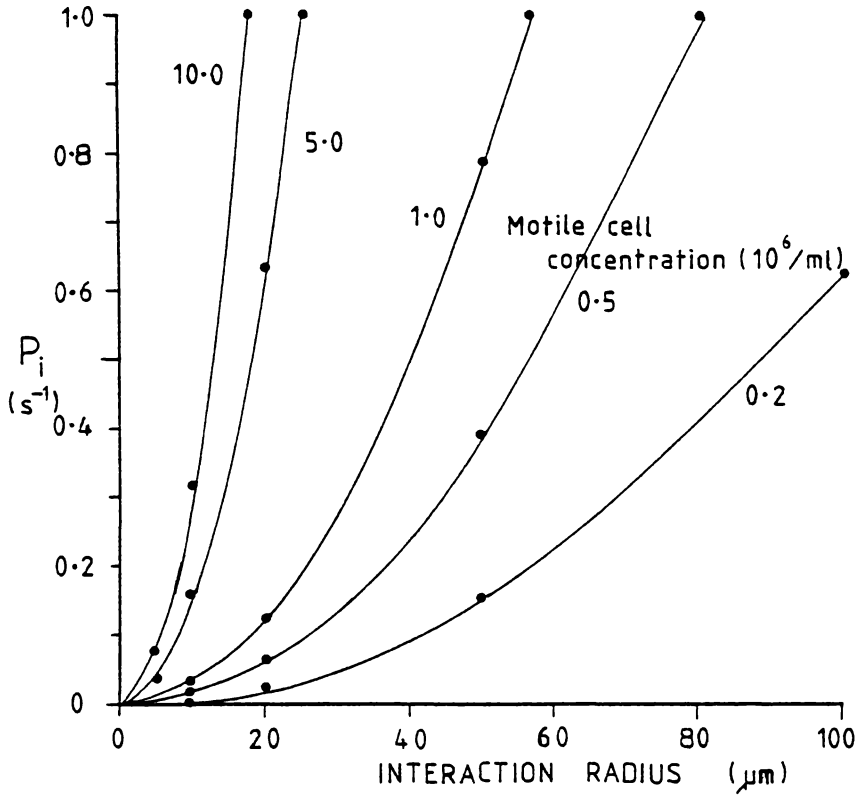

Fig. 5-41. Probability P_i that an immotile cell will experience an interaction with a passing motile cell for a typical range of local motile cell concentration and hydrodynamic interaction radius. A swimming speed of 100μm/s has been assumed.

The correlation functions of figs. 5-37 and 5-38 indicate a value of ∿ 30μm for the interaction radius when located on the above plot.

The orientation which the immotile cell undergoes while probably randomly distributed, is also of uncertain mean amplitude, although in order to generate the truncation effects or to influence the AAR, it need only be reoriented through an angle $\gamma > 2\ \alpha_m$.

For the purposes of the following computations, it will thus be assumed that the reorientations γ are randomly distributed over the angular range $0 < \gamma < \pi/2$.

In undergoing interactions, cells may be reoriented out of or into the visible range of tilt-angles, or may remain within the visible limits.

(iii) *Geotactic relaxation.*

Cells disturbed and reoriented away from the vertical head-down position, relax back to the vertical at an average rate in the range 0.0075 rad/s (from data of section 5.5.3) to $d\gamma/dt = 0.015 \sin\theta$ (Roberts, 1972; Katz and Pedrotti, 1977). A cell relaxing back from an angle of $\gamma = 40^\circ$ would, therefore, take $\sim$ 47s to reach the visible range again (i.e., $\Delta\gamma = 20^\circ$).

(iv) *Surface swimming.*

Accumulation of motile cells on the internal cell surfaces will result in a depletion of the motile cell concentration among the dead cells which are assumed to be more or less uniformly distributed throughout the bulk of the medium.

The exact extent of this depletion is uncertain although on the basis of Rothschild's data, factors of the order of $\alpha = 0.4$ (table 5-1) seem reasonable at high concentrations where;

$$\rho_m = \alpha \bar{\rho}_m$$

ρ_m being the localised concentration of motile cells at some point in the bulk of the medium and $\bar{\rho}_m$ the overall concentration of motile cells in the sample.

It seems likely that α should be a function of $\bar{\rho}_m$ and can reasonably be expected to be < 0.4 at the light scattering concentrations of interest but probably $\rightarrow 1$ at ejaculate concentrations. In addition, α may depend on the sample cell geometry, surface texture, cell dimensions (etc.).

Probably the surface density of swimming cells on the cell surfaces reaches an equilibrium situation where the flux of cells colliding inelastically with the surface equals the flux of cells redirected away from the surface due to motile-motile interactions.

A concentration dependence of α will clearly generate an AAR - concentration interaction and may well be one of the major factors which contributed to the data of figs. 4-9 and 4-19.

In the calculations which follow α will be considered a parameter independent of $\bar{\rho}_m$ so as to explore the concentration effects resulting from reorientational effects.

(v) *Calculations on the basis of the models.*

Consider the number of *immotile* spermatozoa N_v (per unit volume) oriented at visible tilt-angles (instantaneously any given cell may not be visible due to axial rotation).

The time dependence of N_v is given by;

$$\frac{d}{dt} N_v(t) = (N - N_v) P_g + (N - N_v) P_{in} - N_v P_{out} \qquad (5\text{-}9)$$

where N is the total concentration of immotile cells.

P_g is the probability of any given cell *orienting* back *into* the visible range of tilt-angles, per unit time, through geotaxis.

P_{in} is the total probability of an initially *invisible* cell experiencing an interaction and being *reoriented into* the visible region, per unit time.

P_{out} is similarly defined for *visible* cells which are *reoriented out of* the visible range.

The explicit expressions for these probabilities depend on the geometry of the visible range of orientations as previously illustrated in fig. 5-27. However, for purposes of a simple qualitative exploration

of the AAR - concentration effect the three-dimensional nature of the problem will not be considered.

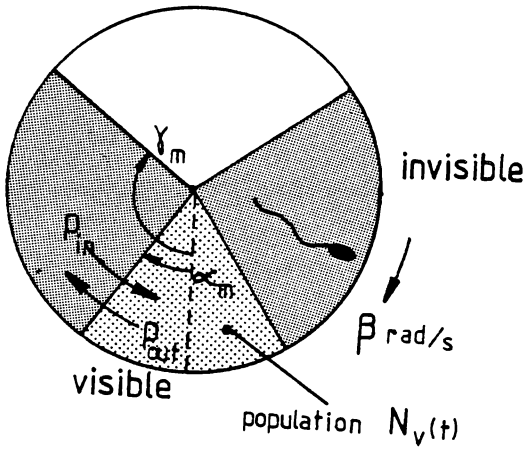

Fig. 5-42. Simple two dimensional model of optical orientational effects. The maximum visible tilt-angle is α_m, geotactic reorientation rate is β rad/s and the maximum angular reorientation is γ_m. Probabilities of relations 5-10 define the flux of cells into and out of the visible region (dotted).

In the simple two dimensional case of fig. 5-42, let us assume that when an immotile cell experiences an interaction (within its reorientational interaction radius), it undergoes a reorientation γ, the amplitude of which is randomly distributed (uniform probability distribution), over the range $o < \gamma < \gamma_m$.

The probability coefficients for relation (5-9) are then;

$$\begin{aligned} P_g &= \beta/(\gamma_m - \gamma_m) \\ P_{in} &= (\alpha_m/\gamma_m)\ P_i \\ P_{out} &\quad (\gamma_m - \alpha_m)\ P_i/\gamma_m \end{aligned} \qquad (5\text{-}10)$$

where P_i was the interaction probability previously defined by relation 5-8. In the steady state condition, $dN_v(t)/dt = 0$ and the distribution of the immotile population between the visible and invisible tilt-angle ranges reaches an equilibrium situation, depending strongly on the geotactic reorientation rate β, and the interaction probability P_i (equation 5-7) i.e.,

$$(N - N_v)\ \beta/(\gamma_m - \alpha_m) + (N - N_v)\ \alpha_m\ P_i/\gamma_m - N_v\ (\gamma_m - \alpha_m)\ P_i/\gamma_m = 0$$

which gives $N_v = N/(1 + I)$ (5-11)

where I, defined as the interaction factor and is given by

$$I = \frac{(\gamma_m - \alpha_m)^2 P_i}{\beta \gamma_m + \alpha_m P_i (\gamma_m - \alpha_m)} \quad (5\text{-}12)$$

looking at the limits of these expressions to check the validity of their functional form;

(a) $P_i \to 0$ (equation 5-8) $I \to 0$ $N_v = N$: no interactions.

(b) $\alpha_m = \gamma_m$ $I = 0$ $N_v = N$: no tilt-angle limitation of the fraction of immotile cells visible.

(c) $\beta \to \infty$ $I \to 0$: rapid geotaxis maintains immotile cell population in the visible range.

(d) $P_i \to \infty$, $\beta \to 0$ $I \to \left(\frac{\gamma_m}{\alpha_m}\right) - 1$ $N_v \to \left(\frac{\alpha_m}{\gamma_m}\right)$: rapid interactions, or zero geotactic relaxation result in a proportionate distribution of immotile cells between visible and invisible tilt-angles.

Incorporating results 5-11 and 5-12 into the expression for the AAR we obtain;

$$AAR = \frac{\rho_d/(1 + I)}{\rho_d/(2 + I) + 2 \rho'_\ell \alpha_m/\pi} \quad (5\text{-}13)$$

where ρ'_ℓ is the local concentration of motile cells within the scattering volume and depends on the wall swimming effect and the relative location and geometry of the scattering volume.

$$\rho'_\ell = (1 - W) \bar{\rho}_\ell \quad (5\text{-}14)$$

where W is the wall swimming factor, $\bar{\rho}_\ell$ is the mean concentration of

motile cells in the sample. The wall factor is probably a function of motile cell concentration, i.e., $W = W_{(\bar{\rho}_\ell)}$, although the exact form of the relationship is uncertain apart from its probable limits (from observations) for a scattering volume remote from the cell walls, i.e.,

$$W \to 1 \text{ for } \bar{\rho}_\ell \to 0 \text{ (or } < 10^5/\text{ml)}$$

$$\text{and } W \to 0 \text{ for } \bar{\rho}_\ell \to \rho$$

It is also very likely that the value of W depends on the sample cell geometry through its linear dimensions and ratio of internal surface area to volume. A scattering volume located close to a surface would effectively correspond to a negative value for W.

Fig. 5-43 shows the relationship between the AAR and total sperm concentration calculated from equation 5-13, for the typical or estimated values of the parameters as given in table 5-3.

Hydrodynamic interaction radius	r_i	= 20μm
Maximum angular reorientation	γ_m	= π/2 rad
Mean geotactic reorientation rate (from $\gamma_m = \pi/2$)	β	= 0.015 rad/s
Maximum visible tilt-angle for immotile cells	α_m	= 0.174 rad
Maximum visible tilt-angle for motile cells	α_ℓ	= 0.348 rad
Mean swimming speed	$\bar{v}$	= 100μm/s
Wall factor	W	= 0.6

Table 5-3. Parameters of the model used in calculations.

The set of curves calculated on the basis of this model (fig. 5-43) clearly resembles the set of experimental curves obtained in the earliest AAR - concentration studies of fig. 4-10. While the simple model employed here does not specify the relationships of the system in quantitative

detail, the phenomenological basis for the model, which has been the subject of much of chapter 5, would appear to confer some degree of qualitative validity.

The parameters used to calculate these curves are all reasonably realistic and are based on experimental data or estimated from observations.

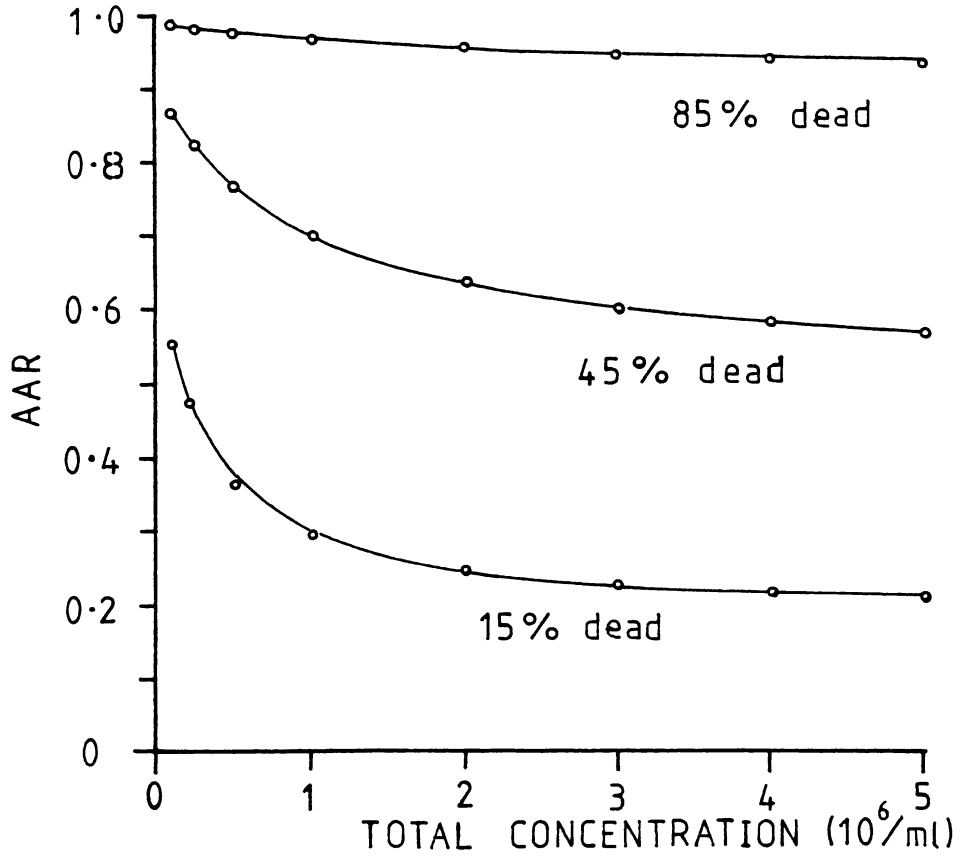

Fig. 5-43. AAR values computed for the model defined by relations 5-12, 5-13 for the parameters of table 5-3, over a typical experimental range of sperm concentration levels (motile + immotile cells). Compare with the early data of fig. 4-10.

The results of fig. 4-10 and fig. 4-19 can certainly be understood on the basis of this interaction model. The optical and dynamic properties of real samples of spermatozoa in real light scattering cells, are considerably more complex than this simple treatment. Nevertheless,

the essential features of the system behaviour appear to be well expressed even in semi-quantitative terms by this two-dimensional model.

AAR - concentration relationships (apart from any immobilisation occurring on dilution) may be understood on the basis of perturbative reorientations of immotile cells to attitudes outside the visible range of tilt-angles. However, a further factor which may also contribute, is the probable concentration dependence of the wall swimming factor (W). In the preceding calculation, the value of W = 0.6 derived from Rothschild's data was employed and was maintained constant over the concentration range. If, as seems probable, the wall swimming phenomenon becomes less pronounced with increasing motile cell concentration, the curves of fig. 5-43 may well more closely approach the form of fig. 4-10. Neither the relationship between the ACF decay constant and the concentration of motile cells (figs. 4-20 and 5-37) nor the scattering angle scaling properties of the decay constant, have been included in the model. These effects probably also result from motile/immotile interactions but with rather different mechanisms being involved. In particular, the collective effect of creeping flow or medium displacements induced by the motile fraction, can be expected to induce very small axial disturbances of visible immotile cells with associated fluctuations in their scattered intensity at the photodetector. These fluctuations clearly arise from the sharply peaked scattering lobe of the spermatozoon head.

Such an interaction mechanism requires definition of the amplitude and range of disturbances induced by motile cells before a useful model can be defined.

5.13 Implications of phenomena within sperm suspensions for sample cell design and scattering geometry.

The previous section discussed the results and phenomenology described in chapter 5 in terms of an optical-dynamical model of

spermatozoa suspensions when used for laser light scattering experiments. It is now appropriate to examine the implications of this phenomenology for the design of the light scattering system, with a view to capitalising on the observed effects.

5.13.1 Surface swimming and sedimentation effects.

The migration of motile cells to the internal surfaces of the light scattering sample chamber, has been found to result in an accumulation of spermatozoa on these surfaces through inelastic collisions. As a result, the observed motile population of the scattering volume may become time dependent although the AAR and variations which it shows may depend on the specific location of the scattering volume within the illuminated region of the sample. Depletion effects could be expected to be most apparent in the mid-region of the sample, using,for example, a horizontal plane type B-1 or type B-2 sample cell.

This effect is illustrated in the data of fig. 5-44 which shows the time dependence of AAR values at various strategic locations within a type B-2 sample cell (*experimental methods as per previous studies but sequentially shifting the scattering volume between the floor, mid-region and roof of the cell*). These AAR levels show lower initial values at the surface sites, consistent with localised surface swimming effects and a rapid depletion of the centrally located scattering volume. A progressive rise in AAR at the bottom of the cell is symptomatic of a sedimentary accumulation of immotile cells. Further interpretation of these trends, particularly in the $t \cong$ 30 min region, is not straight-forward due to a very much diminished signal level (fig. 4-27 for example).

However, the data does provide evidence showing the significance of surface swimming effects to the interpretation of light scattering data, the AAR in particular and the design of the sample chamber.

For this reason, a simple but subtle variation of sample cell geometry

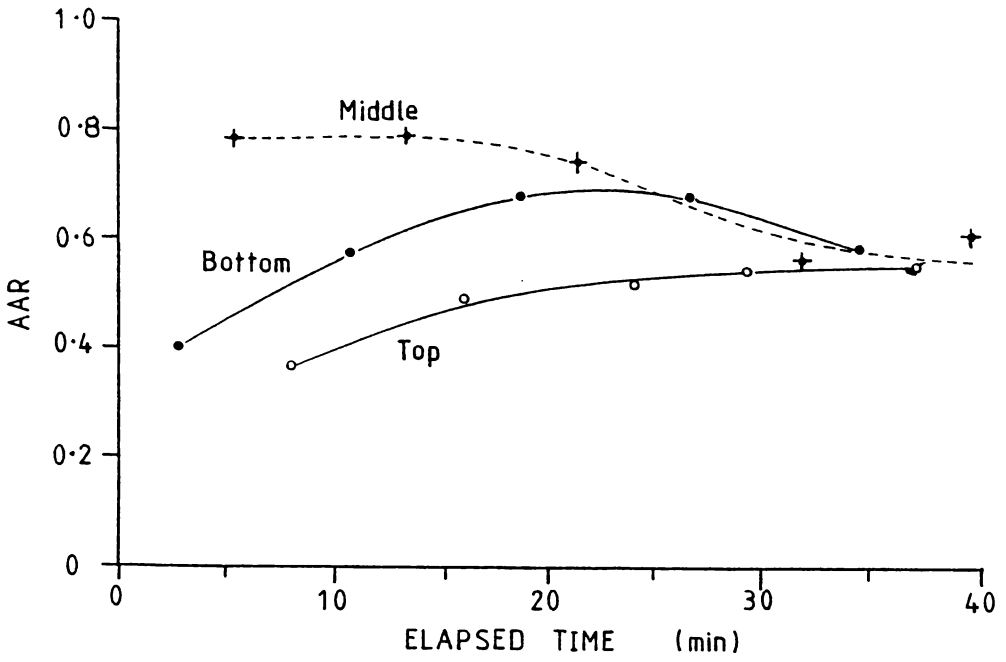

Fig. 5-44. AAR levels and trends at the bottom, mid-region and roof of a horizontal plane type B-2 sample cell (sample concentration 2 x 10^6 sperm/ml in 0.01% CEY).

was devised, which utilised vertical plane window surfaces and a short path-length, the so-called type C cell (refer section 3.17.3). The concept of this geometry was that of creating a scattering volume comprising a sandwich of surface swimming motile cells with dead cells randomly distributed in-between as is illustrated here in fig. 5-45. Using such a system, the phototube aperture was of sufficient diameter to collect light from all illuminated regions within this sandwich. Consequently, it was necessary to use a short beam pathlength through the cell (typically 1mm) so that the projected image of the illuminated region within the sample, at the detector screen (fig. 3-9), was of small linear dimensions and could be completely encompassed (fig. 3-16) by a suitably sized phototube aperture (typically 800μm diameter). Further, the depth of

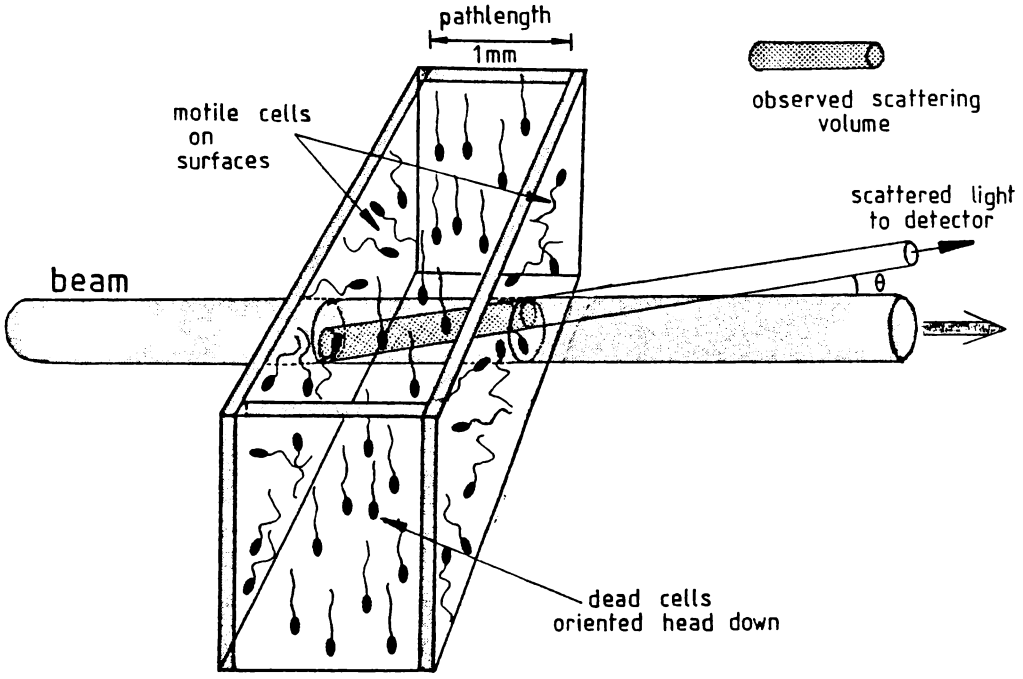

Fig. 5-45. Geometry of the vertical plane short-pathlength sample cell. The detector, using a small lens aperture and a large (800μm) phototube aperture collects light from surface swimming motile cells on both front and back windows of the cell and from the suspension of immotile cells sedimenting head-down in between.

focus of the detection system was required to be at least equal to the beam pathlength through the sample and for this reason a small lens aperture(fig. 3-9)was employed (typically 1mm, as had been normal practice). The use of a relatively large phototube aperture also depended on the realisation that coherence was not primarily involved in the formation of the detected signal (see section 5.6). Since such aperture sizes were considerably in excess of the coherence area at the phototube, the signal/noise ratio of a detected *optical beat-spectrum* would have been considerably degraded.

Further, the spatial distribution and hence the relative numbers of motile and immotile cells in the scattering volume, could be expected to differ for the two cell geometries (horizontal plane B - type and vertical plane C - type), and different AAR values were expected.

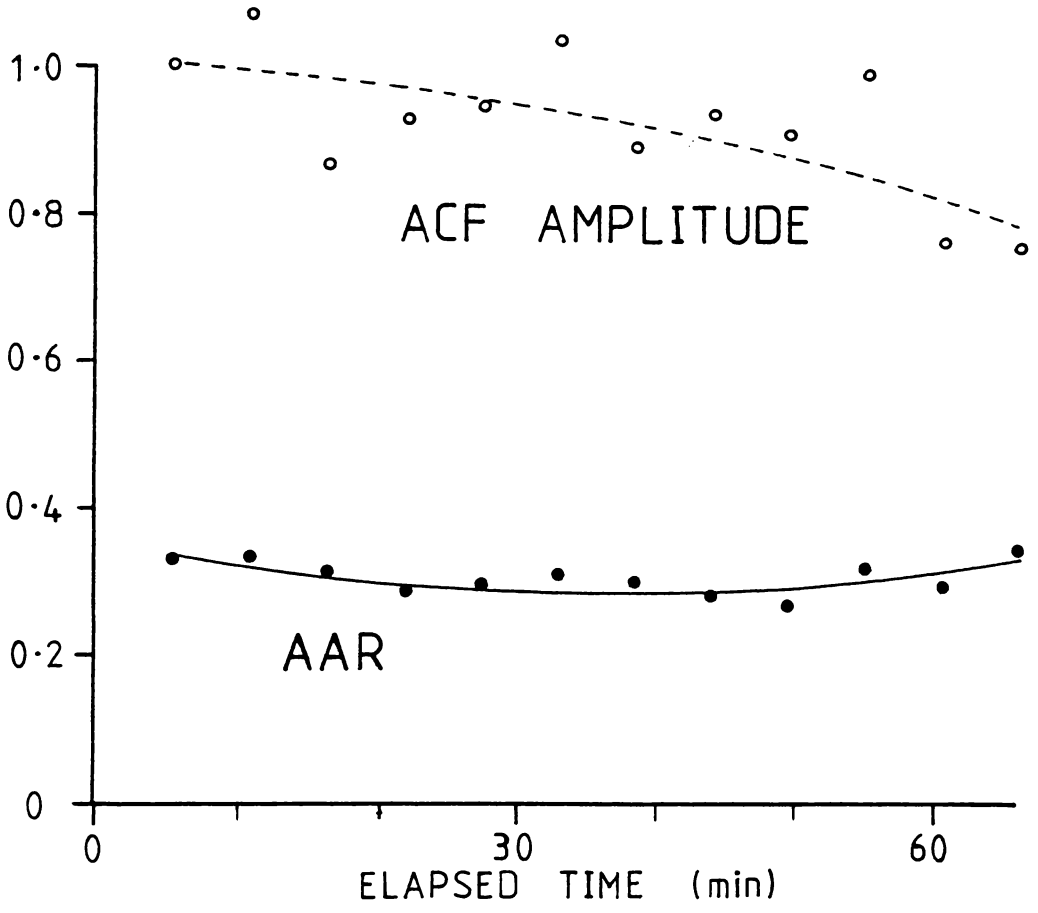

Fig. 5-46. Time dependence of the AAR and ACF amplitude for a sample of concentration 5 x 10^6 sperm/ml in a vertical plane type C sample cell having a path-length of 1mm.

Results such as that given here in fig. 5-46, confirmed that both the AAR and the signal amplitude showed a reduced time-dependence in the type C cell design, presumably due to a reduced sensitivity to wall swimming and sedimentation effects. The trends of fig. 5-46 might be referred back to those previously evident in fig. 4-27 using a horizontal

plane type B cell with a 1cm path-length.

In general, lower AAR values were obtained with type C cells than with type B cells. For example, AAR values of 0.60 and 0.20 for type B and type C cells, respectively, were obtained in one comparative experiment.

The greater vertical depth of a type C cell (typically 10mm), together with a centrally located scattering volume, would appear to give less variability in AAR values which may fluctuate due to sedimentation effects in shallow cells.

5.13.2 Optical geometry

The questionable contribution of optical coherence to the detected signal suggested that other scattering geometries may be profitably considered. The conventional LBS scattering geometry employed a small aperture detector aligned at a small forward scattering angle ($\sim 10^{\circ}$) in the horizontal scattering plane. The detector hence sampled the scattered field at a point. The sharp lobular structure of the scattered field resulted in strong orientational effects wherein the scattering lobe was only seen by the detector for cells swimming close to the normal to the scattering plane (within the angular limits defined by the scattering lobe).

In view of the apparent intensity fluctuation origin of the fast autocorrelation component which was probably also the case for the slow ACF component, a scattering geometry was examined wherein (using a type C sample cell), *the detector was able to receive intensity fluctuations from surface swimming spermatozoa regardless of the direction of translation and from immotile cells regardless of their attitude during geotactic or interactive orientations.*

The geometry considered was that of a semi-annular aperture placed in front of the photodetector lens with the axis of the detector aligned

to be colinear with the laser beam, the system is illustrated diagrammatically here in fig. 5-47.

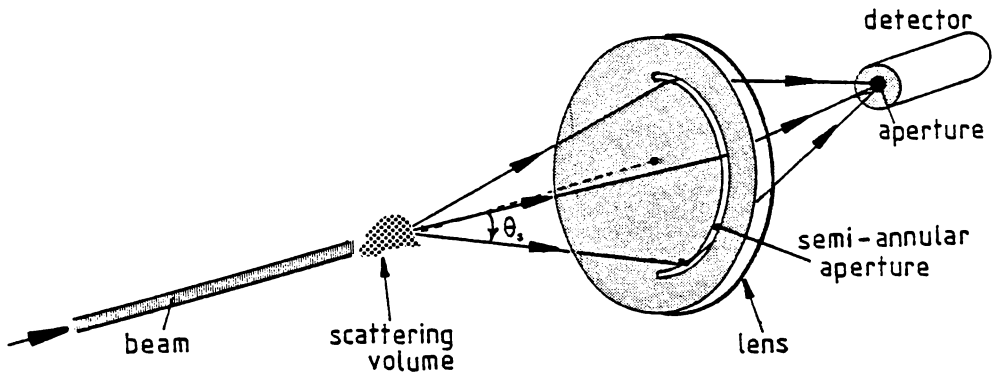

Fig. 5-47. Detector geometry using a semi-annular aperture to reduce orientational effects.

The detector system, therefore, collects light around the length of the semi-annular aperture which was of narrow width ($\sim$ 1mm) and all points on which were located at the same forward scattering angle of 8° with respect to the incident beam.

This system was a variation of conventional LBS optical geometry which was suggested by the phenomenology of chapter 5, although at the time of writing it is still very much an exploratory development. For this reason, comprehensive and detailed results using the semi-annular detector system are not presented. A set of preliminary data are given in the following figures and these illustrate the general behaviour of the system, although a detailed interpretation is not yet available. In some respects, the system gave the results which might be expected of it, in that the detector system was found to generate individual flash trains of longer duration since cells rotating or changing direction in traversing the observed scattering volume were effectively tracked as the equational scattering plane of the swimming cell moved around the

annular orifice. For this reason, autocorrelation functions showed a much more pronounced periodicity (∿ 10Hz) than did previous functions obtained with a point aperture.

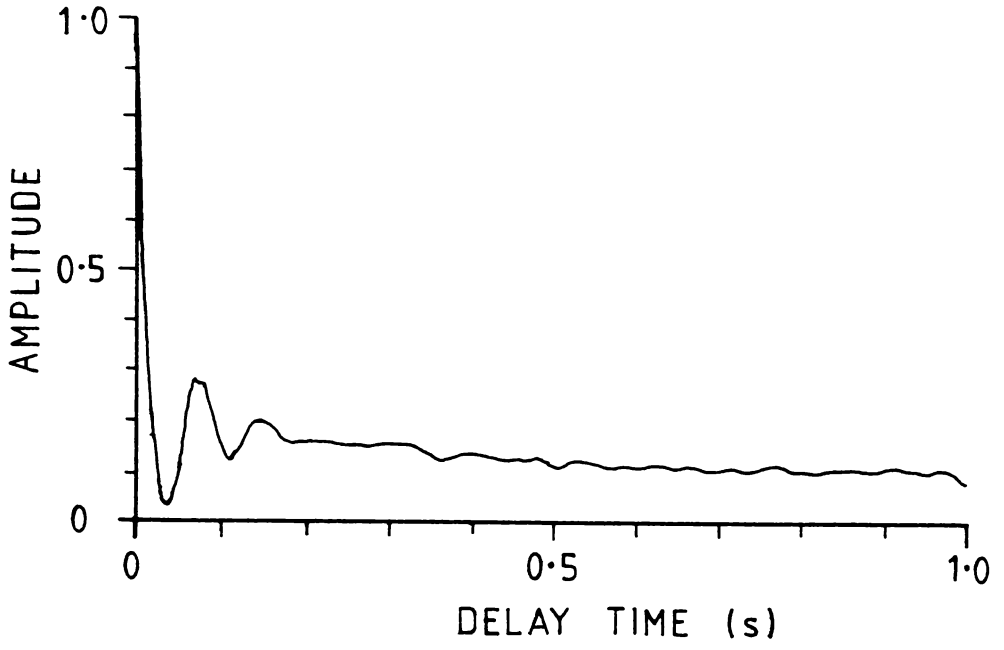

Fig. 5-48. The strongly periodic autocorrelation function for a highly motile sample (6% dead) of spermatozoa, using a semi-annular detector aperture. The period of the oscillatory feature is ∿ 75mS. (The slow exponential feature has been removed after RLQF fitting) ($\rho = 5 \times 10^6$ sperm/ml).

The flash peak trains, as previously seen in fig. 5-20 (for a point detector aperture), were less susceptible to amplitude changes resulting from changes in the swimming trajectory or off-axial head rotations, both of which tend to broaden the distribution of flash periods. This is illustrated in the residual autocorrelation function of fig. 5-48, from a highly motile sample of 94% motile cells, after fitting and removal of the slow ACF exponential. This sample comprised one of a sequence having various levels of percent motile cells, the power spectra for which are shown in fig. 5-49.

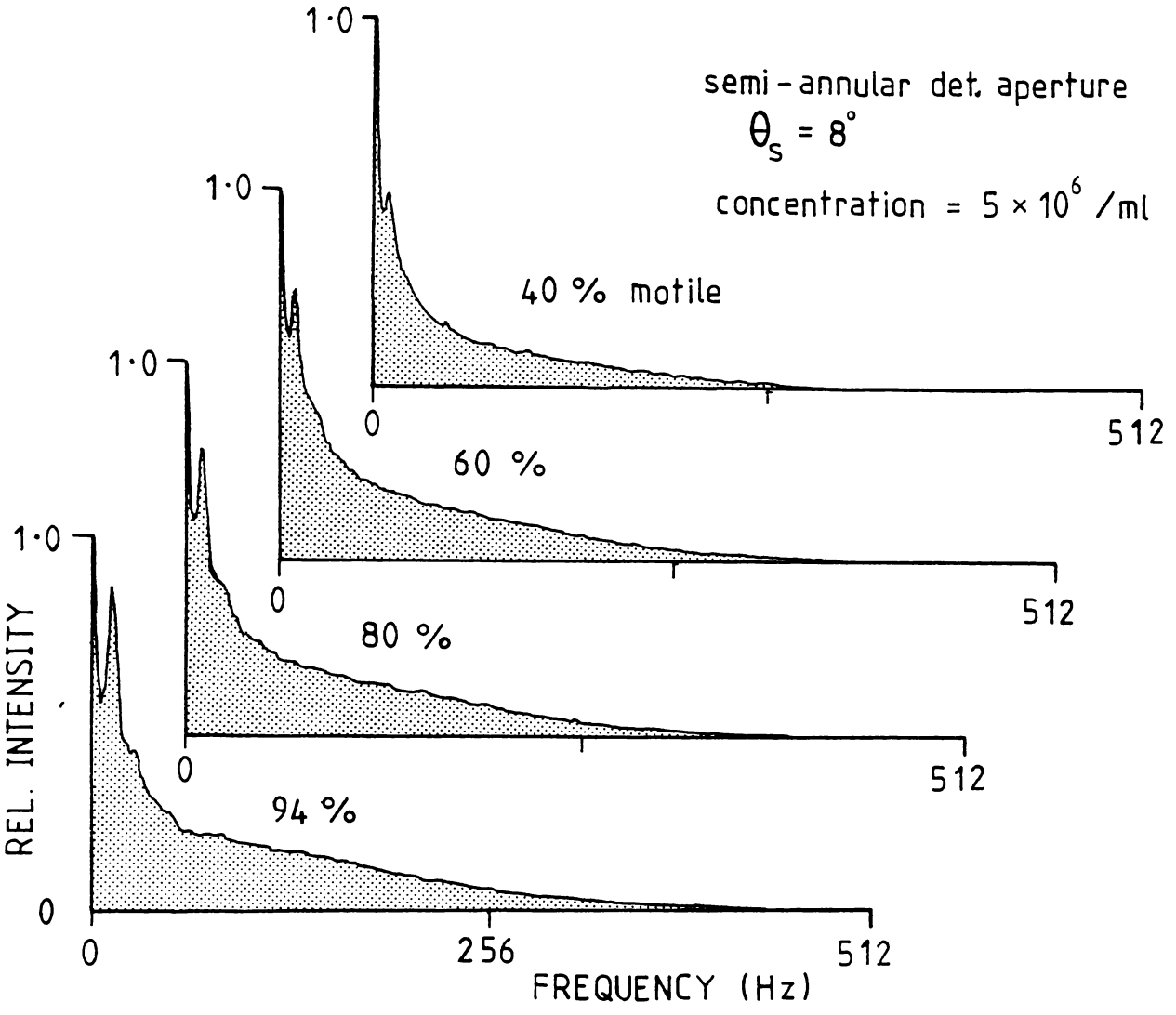

Fig. 5-49. Power spectra at various levels of percent immotile cells using a semi-annular detector aperture. Scattering angle 8°, concentration 5 x 10^6 sperm/ml. Signal sampling time, 113s/spectrum. Phototube aperture diameter was 800μm.

These power spectra show an increasing prominence of the motile cell flash peak, as the percentage of motile cells was increased. The high frequency tail of the spectrum is attributable to the randomly phased super-position of intensity peaks and the low frequency peak in the region $\lesssim$ 6Hz arises from the low frequency intensity fluctuations generated by the immotile cells.

A characterisation of these changes as a function of percent motile cells, is shown in fig. 5-50 where the ratio of areas under the spectra

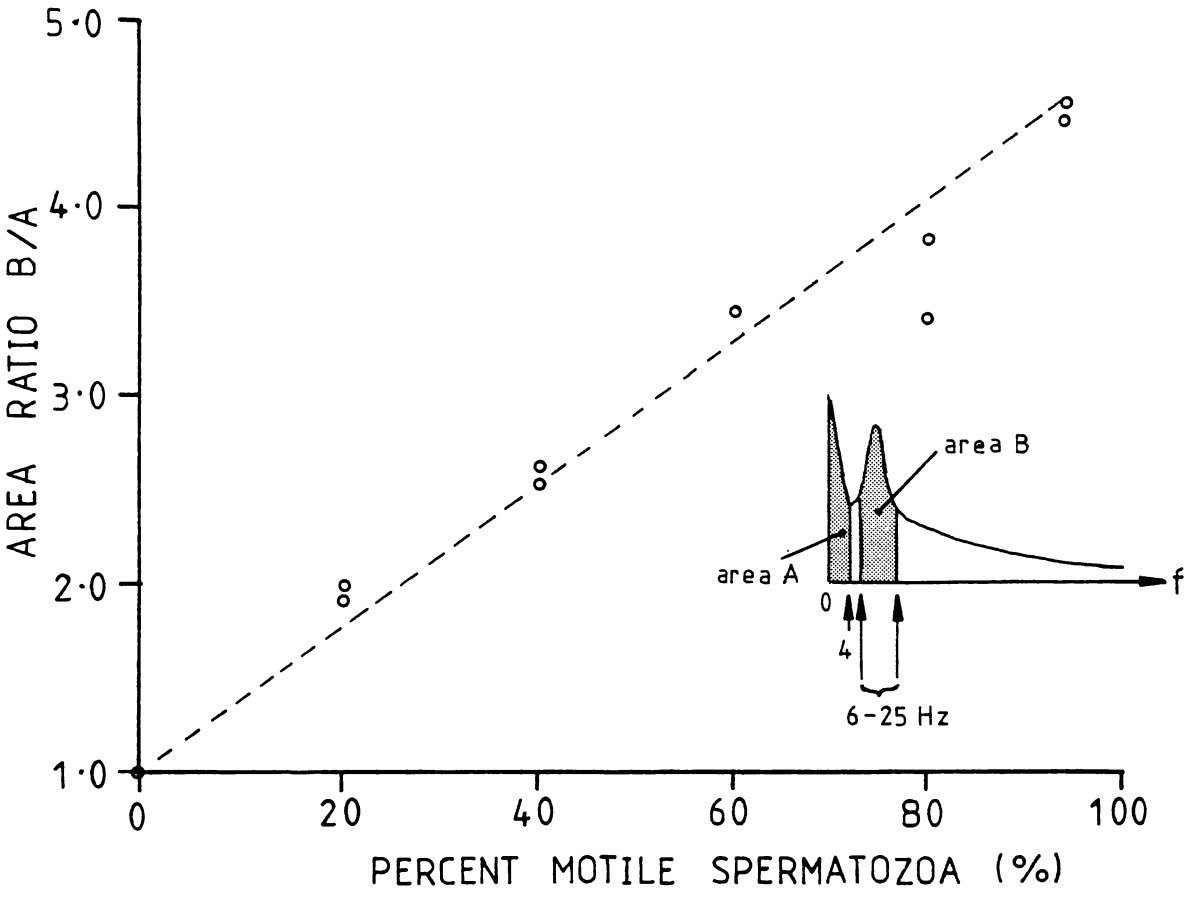

Fig. 5-50. A simple characterisation of the changes evident in the power spectra of fig. 5-49 as the percent immotile spermatozoa was varied.

over the frequency ranges 0 - 4Hz and 6 - 25Hz (expressed relative to the ratio at 100% dead cells) has been plotted against percent motile spermatozoa. The strong flash peak evident in the 94% motile sample was associated with the oscillatory autocorrelation function of fig. 5-48, both being generated by parallel time and frequency domain processing of the same sample.

The optical orientation effects, which have been shown to be associated with the AAR - concentration interaction, were not expected with the semi-annular detector aperture which is able to *track* orienting immotile cells. Autocorrelation functions of fig. 5-50, taken at two total sperm concentrations (1 x 10^6/ml and 4 x 10^6/ml), show no significant

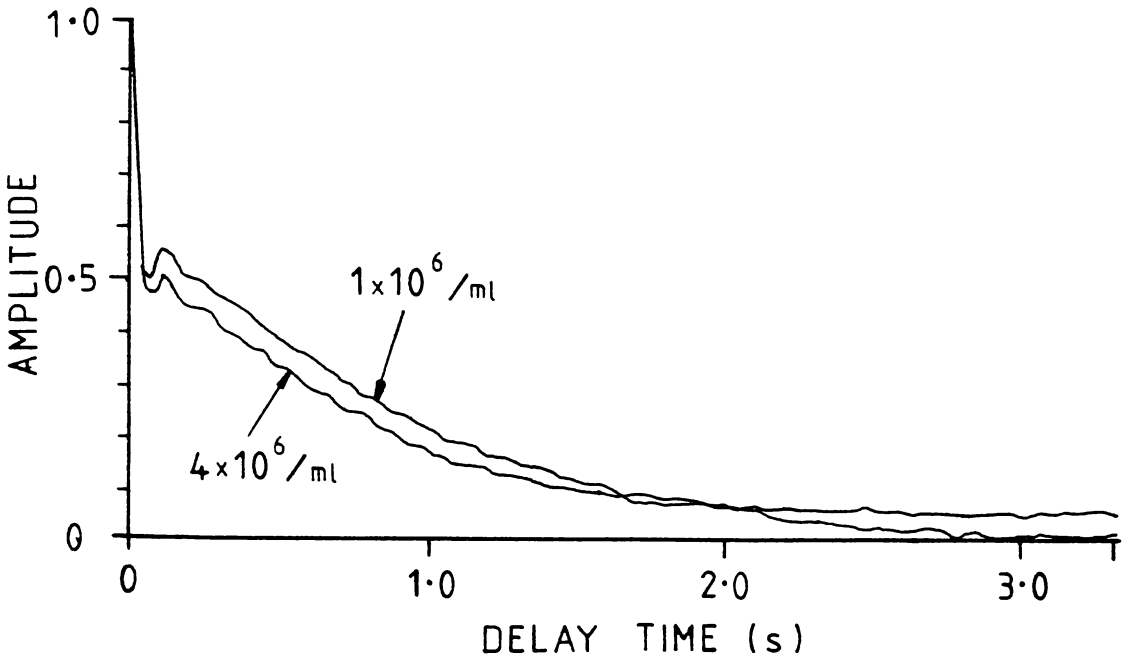

Fig. 5-51. A preliminary study of the concentration dependence of the AAR using a semi-annular detector aperture. These functions in terms of both AAR and decay time might be compared with the results of section 5.11.3 (scattering angle 8°).

evidence of either AAR or decay constant differences between the two concentration levels. This gives an interesting contrast with the corresponding functions in fig. 4-12 and the results of 5.11 at the same concentrations.

However, while such variations in optical geometry look promising, they are currently still of an exploratory nature.

SUMMARY AND CONCLUSIONS

A sequence of experimental studies has been described which progressively revealed a complex optical and dynamical phenomenology within suspensions of bull spermatozoa when used for LBS experiments. The results indicated that previously published interpretations at laser light scattering data in terms of the dynamics of bull sperm suspensions had been simplistic and that the agreements obtained with swimming speed values and distributions were largely fortuitous.

In the case of bull spermatozoa, ram spermatozoa, which has a similar conformation, and possibly even human spermatozoa, the distribution of the scattered intensity is grossly asymmetric. At experimentally accessible forward scattering angles the field intensity is dominated by the light scattered from the sperm head and shows large fluctuations as the head rotates. These fluctuations are of such magnitude that the detected photocurrent at typical scattering angles in the field is completely dominated by the fluctuating intensity (fig. 5-20) and any Doppler-beat component would appear to be undetectable.

The existence of a significant Doppler-beat component in the low frequency signal generated by immotile cells, is still a possibility. However, the autocorrelation functions generated by incoherent light (section 5.6.3), bear a remarkable similarity of form and timescale to those obtained using a coherent light source and strongly suggest that intensity fluctuations form at least a major component of the low frequency signal. With the doubtful rôle of coherence, expedient variations of the geometry became possible in efforts to circumvent some of the undesirable characteristics arising from the optical phenomena and the annular detector-aperture was therefore devised.

The important result arising out of this research programme was the model of optical and dynamic effects within the sperm suspension. The principal phenomena which determine the characteristics of the scattered light field for bull spermatozoa are:

(i) *a sharply peaked scattering lobe generated by the head of the spermatozoa.*

(ii) *geotaxis and sedimentation of immotile cells.*

(iii) *the tendency of motile cells to swim on surfaces.*

(iv) *interactions between motile and immotile cells.*

These four phenomena were presented as a simple model in section 5.12 which proved capable of predicting the form of the AAR - concentration interaction which had resulted from the first experiment of chapter 4. It is accepted that this model is highly simplified and that there is certain to be a contribution from other phenomena such as surface swimming and possibly a real immobilisation on dilution. The important point is that it provides a more realistic model on which to base the interpretation of the light scattering measurements.

The interpretation of other experimental results, largely those of chapter 4, on the basis of this model is summarised in table 5-4.

The only result which is not easily understood on this basis is the k^2t scaling of the slow autocorrelation component with scattering angle, shown in figs. 4-26 and 4-27. Interpretation of this result, which supports a Doppler-based Brownian motion model must await further calculations, those of the angle dependence of the scattering lobe width.

There appears to be little hope of achieving the desirable point-scatter behaviour for bull spermatozoa. Long wavelengths such as the 10.6μm line from the CO_2 laser would be more appropriate in dimensional terms but probably experimentally impractical for liquid suspensions. However, the characteristics of the existing geometry and dimensional/wavelength features are probably capable of further exploitation and in the present form are certainly capable of giving useful analytical results.

The work has dealt largely with bull spermatozoa. Clearly the

Table 5-4. Brief interpretation of the experimental results of chapter 4 in terms of the model described in section 5.12.

GENERAL TABULATION SHOWING PHENOMENOLOGICAL

INTERPRETATION OF INITIAL RESULTS

Section or data ref.	Results Obtained	Brief Interpretation in terms of phenomenological Model.	Reference Sections
1. 4.2/4.3/4.8 figs. 4-11, 4-12.	AAR decreased with increasing total sperm concentration.	1. Motile-immotile interactions reorient dead cells outside range of visible tilt-angles increased frequency with conc. cells. 2. Concentration dependence of fraction of surface swimming motile spermatozoa.	5.12 2.8 5.2
2. 4.3/fig. 4-20.	Increase in slow ACF decay constant with increased conc. of motile spermatozoa.	Long range interactions or general hydrodynamic disturbances of the medium created by motile cells, enhance random Brownian perturbations of dead cells. Sharp scattered intensity lobe generates associated intensity fluctuations.	5.9 fig. 5-25. 5.6.3
3. 4.5 fig. 4-14.	AAR $\sim$ independence of scattering volume population over wide range.	Intensity fluctuations due to scattering volume population changes not an added amplitude component in Doppler spectrum since signal primarily arises from intensity fluctuations induced by the moving scattering lobes.	figs. 5-8/12 5.6
4. 4.6.	Conc. dependence of AAR vanished at sample temperature 28.4°c.	A decreased concentration of motile cells and lower swimming speeds decrease the interaction probability to low level.	5.12 and fig. 5-37.
5. 4.7, fig. 4-17.	AAR rises with decreasing sample temperature.	Few cells motile and decreased interactions.	5.12
6. Fig. 4-17.	Increase in slow ACF decay constant with increasing temperature.	Increase in concentration of motile cells with increasing temperature giving a higher level of medium disturbance and enhancing random motion of dead cells.	5.9
7. Figs. 4-23/24.	Decrease in AAR with increasing scattering angle.	At larger angles an increasing contribution to the scattered field from the flagella and possibly any protein components of the medium. May be an increased contribution from dead cells as visible tilt-angle range increases at low angles and a greater proportion of the dead population (perturbed cells) becomes visible.	fig. 5-24. table 4-5 5.12
8. Table 4-2.	Amplitude of slow ACF component α percent dead cells but ACF component from motile cells of much smaller amplitude than that for same conc. of dead cells.	Fraction of motile cells visible to the detector system much smaller than for immotile cells most of which, depending on specific gravity of medium, orient into the visible range of tilt-angles.	fig. 5-18. fig. 5-17. 5.4
9. Figs.4-28/30/31.	Time dependence of AAR and ACF amplitude.	Geotactic orientation of dead cells into visible tilt-angle range. Sedimentation of cells over extended periods. Migration of cells to internal surfaces of chamber.	5.2 fig. 5-18. fig. 5-19.
10. Figs. 5-1/2.	Detector alignment in vertical or horizontal plane gives significant differences for translating cells but not for non-translating active cells.	Optical-geotactic effects interact. Horizontal aligned detector sees motile and immotile cells. Immotile cells vertical aligned and hence visible. Vertical aligned detector sees only motile cells. Irregularly waving live cells appear the same to both detector alignments.	fig. 5-18. 5.12.

optical-dynamical model for small spherical headed spermatozoa is likely to be quite different (section 5.8). Optically, starfish spermatozoa appeared to give a constant light scattering cross-section, although the surface swimming characteristic still appeared to be present. The extrapolation of the methods to other spermatozoa of interest is uncertain and the interpretation of light scattering data will be dependent on the individual geometry and swimming behaviour of the various species of cells. Human sperm, which has been studied in the light scattering literature, has a rather more symmetric conformation and is of smaller dimensions than bull spermatozoa. In view of the results presented here, a close re-examination of the scattered field from the human spermatozoon head is certainly called for.

In the case of ram spermatozoa, conformation and dimensions are similar to those for bull sperm and similar results can be expected. Experiments, not reported here, show that samples of ram sperm give autocorrelation functions very similar to those for bull sperm, but on a shorter timescale due to higher translational speeds and rotation rates. Further, studies showed a similar concentration - AAR interaction and trends in ACF decay constants to those described in section 4.3 and 4.8.

For swimming and rotating bull spermatozoa the coherence of the incident light appears to be unimportant, the intrinsic brightness and collimation of the laser beam being its most significant attributes. Ironically, under these circumstances, the system does not operate within the realm of *light beating spectroscopy* but is largely a variation of the photoelectric method first described by Bosselaar and Spronk (1952) then later by Rikmenspoel and van Herpen (1957). Their techniques of $\sim$ 20 years before,detected the intensity fluctuations as microscopically projected images of swimming cells, traversed a photo-tube aperture in a screen, (see fig. 3-4 and 3-5) using dark-field illumination. In fact, the intensity peaks of fig. 3-6 (Rikmenspoel and van Herpen, 1957) bear

a striking resemblance to those obtained with the laser light scattering geometry and illustrated in fig. 5-20. The intensity peaks from the laser system would appear to be somewhat sharper and longer pulse trains may be obtained due to the larger effective scattering volume (and hence time over which the detector tracks a spermatozoon) and the better collimation of the incident beam which gives a sharper reflective peak. In the photoelectric apparatus (of both Bosselaar and Spronk, and Rikmenspoel and van Herpen), the illuminating beam (the dark-field optics of a microscope; fig. 3-5) comprised an annular sheet of light focussed to a small scattering volume within the sample. The light scattered into a small solid angle colinear with the axis of the system was then focussed onto the detector. The effective scattering angle was then the semi-angle of the illuminating conical sheet but had an associated uncertainty due to the effective annular aperture of the light source and the aperture of the detector lens. Nevertheless, even with a spread in the effective scattering angle, well defined intensity peaks were obtained and the measurement of the interval between these, gave the head rotation rate.

We might well ask, what exactly does the laser scattering system achieve in comparison with this early photoelectric apparatus? It had initially been expected that Doppler-beat spectra would give direct velocity measurements and estimates of percent normal swimmers. Such is clearly not the case, the high frequency photodetector output signal being a superposition of intensity peaks (fig. 5-20) rather than of Doppler origin. Those features of the laser system which differ from the early photoelectric apparatus may be listed as:

(i) *The laser system shows a smaller spread in effective scattering angles* and this may be responsible for the sharper intensity peaks (fig. 5-20) and the dot-like photographic images (figs. 5-8/12) generated by the laser geometry.

A sperm head following a slightly helical trajectory could be expected to scatter light to the detector or photographic film over a longer segment of its trajectory when illuminated by an annular dark-field microscopic source. This probably accounts for the smeared images left on time exposures (e.g., fig. 5-6) which, even in the best examples obtained by Rothschild, were described as 'duck-footed'.

(ii) *In the laser geometry, the detector collects light at a single point in the scattered field.* Similarly, the time exposure photomicrographs of figs. 5-8 through 5-12, represent images at a point in the scattered field. Since the angular width of the scattered intensity lobe is rather small ($\sim 18^{\circ}$), it does not traverse the detector aperture unless the spermatozoon is swimming within $\sim 20^{\circ}$ of the normal to the plane defined by the detector and the incident beam. The conventional laser scattering geometry does not, therefore, see all motile cells, only an estimated 20% of them. On the other hand, the dark-field photo-electric (DFPE) apparatus collects light from cells swimming in all directions due to its annular light source and axial symmetry.

(iii) The phototube aperture used in the DFPE apparatus by Rikmenspoel and van Herpen (1957) was said to be about the dimensions of the projected image of a sperm head, hence the short double-intensity peak recording of fig. 3-6(a). *This effectively corresponds to a scattering volume of very small dimensions, whereas the laser light scattering geometry has generally utilised relatively large scattering volumes* with populations of the order of hundreds of spermatozoa. The DFPE apparatus has in contrast, been used to analyse single spermatozoon transits of the observed scattering volume. The laser scattering system has subsequently proved capable of operating in this regime (Hawley and Woolford; unpublished, refer appendix IV and also fig. 5-20) and generating similar absolute measurements of head rotation rate and scattering volume transit times. However, the laser system used with

autocorrelation or spectral analysis of the detected signal, can produce information on the collective dynamics of large populations. In this case the characteristic width of the fast ACF component or the extent of the high frequency region of the spectrum is determined by the mean transit time of rotating scattering lobes across the solid angle projected by the detector.

(iv) *The DFPE system, due to its event oriented nature, is not appropriate for obtaining information from the immotile fraction of the sperm suspension.* In contrast the laser scattering system yields substantial information on the concentration of immotile cells and the interactions of motile cells with them. The decay time of the slow ACF component is closely related to the concentration of motile spermatozoa and the perturbations that they induce of immotile cells.

The AAR measurement with the laser system gives an empirical measure of the ratio of motile to immotile spermatozoa.

(v) The collection of data from individual spermatozoon transits of the scattering volume gives more detailed information but involves an extended experimental time-scale for the collection of statistical distributions with both the DFPE and the laser scattering systems (Hawley, 1980). *Using the laser system, the use of larger scattering volumes allows processing of the resultant intensity fluctuations from a population of hundreds of spermatozoa. The motility of the population may therefore be characterised over a timescale of minutes* (typically 5-10 min.), also allowing greater flexibility in the selection of sample concentrations.

These five points compare the laser light scattering approach to motility assessment with the most successful *conventional method*. The DFPE method can be considered the most successful technique developed over the past thirty years on the basis of its contribution of absolute

measurements of rotation rates, swimming speeds and motile cell concentrations (Rikmenspoel, 1960; Van Duijn, 1962). It has not found any significant general application as a routine method, but technically it appears to have given a reasonable compromise between convenience, objectivity and useful kinetic parameters.

The laser light scattering approach has been demonstrated in this thesis to be closely related to the DFPE method, and the semi-annular detector system of fig. 5-47 is essentially the geometrical inverse of the DFPE geometry. However, the laser scattering system does appear to have significant advantages and has the promise of being a more flexible measurement system, more readily adapted to routine use. Already the method has been employed in a large scale field application and has shown extremely promising results as a predictor of fertility between bulls (appendix V). The important feature of this preliminary application, and one responsible for its promising result, has been the recognition through the studies described in this thesis, of the experimental variables procedures and interpretations which must be considered when the technique is used as a motile assay.

Progressing from an initial concept of the laser scattering system as being Doppler-based, a complex phenomenology arising from scattered intensity fluctuations has been defined. The early results of chapter 4 were generally seen as inconsistent with the contemporary point-source at low scattering-angles model accepted in the literature. While the final model of section 5.12 might, in retrospect, have been anticipated from traditional and historical results, it is a reality of experimentation that the optimum course of events in a field of research is not often achieved. In this case, the key results were revealed, not by sophisticated experimental techniques and data analyses, but by simple visual observation, which throughout history has been the keystone of science and our most important contact with the wonders of nature.

APPENDIX I

The formulation and preparation of the buffer and egg-yolk based 'Caprogen' extender used throughout the experiments of chapters 4 and 5.

In addition to this preparation procedure both the buffer and the egg-yolk extender were cleared and filtered prior to use for light scattering experiments.

THE NEW ZEALAND DAIRY BOARD ARTIFICIAL BREEDING SERVICE

PREPARATION OF "CAPROGEN" EXTENDER FOR THE DILUTION AND STORAGE OF BOVINE SEMEN AT AMBIENT TEMPERATURE.

SECTION 1 - BUFFER SOLUTION

Chemical	Quantity Per Litre	Grade
Tri-Sodium Citrate	20.0 gms	B.D.H. Analar
Glycine (Aminoacetic Acid)	10.0 gms	B.D.H. Analar
D-Glucose (Dextrose)	3.0 gms	B.D.H. Analar

Weigh chemicals into sterile graduated cylinder (Pyrex 1,000 ml). Add 250 ml boiling glass-distilled water and shake to dissolve chemicals. Immediately add cold distilled water (previously stored in refrigerator) to ensure rapid cooling and bring volume to approximately 960 ml.

The following should now be added to the cool solution:-

	Quantity Per Litre	Grade
Glycerol	12.5 ml	B.D.H. Analar
Sodium Sulphacetamide	0.025 gms	B.D.H. Laboratory Reagent
Penicillin	1,250,000 units	Glaxo Crystalline Benzylpenicillin B.P. (Sodium Salt)
Streptomycin	1,250,000 units	Glaxo Streptomycin Sulphate B.P.

For convenience, particularly in view of the high viscosity of glycerol, these four are added together in the form of 25 ml of a single solution prepared in the following manner:-

Weigh 0.1 gms sodium sulphacetamide into graduated cylinder (Pyrex 100 ml). Dissolve one 5 mega vial Penicillin in 10 ml distilled water and one 5 grm vial streptomycin in 20 ml distilled water and pour into cylinder thereby dissolving sodium sulphacetamide. Bring volume to 50 ml by adding distilled water as required. Add 50 ml glycerol to complete 100 ml of solution and mix thoroughly.

N.B. This volume (100 ml) is prepared to accommodate standard packs of antibiotics and is sufficient for four litres of buffer solution.

Following the addition of glycerol/antibiotics solution add further distilled water to bring each cylinder up to final volume, i.e. 1 litre.

The pH of freshly prepared buffer solution should be between pH 7.35 and pH 7.50, the day to day variations being due mainly to changes in climatic conditions. The variation in pH between batches of buffer solution prepared on the same day should in no circumstances exceed 0.04.

This buffer solution may be stored under refrigeration for periods up to seven days.

SECTION 2 - "CAPROGEN" EXTENDER

"CAPROGEN" EXTENDER is prepared daily as required in two forms:-

(a) 20% Egg Yolk "CAPROGEN" for PRIMARY dilution.

(b) 5% Egg Yolk "CAPROGEN" for SECONDARY dilution.

(a) 20% Egg Yolk "CAPROGEN"

	Quantity Per Litre	Grade
77 parts buffer solution	770 ml	
1 part 2.5% n-Caproic (n-Hexoic Acid)	10 ml	B.D.H. Laboratory Reagent
1 part 0.05% Chloromycetin	10 ml	Parke-Davis Chloramphenicol.
1 part Catalase solution	10 ml	
20 parts fresh egg yolk	200 ml	

(b) 5% Egg Yolk "CAPROGEN"

Citric Acid	0.14 g	B.D.H. Analar
92 parts buffer solution	920 ml	
1 part 2.5% Caproic Acid	10 ml	B.D.H. Laboratory Reagent
1 part 0.05 Chloromycetin	10 ml	Parke-Davis Chloramphenicol.
1 part Catalase solution	10 ml	
5 parts fresh egg yolk	50 ml	

In each case the egg yolk should be added last following careful mixing of the additive solutions with the buffer solution. The additive solutions are prepared in the following manner:-

2.5% Caproic Acid is prepared by adding 2.5 parts Caproic Acid to 97.5 parts buffer solution and shaking vigorously immediately before use. This solution may be stored under refrigeration for up to seven days provided vigorous shaking is always repeated before use.

0.05% Chloromycetin is prepared by dissolving the contents of one 250 mg Chloramphenicol capsule in 500 ml distilled water.

The catalase solution used contains 45 mg beef liver catalase in 100 ml buffer solution resulting in a final concentration of 4.5 mg catalase per litre of Caprogen.

Following the addition of the egg yolk further mixing is needed to ensure that the egg yolk is in even suspension throughout the Caprogen which should then be chilled to 2° - 5° prior to saturation with dry nitrogen. Chilling at this stage is necessary to facilitate absorption by the Caprogen of the nitrogen gas and to reduce frothing during the period of nitrogen saturation.

Nitrogen saturation is carried out by bubbling dry nitrogen through the Caprogen for a period of thirty minutes at the end of which time cylinder stoppers should be replaced under a jet of nitrogen and firmly taped down to exclude air.

Finally the Caprogen must be allowed to warm up to the ambient temperature of the laboratory before proceeding with semen dilution operations.

New Zealand Dairy Board Artificial Breeding Centre,
Newstead, R.D. 4,
Hamilton, NEW ZEALAND.

December, 1971.

APPENDIX II

A paper giving the principal results of chapter 5 published by the author jointly with Dr. J. D. Harvey of Auckland University in Biophysical Journal, Volume 31, 1980.

This paper is entitled

I. Orientational Effects

and it is intended that a second paper currently in preparation will form a second part;

II. Interaction Effects.

LASER LIGHT-SCATTERING STUDIES OF BULL SPERMATOZOA

I. ORIENTATIONAL EFFECTS

J. D. HARVEY, *Department of Physics, University of Auckland, Auckland, New Zealand*
M. W. WOOLFORD, *Ruakura Agricultural Research Centre, Hamilton, New Zealand*

ABSTRACT Calculations based on the known dimensions of bull spermatozoa show that the scattered light intensity is strongly dependent upon the relative orientation of the particle to the incident beam. The magnitude of this effect is apparently much greater than for other systems where motility has been investigated by dynamic light scattering. The calculations show that the scattering source can be approximated by a small spinning mirror, and consequently the greatest light intensity at the detector results from cells swimming in a direction perpendicular to the scattering vector. The calculations are in substantial agreement with photographic observations, as well as direct measurements of the scattered intensity. Previous treatments of dynamic light scattering from swimming bull spermatozoa based on point scattering models are shown to be incorrect.

INTRODUCTION

Laser light scattering has been used for some years now to study the motility of small swimming organisms. The earliest work on spermatozoa (Bergé et al, 1967) showed that the homodyne spectrum, for light scattered from fish and rabbit sperm, was strongly influenced by the motility of the sample, indicating the value of laser light scattering as an assay of motility. Subsequent work has dealt with a variety of sperm species and analysis techniques (Adam et al., 1969; Dubois et al., 1975; Cooke et al., 1976; Shimizu and Matsumoto, 1976; and Hallett et al., 1978). These studies have largely been concerned with attempts to characterize the swimming speed distribution from autocorrelation of the scattered light intensity.

Generally it has been assumed that spermatozoa behave as point particles moving with constant velocity. This type of analysis is reasonable for motile bacteria, but even in this size range (1–2 μm long) the internal degrees of freedom (wiggling, etc.) can affect the spectrum of the scattered light (Stock and Carlson, 1975; Boon et al., 1974).

Spermatozoa are an order of magnitude larger than bacteria, and in the case of bull or ram sperm, far from spherical. Under these conditions the assumption of point scatterers must be closely examined. Experimental observations of other large-sized flagellates, *Euglena gracilis* (Ascoli et al., 1978), have also pointed to the inadequacy of the point scatterer model.

We have collected correlation data on light scattered from motile bovine spermatozoa for some years now, and have found that the interpretation of the correlation functions requires a

scattering model which takes account of the size, shape, and unusual swimming behaviors of these cells. In this paper the implications of the size and shape of spermatozoan cells for light-scattering experiments are investigated with the use of approximate techniques for the calculation of the scattering amplitude. While these techniques may prove inadequate in their detailed predictions, the general features of the angular distribution of the scattered light are not limited by the approximations. It is found that the cells exhibit a very strong orientational effect, such that the scattered intensity is dominated by the light from those cells swimming in a narrow range of angles which are almost perpendicular to the scattering vector.

THEORY

The simplest way to treat the light scattered from a particle that is large compared with the wavelength of light is to use the Rayleigh-Gans approximation. While this approach may not be adequate to describe accurately the amplitude of the light scattered from a spermatozoa cell in view of its large dimensions, it can be expected that the general features of the scattered amplitude will be apparent from such a treatment. For any scattering particle, the far field amplitude of the scattered electric field from the ith particle may be written

$$A_i(\underset{\sim}{k}) = A_i^0 P_i(\underset{\sim}{k}), \tag{1}$$

where A_i^0 is the Rayleigh limit for small-angle scattering and $P_i(k)$ is a form facter which takes into account the spatial extent of the particle. The Rayleigh-Gans approximation yields $P_i(k)$ in the form

$$P_i(\underset{\sim}{k}) = (1/V_i) \int_{V_i} e^{i\underset{\sim}{k}\cdot\underset{\sim}{r}}\, dV. \tag{2}$$

In this approximation the integration over the volume of the particle assumes that all regions of the particle scatter equally and that the incident plane wave is unaffected by the presence of the scattering particles (i.e., it assumes negligible attenuation of the incident beam). Wyatt (1970) found, for example, that scattering from bacteria (*S. aureus*) was well described by the Rayleigh-Gans theory. Light scattered from spermatozoa is quite exceptional in its angular distribution because of the shape of the primary scattering center (the nucleic-acid-containing head). Bull spermatozoa and several other types of mammalian spermatozoa have a flat leaf-shaped head, and a long thin flagellum. We have found that the scattering pattern can be understood as deriving mainly from scattering from the head of the cell, which has a much greater volume than the flagellum. The major dimensions of the head are well defined (8 μm $\times$ 4.5 μm) and the shape is quite satisfactorily represented by a flat ellipse. The thickness of the head has been variously estimated as 0.7–1.0 μm and in the calculations reported here two models have been used. The head has been represented as either an elliptical slab (semiaxes a and b) of constant thickness (c) or an ellipsoid (of semiaxes a, b, and c).

In the case of the elliptical slab model, the integration over the volume of the particle has been performed numerically by integrating over an elliptical plane section and then summing the amplitudes from separate sections to model the particle as a multielement sandwich. If the head of the cell is modeled as an ellipsoid, the Rayleigh-Gans amplitude can be obtained

analytically. The integral in Eq. 2 can be written as

$$P_i(k) = (1/V)\int_{-r}^{r} e^{ikp} A(p)\, dp, \tag{3}$$

where r is the perpendicular distance from the center of the ellipsoid to a tangent plane normal to $\hat{k}$, p is the perpendicular distance of an arbitrary plane normal to $\hat{k}$ which cuts the ellipsoid with an elliptical cross section of area $A(p)$. A geometrical investigation shows that the area of the ellipse formed by the intersection of the plane $lx + my + nz = p$ with the ellipsoid $x^2/a^2 + y^2/b^2 + z^2/c^2 = 1$ is given by

$$A(p) = (\pi abc/r^3)(r^2 - p^2), \tag{4}$$

where $r = (a^2l^2 + b^2m^2 + c^2n^2)^{1/2}$. From Eqs. 3 and 4, the Rayleigh-Gans amplitude may be written

$$\begin{aligned} P_i(k) &= 3\,[\sin(kr) - kr\cos(kr)]/(kr)^3 \\ &= [9\pi/2(kr)^3]^{1/2} J_{3/2}(kr) \end{aligned} \tag{5}$$

which is the same as that for a sphere of radius r. This result was first obtained for ellipsoids of revolution by Guinier (1939).

For scattering from particles which are very large compared with the wavelength, a quite different approach to calculating the scattering amplitude can be used. The incident wavefront can be divided into a set of rays incident on the particle, each ray being partially reflected and transmitted at the surface of the particle. The resultant scattering pattern is calculated by summing the amplitudes of rays passing through and reflected from the particle, and the amplitude for diffraction around the particle (e.g., Van De Hulst, 1958). In the case of a parallel-sided slab, it can be seen that this approach will lead to a scattered intensity which is dominated by the reflection from the surfaces of the head at most scattering angles, since rays passing through the slab are undeviated and diffraction is concentrated in the forward angle region. Under these circumstances, the scattering can be very usefully approximated by that from a mirror (whose reflectivity may vary with scattering angle due to interference between reflections from both surfaces). The same computational strategy employed to evaluate the Rayleigh-Gans amplitude yields the amplitude from a mirror by using a single element elliptical slab and evaluating the amplitude only for orientations of the head, such that the illuminated side of the head is visible to the detector.

Scattering Calculations

The results of a series of numerical calculations on the scattered intensity as a function of the orientation of a swimming spermatozoan are shown in Fig. 2. The intensity plotted in this figure has been averaged over a rotation of 2π about the long axis of the head, since the cell rotates about this axis as it swims. The averaging was performed by numerical integration of the scattered intensity as a function of head rotation, obtained by repeated evaluation of Eq. 2 either by numerical integration for the elliptical slab model or by use of Eq. 5 for the ellipsoidal model.

The swimming velocity vectors have all been taken to lie in a plane normal to the incident

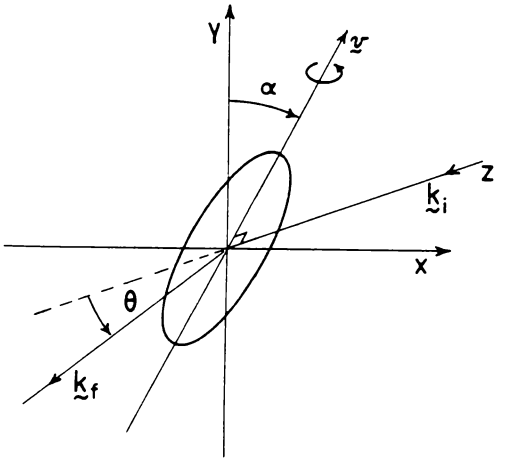

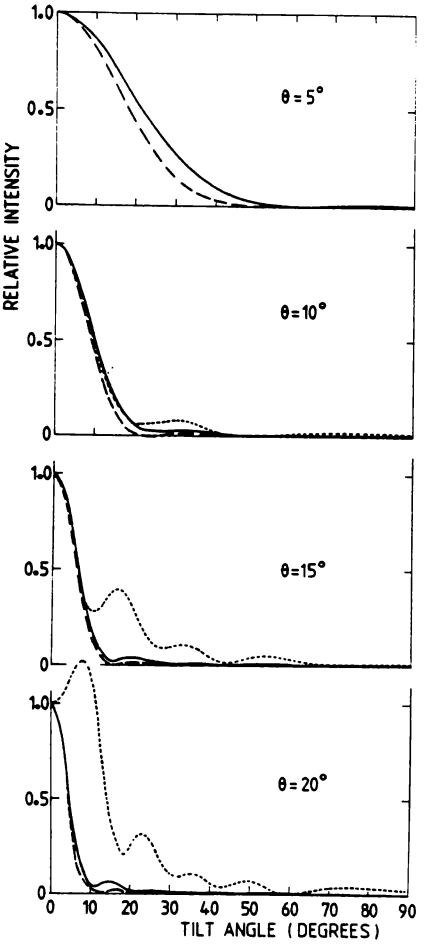

FIGURE 1

FIGURE 2

FIGURE 1 Coordinate system used to model the light from a swimming ellipsoidal spermatozoa. The cell is assumed to rotate about its direction of motion (v). The average intensity is calculated as a function of tilt-angle (α) for various scattering angles.

FIGURE 2 Average scattered intensity at various scattering angles (θ) as a function of tilt-angle (α in Fig. 1) for various theoretical models. Ellipsoid of semiaxes 4.0, 2.25, and 0.5 μm (—). Ellipsoid of semiaxes 4.0, 2.25, and 1.0 μm (---). Spinning opaque elliptical mirror of semiaxes 4.0 and 2.25 μm (— —). The two ellipsoidal models are indistinguishable at $\theta = 5°$. Calculations using a multiple sandwich elliptical slab model of thickness 1.0 μm give results almost indistinguishable from the solid line.

beam, and the scattered intensities are plotted as a function of the tilt-angle defined in Fig. 1. Our observations indicate that motile sperm show a strong tendency to swim on the internal surfaces of the scattering chamber. This is why our analysis deals only with velocities in a plane whose normal is parallel to the incident beam. This marked wall swimming phenomenon has been noted previously (Rothschild, 1963) and more recently analyzed in hydrodynamic terms by Katz and Blake (1975). Its implications for dynamic light-scattering calculations will be considered further elsewhere.

From Fig. 2 it can be seen that the scattered intensity is strongly peaked in the plane whose normal lies along the translation vector. This is true for both elliptical slabs and ellipsoidal shaped heads at forward scattering angles. The differences between the Rayleigh-Gans amplitudes become apparent only at scattering angles such that destructive interference can arise from light scattered from opposite sides of the head. For a head thickness of <1 μm and scattering angles typically employed in dynamic light-scattering studies ($\sim 10°$), the scattering amplitude is essentially the same function of tilt-angle for ellipsoidal and elliptical slab models. Under these circumstances the curve is very close to that given by an opaque spinning mirror of elliptical shape, (i.e., to the amplitude given by the large particle approach discussed earlier, when the scattering is obtained by adding the contributions from different rays reflected and refracted by the cell). The origin of the peaking in the intensity distribution as a function of tilt-angle lies in the strong peak in the curve of intensity versus head rotation angle which arises for specular reflection from the head at a tilt-angle near zero. Detailed investigation shows that the average intensity is dominated by the strength of this "reflective peak," and the average intensity is thus substantially increased for those cells which are swimming in a direction perpendicular to the scattering vector. Eq. 5 permits a simple geometrical interpretation of this effect, since $P_i(k)$ is a maximum when (kr) tends to zero. This maximum value, attained when all scattering elements scatter in phase, occurs either when k tends to zero or when the two tangent planes perpendicular to k become very closely spaced (i.e., when r tends to zero). The minimum value of r is the shortest semiaxis of the ellipsoid and is attained only for vertical orientation of the cell.

As the scattering angle decreases, the intensity versus tilt-angle relationship becomes less sharply peaked; furthermore, all models give similar results, since the thickness of the head is too small to give significant phase differences between rays scattered from opposite sides of the head. It is often asserted that orientational effects can be ignored by performing experiments at a sufficiently small scattering angle, since the form factor $P_i(k)$ tends to unity as θ_{scat} tends to zero. In the case of bull spermatozoa, however, the scattering angles where orientational effects become negligible are experimentally inaccessible. Our calculations show that even at 1° scattering angle the angular distribution of scattered intensity varies significantly with tilt-angle, and that scattering angles below 1° lead to correlation functions which take unreasonable lengths of time to collect and demand extremely high levels of hydrodynamic stability in the suspending medium.

The calculations are sensitive to the detailed geometry of the head (which has not been closely defined) in relation to wavelength and scattering angle, and the secondary peaks in the intensity distributions shown in Fig. 2 should not be accorded any great significance at this stage. In general, the calculations show that because of their small thickness and flat shape, spermatozoan heads can be modeled as rotating mirrors and that a maximum scattered intensity will occur only for cells swimming in such a direction that the normal to the flat surfaces of the head lies close to the direction of the scattering vector at some point during each rotation. Such cells, however, (with $\underset{\sim}{v}$ nearly perpendicular to $\underset{\sim}{k}$) are traveling in such a direction that they impress little or no Doppler shift on the scattered light.

The "spinning mirror" model predicts that the autocorrelation function should exhibit an oscillatory feature with a period corresponding to twice the head rotation rate, since the swimming cells will "flash" when observed by scattered laser light. Weak periodicities on the

appropriate time scale have frequently been observed in the autocorrelation functions we have obtained. These oscillatory features are strongly damped, as would be expected where a spread in velocities (and hence a spread in rotation rates) exists, and generally correspond to a mean rotation rate close to that reported by Gray (1958), who measured the frequency of waves on the flagellum at 9.1 ± 2.9 Hz, and noted that the head rotation was synchronous with these waves.

Photographic Observations

Replacing the photodetector generally used in laser light-scattering studies of sperm motility, with a low power (×30) microscope similarly aligned, provides a dramatic verification of the orientational effect discussed above. The scattering cell used in these experiments was of 1-mm path length having walls oriented normally to the incident beam. After sample insertion, migration of motile cells to the internal surfaces of the cell occurred rapidly (in a time comparable to that required for temperature equilibration). All measurements were performed at a sample temperature of 37°C.

For a scattering vector in the horizontal plane, the majority of sperm cells are observed to swim along trajectories having tilt-angles within ±20% of the vertical for scattering angles in the range 10–30°, with velocities being both upwards and downwards. So marked is the effect that it could easily be mistaken for geotaxis. However, alignment of the scattering vector (and hence the microscope) in the vertical plane results in the cells appearing to swim within a small angle of the horizontal.

These effects are apparent in Fig. 3, which shows a typical microphotograph time exposure (20 s) for swimming bull spermatozoa illuminated with a 628-nm He-Ne laser and observed at a scattering angle of 18.8°. Swimming trajectories appear on the film as a string of dots (a consequence of the flashing effect) and 80% of trajectories fall in the range of tilt-angles $0° < \theta < 20°$.

The range of tilt-angles actually observed can be investigated by counting those tracks on the film which can be distinguished without ambiguity and classifying them according to their angle from the vertical direction. A histogram constructed from the analysis of 171 such tracks on a set of photographs (of which Fig. 3 is one member) is shown in Fig. 4. A detailed agreement between theory and the experimental histogram should not be expected, since the histogram does not measure exactly the average scattered intensity as a function of angle; furthermore, any wobbling or helical motion of the head which causes the long axis to deviate from the translation vector will cause the range of track angles observed to be broadened from that expected for pure spinning motion about this long axis. It is known that spermatozoa swim in approximately helical trajectories, but we have found that the deviation from linear motion, while pronounced at lower temperatures, is not great at 37°C.

Further evidence of the orientational phenomenon may be obtained by viewing immotile cells whose heads become adhered to the cell window. It is usually possible by manipulating the suspending medium in the cell to rotate the spermatozoan about its attachment point by ±90°. The variation so observed in scattered intensity is such that the image formed by the scattered light becomes invisible for tilt-angles >20°.

Examination of the tracks in the photograph of Fig. 3 shows that they all lie in the same focal plane, which was observed to have a depth of field of the order of a few tenths of a

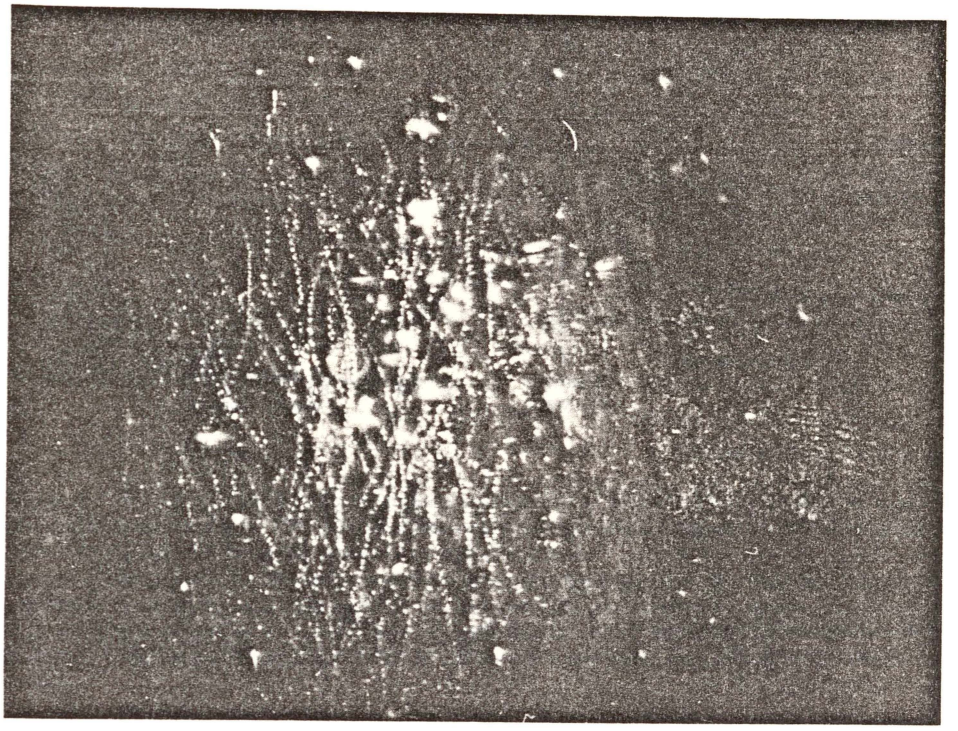

FIGURE 3 Microphotograph time exposure (20 s) of the scattering volume at a scattering angle of 19°, illuminated with a low power He-Ne laser. Swimming trajectories of bull spermatozoa appear as a line of dots. The microscope used was focused on the internal surface of the scattering cells, and the overexposed "flares" on the film were observed to be generated by immotile sperm.

millimeter. This demonstrates the previously mentioned tendency for motile cells to swim on the internal surfaces of the cell (i.e., in the plane normal to the incident beam).

Time Dependence of the Mean Scattered Intensity

Immotile sperm cells sediment at a slow but detectable rate under the influence of gravity. The density of the head is so much greater than that of the flagellum that immotile cells in equilibrium are distributed about a small range of tilt-angles close to 0°. The rate of relaxation back to the equilibrium position has been estimated as $\sim(0.03)\ \sin\phi$ rad s^{-1} (Roberts, 1970), where ϕ is the angle between the tail and the vertical. The calculations reported here imply that the mean scattered intensity for immotile cells will be much greater when this is observed with the scattering vector oriented in the horizontal plane than when it is observed with the scattering vector in the vertical plane (tilt-angles close to 90°). The averaging over all angles of the head in this case will be obtained by the statistical distribution of orientations of dead cells.

The experimentally observed intensity for horizontal and vertical scattering vectors as a function of time after insertion of the sample in the scattering cell (when all orientations of dead cells can be expected in view of turbulent mixing of the sample) is shown in Fig. 5. The shape of these curves is as expected, it being necessary to wait for ~10 min for the immotile

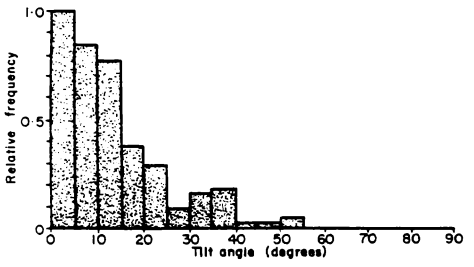

FIGURE 4

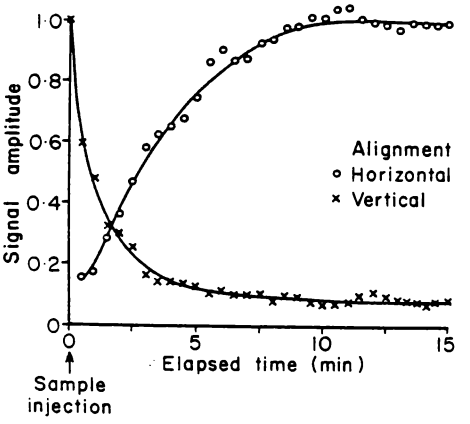

FIGURE 5

FIGURE 4 Histogram of the number of trajectories observed as a function of track angle on a set of photographs similar to Fig. 3. The majority of observed trajectories fall in a narrow range of angles close to the vertical direction for scattering vectors in the horizontal plane.

FIGURE 5 Mean intensity recorded by a detector at a scattering angle of 8° as a function of time after sample insertion with the scattering vector in the horizontal (O) and vertical (X) planes. The change in mean intensity is caused by the relaxation of immotile sperm towards their equilibrium distribution of tilt-angles. After several minutes all immotile sperm are sedimenting with orientations close to the vertical.

cells to reach an equilibrium distribution of orientations. The mean intensity for horizontal alignment is ~80 times greater than that for vertical alignment at a scattering angle of 8°.

DISCUSSION

It has been shown that the intensity of laser light scattered by swimming bull sperm is strongly dependent on the relative orientations of the trajectory and the scattering vector. The intensity distribution as a function of tilt-angle is such that negligible light is scattered to the detector for tilt-angles $\gtrsim 30°$, at the scattering angles generally employed for laser light-scattering experiments.

The phenomenon is most marked where all cells swim in the one plane. This frequently occurs in light-scattering cells as a result of the pronounced tendency for motile spermatozoa to remain swimming close to the internal surfaces. Occasionally, a cell is recorded photographically to be swimming at a large apparent tilt-angle; such cells are inferred to be swimming perpendicular to the scattering vector in the body of the medium.

In dynamic light-scattering (intensity fluctuation spectroscopy) experiments orientational effects will bias the distribution of swimming speeds apparent to the detector and would be expected to significantly increase the autocorrelation decay time. Further serious implications arise from immotile cells, since these rapidly align themselves in a vertical direction (head downwards). Such vertically aligned cells, while visible to a detector aligned at a scattering angle in the horizontal plane, are virtually invisible to a detector aligned at the same scattering angle in the vertical plane. Furthermore, a detector aligned in the horizontal plane will collect

scattered light from almost all immotile cells (as they diffuse rotationally about their long axis) but can receive light from only a small proportion (perhaps 20%) of the motile population. The ratio of the amplitudes of the correlation function components arising from motile and immotile cells cannot thus be expected to yield an absolute estimate of the proportion of live cells unless the orientational effects are fully accounted for.

We conclude, therefore, that neither the swimming speed distribution nor the proportion of motile cells in a sample of bull spermatozoa can be measured by laser light-scattering techniques unless orientational effects are included in the data analysis of the autocorrelation functions. The apparent agreement obtained in some cases between speed distributions derived using a simple point-scattering model at low scattering angles and those obtained by other methods must, therefore, be considered fortuitous.

The calculations reported here can clearly be extended to yield predicted autocorrelation functions. While such an extention may yield useful information on the origin of the fast decaying components of the autocorrelation function of the scattered light, such calculations will depend sensitively upon the precise geometry of the sperm cells, and upon the validity of the Rayleigh-Gans approximation for scattering centers of this size. After submission of this work we learned of the recent paper by Craig et al. (1979) in which it is found by direct numerical computation, using the Reyleigh-Gans approximation and realistic models for the shape and swimming motion of spermatozoa, that the decay of the autocorrelation function of the scattered light is determined predominantly by the rotation rate and not by the translation rate of the cells. This result can be understood readily on the basis of the scattering phenomena described here.

The authors would like to thank Dr. P. Shannon of the New Zealand Dairy Board, Dr. R. Sherlock of the University of Waikato, and Mr. B. Phease of the University of Auckland for helpful discussions during the course of this work.

Received for publication 14 December 1979 and in revised form 1 April 1980.

REFERENCES

ADAM, A., A. HAMELIN, P. BERGÉ, and M. GOFFAUX. 1969. Possibilité d'application de la technique de diffusion inélastique de la lumiere a létude de la vitali té des spermatozoides de taureaux. *Ann. Biol. Anim. Biochim. Biophys.* **9**:657–665.

ASCOLI, C., M. BARBI, C. FREDIANI, and A. MURE. 1978. Measurements of *Euglena* motion parameters by laser light scattering. *Biophys. J.* **24**:585–599.

BERGÉ, P., B. VOLOCHINE, R. BILLARD, and A. HAMELIN. 1967. Mise en évidence du mouvement propre de microorganisms vivants grâce â l'étude de la diffusion inélastique de lumière. *C. R. Acad. Sci. (Paris) Ser. D.* **265**:889–892.

BOON, J. P., R. NOSSAL, and S. O. H. CHEN. 1974. Light scattering due to wiggling motion of bacteria. *Biophys. J.* **14**:847–864.

COOKE, D., F. R. HALLETT, and C. A. V. BARKER. 1976. Motility evaluation of bull spermatozoa by photon correlation spectroscopy. *J. Mechanochem. Cell Motil.* **3**:219–223.

CRAIG, T., F. R. HALLETT, and B. NICKEL 1979. Quasi-elastic light-scattering spectra of swimming spermatozoa. Rotational and translational effects. *Biophys. J.* **28**:457–472.

DUBOIS, M., P. JOUANET, P. BERGÉ, B. VOLOCHINE, C. SERRES, and G. DAVID. 1975. Méthode et apareillage de mesure objective de la mobilite des spermatozoides humains. *Ann. Phys. Biol. Med.* **9**:19–41.

GRAY, J. 1958. The movement of the spermatozoa of the bull. *J. Exp. Biol.* **35**:96–108.

GUINIER, A. 1939. La diffraction des rayons X aux très petits angles: application a l'étude phénomènes ultramicroscopiques. *Ann. Phys. (Paris).* **12**:161–237.

HALLETT, F. R., T. CRAIG, and J. MARSH. 1978. Swimming speed distributions of bull spermatozoa as determined by quasi-elastic light scattering. *Biophys. J.* **21**:203–216.

KATZ, D. F., and J. R. BLAKE. 1975. Flagellar motion near walls. *In* Symposium on Swimming and Flying in Nature. Plenum Press, New York. 173–184.

ROBERTS, A. M. 1970. Motion of spermatozoa in fluid streams. *Nature (Lond.)*. **228**:375–376.

ROTHSCHILD, LORD. 1963. Non random distribution of bull spermatozoa in a drop of sperm suspension. *Nature (Lond.)*. **198**:1221–1222.

SHIMIZU, H., and G. MATSUMOTO. 1976. Photon statistics of laser light scattered by motile spermatozoa. *Opt. Commun.* **16**:197–201.

STOCK, G. B., and F. D. CARLSON. 1975. Photon autocorrelation spectra of wobbling and translating bacteria. *In* Symposium on Swimming and Flying in Nature. Plenum Press, New York. 57–68.

VAN DE HULST, H. C. 1958. Light Scattering by Small Particles. Chapter 8. John Wiley & Sons, Inc., New York.

WYATT, P. J. 1970. Cell wall thickness, size distribution, refractive index ratio and dry weight content of living bacteria. *Nature (Lond.)*. **226**:277–279.

APPENDIX III

A paper prepared and presented by the author at the annual conference of the *New Zealand Society of Animal Production, Lincoln College, Christchurch, New Zealand, February 1980*. This paper outlines very briefly the basis of the technique and acknowledges the participation of others concerned with the project.

Proc. N.Z. Soc. Anim. Prod., 40, 124-129.

LASER LIGHT SCATTERING AS A PROBE OF SPERM MOTILITY

M. W. WOOLFORD,* J. K. WOOLHOUSE,* D S. M. PHILLIPS,* S. A. HAWLEY,** J. D. HARVEY,† P. SHANNON‡ and B. CURSON‡

SUMMARY

Practical aspects of assaying live and dead fractions of bull spermatazoa, as well as concentration effects and organism survival, are briefly discussed. The technique and physical basis for the use of laser light scattering in the assay is presented. Previous work assumes that the high frequency signal components arise from translation motion. Our recent work demonstrates that sperm rotation is responsible for the high frequency photomultiplier-detector signals.

INTRODUCTION

The quantitative measurement of sperm motility has been a long-standing problem, and visual assessment has become the only widely used routine technique.

Recently laser light beating spectroscopy has become recognized as an appropriate tool in this field (Berge *et al.*, 1967; Nossal, 1971; Dubois *et al.*, 1975; Cook *et al.*, 1976; Shimizu and Matsumoto, 1976; Finsey *et al.*, 1979). The only substantial application of this technique to bull sperm in the context of artificial breeding is that of Hallet *et al.* (1978).

The technique has been based on the principle that the speed of a microscopic object which scatters light can be determined by measuring the associated Doppler shift induced in the scattered light field.

Basic to all these studies have been the assumptions that the size and shape of the spermatazoon are unimportant, the swimming velocity distribution is isotropic, and the fluctuating photocurrent results from beats between Doppler components. However, recent studies (Harvey and Woolford, 1980) have cast serious doubt on the validity of these assumptions and the associated interpretations of previous light scattering results.

* Ruakura Agricultural Research Centre, Hamilton.
**Ruakura Agricultural Research Centre. On leave from Eye Research Institute, Boston, Mass., U.S.A.
† University of Auckland.
‡ New Zealand Dairy Board, Newstead, Hamilton

Reprinted from *Proceedings of the New Zealand Society of Animal Production*, *40*: 124-9 (1980)

This paper briefly describes the basic technique, outlines several important factors which must be considered, and presents some illustrative data.

METHODOLOGY

Sperm cells within a defined volume of the sample (typically < 0.5 mm^3) scatter light from an incident laser beam to a photodetector (Fig. 1).

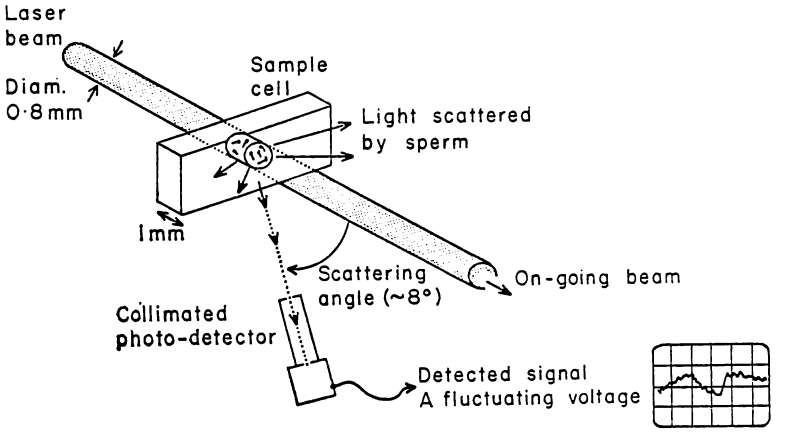

FIG. 1: *Geometry of the laser light scattering system.*

Harvey and Woolford (1980) have shown that the scattered light arises largely from the head region, which behaves as a spinning mirror, giving large intensity peaks as the head rotates.

The resultant photocurrent exhibits fluctuations which appear to arise not from the beating of Doppler shifts in the scattered light, but from intensity fluctuations generated as the cells rotate or otherwise move.

At small scattering angles the photocurrent fluctuations may be characterized by two overlapping frequency domains, a low range 0-10 Hz generated by immotile sperm and a high range 0-500 Hz generated by motile cells.

Analysis of this signal has been carried out in the time domain by forming the autocorrelation function, and in the frequency domain using spectral analysis to derive the power spectrum. Both the autocorrelation function and the power spectrum are of a two-component form arising from the motile and immotile fractions, and features of these functions can be related to certain

kinetic attributes of the sperm sample. In particular, the amplitude ratio (AAR) of the two autocorrelation components is related to the percent motile cells, the autocorrelation decay time is determined by random motions of dead cells, and the high frequency range of the power spectrum appears closely related to the head rotation rates among the motile fraction.

Sperm samples (both bull and ram sperm have been successfully used) are diluted to a standard concentration (usually $< 10^7$/ml) in an optically clear medium. Sodium citrate based buffer (2%) or citrate solubilized milk powder and egg yolk based extenders have been found satisfactory. Egg yolk concentrations up to 5% have been found usable provided the scattering angle is small ($< 10°$).

Large protein aggregates and contaminants must be excluded by filtering to 0.22 μm.

Sample temperature is controlled to close limits (± 0.05 °C) at 37°C to prevent convective motions of the medium.

RESULTS AND DISCUSSION

The two-component nature of the correlation function for a mixture of motile and immotile sperm is evident in Fig. 2. Motile cells generate a characteristic peak arising from the short correlation times for the high frequency components in the signal, and this peak progressively diminishes as the sample ages. The slowly

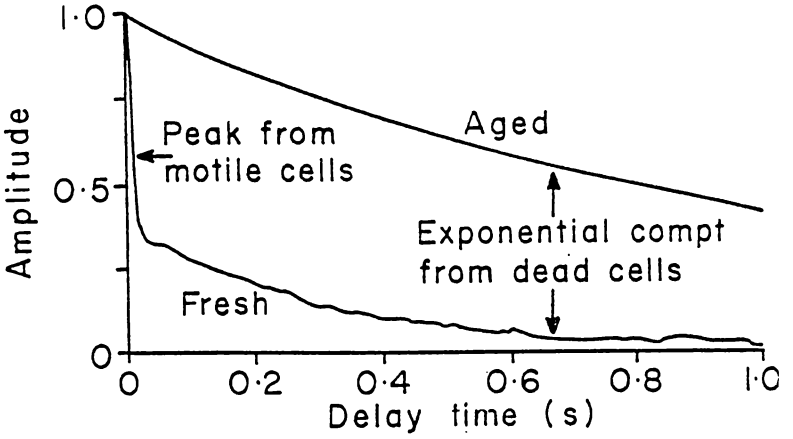

FIG. 2: *Correlation functions for fresh (2 h) and aged (incubated 72 h at 37°C) sperm samples.*

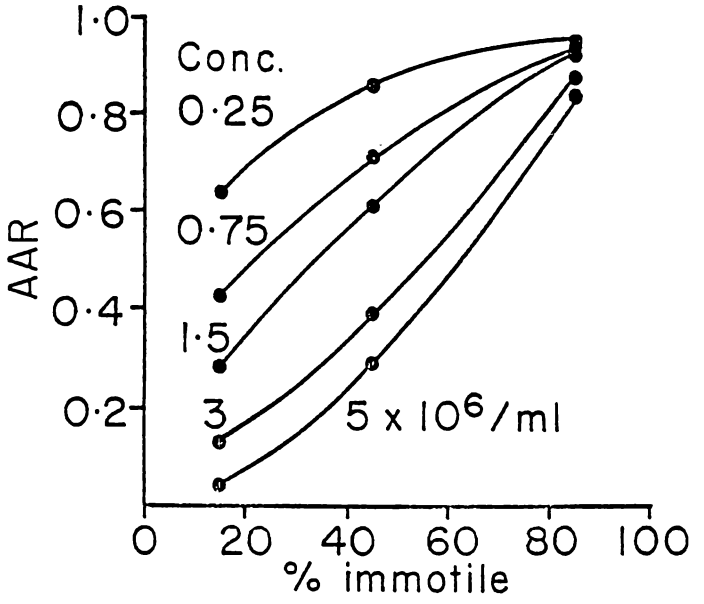

FIG. 3: *Relationship between the autocorrelation amplitude ratio (AAR) for the motile and immotile components and the percent dead cells, over a range of total sperm concentration.*

decaying exponential feature arises from motions of the dead or immotile cells.

The AAR of the two autocorrelation components has been found to give a useful measure of the percent immotile cells, although the relationship is strongly dependent on the total sperm concentration (Fig. 3). While the measurement is clearly empirical, repeatability is generally better than ±5% for a sample analysis time of 5.5 min.

The apparent increase in the percent immotile cells with decreasing sperm concentration is partially a real effect, since adding typically 5% seminal plasma to the diluent was generally found to give a decrease in AAR, particularly at high sperm dilutions. Concentration-dependent changes consistent with collisional perturbations of dead cells have also been observed in the immotile component of the autocorrelation function. Immotile or dead cells normally become vertically oriented, head down, due to geotaxis. Collisional interactions may then decrease the AAR as a consequence of the markedly anisotropic intensity distribution in the light scattered from spermatozoa (Harvey and Woolford, 1980),

since perturbed cells may become reoriented so that they do not contribute to the scattered intensity at the detector.

The scattering anisotropy has been found to be of such magnitude that the detector observes only those spermatozoa either aligned or swimming within $\pm 20°$ of the normal to the plane defined by the laser beam and the detector.

Spermatazoa have also been found to exhibit a remarkable tendency to swim in close proximity to the internal surfaces of the sample chamber. This results in a spatial separation of the motile and immotile cells in the sample, and with inappropriate cell geometry can contribute to both concentration and time dependence of the AAR. These effects confound the absolute measurement of the percent motile cells, unless they are appropriately considered in the experimental design.

Information on the vigour of the motile fraction is often more conveniently derived from the power spectrum than from the autocorrelation function.

Typical time-dependent changes in the spectrum are illustrated in Fig. 4 for samples incubated at both 37 and 20°C. The exponential feature extending to several hundred Hertz is generated by rotational motions of motile cells which produce rapid intensity fluctuations.

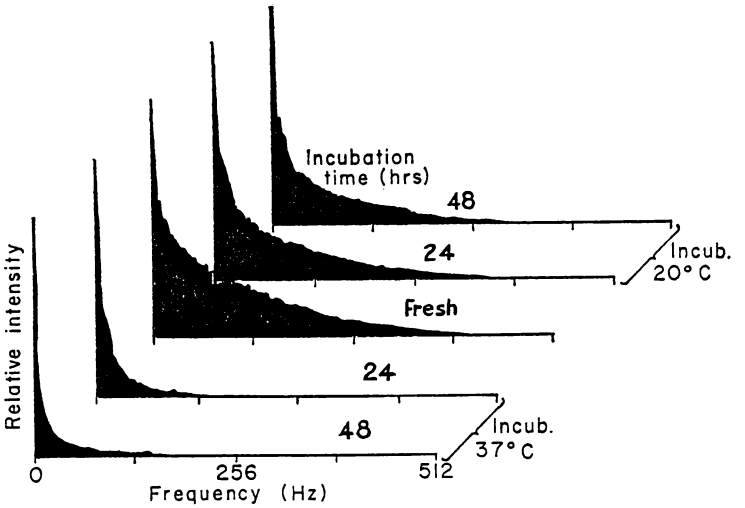

FIG. 4: *Power spectra for fresh and incubated samples.*

The decreasing prominence of the high frequency region with incubation is associated with a decrease in both the number and vigour of swimming cells. Changes in the spectrum are characterized by computing the power distribution between the frequency ranges 0-10 Hz (immotile cells), 10-100 Hz (defective or weak swimmers) and 100-500 Hz (vigorous swimmers).

Data collection and processing time is typically 5 min, allowing motility changes to be followed over a short time scale if desired.

Results to date clearly demonstrate that the light scattering technique gives a rapid, objective and repeatable measure of sperm motility. Further development of the optical geometry and data analysis should establish the technique as a routine laboratory assay.

ACKNOWLEDGEMENTS

The authors would like to thank Dr R. Sherlock for helpful discussions during the course of this work, and recognize the general support for the programme given by the University of Waikato.

REFERENCES

Berge, P.; Volochine, B.; Billard, R.; Hamelin, A., 1967. *C. R. Acad. Sci., Paris, 265*: 889, Series D.

Cook, D.; Hallet, F. R.; Barker, C. A. V., 1976. *J. Mechanochem. Cell Motility, 3*: 219.

Dubois, M.; Jouanet, P.; Berge, P.; Volochine, B.; Serres, C.; David, G., 1975. *Ann. Phys. Biol. Med., 9*: 19.

Finsey, R.; Peetermans, J.; Lekkerkerker, H., 1979. *Biophys. J., 27*: 187.

Hallet, F.; Craig, T.; Marsh, J., 1978. *Biophys. J., 21*: 203.

Harvey, J. D.; Woolford, M. W., 1980. *Biophys. J.* (in press).

Nossal, R., 1971. *Biophys. J., 11*: 341.

Shimizu, H.; Matsumoto, G., 1976. *Opt. Commun., 16*: 197.

APPENDIX IV

Relevant data collected by Dr. S. A. Hawley† during a period of collaborative research at the Ruakura Agricultural Research Centre, based on the experimental concepts developed in this thesis and using the apparatus described in chapter 3, part 2.

† current address:

Eye Research Institute of Retina Foundation,
Boston, U.S.A.

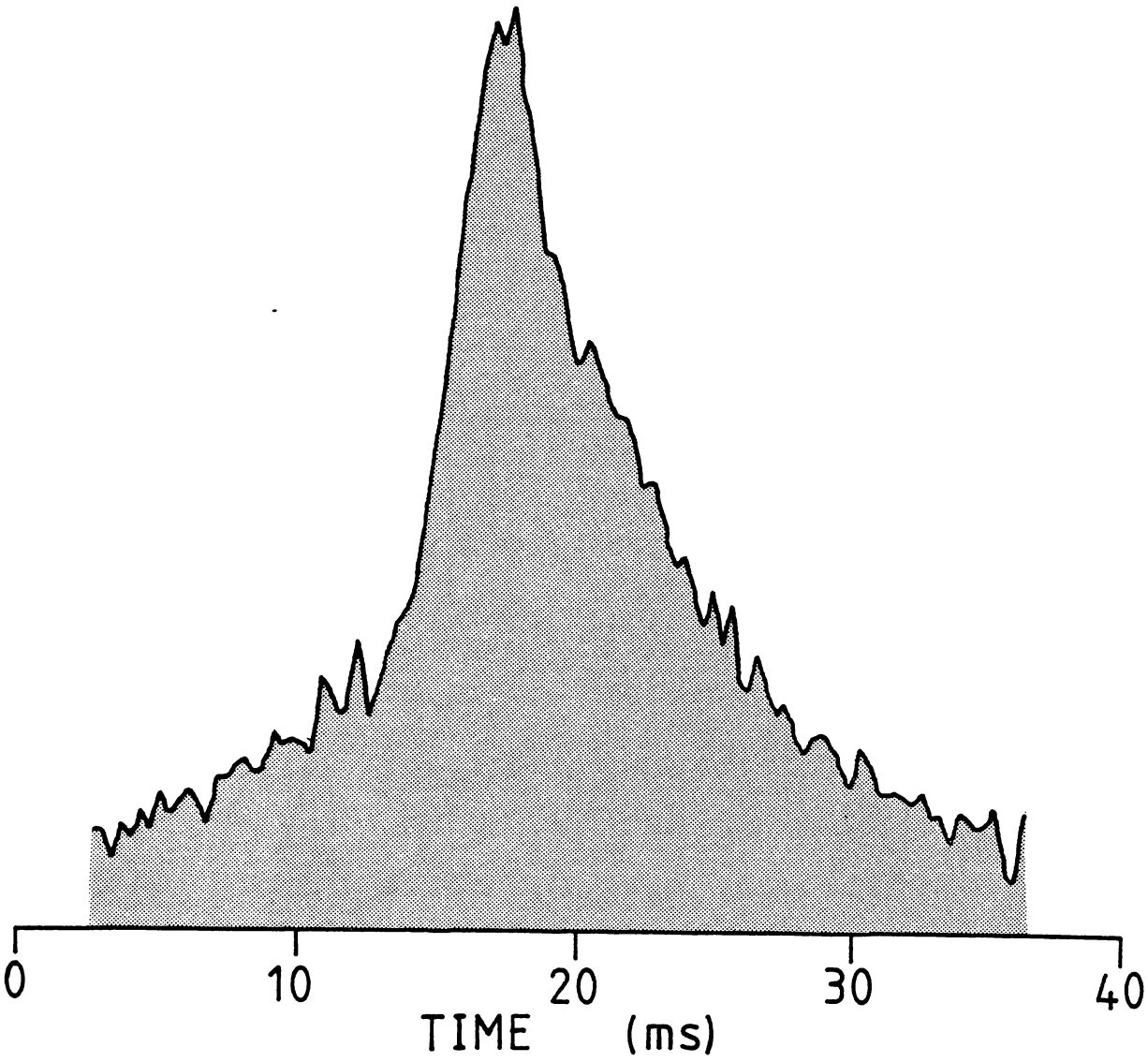

A computer averaged intensity peak profile derived from 341 singular sperm transits of the scattering volume. The average number of flashes per transit (fig. 5-20 for example) was 7.5. The sample concentration was 10^5 sperm/ml and was 'normally' motile. The vertical plane C-type light scattering cell was employed, and the flashes arise largely from spermatozoa swimming on the internal window surfaces of the cell. The peak width at half-intensity is 7.1mS.

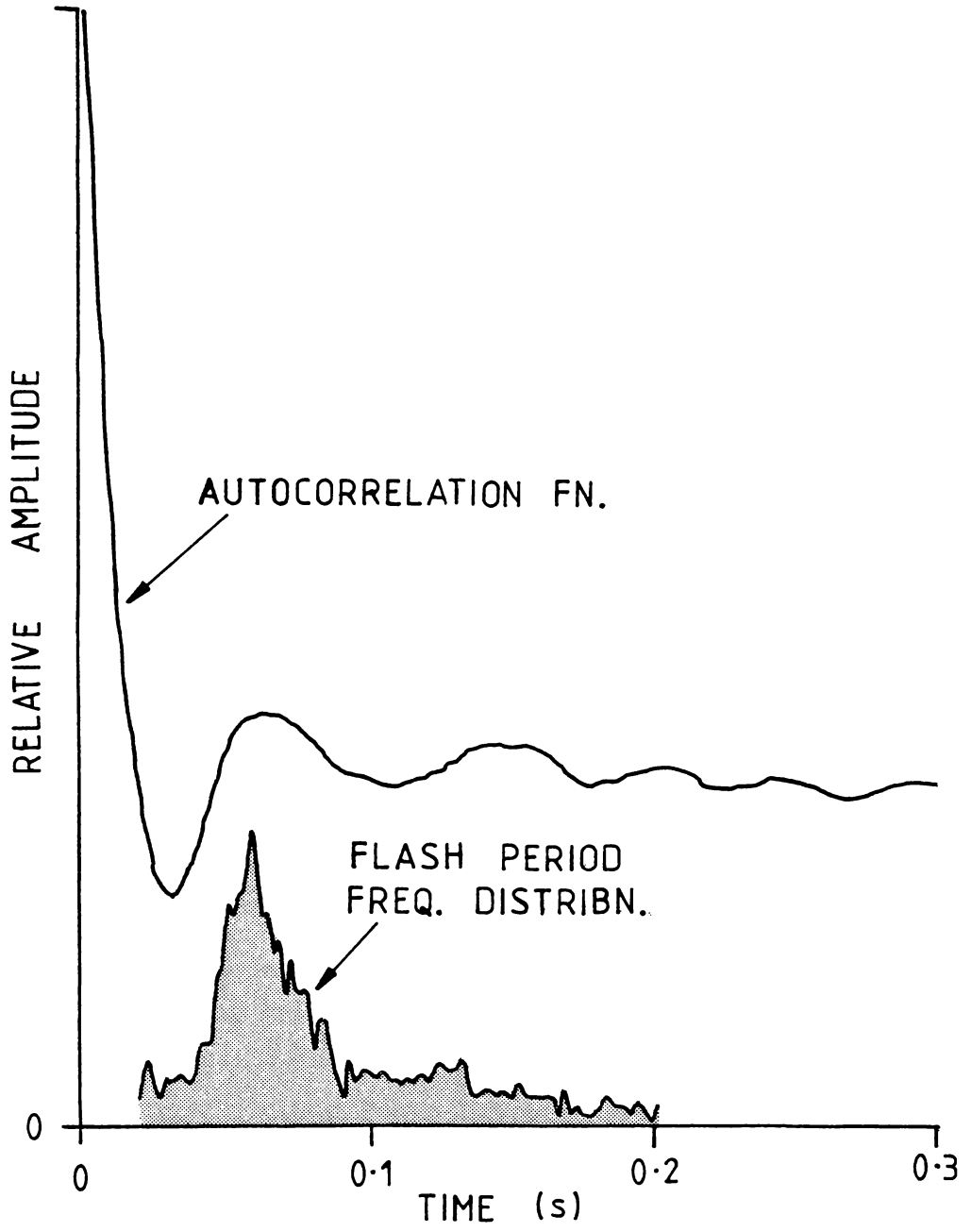

An autocorrelation function obtained by using gated autocorrelation signal analysis showing the flash-induced periodicity and the frequency distribution of flash periods determined by parallel computer sampling and processing. The flash period frequency distribution peaks at 58.4mS corresponding to a head rotation rate of 8.6Hz (on the assumption of 2 flashes/rotation). Both the autocorrelation function and the frequency distribution of periods are on the same timescale.

APPENDIX V

Application of light scattering motility measurements to field studies within the context of the artificial breeding industry in New Zealand.

The objective in presenting this final appendix, is to illustrate that the basic research described in chapters 4 and 5, while it revealed gross errors in the traditional interpretations placed on the results of light scattering experiments with spermatozoa, did nevertheless not detract from the potential value of the technique. An understanding of the phenomena involved and a more realistic interpretation placed on results lead to a standardisation of experimental methods which allowed the assay to be of practical value.

Accordingly a field experiment was designed to assess the value of objective motility measurements, as provided by the technique, in predicting the field performance of batches of liquid semen under commercial artificial breeding conditions.

This experiment was the result of the contributions and the hard work of many people, and is not the exclusive work of the author. However, since the author (M.W.W.) was primarily responsible for the planning, design and conduct of the experiment, a brief description and a few principal results are presented here as evidence of the successful application of the light scattering concepts developed in this thesis.

The following pages contain excerpts from a general project description written by the author (M.W.W.) for research administration purposes and which details the background and methods used in the experiment.

The data presented is the result of a preliminary analysis by Dr. S. A. Hawley[1] in cooperation with Mr. P. Shannon of the New Zealand Dairy Board and Mr. J. K. Woolhouse[2].

This project description was dated 30.7.79.

(1) Research Fellow with Biophysics group of Ruakura Animal Research Centre.

(2) Ruakura Animal Research Centre.

PROJECT DESCRIPTION

Introduction

This project involves the practical application of recently developed laser light scattering technology to assessments of semen 'quality' in the NZDB artificial breeding program. In particular correlations are sought between various light scattering measurements made on commercial AI services and the corresponding conception or non-return rates for the various bulls employed. The study is a preliminary attempt to evaluate light scattering motility measurements as a predictor of semen quality and conception rate.

Such laser techniques originate in the field of light beating spectroscopy (LBS) which over the past decade has progressively evolved as a powerful probe of the dynamics in microscopic systems. Variations of the general method have found diverse application.

Molecular diffusion (Cummins, 1973), electrophoresis of macromolecules (Ware and Flygare, 1972; Harvey,Walls and Woolford, 1976) fluid hydrodynamics (Yeh and Cummins, 1964), intra-cellular motion (Mustacich and Ware, 1974), phase changes and entropy fluctuations (Swinney, 1973) are examples. In many such applications data unavailable by other methods has been obtained.

Not unexpectedly, the characterisation of motility for flagellated micro-organisms has received significant attention. Berge *et al.*, (1967) first noted spectral broadening in the light scattered from rabbit and fish sperm, the level of broadening depending subjectively on the degree of motility. Subsequent reports have dealt with motility. Subsequent reports have dealt with motile bacteria (Nossal and Chen, 1972), sea urchin sperm (Matsumoto *et al.*, 1977) and bovine sperm (Hallett *et al.*, 1978).

Relatively little definitive work has been carried out on sperm due to continuing doubts over interpretation of correlation or spectral data in terms of particle kinetics.

Our own basic development program has evolved objective light scattering measurements which appear to repeatably characterise motility at high dilutions in a comparative but as yet not in an absolute sense.

General Technique

In principle, LBS can give objective quantitative measurements of the swimming motions of motile micro-organisms.

Movement of a sub-micron sized object can be characterised by the Doppler shift which it creates in the scattered light field. For a single object the motion is not uniquely determined since only that velocity component which lies along the scattering vector (towards the detector or observer) produces a measurable Doppler shift.

The scattered light from a large number of randomly moving scatterers contains a distribution of Doppler shifts representing all possible velocities. This scattered light field is collected by a non-linear photodetector which induces beats between the Doppler shifted frequencies in the light field. The detector thus generates a fluctuating electrical signal the frequency spectrum of which is simply the distribution of Doppler shifts in the scattered light. The distribution of velocities among the scattering particles may thus be deduced.

Depending on the optical geometry employed, measurement of either relative or absolute velocities of the scatterers is possible.

Further, where-as with sperm a certain fraction of the population is immotile, an estimate of % motile scatterers is possible by looking at the relative signal power in the high and low frequency domains. Dead sperm having only very low diffusional velocities, produce very small Doppler shifts while translating motile sperm generate very large Doppler shifts and hence high frequency components in the output of the photo-detector.

The above outline of the principles of the technique is however naive. While published work is still largely based on this simplistic model recent work by ourselves has already shown it to be an over-simplification. Problems arise as a consequence of the relatively large size of the spermatozoa. The wavelength of the laser light (e.g., 0.488μm) is considerably less than the major dimensions of the flat elliptical sperm head (approximately 8.6 x 4.6 x 1.0μm) and this results in a sharply peaked angular distribution of the scattered light intensity. One can therefore only measure those motions which are visible in the scattered light. Further, a homogeneous spatial distribution of sperm in the sample is difficult to achieve due to rapid sedimentation of dead cells and migration of motile cells to the internal surfaces.

Nevertheless, methods have been developed which either reduce or capitalise on these problems. Current methods yield objective data which appear to usefully characterise certain aspects of sperm motility. Sufficient understanding of the phenomena involved now exists to allow a

pilot application of these methods within the artificial breeding system. Significant future development of these techniques is however very probable now that the problems have been defined.

Applications of LBS Motility Assay

Two principal areas of application for light scattering motility methods are envisaged.

(i) Use of LBS assays in laboratory studies. These may involve comparative studies of extenders, freezing methods or basic aspects of sperm motility for either bull or ram sperm.

(ii) Studies aimed at characterising motility for bulls and rams, and defining predictive relationships for conception rate or developing screening tests for acceptable levels of semen "activity".

This proposal details a pilot experiment in the area described by (ii) above based on current technology.

Studies using alternative methods

It is not generally known whether the various kinetic attributes and behaviours of sperm are predictably related to conception rates. Intuitively there must be a positive correlation between motility and the probability of fertilisation, the question being rather, whether there is a correlation over the normal range of motility found in commercial ejaculates.

A survey by van Duijn (1964) showed that a relationship of the form

$$t_{\frac{1}{2}} \ (N \ . \ \bar{V}) \ (\log \ (N \ . \ \bar{V}))$$

where N = number of normally translating sperm with mean velocity $\bar{V}$.

$t_{\frac{1}{2}}$ = half life period.

closely fitted the seasonal variations in AI non-returns ($P < 0.002$).

The technique utilised the photo-electric method of measuring sperm velocity where the time taken to traverse an illuminated aperture is measured (Rikmenspoel, 1957).

A more recent study by Linford *et al.*, (1976) attempted to correlate various laboratory assessments of "semen quality" with field conception data based on the 112 day non-return percentage. Small numbers of ejaculates used and a high expectation of quality for the bulls employed,

mitigated against conclusive results.

Of the nine motility measures evaluated, only one was an objective technique and most involved measurements on undiluted semen.

The objective measure employed a 'motility meter' which through imposing viscous shearing forces, erased the normal cooperative wave motion in the undiluted ejaculate. The time required for the pattern to become re-established was then measured and taken to be an indicator of motility.

The best correlation with conception frequency was obtained using a subjective assessment of % translatory motion at 40°c after a 20 fold dilution into 0.9% NaCl ($r = + 0.698^{***}$). While "poor" quality semen was generally identified by most motility tests, prediction of non-return for normal or higher quality bulls was inadequate for routine use.

There are several aspects of such experiments which, very plausibly may have impeded the detection of any motility/conception relationships.

(a) Motility assessments have most usually been carried out at the high sperm concentrations existing in the basic ejaculate.

(b) Motility assessments on undiluted or even moderately diluted ejaculates (up to 1:50) are likely to be unrealistically over-estimated owing to the presence of seminal plasma at relatively high concentration (Shannon, 1979 pers. comm.).

(c) Sperm survival in a dilute environment as a function of time is difficult to estimate repeatably using subjective techniques.

(d) Subjective motility assessments and even most objective methods, tend to give reasonable characterisation of extremes but inadequate resolution between samples in the intermediate ranges.

The use of the present light scattering methods for motility assessment in field conception rate experiments, offers significant advantages:

(1) Measurements currently give results for sperm in dilute suspension (useable range 0.25 - 10 x 10^6 cells/ml) in either a citrate based buffer or optically cleared Caprogen extender with up to 5% cleared egg yolk.

(2) Measurements are highly repeatable (typically $\pm$ 5%) and can be carried out at any desired temperature over any desired time scale.

(3) Standardised methods virtually eliminate variability between operators.

(4) High repeatability over a time scale of days allows long term changes to be measured.

(5) Measurements at high dilution remove the "artificial" motility in the basic ejaculate promoted by the presence of the seminal plasma.

(6) Measurements may be made in any extender or environment which is optically clear.

While the interpretation of the light scattering measurements is still the subject of basic studies, the general understanding of the phenomena involved is sufficiently far advanced as to make the proposed experiment a worthwhile proposition.

It is likely that a further 12 - 18 months development of the current techniques, particularly with additional input from NRAC fellow Dr. S. Hawley, will see significant improvements and a closer approach to absolute measurements of motility. The proposed experiment is therefore intended as a pilot trial for the 1979 mating period in anticipation of a larger and more definitive study for the 1980 season.

Development Status of LBS Motility Technique

Information on the technical aspects of these laser light scattering methods and their historical development has been variously described as under project RA330.

Recent work has uncovered various interesting aspects of sperm motion which account for data not previously understood.

The central feature of these phenomena is that they all generate gross spatial or orientational inhomogeneities in the sperm suspension and introduce confounding variables. To date, no other published work cites these effects.

In brief the effects involved are:

(i) a remarkable and very pronounced tendency for motile sperm to accumulate on the internal surfaces of the sample chamber. It appears that motile sperm approaching a surface undergo a change in their swimming mechanics which precludes the flagellar motion from generating a force component normal to the surface. Swimming cells therefore tend to swim along the surface rather than move back into the bulk of the sample.

(ii) The high specific gravity of sperm heads (variously measured in the range 1.02 - 1.25) results in a high rate of sedimentation of dead cells unless the specific gravity and/or viscosity of the medium is suitably adjusted. It also results in a tendency for motile sperm to swim downwards.

(iii) Geotaxis results from the higher specific gravity of the sperm head relative to the tail. Dead cells therefore rapidly became vertically oriented, head down.

(iv) The swimming fraction imparts hydrodynamic disturbances to the suspending medium which perturb the normal Brownian motion of suspended dead cells.

(v) Strong optical orientation effects arise as a consequence of the flat elliptical shape of the sperm head which generates a sharply peaked scattering lobe.

Light scattered from different regions of the sperm head interfere constructively and destructively as the head rotates, producing a flashing effect.

(vi) The scattered light intensity depends on the direction of translation and only those sperm swimming or orientated within 20 - 30° of the normal to the plane defined by the beam and the observer (or detector), are visible.

The identification of these has significantly improved our understanding of the current techniques and their limitations. A new sample cell and beam geometry has been devised to minimise the effect of surface swimming and sedimentation. The orientational effects have serious implications for measurement of both % motile cells and swimming speeds. New beam geometries will need to be devised in order to measure swimming speeds although this is not considered a serious problem. However, orientational effects do confound the current measurement of % motile cells, and preclude absolute measurements of % motility. This arises since a detector aligned in the *horizontal plane* sees most of the dead cells most of which have become *vertically orientated,* but sees only a small fraction (perhaps 15 - 20%) of the motile cells, *those* that happen to be *swimming within 20 - 30° of the vertical.* On the other hand, a detector aligned in the vertical plane sees *no* dead cells (since these have become vertically orientated) and sees only 15 - 20% of the swimmers, *those* that happen to be *moving within 20 - 30° of the horizontal.*

Notwithstanding these peculiar problems, current methods can provide

comparative measurements of % motile cells, which even if not absolute, are repeatable and objective.

To be comparative, these measurements must be carried out at a specific sample temperature (nominally 37°c), sperm concentration (in the range 0.1 - 10 x 10^6/ml) and scattering angle (typically 5° - 10°).

Samples are usually suspended in either a citrate based buffer or optically cleared Caprogen extender diluted to a 5% concentration with buffer. The suspending medium contributes at a negligible level to the scattered light if filtered to 0.22µm.

Sample throughput is an important aspect of the technique highly relevant to the proposed experiment. The time/sample is determined by the time required for a newly injected sample to attain thermal equilibrium (a minimum of 3 min) and then the time for the autocorrelator to collect sufficient signal samples to give acceptable correlation statistics (typically 5.5 min). Allowing for sample changing, a throughput of around 7 samples/hour is currently attainable.

Software is being developed which will to some extent automate the data collection, monitor the signal level and provide prompts for experimental operations.

Experimental Objectives

This pilot study will compare semen motility for bulls used in the NZDB spring mating program (1979), on the basis of laser light scattering measurements.

Correlations between various motility measures and field conception rates will be sought.

The value of current light scattering measurement techniques for sperm motility as predictors of bull performance will be assessed.

Ejaculate subsamples will be subjected to as many motility measurements as current techniques and resources permit.

Semen samples will be diluted to levels used for field distribution (4 x 10^6/ml) and split into three subsamples. These will be held under nitrogen at temperatures of 20°c and 37.4°c for nominal intervals of 2, 30, 78 hrs before motility assessment.

Further dilution of the samples will occur immediately prior to the light scattering measurements, to a level of 2 x 10^6/ml.

For individual samples, single light scattering measurements will be made of the autocorrelation AAR and decay constant. Simultaneous with the autocorrelation data collection, spectral analysis of the high frequency fraction will be carried out in an attempt to obtain additional data related to the swimming kinetics. Both autocorrelation functions and frequency spectra will be stored on floppy disc files for subsequent analyses.

These general procedures will give objective but empirical data on:

(i) initial % motile cells at 37°c.

(ii) initial 'vigour' of the motile fraction at 37°c.

(iii) trends in (i) and (ii) over a 3 day period for incubation at both 20°c and 37°c which will give an indicator of sperm survivability.

(iv) frequency spectrum generated by the motile fraction which has yet to be correlated with swimming motions. (This will enable retrospective studies when suitable methods of characterising frequency spectra have been developed).

In addition routine assessments made at Newstead on the basic ejaculate will give estimates of wave motion score, % live sperm and abnormal morphology.

Experimental Procedures

The following procedures relate to the daily collection, processing and measurements on semen samples.

(1) Ejaculates used will be those collected at Newstead AB Centre during the normal course of commercial operations. An artificial vagina and associated procedures as currently used for field distribution of semen will be employed. Collection time will be 0400 - 0800 hrs. Total number of bulls in daily use will vary in the range 6 - 9.

(2) Ejaculate subsamples will be assessed microscopically by experienced technicians and scored for wave motion and morphology. A differential stain count of % live cells will be carried out. This phase of the motility assessment together with the primary dilutions will be carried out at Newstead AB Centre by NZDB staff.

Samples supplied ex Newstead for each bull will be in five separate subsamples each sealed under nitrogen at a concentration of 4×10^6 sperm/ml.

One sample will be analysed on the day of collection, the other four being held, two at 37°c, two at 20°c, for analysis at 30 and 72 hrs.

(3) Primary dilutions carried out at Newstead will be to a concentration of 4 x 10^6 sperm/ml in 1% cleared egg yolk (CEY) extender. The CEY will be pre-filtered to 0.22μm after dilution with citrate based buffer to a 1% CEY level. The dilution will be divided into three portions each being sealed under nitrogen.

(4) Laser motility assessments will be carried out for each bull 2 hrs, 30 hrs, and 78 hrs, after collection at the Biophysics light scattering laboratory, Ruakura after collection. These timings in practice will be subject to variations of no more than ± 2 hrs. The 30 hr and 78 hr samples will be incubated at temperatures of 20°c and 37°c.

(5) Each sample will be opened to air no more than 5 min prior to use. Secondary dilution to 2 x 10^6 sperm/ml will be carried out using pre-filtered (0.22μm) 1% CEY.

(6) After secondary dilution the sample will be injected into the light scattering cell and a period of 4 min allowed for the sample to come to thermal equilibrium and sperm activation to occur.

The detected light scattering signal will then be sampled for a period of 5.5 min by both the autocorrelator and the computer spectral analysis system.

(7) At the conclusion of the sampling interval both the 100 point correlation function and the 256 point power spectrum will be stored on floppy disc together with the date, time and experimental parameters.

Operators' comments may also be entered.

While preliminary on-line analysis of the autocorrelation functions will be carried out during the experiment, the majority of the data processing will be carried out at a later date.

(8) Appropriate measures will be taken to ensure all glassware and sample handling equipment is free of contaminants. The light scattering cell will be flushed with 0.22μm filtered buffer between samples.

(9) Subsamples of the 1% CEY extender used for secondary dilutions will be checked for aggregates on the day of preparation and use then held over for 30 and 78 hr. periods to estimate the degree of protein aggregation in the incubating sperm samples.

(10) Experimental parameters such as laser beam geometry, focussing,

scattering angle, beam power, detector apertures, system gain and data collection statistics will be maintained constant throughout the six week experimental period.

Bulls

These studies will involve only proven bulls used in Premium Sire Service (PSS), predominently of Jersey and Friesian breed. These bulls will contribute semen to a range of Livestock Improvement Associations.

Cycling of bulls through the service team over the six week duration of the trial will give useful data on within bull variations in motility characteristics.

Analysis of Data

Analysis of variance and covariance will be employed to relate light scattering data to 49-day non-return rate and other relevant variates. Analysis will be carried out within associations, within bulls and between bulls using the well known factors which influence conception rate as covariates.

In view of the volume of field data involved it would appear most expedient for the analysis to be carried out on the NZDB computer system using existing statistical packages which have been specifically set up for trials of this format.

As previously discussed, final analysis of the light scattering autocorrelation data will be carried out after completion of the experimental phase of the trial. This will enable the operators full attention to be devoted to experimental procedures and will allow closer consideration of the data and associated factors.

It is anticipated that analysis of the data from the trial will be available in approximately March - April 1980, depending on the time required by NZDB to collate the 49-day non-returns and other associated data.

Analysis and collation of the light scattering autocorrelation and spectral data will be carried out by M. W. Woolford using the Biophysics computer system over the period January - February 1980. Results from the light scattering analysis will then be appropriately coded and fed into the NZDB analysis system, possibly via suitably formatted paper tape punched by the Biophysics computer.

Mr. Duganzich will be statistical consultant for the Ruakura involvement and appropriate meetings will be arranged between all parties to achieve a general concensus of analysis.

Further Work

As previously discussed the application of light scattering motility measurements to conception rate studies is to some extent premature and must be regarded as a pilot experiment.

It will depend on state-of-the-art techniques and equipment which should see substantial development over the next 12 months. In all probability development work will lead to more absolute measurements of % live cells free from the confounding problems previously discussed. Further, the implementation of alternative scattering geometrics will allow translation swimming speeds to be measured. Improved data collection efficiency should allow increased sample throughput.

However, even with current light scattering technology and despite it being a pilot trial, this experiment will rank as one of the most comprehensive and definitive studies which has attempted to uncover any relationship which may exist between motility and conception rate.

As has already been discussed in this proposal, current light scattering methods have technical problems which continue to relegate the method to the list of "empirical techniques". We have only recently come to understand what the problems are.

Now that the deficiencies of the method have been defined it is very likely that continuing development will lead to substantial advances in the near future.

The experiment outlined in this proposal is therefore intended as a fore-runner to a more comprehensive and definative trial during the 1980 spring mating period.

Nevertheless, the study proposed for 1979 has every chance of yielding useful data and giving an indication of any correlation which may exist between motility and conception rate.

A separate proposal will be submitted for any further studies which may be considered for the 1980 mating season.

REFERENCES

Berge, P., B. Volochine, R. Billard and A. Hamelin, (1967): Acad. Sci. Paris D265, 889.

Cummins, H. Z. (1973): Proc. NATO Advanced Study Institute, Capri, Italy.

Hallett, F. R., T. Craig, and J. Marsh. (1978): Biophysical Journal, *21*, 203-216.

Harvey, J. D., D. F. Walls and M. W. Woolford. (1976): Optics. Commun.

Linford, Eileen, F. A. Glover, C. Bishop and D. L. Stewart. J. Reprod. Fert. (1976): *47*, 283-291.

Matsumoto, Shimuzu, Shimada and Wada. (1977): Optics. Commun. *22*, 3, 369-373.

Mustacich, R. V. and B. R. Ware. (1974): Phys. Rev. Lett. *33*, 617.

Nossal, R. and S. H. Chen. (1972): Optics, Commun. *5*, 117.

Rikmenspoel, R. (1957): Thesis, Utrecht.

Swinney, H. L. (1973): Proc. NATO Advanced Study Institute, Capri, Italy.

van Duijn, C. (Jr.), 1964: 5th Int. Conf. on Animal Prod. and AI, Trento.

Ware, B. R. and W. H. Flygare. (1972): J. Coll. Interf. Sci. *39*, 670.

Yeh, Y. and H. Z. Cummins. (1964): Appl. Phys. Letters, *4*, 176.

RESULTS

The following figures illustrate the basic results obtained in this experiment for one of the light scattering parameters measured, the AAR. The results are given for individual sires (32) across semen batches (142) and for individual semen batches across sires. The AAR in these figures is plotted against field conception rate averages for sires and semen batches after standard adjustments for seasonal and geographical variables (MacMillan and Curnow, 1977).

Other experimental data included measurements of the power spectrum and involved characterisation of the power distribution in the spectrum.

The survival of semen when incubated at both 37°c and 20°c was also studied for all batches using both autocorrelation and FFT spectral analysis. (These results to be published).

It is highly significant that this experiment relates to semen from sires which have been highly selected for artificial breeding purposes. Such bulls give semen having an extremely high level of fertility with a small variance in conception rates. The standard deviation in conception rate in this experiment was approximately 3% and it was within this extremely small range that the following relationships were obtained (minimum C.R. was 57%).

Previous experiments of a similar nature (Bishop, *et al.*, 1954 and Linford, *et al.*, 1976) had obtained significant correlations between conception rate and motility measurements (e.g., visual estimates, wavemotion scaning) in some circumstances, but over a very much wider range of conception rates, (e.g., for Linford, *et al.*, mean C.R. was 57.9%, standard deviation 10.7% with a range of < 30% - 80%).

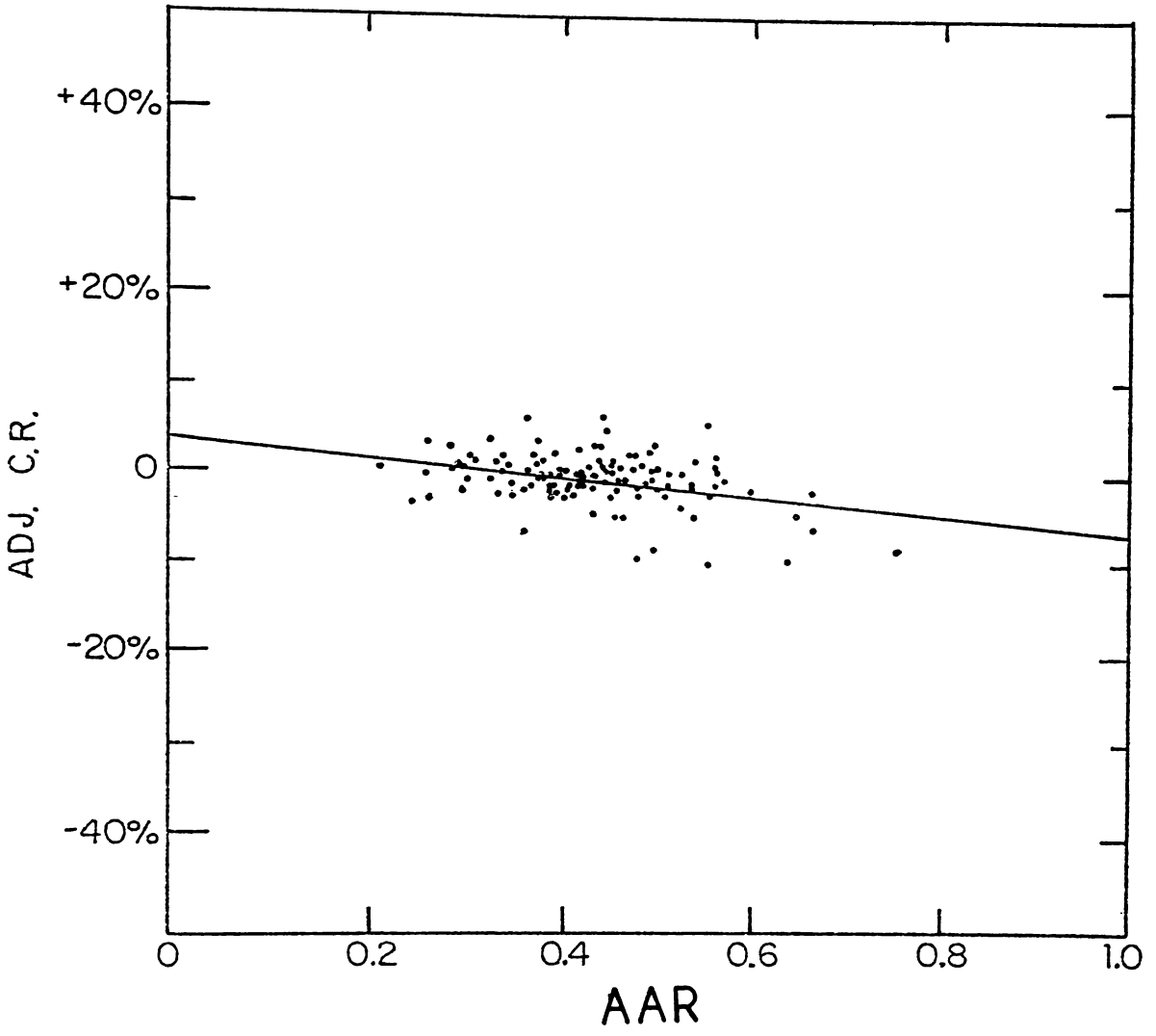

Fig. (i). Relationship between conception rate (CR) expressed as a deviation from the mean (∿ 66%), adjusted for seasonal and geographical factors, and laser light scattering measurements of AAR for batches of semen. In total 142 batches of semen were assayed and the data points shown are those for the fresh samples (< 10 hrs old) at an assay concentration of 2 x 10^6 sperm/ml in 1% CEY.

The data points shown represent samples across 32 sires. (Correlation coefficient - 0.37).

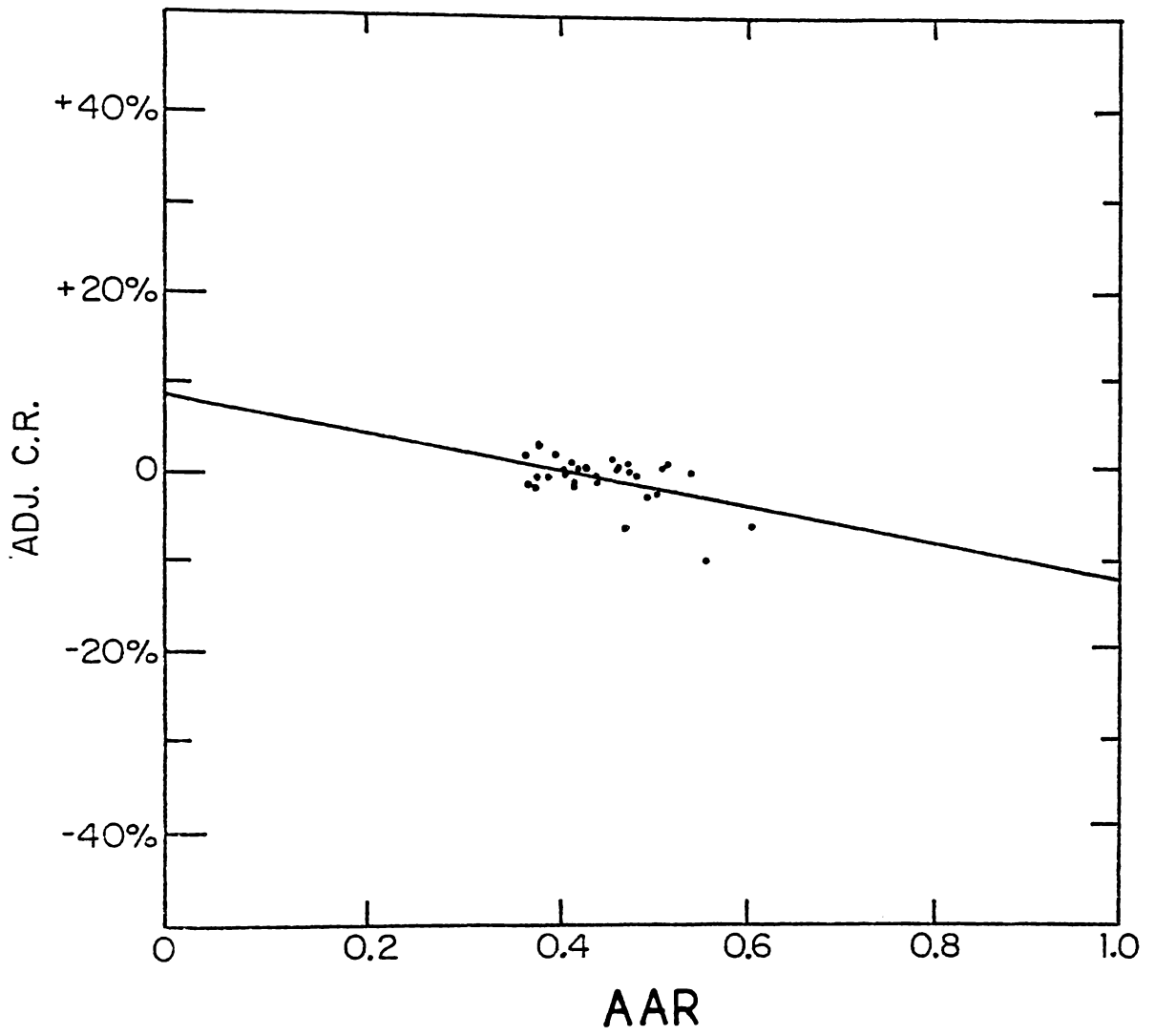

Fig. (ii). The mean AAR values for the 32 sires involved in the experiment plotted against field conception rates which had been adjusted for seasonal and geographic factors, and are expressed as a deviation from the mean (∿ 66%). Preliminary simple correlations show the individual sire averages when weighted by the number of inseminations gave a correlation coefficient of - 0.60 between AAR and conception rate.

Over all sires, a total of 217,000 cow-inseminations generated these data points.

APPENDIX VI

The FORTRAN RLQF least squares fitting algorithm used to characterise the slow autocorrelation component.Tindel (1977).

```
0001        SUBROUTINE RLQF(X,Y,YF,W,E1,E2,P,WZ,N,M,NI,ND,EP,AUX,MD)
0002        DIMENSION X(1),Y(1),YF(1),W(1)
0003        DIMENSION P(10),E1(10),E2(10),D(10),MD(10)
0004        DIMENSION C(55),V(10),CC(10,10),VV(10,1),U(10)
0005        EQUIVALENCE (V(1),VV(1,1))
0006        COMMON /RLQF/ S
0007        ND=1
0008        WRITE(6,2)
0009      2 FORMAT(/53H INTERMEDIATE ESTIMATES OF PARAMETERS, SUM OF SQUARES)
0010        LM=0
0011        DO 4 IM=1,M
0012        IF(MD(IM).EQ.0) GOTO 4
0013        LM=LM+1
0014        MD(LM)=IM
0015      4 CONTINUE
0016        SXX=1.E20
0017        NT=0
0018        IV=0
0019      5 IJ=0
0020        NT=NT+1
0021        DO 10 I=1,LM
0022        V(I)=0.
0023        DO 10 J=1,I
0024        IJ=IJ+1
0025     10 C(IJ)=0.
0026        XX=0.
0027        TT=0.
0028        DO 40 L=1,N
0029        IF(WZ)15,25,15
0030     15 WT=W(L)
0031        IF(WT) 28,40,28
0032     25 WT=1.
0033     28 CALL AUX(F,P,D,X(L),L)
0034        A=F-Y(L)
0035        XX=XX+A*A
0036        IJ=0
0037        DO 40 I=1,LM
0038        K=MD(I)
0039        DO 30 J=1,LM
0040        KJ=MD(J)
0041        IJ=IJ+1
0042     30 C(IJ)=C(IJ)+WT*D(K)*D(KJ)
0043        V(I)=V(I)-WT*A*D(K)
0044     40 CONTINUE
0045        WRITE(6,55) (P(J),J=1,M),XX
0046     55 FORMAT(1X,8E15.5)
0047        IF(IV.EQ.1) GOTO 78
0048        IF(NT.GT.NI) GOTO 125
0049        IF(XX.GT.SXX) GOTO 71
0050        SXX=XX
```

```
0051        CALL  SOLMT(C,VV,1,IJ,LM,KEY)
0052        IF(KEY.EQ.1) GOTO 120
0053        PMAX=ABS(P(MD(1)))
0054        DO 70 I=2,LM
0055        PK=ABS(P(MD(I)))
0056        IF(PK.GT.PMAX) PMAX=PK
0057     70 CONTINUE
0058        PMAX=PMAX*1.E-8
0059        GOTO 73
0060     71 DO 72 I=1,LM
0061        K=MD(I)
0062        P(K)=P(K)-U(I)
0063     72 V(I)=U(I)*.3
0064     73 DO 75 I=1,LM
0065        K=MD(I)
0066        P(K)=P(K)+V(I)
0067        U(I)=V(I)
0068        IF(ABS(P(K)).LT.PMAX) GOTO 75
0069        TC=ABS(V(I)/P(I))
0070        IF(TC.LE.TT) GOTO 75
0071        TT=TC
0072     75 CONTINUE
0073        IF(EP.GT.TT) IV=1
0074        GOTO 5
0075     78 DO 80 I=1,LM
0076        DO 80 J=1,LM
0077     80 CU(I,J)=0.
0078        DO 82 I=1,LM
0079     82 CU(I,I)=1.
0080        CALL  SOLMT(C,CU,M,IJ,LM,KEY)
0081        IF(KEY.EQ.1) GOTO 120
0082        DO 85 I=1,LM
0083        K=MD(I)
0084        DO 85 J=1,LM
0085     85 P(K)=P(K)+CU(I,J)*V(J)
0086        DO 91 I=1,M
0087     91 E1(I)=0.
0088        DO 95 I=1,LM
0089        K=MD(I)
0090     95 E1(K)=SQRT(CU(I,I))
0091        WRITE(6,96) NT
0092     96 FORMAT(/30H FINAL ESTIMATES OF PARAMETERS35X,11HITERATIONS=,I5)
0093        WRITE(6,55) (P(I),I=1,M)
0094        SS=0.
0095        S=0.
0096        DO 105 L=1,N
0097        IF(WZ.EQ.0.) GOTO 100
0098        WT=W(L)
0099        GOTO 102
0100    100 WT=1.
```

```
0101   102 CALL  AUX(F,P,N,X(L),L)
0102       YF(L)=F
0103       XX=(Y(L)-F)**2
0104       S=XX*WT+S
0105       SS=XX+SS
0106   105 CONTINUE
0107       PP=N-M
0108       FI=SQRT(S/PP)
0109       DO 115 I=1,M
0110   115 E2(I)=FI*E1(I)
0111       WRITE(6,117) SS,S
0112   117 FORMAT('0SUM OF SQUARES',E15.5,'  WEIGHTED S S',E15.5)
0113       WRITE(6,118)
0114   118 FORMAT('0RMS STATISTICAL ERRORS')
0115       WRITE(6,55) (E1(I),I=1,M)
0116       WRITE(6,119)
0117   119 FORMAT('0RMS TOTAL ERRORS')
0118       WRITE(6,55) (E2(I),I=1,M)
0119       RETURN
0120   120 WRITE(6,121)
0121   121 FORMAT(22H LINEAR EQUATIONS FAIL)
0122       NN=0
0123       RETURN
0124   125 WRITE(6,126)
0125   126 FORMAT('0NO CONVERGENCE')
0126       RETURN
0127       END
0128       SUBROUTINE  SOLMT(A,B,L,M,N,KEY)
0129       DIMENSION A(1),B(10,1)
0130       IF(A(1).EQ.0.) GOTO 150
0131       IF(M.EQ.1) GOTO 160
0132       A(1)=1./SQRT(A(1))
0133       DO 10 I=2,N
0134    10 A(I)=A(I)*A(1)
0135       INC=N
0136       I1=1
0137       IN=N
0138       NM1=N-1
0139    20 INC=INC-1
0140       I1=IN+1
0141       IN=IN+INC
0142       NS=N-INC
0143       X=0.
0144       ISUB=I1
0145       DO 30 I=INC,NM1
0146       ISUB=ISUB-I
0147    30 X=X+A(ISUB)**2
0148       IF(A(I1).LT.X) GOTO 150
0149       A(I1)=SQRT(A(I1)-X)
0150       IF(A(I1).EQ.0.) GOTO 150
```

```
0151        A(I1)=1./A(I1)
0152        IF(INC.EQ.1) GOTO 90
0153        I11=I1+1
0154        L11=I1-INC
0155        DO 50 I=I11,IN
0156        X=0.
0157        L1=L11
0158        L2=I-INC
0159        DO 40 J=1,NS
0160        X=X+A(L1)*A(L2)
0161        L1=L1-INC-J
0162     40 L2=L2-INC-J
0163     50 A(I)=A(I1)*(A(I)-X)
0164        GOTO 20
0165     90 DO 130 K=1,L
0166        B(1,K)=B(1,K)*A(1)
0167        DO 110 I=2,N
0168        JM=I-1
0169        ISUB=I
0170        INC=N
0171        X=0.
0172        DO 100 J=1,JM
0173        X=A(ISUB)*B(J,K)+X
0174        INC=INC-1
0175    100 ISUB=ISUB+INC
0176    110 B(I,K)=A(ISUB)*(B(I,K)-X)
0177        B(N,K)=B(N,K)*A(M)
0178        INC=-1
0179        J1=M+1
0180        DO 125 I=2,N
0181        INC=INC+1
0182        JM=J1-2
0183        J1=JM-INC
0184        JSUB=N-INC-1
0185        II=JSUB
0186        X=0.
0187        DO 120 J=J1,JM
0188        JSUB=JSUB+1
0189    120 X=X+A(J)*B(JSUB,K)
0190    125 B(I1,K)=A(J1-1)*(B(II,K)-X)
0191    130 CONTINUE
0192        KEY=0
0193        RETURN
0194    150 KEY=1
0195        RETURN
0196    160 B(1,1)=B(1,1)/A(1)
0197        KEY=0
0198        RETURN
0199        END
0200        SUBROUTINE   AUX(F,P,D,X,L)
0201        DIMENSION  P(10), D(10)
0202        F=P(1)*EXP(X*P(2))+P(3)
0203        D(1)=EXP(X*P(2))
0204        D(2)=P(1)*EXP(X*P(2))*X
0205        D(3)=1
0206        RETURN
0207        END
```

BIBLIOGRAPHY

Adam, M., A. Hamelin, P. Berge and M. Goffaux. (1969). Possibilité d'application de la technique de diffusion inélastique de la lumière à l'étude de la vitalité des spermatozoides de tareaux. *Ann. Biol. Anim. Biochem. Biophys.*, 9, 651-655.

Allison, A. J. and T. J. Robinson. (1972). The recovery of spermatozoa from the reproductive tract of the spayed ewe treated with progesterone and oestrogen. *J. Reprod. Fert.*, 31, 215-224.

Asano, S., and G. Yamamoto. (1975). Light scattering by a spheroidal particle. *Appl. Optics,* 14, 29-49.

Ascoli, C., M. Barbi, C. Frediani and A. Mure. (1978). Measurements of *Euglena* motion by laser light scattering. *Biophys. J.*, 24, 585-599.

Ascoli, C., M. Barbi, C. Frediani and D. Petracchi. (1978). Effects of electromagnetic fields on the motion of *Euglena Gracilis*. *Biophys. J.*, 24, 601-612.

Atherton, R. W. (1975). An objective method for evaluating Angus and Hereford sperm motility. *Int. J. Fertil.*, 20, 109-112.

Atherton, R. W. (1979). *In* D. W. Fawcett and J. M. Bedford. *The Spermatozoon.*, Urban and Schwarzenberg, Inc. Baltimore-Munic.

Bahr, G. F. and E. Zeitler. (1964). Study of bull spermatozoa. *J. Cell. Biol.*, 21, 175-189.

Baker, F., R. G. Cragle, G. W. Salisbury and N. L. Van Demark. (1957). Spermatozoa velocities *in vitro*. A simple method of measurement. *Fert. Steril.*, 8, 149-155.

Baker, F. N. and G. W. Salisbury. (1963). Nuclear size of live and dead bovine spermatozoa. *Nature,* 197, 820.

Berg, H. C. (1971). How to track bacteria. *Rev. Sci. Instrum.*, 42, 868-871.

Berg, H. C. and D. A. Brown (1972). Chemotaxis in *Escherichia coli* analysed by three dimensional tracking. *Nature,* 239, 500-504.

Bergé, P., B. Volochine, R. Billard and A. Hamelin. (1967). Mise en évidence du mouvement propre de microorganismes vivants grâce à l'étude de la diffusion inélastique de la lumière. *C. R. Acad. Sc. Paris,* 265, 889-892.

Berne, B. J. and R. Nossal. (1974). Inelastic light scattering by large structural particles. *Biophys. J.*, 14, 865.

Berne, B. J. and R. Pecora. (1976). *Dynamic Light Scattering*, Wiley & Sons, Inc., New York.

Bishop, D. W. (1962). Sperm Motility. *Physiological Reviews*, 42, 1-59.

Bishop, M. W. H., R. C. Campbell, J. L. Hancock and A. Walton. (1954). Semen characteristics and fertility in the bull. *J. Agric. Sci., Camb.*, 44, 227-248.

Bishop, M. W. H. and A. Walton. (1960). Metabolism and motility of mammalian spermatozoa. *In* A. S. Parkes (Ed.), *Marshall's Physiology of Reproduction*. Green and Co., Ltd., London.

Blackshaw, A. W. (1953). The motility of ram and bull spermatozoa in dilute suspension. *J. Gen. Physiol.*, 36, 449-462.

Blau, H. H., D. J. McCleese and D. Watson. (1970). Scattering by individual transparent spheres. *Appl. Optics*, 9, 2522-2528.

Blokhuis, E. W. M. (1961). Optical investigations on the movement of bull spermatozoa. *Proc. IV Int. Congr. Anim. Reprod.*, 243-248.

Blokhuis, E. W. M. (1972). Types of movement of bull spermatozoa and semen quality. *Proc. VII Int. Congr. Anim. Reprod. and A.I., Munich*, 1289-1293.

Blom, E. (1946). A comparing-chamber for microscopic examination of undiluted bull semen. *Vet. J.*, 102, 252.

Blumer, H. (1926). *Z. Physik*, 32, 119.

Boon, J. P. (1975). Theoretical models for bacterial motion and chemotaxis. *Adv. Chem. Phys.*, 29, 169-190.

Boon, J. P., R. Nossal and S. H. Chen. (1974). Light scattering spectrum due to wiggling motions of bacteria. *Biophys. J.*, 14, 847.

Bosselaar, C. A. and N. Spronk. (1952). A physical method for determination of the motility and concentration of spermatozoa. *Nature*, 169, 18-19.

Botella, L. (1956). Measurement of linear progression of the human spermatozoon as an index of male fertility. *Int. J. Fertil.*, 1, 113.

Brigham, E. O. (1974). *The Fast Fourier Transform*. Prentice-Hall, Inc., Englewood Cliffs, N.J.

Brokaw, C. J. and I. R. Gibbons. (1975). Mechanisms of movement in flagella and cilia. *In* T. Y. T. Wu, C. J. Brokaw and C. Brennan, *Swimming and Flying in Nature*, 1, 89-126, Plennum Press, New York.

Campbell, R. C., J. L. Hancock and I. G. Shaw. (1960). Cytological characteristics and fertilising capacity of bull spermatozoa. *J. Agric. Sci.*, 55, 91-99.

Chan, J. H. C. and E. A. Ballik. (1975). SNR in optical velocimeters: effect of particle number density. *Appl. Optics*, 14, 1839-1846.

Chandrasekhar, S. (1943). Stocastic problems in physics and astronomy. *Rev. Mod. Physics*, 15, 1-89.

Chu, B. (1974). *Laser Light Scattering*. Academic Press, New York.

Cohen, S. C. (1975). Heterodyne detection: phase front alignment, beam spot size, and detector uniformity. *Appl. Optics*, 14, 1953-1959.

Collins, E. R. (1976). The optical collimator system employed in these experiments was originally designed by Prof. E. R. Collins of Auckland University for use in laser Doppler velocimetry studies in wind tunnels.

Commoner, B. (1949). On the interpretation of the absorption of ultra-violet light by cellular nucleic acids. *Science*, 110, 31-40.

Cooke, D. F., F. R. Hallett and C. A. V. Barker. (1976). Motility evaluation of bull spermatozoa by photon correlation spectroscopy. *J. Mechanochem. Cell Motility*, 3, 219-223.

Craig, T., F. R. Hallett and B. Nickel. (1979). Quasi-elastic light scattering spectra of swimming spermatozoa. *Biophys. J.*, 28, 457-472.

Cross, D. A. and P. Latimer. (1972). Angular dependence of scattering from *Escherichia coli* cells. *Appl. Optics*, 11, 1225-1228.

Cummins, H. Z. (1973). *Proc. NATO Adv. Study Institute, Capri, Italy. Edited by H. Z. Cummins and E. R. Pike, Plenum, New York.*

Cummins, H. Z., F. D. Carlson, T. J. Herbert and G. Woods. (1969). Translational and rotational diffusion constants of Tobacco Mosaic Virus from Rayleigh linewidths. *Biophys. J.*, 9, 518-546.

Cummins, H. Z., N. Knable and Y. Yeh. (1964). Observation of diffusion broadening of Rayleigh scattered light. *Phys. Rev. Lett.*, 12, 150.

Cummins, H. Z. and E. R. Pike. (1976). *Photon Correlation and Light Beating Spectroscopy*. NATO Advanced Study Institute Series, Plenum Press, New York.

Dannon, D. and V. Marikovsky. (1964). Determination of density distribution of red cell population. *J. Lab. Clin. Med.*, 64, 668.

Debye, P. (1909). *Ann. Physik.*, 30, 59.

Desjardins, C. and H. D. Hafs. (1961). Enzymic degradation of hydrogen peroxide in egg-yolk. *J. Dairy Sci.*, 44, 1183.

Dott, H. and A. Walton. (1953). Apparatus for studying semen metabolism and sperm motility under constant fluid perfusion and known gaseous partial pressures. *J. Physiol.*, 122, 1P.

Drevius, L. O. (1972). Water content, specific gravity and concentrations of electrolytes in bull spermatozoa. *J. Reprod. Fert.*, 28, 15.

Dubin, S. B., J. H. Lunacek and G. B. Benedek. (1967). Observation of the spectrum of light scattered by solutions of biological macromolecules. *Proc. Nat. Acad. Sci. (Physics)*, 57, 1164-1171.

Dyott, R. B. (1978). The fibre-optic Doppler anemometer. *Microwaves, Optics and Acoustics*, 2, 1.

Foote, R. H. (1967). Influence of light and agitation on bovine spermatozoa stored with preservative agents. *J. Dairy Sci.*, 50, 1468-1474.

Frost, J. W. (1977). *Photon correlation studies of motile microorganisms*. Ph.D. Thesis, New York University.

Gans, R. (1925). *Ann. Physik.*, 76, 29.

Gassner, F. X., J. W. Goldzieher, J. F. Masken and M. L. Hopwood. (1959). The objective measurement of sperm motility. *Fertil. Steril.*, 10, 488-501.

Gibbons, I. R. (1962). Observations on the circular movement of sperm at an interface. *Proc. V. Int. Congr. for Electron Microscopy - M2*.

Glauber, R. J. (1963). Coherent and incoherent states of the radiation field. *Phys. Rev.*, 131, 2766.

Glover, F. A. (1968a). Physical method of measuring the motility of bull spermatozoa. *Nature, Lond.*, 219, 1263-1264.

Glover, F. A. (1968b). A new physical method of measuring the motility of bull spermatozoa. *Proc. VI Int. Congr. Anim. Reprod. and A.I.*, Paris.

Gray, J. (1958). The movement of the spermatozoa of the bull. *J. Exp. Biol.*, 35, 96-108.

Guinier, A. (1939). La diffraction des rayons X aux très petits angles: application a l'étude phénomènes ultra microscopiques. *Ann. Phys. (Paris)*, 12, 161-237.

Hackett, A. J. and J. W. MacPherson. (1965). Some staining procedures for spermatozoa; a review. *Canadian Vet. J.*, 6, 55-62.

Hafs, H. D., R. S. Hoyt, and R. W. Bratton. (1959). Libido, sperm characteristics, sperm output and fertility of mature dairy bulls ejaculated daily or weekly for thirty-two weeks. *J. Dairy Sci.*, 42, 626.

Hale, E. B. and J. O. Almquist. (1960). Relation of sexual behaviour to germ cell output in farm animals. *J. Dairy Sci.*, 43, (*Suppl.*), 145.

Hallett, F. R., T. Craig and J. Marsh. (1978). Swimming speed distributions of bull spermatozoa as determined by quasi-elastic light scattering. *Biophys. J.*, 21, 203-212.

Hamner, C. E. and W. L. Williams. (1961). *Biochem. Biophys. Res. Comm.*, 5, 316.

Hancock, J. L. (1952). The morphology of bull spermatozoa. *J. Exp. Biol.*, 29, 445-453.

Hancock, J. L. (1956). The morphology of boar spermatozoa. *J. Roy. Microsc. Soc.*, 76, 84-97.

Hancock, J. L. (1966). The ultra-structure of mammalian spermatozoa. *In* A. McLaren (Ed.). *Advances in Reproductive Physiology*, 1, p.28.

Hancock, J. L. and M. Paraschivescu. (1965). The motility of spermatozoa under glass and under polyethylene. *Vet. Rec.*, 77, 734-735.

Harvey, C. (1960). The speed of human spermatozoa and the effect on it of various diluents with some preliminary observations on clinical material. *J. Reprod. Fertil.*, 1, 84-95.

Harvey, J. D., D. F. Walls and M. W. Woolford. (1976). Electrophoretic investigations by laser light scattering. *Optics Commun.*, 18, 367-370.

Harvey, J. D. (1976). University of Auckland. Developed computer software enabling the Computer Automation LSI-2 computer system to sample a 16-bit input port at intervals determined by the system real time clock. The software via the same I/O module allowed control and sampling of the autocorrelator.

Harvey, J. D. and M. W. Woolford. (1980). Light scattering studies of bull spermatozoa. I. Orientational effects. *Biophys. J.*, 31, 147-156.

Hawley, S. A. (1980). *Unpublished research fellowship report* to Research Division of N.Z. Ministry of Agriculture and Fisheries.

Hodge, A. J. (1949). Electron microscopic studies of spermatozoa II. The morphology of human spermatozoa. *Australian J. Sci. Res., (B)*, 2, 368.

Holwill, M. E. J. (1966). Physical aspects of flagellar movement. *Physiological Reviews*, 46, 696-785.

Jakeman, E. (1974). Photon correlation. In H. Z. Cummins and E. R. Pike (Ed.), *Photon Correlation and Light Beating Spectroscopy*, Plenum, New York.

Janick, J. and J. MacLeod. (1970). The measurement of human sperm Motility. *Fertil. and Steril.*, 21, 140-146.

Jouannet, P., B. Volochine, P. Deguent, C. Serres and G. David. (1977). Light scattering determination of various characteristic parameters of spermatozoa motility in a series of human sperm. *Andrologia*, 9, 36.

Kampschmidt, R. F., D. T. Mayer and H. A. Herman. (1953). Lipid and lipo-protein constituents of egg-yolk in the resistance and storage of bull spermatozoa. *J. Dairy Sci.*, 36, 733-742.

Katz, D. F. (1974). On the propulsion of micro-organisms near solid boundaries. *J. Fluid Mech.*, 64, 33-49.

Katz, D. F. and J. R. Blake. (1974). Flagellar motions near walls. In T. Y. T. Wu, C. J. Brokaw and C. Brennan (Ed.), *Swimming and Flying in Nature*, 1.

Katz, D. F. and H. M. Dott. (1975). Methods of measuring swimming speed of spermatozoa. *J. Reprod. Fert.*, 45, 263-272.

Katz, D. F. and L. Pedrotti. (1977). Geotaxis by motile spermatozoa: hydrodynamic reorientation. *J. Theoretical Biol.*, 67, 723-732.

Keller, E. F. and L. A. Segel. (1971). Model for chemotaxis. *J. Theoretical Biol.*, 30, 225-234.

Kinosita, H. and A. Murakama. (1967). *Physiol. Rev.*, 47, 53.

Kirton, K. T. and H. D. Hafs. (1964). Sperm output of dairy bulls by repetitive ejaculation. *V. Int. Cong. Anim. Reprod.*, 4-5, 507-511.

Lamar, J. K., L. B. Shettles and E. Delfs. (1940). Cyclic penetration of human cervical mucus to spermatozoa *in vitro*. *Amer. J. Physiol.*, 13, 234.

Lavon, U., R. Volcani, D. Amir and D. Danon. (1966). The specific gravity of bull spermatozoa and seminal plasma. *J. Reprod. Fert.*, 11, 447-449.

Lindahl, P. E. and J. E. Kihlström. (1952). Alterations in specific gravity during the ripening of bull spermatozoa. *J. Dairy Sci.*, 35, 393.

Lindahl, P. E., J. E. Kihlström and B. Ström. (1952). *J. Agric. Sci.*, 42, 184.

Lindahl, P. E. and L. O. Thunqvist. (1965). Specific gravity of epididymal and ejaculated bull spermatozoa and their parts. *Experimentia*, 21, 94.

Linford, E., F. A. Glover, C. Bishop and D. L. Stewart. (1976). The relationship between semen evaluation methods and fertility in the bull. *J. Reprod. Fert.*, 47, 283-291.

Lobb, R. J. (1976). Wrote a 1024 point FFT algorithm in assembler code for the Computer Automation LSI-2 computer at Auckland University Physics Dept.

MacMillan, K. L. and R. J. Curnow. (1977). Factors influencing A. B. Conception rates. *N. Z. J. Exptl. Agric.*, 5, 279-285.

MacMillan, K. L. and J. D. Watson. (1975). Fertility differences between groups of sires relative to the stage of oestrus at the time of insemination. *Animal Production*, 21, 243.

Mann, T. (1945). Studies on the metabolism of semen. *Biochem. J.*, 39, 451-465.

Mann, T. (1964). *The Biochemistry of semen and of the Male Reproductive Tract*. Methuen and Co. Ltd., London.

Matsumoto, G., H. Shimizu, J. Shimada and A. Wada. (1977). Depolarised laser light scattered by motile spermatozoa. *Optics Commun.*, 22, 369-373.

Maude, A. D. (1963). Non-random distribution of bull spermatozoa in a drop of sperm suspension. *Nature*, 200, 381.

Mayer, D. T., D. Squires and R. Bogart. (1947). An investigation of the staining principle and the background stain in the differentiation of live from dead spermatozoa. *J. Anim. Sci.*, 6, 499.

Mie, G. (1908). *Ann. Physik*, 25, 377.

Moeller, A. N. (1955). *In vitro* speeds of bovine spermatozoa. *Fertil. and Steril.*, 6, 506-512.

Mukherjee, D. P. and H. M. Dott. (1960). Effects of egg-yolk citrate and egg-yolk glycine dilutors on the morphology of bovine spermatozoa. *J. Agric. Sci.*, 55, 225-228.

Nelson, L. (1967). Sperm Motility. *In* C. B. Metz and A. Monroy (Ed.). *Fertilisation*. Academic Press, New York-London.

Nevo, A. C. and R. Mohan. (1969). Migration of motile spermatozoa into sperm-free medium and the 'dilution effect'. *J. Reprod. Fert.*, 18, 379-381.

Norman, C. and E. Goldberg. (1959). Effect of light on motility, lifespan and respiration of bovine spermatozoa. *Science*, 130, 624-625.

Norman, C., E. Goldberg and I. D. Porterfield. (1962). The effect of visible radiation on the functional lifespan of mammalian and avian spermatozoa. *Exp. Cell. Res.*, 28, 69-84.

Nossal, R. (1971). Spectral analysis of laser light scattered from motile microorganisms. *Biophys. J.*, 11, 341-354.

Nossal, R., S. H. Chen and C. Lai. (1971). Use of laser scattering for quantitative determinations of bacterial motility. *Optics Communications*, 4, 35.

Nossal, R. and S. H. Chen. (1972a). Light scattering from motile bacteria. *J. Phys. (Paris)*, 33, C1: 171-176.

Nossal, R. and S. H. Chen. (1972b). Laser measurements of chemotactic response of bacteria. *Optics Comm.*, 5, 117-122.

Oster, G. (1950). The Scattering of light and its applications to chemistry. *Chem. Rev.*, 43, 319-365.

Pecora, R. (1964). *J. Chem. Phys.* 40, 1604.

Pecora, R. (1968). Spectral distribution of light scattered by monodisperse rigid rods. *J. Chem. Phys.*, 48, 4126-4128.

Perry, R., B. Thorell, L. Akerman and B. Chance. (1960). Microspectrophotometric measurements of the cytochromes in a mitochondrial aggregate *in vivo*. *Biochim. Biophys. Acta.*, 39, 24-32.

Phillips, D. M. (1970). Cinematographic analysis of mammalian spermatozoa. *J. Cell. Biol.*, 47, 238.

Phillips, D. M. (1972). Comparative analysis of mammalian sperm motility. *J. Cell. Biol.*, 53, 561-573.

Phillips, P. H. (1939). Preservation of bull semen. *J. Biol. Chem.*, 130, 145.

Phillips, R. and F. Andrews. (1937). The speed of travel of ram spermatozoa. *Anat. Rec.*, 68, 127.

Pike, E. R. (1970). *Review of Physics in Technology,* 180-194.

Rayleigh, Lord. (1871). *Phil. Mag.*, 41, 447.

Rayleigh, Lord. (1881). *Phil. Mag.*, 12, 81.

Rayleigh, Lord. (1910). The incidence of light upon a transparent sphere of dimensions comparable with the wavelength. *Proc. Roy. Soc.*, A84, 25-46.

Rayleigh, Lord. (1914). *Proc. Roy. Soc.*, A90, 219.

Rayleigh, Lord. (1918). *Proc. Roy. Soc.*, A94, 296.

Reynolds, A. J. (1965). The swimming of minute organisms. *J. Fluid Mech.*, 23, 241-260.

Reynolds, A. J. and Lord Rothschild. (1963). The stirring of the medium by bull spermatozoa. *Proc. Roy. Soc.*, B157, 461-472.

Rikmenspoel, R. (1957). *Experimentia,* 13, 124.

Rikmenspoel, R. (1960). Measurements of the motility of bull sperm cells under various conditions. *J. Agric. Sci.*, 54, 399-409.

Rikmenspoel, R. (1962). Biophysical approaches to the measurement of sperm motility. *In* D. W. Bishop (Ed.), *Spermatozoan Motility, Am. Assoc. Adv. Sci.*, Washington, D. C.

Rikmenspoel, R. (1964). Electronic analyser for measuring velocities and the concentration of spermatozoa. *Rev. Sci. Instrum.*, 35, 52-57.

Rikmenspoel, R. (1965). The tail movement of bull spermatozoa. Observations and model calculations. *Biophys. J.*, 5, 365-392.

Rikmenspoel, R. and van Herpen. (1957). Photoelectric and cinematographic measurements of the motility of bull sperm cells. *Phys. Med. Biol.*, 2, 54-63.

Roberts, A. M. (1970). Motion of spermatozoa in fluid streams. *Nature*, 228, 375-376.

Roberts, A. M. (1972). Gravitational separation of X and Y spermatozoa. *Nature*, 238, 223-225.

Roberts, A. M. (1974). The biased random walk and the analysis of microorganism movement. *In* T. Y. T. Wu, C. J. Brokaw and C. Brennan, *Proc. Symp. on Swimming and Flying in Nature*, 377-393.

Ross, D. A., H. S. Dhadwal and R. B. Dyott. (1978). The determination of the mean and standard deviation of the size distribution of a colloidal suspension of submicron particles using the fibre optic Doppler anemometer. *J. Colloid and Interface Sci.*, 64, 533-542.

Rothschild, Lord. (1948a). The activity of ram spermatozoa. *J. Exptl. Biol.*, 25, 219-226.

Rothschild, Lord. (1948b). The physiology of sea-urchin spermatozoa: senescence and the dilution effect. *J. Exptl. Biol.*, 25, 353-368.

Rothschild, Lord. (1949). Measurement of sperm activity before artificial insemination. *Nature*, 163, 358-359.

Rothschild, Lord. (1950a). Electrical measurement of bull sperm activity. *J. Agric. Sci.*, 40, 82-83.

Rothschild, Lord. (1950b). Cytochrome - catalysis of the movements of bracken spermatozoids. *Proc. Roy. Soc. B*, 138, 272-277.

Rothschild, Lord. (1951). Sea-urchin spermatozoa. *Biol. Rev.*, 26, 1-27.

Rothschild, Lord. (1953a). A new method of measuring the activity of spermatozoa. *J. Exptl. Biol.*, 30, 178-199.

Rothschild, Lord. (1953b). *In the movements of spermatozoa in mammalian germ cells.* Edited by Wolstenholme, The Ciba Foundation, J. A. Churchill Ltd.

Rothschild, Lord. (1961). *A Classification of Living Animals.* Longmans, Green, London.

Rothschild, Lord. (1962). Spermatozoa. *British Medical Journal,* 743-817.

Rothschild, Lord. (1963a). *In* D. W. Bishop (Ed.), *Spermatozoan Motility, Am. Assoc. Adv. Sci.*, Washington, D.C.

Rothschild, Lord. (1963b). Non-random distribution of bull spermatozoa in a drop of sperm suspension. *Nature,* 198, 1221-1222.

Rothschild, Lord, and G. Swann. (1949). The fertilisation reaction in sea-urchin egg. A propagated response to sperm attachment. *J. Exptl. Biol.*, 26, 164.

Rozin, S. (1960). Studies on seminal plasma: I. The role of seminal plasma in the motility of spermatozoa. *Fertil. and Steril.*, 11, 278-285.

Saake, R. G. and J. O. Almquist. (1964). Ultra-structure of bovine spermatozoa: I. The head of normal ejaculated sperm. *J. Dairy Sci.*, 115, 143-161.

Salisbury, G. W. (1957). Recent developments with bull semen diluents. *Anim. Breeding Abstr.: A review article,* 25, 111-123.

Salisbury, G. W. and C. G. van Dongen. (1965). A comparison of several methods of estimating nuclear size of bovine spermatozoa. *J. Anim. Sci.*, 23, 1098-1101.

Salisbury, G. W., E. L. Willett and I. C. Gunsalus. (1939). Some problems in bull semen storage. *Conf. on Artif. Insem. Proc. Amer. Soc. Anim. Prod.*

Salisbury, G. W., J. A. Zelaya and N. L. Vandemark. (1945). Livability and glycolysis of bovine spermatozoa in yolk-citrate, incubated eggs or chick embryo diluters. *J. Anim. Sci.*, 4, 270-276.

Schaefer, D. W. (1973). Dynamics of number fluctuations: motile microorganisms. *Science*, 180, 1293-1295.

Schaefer, D. W. and B. J. Berne. (1972). Light scattering from non-Gaussian concentration fluctuations. *Phys. Rev. Lett.*, 28, 475.

Schwartz, R. and H. H. Zinsser. (1955). Some factors modifying sperm progression. *Fertil. and Steril.* 6, 450.

Shannon, P. (1965). Contribution of seminal plasma, sperm numbers and gas phase to dilution effects of bovine spermatozoa. *J. Dairy Sci.*, 55, 1-7.

Shannon, P. (1973). Factors affecting storage of semen. *Proc. N.Z. Soc. Anim. Prod.*, 33, 40.

Shannon, P. and B. Curson. (1972). Toxic effect and action of dead sperm on diluted bovine semen. *J. Dairy Sci.*, 55, 614-620.

Shannon, P. (1980). Personal communication based on commercial A.I. practice at NZDB Artificial Breeding Laboratory.

Shimizu, H. and G. Matsumoto. (1977). Light scattering study on motile spermatozoa. *I.E.E.E. Trans. Biomed. Eng.*, BME-24, 153-157.

Shimizu, H. and G. Matsumoto. (1980). Observation of flagellation of spermatozoa by depolarised light scattering. *Biophys. J.*, 29, 167-176.

Smith, J. T., D. T. Mayer and C. P. Merilan. (1956). Effect of egg-yolk and its isolated constituents upon the dehydrogenase activity of bovine spermatozoa. *J. Dairy Sci.*, 39, 552-560.

Smith, S. E. and R. Newman. (1961). A qualitative method of determining sperm motility. *Fertil. and Steril.*, 12, 486-487.

Stock, G. B. (1976). Application of splines to the calculation of bacterial swimming speed distributions. *Biophys. J.*, 16, 535-540.

Stock, G. B. and Carlson, F. D. (1974). Photon autocorrelation spectra of wobbling and translating bacteria. *In* T. Y. T. Wu, C. J. Brokaw and C. Brennen, (Ed.). *Proc. Symp. on Swimming and Flying in Nature*, 57-68, Plenum, New York.

Swan, A. M. (1969). An equation relating the speed of ram spermatozoa to tail wave parameters. *J. Anat.*, 104, 410.

Szollosi, D. G. and H. Ris. (1961). Observations on sperm penetration in the rat. *J. Biophys. Biochem. Cytol.*, 10, 275.

Tampion, D. and R. A. Gibbons. (1962). Swimming rate of bull spermatozoa. *Nature*, 194, 695.

Tampion, D. and R. A. Gibbons. (1963). Swimming rate of bull spermatozoa in various media and the effect of dilution. *J. Reprod. Fertil.*, 5, 259-275.

Tanaka, T. and G. B. Benedek. (1975). Measurement of the velocity of blood flow (*in vivo*) using a fibre optic catheter and optical spectroscopy. *Appl. Optics*, 14, 189-196.

Taylor, Sir Geoffrey. (1951). The action of waving cylindrical tails in propelling microscopic organisms. *Proc. Royal Soc. (Lond.)*, A211, 225-239.

Tervitt, R. (1980). Unpublished data from an *in vivo* motility assay using ram semen inseminated into ewes. *Ruakura Agricultural Research Centre*, Hamilton, N.Z.

Timourian, H. and G. Watchmaker. (1970). Determination of spermatozoan motility. *Dev. Biol.*, 21, 62-72.

Tindel, C. (1977). Made available a FORTRAN routine RLQF, (originally written at the University of British Columbia) which gave a multi-function least squares fit.

Torre, L. de la, and G. W. Salisbury. (1964). Feulgen - DNA cytophotometry of bovine spermatozoa. *J. Dairy Sci.*, 47, 284.

Troll, J. and J. W. Goldzieher. (1962). Quantitative evaluation of the motility of spermatozoa. *Fertil. and Steril.*, 13, 72-83.

Uzgiris, E. E. (1972). Electrophoresis of particles and biological cells measured by the Doppler shift of scattered laser light. *Optics Commun.*, 6, 55-57.

van Demark, N. L., G. W. Salisbury and R. W. Bratton. (1949). Oxygen damage in bull spermatozoa and its prevention by catalase. *J. Dairy Sci.*, 32, 353-360.

van Dongen. (1963). Basis for an objective method of determining the physiological age of bovine spermatozoa. *J. Dairy Sci.*, 46, 618.

van Duijn, C. (1961). Effects of light and photosensitisation by some vital stains and fluorochromes on living bull spermatozoa. *4th Int. Congr. Anim. Reprod. & A.I.*, 249-254.

van Duijn, C. and R. Rikmenspoel. (1960). The mean velocity and velocity frequency distributions of normal bull spermatozoa at different hydrogen-ion concentrations, derived from photo-electric measurements. *J. Agric. Sci.*, 54, 300-309.

van Duijn, C. Jr. (1960). Measuration of the heads of bull spermatozoa. *Mikroskopie*, 14, 265.

van Duijn, C. Jr. (1962). Velocity characteristics and numbers of bull spermatozoa in relation to ageing, determined by photoelectric methods. *J. Reprod. Fertil.*, 4, 277-290.

van Duijn, C. and C. van Voorst. (1971). Precision measurements of dimensions, refractive index and mass of bull spermatozoa. *Mikroskopie*, 27, 142-167.

van Duijn, C. Jr. (1973). Positive hydrodynamic interaction between swimming bull spermatozoa. *Ann. Biol. Anim. Bioch. Biophys.*, 13, 7-15.

van Herpen, G. and R. Rikmenspoel. (1969). *Biophys. J.*, 9, 822.

van de Hulst, H. C. (1962). *Light Scattering by Small Particles, 2nd Edition*, Wiley, Inc., New York - London.

Veres, I. (1964). Electron microscopical investigations on bull sperm. *Proc. V Int. Congr. Anim. Reprod. and A.I. Trento*, 582-586.

Wales, R. G. and C. H. Choong. (1963). The effect of ultraviolet radiation on ram and bull spermatozoa. *Australian J. Biol. Sci.*, 16, 885-895.

Wall, K. A. and M. A. Boone. (1973). Objective measurement of sperm motility. *Poultry Sci.*, 52, 657-660.

Walton, A. (1952). Flow orientation as a possible explanation of 'wave-motion' and 'rheotaxis' of spermatozoa. *J. Experimental Biol.*, 29, 520-531.

Wang, C. P. and D. Snyder. (1974). Laser Doppler velocimetry: Experimental study. *Appl. Optics*, 13, 98-103.

Warner, F. D. (1973). The fine structure of the ciliary and flagellar axoneme. *In* M. A. Sleigh, *Cilia and Flagella*, Academic Press, London.

Watson, P. F. (1975). The interaction of egg-yolk and ram spermatozoa studied with a fluorescent probe. *J. Reprod. Fert.*, 42, 105-111.

Weihs, D. (1975). Some hydrodynamical aspects of fish schooling. *In* T. Y. Y. Wu, C. J. Brokaw and C. Brennan, *Proc. Symp. Swimming and Flying in Nature*, Plenum Press, New York.

Woolford, M. W., J. K. Woolhouse, D. S. M. Phillips, S. A. Hawley, J. D. Harvey, P. Shannon and B. Curson. (1980). Laser light scattering as a probe of sperm motility. *Proc. N.Z. Soc. Anim. Prod.*, 40, 124-129.

Woolhouse, J. K. (1976). *Bovine sperm motility studies by laser light beating spectroscopy*. M.Sc. Thesis, University of Waikato.

Wu, S. H. and J. D. Newstead. (1963). Electron microscope studies of bovine epididymal spermatozoa. (Abstr.). *J. Anim. Sci.*, 22, 867.

Wyatt, P. J. (1962). Scattering of electromagnetic plane waves from inhomogeneous spherically symmetric objects. *Phys. Rev.*, 127, 1837-1843.

Wyatt, P. J. (1968). Differential light scattering: A physical method for identifying living bacterial cells. *Appl. Optics*, 7, 1879.

Wyatt, P. J. (1972a). Light scattering in the microbial world. *J. Colloid and Interface Sci.*, 39, 479-491.

Wyatt, P. J. (1973). Differential light scattering techniques for microbiology. In *Methods in Microbiology*, 8, edited by Norris and Ribbons, Academic Press, New York.

Wyatt, P. J. and D. T. Phillips. (1972). Structure of a single bacteria from light scattering. *J. Theoretical Biol.*, 37, 493-501.

Yeh, Y. and R. N. Keeler. (1969). A new probe for reaction kinetics - the spectrum of scattered light. *Quarterly Reviews of Biophysics*. 2, 315-349.

Zittle, C. A. and B. Zittin. (1942). *J. Biol. Chem.*, 144, 99.

Zorgniotti, A. W., R. S. Hotchkiss and L. C. Wall. (1958). High speed cinephotomicrography of human spermatozoa. *Med. Rad. and Photography*, 34, 44-49.